THE FORMATION OF POLYCYCLIC AROMATIC HYDROCARBONS AND SOOT IN A JET-STIRRED/PLUG-FLOW REACTOR

BY

FREDERICK WARREN LAM

B.S. Chemical Engineering, University of California, Berkeley (1983)

SUBMITTED TO THE
DEPARTMENT OF CHEMICAL ENGINEERING
IN PARTIAL FULFILLMENT
OF THE REQUIREMENTS FOR THE DEGREE OF

DOCTOR OF PHILOSOPHY

at the

MASSACHUSETTS INSTITUTE OF TECHNOLOGY

December, 1988

Signature of author _____
Department of Chemical Engineering
December 21, 1988

Certified by _____
John P. Longwell
Thesis Supervisor

_____
Jack B. Howard
Thesis Supervisor

Accepted by _____
Robert C. Armstrong
Chairman, Departmental Graduate Committee

Vol. 1

THE FORMATION OF POLYCYCLIC AROMATIC HYDROCARBONS AND SOOT IN A JET-STIRRED/PLUG-FLOW REACTOR

BY

FREDERICK WARREN LAM

Submitted to the Department of Chemical Engineering on December 21, 1988, in partial fulfillment of the requirements for the Degree of Doctor of Philosophy in Chemical Engineering.

ABSTRACT

An experimental investigation of Polycyclic Aromatic Hydrocarbon (PAH) and soot formation in a Jet-Stirred/Plug-Flow Reactor (JSR/PFR) involved measurement of PFR stable species concentration profiles of fixed gases, light hydrocarbons, aromatics, PAH, tar and soot. At 1630K, 1 atm, for fuel-rich (ϕ=2.18) and sooting (ϕ=2.37) conditions in the JSR, $C_2H_4/O_2/N_2$ mixtures were combusted with typical residence times of 5 ms in the JSR and 15 ms in the PFR. Injection of C_2H_4 and C_6H_6 into the upsteam end of the PFR tested the effect of aliphatic and aromatic species on PAH and soot formation.

As expected, the concentration profiles of fixed gases and major light hydrocarbon species changed little in the PFR as the equivalence ratio was increased from non-sooting to incipient sooting conditions in the JSR; but for the sooting condition, the tar concentration increased 5-fold, and the soot concentration increased 10-fold. At the end of the PFR, the combined mass concentration of PAH species with 2-5 rings is comparable that of the high molecular weight tar material (≥6 rings and CH_2Cl_2-soluble).

Injection of C_2H_4 (8200 ppm at ϕ=2.37, 10,000 ppm at ϕ=2.18) into the PFR results predominantly in conversion to C_2H_2, but also increases the concentrations of benzene and PAH. An incremental amount of C_2H_4 injected into the PFR is not as effective in enhancing PAH and soot production as the same incremental amount of C_2H_4 fed to the JSR. Injection of a small amount of C_6H_6 (1800 ppm) into the PFR caused a 10-fold increase in the PAH and soot concentrations in the PFR for the ϕ = 2.18 condition studied. Assuming the 10-fold increase in tar and soot concentration comes from benzene, then these data indicate that 16% of the injected benzene was converted to tar and 11% to soot. Oxidation of C_6H_6 to CO and C_2H_2 was also occurring. Benzene promoted tar and soot formation by causing a 10-fold increase in the benzene concentration at the beginning of the PFR. This observation is consistent with the hypothesis that the number concentration of single-ring aromatics in a combustion environment with high C_2H_2 concentrations controls the growth of higher aromatics. An increase in benzene concentration increases the production of 2-ring aromatics, and is the major source of new moles of PAH material.

PAH species which contain 5-membered ring structures account for more than half of the total PAH inventory from indene (C_9H_8) to benzo(ghi)perylene ($C_{22}H_{12}$). These PAH species with 5-membered ring structures consisted of 2 types: 1) 5-membered rings containing a methylene group, which may be oxidation products of 6-membered ring

species, and 2) "acenaphthylene bridge" structures, which may be growth products from acetylene addition.

Acetylenic-substituted PAH species, which have been proposed as important intermediates in PAH formation, were positively identified by the use of Gas Chromatography/Fourier Transform Infrared Spectroscopy (GC/FTIR). Phenylacetylene formation from the injected benzene is rapid, and the ratio of phenylacetylene to benzene is near that predicted from equilibration of the reaction $C_6H_6 + C_2H_2 = C_8H_6 + H_2$.

Fixed gases and major hydrocarbon species (CO, CO_2, H_2, CH_4, C_2H_2, C_2H_4) can be modelled assuming a perfectly-stirred/plug-flow reactor system using an elementary reaction mechanism proposed by Glarborg (1986a), which contains 134 reactions, and 29 chemical species, or by a mechanism proposed by Harris (1988a) consisting of 193 reactions and 49 species.

Thermodynamics analysis of the PAH reveals that, with the exception of the ethynyl-acenaphthylenes, the most abundant PAH species observed experimentally are the stabilomers predicted by Stein (1985), which are the most thermodynamically stable species for a given carbon and hydrogen number. Aliphatic hydrocarbons with the general formula $C_{2n}H_{2m}$ are produced in excess concentrations in the JSR for equilibration of the C_2H_2-H_2-$C_{2n}H_{2m}$ system, and these species decay towards their equilibrium limits in the PFR. Aromatic species, including PAH, with the general formula $C_{2n}H_{2m}$ are far below their equilibrium limit, but are increasing towards their predicted thermodynamic limits in the PFR.

A kinetics model of PAH (2-5 rings species) formation successfully predicted the concentration profile of the PAH inventory in the PFR at ϕ=2.18, as well as the perturbation to the PAH profiles from the injection of additional ethylene and benzene. The model includes pathways for mass flux into the PAH inventory due to 1) C_2H_2 addition reactions with single-ring aromatics and 2) C_2H_2 addition reactions with PAH; and pathways for mass flux out of the PAH inventory by 3) C_2H_2 addition reactions with 5-ring PAH, 4) coagulation reactions between PAH, 5) coagulation of PAH with high molecular weight tar, 6) coagulation of PAH with soot, and 7) oxidation reactions of PAH with OH. Acetylene addition to aromatic species provided the major source of mass flux into the PAH inventory, while oxidation was the main route of mass loss from the PAH inventory. PAH coagulation reactions, consisting of bimolecular reactions of aryl species reacting with intact aromatic rings, is not the dominant mechanism of PAH formation. Coagulation of PAH with soot was predicted to have low collision efficiencies ($\approx$ 1%). A collision efficiency, γ, of 0.2 for OH with PAH (based on γ = 0.2 for OH reaction with soot) was necessary in order to successfully predict the experimental trends. This rate is $\approx$40 times higher than the rate of benzene oxidation by reaction with OH.

Thesis Supervisors: Professor John P. Longwell
Professor Jack B. Howard

ACKNOWLEDGEMENTS

I would like to express my most sincere appreciation to my thesis advisors, Professor John Longwell and Professor Jack Howard for their guidance and support through the years. To Professor Longwell, I thank him for his irrepressible enthusiasm, extensive knowledge, and keen sense of humor, all of which were usually displayed during our (sometimes) very long meetings. My apologies to Mrs. Longwell for her dinners I've spoiled by keeping Professor Longwell late. To Professor Howard, I thank him for his patience, encouragement of careful and rigorous analysis, and gracious manner.

I would like to thank Professor Robert Alberty for invigorating PAH thermodynamic discussions, and Dr. Steve Stein for the computer programs to estimate PAH thermochemistry.

Many thanks go to members of the Center: Art Lafleur, Pete Monchamp, and Elaine Plummer of the Analytical Chemistry Group for their assistance with the PAH chemical analysis and for discussions of what we see and don't see in those bloody complicated chromatograms; Tony Modestino for his overall experimental expertise (especially with cranky GC's); Ed Kruzel for helping me get started with the PAH sampling; Andy Braun and Lata Shirname-More for the bioassays and discussions on how to interpret those results.

To all the guys in the lab and the office, Tom McKinnon, Craig Vaughn, Andreas Kridiotis, Tom Griffin, Glen Ko, Alain Bourhis, Derek Mess, George Darivakis, Bob Barat, Joe Marr, and Steve Hsu; thanks for your advice, friendship and support; and to the other members of our 10.731 group, Carl Wikstrom, Rich Shandross, Chris Pope, and the one and only, Phil Westmoreland. The technical contributions of UROP students Martha Morgan and Dave Wright were also appreciated.

Many others have made my stay at M.I.T. enjoyable, so thanks to all those who joined me for the "Worthless and Weak" team tradition of intramural sports, for poker games at the top of Tang, and of course, Fridays at the Muddy and all the festivities which that usually entailed. Special thanks to our close friends for the good times here in Boston. Cindy and I will always have terrific memories of our times together. I would also like to let my family know my appreciation for their support during my tenure here at M.I.T.

Finally, I would like to let my fiánce, Cindy, know how much I love her, and for being my joy and support always.

I am grateful to the National Institute of Environmental Health Sciences (N.I.E.H.S.) for sponsoring this research.

TABLE OF CONTENTS

LIST OF FIGURES

LIST OF TABLES

S. SUMMARY

S.1 INTRODUCTION

Polycyclic aromatic hydrocarbons (PAH) and soot are undesirable products of fuel-rich combustion that pose biological and environmental hazards. Certain PAH are known to be mutagenic to bacterial cells (Kaden, 1979) and human cells (Thilly, 1986) and may adsorb onto soot particles and be transported into the human body by inhalation. Practical combustors, such as large industrial furnaces, do not have control strategies to minimize PAH formation, and may actually enhance the production of PAH. For example, in large furnaces staged combustion is used to control NO_x emissions, and soot is allowed to form in the primary chamber under fuel-rich conditions. Soot enhances radiative heat transfer to the walls of the furnace, but PAH are also formed under fuel rich conditions, and PAH destruction in the secondary chamber is not certain. In order to identify PAH reduction strategies in practical combustors, their formation chemistry must be understood.

The chemistry of lean combustion is fairly well understood, and networks of elementary reactions predict experimental observations with surprising accuracy. Rich combustion chemistry is not so well understood, probably because of the large number of species, including PAH, which are generated. Many of these species have molecular weights higher than the parent fuel molecule, and molecular-weight growth processes must be responsible for their formation. Although the tremendous number of individual species complicates chemical analysis, measurements for chemical species of molecular weights higher and lower than the parent fuel molecule must be obtained in order to gain an understanding of molecular weight growth.

The field of soot formation has been studied by many, but the amount of research which has been focused on the formation and destruction of PAH is small, mainly because the problem has been identified only recently as a biological hazard. Recent reviews of the field of PAH formation (Longwell, 1982; Homann, 1984) and soot formation (Haynes and Wagner, 1980) have highlighted the importance of temperature, fuel-type, mixing, ions, and radical species in deter-

mining different pathways for molecular-weight growth. These factors influence the production of aromatic and aliphatic species, and there is much evidence, both experimental (Scully, 1964; Davies, 1965; Asaba, 1971, Bauer, 1983; Bittner, 1981a, 1981b, 1981c; Cole, 1984; Frenklach, 1983, 1985a; and Bockhorn, 1983) and theoretical (Bauer, 1987; Frenklach, 1985b, 1987, 1988; Harris 1988b; and Stein, 1985) that the molecular-weight growth process is determined by reactions between the aromatic and aliphatic species.

The general goals of this research are to obtain a better understanding of the molecular weight growth process which forms PAH and eventually soot during combustion. The specific objectives of this dissertation are to:

1) Obtain experimental measurements for fixed gases, light hydrocarbons, PAH and soot in a plug-flow reactor for $C_2H_4/O_2/N_2$ combustion under non-sooting and sooting conditions in an upstream jet-stirred reactor;
2) Investigate the effects of aliphatic and aromatic species on molecular-weight growth;
3) Model the hydrocarbon chemistry at the elementary reaction level;
4) Develop a kinetics model for the formation of PAH;
5) Identify and assess the mutagenicity of PAH produced during combustion through collaborative efforts with researchers in the Analytical Chemistry and Toxicology departments.

S.2 EXPERIMENTAL

Figure S.1 shows a schematic of the Jet-Stirred/Plug-Flow Reactor (JSR/PFR) used in this research. Pre-mixed fuel and air are fed through 32 sonic jets, located on the outside circumference of the toroidal JSR, to produce a intensely back-mixed, turbulent combustion zone in the JSR. The burned gases exit the JSR and proceed through eight exhaust ports, a flow straightener, and the PFR in turbulent flow. Flow visualization studies were performed using a plexiglass reactor and revealed a corkscrew flow pattern in the PFR which

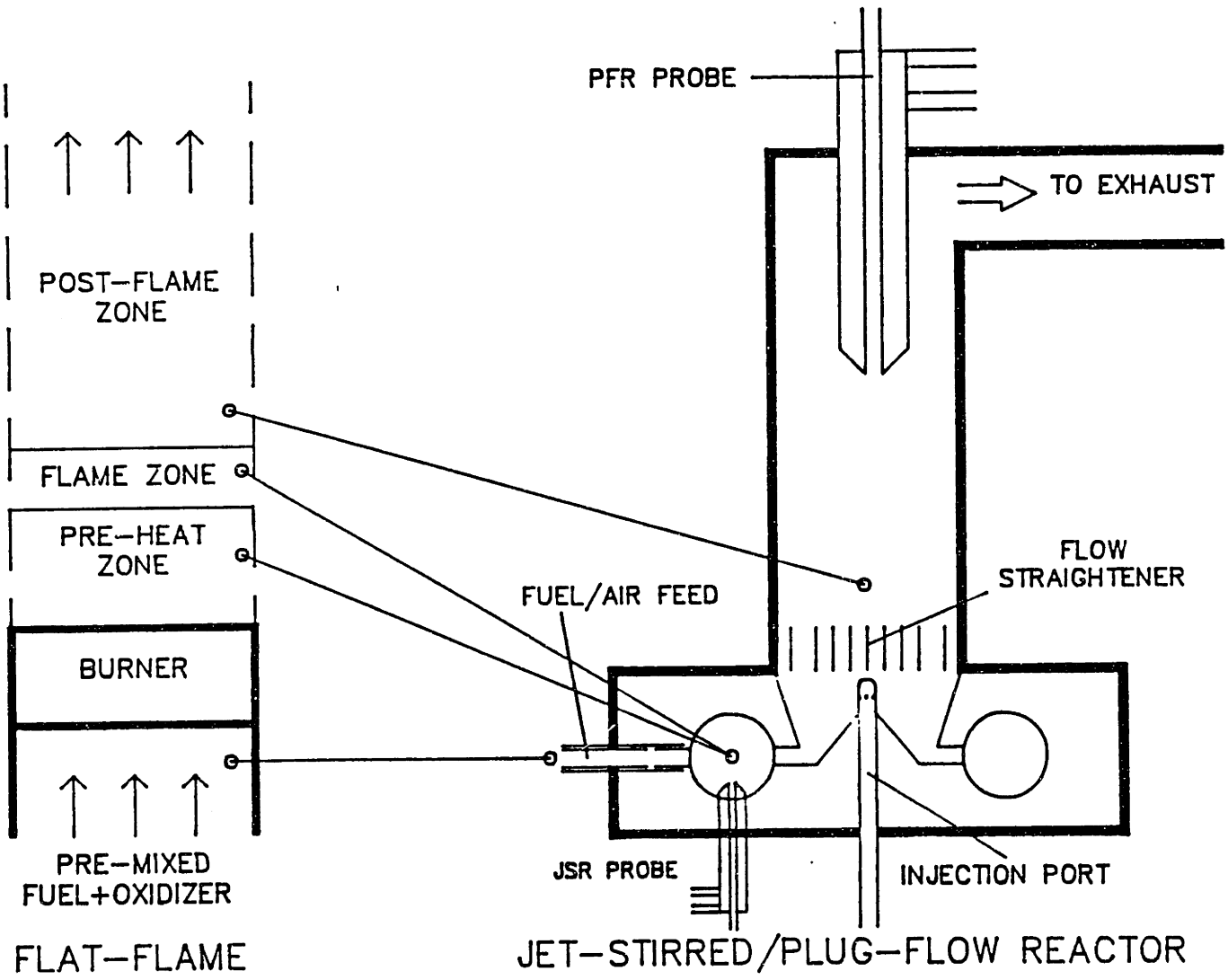

Figure S.1 Schematic of Jet-Stirred/Plug-Flow Reactor (JSR/PFR) and comparison to laminar flat-flame.

necessitated the design of the flow straightener. An additive system was built to allow the injection of either gaseous or liquid species into the PFR to test the effect of an incremental amount (≈1% of total flow) of an aliphatic (C_2H_4) and an aromatic (C_6H_6) species on the formation of PAH and soot. An injection port allows the addition of chemical species through 8 radial jets directly into the upstream end of the PFR. Details of the JSR/PFR may be found elsewhere (Nenniger, 1983, 1985; Sun, 1985).

The JSR/PFR operates at atmospheric pressure, and typical residence times in the JSR range from 5-7 ms, and in the PFR from 15-20 ms. Temperature was measured using type R (Pt/Pt87%-Rh13%) thermocouples. Stable species are sampled in the JSR/PFR using stainless steel water-cooled probes. Residence time in the PFR is varied by varying probe position along the reactor centerline.

The JSR/PFR system has several advantages over laminar flat-flames. Analysis of the chemistry of PAH and soot during the early stages of soot formation in laminar flat-flames is complicated by steep concentration gradients, difficulty in obtaining sufficient spatial resolution, and probe disturbances to the flame. The velocity of the gas in the PFR is 25 m/s (Reynolds number = 4×10^5), so axial diffusion of species is negligible (Taylor dispersion coefficient = 0.033). Thus, reaction rates may be obtained by differentiation of the concentration versus time profiles. The total PFR residence time of 15 msec is spread over a PFR length of 0.3 m, so spatial resolution is excellent. Probe disturbances are small because the PFR does not have flame stabilization problems. The PFR is nearly isothermal. Finally, the injection system allows one to test the effect of additive species, without those species being destroyed passing through an oxidation zone.

Stable species data were collected for fixed gases, light hydrocarbons, aromatics, polycyclic aromatic hydrocarbons (PAH), and soot at incipient (ϕ^*=2.37, T=1630K) and non-sooting (ϕ=2.18, T=1630K)

---

* where ϕ is equivalence ratio = $\frac{\text{(mole fuel/mole air)}}{\text{(mole fuel/mole air)}_{\text{stoichiometric}}}$

conditions for $C_2H_4/O_2/N_2$ combustion in the JSR. A PAH sampling system (Fig. S.2) was developed, and a variety of analytical techniques were used for species quantification (Tables S.1 and S.2). Concentration profiles for 16 aliphatic species, 21 individual aromatic and polyaromatic species (1-5 rings), total tar (CH_2Cl_2-soluble material with masses ≥128 amu) and soot (CH_2Cl_2-insoluble material) were obtained.

S.3 CHEMICAL SPECIES CHARACTERIZATION

A tremendous number and variety of species are observed in the JSR-PFR under our fuel-rich (sooting) experimental conditions. Figure S.3 shows the types and relative amounts of the major stable species which are measured in the PFR. It is convenient to categorize these species into three general classes:

- -aliphatic (acyclic) species
- -unsubstituted aromatic species
- -substituted aromatic species

The first class of species includes the fixed gases and light hydrocarbons, and accounts for most of the carbon mass; the second class contains most of the mass of the PAH inventory; and the third class is dominated by methyl- and ethynyl-substituted aromatics.

A total of 16 acyclic hydrocarbons are routinely measured and more than 130 individual PAH species are observed, and Table S.3 shows identifications for 35 species and tentative identifications for 32 species. Although a large number of PAH species are not identified, the identified species constitute more than 98% of the total GC chromatogram area. The unidentified species appear as very small peaks on the chromatogram (Fig. S.4), and it is difficult to distinguish these peaks from the baseline noise.

The substituted aromatic species are usually found in concentrations 1-2 orders of magnitude lower than the parent unsubstituted species. Acetylenic-substituted PAH species, which have been proposed as important intermediates in PAH formation, were positively

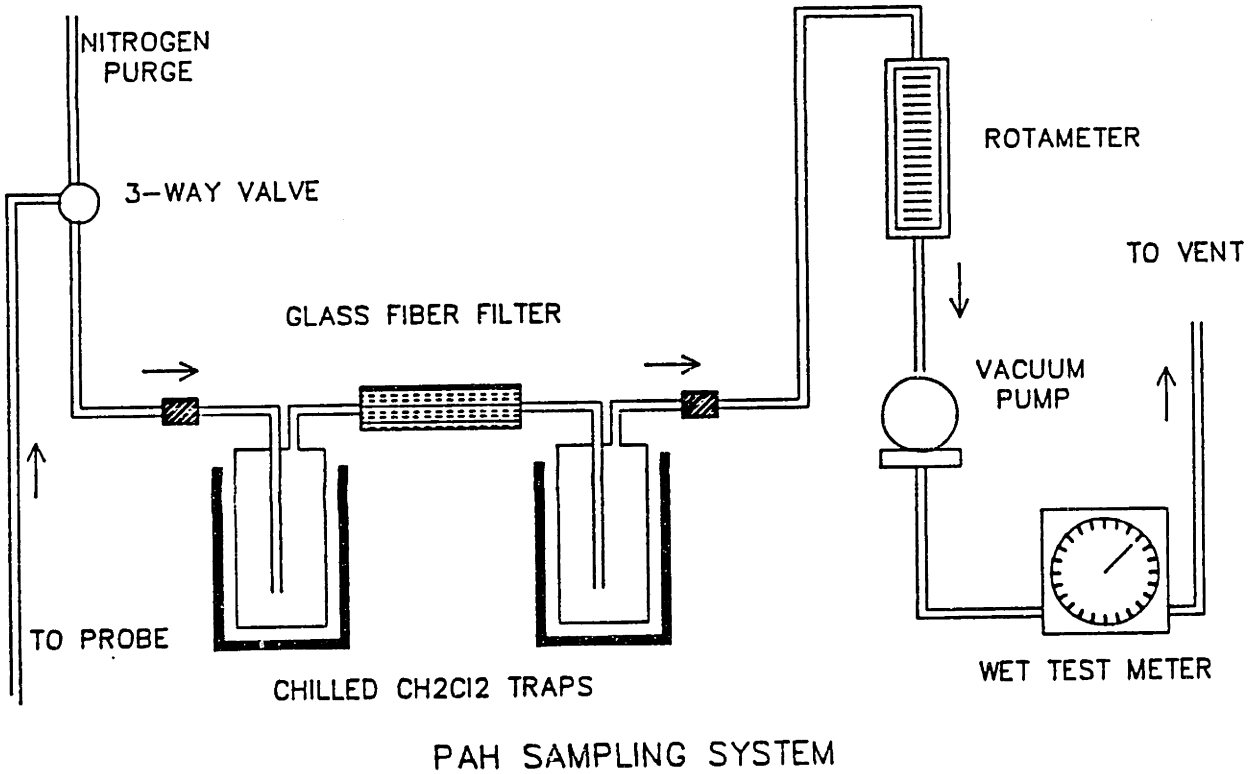

Figure S.2 Polycyclic aromatic hydrocarbon sampling system.

TABLE S.1 - SUMMARY OF EXPERIMENTAL METHODS

SPECIES	SAMPLING METHOD	ANALYSIS METHOD
Fixed gases		
(H_2, CO)	Glass Sampling Bulb	GC-mole sieve (5Å)
(CO_2)	Glass Sampling Bulb	GC-Spherocarb
Light Hydrocarbons		
(CH_4, C_2H_2, C_2H_4, C_2H_6)	Glass Sampling Bulb	GC-Poropak T
(C3 - C4)	Glass Sampling Bulb	GC-0.19% Picric Acid on Graphpac
Aromatics		
(C4 - C8)	Glass Sampling Bulb	GC-DB5 capillary
PAH		
(C6H6-C22H10)	CH_2Cl_2 Liquid Traps	GC-DB5 capillary
Total Tar		
(CH_2Cl_2 solubles)	CH_2Cl_2 Liquid Traps	Microgravimetric evaporation
Soot		
(CH_2Cl_2 insolubles)	Fluorocarbon coated Fibrous filters	Analytical Balance

TABLE S.2 - HIGH MOLECULAR WEIGHT SPECIES

Measurement	Species Range	MW Range
ΣGC PAH	Naphthalene - Cyclopenta(cd)pyrene	128 - 226 amu
High MW TAR	Benzopyrenes - solubility limit in CH_2Cl_2	252 - ≈1000 amu
SOOT	CH_2Cl_2 non-solubles - solid particulates	≈1000 - ∞ amu

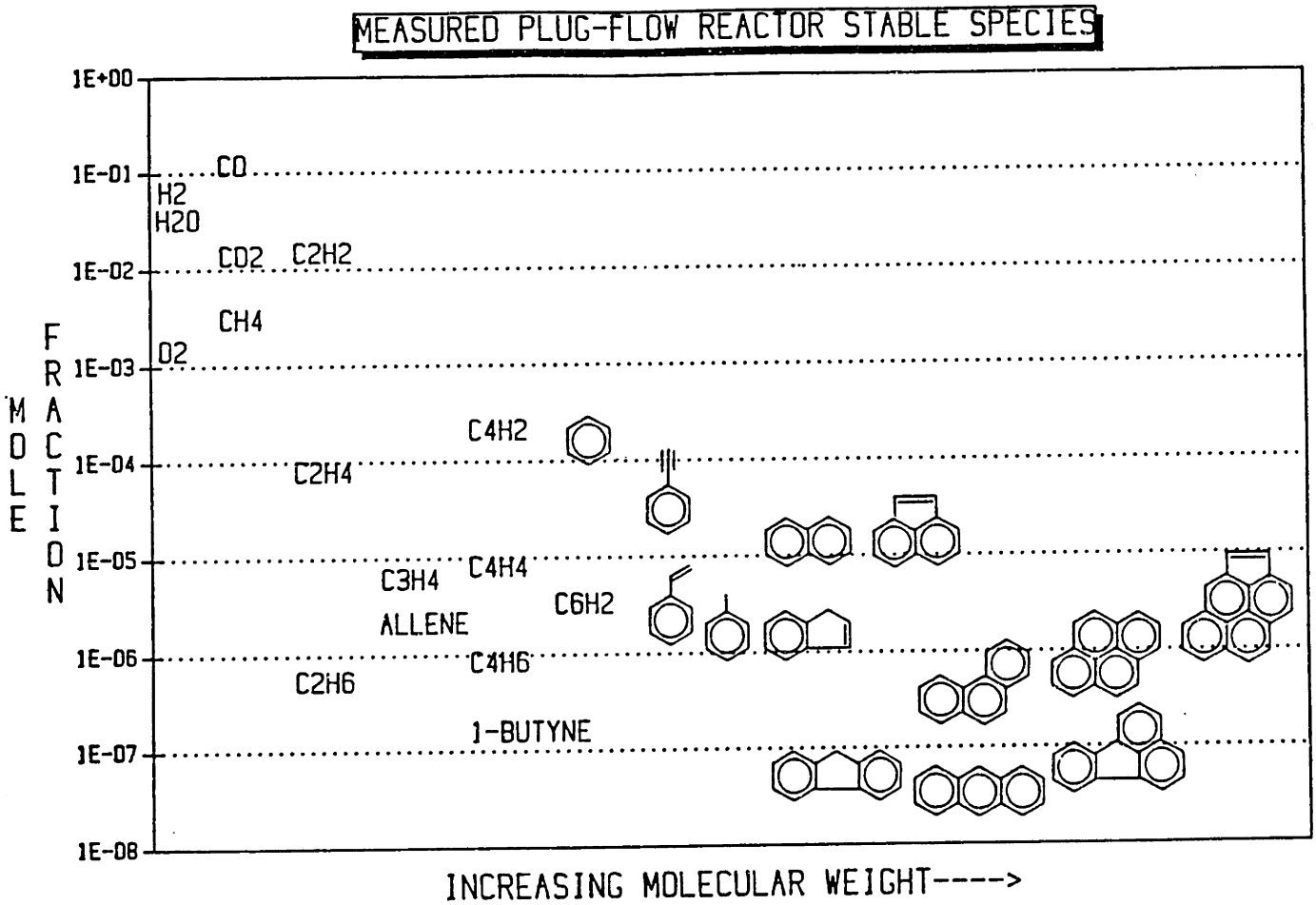

Figure S.3 Relative Concentrations of measured PFR stable species.

identified (Lafleur, 1988a) by the use of Gas Chromatography/Fourier Transform Infrared Spectroscopy (GC/FTIR). The IR spectra of acetylenic-substituted species, such as 2-ethynyl naphthalene (Fig. S.5) show a very strong absorbance at 3300 cm^{-1} due to (≡C-H) stretching, and isomer differentiation was possible by inspection of the aromatic C-H bending modes (700-1000 cm^{-1}). Other identified acetylenic-substituted PAH species include phenylacetylene (C_8H_6), 1,2-, 1,3-, and 1,4-di-ethynyl-benzene ($C_{10}H_6$), and 3 different ethynyl-acenaphthylene isomers.

PAH species which contain 5-membered ring structures account for more than half of the total PAH inventory from indene (C_9H_8) to benzo(ghi)perylene ($C_{22}H_{12}$), on either a mass or mole basis. These PAH species with 5-membered ring structures consisted of 2 types: 1) 5-membered rings containing a methylene group which may be oxidation products of 6-membered ring PAH (e.g., cyclopentadiene, indene, fluorene, and 4H-cyclopenta(def)phenanthrene); and 2) "acenaphthylene bridge" structures which may result from C_2H_2 addition reactions to PAH followed by cyclization (e.g., acenaphthylene, acephenanthrylene, aceanthrylene, and cyclopenta(cd)pyrene).

In addition to characterization of the stable chemical species, soot particles were examined using Transmission Electron Microscopy (TEM), and elemental (C/H/O) analyses of the soot were performed.

S.4 DATA OVERVIEW

Two different baseline experimental conditions (Table S.4) were studied (ϕ=2.18 and ϕ=2.37, T=1630K in JSR), and the effect of an aromatic and aliphatic species as additives for the ϕ=2.18 condition will be discussed in this overview. For ϕ=2.18, the flow rate of injected C_2H_4 into the PFR was the same as the difference between the ϕ=2.18 and ϕ=2.37 C_2H_4 flow rates into the JSR. Complete conversion of the injected C_2H_4 would increase the carbon atom mole fraction by 1.9×10^{-2} mole C-atom/mole flame gas, or mass concentration by 1.7×10^{-6} gram C-atom/cm^3 flame gas. Complete conversion of the injected C_6H_6 would increase mole fraction by 1.1×10^{-2} mole C-atom/mole flame gas, or 1.0×10^{-6} gram C-atom/cm^3 flame gas. On either a mole or mass

TABLE S.3 - DETAILED PAH SPECIES IDENTIFICATION

PEAK #	RETENTION INDEX	MW	FORMULA	SPECIES NAME (if known)	IDENTIFIED BY METHOD# 1	2	3	4
1	95.92							
2	96.75							
3	97.70							
4	100.00	78	C6H6	BENZENE	X	X	X	X
5	104.19							
6	105.34							
7	105.97	76	C6H4	HEXENE-DIYNE		X	X	
8	108.27	72	C6H2	TRIACETYLENE		X	X	
9	116.44							
10	119.27	92	C7H8	TOLUENE		X		X
11	121.47	90	C7H6			X		
12	127.64	90	C7H6			X		
13	131.20							
14	132.25							
15	133.40							
16	138.95							
17	140.73	106	C8H10	ETHYLBENZENE, XYLENE		X		X
18	142.62	102	C8H6	PHENYLACETYLENE		X	X	X
19	144.92	104	C8H8	STYRENE		X	X	X
20	150.26	88	C7H4	METHYL TRIACETYLENE		X	X	
21	152.25							
22	152.98							
23	155.81							
24	161.88	98	C8H2	TETRA-ACETYLENE		X	X	
25	171.20							
26	175.08	116	C9H8	INDENE		X	X	X
27	178.22							
28	180.00	126	C10H6	1,3-DIETHYNYL-BENZENE		X	X	
29	183.77	126	C10H6	1,4-DIETHYNYL-BENZENE		X	X	
30	186.49							
31	192.04							
32	195.08	128	C10H8			X		
33	197.59	126	C10H6	1,2-DIETHYNYL-BENZENE		X	X	
34	200.00	128	C10H8	NAPHTHALENE	X	X	X	X
35	209.61							
36	215.27	140	C11H8	ETHYNYL INDENE ISOMER		X	X	
37	217.49	140	C11H8	ETHYNYL INDENE ISOMER		X	X	
38	221.06	142	C11H10	2-METHYL NAPHTHALENE		X		X
39	224.26	142	C11H10	1-METHYL NAPHTHALENE		X		X
40	230.54							
41	236.21							
42	240.64	152	C12H8	2-ETHYNYL NAPHTHYLENE		X	X	
43	248.40	152	C12H8	ACENAPHTHYLENE	X	X	X	X
44	267.36	166	C13H10			X		
45	270.32	166	C13H10	FLUORENE	X	X		X
46	273.65							
47	275.99							

TABLE S.3 - DETAILED PAH SPECIES IDENTIFICATION (cont.)

PEAK #	RETENTION INDEX	MW	FORMULA	SPECIES NAME (if known)	IDENTIFIED BY METHOD# 1	2	3	4
49	282.51	176	C14H8	ETHYNYL-ACENAPHTHYLENE		X	X	
50	284.24	176	C14H8	ETHYNYL-ACENAPHTHYLENE		X	X	
51	285.59	176	C14H8	ETHYNYL-ACENAPHTHYLENE		X	X	
52	289.41							
53	292.98	176	C14H8			X		
54	294.46							
55	300.00	178	C14H10	PHENANTHRENE	X	X		X
56	301.76	178	C14H10	ANTHRACENE	X	X		X
57	304.40							
58	306.59							
59	310.99							
60	312.45							
61	314.06							
62	317.29							
63	318.75							
64	321.24							
65	322.56	190	C15H10	4H-CYCLOPENTA(def)-	X	X		X
66	324.61			PHENANTHRENE				
67	326.37							
68	330.62	204	C16H12			X		
69	333.84							
70	336.04	202	C16H10			X		
71	337.36	202	C16H10			X		
72	339.12							
73	341.02							
74	343.07	204	C16H12			X		
75	344.83	202	C16H10	FLUORANTHENE	X	X		X
76	348.49	202	C16H10	ACEPHENANTHRYLENE		X		X
77	351.28	202	C16H10	ACEANTHRYLENE		X		X
78	353.18	202	C16H10	PYRENE	X	X		X
79	358.60							
80	359.34							
81	360.80	214	C17H10			X		
82	362.12							
83	366.51							
84	367.54							
85	369.01	216	C17H12			X		
86	369.88							
87	372.67	214	C17H10			X		
88	374.13	228	C18H12			X		
89	375.89	226	C18H10			X		
90	378.09	226	C18H10			X		
91	379.11	226	C18H10			X		
92	380.29	226	C18H10			X		
93	382.04							
94	382.92							
95	384.54	226	C18H10			X		

TABLE S.3 - DETAILED PAH SPECIES IDENTIFICATION (cont.)

PEAK #	RETENTION INDEX	MW	FORMULA	SPECIES NAME (if known)	IDENTIFIED BY METHOD# 1	2	3	4
96	386.29							
97	389.37							
98	390.84	226	C18H10	BENZO(ghi)FLUORANTHENE		X		X
99	391.86	226	C18H10			X		
100	393.77	226	C18H10			X		
101	396.11	226	C18H10			X		
102	398.60	226	C18H10	CYCLOPENTA(cd)PYRENE		X		X
103	402.41	228	C18H12			X		
104	404.46							
105	405.49							
106	407.10							
107	408.71							
108	409.88							
109	412.66							
110	413.84							
111	415.89							
112	417.21							
113	418.09							
114	419.11							
115	424.68							
116	425.41							
117	427.32	250	C20H10			X		
118	434.93							
119	436.25							
120	439.77	250	C20H10			X		
121	441.53	250	C20H10			X		
122	445.92	252	C20H12			X		
123	452.52	252	C20H12			X		
124	455.74	252	C20H12			X		
125	459.84							
126	475.96							
127	483.87	264	C21H12			X		
128	491.63							
129	514.93	276	C22H12			X		
130	521.37	276	C22H12			X		
131	528.85	276	C22H12			X		
132	548.48	276	C22H12	BENZO(ghi)PERYLENE		X		X
133	562.40							

Identification Methods:
1 = Species in PAH standard
2 = GC/MS
3 = GC/FTIR
4 = Correlation of Retention Indices

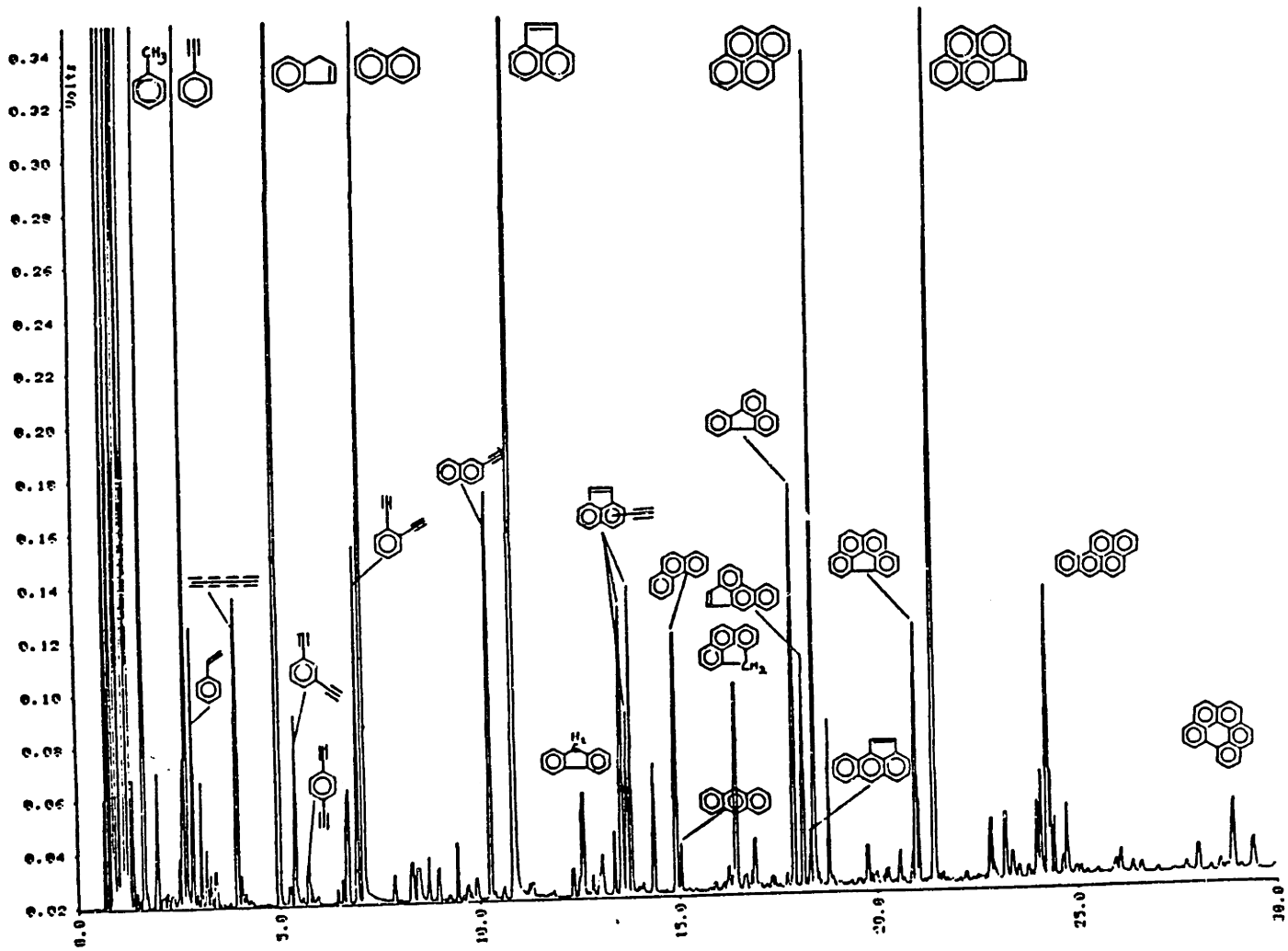

Figure S.4 Gas Chromatogram of PAH species, at PFR residence time of 12.7 msec for ϕ=2.37, JSR T=1630K, $C_2H_4/O_2/N_2$ combustion.

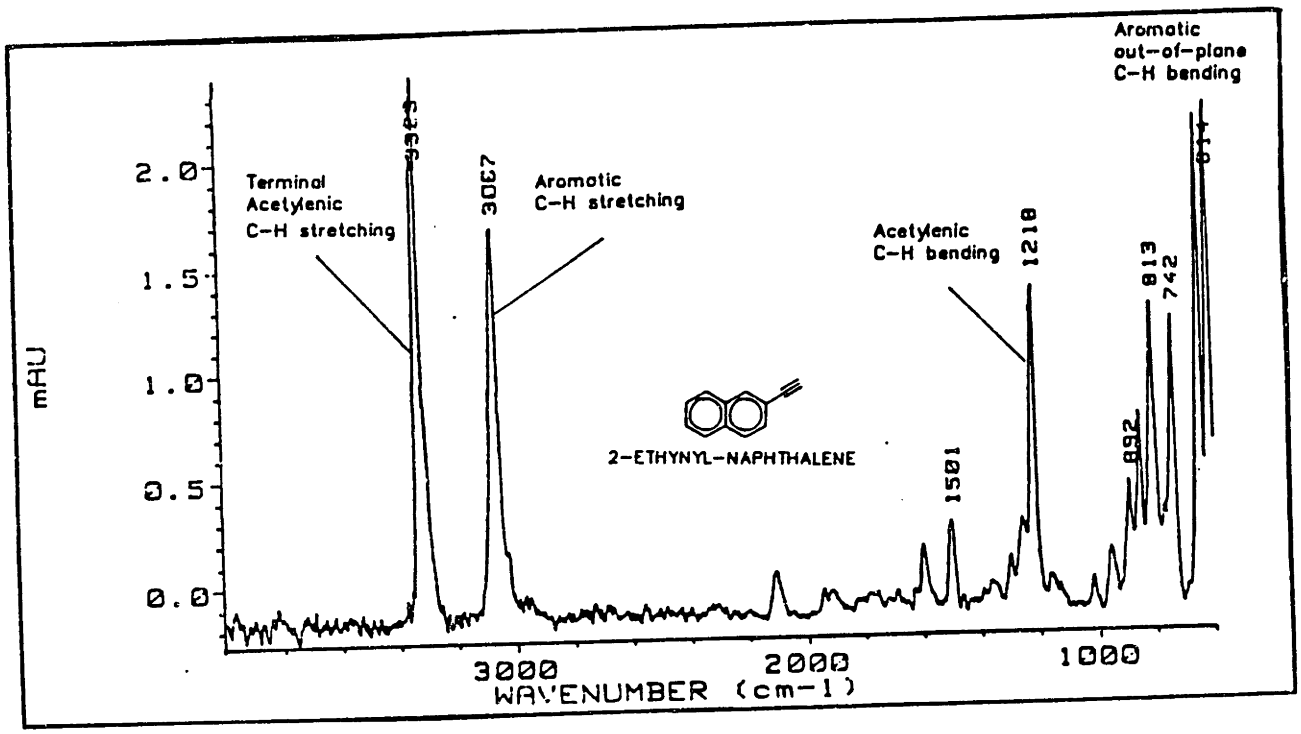

Figure S.5 IR spectra of 2-ethynyl-naphthalene.

TABLE S.4 - SUMMARY OF EXPERIMENTAL CONDITIONS

	Case 1	Case 2	Case 3	Case 4	Case 5
Feed to JSR Flow rates (moles/sec)					
C_2H_4	4.44×10^{-2}	4.44×10^{-2}	4.08×10^{-2}	4.08×10^{-2}	4.08×10^{-2}
O_2	5.60×10^{-2}	5.60×10^{-2}	5.60×10^{-2}	5.60×10^{-2}	5.60×10^{-2}
N_2	2.23×10^{-1}	2.23×10^{-1}	2.45×10^{-1}	2.45×10^{-1}	2.45×10^{-1}
Ar	2.29×10^{-3}	2.29×10^{-3}	2.29×10^{-3}	2.29×10^{-3}	2.29×10^{-3}
Injection Flow Rates (moles/sec)					
N_2	2.48×10^{-3}	0	2.48×10^{-3}	0	2.48×10^{-3}
C_2H_4	0	2.67×10^{-3}	0	3.61×10^{-3}	0
C_6H_6	0	0	0	0	7.08×10^{-4}
Experimental Conditions					
ϕ	2.37	2.37	2.18	2.18	2.18
JSR T(K)	1630	1630	1630	1630	1630
JSR τ(ms)	5.74	5.74	5.38	5.38	5.38

basis, the amount of C_6H_6 injected was less than injected C_2H_4.

S.4.1 Light Hydrocarbons

Acetylene is the dominant hydrocarbon species present (Fig. S.6), and its concentration at ϕ=2.18 is greatly affected by C_2H_4 injection. Almost 70% of the injected C_2H_4 is converted to C_2H_2, and most of this conversion occurs rapidly at the beginning of the PFR before the first PFR data point, where the C_2H_4 mole fraction (Fig. S.7) drops very rapidly from $1.0x10^{-2}$ at the injection point to $2.3x10^{-3}$ at the first PFR data point. Acetylene is not affected much by C_6H_6 injection, indicating that C_2H_2 formation is not the major sink for C_6H_6 under these conditions.

Methane (Fig. S.6) is the second most abundant hydrocarbon and shows only a small sensitivity to C_2H_4 and C_6H_6 injection. Ethylene concentration is also relatively insensitive to C_6H_6 injection.

S.4.2 Aromatics and PAH

Figure S.8 shows that C_2H_4 injection increases benzene concentration by about 50% at the end of the PFR. The injection of C_6H_6 results in an inititally high benzene mole fraction ($1.3x10^{-3}$) at the first PFR data point, which rapidly decays to $5.0x10^{-4}$ in the PFR. Of the initial C_6H_6 injected, 30% is consumed prior to the first sampling point in the PFR; and by the end of the PFR, 16% is converted to tar, 11% is converted to soot, and 18% remains as benzene. The rest of the benzene consumption is probably oxidation to CO and perhaps decomposition to C_2H_2, although we cannot accurately determine the small expected increases in CO and C_2H_2 concentrations. At early PFR residence times, the rates of tar and soot formation are equal to 29% and 12%, respectively, of the C_6H_6 dissappearance rate. A kinetic calculation assuming oxidation of C_6H_6 by OH with a rate constant given by He et al. (1988b) for C_6H_6+OH, $k_{(1600K)}$=$2.5x10^{12}$ $cm^3/mol \cdot s$, is able to account for the rate of C_6H_6 disappearance in the PFR. Thus, besides growth to larger species, a large part of the benzene consumption in the PFR is probably from oxidation.

Phenylacetylene (C_8H_6) concentration profiles (Fig. S.9) show

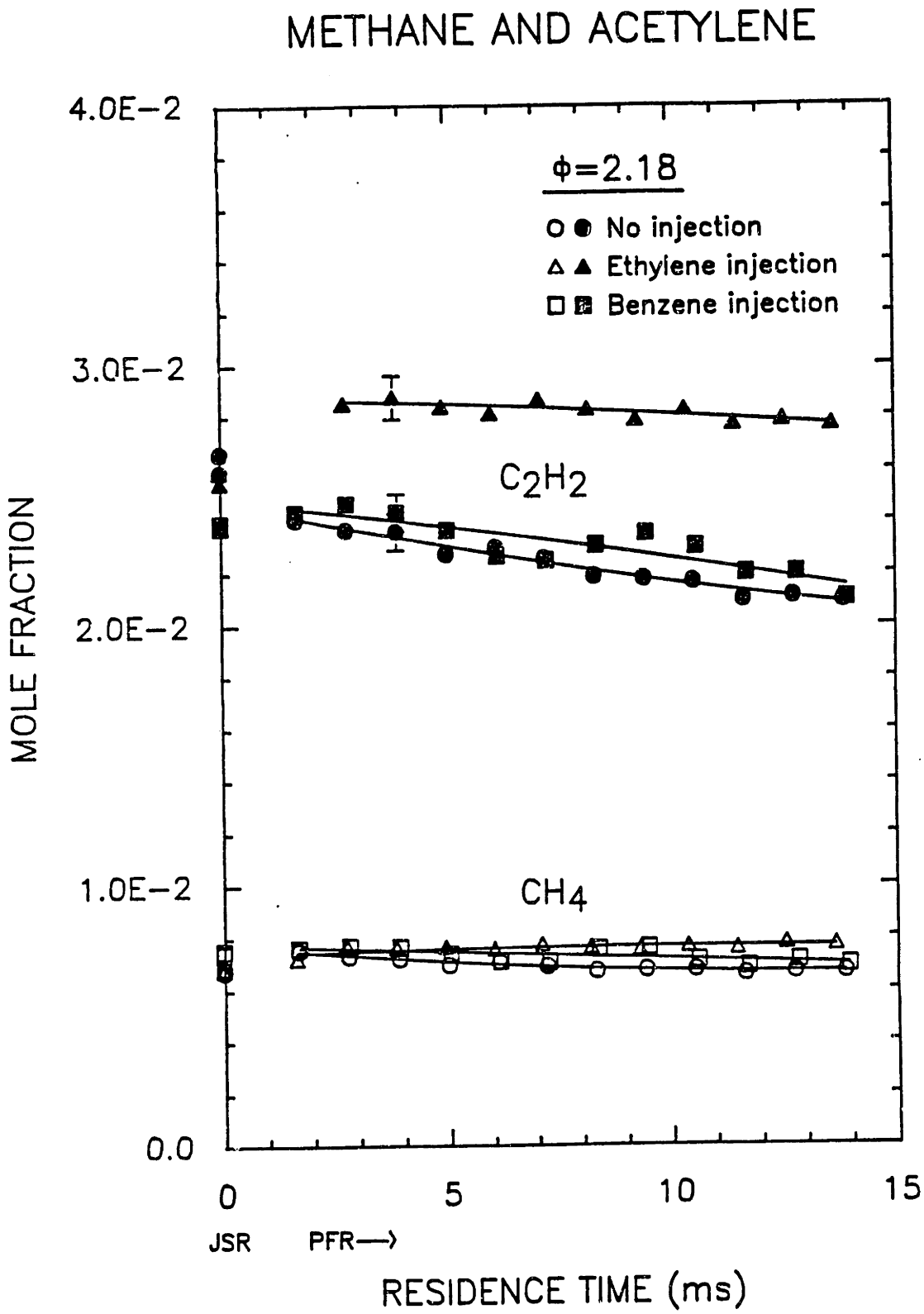

Figure S.6 Concentration profiles for methane (CH_4) and acetylene (C_2H_2) in JSR/PFR for ϕ=2.18, for no injection, C_2H_4 injection and C_6H_6 injection cases as defined in Table S.4.

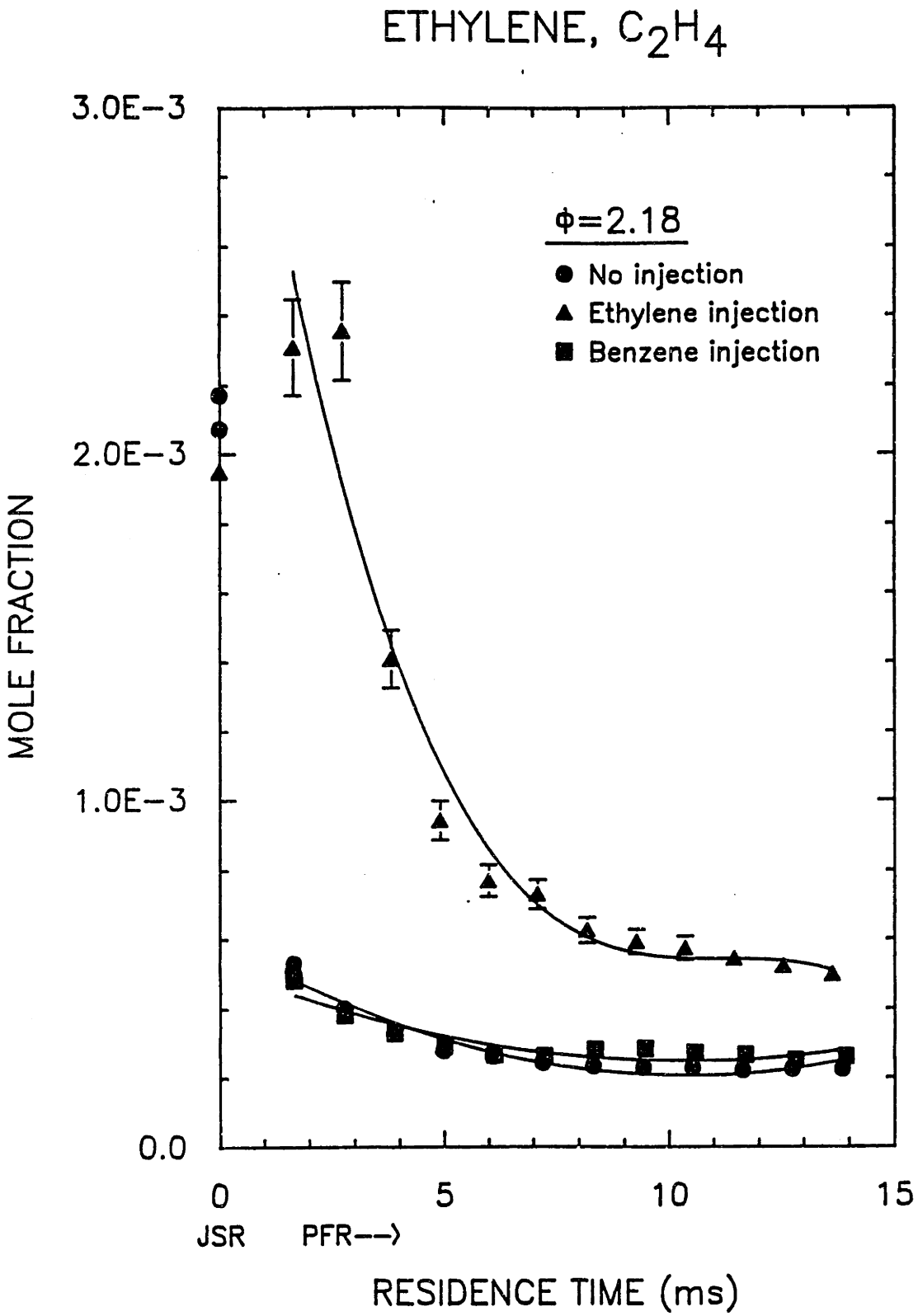

Figure S.7 Concentration profiles for ethylene (C_2H_4) in JSR/PFR for ϕ=2.18, for no injection, C_2H_4 injection and C_6H_6 injection cases as defined in Table S.4.

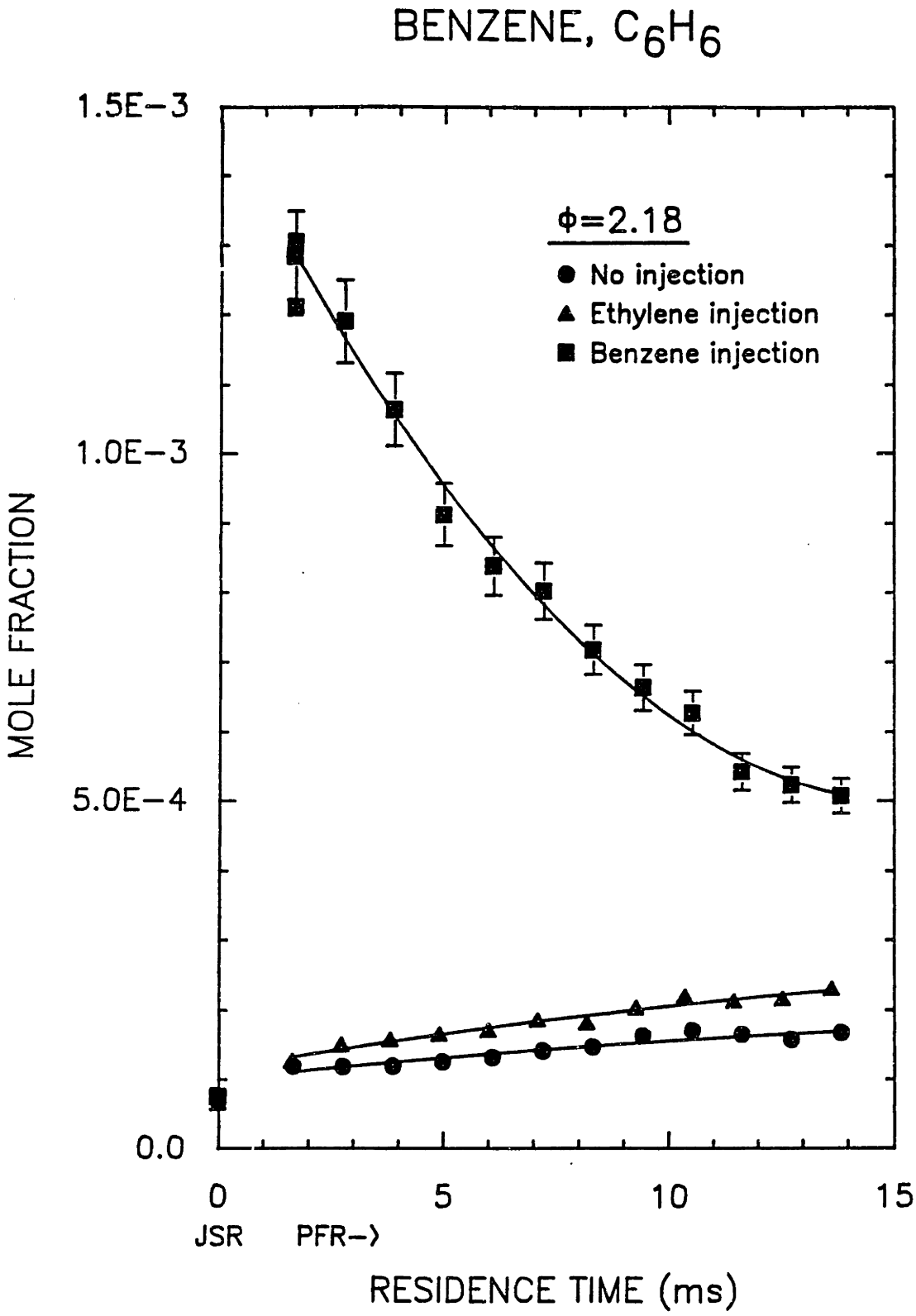

Figure S.8 Concentration profiles for benzene (C_6H_6) in JSR/PFR for ϕ=2.18, for no injection, C_2H_4 injection and C_6H_6 injection cases as defined in Table S.4.

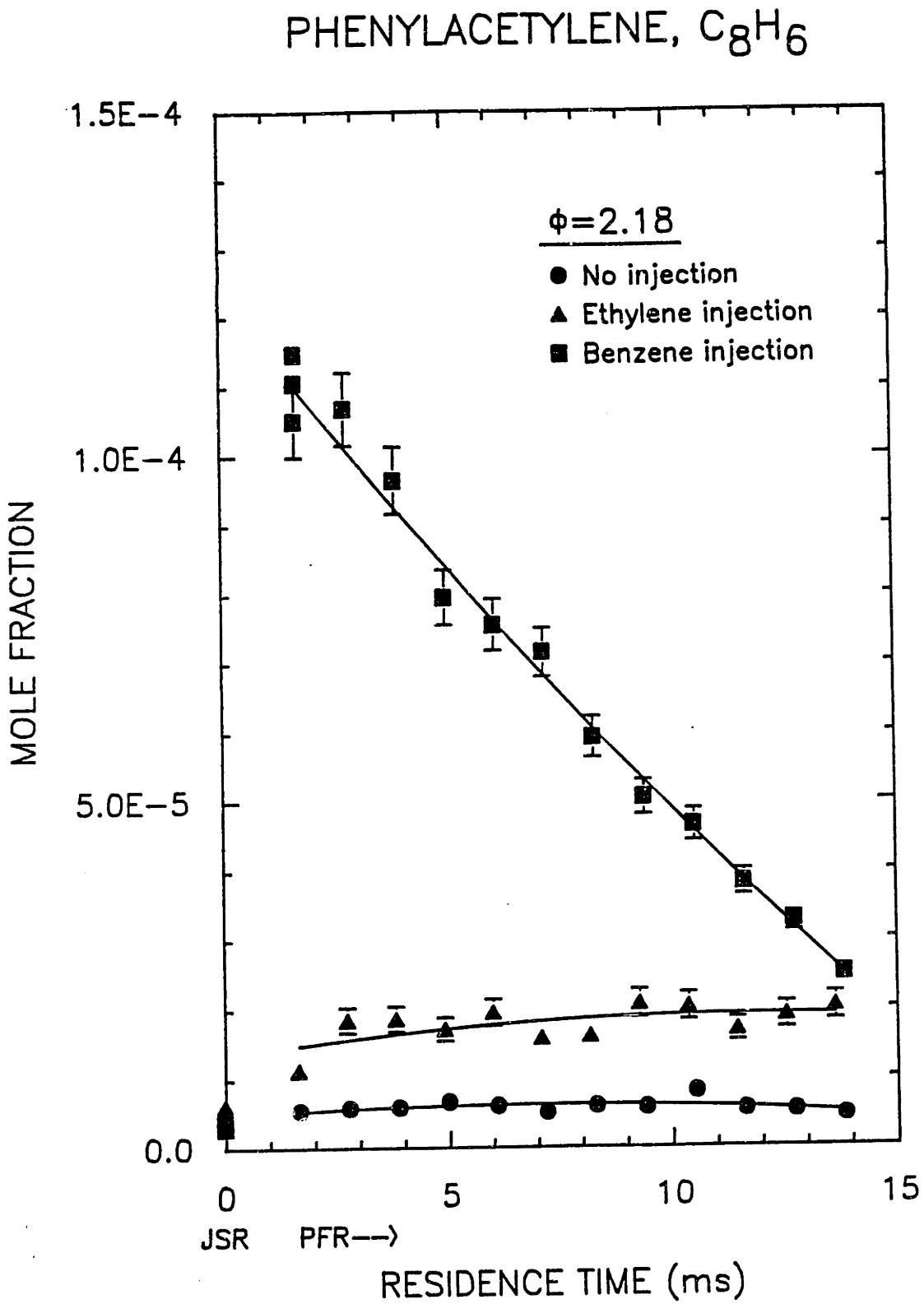

Figure S.9 Concentration profiles for phenylacetylene (C_8H_6) in JSR/PFR for ϕ=2.18, for no injection, C_2H_4 injection and C_6H_6 injection cases as defined in Table S.4.

similar perturbations as benzene for no injection, C_2H_4 injection, and C_6H_6 injection cases. The response of the C_8H_6 profile to C_6H_6 injection indicates that conversion of C_6H_6 to C_8H_6 is rapid compared with the total residence time in the PFR, and a rapid equilibrium may exist between the two species.

The concentration profiles of naphthalene ($C_{10}H_8$) (Fig. S.10) show that both C_2H_4 and C_6H_6 addition enhances production of $C_{10}H_8$. The 4 and 5 ring PAH species, such as cyclopenta(cd)pyrene ($C_{18}H_{10}$) (Fig. S.11), have the same general shape, and the injection of C_2H_4 enhances slightly the production of individual PAH, while the injection of benzene greatly enhances individual PAH species production.

S.4.3 Tar and Soot

The injection of C_2H_4 results in an increase in the tar concentration (Fig. S.12) at the end of the PFR by a factor of 2, and C_6H_6 injection results in a 10-fold increase. The soot concentration at ϕ=2.18 (Fig. S.13) is almost the same for C_2H_4 injection as for no injection. The injection of benzene, however, results in a 10-fold increase in soot concentration at the end of the PFR.

Ethylene may promote the formation of high-molecular weight species through aliphatic addition reactions to aromatic structures by increasing the concentration of C_2H_2, but a secondary effect of C_2H_4 injection is to increase the formation of single-ring aromatics, presumably by reactions between C_2 and C_4 species. Figure S.8 shows that the benzene concentration is increased by C_2H_4 injection.

The observed increase in tar concentration resulting from the injection of C_6H_6 strongly suggests that the concentration of single-ring aromatics in a combustion environment in the presence of high concentrations of C_2H_2 controls the production of high molecular weight material. In a combustion environment with high concentrations of aliphatic species already present, the addition of C_2H_4 will have a much smaller effect than C_6H_6 on tar formation. Soot formation may be promoted by high concentrations of intact aromatic rings, perhaps indirectly through production of tar species.

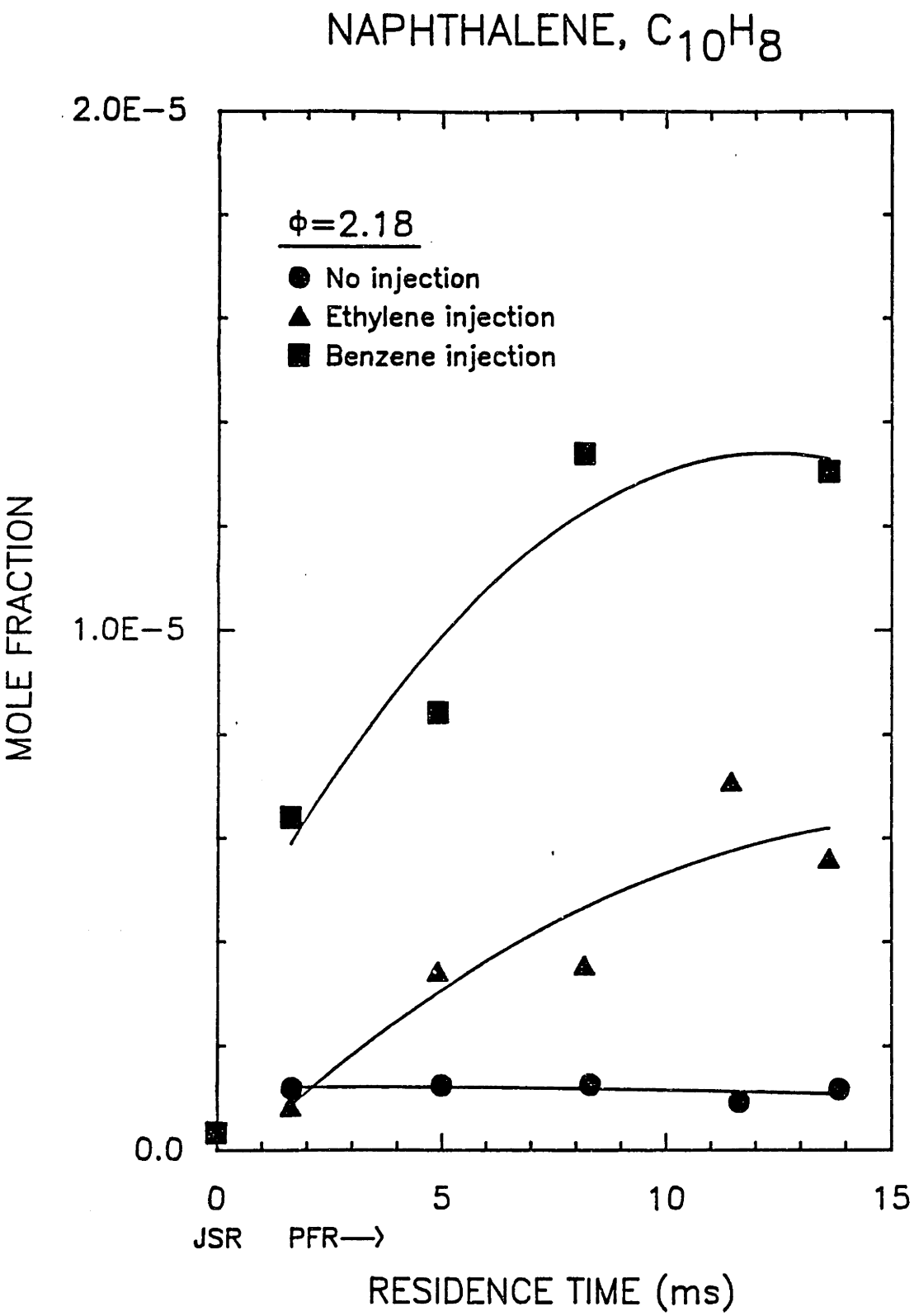

Figure S.10 Concentration profiles for naphthalene ($C_{10}H_8$) in JSR/PFR for ϕ=2.18, for no injection, C_2H_4 injection and C_6H_6 injection cases as defined in Table S.4.

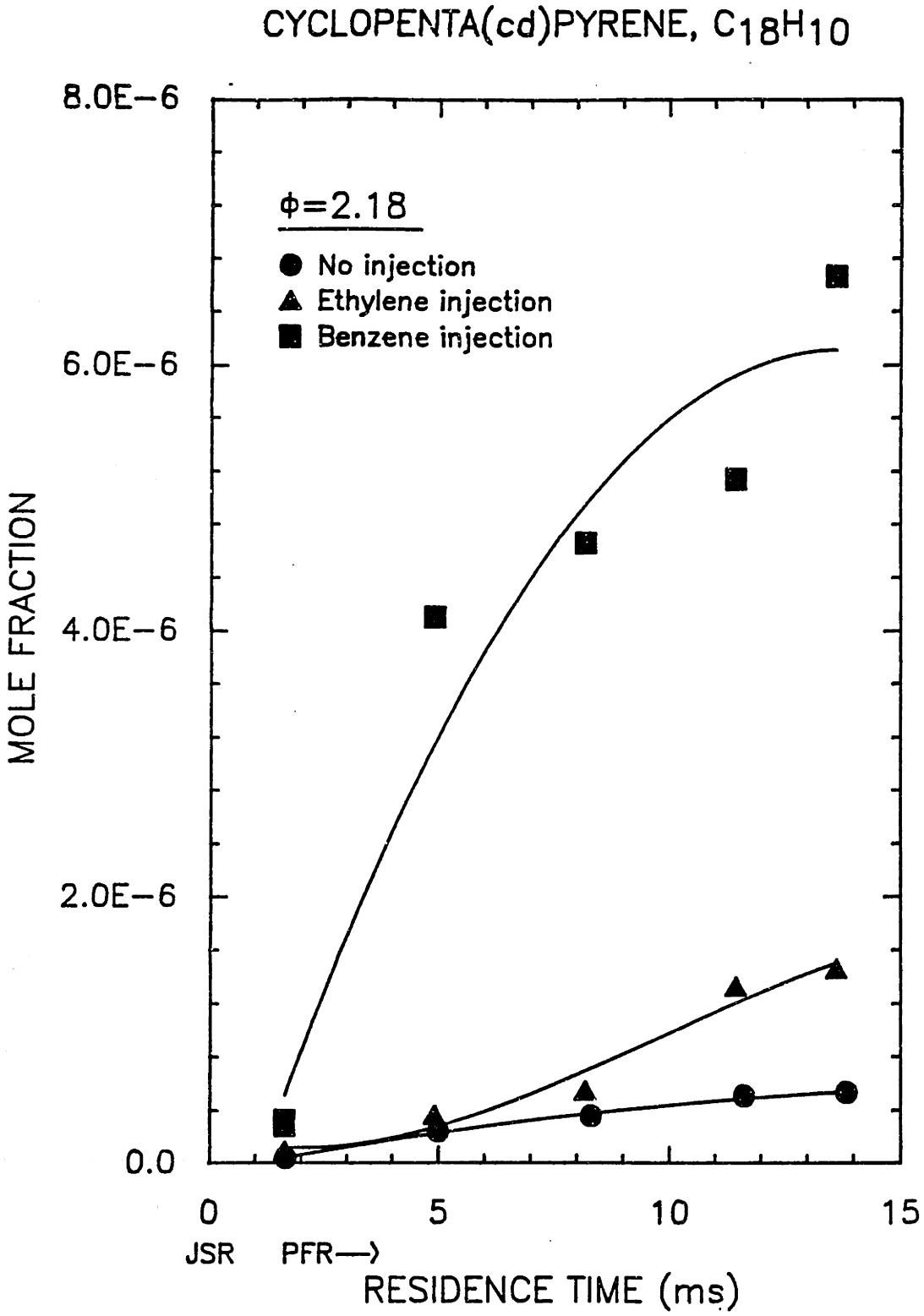

Figure S.11 Concentration profiles for cyclopenta(cd)pyrene in JSR/PFR for ϕ=2.18, for no injection, C_2H_4 injection and C_6H_6 injection cases as defined in Table S.4.

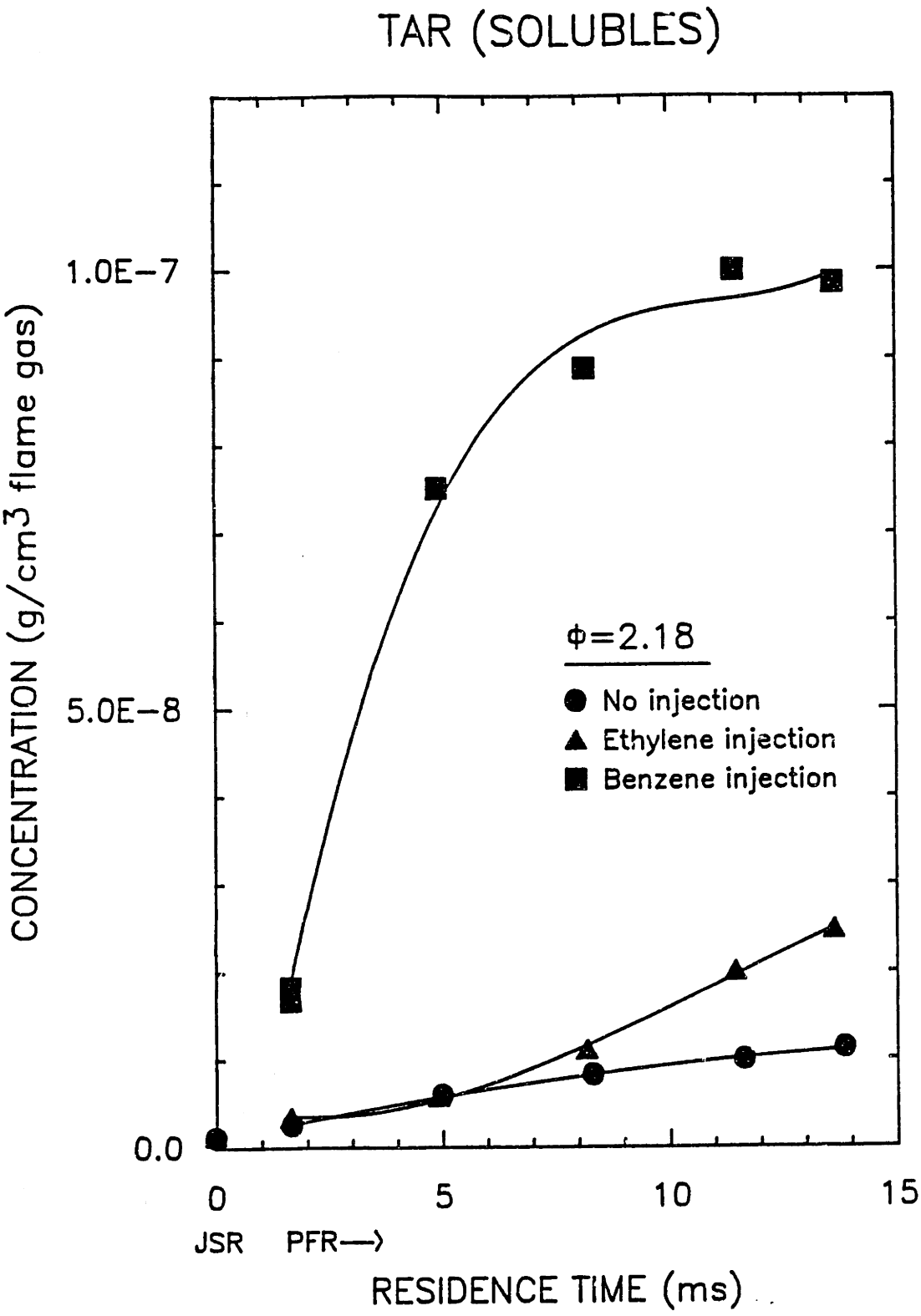

Figure S.12 Concentration profiles for tar (defined as CH_2Cl_2-soluble material with mass ≥ naphthalene) in JSR/PFR for ϕ=2.18, for no injection, C_2H_4 injection and C_6H_6 injection cases as defined in Table S.4.

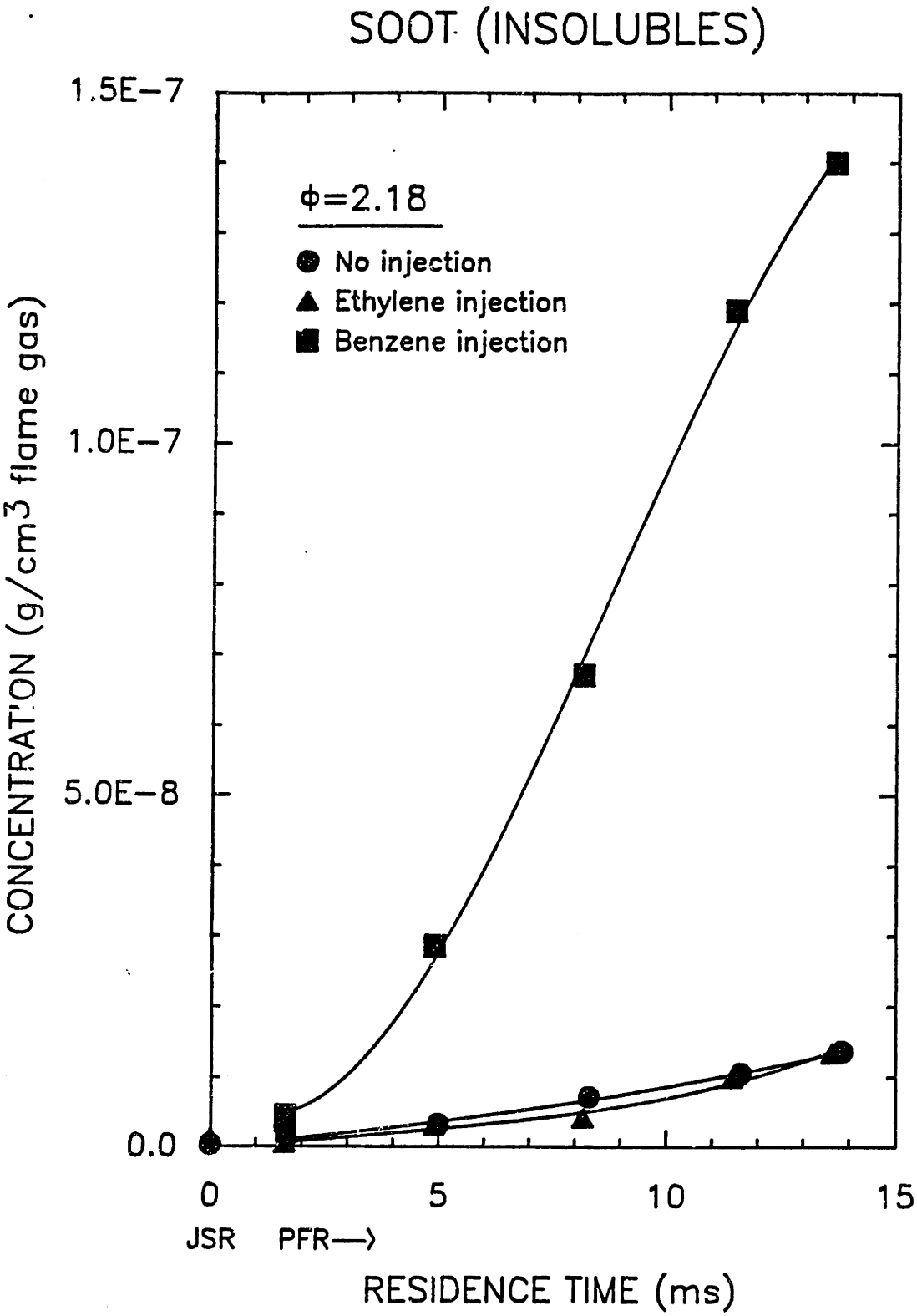

Figure S.13 Concentration profiles for soot (defined as CH_2Cl_2-insoluble material) in JSR/PFR for ϕ=2.18, for no injection, C_2H_4 injection and C_6H_6 injection cases as defined in Table S.4.

The effect of fuel equivalence ratio on tar and soot formation is shown in Figures S.14 and S.15, where the mass concentrations are plotted on a logarithmic scale. An increase in ϕ from 2.18 to 2.37 increases tar by a factor of 8 at the JSR and a factor of 5 at the end of the PFR. Increasing ϕ from 2.18 to 2.37 results in a sooting condition in the JSR, and increases soot by a factor of 10 at the end of the PFR. The ϕ=2.18, C_2H_4 injection case produces much less tar and soot than the ϕ=2.37 case with no injection, although the total amount of C_2H_4 fuel is the same. It should be noted that the JSR benzene concentrations for ϕ=2.37, no injection are higher than ϕ=2.18 with C_2H_4 injection.

S.5 LIGHT HYDROCARBON KINETIC MODELLING

The species concentration profiles for H_2, CO, CO_2, C_2H_2, C_2H_4, and CH_4 were modelled at the elementary reaction level using literature mechanisms proposed by Glarborg et al. (1986a) (29 species, 134 reactions) and Harris (1988) (193 reactions, 49 species).

The problem was modelled assuming a completely-stirred tank reactor (CSTR) condition applies in the JSR, and perfect plug flow behavior is assumed for the PFR. The governing equations are simply the CSTR and PFR equations for energy and mass conservation. Because the measured reactor temperature is used as an input parameter, the energy conservation equations are decoupled from the species conservation equations, and only the mass balance for each species needs to be solved. In the PFR, the measured temperature profile was initially used. The assumption of an isothermal temperature did not change the model predictions and so a temperature of 1600K was used. In the JSR, a mass balance on each chemical species k gives

$$\dot{m} \cdot (Y_k - Y_k^{in}) = w_k \cdot W_k \cdot V \qquad \text{(Eq. S.1)}$$

where $\dot{m}$ = the mass flow rate
Y_k = the mass fraction of the kth species in the JSR
Y_k^{in} = the mass fraction of the kth species input into the JSR
W_k = the molecular weight of the kth species
V = the volume of the reactor
w_k = the molar production rate of the kth species per unit volume.

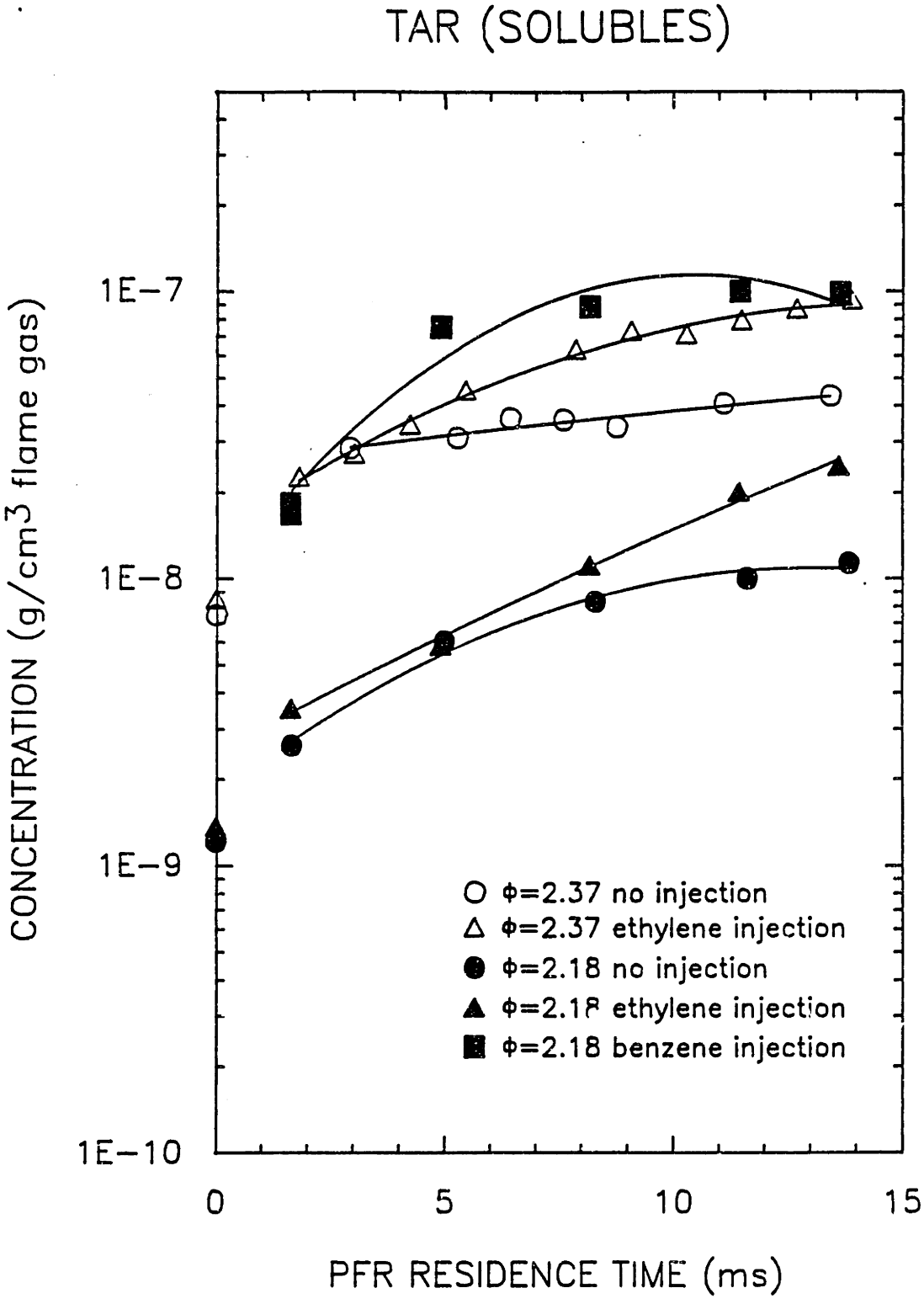

Figure S.14 Concentration profiles for tar (defined as CH_2Cl_2-soluble material with mass ≥ naphthalene) in JSR/PFR for experimental conditions given in Table S.4.

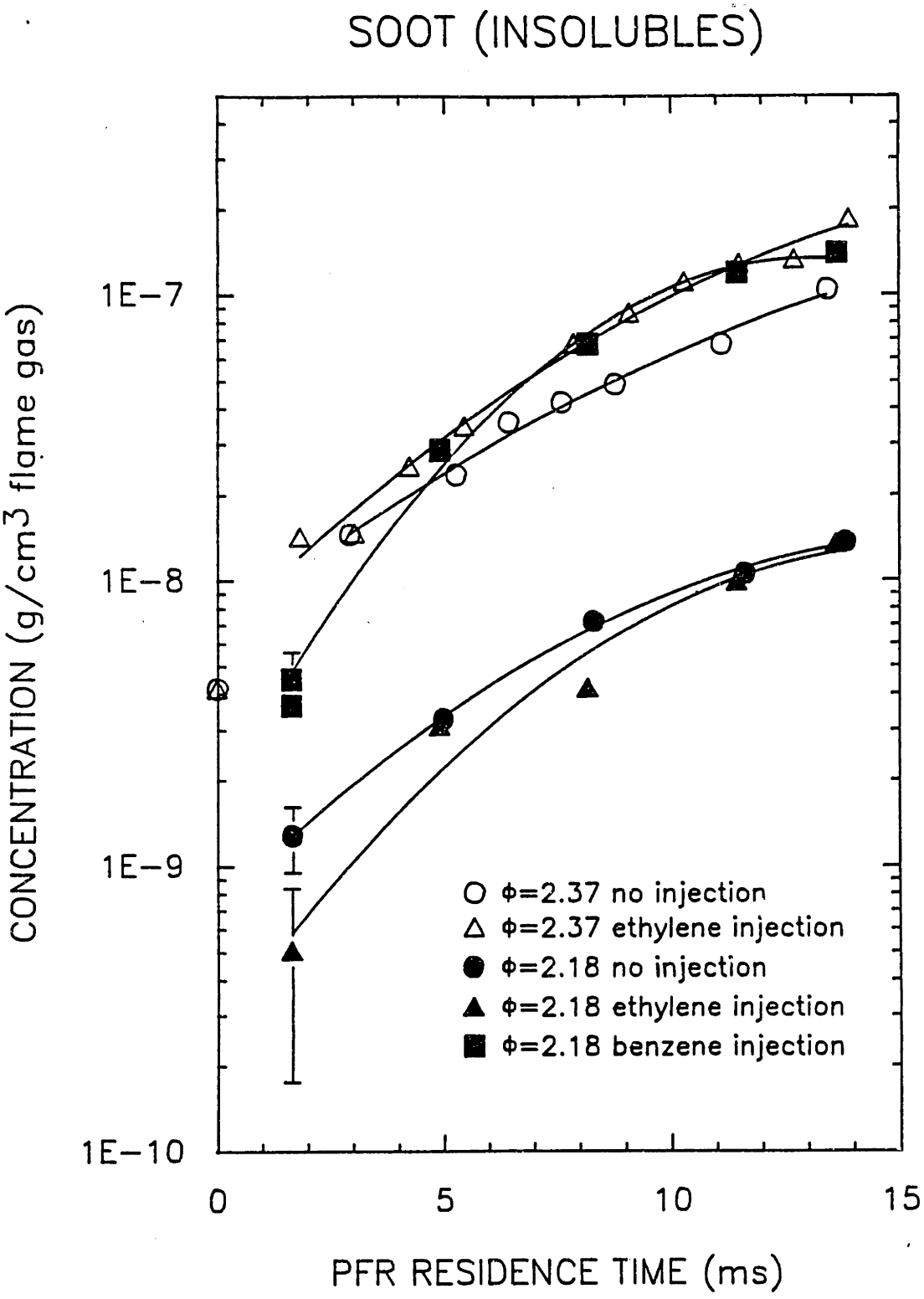

Figure S.15 Concentration profiles for soot (defined as CH_2Cl_2-insoluble material) in JSR/PFR for experimental conditions given in Table S.4.

The w_k term is dependent upon the reaction mechanism chosen for the problem. Solving the resulting set of k algebraic equations yields the solution vector [Y_k], the mass fractions of each species in the WSR. The solution is used as the starting point for the PFR problem.

In the PFR, the concentration of each species will change as a function of residence time. The mass fraction of each species k is obtained by solving the expression

$$(1/\tau)\ (Y_k^{t2} - Y_k^{t1}) = (w_k W_k/\rho) \qquad \text{(Eq. S.2)}$$

where the residence time, τ, is given by

$$\tau = (\rho V/m) \qquad \text{(Eq. S.3)}$$

and the mass density, ρ, is calculated from the ideal gas equation of state,

$$\rho = PW_{mean}/RT \qquad \text{(Eq. S.4)}$$

Modelling work was facilitated by use of the computer program CHEMKIN (Kee et al. 1980), which is a FORTRAN transportable chemical kinetics computer code package. The CSTR problem was solved using the Perfectly-Stirred Reactor (PSR) code written by Glarborg et al. (1986b) which uses a hybrid Newton/time-integration procedure. The governing differential equations for the PFR problem were solved using the Livermore Solver for Ordinary Differential Equations, LSODE, (Hindmarsh, 1983), an efficient numerical integration routine which is based on Gear and Gearb packages. LSODE is especially efficient at solving the initial value problem for systems of first order ordinary differential equations for combustion problems. The computations were performed on a VAX 11/785.

The solution vector of species concentrations for the CSTR problem was used as the initial value for the PFR problem. It should be emphasized that for the kinetics modelling of light hydrocarbons, no adjustable parameters were used. The rate constants from the published literature mechanisms were used, except for reactions which have been corrected for typographical errors and computational limitations of the VAX 11/785 (no numbers larger than 10^{38} allowed).

The two baseline cases (ϕ=2.18 and ϕ=2.37) were modelled using the Glarborg and Harris mechanisms, and the comparison of the model predictions to the experimental data for fixed gases and acetylene are shown in Figures S.16 and S.17. The differences in major species concentrations between the two fuel equivalence ratios are not large. Both models predict the species profiles quite well, although the Harris mechanism under-predicts C_2H_2 by about a factor of 2 at the end of the PFR for ϕ=2.18.

Besides being able to model fixed gases and major stable species, an important feature of extending these elementary chemical mechanisms to our sooting conditions is that we can use the predictions for important radical species concentrations, such as H, OH, and O. Since we do not have any way of experimentally determining the radical concentrations, this modeling approach allows us to make an estimation of the radical concentrations. We do not try to extend the model predictions for hydrocarbon radical species, because Westmoreland (1986c) has shown that hydrocarbon mechanisms do not predict these hydrocarbon radical species with the same accuracy as the H, OH, and O radicals for fuel-rich conditions.

S.6 THERMODYNAMICS

The equilibrium distribution of PAH isomers in each $C_{2n}H_{2m}$ class of species will favor the PAH isomer with the lowest ΔG_f. These have been defined as "stabilomers". Alberty (1988) has identified the most stable isomers in each class of the benzenoid series up to 5 aromatic rings and has calculated the equilibrium distribution among the PAH isomers at flame temperatures. Based on theoretical considerations, Stein (1985) has predicted the stabilomer in each $C_{2n}H_{2m}$ class of species up to $C_{42}H_{16}$ at 1500K. Figure S.18 shows the experimentally most abundant $C_{2n}H_{2m}$ PAH species up to cyclopenta(cd)pyrene ($C_{18}H_{10}$) which we observe for our reactor conditions. With the exception of the ethynyl-acenaphthylenes ($C_{14}H_8$), all of the species are the stabilomers which have been predicted by Stein. Pyracyclene, or "diacenaphthylene" is the predicted $C_{14}H_8$ stabilomer.

Following the development of Stein, if we assume partial

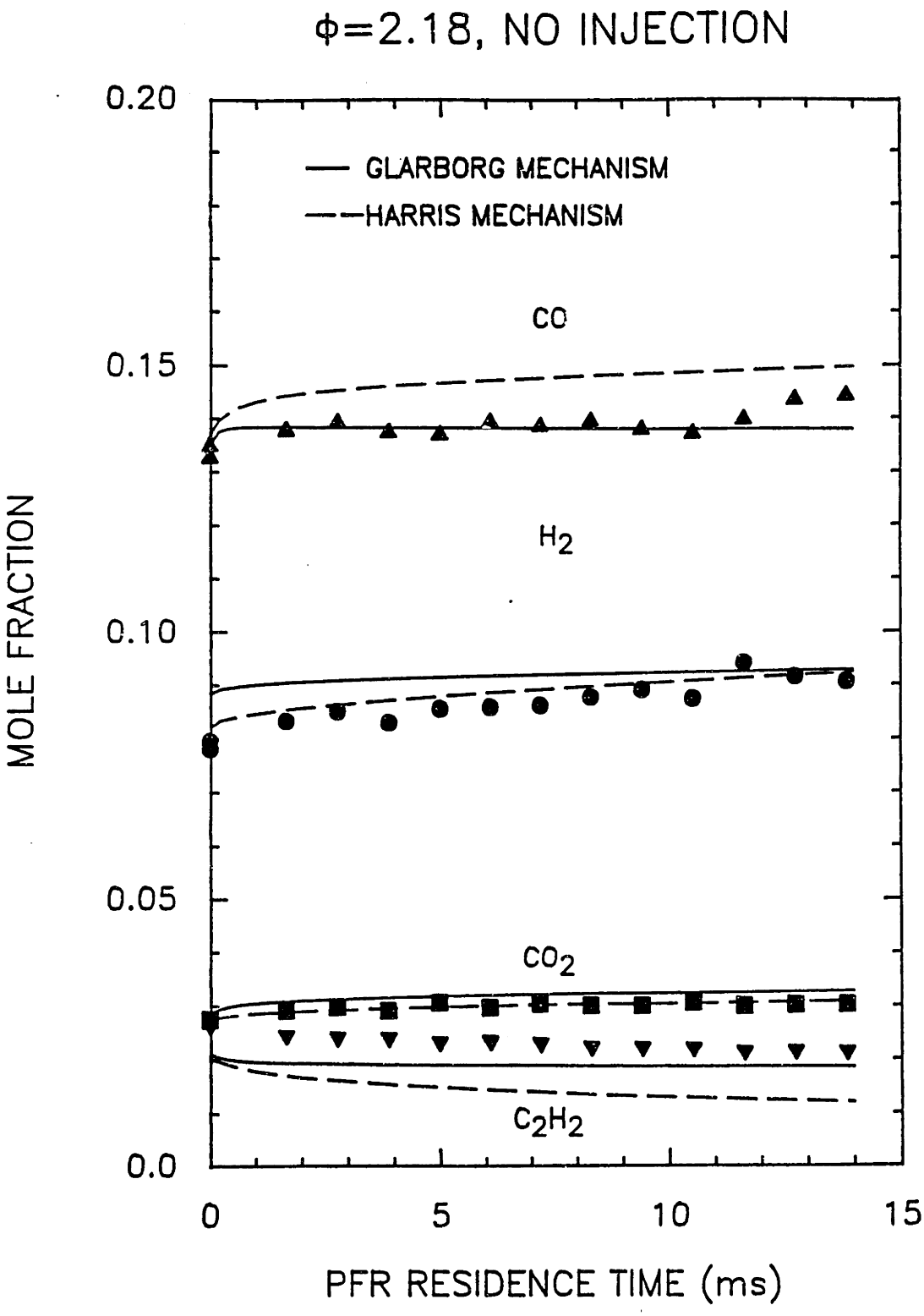

Figure S.16 Comparison of Glarborg mechanism and Harris mechanism predictions with experimental concentration profiles for CO, H_2, CO_2, and C_2H_2 in JSR/PFR at ϕ=2.18.

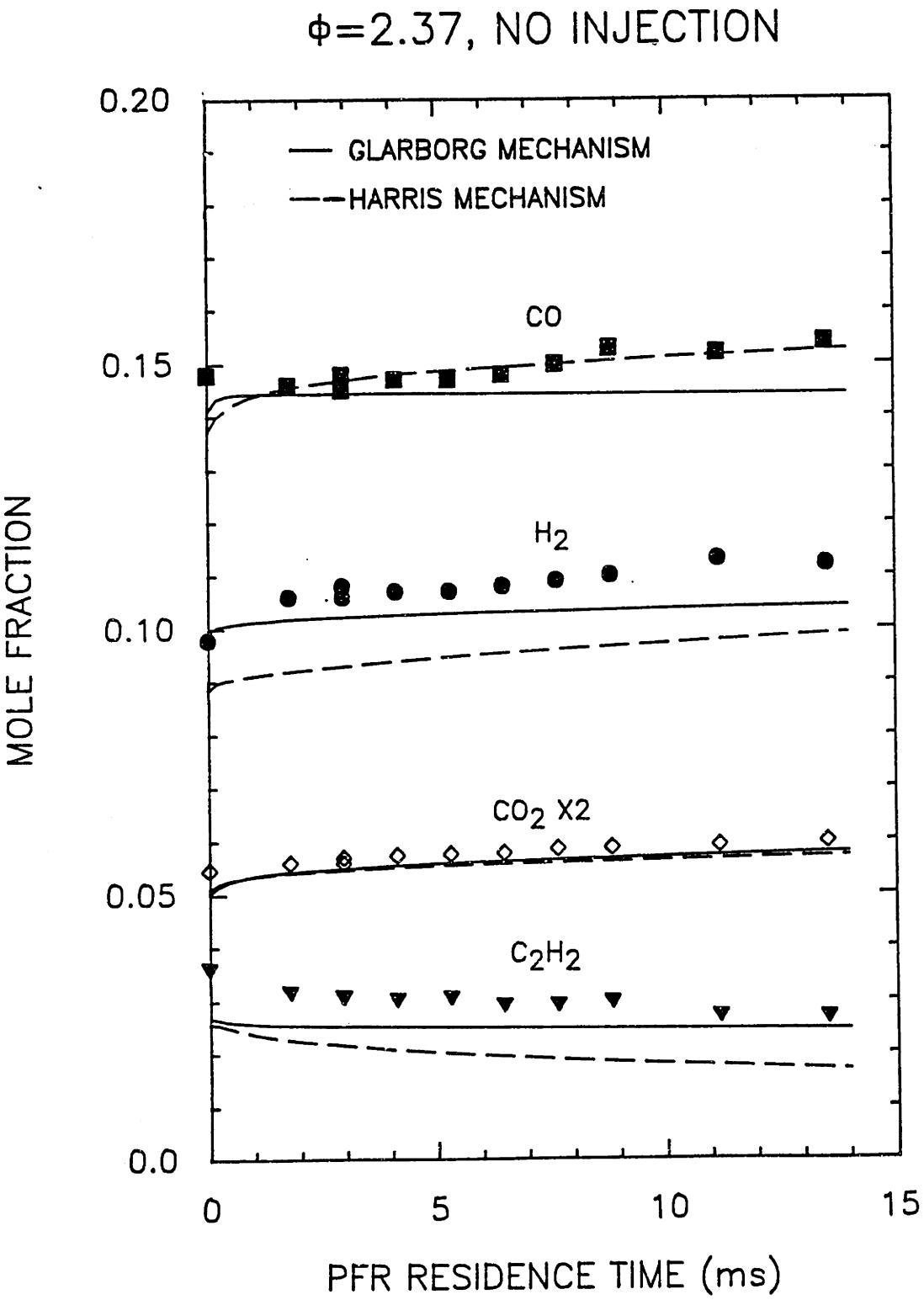

Figure S.17 Comparison of Glarborg mechanism and Harris mechanism predictions with experimental concentration profiles for CO, H_2, CO_2, and C_2H_2 in JSR/PFR at ϕ=2.37.

equilibration of the C_2H_2-H_2-PAH system, then the equilibrium concentration of an individual PAH species could be predicted by finding K_p for the reaction

$$nC_2H_2 = C_{2n}H_{2m} + (n-m)H_2 \qquad n,m = 1,2,3... \qquad \text{(Rxn. S.1)}$$

and so

$$[C_{2n}H_{2m}] = K_p \cdot [C_2H_2]^n \cdot [H_2]^{(m-n)} \qquad \text{(Eq. S.5)}$$

Thus we see that the equilibrium concentration of PAH species will be a function of temperature, C_2H_2 concentration, and H_2 concentration. For $n/m > 1$, which is the case for the most stable PAH species, increasing H_2 inhibits PAH formation. Increasing C_2H_2 favors PAH formation.

Figure S.18 also shows the most favored thermodynamic path (in bold arrows) which leads from C_2H_2 to large PAH for our experimental conditions of ϕ=2.18, T=1600K, with C_2H_2 and H_2 mole fractions of 2×10^{-3} and 9×10^{-2}, respectively. Polymerization along this path occurs by a logical series of steps, each involving addition of H_2 (vertical step), addition of C_2H_2 (diagonal step), or addition of C_2H_2 and loss of H_2 (horizontal step). The number associated with each step is the ratio of product to reactant, R, for the 3 different steps and is given by

$$[C_{2n}H_{2m+2}]/[C_{2n}H_{2m}] = K_p \cdot [H_2] \qquad \text{(vertical step)} \qquad \text{(Eq. S.6)}$$

$$[C_{2n+2}H_{2m+2}]/[C_{2n}H_{2m}] = K_p \cdot [C_2H_2] \qquad \text{(diagonal step)} \qquad \text{(Eq. S.7)}$$

$$[C_{2n+2}H_{2m}]/[C_{2n}H_{2m}] = K_p \cdot [C_2H_2]/[H_2] \qquad \text{(horizontal step)} \qquad \text{(Eq. S.8)}$$

For R values greater than 1, product formation, and therefore molecular weight growth, will be favorable. The path indicated by the bold arrows in Figure S.18 does not represent a kinetic pathway, but rather a thermodynamic pathway. However, if a state of partial equilibration exists, then the concentration of the product available for further growth reactions will be determined by the thermodynamics for each step, through reversibility.

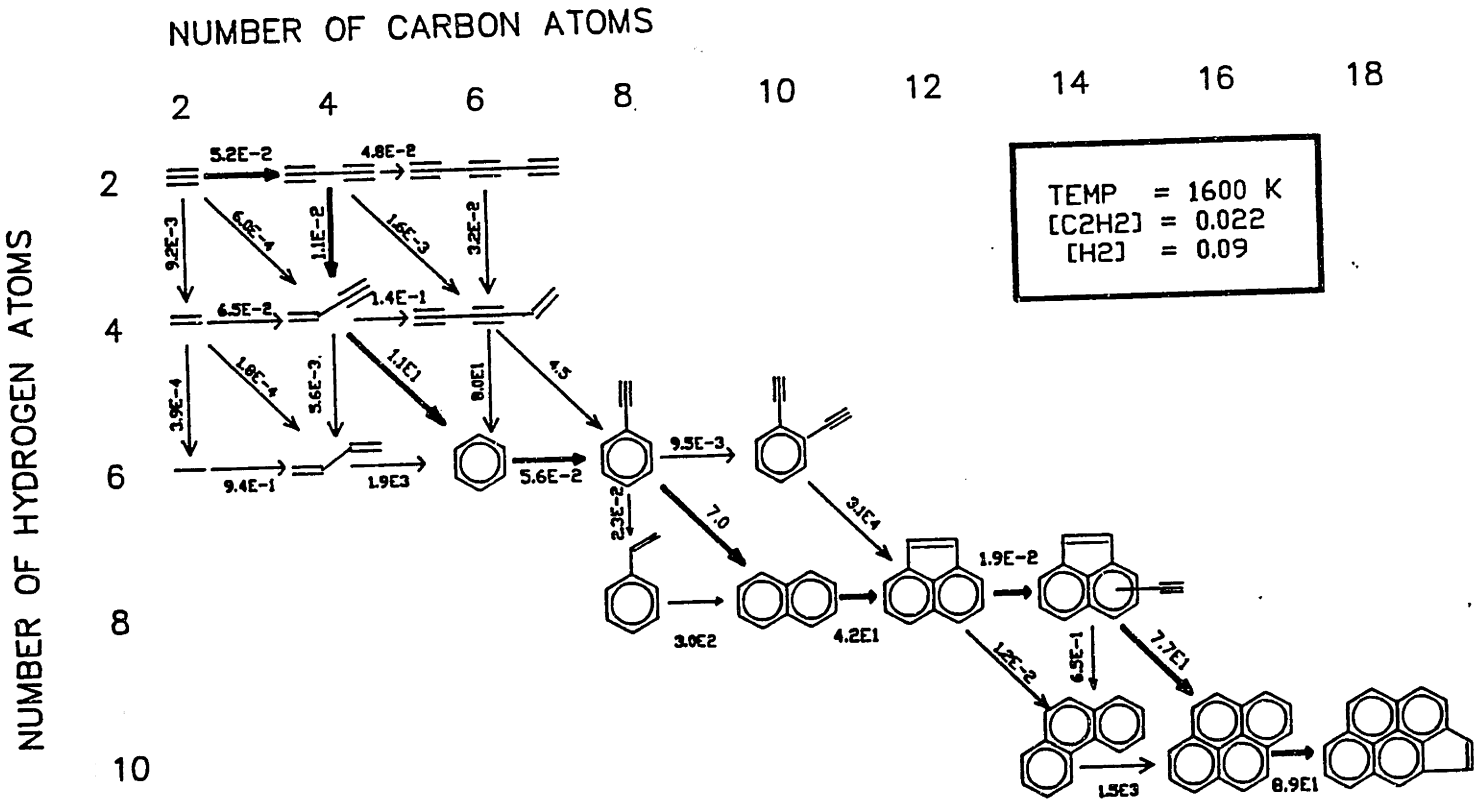

Figure S.18 Most abundant experimentally observed PAH species in the PFR, and most favored thermodynamic pathway. Numbers are the ratio of product to reactant, assuming equilibration of the C_2H_2-H_2-$C_{2n}H_{2m}$ system. See text for discussion.

The aliphatic light hydrocarbon species, except diacetylene, are produced in the JSR in super-equilibrium quantities, and then decay in the PFR towards their equilibrium limits, as calculated by Eq. S.5, (Fig. S.19). The diacetylene concentration increases slightly towards its equilibrium limit.In contrast, the aromatic species (Fig. S.20) are far below their equilibrium concentrations in the JSR, but are increasing rapidly in the PFR towards their thermodynamic limits. Similar trends are observed for the sooting ϕ=2.37 conditions (Lam, 1988). Clearly the formation of PAH species is kinetically controlled.

Although the entire C_2H_2-H_2-$C_{2n}H_{2m}$ system is not equilibrated, the possibility exists for some species to be partially equilibrated. A possible free radical mechanism for the formation of two-ring PAH involving cyclization across a triple bond (Fig. S.21), as proposed by Frenklach (1985b), includes phenylacetylene as an intermediate. Using the experimentally measured C_6H_6, C_2H_2, and H_2 concentrations and equilibrium constants calculated for our temperature profile in the PFR, we find that C_8H_6 is near partial equilibrium with C_6H_6 (Figure S.22). Similarly, 2-ethynyl naphthalene is nearly partially equilibrated with naphthalene. Naphthalene is <u>not</u> equilibrated with phenylacetylene, and is substantially below its equilibrium concentration. Although the C_2H_2 addition reactions to form ethynyl-substituted PAH appear to be partially equilibrated, C_2H_2 addition reactions which result in ring closure are not. This experimental finding is consistent with the conclusion determined from kinetic modelling studies (Frenklach, 1985b) that ring cyclization reactions to form fused ring PAH are essentially irreversible and provide the driving force for molecular weight growth by "pulling" chains of reversible reactions.

S.7 PAH GLOBAL KINETIC MODELLING

S.7.1 Model Formulation

In order to model the formation of PAH, we must first realize that PAH are intermediates in the molecular weight growth process. Since it is necessary to form PAH structures between the fuel and the

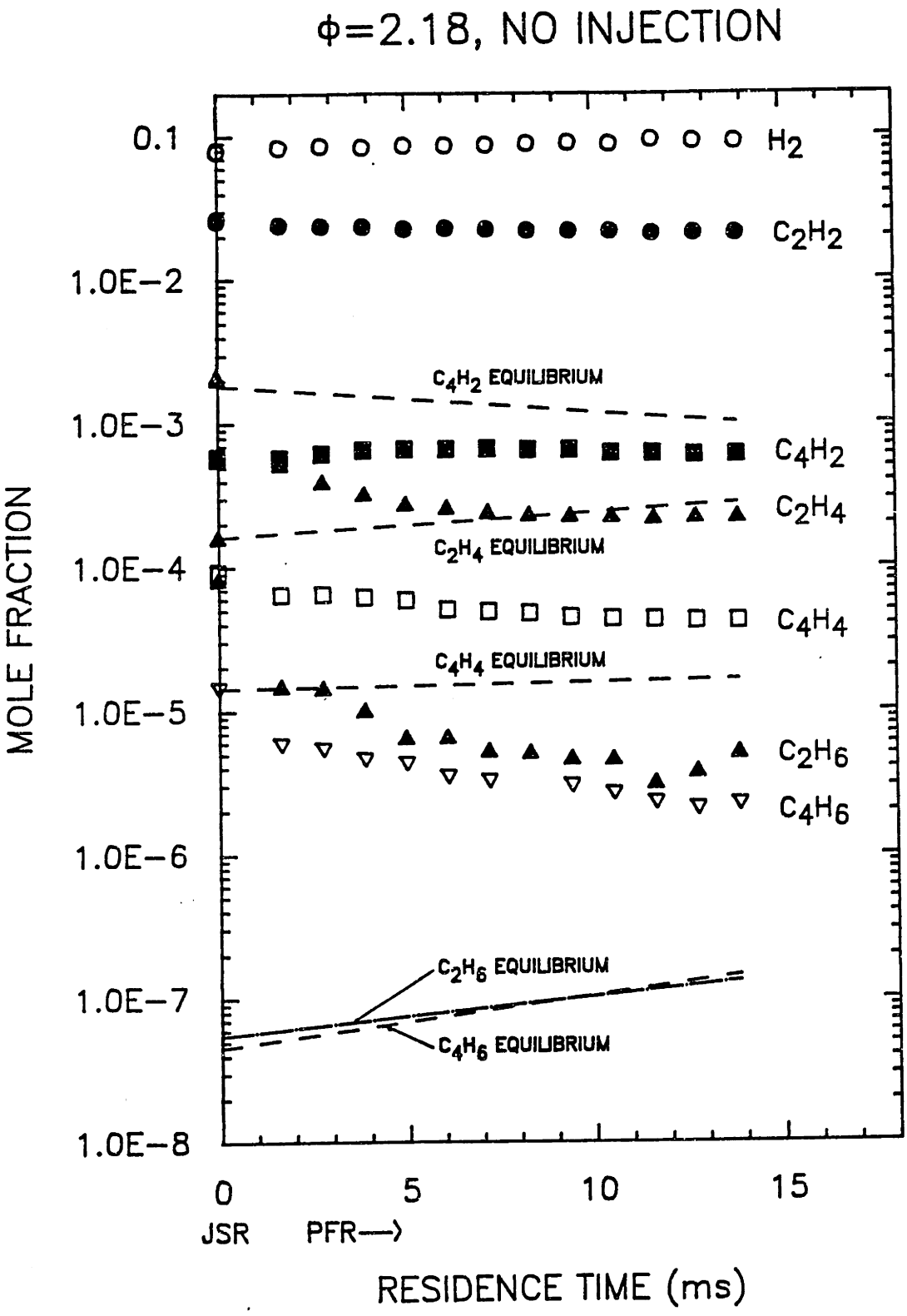

Figure S.19 Aliphatic $C_{2n}H_{2m}$ species concentrations and equilibrium concentrations predicted from equilibration of the C_2H_2-H_2-$C_{2n}H_{2m}$ system, using measured C_2H_2 and H_2 concentrations.

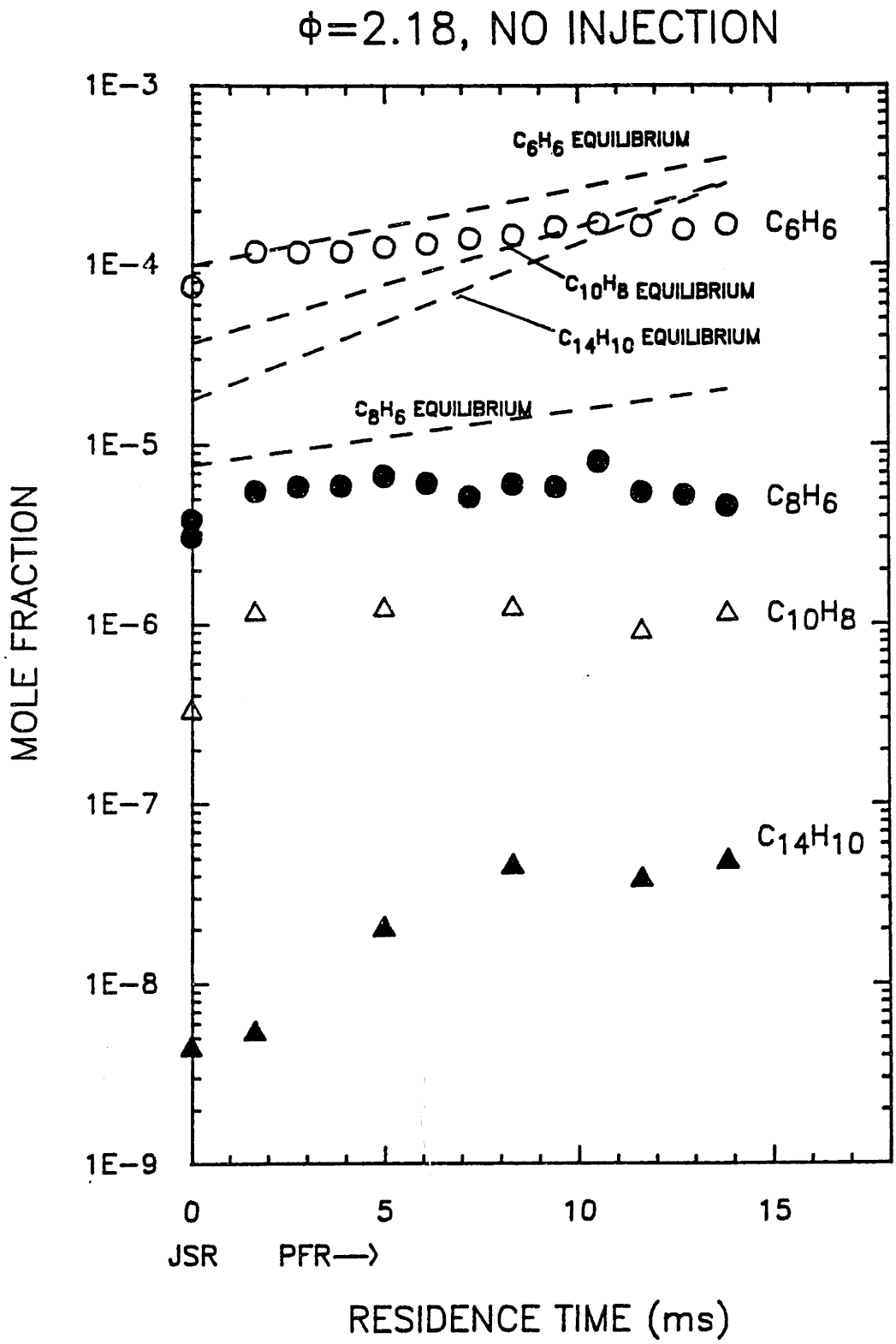

Figure S.20 Aromatic $C_{2n}H_{2m}$ species concentrations and equilibrium concentrations predicted from equilibration of the C_2H_2-H_2-$C_{2n}H_{2m}$ system, using measured C_2H_2 and H_2 concentrations.

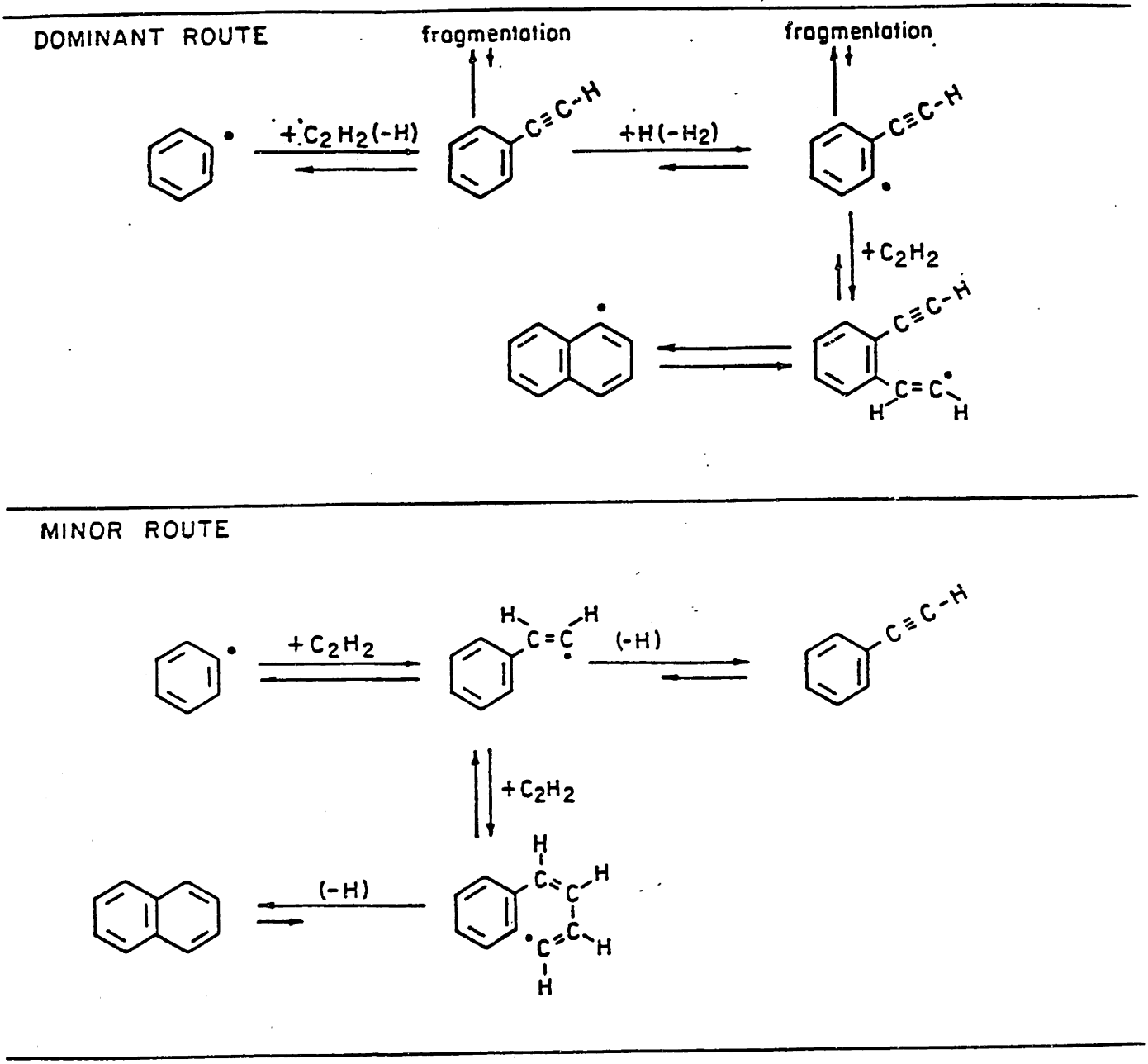

Figure S.21 Possible mechanism for formation of two-ring aromatics. Dominant route was determined from computer simulations (taken from Frenklach, 1985b).

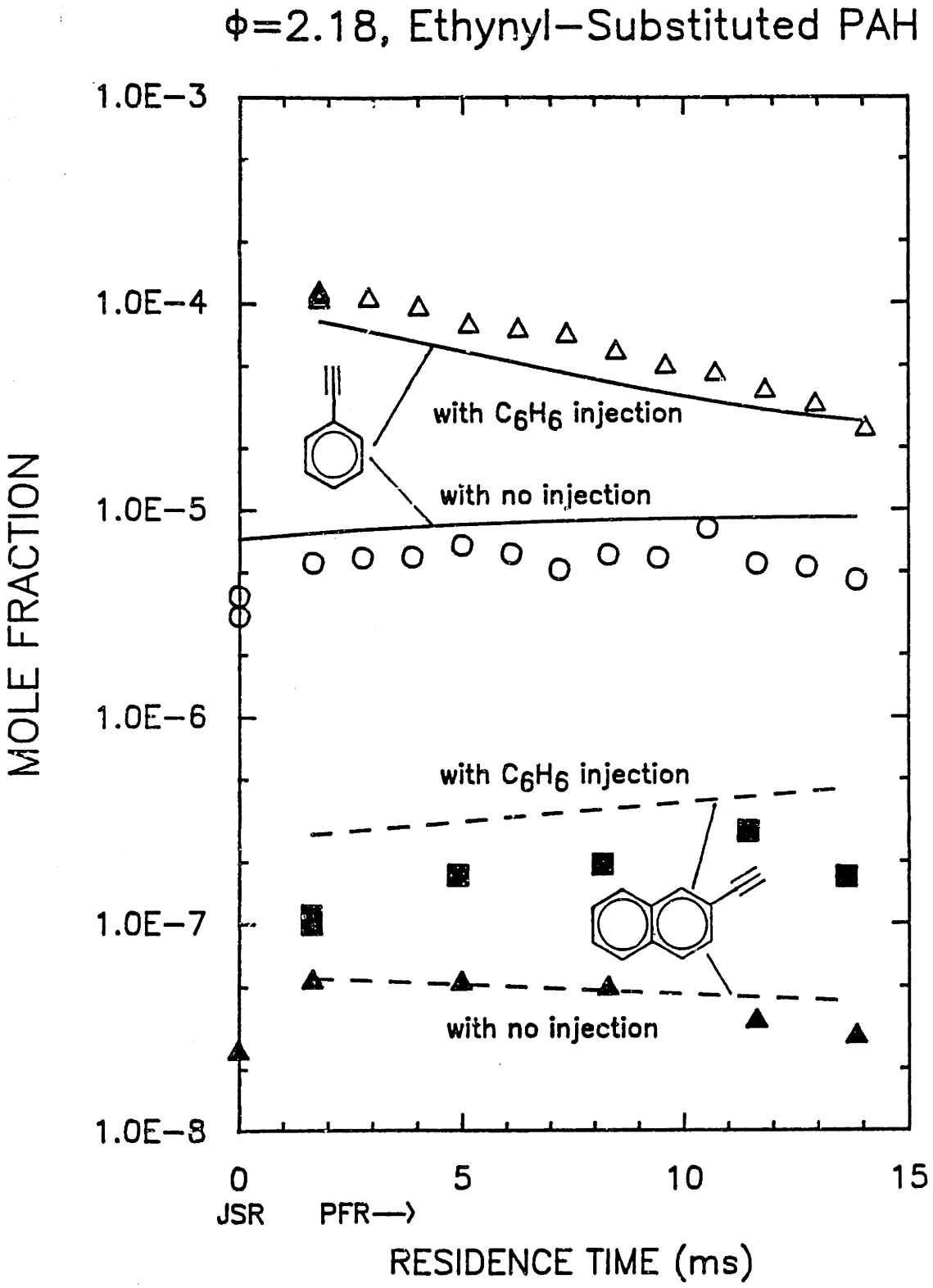

Figure S.22 Ethynyl-aromatic $C_{2n}H_{2m}$ species concentrations and equilibrium concentrations predicted from equilibration of the reactions $C_6H_6+C_2H_2=C_8H_6+H_2$ and $C_{10}H_8+C_2H_2=C_{12}H_8+H_2$, using measured $C_{10}H_8$, C_6H_6, C_2H_2, H_2 concentrations.

soot forming reactions. The PAH inventory is by definition bounded at both ends of the molecular weight scale, and species may enter through the lower bound and exit through the upper bound, so that at any formation of the first soot nuclei, the PAH inventory is being simultaneously formed from fuel decomposition and consumed through position in the PFR the rate of change of mass concentration of PAH is determined by the net of these rates. Figure S.23 shows a representation of these rates for the ΣGC PAH inventory.

The change in the mass concentration, C, of the ΣGC PAH inventory with respect to time is given by

$$dC/dt = R_i + R_{add} - R_{ox} - R_o \qquad \text{(Eq. S.9)}$$

where R_i is the initiation rate ($g/cm^3 \cdot s$) for the formation of species at the low molecular weight limit (ie. naphthalene, the smallest species in the ΣGC PAH inventory); R_{add} is the net rate of addition of aliphatic species (assumed to be primarily C_2H_2) to the PAH inventory; R_{ox} is the rate of oxidation of species to form CO (OH is assumed to be the primary oxidizing species); and R_o is the net rate at which mass is lost through the high molecular weight limit of the ΣGC PAH inventory. This last term, R_o, is comprised of 4 different components as given by

$$R_o = R_{C_2H_2} + R_{coag\text{-}PAH} + R_{coag\text{-}tar} + R_{coag\text{-}soot} \qquad \text{(Eq. S.10)}$$

where $R_{C_2H_2}$ is the rate at which a 5 ring PAH species (mostly cyclopenta(cd)pyrene) adds C_2H_2 and leaves the ΣGC PAH pool through the high MW limit, $R_{coag\text{-}PAH}$ is the rate at which two small PAH (2-5 rings) coagulate to form a PAH species larger than 5 rings, $R_{coag\text{-}tar}$ is the rate at which PAH coagulate with high MW tar species (≥ 6 rings) and are removed from the ΣGC PAH inventory, and $R_{coag\text{-}soot}$ is the rate at which soot particles scavenge PAH molecules.

For each of the terms given in Equations S.9 and S.10, we can write rate expressions ($g/cm^3 \cdot s$) in terms of a rate constant (or collision efficiency times collision frequency), molar concentrations

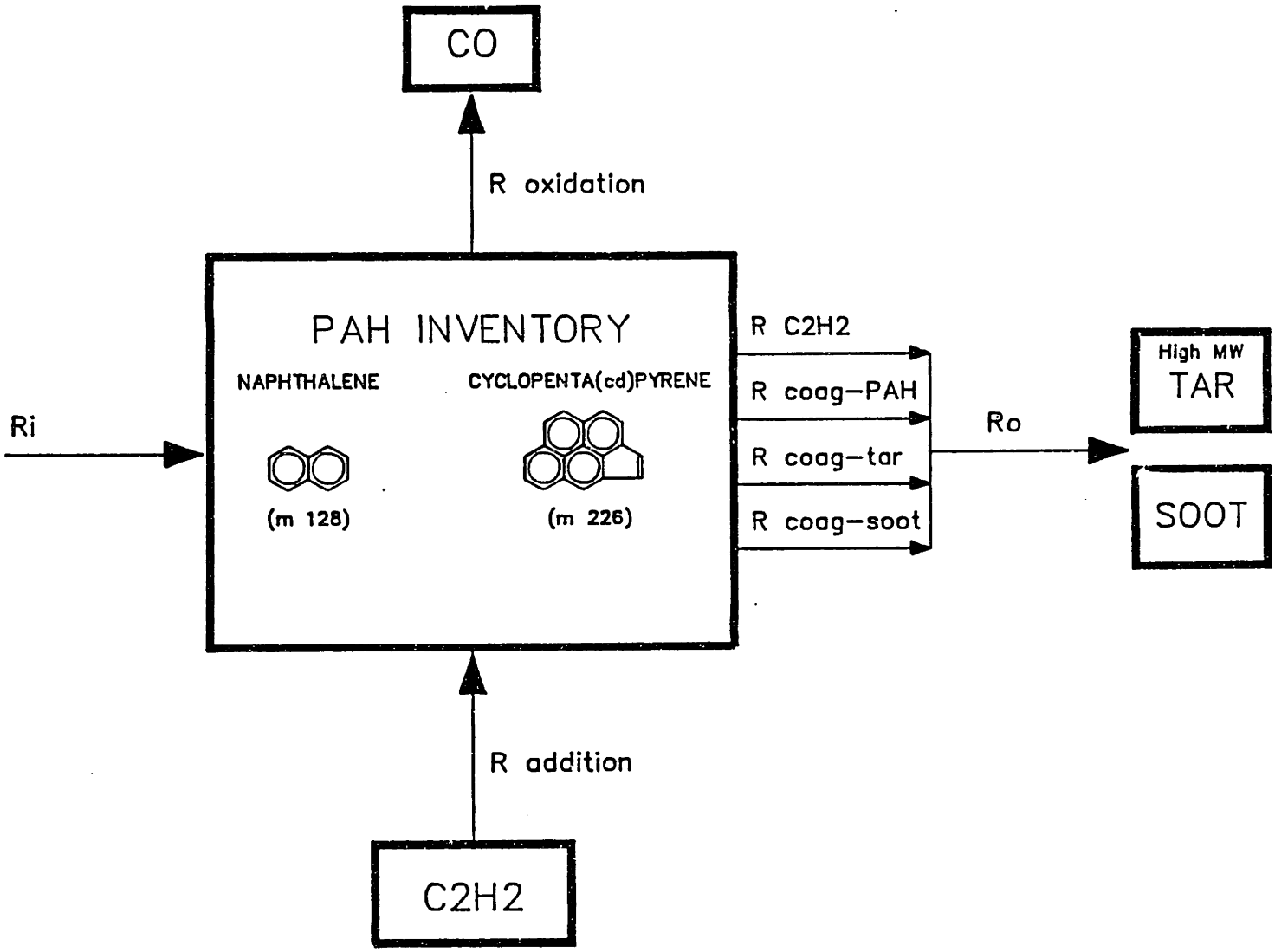

Figure S.23 Representation of ΣGC PAH formation and destruction pathways.

of species, and mass transferred in or out of the PAH inventory. These expressions are given in Equations S.11 through S.17,

$$R_i = k_i \cdot [C_8H_6] \cdot [C_2H_2] \cdot 128 \quad \text{(Eq.S.11)}$$

$$R_{addition} = k_{add} \cdot [\Sigma GC\ PAH] \cdot [C_2H_2] \cdot 24 \quad \text{(Eq.S.12)}$$

$$R_{oxidation} = k_{ox} \cdot [\Sigma GC\ PAH] \cdot [OH] \cdot 12 \quad \text{(Eq.S.13)}$$

$$Rc_2H_2 = kc_2H_2 \cdot [\Sigma GC\ PAH] \cdot [C_2H_2] \cdot 226 \quad \text{(Eq.S.14)}$$

$$R_{coag\text{-}PAH} = \gamma_{PAH} \cdot (Z_{PAH}/N_{av}) \cdot [\Sigma GC\ PAH] \cdot [\Sigma GC\ PAH] \cdot MW_{PAH} \quad \text{(Eq.S.15)}$$

$$R_{coag\text{-}tar} = \gamma_{tar} \cdot (Z_{tar}/N_{av}) \cdot [tar] \cdot [\Sigma GC\ PAH] \cdot MW_{PAH} \quad \text{(Eq.S.16)}$$

$$R_{coag\text{-}soot} = \gamma_{soot} \cdot (Z_{soot}/N_{av}) \cdot [soot] \cdot [\Sigma GC\ PAH] \cdot MW_{PAH} \quad \text{(Eq.S.17)}$$

where k's are rate constants, γ's are collision efficiencies, and Z's are collision frequencies for the coagulation-type reactions. If we can find or calculate the rate constants (or equivalently $\gamma \cdot Z$'s), we will be able to model the formation of PAH because we measure or model the species concentrations given in Equations S.11 - S.17.

S.7.2 Mathematical Formulation

The expression for dC/dt can be rearranged to give an equation of the form

$$dC/dt = a(t) + b(t) \cdot C + c(t) \cdot C^2 \quad \text{(Eq.S.18)}$$

where

$$a(t) = Ri$$
$$b(t) = F_{add} - F_{ox} - Fc_2H_2 - F_{coag\text{-}tar} - F_{coag\text{-}soot}$$
$$c(t) = F_{coag\text{-}PAH}$$

and

$$F_{add} = k_{add} \cdot [C_2H_2] \cdot 24 / MW_{PAH}$$
$$F_{ox} = k_{ox} \cdot [OH] \cdot 12 / MW_{PAH}$$
$$Fc_2H_2 = f_{5\ rings} \cdot k_{add} \cdot [C_2H_2] \cdot 226 / MW_{PAH}$$
$$F_{coag\text{-}tar} = \gamma_{tar} \cdot Z_{tar} \cdot [tar]$$
$$F_{coag\text{-}soot} = \gamma_{soot} \cdot Z_{soot} \cdot [soot]$$
$$F_{coag\text{-}PAH} = \gamma_{PAH} \cdot Z_{PAH} \cdot fraction(PAH+PAH \geq 6 rings)$$

which is a first-order, non-linear ordinary differential equation. Since the functions a(t), b(t) and c(t) are obtained from experimental data, as well as literature rate constants and estimated radical

concentrations, we can solve this equation numerically using a fourth-order Runga-Kutta integration technique. The initial value is the measured concentration of the ΣGC PAH inventory at the first PFR data point. A constant time-step size of 1.5×10^{-5} s was used, and when we doubled the step size, we observed no change in the predicted concentration profile. Thus our predictions are not sensitive to the particular time-step size we selected.

S.7.3 Discussion of Model Features

An aromatic coagulation mechanism for PAH formation, consisting of bimolecular reactions of aryl species reacting with intact aromatic rings, is not the dominant mechanism of PAH formation for our experimental conditions. This conclusion is based on the following three facts: 1) the expected products of such a mechanism, namely biphenyl, terphenyl and triphenylene, are not observed; 2) a coagulation mechanism of aryl radicals with aromatics cannot explain formation of PAH structures such as phenylacetylene, naphthalene and acenaphthylene which are observed in the JSR/PFR; and 3) coagulation of aromatics alone cannot explain the observed increase in molar concentration of the PAH inventory in the PFR.

The rate constant for C_2H_2 addition to aryl species is based on the value determined from an interpretation (McKinnon, 1988a) of Fahr and Stein's (1986) rate constant for the addition of C_2H_2 to phenyl ($k=4.4 \times 10^{12} \cdot \exp(-3400/T)$, $cm^3/mol \cdot s$, T[K]). Aryl species concentrations were calculated by assuming partial equilibrium of

$$\text{Aromatic} + H = \text{Aryl} + H_2 \qquad \text{(Rxn.S.2)}$$

The oxidation rate was determined assuming a collision efficiency of 0.2 for OH oxidation of ΣGC PAH, based on Neoh's observation of the same collision efficiency of OH with soot. The H and OH concentrations were determined from the light hydrocarbon kinetics modelling using the Glarborg and Harris mechanisms.

S.7.4 Model Results

Figure S.24 shows the experimental data and the predictions from our model for ϕ=2.18 with no injection, C_2H_4 injection and C_6H_6 injection. It was found that the shape of the curves was best predicted assuming low collision efficiencies (<1%) for the ΣGC PAH with the soot particles and tar molecules. The coagulation of PAH molecules to form species larger than 5 aromatic rings was not important, and so $R_{coag-PAH}$ was equal to zero. The rate at which C_2H_2 adds to the 5 ring aromatic species, $R_{C_2H_2}$, does contribute to the net rate, especially at long residence times in the PFR when the fraction of 5 ring aromatic species approaches 10% of the total ΣGC PAH.

The most successful feature of the model is the ability to predict the changes in the ΣGC PAH inventory due to the addition of either aliphatic or aromatic species. We expect the injection of ethylene to increase the C_2H_2 concentration and thus increase R_{add}. If we increase R_{add}, we will also increase the rate at which mass is lost at the high molecular weight limit, $R_{C_2H_2}$. A secondary effect of the ethylene addition is an increased benzene profile, and so we expect a slightly increased R_i as well. These factors result in a higher rate of ΣGC PAH mass production, and consequently higher concentrations. The injection of benzene should have a large effect on the initiation rate, R_i, because the phenylacetylene mole fraction is increased dramatically by the benzene injection. From our phenylacetylene profile we know that R_i is high at early PFR residence times, and decreases at later times, so we expect the ΣGC PAH concentration profile to be increasing steeply at early times in the PFR, and then leveling out at later times.

Figures S.25-S.27 show the predicted contributions to the net rate from the different pathways in the model. For the no injection case (Fig. S.25), at early residence times, the major contributor to the mass of the ΣGC PAH inventory is R_i, and at later times R_{add} is dominant. The dominant pathway for destruction is R_{ox}. $R_{coag-soot}$ and R_{C2H2} are increasing, but remain much less than R_{ox} in the PFR. The ethylene injection case has a balance of rate contributions (Fig. S.26) similar to the no injection case, but each component has a

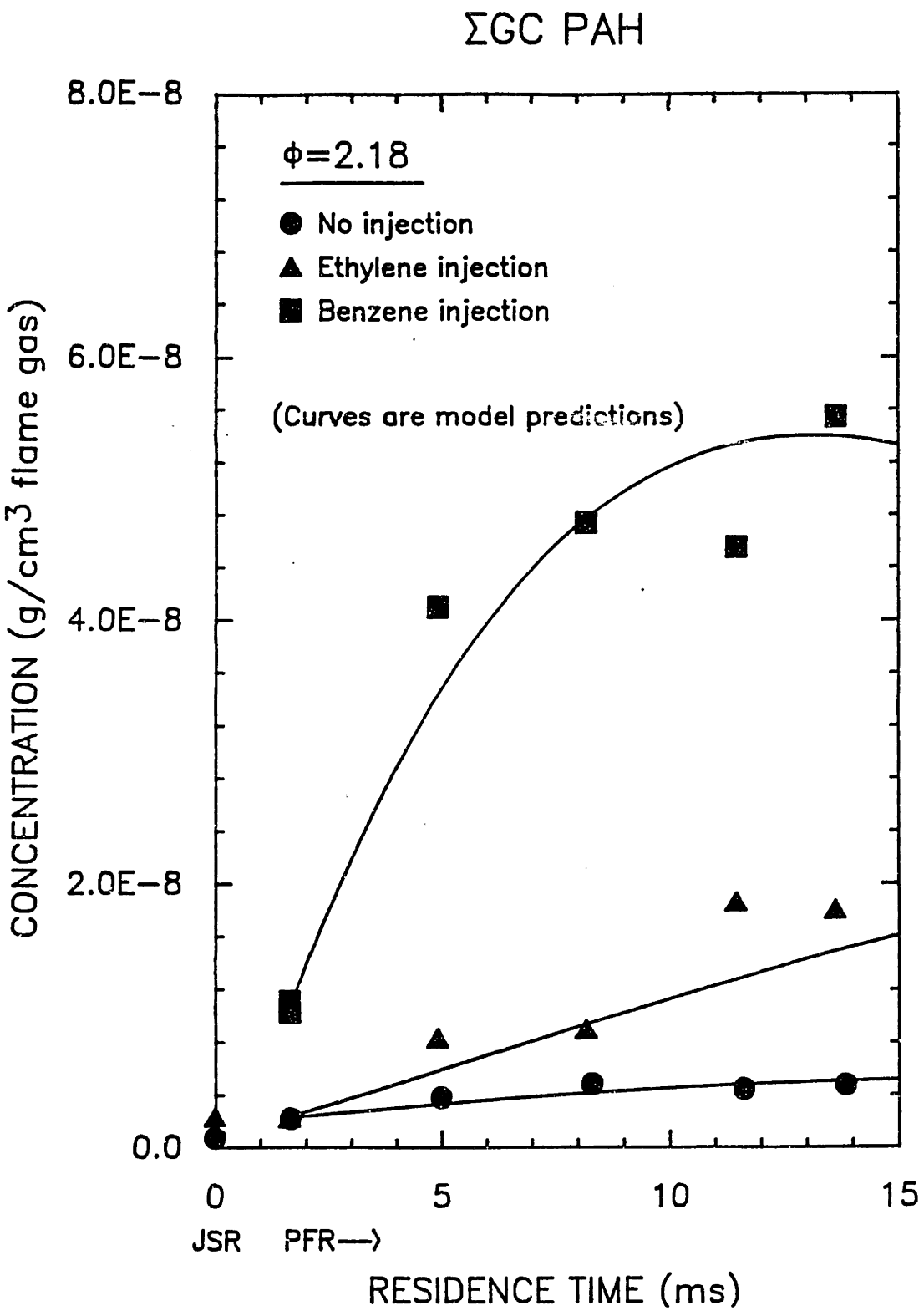

Figure S.24 Comparison of global PAH kinetic model predictions with experimental data for ΣGC PAH species for ϕ=2.18, no injection, C_2H_4 injection and C_6H_6 injection cases as defined in Table S.4.

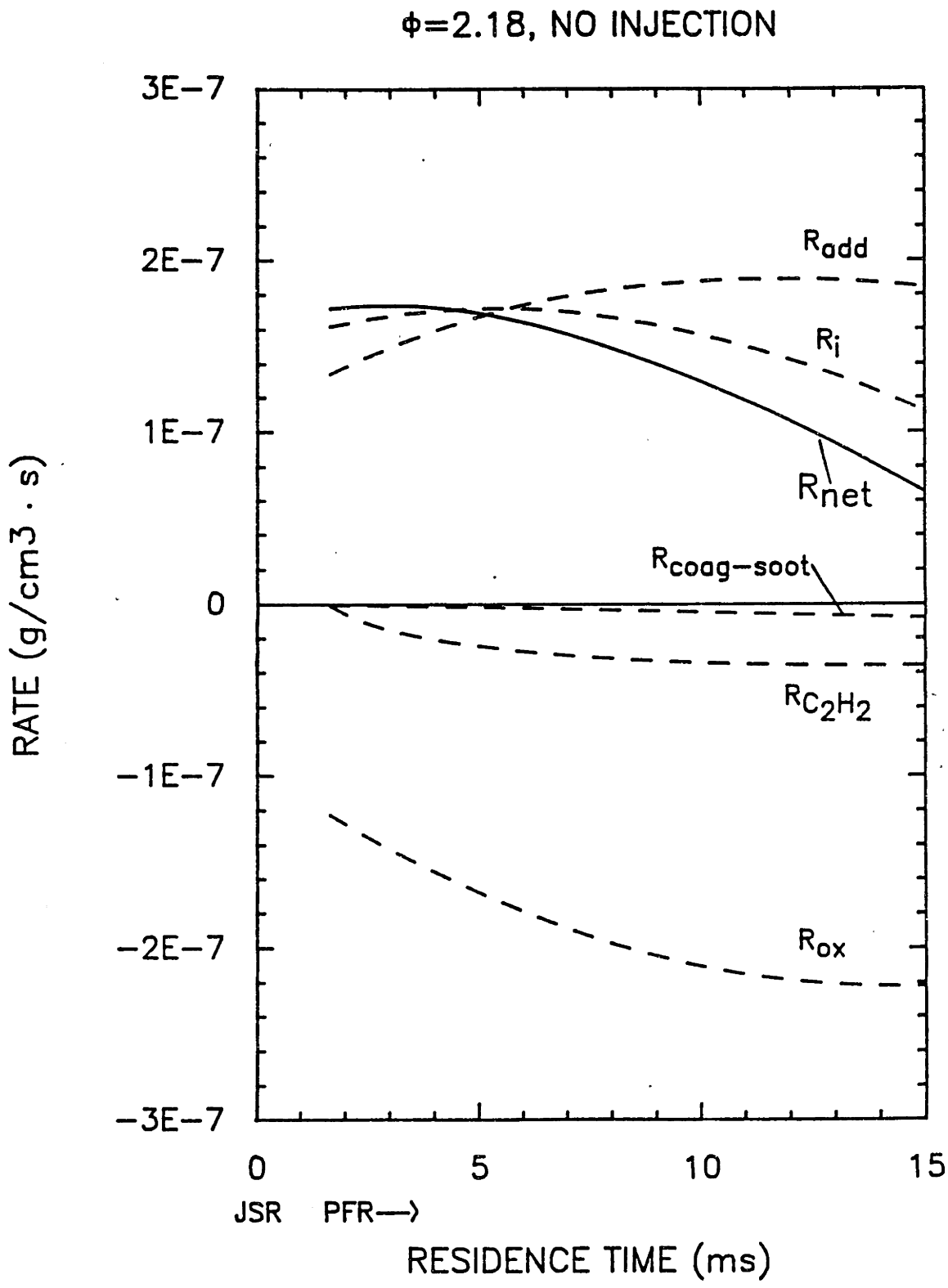

Figure S.25 Rates of formation and destruction of ΣGC PAH inventory for ϕ=2.18, no injection.

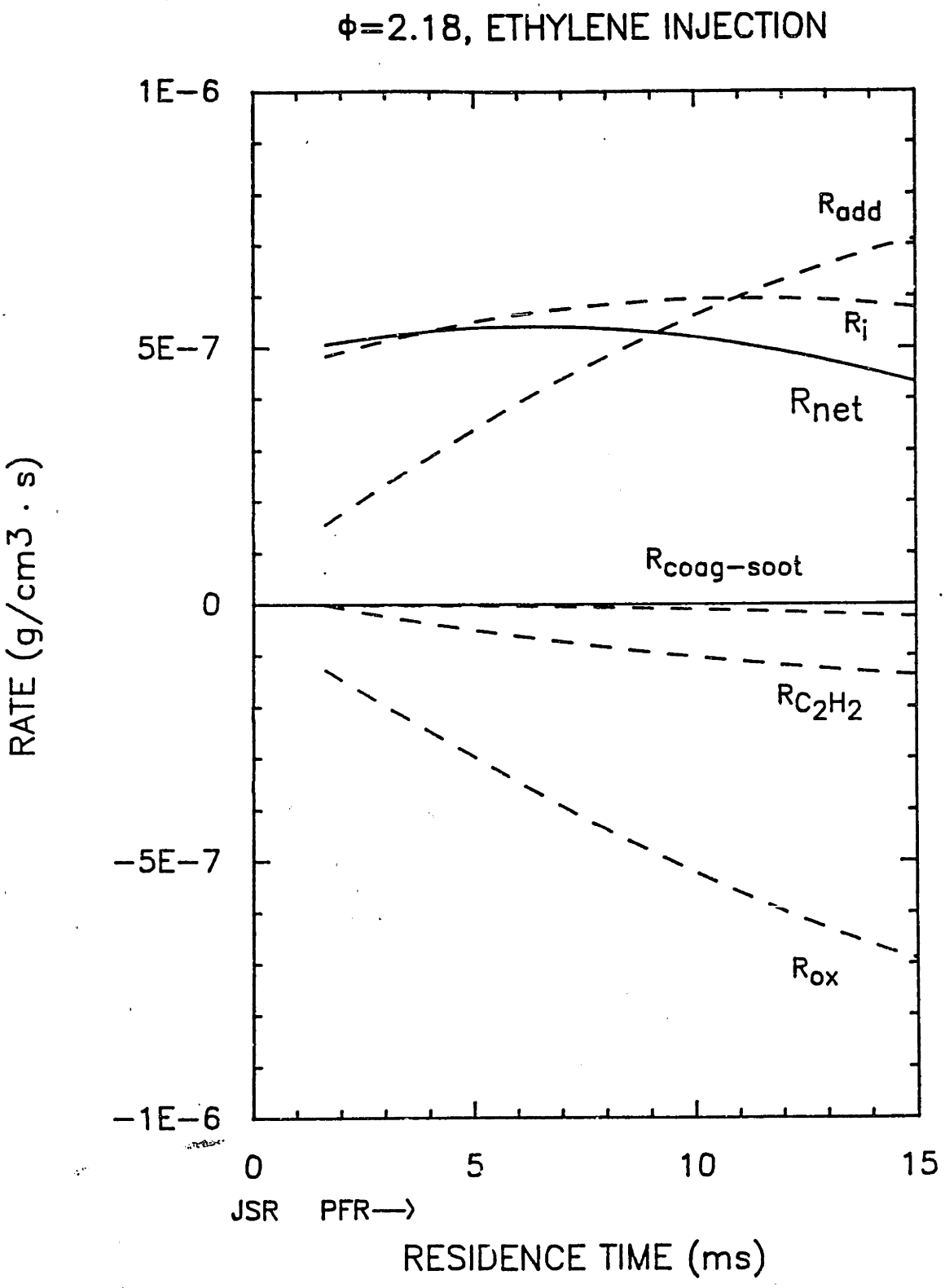

Figure S.26 Rates of formation and destruction of ΣGC PAH inventory for ϕ=2.18, C_2H_4 injection.

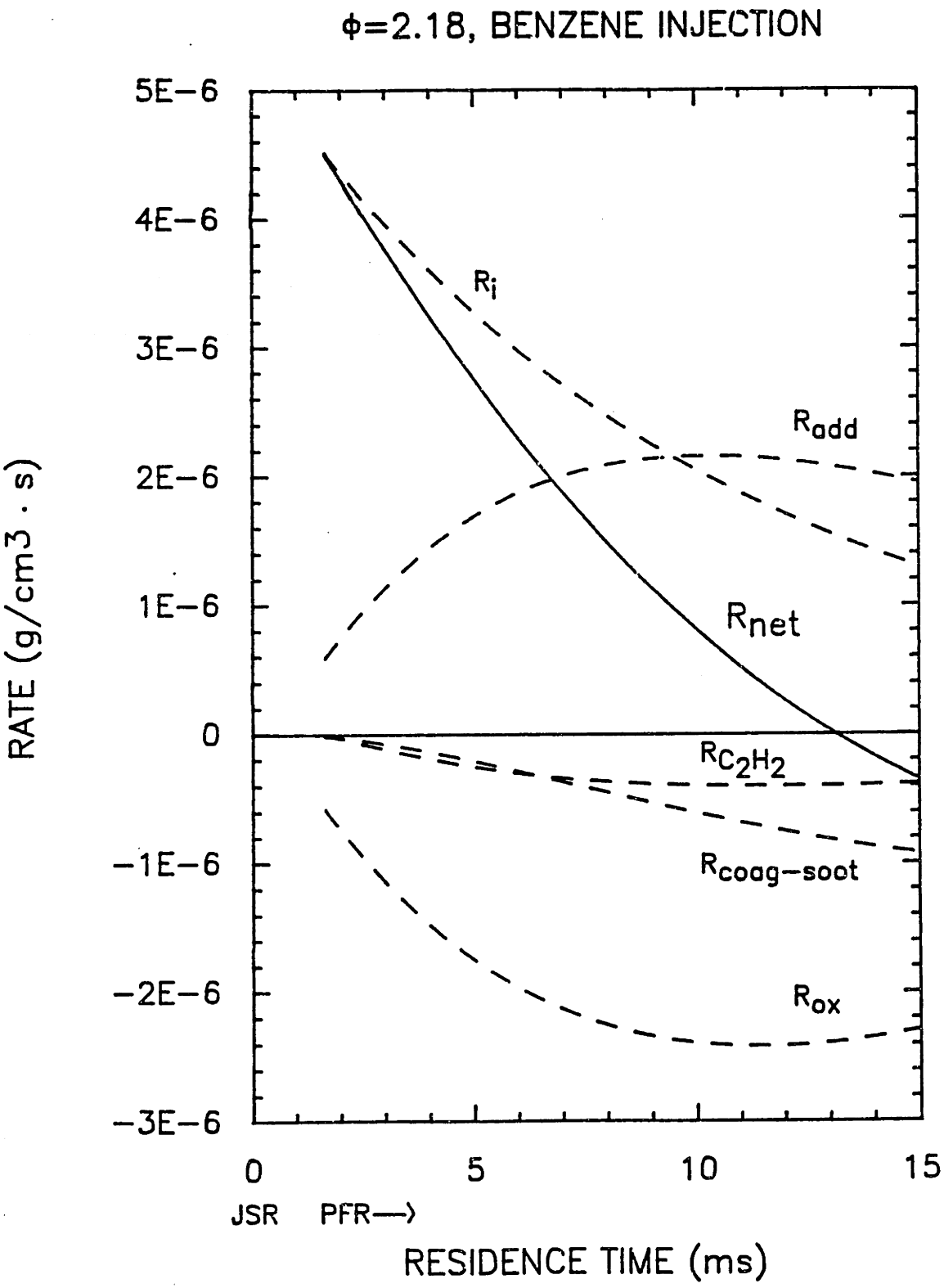

Figure S.27 Rates of formation and destruction of ΣGC PAH inventory for ϕ=2.18, C_6H_6 injection.

higher rate than the corresponding component for the no injection case.

The individual rates for the C_6H_6 injection case (Fig. S.27) show that R_1 is the dominant pathway for mass addition to the ΣGC PAH inventory. The sharply decreasing C_6H_6 concentration profile causes R_1, and therefore R_{net}, to decrease in the PFR. The contribution of intact single-ring aromatics on the formation of PAH is to provide additional moles and mass into the PAH inventory through reactions with C_2H_2.

For the chosen parameters of the model, based on available literature rate constants for the growth reactions, oxidation was required to successfully predict the shape and magnitude of the ΣGC PAH concentration profiles. As previously mentioned, the decay of the benzene concentration profile for the C_6H_6 injection case could be explained by the literature rate constant for oxidation of benzene by OH ($k_{(1600K)}$=2.5x10^{12} cm^3/mol•s), but a higher oxidation rate was required for the ΣGC PAH. Assuming constant collision efficiency, extrapolation to benzene of Neoh's collision efficiency of 0.2 for OH reacting with soot particles gives a bimolecular rate constant for C_6H_6+OH of 9.5x10^{13} cm^3/mol•s at 1600K, or almost a factor of 40 higher than the benzene oxidation rate. The oxidation rate constant for species in the ΣGC PAH inventory will be between these two values, and will probably increase with increasing molecular weight.

S.8 SUMMARY AND CONCLUSIONS

From our experimental observations of PAH and soot formation for fuel-rich (ϕ=2.18, 2.37) combustion of $C_2H_4/O_2/N_2$ in a JSR/PFR, we reach the following conclusions:

(1) The concentration profiles of fixed gases and major light hydrocarbon species change little in the PFR as equivalence ratio is increased from non-sooting to incipient sooting conditions in the JSR, but for the sooting condition, the tar concentrations are 5 times higher, and soot concentration is 10 times higher.

(2) At the end of the PFR, the combined mass concentration of PAH species with 2-5 rings is comparable that of the high molecular weight tar material (≥6 rings and CH_2Cl_2-soluble).

(3) Injection of C_2H_4 ($8.2x10^{-3}$ moles/mole total flow at ϕ=2.37, $1.0x10^{-2}$ moles/mole total flow at ϕ=2.18) into the PFR results predominantly in conversion to C_2H_2, but also increases the concentrations of benzene and PAH. An incremental amount of C_2H_4 injected into the PFR is not as effective in enhancing PAH and soot production as the same incremental amount of C_2H_4 fed to the JSR.

(4) Injection of a small amount of C_6H_6 (≈1800 ppm) into the PFR caused a 10-fold increase in the PAH and soot concentrations in the PFR for the ϕ = 2.18 condition studied. Assuming the 10-fold increase in tar and soot concentration comes from benzene, then these data indicate that 16% of the injected benzene is converted to tar and 11% to soot. Oxidation of C_6H_6 to CO and C_2H_2 is also occurring. Benzene promotes tar and soot formation by causing a 10-fold increase in the benzene concentration at the beginning of the PFR. This observation is consistent with the hypothesis that the number concentration of single-ring aromatics in a combustion environment with high C_2H_2 concentrations controls the growth of higher aromatics. An increase in benzene concentration increases the production of 2-ring aromatics, and is the major source of new moles of PAH material.

(5) Acetylenic-substituted PAH species, which have been proposed as important intermediates in PAH formation, were positively identified by the use of Gas Chromatography/Fourier Transform Infrared Spectroscopy (GC/FTIR).

(6) PAH species which contain 5-membered ring structures account for more than half of the total PAH inventory from indene (C_9H_8) to benzo(ghi)perylene ($C_{22}H_{12}$). These PAH species with 5-membered ring structures consisted of 2 types: 1) 5-membered rings containing a methylene group, and 2) "acenaphthylene bridge" structures.

(7) Phenylacetylene formation from the injected benzene is rapid, and the ratio of phenylacetylene to benzene is near that predicted from equilibration of the reaction $C_6H_6 + C_2H_2 = C_8H_6 + H_2$.

For the fixed gases and light hydrocarbons, kinetics modeling was done at the elementary reaction level; and for PAH both thermodynamics and global kinetics modelling efforts proved insightful. The major conclusions from the modelling work are:

(8) Fixed gases and major hydrocarbon species (CO, CO_2, H_2, CH_4, C_2H_2, C_2H_4) can be modelled assuming a perfectly-stirred/plug-flow reactor system using an elementary reaction mechanism proposed by Glarborg (1986a), which contains 134 reactions, and 29 chemical species, or by a mechanism proposed by Harris (1988) consisting of 193 reactions and 49 species.

(9) Thermodynamics analysis of the PAH reveals that, with the exception of the ethynyl-acenaphthylenes, the most abundant PAH species observed experimentally are the stabilomers predicted by Stein, which are the most thermodynamically stable species for a given carbon and hydrogen number.

(10) Aliphatic hydrocarbons with the general formula $C_{2n}H_{2m}$ are produced in excess concentrations in the JSR for equilibration of the C_2H_2-H_2-$C_{2n}H_{2m}$ system, and these species decay towards their equilibrium limits in the PFR. Aromatic species, including PAH, with the general formula $C_{2n}H_{2m}$ are far below their equilibrium limit, but are increasing towards their predicted thermodynamic limits in the PFR.

(11) An aromatic coagulation mechanism for PAH formation, consisting of bimolecular reactions of aryl species reacting with intact aromatic rings, is not the dominant mechanism of PAH formation for our experimental conditions.

(12) A global kinetics model of the PAH inventory (2-5 rings species) successfully predicted the concentration profile of the PAH inventory in the PFR at ϕ=2.18, as well as the perturbation to the PAH profiles from the injection of additional ethylene and benzene. The model includes pathways for mass flux into the PAH inventory due to 1) C_2H_2 addition reactions with single-ring aromatics and 2) C_2H_2 addition reactions with PAH; and pathways for mass flux out of the PAH inventory by 3) C_2H_2 addition reactions with 5-ring PAH, 4) coagulation reactions between PAH, 5) coagulation of PAH with high molecular weight tar, 6) coagulation of PAH with soot, and 7) oxidation reactions of PAH with OH. Acetylene addition to aromatic species provided the major source of mass flux into the PAH inventory, while oxidation was the main route of mass loss from the PAH inventory. Coagulation of PAH with soot was predicted to have low collision efficiencies ($\approx$ 1%). A collision efficiency, γ, of 0.2 for OH with PAH (based on γ = 0.2 for OH reaction with soot) was necessary in order to successfully predict the experimental trends. This rate is $\approx$40 times higher than the rate of benzene oxidation by reaction with OH.

S.9 RECOMMENDATIONS FOR FUTURE WORK

The use of the injection system along with the unique capabilities of the JSR/PFR should enable further progress to be made in the acquisition of experimental data in order to better understand PAH formation. Specific areas for further research include:

(1) Further injection studies on the effect of multi-ring aromatics on the formation of PAH would be useful in identifying pathways for PAH (as well as soot) formation and destruction. Since PAH are destroyed as well as formed, the destruction of large PAH to smaller PAH needs to be investigated.

(2) The effect of temperature on PAH formation should be investigated further by obtaining experimental data at higher temperatures closer to those found in typical laminar flat-flames.

(3) The measurement of radical species, especially aromatic radicals, by molecular beam-mass spectrometry would be very valuable in evaluating elementary kinetic models for PAH formation.

(4) The modelling of PAH at the elementary reaction level is not possible until more rate constants become available from isolated kinetic studies at high temperatures. In particular, kinetics experiments to determine the high temperature rate parameters for PAH oxidation reactions, as well as further studies on aliphatic addition reactions to PAH, should be performed. Chemically activated pathways for PAH formation should be considered.

(5) Hydrocarbon combustion mechanisms for formation of C_4 species and aromatic species should be tested against this data set.

(6) Additional characterization of the high molecular weight tar material which is soluble in CH_2Cl_2 but not amenable to GC analysis, should provide information necessary to obtain a better understanding of soot formation.

1. INTRODUCTION

1.1 BACKGROUND

Polycyclic aromatic hydrocarbons (PAH) are undesirable combustion products that pose biological and environmental hazards. Practical combustors, such as domestic oil burners, form significant amounts of PAH, and certain individual species are known to be mutagenic in bacterial cell assays. Other practical combustors, such as industrial furnaces, do not have control strategies to minimize PAH formation and may in fact actually enhance the production of PAH. For example, in large furnaces staged combustion is used to control NO_x emissions, and soot is allowed to form in the primary chamber under fuel rich conditions. Soot enhances radiative heat transfer to the walls of the furnace, but PAH is also formed under fuel rich conditions, and the destruction of the PAH in the secondary chamber is not certain.

Because of complex flow patterns in practical combustors, it is difficult to separate the fluid mechanics, transport processes, and chemistry which occurs. It is therefore necessary to study the problem in well-characterized laboratory combustors in order to focus attention on the effects of chemistry.

The chemistry of lean combustion is fairly well understood, and reaction networks composed of elementary reactions predict experimental observations with surprising accuracy. Rich combustion chemistry is not so well understood, probably because of the large number of species which are generated. These species may have molecular weights higher that the parent fuel molecule, and a "mole-

cular-weight growth" process must be responsible for the formation of PAH. A tremendous number of individual PAH species are generated, which further complicates analysis. In order to gain an understanding of "molecular weight growth", measurements for chemical species of molecular weights higher and lower than the parent fuel molecule must be obtained.

The role of PAH in the formation of soot is also an interesting topic of research. The relationship between the formation of PAH and soot may be described as either competitive or sequential. One view is that PAH must be formed prior to the formation of the first incipient soot particle, and so therefore the PAH act as gas-phase precursors to soot particles. Another view is that PAH compete with incipient soot particles for gas-phase species which are prone to form soot. Of course, it is entirely possible that different classes of PAH perform in both these ways. The role of PAH in soot formation needs further investigation.

The amount of research which has been focused on the formation and destruction of PAH is small, mainly because the problem has been identified only recently as a biological hazard. The formation and destruction of soot, however, has been well-studied, and a vast amount of literature exists. An unfortunate problem with most of the soot literature is that the quantification of chemical species generated during combustion or pyrolysis is inadequate.

1.2 THESIS OBJECTIVES

The general goals of this research are to obtain a better under-

standing of the molecular weight growth process which forms PAH and eventually soot during combustion. The specific objectives of this dissertation are to:

1) Obtain experimental measurements for fixed gases, light hydrocarbons, PAH and soot in a plug-flow reactor for $C_2H_4/O_2/N_2$ combustion under non-sooting and sooting conditions in an upstream jet-stirred reactor;
2) Investigate the effects of aliphatic and aromatic species on molecular-weight growth;
3) Model the hydrocarbon chemistry at the elementary reaction level;
4) Develop a kinetics model for the formation of PAH;
5) Identify and assess the mutagenicity of PAH produced during combustion through collaborative efforts with researchers in the Analytical Chemistry and Toxicology departments.

2. LITERATURE SURVEY

2.1 EXPERIMENTAL OBSERVATIONS

The field of soot formation has been reviewed periodically by various authors. An early review article written by Street and Thomas (1955) summarized the literature on soot formation prior to 1955, and the authors presented a good provocative discussion on the nature of soot formation mechanisms. Palmer and Cullis (1965) summarized the main experimental observations on carbon formation from gaseous fuels and included a survey of kinetic mechanisms in their classic review. Haynes and Wagner (1980) presented an updated and comprehensive review on soot formation which included premixed flames, diffusion flames, fuel spray flames, as well as soot oxidation and the influence of additives, but did not review literature in the carbon black field. The authors also summarized models for soot formation, concentrating on the chemistry which occurs prior to the appearance of the first incipient soot particle. A review of work in the carbon black field is presented in Lahaye and Prado (1978). Calcote (1978) reviews the literature which postulates an ionic mechanism of soot formation. An ionic mechanism is appealing because it bypasses some of the restrictions to molecular weight growth inherent in a free-radical mechanism, and ionic reactions are known to proceed at rates approaching collision rates.

The amount of research focused on the PAH and aromatic material formation in combustion is much more scarce than the work on soot formation. Longwell (1982) has written an excellent review article on PAH formation and examines the role of PAH in soot formation as well

as mechanisms by which parent fuel molecules form PAH. Homann (1984) reviewed some of the more recent work on large ions and particulates. Bittner and Howard (1978) examined the role of the aromatic ring in soot formation and discussed the possible growth mechanisms which lead to higher aromatics. Finally, Longwell (1983) has examined the mutagenicity and toxicity of PAH produced in practical combustors.

In order to study the mechanism of PAH formation properly, chemical species quantification is required. Early soot formation studies unfortunately lacked information about concentrations of the chemical species which were present in the gas. In the molecular weight growth process, both species of molecular weight lower and higher than the parent fuel molecules will be important. The formation of PAH and soot has been investigated in both combustion systems (with oxygen) and pyrolysis systems (without oxygen). The purpose of this survey is to highlight the experimental observations in systems in which chemical species quantification allows insight into the chemical pathways of the formation of PAH and soot.

2.1.1 Combustion Systems -- Laminar Flat Flames

In a pioneering study by Bonne, Homann, and Wagner (1965) a low pressure (20 torr) laminar flat flame was sampled using a molecular-beam/mass spectrometry system. This allowed quantification of chemical species, both stable and radical, found present in the flames studied: acetylene, ethylene, propane, benzene and ethanol. Soot was detected optically by monitoring absorption at a wavelength of 6500 angstroms. Concentration profiles were obtained for fixed gases, such

as CO, H_2, H_2O, O_2, and CO_2; light hydrocarbon species, such as CH_4, C_2H_2; as well as polyacetylenes up to $C_{12}H_2$. The polyacetylene concentrations, excluding acetylene, maximized in the oxidation zone where radical concentrations were high, and then decreased to steady, or gradually falling, concentrations in the burned gases in the hydrocarbon flames studied. The authors chose to study acetylene in more detail. They found that soot was observed to first form in the region where polyacetylene concentrations were high, and the number concentration of soot particles was constant in the region where polyacetylene concentrations were relatively constant. On the basis of these observations, the authors concluded that polyacetylenes played a critical role in soot formation.

Two years later, Homann and Wagner (1967) presented another paper in which their interpretation of the data changed to include PAH in the reaction growth scheme. They studied benzene flames and found a high concentration of PAH in the oxidation zone where soot first appeared. From the acetylene experiments, the authors had concluded that PAH were by-products of soot formation rather than intermediates. From the benzene experiments they concluded that PAH could add to certain "bulky reactive radical intermediates" in the oxidation zone. They proposed that three different classes of compounds were important in formation of carbon. They are 1) acetylene and polyacetylenes, 2) unreactive PAH without sidechains, and 3) reactive PAH with sidechains. Thus, in the benzene flame, the compounds in class 3 would add to the growing polyacetylene polymer. The total concentration of PAH in the acetylene flame was 10^{-2} mole percent, and the

benzene flame had a total PAH concentration about 100 times greater.

Another study in which individual PAH species were identified was by Tompkins and Long (1969). The authors studied acetylene-oxygen flat flames and characterized their chemical measurements into 3 classes of compounds: 1) total polymeric material, 2) chloroform insoluble material, and 3) chloroform soluble material, which was then analyzed by GC to yield 20 PAH species. The authors did not make measurements of lower molecular weight species.

Tompkins and Long found two distinct regions of PAH formation. The first region was characterized by a sharp increase followed by a sharp decrease by the end of the oxidation zone. The second region was higher in the flame where the temperature was falling over a range 1173 K to 923 K, and the PAH concentration gradually increased. The authors concluded that the PAH formed in this secondary region were formed from pyrolysis of the residual acetylene. Because the PAH formed in the primary region does not have side chains and goes through a maximum where incipient sooting occurs, Tompkins and Long concluded that PAH may be important in the formation of soot. This statement is in contradiction to that made by Homann and Wagner in 1965.

D'Alessio, et. al. (1974) studied the burned gas of a methane-oxygen atmospheric flat flame. Soot production began in the region of falling acetylene concentration and where benzene, C_4H_2, and C_4H_4 maximized. PAH first appeared in the region of soot production and increased slightly after which it remained constant. Individual species of PAH such as pyrene, fluoranthene, anthracene and phenanth-

rene increased steadily through the burned gas zone. In contrast, coronene, 3,4-benzopyrene, 1,2-benzopyrene and benzoperylene showed maxima in their concentration profiles. D'Alessio calculated that the PAH could only account for 2-3% of the total soot formed, and hence agreed with Homann and Wagner that PAH were by-products and not intermediates to soot production.

In a second paper by the same group (D'Alessio et al. 1976) they probed the oxidation zone of their atmospheric methane-oxygen flat flame. From this study the authors concluded that evolution of C_2, C_3, and C_4 unsaturated species did not occur before the evolution of soot. This result has been criticized because of the sampling technique used. Soot was detected optically, and probe interference in the oxidation zone, where concentration gradients were steep, may have caused a misalignment in the soot and hydrocarbon profiles.

Bittner and Howard (1981a, 1981b, 1981c) used a molecular-beam/mass spectrometry sampling system to study 20 torr benzene flames. They presented experimental evidence for molecular weight growth in the flame for both non-sooting (ϕ = 1.8) and sooting (ϕ = 2.0) conditions. Data was collected by operating the mass spectrometer as a high pass filter to detect molecules above a certain cut-off mass, and this data is shown in Figure 2.1. The most striking observation is that the maximum peak concentration for the high mass (I_M > 700) material at sooting conditions is 2 orders of magnitude larger than the maximum concentration for the non-sooting condition. Since the formation of soot is a balance of growth reactions versus oxidation or destruction reactions, the high concentration of high

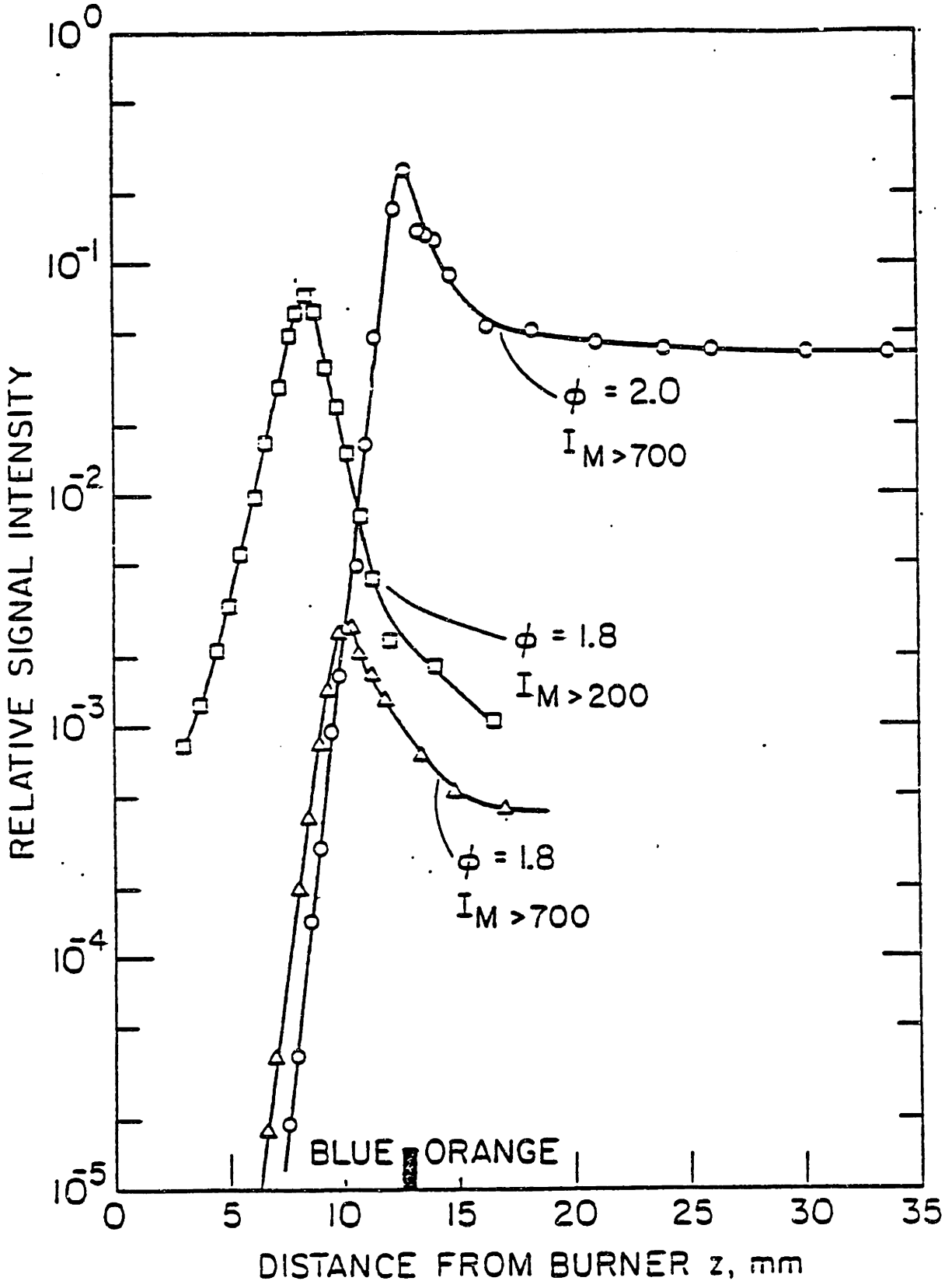

Figure 2.1 Relative Intensities of High Mass Signals vs. Distance from Burner in Nearly Sooting (ϕ = 1.8) and Sooting (ϕ = 2.0) Benzene-Oxygen-30 mol % Argon Flames. (From Bittner and Howard, 1981a.)

molecular weight material which builds up at low burner heights, may not be completely destroyed passing through the oxidation zone, and thus producing soot in the secondary zone of the flame.

Another observation is that the concentration of material larger than 200 amu peaks before the maximum of the material larger than 700 amu. The relative positions of these concentration maxima implies sequential growth of lower molecular weight material into higher molecular weight material. This trend is shown more clearly in Figure 2.2 where the mass of material is presented on an incremental basis instead of a cumulative basis. At low burner heights, Bittner states that the constant slopes on the formation side of the peaks can be described by a balance of convection and diffusion. This implies that the region of formation of high molecular weight material is in the vicinity of the peak concentrations. At higher burner heights, preferential destruction of the low molecular weight material indicates that the lower molecular weight species are more rapidly destroyed, or the destruction of the lower molecular weight material leads to the production of the higher molecular weight material. The observed trend of the low molecular weight material peaking in concentration while the high molecular weight material is increasing indicates that the molecular weight distribution shifts towards higher molecular weight.

As shown in Figure 2.4, if the data in Figure 2.3 is plotted as a function of molecular weight for various burner heights, and we can see quite clearly the shift in distribution of molecular weight to higher masses at higher burner heights. At a burner height of 7.2 mm,

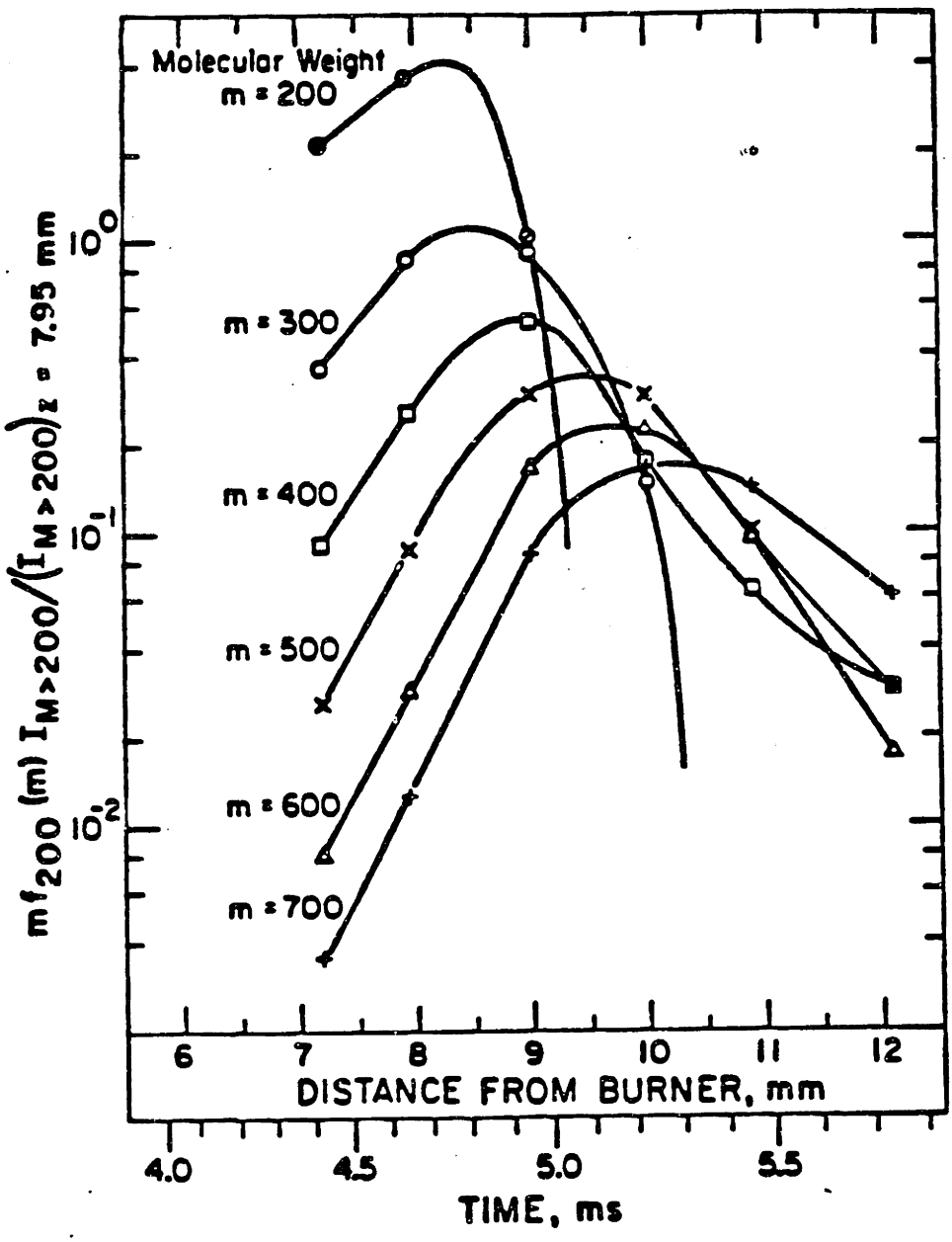

Figure 2.2 Variation with Distance from Burner of Mass of Material in Molecular Weight Range m to m+dm at Different Molecular Weights, Normalized with Number of Moles of M>200 amu material at 7.95 mm above Burner in a Near Sooting (ϕ = 1.8) Benzene (13.5 mol %) - Oxygen (56.5 mol %) - Argon (30.0 mol %) Flame. (From Howard and Bittner, 1981).

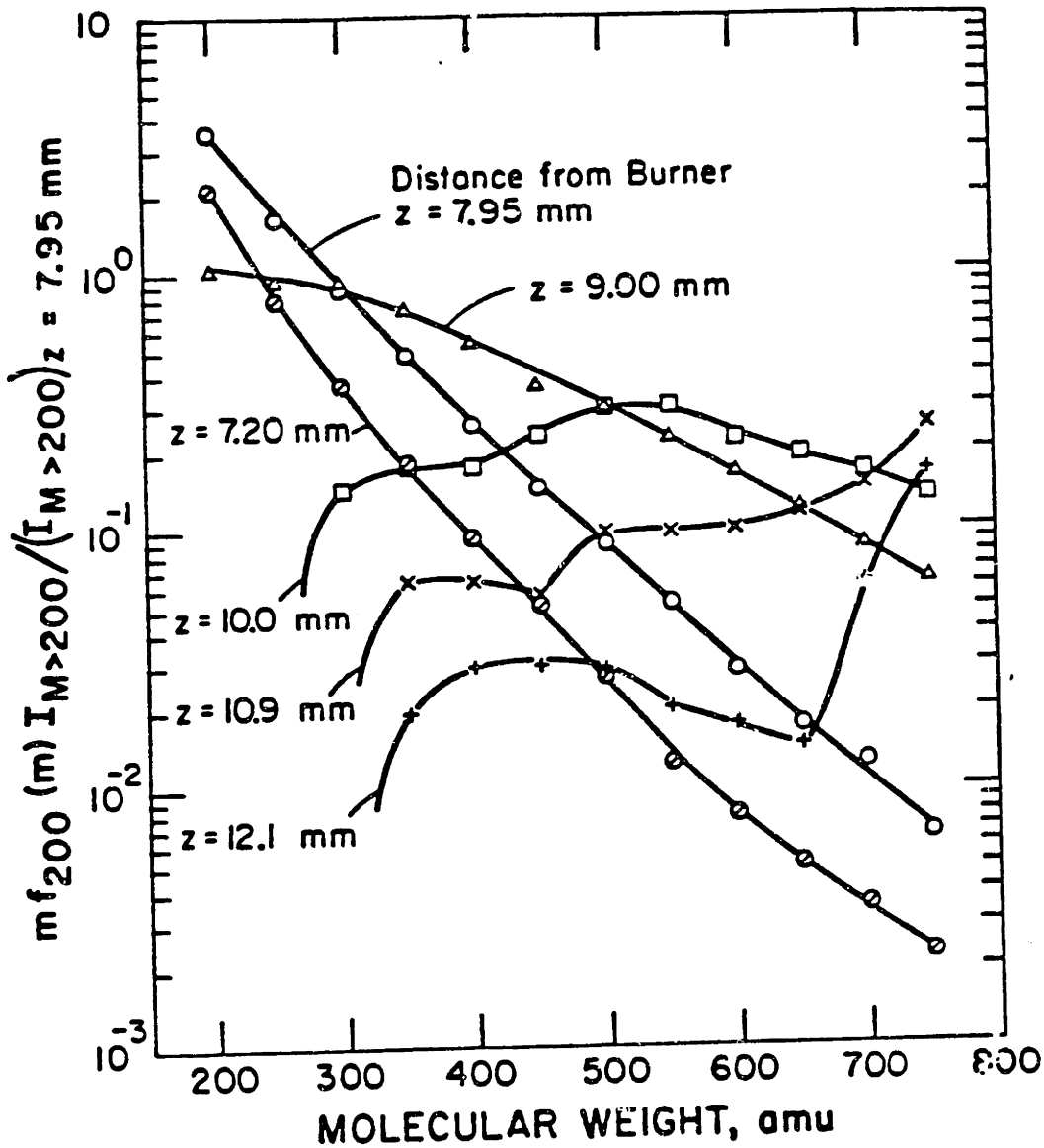

Figure 2.3 Mass of Material as Function of Molecular Weight at Different Heights above Burner, Normalized with Number of Moles of M > 200 amu Material at 7.95 mm above Burner in a Near Sooting (ϕ = 1.8) Benzene (13.5 mol %) - Oxygen (56.5 mol %) - Argon (30.0 mol %) Flame. (From Howard and Bittner, 1981).

the PAH distribution is heavily weighted towards the 200 amu material, but at a height of 12.1 mm, the lower molecular weight material has been depleted by 3 orders of magnitude, and the higher molecular weight material is increased by 2 orders of magnitude, resulting in a profile which is actually weighted towards the 700 amu material. Further numerical analysis of this unique data set has been performed by Pope (1988).

Although identification of these high mass species was not obtained, thorough quantification of the lower mass species enabled the authors to postulate possible molecular weight growth mechanisms. Figure 2.4 shows some of the PAH species profiles obtained by Bittner for the non-sooting benzene flame. All of the profiles show an increase to a maximum concentration between 7.5 and 9.0 mm, followed by a sharp decrease to below detectable limits. Other than phenyl radical, no PAH radical species measurements were obtained, probably because of their low concentrations. It should be noted that the identifications by Bittner were only possible structures consistent with the GC/MS data. For example, the structure shown for the $C_{14}H_8$ species is pyracylene, but it is impossible to distinguish pyracylene from an ethynyl-substituted acenaphthylene based solely on GC/MS data.

A study by Bockhorn, Fetting and Wenz (1983) used low pressure flat flames burning propane, acetylene and benzene as fuels. It was seen that for propane, the concentration of PAH went through a sharp maximum and then a steady increase higher in the flame. For acetylene, this second rise in PAH concentration was less pronounced, and for benzene it was missed altogether. The authors explain these

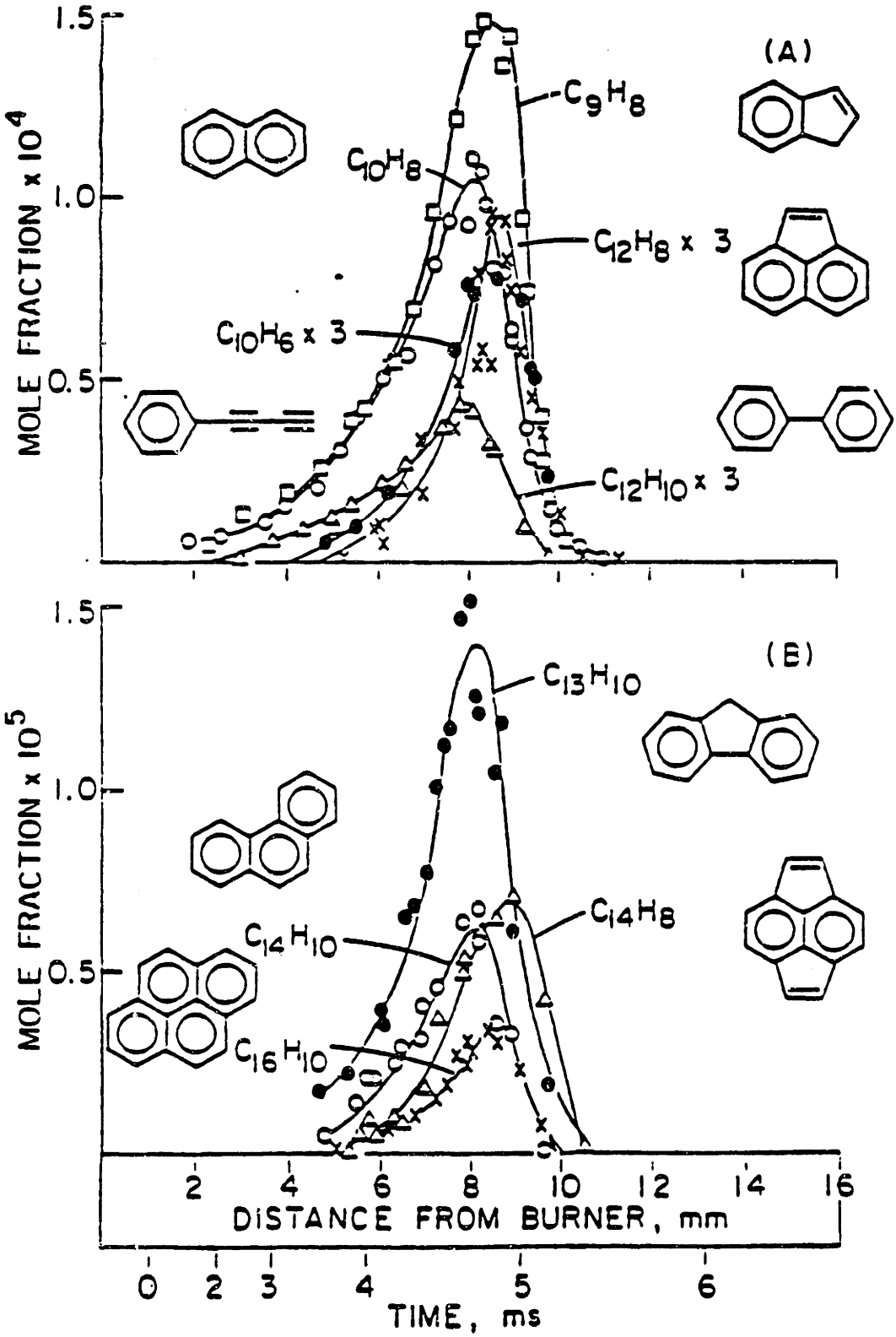

Figure 2.4 Mole Fractions of Polycyclic Aromatic Hydrocarbons vs. Distance from Burner in a Near Sooting (ϕ = 1.8) Benzene (13.5 mol %) - Oxygen (56.5 mol %) - Argon (30.0 mol %) Flame. (From Bittner and Howard, 1981a).

observations by pointing to temperature differences in the three flames. At the start of the postflame zone, the temperature was 1700 K for propane, 1850 K for acetylene, and 2050 K for benzene. The logical explanation would be that the lower temperatures promote PAH formation.

2.1.2 Well-Stirred Reactors

Well-stirred reactors are ideal for studying the intrinsic kinetics of combustion reactions if the perfectly stirred criterion can be met. Nenniger (1983) studied PAH production in a jet-stirred reactor for ethylene and toluene fuels. For both ethylene and toluene, PAH concentration increased with equivalence ratio until heavily sooting conditions, in which case the yields slightly decreased. For ethylene, this limit occurred at an equivalence ratio of 2.8, and for toluene the limit was around 1.9-2.0. Soot yields showed a maximum with temperature at 1800 K for a given equivalence ratio. This type of behavior has been observed in pyrolysis systems, such as shock tubes, but not in combustion systems.

Vaughn (1988) studied the formation and destruction of single-ring aromatics in the same Jet-stirred reactor used in this study, but was also able obtain PAH and soot data. Fuel mixtures of toluene with ethylene or benzene with ethylene were studied. By varying the aromatic/ethylene ratio, Vaughn found that the PAH concentrations increased as the aromatic/ethylene ratio was increased. The increases in concentrations of PAH species was roughly the same as the increase in the concentrations of the single ring aromatics which were not

destroyed in the JSR. For a fixed equivalence ratio, soot was also observed to increase as the benzene or toluene fraction was increased.

2.1.3 Turbulent Diffusion Flame

Toqan (1985) studied PAH and soot formation in a turbulent diffusion flame using two fuels: a coal-derived liquid (Exxon Donor Solvent) and natural gas. Time-averaged axial flux profiles showed sequential maxima in the ethane, ethylene, and acetylene profiles. Benzene and PAH maximized even further downstream, indicating a molecular weight growth sequence similar to that observed in flat flames.

2.1.4 Flow Reactors

Early flow reactor studies concentrated on the pyrolysis of hydrocarbon fuels in an inert carrier gas, such as He, Ne, or N_2. A tremendous amount of work was done in this area by Badger and coworkers (Badger et al. 1958-1967, 29 papers), but their studies were confined to temperatures below 973 K, with long residence times. Hou and Anderson (1963) studied the pyrolysis of acetylene, vinylacetylene and diacetylene using a flow reactor with 25 mole % hydrocarbon in He. Again, low temperatures (less than 973 K) and long residence times (9 seconds) make the results of this study not directly applicable. Some of the mechanisms and observed species, however, may be of value when looking at high temperature behavior of PAH.

Hou and Palmer (1965a, 1965b) pyrolyzed diacetylene and benzene in a high temperature, atmospheric pressure reactor (up to 1523 K),

with lower residence times (30-250 msec). The diacetylene study extended the earlier work of Hou at lower temperatures. It was found that the decomposition of diacetylene exhibited a strong similarity to that of acetylene. The benzene study showed a mixed order reaction for the decomposition of benzene. It was postulated that the first order reaction was due to benzene decomposition due to wall interactions. The second order behavior was explained by the reaction of two benzenes going to biphenyl and hydrogen. This low temperature behavior is consistent with the findings of Kinney and Slysh (1960).

2.1.5 Shock Tubes

Shock tubes have been used in numerous studies of soot formation using optical diagnostics, but relatively few studies have included product species identification, probably because of sampling difficulties. Vaughn (1980) studied benzene pyrolysis using a 5.08 cm id single pulse shock tube in which batch gas samples were taken after pyrolysing benzene over a temperature range of T_5=1100 K to 2400K. Vaughn was unable to detect any species larger than styrene, and postulated that the first step to soot formation was the addition of acetylene to benzene to form styrene. Styrene and acetylene were the major products observed, and trace amounts of vinylacetylene, methane, and toluene were also detected. Sensitivity limited the detection of biphenyl to 1% by mass of the original benzene fuel, and none was detected.

Kern et al. (1982a) studied toluene, benzene, butadiene, and acetylene pyrolysis using a time-of-flight mass spectrometer sampling

from the reflected shock zone. For benzene and toluene, over a temperature range of 1400-2300 K and pressure range of 0.21-0.57 atm, the major products were acetylene and polyacetylenes up to C_8H_2. No products with masses greater than the original benzene or toluene fuel were detected, although the detection range was reported to extend to m/e 300 with a sensitivity of 5000 ppm with respect to the original fuel concentration. The onset of sooting was not observed, but an upper limit of 10% was set as the soot yield from toluene. In a later paper, Kern and Singh (1982b) show a peak at m/e 152 for higher benzene concentrations (5%) which could be attributed to acenaphthylene. Because of low carbon atom concentrations relative to combustion systems, shock tubes are not well suited for detection of higher aromatic species which occur in very low concentrations. The shock tube environment is ideal, however, for studying the inherent chemistry of PAH formation, because of the homogeneity of the system, and the ability to vary temperature and chemical species effects separately.

Bauer and Jeffers (1984) studied shock tube pyrolysis of di- and tri-cyclic aromatic hydrocarbons. Ten different test samples were pyrolyzed, and a minimal mechanism for soot formation was postulated. Some of the key observations were that while acetylene, tetramethylpentane, acenaphthylene, and acenaphthene when tested individually produced no soot, mixtures of either of the two aliphatics with either of the two aromatics produced copious amounts of soot. The author interpreted these observations to imply that two different classes of species were necessary for soot initiation:

adduct species such as C_2H_2, C_4H_2, C_4H_3, C_2H, etc., and aromatic radicals such as phenyl, naphthyl, etc.

2.1.6 Knudsen Cell

Using a high temperature (2173 K), low pressure (10^{-5} to 10^{-1} torr) Knudsen cell, Smith (1979a) measured chemical species generated during the pyrolysis of toluene. A modulated molecular beam mass spectrometer was used to analyze chemical species. He found that high-molecular weight compounds were produced most efficiently at temperatures between 1473-1773 K, and that at temperatures above 1973K no species larger than C_6H_6 were found at any pressure. At temperatures between 1473-1673 K, species such as C_3H_4, C_4H_2, C_4H_3, C_5H_3, C_5H_5, C_6H_4, C_6H_4, C_6H_5, C_7H_5, C_7H_6, C_7H_7, exhibited maxima in their concentration profiles as a function of pressure, and Smith concluded that these species played a role in the formation of higher molecular weight compounds.

2.1.7 Additive Studies

A substantial amount of experimental work was presented by Davies and Scully (1964, 1965) studying soot formation from 25 different hydrocarbons injected into the burned gas of a H_2-CO flame. The temperature range was 800-1100 °C and the experimental data obtained was only semi-quantitative, but the experiments provided interesting points for discussion. Davies and Scully concluded that an intact aromatic ring was essential for the onset of soot formation. This statement was based on the sooting behavior of a

homologous series of heteroatomic aromatic molecules. Compounds which had a heteroatom in the aromatic ring did not form soot under the conditions of the experiment, while those compounds which had the heteroatom outside the ring or no heteroatom, formed copious amounts of soot. Also, the authors concluded that methyl-substituted aromatics yielded higher amounts of soot than non-substituted aromatics, even allowing for extra carbon in the fuel.

Harris (1984) added an incremental amount (≈1% of the total flow) of either toluene or ethylene as fuel to an $C_2H_4/O_2/Ar$ laminar flat flame. As Figure 2.5 shows, soot production was increased from the baseline case (Flame 1) by the same amount for either toluene (Flame 2) or ethylene (Flame 3) addition. The peak temperature was increased by 30°C for the ethylene addition, so Harris also studied a hotter ethylene flame (Flame 4) by increasing the total flow rate, but keeping the equivalence ratio the same. The effect of the 30°C temperature difference on soot production was negligible. Harris concluded that the soot formation process in his ethylene flame was not limited by the concentration of benzene or toluene, and that the flame environment, not fuel structure dominates in determining the sooting propensity.

A factor which complicates the analysis by Harris is the almost complete destruction of the additional toluene before it reaches the post-flame zone. Although toluene comprises 3500 ppm of the fuel in the toluene-doped flame, its concentration is only 150 ppm at a height above burner below where the first optical measurement was taken. The

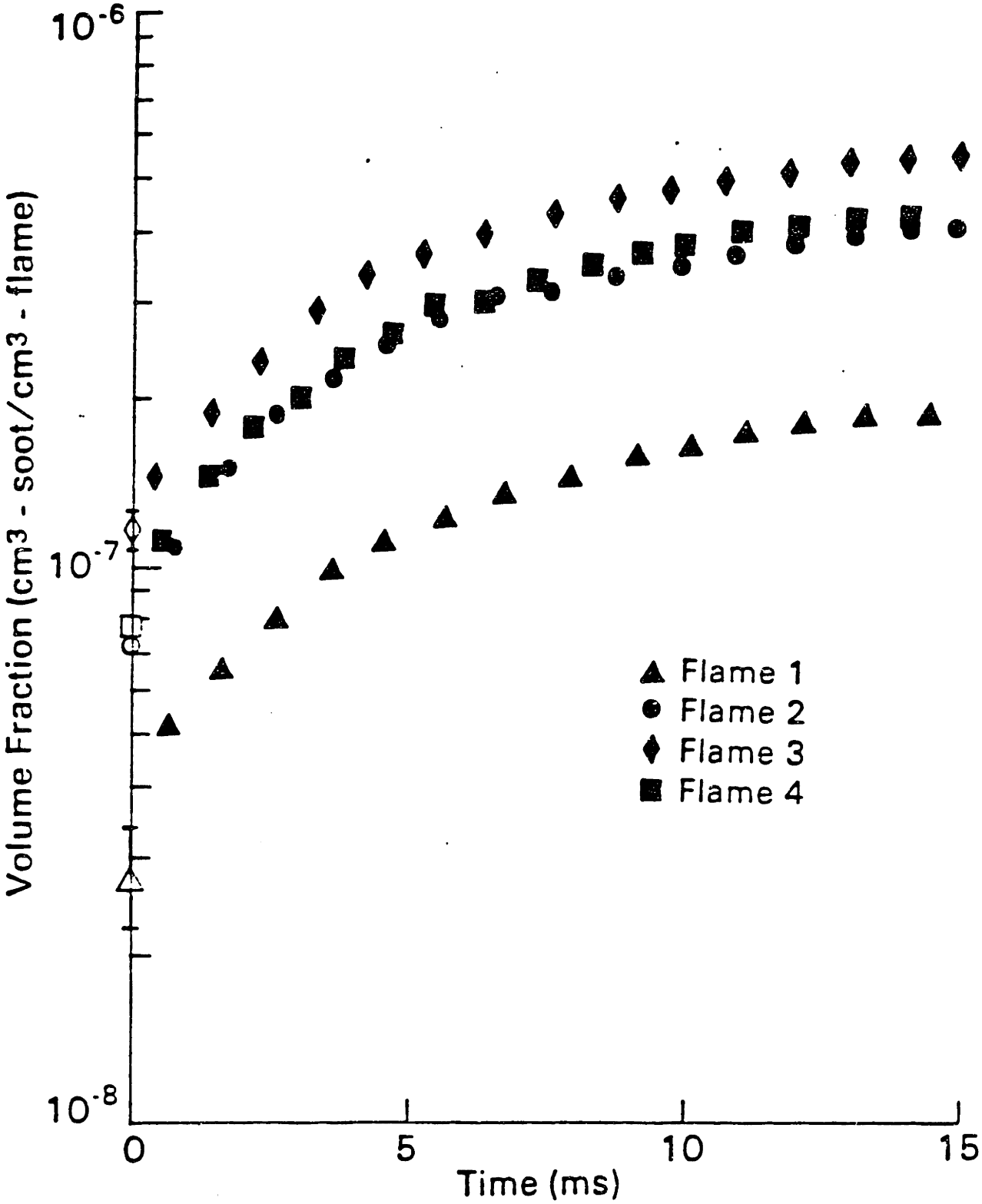

Figure 2.5 Soot Volume Fraction Profiles for Flames 1-4. Flame 1 is the baseline case (C/O=0.82), Flame 2 is the toluene-doped flame (C/O=0.89), Flame 3 is the ethylene-doped flame (C/O=0.89), and Flame 4 is a slightly higher temperature flame for ethylene-doping (C/O=0.89). (From Harris, 1984).

benzene concentration is very low for the undoped case (50 ppm), and only increases to 200 ppm at the same height for the toluene addition case. The almost complete destruction of the aromatic ring structure (probably to C2 fragments) in passing through the oxidation zone of the flat-flame makes it difficult to interpret the actual chemical effect of toluene.

2.2 LITERATURE SURVEY -- PROPOSED MECHANISMS

A number of mechanisms for the formation of soot have been proposed, and Figure 2.6 shows a summary of the possible soot forming routes (Bittner 1978). The two extreme routes, which are a pure agglomeration route and a pure dehydrogenation route, are generally not applicable at flame temperatures. The agglomeration route which involves polymerization of fuel molecules followed by dehydrogenation of the polymer, generally occurs at temperatures lower than 700 K. This reaction pathway has been studied in a large number of papers by Badger and coworkers (1958-1967). The extreme dehydrogenation route involves intermediate C_2 molecules (Smith, 1940) formed from fuel molecules, which can then condense to form soot-like particles. This dehydrogenation route usually occurs only at temperatures greater than 3000 K, because of the high endothermicity of the initial fuel dehydrogenation reactions to form the C_2 molecules. The central section of Figure 2.6 which involves various intermediate species such as biphenyl, acetylene, polyacetylene, hydrocarbon ions, and PAH, are likely to occur in the temperature range 1500 - 2500 K, typical of most combustion systems.

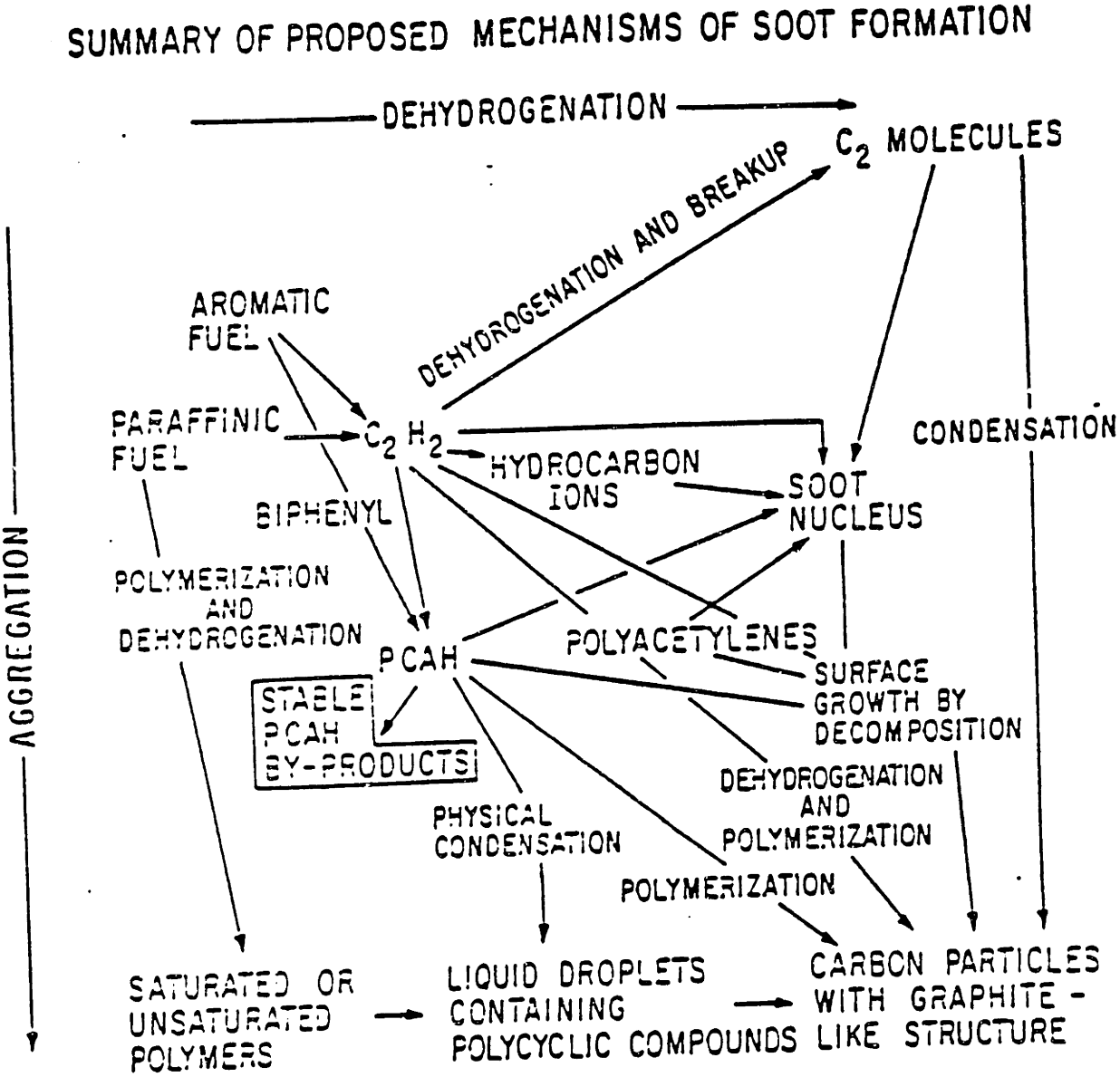

Figure 2.6 Summary of Proposed Soot Formation Mechanisms. (From Bittner, 1978).

2.2.1 Early Proposed Mechanisms

In a paper by Stehling, Frazee, and Anderson (1956) the authors concluded from benzene pyrolysis studies in a flow reactor that acetylene was important in the growth reactions. This conclusion was based on the observation that the rate of benzene disappearance was accelerated by the presence of C_2H_2, yet the C_2H_2 rate of disappearance was not affected by the presence of benzene. The authors proposed a two step mechanism of H-abstraction from phenyl radical to form a diradical, followed by addition of two C_2H_2 molecules to form naphthalene. Although the tri-molecular reaction of phenyl diradical plus two acetylenes must be viewed with skepticism, this paper attempted a mechanistic explanation of soot formation.

Davies and Scully (1965) proposed that an intact aromatic ring was necessary for the formation of soot. In their experiments, previously described, aromatic compounds which contained a hetero-atom in the ring did not soot, while aromatics with no hetero atom, or hetero-atom outside the aromatic ring produced soot. Thus the authors conclusions seemed justified, based on their assumption that the heteroatom promotes ring rupture.

About the same time as Davies and Scully's paper was presented, Bonne, Homann, and Wagner (1965) concluded that soot formation was strongly influenced by the polyacetylene concentration in the flame. Based on molecular-beam/mass spectrometry sampling of a low pressure laminar flat flame, Bonne et.al. proposed a mechanism in which the propagating polyacetylene radicals either add to existing polyacetylene molecules and continue molecular weight growth, or

stabilize by hydrogen elimination. This proposed mechanism did not require the presence of an initial aromatic ring, and contradicts the findings of Davies and Scully (1964, 1965). In fact, because the polyacetylene mechanism does not explicitly include an initial aromatic ring in the reaction sequence, it seems that it would be difficult for the mechanism to explain the graphite-like structure observed in soot particles, given the stiff, rod-like structure of polyacetylene molecules. The authors postulated that collisions between polyacetylene radicals and molecules can give branched structures, which could lead to aromatic structures after a certain degree of polymerization.

Asaba and Fujii (1971) performed shock-tube pyrolysis experiments on benzene for the temperature range 1400 -1900 K, and stated that biphenyl, rather than acetylene and diacetylene, was the product of benzene decomposition. The proposed reaction mechanism focused on the initial reactions of benzene, and examined the competition between bimolecular addition of benzene to itself to give biphenyl, and unimolecular fragmentation of benzene to give acetylene and diacetylene products. Because the authors observed, under their experimental conditions, dominance of the biphenyl route, they postulated a reaction mechanism in which phenyl radicals added to biphenyl to give a three-ring aromatic product and so on. The drawback to the mechanism is the noncondensed structure which would be obtained.

Graham, Homer, and Rosenfeld (1975) used light scattering methods to observe soot formation from shock tube pyrolysis of benzene

in the temperature range 1600 - 2300 K and observed a soot yield maximum at 1800 K. The authors offered an interpretation of this rise and fall of soot yield with temperature by proposing a competition between two reaction pathways, both of which lead to soot. The direct route involves condensation reactions of the intact aromatic fuel and leads to rapid soot formation. The other route, the indirect route, involves fragmentation of the aromatic fuel, followed by a slower, less efficient soot-forming route from the chemical fragments. Thus the bell-shaped soot yield curve can be explained as follows: At low temperatures condensation reactions dominate and soot formation is rapid. As the temperature increases, fragmentation reactions become more important, and at temperatures higher than 1800 K begin to dominate and reduce soot yield. An equivalent explanation is that fragmentation reactions have a higher "activation energy" than condensation reactions, where the term "activation energy" is used in a global sense.

2.2.2 Recent Proposed Mechanisms

In order to evaluate chemical mechanisms which describe molecular weight growth, one must obtain knowledge about the chemical species which are formed during the combustion process. Recent experimental efforts have been directed at obtaining information on chemical species found in the soot forming regions of the combustor, with the objective of determining the chemical mechanism of soot and PAH formation. Computer modelling efforts, which have had a degree of success with lean flames, are not as effective in rich flames, because

of the large number of chemical species. Attempts have been made to model growth reactions, however, and these can lend insight into the problem.

Frenklach et al. (1985b) developed an elementary reaction network of 600 reactions and 180 species to model molecular weight growth for benzene shock tube experiments. The core of the model was the hydrocarbon mechanism developed by Tanzawa and Gardiner (1980) for acetylene pyrolysis and reactions of higher molecular weight species were assigned to reaction classes. All of the reactions in a particular reaction class were given the same rate constant. This modeling approach was shown to be successful at predicting the characteristic bell-shaped curve for soot yield as a function of temperature. Although the maximum temperature was shifted 400 K, and the soot yield was 4 times lower than that predicted, it is surprising that the model was able to predict the shape correctly. The modelling efforts of Frenklach et al. represent the first attempt to model soot formation as a chemical reaction network, starting from the initial fuel molecules. While the authors conclude that it is a hopeless task to actually model soot formation at the elementary reaction level, sensitivity analyses provide interesting insights into the reaction network. Ten different pathways for the formation of two-ring aromatics were considered, and one route was shown to be 3 orders of magnitude faster than the next fastest route. The dominant route begins with acetylene adding to phenyl radical followed by H-elimination to give stable phenylacetylene. Hydrogen-abstraction from the ring at a position alpha to the acetylene side chain creates

an "active site" for the addition of a second acetylene. This second acetylene can cyclize across the triple bond to form naphthyl radical. This reaction sequence is shown in Figure 2.7a. The second fastest route involves the same initial step, but without subsequent H-elimination. A second acetylene adds to the reactive acetylene sidechain, followed by unimolecular cyclization and stabilization to give stable naphthalene. This reaction sequence is shown in Figure 2.7b. The reaction sequence in Figure 2.7a was first proposed by Bockhorn et al. (1983) based on their low pressure flat flame studies.

At first it would seem that the dominant reaction sequence, which undergoes a stabilization step followed by a reactivation step, would be slower than the minor route, which does not have these two extra steps. The authors point out the fact that while this may be true for irreversible kinetics, it is not true for reversible kinetics. Using sensitivity analysis, Frenklach et al. determined that the key factor which dictates reaction rates for these growth sequences is the stability of the intermediate aromatics with sidechains. The authors argue that the stable phenylacetylene formed in the dominant reaction sequence has a longer lifetime and is hence more likely to incur a bimolecular addition step. The intermediate formed in the minor route has a reactive acetylene sidechain and is more likely to undergo unimolecular stabilization to form phenylacetylene, rather than adding a second acetylene in a bimolecular step.

It must be said at this point that some of the rate constants

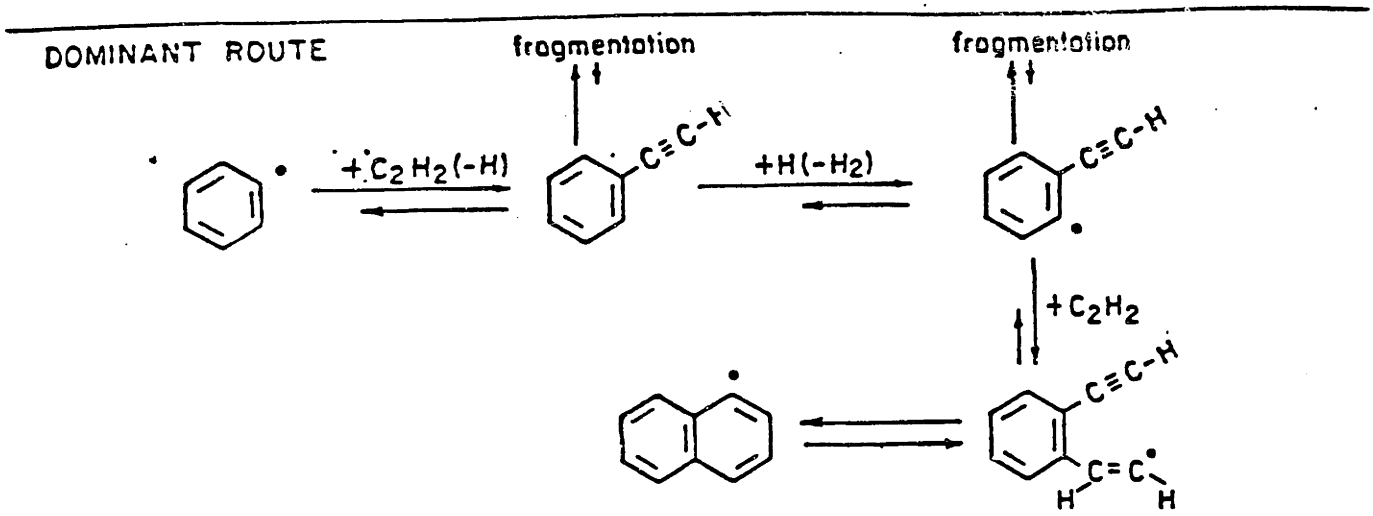

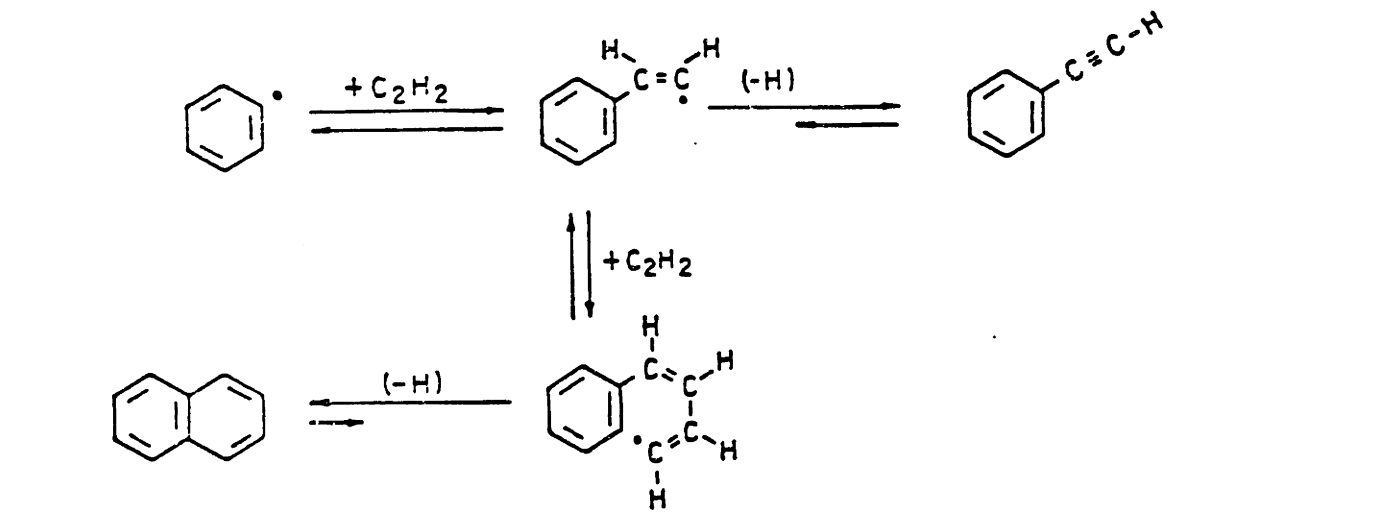

Figure 2.7a Proposed Major Route for Formation of Two-Ring Aromatics. (From Frenklach, 1985b).
Figure 2.7b Proposed Minor Route for Formation of Two-Ring Aromatics. (From Frenklach, 1985b).

used by Frenklach for the computer modelling studies were only estimated. Because of the large number of species, rate constants were designated for different classes of reactions, and the verification of any proposed mechanism must also include a hard look at the rate constants used in the mechanism. The proposed mechanism shown in Figures 2.7a and 2.7b are the results of a particular computer experiment, and are by no means universally accepted. Nevertheless, the work of Frenklach et al. has provided some interesting insights into the understanding of molecular weight growth.

This competition between unimolecular decomposition and bimolecular addition is examined in a theoretical study by Bittner (1981c). Bittner performed analyses, based on heats of reaction, of non-aromatic fragments adding to aromatics to determine the likely reaction pathways for growth. Bittner examined two classes of addition reactions: stable non-aromatics adding to radical aromatics and radical non-aromatics adding to stable aromatics. The species included in this study were selected based on data obtained in a low pressure benzene flat flame. The analysis focused on the decomposition pathways of the adduct formed from the initial addition reaction which would allow for further bimolecular addition reactions to occur and continue the growth sequence. From this analysis only a limited number of reaction pathways are possible, and it was determined that the likely mechanism involves reactions between aromatic radical and stable non-aromatics, such as phenyl and vinylacetylene. From a theoretical analysis of aliphatic addition to

aromatics, it was concluded that the most likely paths to PAH formation started with vinyl-acetylene adding to phenyl radical or allene adding to benzyl radical. The principal role the aromatic played was to stabilize the high energy adduct formed from the addition of the aliphatic fragment.

As mentioned Frenklach's mechanism was developed to explain soot formation, as measured optically. When a modified version of the mechanism (Frenklach and Warnatz, 1987) was applied in modelling the detailed PAH species profiles as measured by Wenz (1983), the mechanism could only approximately predict the general shapes of the PAH profiles. The comparison between model and experiment is shown in Figure 2.8 and 2.9. The model seriously over-predicts the decline of the PAH species after the peak concentration has been reached. Frenklach argues that uncertainties in the thermochemistry, as well as the kinetic rate parameters, may be the cause for the misprediction. Another serious deficiency of the mechanism is the gross misprediction of the benzene profile. The predicted benzene peak concentration is a factor of 10 higher than the experimental data, and decrease in the experimental benzene profile is only about a factor of 2, but the model predicts a decrease of more than 5 orders of magnitude.

Although a total of 93 elementary reactions in 13 reaction classes involving species with 1-6 aromatic rings were included in the Frenklach and Warnatz (1987) mechanism, only 5 different rate constants were used. The 33 aromatic oxidation reactions in the mechanism were all assigned a rate constant of $1x10^{13}$ $cm^3/mole/s$.

Harris has also constructed a elementary reaction mechanism for

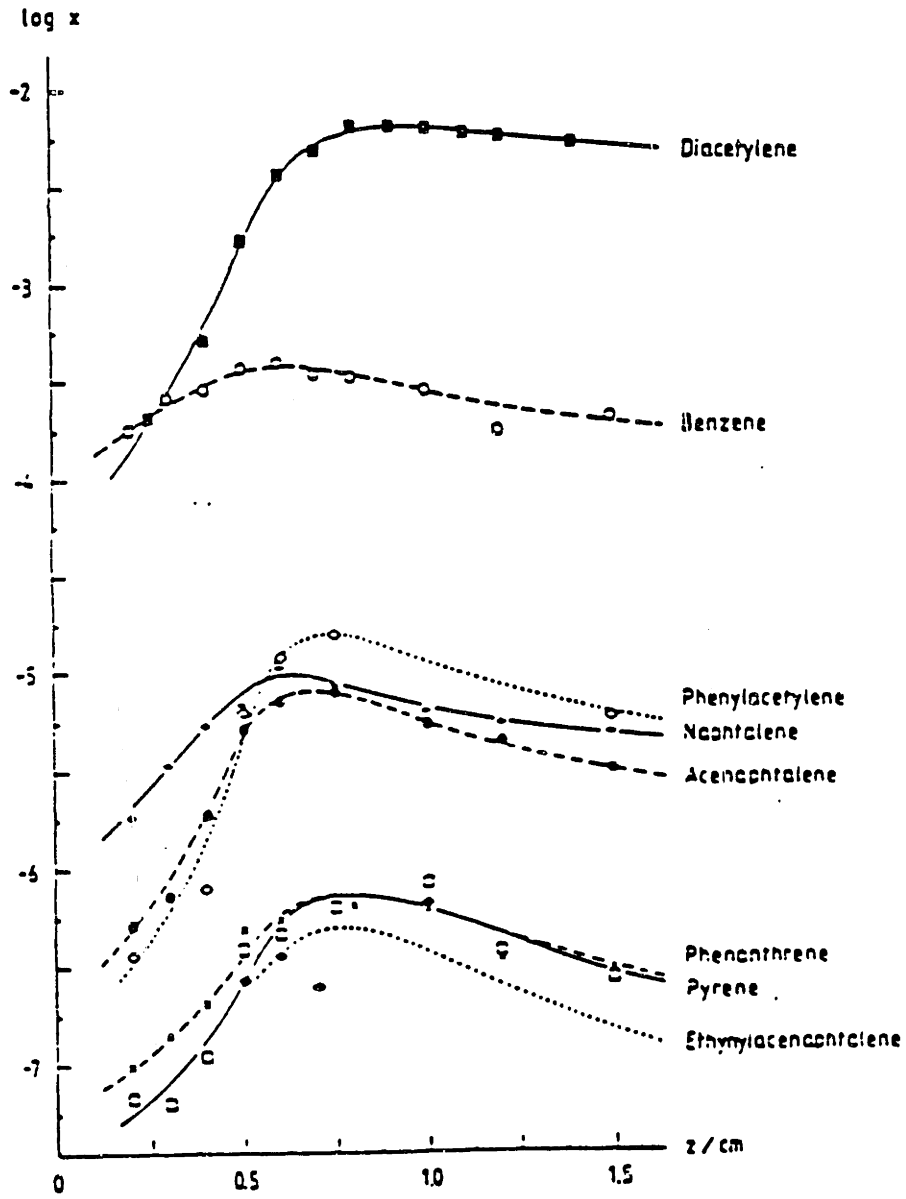

Figure 2.8 Measured (Bockhorn, et al. 1983, Wenz, 1983) Mole Fractions of selected minor and PAH species. (From Frenklach and Warnatz, 1987).

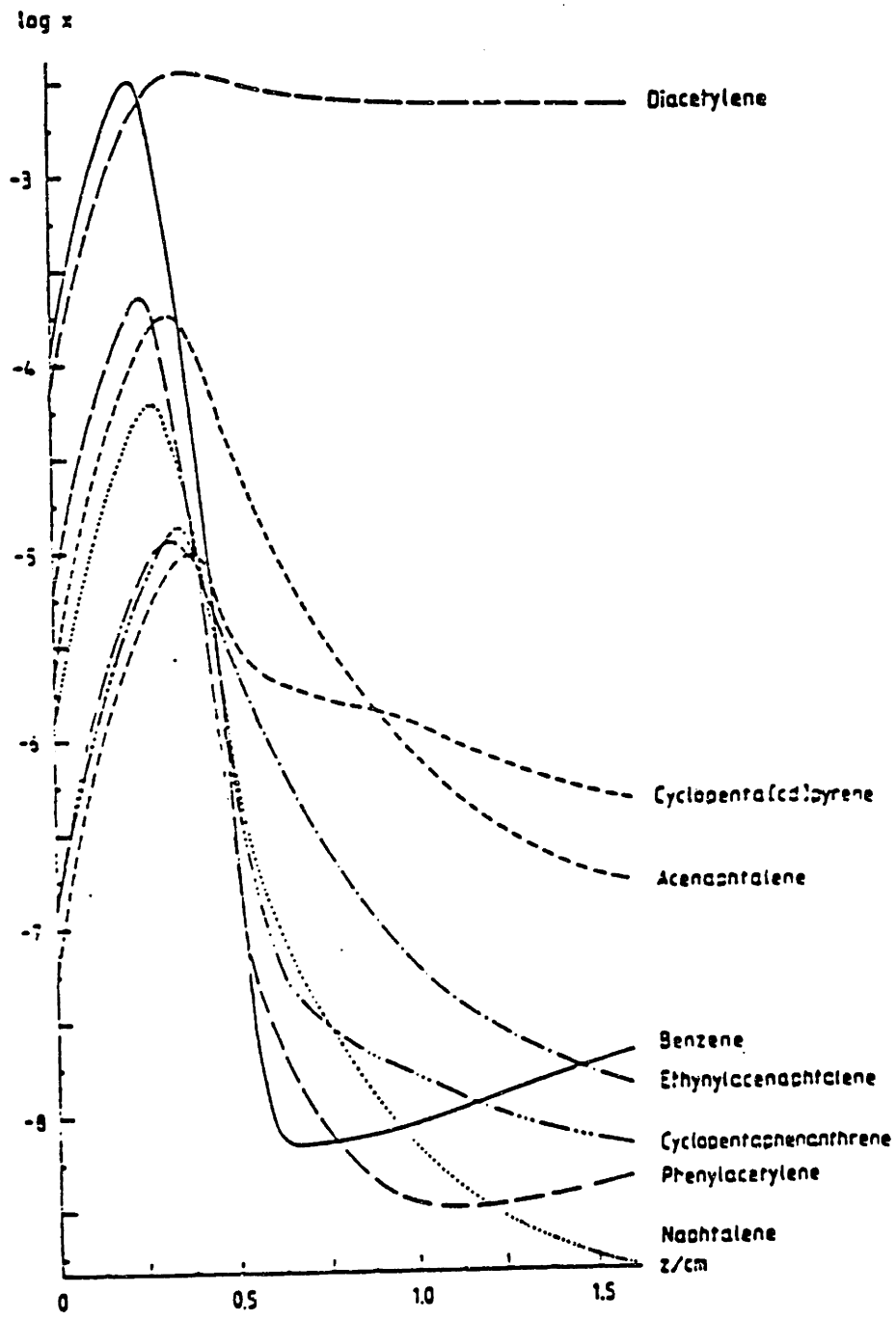

Figure 2.9 Predicted Mole Fractions of selected minor and PAH species using the mechanism proposed in Frenklach and Warnatz (1987). (From Frenklach and Warnatz, 1987).

PAH, although his model was primarily intended to model single-ring aromatic formation, and only includes species up to acenaphthylene. The model was able to predict benzene and styrene profiles adequately, and the phenylacetylene prediction was different from experiment by a factor of 6. Sensitivity analysis identified the key reaction as $C_4H_3 + C_2H_2 = C_6H_5$ which was given a non-activated rate constant of 1.5×10^{12} $cm^3/mol/s$. Since species with molecular weights greater than styrene were not measured for Harris' ethylene flat-flame, the model predictions for PAH could not be tested.

These two PAH modelling investigations (Frenklach and Warnatz, 1987, and Harris, 1988a) show that PAH formation chemistry is not nearly as well understood as lean combustion chemistry. Uncertainties in rate parameter estimations are a source of difficulty in distinguishing between elementary reaction mechanisms. The amount of data, especially for PAH reactions is very scarce, and additional high temperature rate data for some of the possible important reaction pathways for PAH formation should be obtained by kinetics experiments on isolated reactions. The competition between growth and destruction of PAH requires that measurements of PAH destruction rates, either through ring fragmentation reactions or oxidation reactions, also be determined before PAH formation may be accurately modeled. Information obtained on the reactions which lead to the formation of an aromatic ring may shed light on the types of reactions which also result in ring growth. Although usually thermalized free-radical reactions are often postulated in PAH models, ionic and non-thermalized reactions may be important. Significant progress in

modelling aromatics formation for fuel-rich combustion will increase the chances of modeling PAH formation at the elementary kinetic level.

2.3 CURRENT VIEW OF PAH FORMATION

The current picture of PAH formation which emerges from this survey of experimental and theoretical work is that the molecular growth process probably occurs through a free-radical mechanism, although ionic mechanisms cannot unequivocally be ruled out. A number of different individual pathways to PAH formation are possible and the relative concentrations of the key chemical species involved in the growth process, as well as temperature, will promote or inhibit the different pathways. In combustion systems where the radical pool of H, OH, and O is present at high concentrations, bimolecular reactions, which create hydrocarbon radical species, will be fast enough to compete with unimolecular bond fission reactions. In pyrolysis systems where the radical concentrations are low, unimolecular fission reactions will probably be the rate limiting step in the molecular weight growth process.

The relative concentrations of aliphatic and aromatic species is important in determining the different pathways for PAH formation. In a combustion system where the radical pool is well-established and aliphatic hydrocarbons and hydrocarbon radicals are present, the aromatic structure provides the "seed" from which growth reactions can occur through addition of the aliphatic species to the aromatic structure. The aromatic structure may permit unimolecular reactions to occur by stabilizing the initial adduct species, or bimolecular reactions may be responsible for growth. The conclusion that both aliphatic and aromatic species are necessary for PAH formation seems to be well accepted now, and has supporting experimental observations

by Bittner (1981c), Bauer (1983), and Kern (1982a).

In a pyrolysis system starting with only an aliphatic fuel, the decomposition of the fuel to hydrocarbon radicals which can form the first aromatic ring will probably be the rate determining step to PAH formation. Combustion of an aliphatic fuel oxidizes the fuel carbon to CO and CO_2, which effectively removes carbon mass from the PAH growth process, but for fuel-rich conditions hydrocarbon fragments and radicals are produced which can synthesize the first aromatic ring. Once the initial aromatic ring is formed, and there exists an abundance of aliphatic hydrocarbon species, PAH growth should rapidly occur.

In a pyrolysis system starting with only an aromatic species, such as benzene, the decomposition of the aromatic structure to aliphatic fragments which can add to the aromatic structures will cause an induction period before the appearance of high molecular weight species. For systems with a very high concentration of aromatics, a condensation free-radical mechanism which proceeds through biphenyl and terphenyl-type compounds and non-condensed structures may become the dominant channel. This condensation of intact aromatic rings pathway is more likely at low temperatures where unimolecular decomposition of aromatics to produce aryl radicals, which is a highly activated process, is slow.

The effect of fuel type on PAH formation will depend upon the speed and extent with which it is destroyed and consequently determines the aliphatic and aromatic mixture. In laminar flat-flames the fuel is destroyed by passing through the oxidation zone, but for

benzene flat-flames the PAH species reach their maximum before the fuel has been totally consumed. An interpretation of this is that in the relatively cool pre-heat zone of the aromatic laminar flat flames a substantial amount of PAH growth has occurred through reactions of intact aromatic rings such as phenyl radical. For example, the study by Davies and Scully was at relatively low temperatures and the chemical environment into which they injected various aromatics was not representative of the chemical environment found in fuel-rich hydrocarbon combustion. Although individual chemical species measurements were not presented, because they used a H_2/CO flame, no C2 or higher molecular weight fragments would be expected to present in the burned gas, unless they were products of the aromatics destruction. These two factors, low temperature and low concentration of aliphatic fragments, imply that a condensation mechanism of intact aromatic rings was dominant in their system.

The effect of oxidation has not been addressed fully in the PAH formation picture. Oxidation balances the growth reactions and can play an important role in the PAH formation process. In most of the PAH kinetic models proposed, oxidation is not included, or very rough estimates of the oxidation rate are used.

Temperature plays an important role because of the temperature dependence of the reactions. At high temperatures, highly activated processes will be able to compete with processes having lower activation energies. The rate constants of the different pathways depend on temperature, and consequently as different reaction channels are favored, a different product spectrum is produced. In systems

where there is a steep temperature gradient, such as the preheat zone of laminar flat-flames, the multiplicity of temperature dependent reaction channels makes kinetic analysis difficult.

The thermodynamic stability of PAH species, expressed as the Gibbs free energy of formation, is temperature dependent, and at high temperatures, the entropy term will dominate in determining the stability of the PAH molecule. The thermodynamic properties of PAH species are presently obtained through estimation techniques, and it has been shown that small differences in the thermodynamics can greatly influence the kinetic predictions, since the elementary kinetic rate constants are related through the equilibrium constant.

Finally the soot particles themselves may be an important sink of PAH. Soot particles may scavenge PAH species, or the precursors such as C_2H_2 which form PAH, and so the effect of soot on PAH formation must also be considered.

3. EXPERIMENTAL

3.1 JET-STIRRED/PLUG-FLOW (JSR/PFR) REACTOR SYSTEM

The experimental reactor system used in this research is the Jet-Stirred/Plug-Flow (JSR/PFR) Reactor System which was originally constructed at M.I.T. by Nenniger (1983) and is shown in Figure 3.1. For a complete description of the design, construction and operation of the JSR, the reader is referred to Nenniger (1983). Characterization of the JSR is given by Nenniger et al. (1986), a theoretical investigation of the mixing in the JSR is given by Kridiotis (1984), and an experimental characterization of the mixing is given by Barat et al. (1988). A kinetic study of aromatics formation has been investigated by Vaughn (1988) using the JSR, and nitrogen combustion chemistry was studied by Sun (1985).

The JSR is a toroidal reactor in which pre-mixed fuel and air are introduced through 32 sonic jets angled 20 degrees off radius to produce a swirling, highly turbulent, intensely mixed flow which approaches the well-stirred condition for many hydrocarbon reactions. The reactor is constructed from a high temperature castable alumina cement (Norton Co.) using silicon molds for the top and bottom halves of the JSR. The reactor volume is 250 cm^3 and typical residence times in the JSR ranged from 5-7 msec.

The Plug-Flow reactor section is characterized by high Reynolds number flow ($Re=4 \times 10^5$) and nearly isothermal conditions. Axial dispersion is shown to be negligible with a Peclet number of 0.033 (see Appendix 1). Four concentric alumina and zirconia cylinders with 1/2 inch wall thickness (Zircar) are used in the construction of the

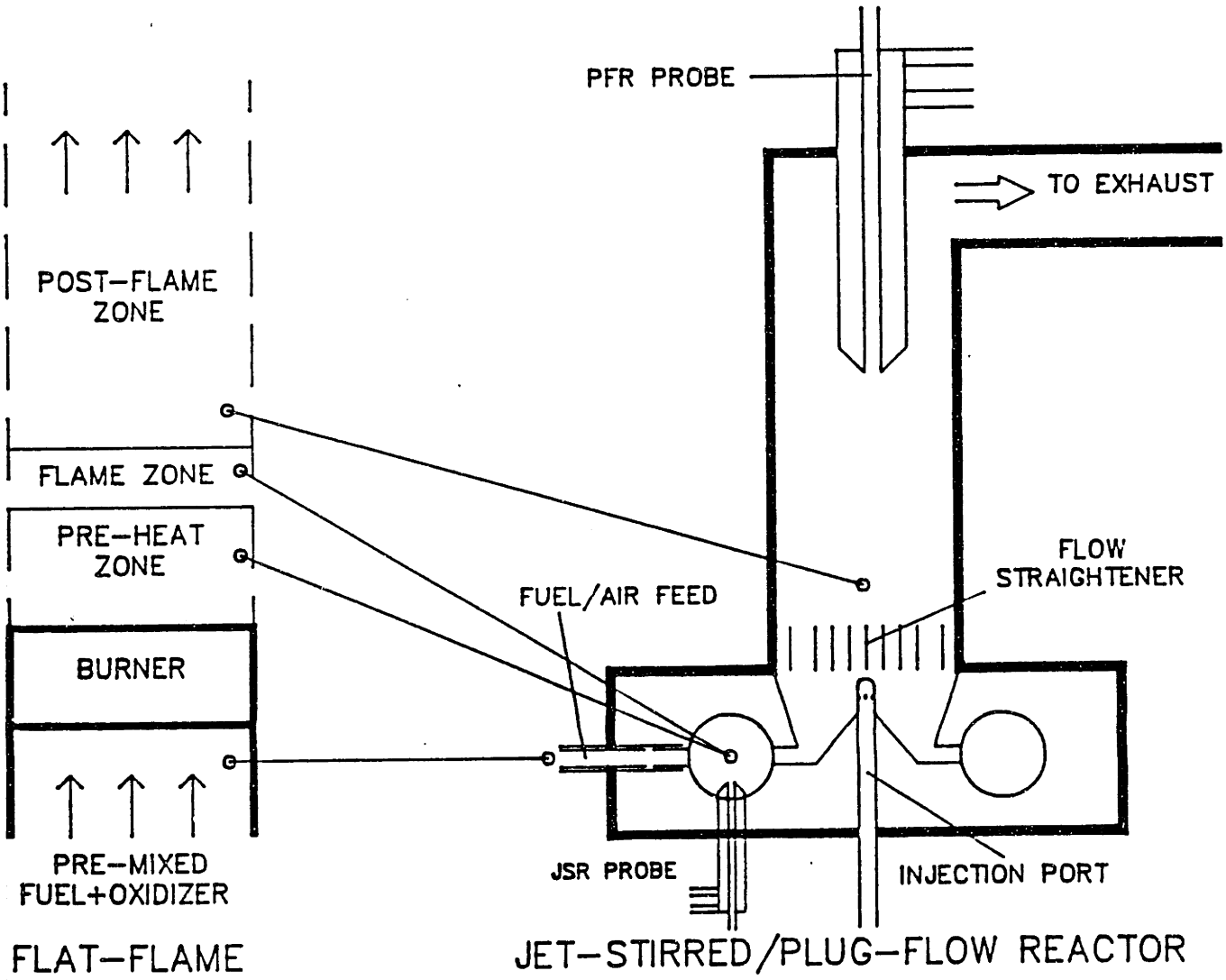

Figure 3.1 Schematic of Jet-Stirred/Plug-Flow Reactor (JSR/PFR) and comparison to laminar flat-flame.

PFR. The outer 3 cylinders are alumina, and the inner cylinder which is exposed to the highest temperature is fabricated from zirconia. Because of thermal stresses, a zirconia rigidizer is used to ensure longer lifetimes of the inner cylinder of the PFR. The total length of the PFR is 30.5 cm and typical residence times in the PFR ranged from 15-20 msec.

Premixed fuel and air are combusted in the JSR, and the exhaust gases exit through 8 ports, through a flow straightening section, into the PFR, and are vented to the hood after dilution with secondary air to complete the combustion. Ethylene and air were premixed and preheated to 200 °C before entering the JSR through the sonic jets. Nitrogen and/or oxygen were added to the main air flow to adjust the temperature independently of the fuel equivalence ratio or residence time. All gas flows were metered through rotameters. Ethylene was supplied at 100 psig, air at 80 psig, nitrogen at 120 psig, and oxygen at 100 psig. Temperature was measured using type R (Pt/Pt87%-Rh13%) thermocouples positioned in the JSR and the PFR.

The JSR/PFR has the capability to add gaseous and liquid species directly to the PFR, bypassing the JSR, through an injection system designed to allow rapid mixing of the added species. The design, construction and testing of the flow straightening section and injection system used in this work is discussed in detail in the following section. Injected gaseous species were metered and injected directly into the PFR, liquid species were vaporized in a saturated hot nitrogen stream and carried to the PFR.

As indicated in Figure 3.1, the PFR may be viewed as similar to

the post-flame zone of a laminar flat-flame. In the JSR, fuel decomposition and hydrocarbon oxidation occur together in the same space. In the flat flame these two processes are spatially distinct, although not without some overlap. The gases entering the PFR are similar to those found in the post-flame zone of the laminar flame and contain fixed gases (CO, CO_2, H_2, and H_2O), aliphatic hydrocarbons (mostly C_2H_2, CH_4, and C_4H_2), small aromatics, PAH, and soot.

The JSR/PFR system has several advantages over the laminar flat-flames. Analysis of the chemistry of PAH and soot during the early stages of soot formation in laminar flat-flames is complicated by steep concentration gradients, difficulty in obtaining sufficient spatial resolution, and probe disturbances to the flame. The velocity of the gas in the PFR is 25 m/s (Reynolds number = $4x10^5$), so axial diffusion of species is negligible (Taylor dispersion coefficient = 0.033). Thus, reaction rates may be obtained by differentiation of the concentration versus time profiles. Spatial resolution is excellent, even at atmospheric pressure because of the high gas velocities. Probe disturbances are small because the PFR does not have flame stabilization problems. Because the PFR is nearly isothermal, kinetic rate constants do not need to be well known over a wide range of temperatures. This is especially important for highly activated reactions. Finally, the injection system allows one to test the effect of additive species, without those species being destroyed by passing through an oxidation zone.

3.2 FLOW STRAIGHTENING AND INJECTION SYSTEM

Early in this research, flow visualization studies using dye injections into a plexiglass water model of the JSR/PFR revealed that a "corkscrew" flow pattern existed in the PFR. This necessitated the design of a flow straightening section to compensate for the large angular momentum generated in the JSR. Several designs of the flow straightening section were considered, and the successful design was then machined from alumina ceramic and cemented into the reactor using a special high-temperature zirconia cement.

The plexiglass water model was also used to help design the injection system. The final design consisted of an alumina ceramic thermocouple well with 8 holes (diameter = 1/32") drilled radially using a diamond tipped drill bit. The alumina tube must be able to withstand temperatures up to 2000K, because the heat transfer to the tube is very high due to the central position of the tube in the JSR. The diameter of the holes was designed by calculating decay profiles for jets in cross flow, for a given total flow rate. From Patrick (1965), the profile of a jet in cross flow is given by

$$y/d_n = 1.91 \cdot [(\rho_o/\rho_m) \cdot (U_o/U_m)]^{0.606} \cdot [x/d_n]^{0.303} \qquad \text{Eq. (3.1)}$$

where

y, x = decay profile of jet
d_n = diameter of jet
ρ_o, ρ_m = density of jet, crossflow fluid
U_o, U_m = velocity of jet, crossflow fluid

Using Equation 3.1, the decay profiles for each of the 8 radial jets

were calculated as a function of total flow through the jets. The selection of a jet diameter of 0.8 mm resulted in jet decay profiles which penetrated into the center-line of the cross-flow within the residence time allowed by the flow straightening section.

The quality of the mixing of the injected species with the gases in the PFR was determined by the following experiment. The JSR was operated at a fuel lean condition (ϕ= 0.4) with a relatively low temperature of 1200K for the combustion of ethylene with air. Additional ethylene added to the PFR under these fuel lean conditions caused a 400 K temperature increase in the PFR. A radial temperature profile was taken at a PFR height of 12.7 cm. If the injected ethylene was poorly mixed, the radial temperature profile would have a maximum near the centerline indicating preferential combustion of ethylene along the centerline. Figure 3.2 shows that the radial temperature profiles are flat indicating good mixing of the injected ethylene.

For this study, since it was desired to inject aromatic species into the PFR, it was necessary to construct a system to allow the injection of liquid and solid PAH species. Since only a small amount would need to be introduced, a vaporizer system was designed in which a nitrogen stream would enter a heated vessel and leave saturated with the species to be injected. The vaporizer was constructed from stainless steel and designed with a maximum operating temperature of 600 °C.

The system, as diagrammed in Figure 3.3, featured a vessel of 1.9 liters, a filter to prevent entrainment and supersaturation, a

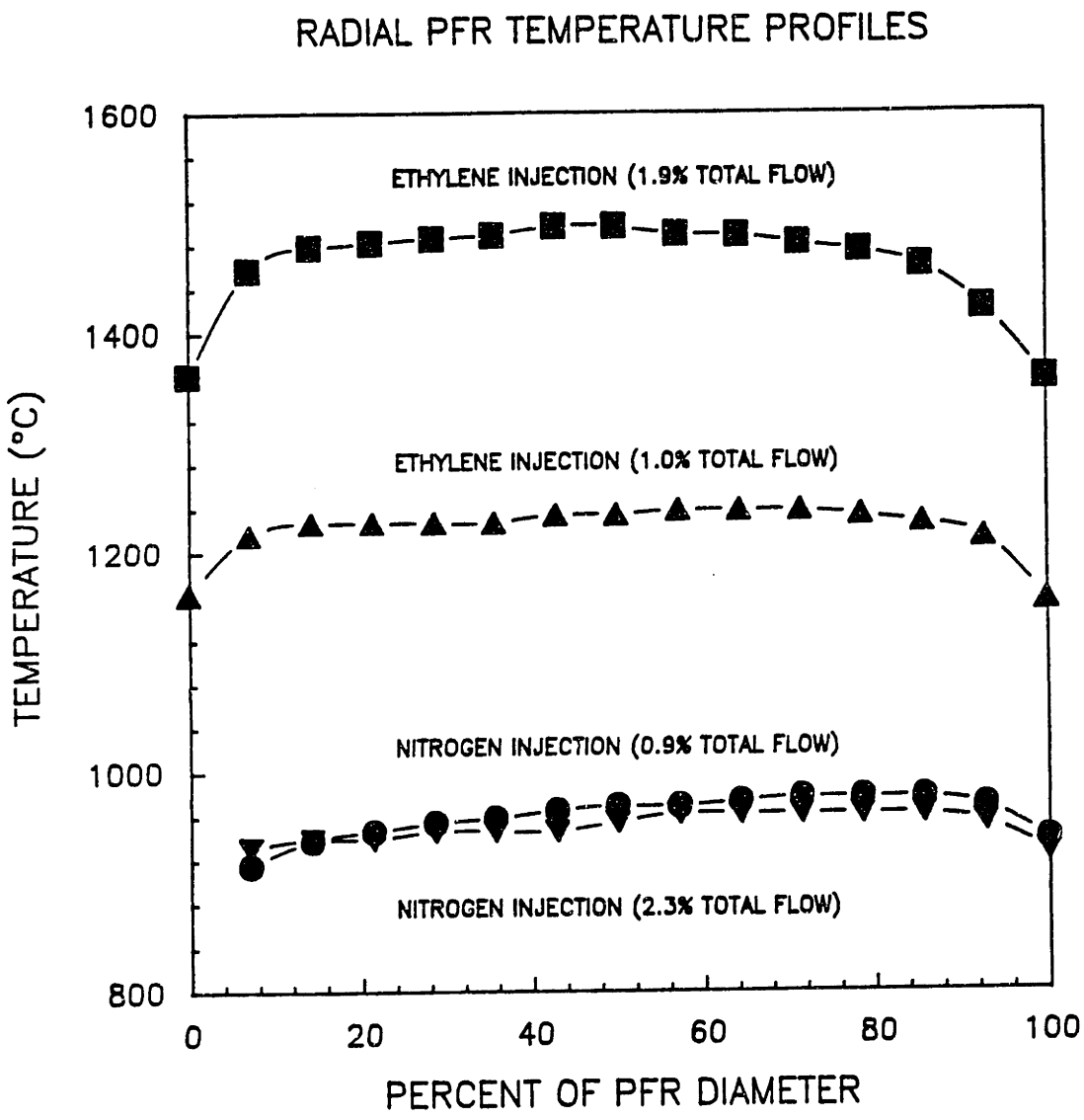

Figure 3.2 PFR Radial Temperature Profiles with Injection of C_2H_4 into ϕ=0.4 $C_2H_4/O_2/N_2$ combustion gas exiting the JSR.

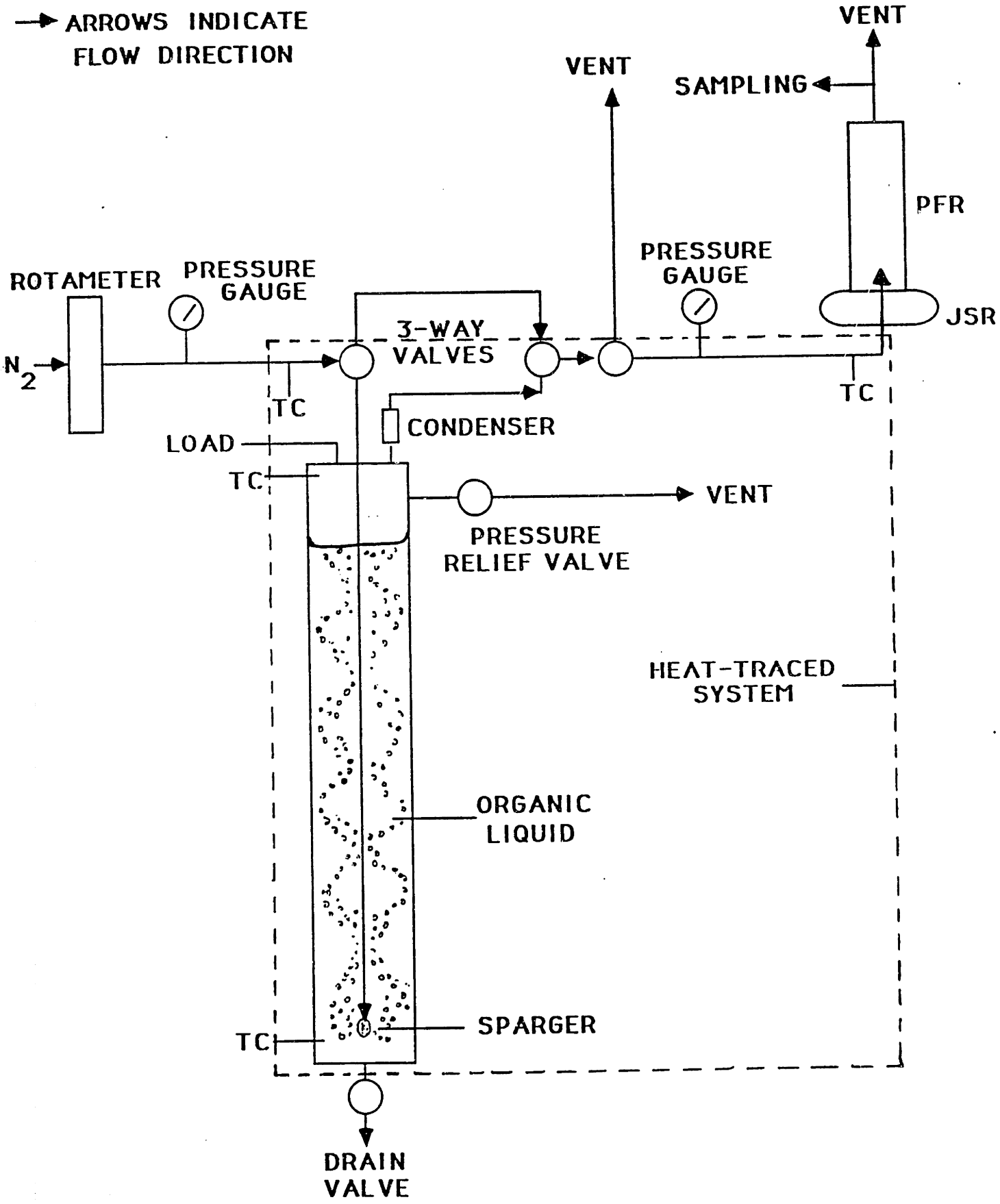

Figure 3.3 Vaporizer and Injection System.

bypass so that nitrogen may be fed to the reactor without passing through the vaporizer, a bypass so that the aromatic additive could be vented before the reactor, and a seven micron sintered stainless steel sparger. This sparger was found to produce the best flow of bubbles, with diameters of 1.0-3.0 mm, as well as excellent mixing. From mass transfer calculations, the bubble rise time was much longer than the time required for saturation of the gas inside the bubble.

The entire vessel and lines were jacketed with electrical resistance heating with active temperature control. Three separate controllers were used to control the temperature of the feed nitrogen, the liquid temperature in the vessel, and the exit line of the vessel leading to the injector port located in the PFR. The exit line was kept at a temperature 5-10°C above the boiling temperature of the liquid species being used as an additive. For benzene, which has a boiling point of 80°C, the exit line was kept at 95°C.

The system was calibrated for benzene and showed benzene saturation of the nitrogen at temperatures below 55°C. At higher temperatures supersaturation was observed. It was believed that this was caused by benzene splashing onto the non-wetted portion of the vessel wall where the temperature was higher. In future experiments, a larger initial charge of liquid to the vessel and repositioning the heating elements lower around the vessel would reduced this problem. At the desired operating temperature (46°C) for our benzene injection studies, the nitrogen was saturated with benzene. Figure 3.4 shows the benzene calibration and the predicted benzene flow based on saturation of the nitrogen stream.

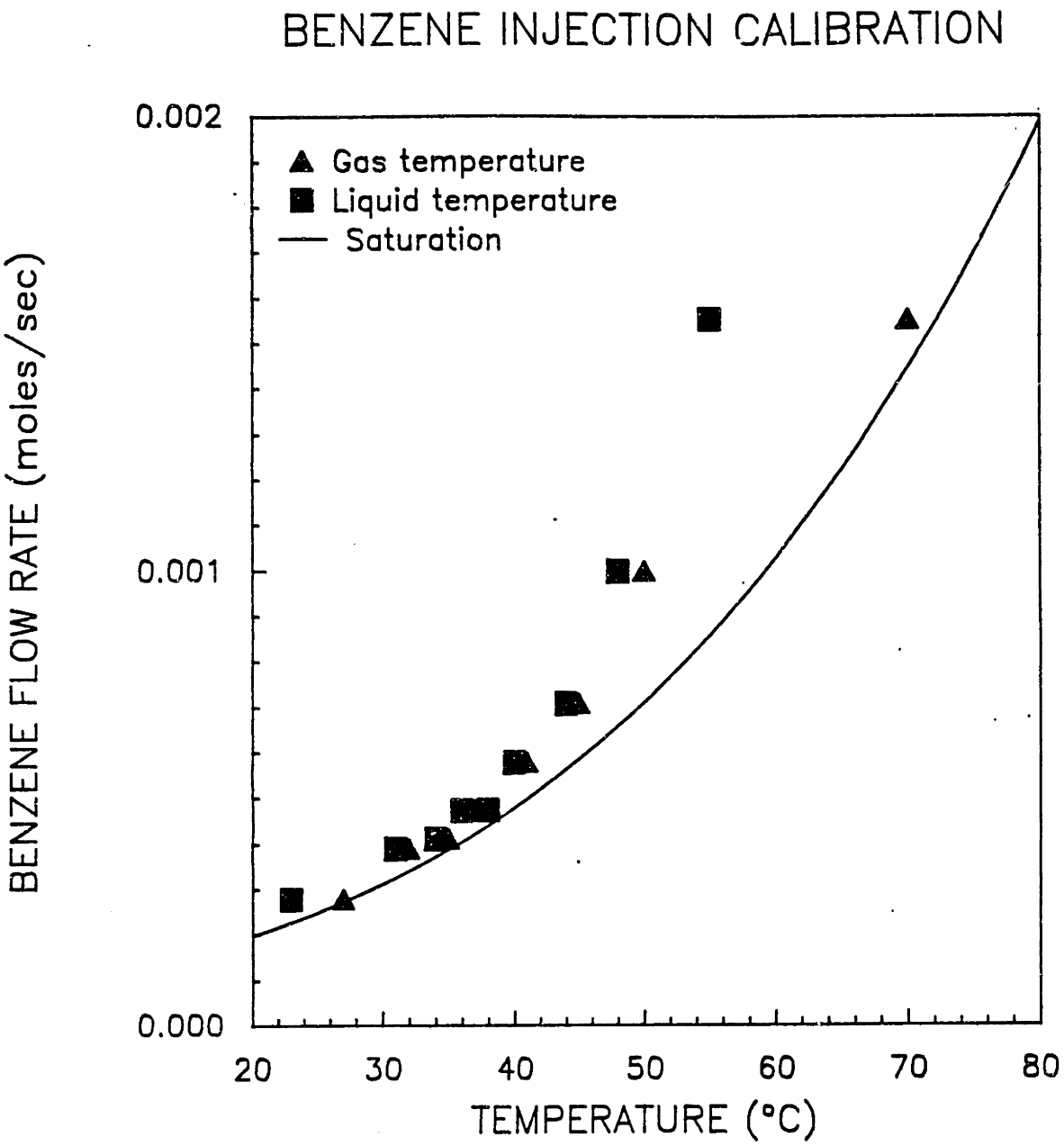

Figure 3.4 Benzene Calibration data and Predicted Saturation Curves.

3.3 SAMPLING AND ANALYSIS

A 1.6mm diameter, constant flow area, water cooled probe was used to sample species in the JSR. The probe was positioned 6mm from the reactor bottom wall as recommended by Vaughn (1988). Samples were taken from the PFR using a water-cooled stainless steel probe with a specially designed conical tip (diameter=3.5mm). The relatively large probe tip diameters of the JSR and PFR probes allows for the collection of large quantities of material in reasonable sampling times, by preventing clogging due to highly sooting conditions.

A large number of species were sampled and analyzed, and Table 3.1 shows a summary of the species sampling and analysis methods. Some species were quantified by more than one method, and this redundancy provided a good check of the experimental accuracy of the data. Fixed gases (CO, CO2, H2, O2), light hydrocarbons (C1-C4), and single ring aromatics were pumped into evacuated glass sampling vials and analyzed directly by GC/FID and GC/MS. PAH species, which are in much lower concentration than the gaseous species, were collected in a sampling train which consisted of two methylene chloride ($CH2Cl_2$) traps in series. Soot and total tar were collected on teflon coated glass fiber filters. Total tar consists of both the ΣGC PAH and high molecular weight tar, and the classification of the high molecular weight material is shown in Table 3.2. These terms will be used throughout this thesis.

TABLE 3.1 - SUMMARY OF EXPERIMENTAL METHODS

SPECIES	SAMPLING METHOD	ANALYSIS METHOD
Fixed gases		
(H_2, CO)	Glass Sampling Bulb	GC-mole sieve (5Å)
(CO_2)	Glass Sampling Bulb	GC-Spherocarb
Light Hydrocarbons		
(CH_4, C_2H_2, C_2H_4, C_2H_6)	Glass Sampling Bulb	GC-Poropak T
(C3 - C4)	Glass Sampling Bulb	GC-0.19% Picric Acid on Graphpac
Aromatics		
(C4 - C8)	Glass Sampling Bulb	GC-DB5 capillary
PAH		
(C6H6-C22H10)	CH_2Cl_2 Liquid Traps	GC-DB5 capillary
Total Tar		
(CH_2Cl_2 solubles)	CH_2Cl_2 Liquid Traps	Microgravimetric evaporation
Soot		
(CH_2Cl_2 insolubles)	Fluorocarbon coated Fibrous filters	Analytical Balance

TABLE 3.2 - HIGH MOLECULAR WEIGHT SPECIES

Measurement	Species Range	M Range
ΣGC PAH	Naphthalene - Cyclopenta(cd)pyrene	128 - 226 amu
High MW TAR	Benzopyrenes - solubility limit in CH_2Cl_2	252 - ≈1000 amu
SOOT	CH_2Cl_2 non-solubles - solid particulates	≈1000 - ∞ amu

3.3.1 Fixed Gases

Fixed gases (H_2, CO and CO_2) were routinely analyzed by gas chromatography (GC). H2 and CO were separated on a molecular sieve (5 Å., Supelco Inc.) column isothermally at 100 °C. At this temperature, H_2 elutes first followed by O_2 and Ar which coelute, followed by N_2, then CH_4 and finally CO. Since CO_2 adsorbs onto the molecular sieve, a Spherocarb (Foxboro/Analabs) column was used isothermally at 200 °C. The order of elution of species on the spherocarb is as follows: H_2 followed by O_2, Ar, CO and N_2 which coelute, and CO_2. These columns are installed in a Perkin Elmer Sigma II GC equipped with a thermal conductivity detector and with helium carrier gas.

Standards from Supelco and Scott specialty gases are injected every time an analysis is performed. Care must be taken to verify that a standard is truly what the label says.

An additional separation was performed between Ar and O_2 on the molecular sieve column and by lowering the isothermal column temperature to -50 C. Since Ar is an inert species, and we can calculate the amount of Ar entering the JSR, we can determine the molar expansion due to combustion reactions by looking at the Ar ratios. This expansion ratio is approximately 1.1 for ϕ=2.37, 1630K based on our Ar measurements.

3.3.2 Light Hydrocarbons

The C_1 and C_2 light hydrocarbon species, CH_4, C_2H_2, C_2H_4 and C_2H_6, were separated on a Porapak T column (Alltech) isothermally at 65 C. The elution order was CH_4, followed by C_2H_4, C_2H_6, and C_2H_2.

The C_2H_6 peak was usually quite small, especially for PFR samples taken at long residence times, and sometimes the C_2H_6 and C_2H_4 peak were not entirely resolved. The experimental uncertainties were estimated to be ±3% for C_{H4}, ±3% for C_2H_2, ±5% for C_2H_4, and ±35% for C_2H_6, based on estimated sampling and GC uncertainty.

The C_3 and C_4 species were separated on a .19% picric acid on graphpac (Alltech) at 65 C. The order of elution at this temperature is as follows: C1 and C2's coelute, followed by two resolved C3 species, and 8 C4 species peaks. Vaughn (1988) has determined the identity and elution order of the C3-C4 species by injecting samples on a cross-linked methyl-silicon capillary column connected to a mass spectrometer. Although the elution order of species on the capillary column did not necessary match the order of elution on the graphpak, the relative areas of the peaks were the same. Using this method, Vaughn determined the order of elution of species on the graphpak which is given in Table 3-3.

TABLE 3.3 - SPECIES IDENTIFICATION AND ELUTION ORDER FOR C3-C4 ANALYSIS

PROPANE, PROPENE, ALLENE
METHYLACETYLENE
ISOBUTANE
1-BUTENE
n-BUTANE
1-BUTYNE, ISOBUTENE, CIS-2-BUTENE
VINYLACETYLENE, TRANS-2-BUTENE
2-BUTYNE
1,3 BUTADIENE
DIACETYLENE

These two columns are installed in series on a Hewlett Packard model 5830A GC equipped with a flame ionization detector and with argon as a carrier gas. When the C_1-C_2 analysis is done, the gas is passed through both columns. The graphpac column will pass the lighter gases without separation but the porapak will not elute the heaver species. When the C_3-C_4 analysis is done, a valve is closed, directing the gas flow through the graphpak only and then on to the detector.

3.3.3 Single Ring Aromatics

Gas samples were also injected on a thick film DB-5 capillary column installed in a Perkin-Elmer Sigma I GC. The column was held at -50 C for 2 minutes, followed by a ramp at 20 degrees/min to 150 C. This analysis was used to quantify species between C_4 and C_8, especially the single ring aromatic species. Three C4 species, vinyl-acetylene (C_4H_4), 1,3-butadiene (C_4H_6), and diacetylene (C_4H_2) elute on both the graphpak and the DB-5 column. This redundancy was useful in evaluating errors in injection technique and response factors. GC/MS analysis and standards were used to identify some of the many peaks seen.

Response factors for the gas samples were obtained from standards. Gas mixtures obtained from Scott Specialty Gases were used. A certified standard consisting of 96 ppm of 1,3 butadiene (Matheson Gas Products) was used to calculate response factors from the C_3-C_4 injections. For gas injections on the Sigma I GC, a benzene standard was used. This standard was obtained from Matheson and

consisted of 228 ppm benzene in nitrogen.

3.3.4 Polycyclic Aromatic Hydrocarbons

Figure 3.5 shows the sampling train we developed to obtain PAH data. Inside the PFR probe is a removable teflon liner which is pre-extracted with dichloromethane (CH_2Cl_2). When we are not sampling, the PFR probe is back-flushed with nitrogen in order to prevent adsorption of species onto the teflon liner. The PAH-laden gases are drawn from the reactor and bubbled through two chilled CH_2Cl_2 traps separated by a glass fiber filter. The glass fiber filter collects fine soot particulates which are entrained through the first trap. A rotameter is used to control the sampling rate (14 cm^3/sec). The teflon liner collects some of the soot and is extracted with CH_2Cl_2 and combined with the CH_2Cl_2 from the first and second traps. Approximately 500 ml of CH_2Cl_2 are concentrated using a Kuderna-Danish evaporative concentrator, and final concentration to approximately 1 ml is achieved by evaporation under a stream of nitrogen.

Analysis on a Perkin Elmer Sigma 1 Gas Chromatograph with FID detector uses a 30 meter methyl-phenyl(5%) silicone capillary column (DB-5, J & W Scientific) with a temperature program beginning at subambient -10 °C with a linear temperature increase to 280 °C and a holding temperature of 280 °C for 10 minutes. A flash vaporization injector was used. A PAH standard consisting of 18 different species with molecular weights from naphthalene up to perylene was injected every day a PAH analysis was performed. All quantitative analysis of PAH species were performed using GC/FID, and supplemental qualitative

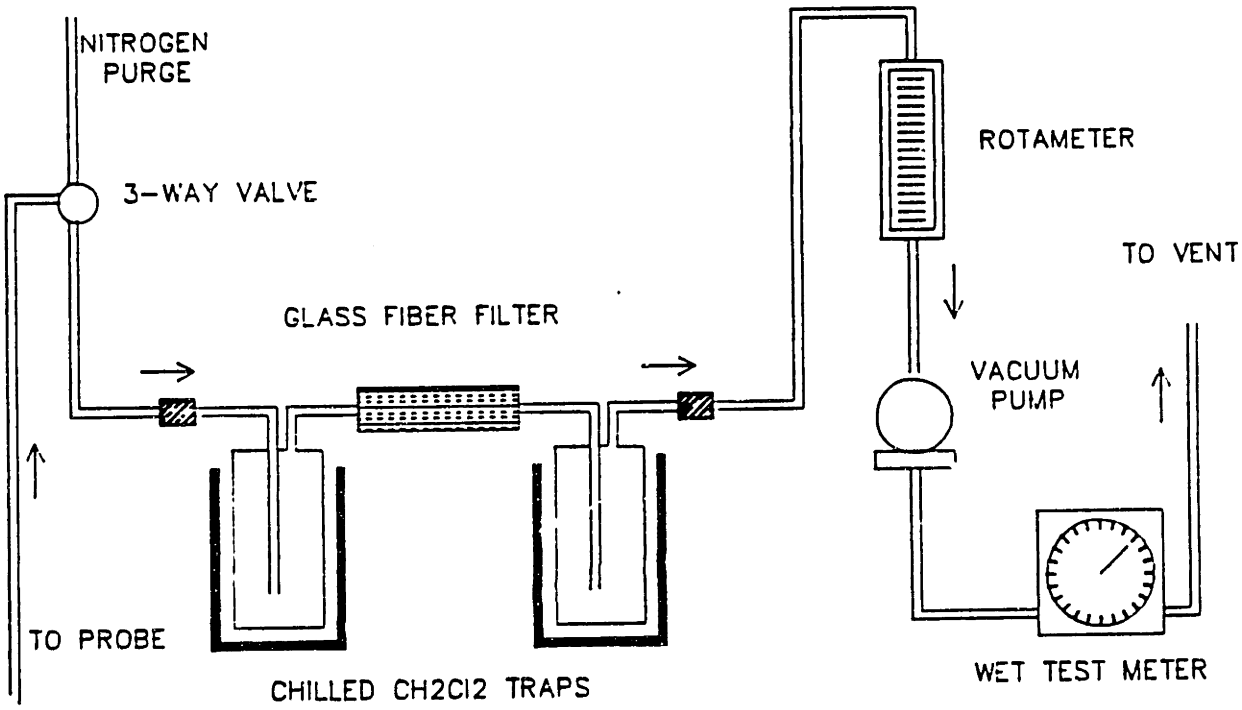

Figure 3.5 PAH sampling system.

PAH identification was also performed. Identification of PAH species used a variety of techniques including 1) injection of known standards, 2) GC/MS, 3) correlation of retention indices (Lee, 1979), and 4) GC/FTIR (Lafleur, 1988a). Acetylenic-substituted species were identified using GC/FTIR and monitoring absorbance at 3330 cm^{-1}, and differentiation of isomers was deduced from the aromatic C-H bending frequencies. Limited measurements using High-Performance Liquid Chromatography (HPLC) to identify large PAH species were also performed.

The detailed chemical characterization of the capillary GC PAH analysis is shown in Table 3.4 for the ϕ = 2.37 baseline case. The peaks are listed by retention index using the formula developed by Lee et al. (1979) for linear temperature programming conditions for capillary GC columns. The use of the retention index helps in the identification of an unknown PAH species, as well as the reproducibility of correlating the retention times of chromatogram peaks between different samples analyzed on different instruments. PAH species whose identification is virtually certain are given a name in Table 3.1, and uncertain identifications are only given a molecular weight and general formula. The method of identification is also shown.

More than 130 individual PAH peaks are separable and quantifiable by GC/FID, for which we have certain identifications for 35 species and tentative identifications for 32 additional PAH species. Although a large number of PAH species are not identified, the ones we have identified make up more than 98% of the total PAH

mass. The unidentified species appear as very small peaks on the chromatogram, and it is difficult to distinguish these peaks from the

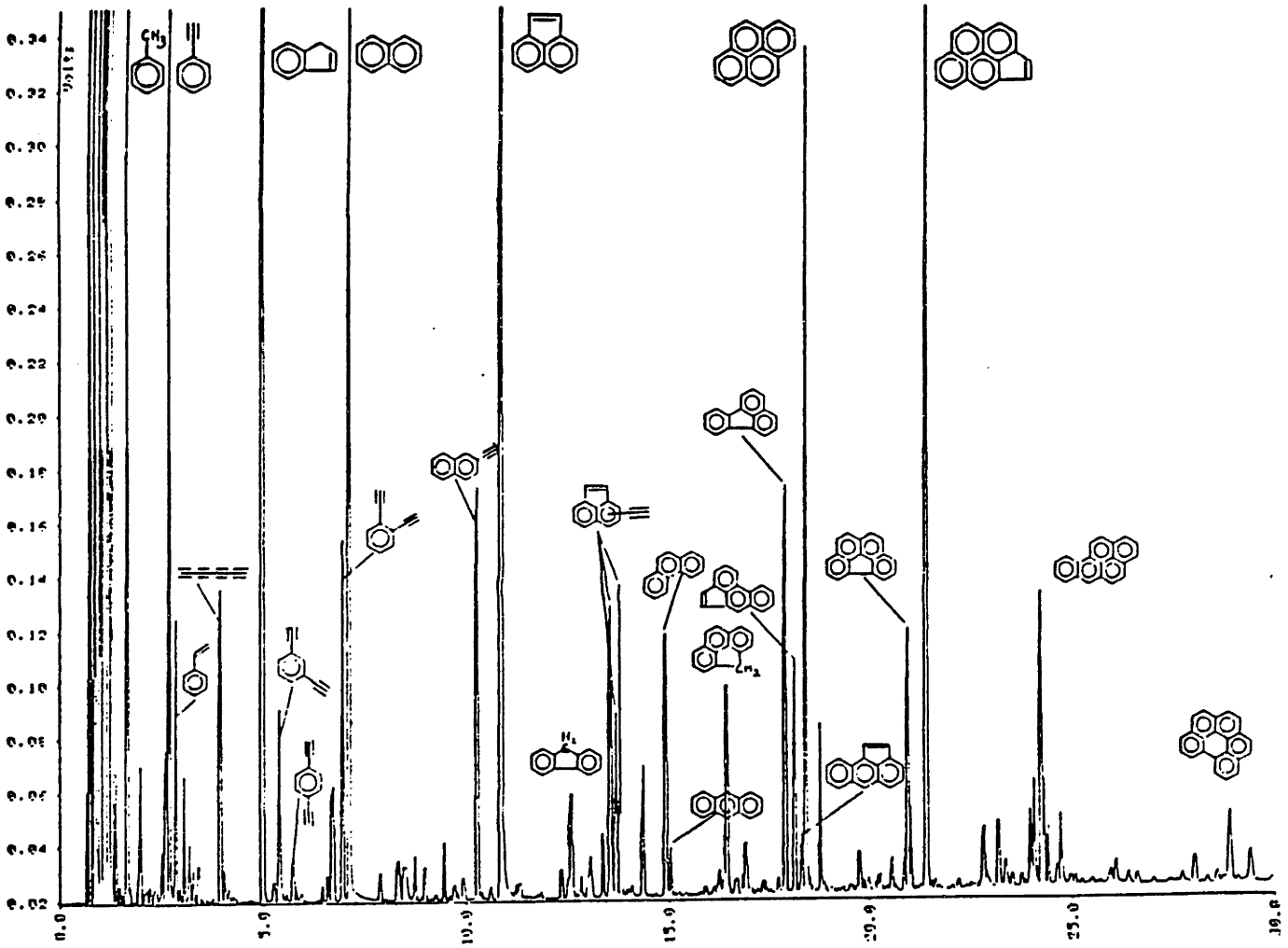

Figure 3.6 Gas Chromatogram of PAH species, at PFR residence time of 12.7 msec, for ϕ=2.37, JSR T=1630K, $C_2H_4/O_2/N_2$ combustion.

TABLE 3.4 - DETAILED PAH SPECIES IDENTIFICATION

PEAK #	RETENTION INDEX	MW	FORMULA	SPECIES NAME (if known)	IDENTIFIED BY METHOD# 1	2	3	4
1	95.92							
2	96.75							
3	97.70							
4	100.00	78	C6H6	BENZENE	X	X	X	X
5	104.19							
6	105.34							
7	105.97	76	C6H4	HEXENE-DIYNE		X	X	
8	108.27	72	C6H2	TRIACETYLENE		X	X	
9	116.44							
10	119.27	92	C7H8	TOLUENE		X		X
11	121.47	90	C7H6			X		
12	127.64	90	C7H6			X		
13	131.20							
14	132.25							
15	133.40							
16	138.95							
17	140.73	106	C8H10	ETHYLBENZENE, XYLENE		X		X
18	142.62	102	C8H6	PHENYLACETYLENE		X	X	X
19	144.92	104	C8H8	STYRENE		X	X	X
20	150.26	88	C7H4	METHYL TRIACETYLENE		X	X	
21	152.25							
22	152.98							
23	155.81							
24	161.88	98	C8H2	TETRA-ACETYLENE		X	X	
25	171.20							
26	175.08	116	C9H8	INDENE		X	X	X
27	178.22							
28	180.00	126	C10H6	1,3-DIETHYNYL-BENZENE		X	X	
29	183.77	126	C10H6	1,4-DIETHYNYL-BENZENE		X	X	
30	186.49							
31	192.04							
32	195.08	128	C10H8			X		
33	197.59	126	C10H6	1,2-DIETHYNYL-BENZENE		X	X	
34	200.00	128	C10H8	NAPHTHALENE	X	X	X	X
35	209.61							
36	215.27	140	C11H8	ETHYNYL INDENE ISOMER		X	X	
37	217.49	140	C11H8	ETHYNYL INDENE ISOMER		X	X	
38	221.06	142	C11H10	2-METHYL NAPHTHALENE		X		X
39	224.26	142	C11H10	1-METHYL NAPHTHALENE		X		X
40	230.54							
41	236.21							
42	240.64	152	C12H8	2-ETHYNYL NAPHTHYLENE		X	X	
43	248.40	152	C12H8	ACENAPHTHYLENE	X	X	X	X
44	267.36	166	C13H10			X		
45	270.32	166	C13H10	FLUORENE	X	X		X
46	273.65							
47	275.99							

TABLE 3.4 - DETAILED PAH SPECIES IDENTIFICATION (cont.)

PEAK #	RETENTION INDEX	MW	FORMULA	SPECIES NAME (if known)	IDENTIFIED BY METHOD# 1	2	3	4
49	282.51	176	C14H8	ETHYNYL-ACENAPHTHYLENE		X	X	
50	284.24	176	C14H8	ETHYNYL-ACENAPHTHYLENE		X	X	
51	285.59	176	C14H8	ETHYNYL-ACENAPHTHYLENE		X	X	
52	289.41							
53	292.98	176	C14H8			X		
54	294.46							
55	300.00	178	C14H10	PHENANTHRENE	X	X		X
56	301.76	178	C14H10	ANTHRACENE	X	X		X
57	304.40							
58	306.59							
59	310.99							
60	312.45							
61	314.06							
62	317.29							
63	318.75							
64	321.24							
65	322.56	190	C15H10	4H-CYCLOPENTA(def)-	X	X		X
66	324.61			PHENANTHRENE				
67	326.37							
68	330.62	204	C16H12			X		
69	333.84							
70	336.04	202	C16H10			X		
71	337.36	202	C16H10			X		
72	339.12							
73	341.02							
74	343.07	204	C16H12			X		
75	344.83	202	C16H10	FLUORANTHENE	X	X		X
76	348.49	202	C16H10	ACEPHENANTHRYLENE		X		X
77	351.28	202	C16H10	ACEANTHRYLENE		X		X
78	353.18	202	C16H10	PYRENE	X	X		X
79	358.60							
80	359.34							
81	360.80	214	C17H10			X		
82	362.12							
83	366.51							
84	367.54							
85	369.01	216	C17H12			X		
86	369.88							
87	372.67	214	C17H10			X		
88	374.13	228	C18H12			X		
89	375.89	226	C18H10			X		
90	378.09	226	C18H10			X		
91	379.11	226	C18H10			X		
92	380.29	226	C18H10			X		
93	382.04							
94	382.92							
95	384.54	226	C18H10			X		

TABLE 3.4 - DETAILED PAH SPECIES IDENTIFICATION (cont.)

PEAK #	RETENTION INDEX	MW	FORMULA	SPECIES NAME (if known)	IDENTIFIED BY METHOD# 1	2	3	4
96	386.29							
97	389.37							
98	390.84	226	C18H10	BENZO(ghi)FLUORANTHENE		X		X
99	391.86	226	C18H10			X		
100	393.77	226	C18H10			X		
101	396.11	226	C18H10			X		
102	398.60	226	C18H10	CYCLOPENTA(cd)PYRENE		X		X
103	402.41	228	C18H12			X		
104	404.46							
105	405.49							
106	407.10							
107	408.71							
108	409.88							
109	412.66							
110	413.84							
111	415.89							
112	417.21							
113	418.09							
114	419.11							
115	424.68							
116	425.41							
117	427.32	250	C20H10			X		
118	434.93							
119	436.25							
120	439.77	250	C20H10			X		
121	441.53	250	C20H10			X		
122	445.92	252	C20H12			X		
123	452.52	252	C20H12			X		
124	455.74	252	C20H12			X		
125	459.84							
126	475.96							
127	483.87	264	C21H12			X		
128	491.63							
129	514.93	276	C22H12			X		
130	521.37	276	C22H12			X		
131	528.85	276	C22H12			X		
132	548.48	276	C22H12	BENZO(ghi)PERYLENE		X		X
133	562.40							

Identification Methods:
1 = Species in PAH standard
2 = GC/MS
3 = GC/FTIR
4 = Correlation of Retention Indices

baseline noise. Some of the major PAH species are shown in a sample chromatagram in Figure 3.6.

We have performed studies to evaluate the performance of the PAH sampling system and analysis techniques. A total recovery study using a standard of 109 ppm toluene in nitrogen was performed successfully. We also concentrated and analyzed CH_2Cl_2 from the teflon probe liner, first trap, filter, second trap separately in order to determine the distribution of PAH compounds between the liner and the traps. From repeated experiments, we know that deviation in reproducibility is less than 25% for most PAH species formed in the JSR/PFR.

Table 3.5 shows the distribution of the PAH species in the sampling train. The first trap collects almost 100% of the PAH smaller than two aromatic rings, and approximately 75% of the larger PAH. The second trap collects some acenaphthylene which is carried through the first trap. The teflon probe liner yields approximately 25% of the larger PAH species when extracted with CH_2Cl_2. Repeated extractions of the probe liner do not yield additional PAH.

TABLE 3.5 - DISTRIBUTION OF PAH IN SAMPLING TRAIN

	YIELDS (ug/g)	1ST TRAP	2ND TRAP	PROBE
1	BENZENE	1295.30	133.74	
2	TRIACETYLENE	217.29		
3	TOLUENE	53.52	21.47	
4	PHENYLACETYLENE	316.71		
5	STYRENE	9.13		
6	PHENOL	2.95		
7	INDENE	50.38		
8	NAPHTHALENE	145.27	15.63	1.52
9	ACENAPHTHYLENE	79.02	38.85	18.21
10	ETHYNYL-ACENAPHTHYLENE	8.95		1.89
11	ETHYNYL-ACENAPHTHYLENE	3.66		0.60
12	ETHYNYL-ACENAPHTHYLENE	3.34		
13	PHENANTHRENE	3.17		1.61
14	4H-CYCLOPENTA(def)PHENANTHRENE	6.29		1.88
15	FLUORANTHENE	12.13		4.33
16	ACEPHENANTHRYLENE	5.95		2.00
17	ACEANTHRYLENE	4.09		
18	PYRENE	28.52		10.29
19	CYCLOPENTA(cd)PYRENE	60.34		16.73

Table 3.6 shows the yields of PAH (sum of first trap, second trap, and probe extract) and the experimental uncertainty in our PAH measurements. The three sources of uncertainty are GC injection technique, sampling technique, and reactor operating setpoint. Data points 1, 2 and 3 are triplicate samples obtained on the same day, and data point 4 is for the same reactor operating conditions 3 months later. The largest source of uncertainty is the reactor operating conditions.

TABLE 3.6 - EXPERIMENTAL UNCERTAINTY IN PAH MEASUREMENTS

	YIELDS (ug/g)	1	2	3	4
1	BENZENE	1429.04	1472.79	1471.14	1202.95
2	TRIACETYLENE	217.29	237.06	233.14	204.97
3	TOLUENE	74.99	38.98	25.64	35.58
4	PHENYLACETYLENE	316.71	293.98	315.54	270.05
5	STYRENE	9.13	8.43	8.19	14.23
6	PHENOL	2.95	1.68	2.77	14.87
7	INDENE	50.38	46.61	47.43	42.05
8	NAPHTHALENE	162.41	143.65	114.16	113.43
9	ACENAPHTHYLENE	136.08	134.38	132.82	120.40
10	ETHYNYL-ACENAPHTHYLENE	10.84	9.96	8.53	12.68
11	ETHYNYL-ACENAPHTHYLENE	4.26	3.96	3.82	8.70
12	ETHYNYL-ACENAPHTHYLENE	3.34	3.67	3.49	6.79
13	PHENANTHRENE	4.78	5.81	5.03	6.20
14	4H-CYCLOPENTA(def)PHENANTHRENE	8.17	8.15	9.23	9.62
15	FLUORANTHENE	16.46	14.46	16.24	22.13
16	ACEPHENANTHRYLENE	7.95	7.10	8.05	10.61
17	ACEANTHRYLENE	4.09	3.75	4.86	
18	PYRENE	38.81	34.45	38.43	50.41
19	CYCLOPENTA(cd)PYRENE	77.06	73.55	83.79	84.11

3.3.5 Tar and Soot

Soot and tar were collected on teflon-coated glass fiber filters (Pallflex), and extraction in CH_2Cl_2 was used to separate the soot from the tar. Soot was defined to be CH_2Cl_2 non-soluble material and tar was defined to be CH_2Cl_2 soluble material. The soot remaining in the filter after extraction was weighed on an analytical balance with precision to 0.01 mg (Mettler H20). Repeated extraction of the soot filters did not yield additional tar, indicating that the initial extraction was sufficient.

Tar yields were determined using a microscale evaporation technique developed by LaFleur (1986). This technique consists of evaporating a 100 μl aliquot of concentrated CH_2Cl_2 containing the tar on a 25 mm diameter aluminum foil disc, and weighing the residue on an analytical balance (Perkin-Elmer Model AD-6 Ultramicrobalance). The CH_2Cl_2 is completely evaporated at ambient conditions in less than 2 minutes, and an evaporation period of 5 minutes was selected to allow for solute and matrix effects that can lengthen evaporation times. The accuracy of this technique depends on the concentration level and boiling point of the solute, but components with boiling points above 200°C are measured with reasonable accuracy using this technique.

3.3.6 High Performance Liquid Chromatography

A limited number of High Performance Liquid Chromatography (HPLC) measurements were performed in order to extend the molecular weight range of the GC/FID measurements. This work was performed in collaboration with the Analytical Chemistry Group in the M.I.T. Center

for Environmental Health Sciences.

Samples collected in CH_2Cl_2 were passed over a cyano gravity column (Analytichem) to remove highly polar compounds which might damage the HPLC column, and concentrated by nitrogen evaporation. The samples were injected onto 3 normal phase cyanopropyl columns (Alltech) in series. Each was 25 cm in length, with an internal diameter of 0.46 cm and packed with 5 μm cyanopropyl material having a 60 Å average pore diameter with a surface area of 400 m^2/g. The HPLC system consisted of a Hewlett-Packard Model 1090 ternary gradient pumping system with 190-600 nm diode-array detector.

3.3.7 GC/FTIR Spectrometry

Gas Chromatography/Fourier-Transform Infrared Spectrometry (GC/FTIR) is a chemical analysis technique which was used in the identification of aromatic alkynes in the JSR (Lafleur et al. 1988a). GC/FTIR was used in combination with our GC/MS data in this study to confirm 1) PAH identifications by comparison of the IR spectra to literature spectra, if available; 2) the existence of ethynyl-substituted PAH; and 3) to distinguish between PAH isomers.

Concentrated CH_2Cl_2 samples which were prepared for the GC/FID analysis were further concentrated by nitrogen evaporation since the sensitivity of the FTIR is about an order of magnitude less than the FID. The samples were injected on a 25 meter methyl-phenyl(5%) silicone open tubular column (Quadrex), with an internal diameter of 0.25 mm and film thickness of 0.25 μm. The column was mounted in a HP5890 GC/HP5970 MS and detected using an HP5965A IRD instrument.

Because the HP was not equipped for subambient operation, the temperature program was not the same as for the GC/FID analysis. Instead, a temperature program starting from 40°C and ramping to 280°C at a rate of 10°C/min was used. Since we were mainly interested in species with molecular weights above phenylacetylene for the GC/FTIR analysis, lack of subambient operation presented no problems.

One of the most powerful advantages to using the GC/FTIR was the unambiguous identification of ethynyl-substituted species, which have been proposed as intermediates in PAH formation mechanisms. Ethynyl groups absorb strongly near 3330 cm^{-1} (≡C-H stretching) and 1220 cm^{-1} (≡C-H bending), and the stretching frequency is independent of the rest of the structure of the PAH.

The use of the GC/FTIR allowed us to confirm many of the identifications made from inspection of the GC/MS fragmentation spectra data. General structural characteristics of unknown PAH could be inferred from the different absorption bands in the IR, and identification could be confirmed by comparison with literature IR spectra. If no literature spectra existed, one could still gain insight into the chemical structure of the PAH species.

GC/FTIR also allowed us to distinguish different isomers, based on the characteristic stretching and bending frequencies. For example, we were able to differentiate between 1-ethynyl naphthalene and 2-ethynyl naphthalene by inspection of the aromatic C-H bending frequencies (700-900 cm^{-1}). The type of substitution group on the aromatic ring does not affect the C-H bending frequencies, and so by comparing the observed IR spectra with the literature IR spectra of 1-

methyl and 2-methyl naphthalene, we deduced that only 2-ethynyl naphthalene was present in the PFR under our experimental conditions.

3.3.8 Transmission Electron Microscopy

Transmission electron microscopy (TEM) was performed on soot samples obtained for the ϕ = 2.37 baseline case. The characterization of soot by TEM was not investigated in great detail, as we were only interested in answering two questions: 1) Are we collecting solid particulate matter in the JSR at ϕ = 2.37 (incipient sooting condition)? and 2) What is the approximate size of the spherules which make up the soot particles?

The first attempts at obtaining TEM samples used a soot filter which had already been extracted in methylene chloride. The filter was sonicated in brown glass jar in methanol for 2 hours, concentrated by evaporation, and then aliquots of soot in methanol were transferred to the electron microgrid. Unfortunately, the coverage of soot on the grid was very sparse and no prints were taken. Contamination, probably from particulate matter in the solvent, also prevented us from obtaining a good sample.

In order to get higher coverage of soot particles on the grid and avoid solvent contamination problems, a direct impact method was used. In this method, 3 electron microgrids were placed directly on the teflon fiber filters and the collected sample gas stream was passed through the filter. Soot particles would directly impact onto the electron microgrids in the areas where the filter was covered by a grid.

Three samples were taken using this method, one from the JSR, one from the beginning of the PFR (height=3.8 cm, residence time=1.8 msec), and one from the near the end of the PFR (height=26.7 cm, residence time=11.2 msec). Total gas volume sampled was approximately the same for the three samples and was 3.4 standard liters over a sampling time of 18 seconds. The sample obtained from the JSR was very light yellow-brown in color. The filter for the PFR h=3.8 cm sample was a very dark yellow-brown in color. The sample obtained from PFR h=26.7 cm was black and had a dry, powdery texture.

The microscope used was the JEOL 200CX which is a 200 KeV, high resolution microscope equipped with a high brightness electron source and free lenses control. The JEOL 200CX is capable of 0.14 nm linie-to-line resolution and 3.0 nm point-to-point resolution. The microscope is located at the Center for Materials Science and Engineering (CMSE) at MIT. The grids used were 3.0 mm in diameter with 200 mesh copper grids with stress-free carbon film purchased from Ladd Research Industry, Inc.

3.4 DATA LIMITATIONS AND ERROR ESTIMATION

The detection sensitivity for the HP GC/FID used for the C1-C4 analyses ends at a mole fraction of about $5x10^{-6}$ ppm. A higher sensitivity is observed for the Perkin Elmer Sigma 1 GC/FID, and mole fractions of about $5x10^{-7}$ could be detected. Species present in lower concentrations were sampled using the chilled CH_2Cl_2 traps, and for the typical volumes of gas sampled (about 14 liters), the lower

detection limit corresponded to a reactor mole fraction of $1x10^{-9}$. The lower limit for the gravimetric measurements was determined by the precision of the analytical balance, and this corresponded to a mass concentration of about $1x10^{-9}$ g/cm^3 in the JSR/PFR.

Reproducibility for GC injections was usually better than 3% for the C1-C4 species, and of the order 10% for the PAH species, depending on the concentration level. Species near the detection limit would have reproducilibities around 25-35%. Other uncertainties in analytical measurements include GC integration errors from peaks which are not completely resolved. This is especially prevalent in the PAH analysis. Obvious integration errors were cause for rejection of data.

Care was taken to minimize sampling errors, but in general the gas samples showed less uncertainty than the liquid samples. Multiple gas samples were taken at the same sampling location to verify that gas sampling errors are small. Liquid samples, because of the involved procedure for concentrating the samples, usually showed a reproducibility of about than 30%. The chemical work-up of the PAH samples introduced other sources of error. If the heating rate for concentration of the CH_2Cl_2 liquid samples was too high, loss of volatile species occurs, and so the gas-phase benzene measurements were used.

Systematic errors which have to be considered are caused by probe sampling. Unstable or reactive species will undergo stabilizing reactions in the probe. For some of the species, the kinetics of these stabilizing reactions may be predicted. Species such as oxygen

are destroyed in the probe by insufficient thermal quenching, and species such as ethane are formed from methyl-methyl recombination reactions which occur in the probe. The result is that measured stable species concentrations will not be representative of the concentrations in the reactor. Vaughn (1988) has modeled the effect of probe quenching for species in the JSR. Probe quenching was important at low equivalence ratios (ϕ=1.3) where the radical concentrations are very high, and less important at higher equivalence ratios. In the PFR, the radical concentrations are much lower than in the JSR and probe quenching will not be as significant as in the JSR.

4. CHEMICAL SPECIES CHARACTERIZATION

4.1 DETAILED PAH IDENTIFICATION

A tremendous number and variety of species are observed in the JSR-PFR under our fuel-rich (sooting) experimental conditions. Figure 4.1 shows the types and relative amounts of the major stable species which are measured in the PFR. It is convenient to categorize these species into three general classes:

-aliphatic (acyclic) species

-unsubstituted aromatic species

-substituted aromatic species

The first class of species includes the fixed gases and light hydrocarbons, and accounts for most of the carbon mass; the second class contains most of the mass of the PAH inventory; and the third class is dominated by methyl- and ethynyl-substitutions.

A total of 20 acyclic hydrocarbons are routinely measured and more than 130 individual PAH peaks are observed, for which we have certain identifications for 35 species and tentative identifications for 32 additional PAH species for a total of 67 species. These identifications have been summarized in Table 3.4. Although a large number of PAH species are not identified, the ones we have identified make up more than 98% of the total PAH mass. The unidentified species appear as very small peaks on the chromatogram, and it is difficult to distinguish these peaks from the baseline noise.

Some of the species disappear after exiting the JSR, and others appear in measurable quantities at long PFR residence times. For example, PAH species containing O atoms, such as phenol (C_6H_5OH) and

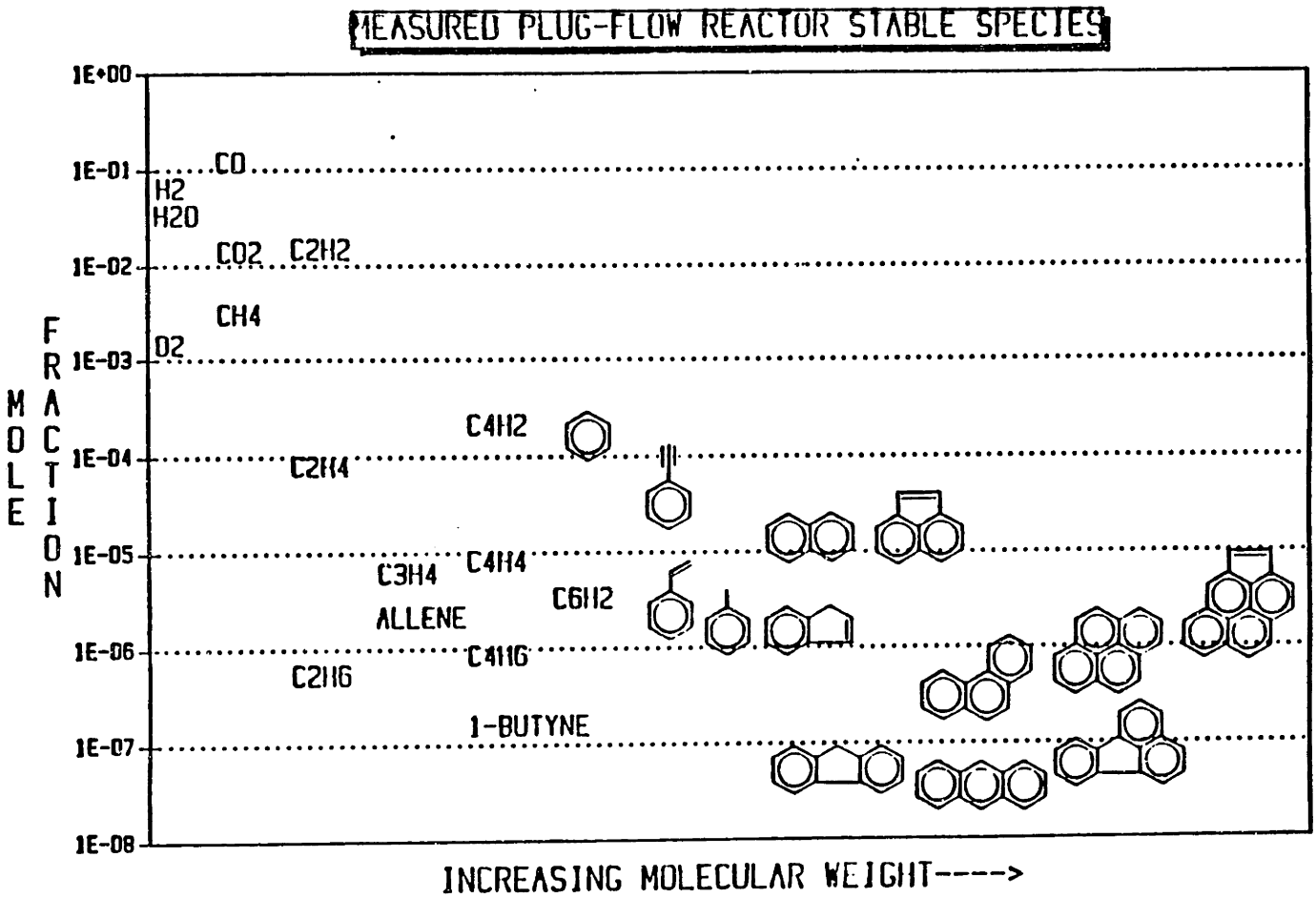

Figure 4.1 Relative Concentrations of measured PFR stable species.

benzaldehyde (C_7H_6O), are observed in samples obtained from the JSR, but these species do not survive into the PFR in detectable quantities. The same phenomenon is observed for species with a high degree of saturation such as propane (C_3H_8) or 1-butene (C_4H_8). On the other hand, very high molecular weight species, such as benzo(ghi)perylene, do not appear in the JSR, but become detectable at long PFR residence times. In general, species with high H/C ratios which are present in the JSR are destroyed in the PFR, especially at long residence times. PAH species which have molecular weights greater than cyclopenta(cd)pyrene begin to appear in detectable quantities at long PFR residence times, for the sooting conditions which we have studied.

4.1.1 Aliphatic (Acyclic) Species

The fixed gases, H_2, H_2O, CO, and CO_2, are the major species present in the reactor by molar concentration. Although H_2O is not directly measured, we can calculate its concentration by O-atom mass balance. The fixed gases H_2O, CO, and CO_2 are relatively unimportant in the molecular weight growth process. They act mainly as a sink for the available O atoms, taking them out of the radical pool. Hydrogen, on the other hand, plays a role in molecular weight growth because it influences the concentration of H atoms. The H atoms are active in abstraction reactions to create hydrocarbon radical species.

The aliphatic hydrocarbons may be classified by degree of conjugation, or H/C ratio. Species with high H/C ratios, such as the alkanes, do not extend into the high molecular weight regime. For example, although methane is present in high concentration (≈10,000 ppm), ethane is in low concentration (≈10 ppm), and propane or butane are not detected (<1 ppm).

The alkenes, such as ethylene, allene, and butadiene are present in larger quantities than their alkane counterparts. These species generally show a decreasing profile in the PFR, indicating a net destruction rate. The normalized net rate of destruction, $(1/-[\text{alkene}])\cdot d[\text{alkene}]/dt$, is much less than the normalized alkane net destruction rate.

Acetylenic species dominate the aliphatic hydrocarbon inventory. Acetylene is the most abundant C2 species, and diacetylene is the most abundant C4 species. These profiles are relatively flat, and do not show the same net destruction rate as the alkanes and alkenes. Higher

polyacetylenes are also observed. Triacetylene (C_6H_2) and tetra-acetylene (C_8H_2) show relatively flat profiles, although the latter compound is near the detection limit.

Species which have both vinylic and acetylenic structures, such as vinylacetylene ($CH{\equiv}C\text{-}CH{=}CH_2$), hexadiene-yne ($CH_2{=}CH\text{-}CH{=}CH\text{-}C{\equiv}CH$ or other C_6H_6 isomer), and hexene-diyne ($CH_2{=}CH\text{-}C{\equiv}C\text{-}C{\equiv}CH$ or other C_6H_4 isomer) are also present. Vinyl acetylene is the second most abundant C4 species, and the C6 vinylic-acetylenic species are minor products compared with the aromatic C6, benzene.

Polyacetylenes have been observed in acetylene flat-flame studies in relatively high concentrations. We also observe the polyacetylenes up to tetra-acetylene, (C_8H_2), and their concentrations decrease by a factor of ≈30 for each addition acetylene group. Acetylene, diacetylene, triacetylene and tetra-acetylene are present in high enough concentrations to be observed in the gas-phase for all conditions studied, although the tetra-acetylene shows a somewhat larger amount of scatter in the data.

4.1.2 Unsubstituted Aromatic Species

The basic building blocks in the molecular weight growth process are the single-ring species. This series starts with benzene and cyclopentadiene, and both species are always observed for all of the different experimental conditions studied. Benzene and cyclopentadiene were unambiguously identified through GC/MS and GC/FTIR, and the identification of cyclopentadiene formed in the JSR was first confirmed by Vaughn (1988) using the GC/FTIR technique.

Benzene
(C_6H_6)

Cyclopentadiene
(C_5H_6)

Cyclopentadiene has been observed as an oxidation product of benzene in a flow reactor (Venkat, 1982) as well as a flat-flame (McKinnon, 1988b).

The two-ring cyclic species which may be formed starting from the single-ring species are numerous, but only two are always observed for our experimental conditions. Naphthalene and indene were positively identified using all four of the identification techniques namely 1) injection of a verified standard, 2) GC/MS, 3) GC/FTIR, and 4) correlation of retention indices (Lee et. al. 1979).

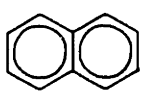

Naphthalene
($C_{10}H_8$)

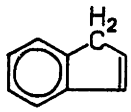

Indene
(C_9H_8)

Other possible two-ring species containing rings larger than 6 atoms, such as azulene, were not observed. Two-ring aromatic species which are not fully condensed, such as biphenyl and bibenzyl, were also not observed experimentally. Both biphenyl and bibenzyl were in our GC standard, and no peak was observed to elute at the retention times corresponding to the two compounds. Biphenyl has been observed in benzene flat-flames before the oxidation zone, where there is a high concentration of intact aromatic structures, such as phenyl. Phenyl-phenyl recombination is the formation pathway for biphenyl, and at the location in the flame where biphenyl is observed, the benzene mole fraction is of order 10 mole percent. We are combusting ethylene, and the benzene concentration never exceeds 300 ppm. Therefore, we do not expect much biphenyl formation.

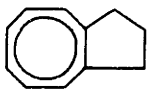

Azulene
($C_{10}H_8$)

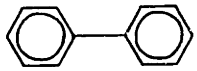

Biphenyl
($C_{12}H_{10}$)

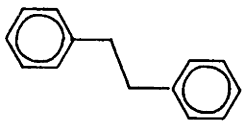

Bibenzyl
($C_{14}H_{14}$)

Three-ring unsubstituted aromatic species include phenanthrene, anthracene, acenaphthylene, and fluorene. Phenanthrene is always found in higher concentration than anthracene, and the ratio varies from 4:1 to 8:1. At 1500K, phenanthrene (ΔG_f=184.8 kcal/mol) is more thermodynamically stable than anthracene (ΔG_f=189.1 kcal/mol), and their equilibrium ratio is calculated to be 0.81/0.19. It is tempting to infer that the ratio of phenanthrene to anthracene is determined

solely by their thermodynamic stabilities, but this rule does not hold for larger multi-ring PAH species.

Acenaphthylene is always found in high concentration relative to the total PAH inventory. Acenaphthylene has a 5-membered ring "bridge" structure which is more thermodynamically stable than an ethynyl-group substitution at combustion temperatures. Using Stein's group additivity method, the heat of formation of the acenaphthylene is 29.8 kcal/mol lower than ethynyl-substituted naphthalene, and the entropy is only 3.7 cal/mol/K lower. Thus at temperatures below 3000K, acenaphthylene is more thermodynamically stable than ethynyl-naphthalene. Fluorene is always observed, although it is a relatively minor species.

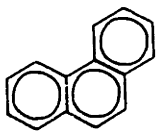

Phenanthrene
($C_{14}H_{10}$)

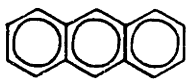

Anthracene
($C_{14}H_{10}$)

Acenaphthylene
($C_{12}H_8$)

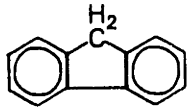

Fluorene
($C_{13}H_{10}$)

Three-ring species which are not observed include acenaphthene, phenalene, and any three-ring PAH containing a hetero-atom.

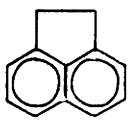

Acenaphthene
($C_{12}H_{10}$)

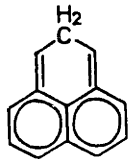

Phenalene
($C_{13}H_9$)

The most abundant four-ring PAH species which is usually

observed in the PFR is pyrene. Pyrene and fluoranthene are commonly found in approximately a 2:1 ratio. From thermodynamic equilibrium, pyrene is predicted to be much more stable than fluoranthene, by a factor of 1000.

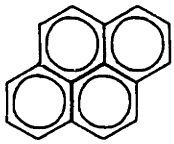

Pyrene
($C_{16}H_{10}$)

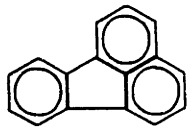

Fluoranthene
($C_{16}H_{10}$)

Other 4-ring PAH species include acephenanthrylene, aceanthrylene, and 4H-cyclopenta(def)phenanthrene. Because of GC separation problems, the aceanthrylene peak is not always distinguishable from the relatively large pyrene peak. Acephenanthrylene and 4H-cyclopenta(def)phenanthrene are always observed.

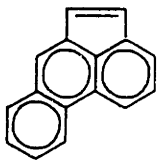

Acephenanthrylene
($C_{16}H_{10}$)

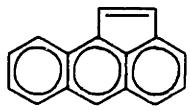

Aceanthrylene
($C_{16}H_{10}$)

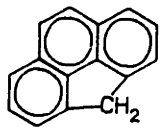

4H-cyclopenta(def)phenanthrene
($C_{15}H_{10}$)

PAH species with 5 rings which are seen experimentally include cyclopenta(cd)pyrene, benzo(ghi)fluoranthene, perylene and numerous benzopyrene isomers. The amount of cyclopenta(cd)pyrene which is formed in the PFR is quite large, and can account for as much as 15% of the total PAH inventory by the end of the PFR.

Cyclopenta(cd)pyrene is always experimentally detected, and always shows an increasing profile in the PFR. Benzo(ghi)fluoranthene is usually detected, although it is near the detection limit in the JSR, especially for the $\phi = 2.18$ case.

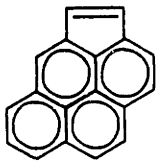

Cyclopenta(cd)pyrene
($C_{18}H_{10}$)

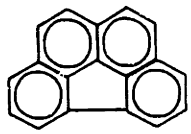

Benzo(ghi)fluoranthene
($C_{18}H_{10}$)

A number of the benzopyrene isomers, including benzo(a)pyrene and benzo(e)pyrene, were not distinguishable or co-eluted with each other on the GC chromatogram. Perylene was not observed, based on retention time comparison with a certified standard.

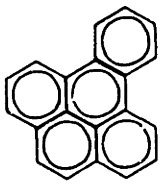

Benzo(e)pyrene
($C_{20}H_{12}$)

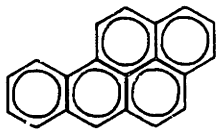

Benzo(a)pyrene
($C_{20}H_{12}$)

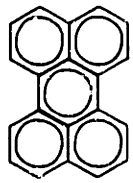

Perylene
($C_{20}H_{12}$)

Larger PAH species, containing 6 or more aromatic rings, were just detectable using the GC/FID. These large species have very low vapor pressures and do not volatilize fully in the GC injection port. Consequently, the total amount of material which gets onto the capillary column is small, the reproducibility is poor; and so quantification of the 6-ring and larger PAH is not reliable. Also, in order to preserve the operating lifetime of the capillary column, a

final maximum temperature of 280°C, instead of the actual allowable maximum temperature of 350°C for the column, was used. A higher final temperature would have helped quantification of 6-ring PAH species. Benzo(ghi)perylene was sometimes observed in PFR samples obtained at long residence times. The use of HPLC allowed identification and quantification of some of the larger PAH species, including coronene and naphtho(8,1,2,abc)coronene.

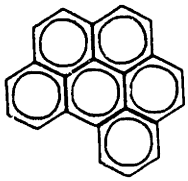

Benzo(ghi)perylene
($C_{22}H_{12}$)

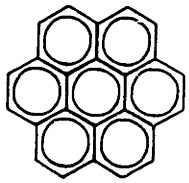

Coronene
($C_{24}H_{12}$)

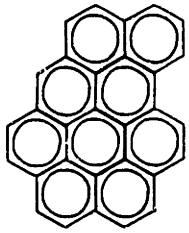

Naphtho(8,1,2,abc)coronene
($C_{30}H_{14}$)

The identification of naphtho(8,1,2,abc)coronene was made by comparison of the UV spectra with a known standard synthesized and provided by Dr. Fetzer (Chevron Research) to the Analytical Chemistry Group in the M.I.T. Center for Environmental Health Sciences.

4.1.3 Substituted Aromatic Species

The substituted aromatic species are usually found in concentrations 1-2 orders of magnitude lower than the parent unsubstituted species. Mono-substituted single ring aromatic species which were observed include toluene, phenylacetylene, styrene, and possibly ethylbenzene, although the latter was not distinguishable from the 3 xylene isomers.

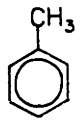

Toluene
(C_7H_8)

Phenylacetylene
(C_8H_6)

Styrene
(C_8H_8)

Two peaks in the chromatogram, listed as peaks #11 and #12 in Table 3.4, show a molecular mass of 90 from the GC/MS and also the existence of terminal acetylene groups from the GC/FTIR. These two peaks are probably two of the ethynyl-cyclopentadiene isomers.

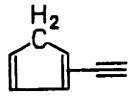

Ethynyl-cyclopentadiene
(C_7H_6)

Disubstituted single-ring PAH species which were positively identified include the three di-ethynyl benzene isomers: 1,2-, 1,3-, and 1,4-diethynyl benzene. These species are separated on the GC column, and the isomers were distinguished by inspection of the

aromatic C-H out-of-plane bending frequencies in the IR spectra (700-1000 cm^{-1}). The type of substitution does not affect these aromatic bending frequencies, and by comparison with library IR spectra for the 3 xylene isomers, the 3 diethynyl benzene isomers could be identified.

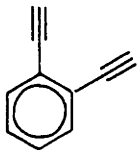

1,2-diethynyl benzene
($C_{10}H_6$)

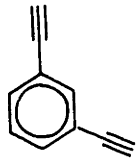

1,3-diethynyl benzene
($C_{10}H_6$)

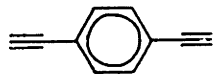

1,4-diethynyl benzene
($C_{10}H_6$)

Other disubstituted mono-aromatic species which were observed are ethynyl-substituted toluene (mostly in the JSR) and probably vinyl-ethynyl-substituted benzene. This last compound is probably peak #32 in Table 3.4, since it was determined to have a terminal acetylene group from the GC/FTIR. Unfortunately, we were unable to identify the specific isomers for either of the two species.

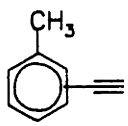

Ethynyl-toluene
(C_9H_8)

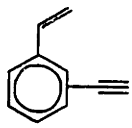

Vinyl-ethynyl-benzene
($C_{10}H_8$)

The mono-substituted 2-ring aromatic species include both 1- and 2-methyl naphthalene. These species were usually present in the JSR samples, but not always present in the PFR samples. Their concentrations were usually a factor of 100 lower than naphthalene.

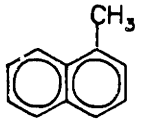

1-Methyl naphthalene
($C_{11}H_{10}$)

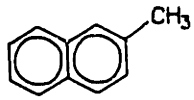

2-Methyl naphthalene
($C_{11}H_{10}$)

The ethynyl-substituted 2-ring aromatics were found in much higher concentrations than the methyl-substituted species. The dominant substituted 2-ring PAH was 2-ethynyl naphthalene. This peak elutes just before acenaphthylene, and was verified by confirmation of a terminal acetylene group, as well as isomer identification by the substitution pattern for the aromatic C-H bending frequencies. Some combustion studies in the literature have identified this peak as biphenylene, but the ethynyl-naphthalene structure was tentatively proposed by Wenz (1983), based on GC/MS fragmentation spectra. Two ethynyl indene isomers were separated and determined to have a terminal acetylene group, but the isomers were not differentiated.

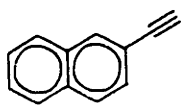

2-Ethynyl naphthalene
($C_{12}H_8$)

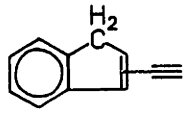

Ethynyl-indene
($C_{11}H_8$)

No di-substituted 2-ring aromatic species were observed.

The low concentrations of the mono-substituted 3-ring aromatic species only permitted the identification of the ethynyl-

acenaphthylene isomers. These species were in surprisingly high concentrations (≈1 ppm), especially for sooting conditions at long residence times in the PFR. Although there are 4 different ethynl-acenaphthylene isomers, only 3 GC peaks could be positively identified as species with masses of 176 amu and having a terminal acetylene group. These 3 peaks are peaks #49, #50, and #51 as given in Table 3.4. Peak #53 also has a mass of 176 amu, but it did not show a strong absorbance at 3330 cm^{-1}, indicating the absence of an ethynyl group. A possible identification for this peak would be pyracylene.

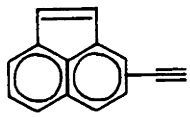

Ethynyl-acenaphthylene
($C_{14}H_8$)

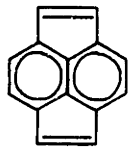

Pyracylene
($C_{14}H_8$)

Pyracylene has been synthesized and reported in the literature (Trost, 1971, Schaden, 1983). Interestingly, one of the pyracylene synthesis techniques involves the oxidation of pyrene to either 1,6-pyrenedione or 1,8-pyrenedione, followed by pyrolysis in a quartz flow tube at 1100°C to yield pyracylene. If peak #53 is indeed pyracylene, then the possibility exists that two of the ethynyl-acenaphthylene isomers co-elute, probably as peak #49, and thus only appearing as 3 chromatographic peaks.

A search for ethynyl-substituted aromatic species with 4 or more rings did not positively show the existence of say, ethynyl-pyrene, but these species, if present, are probably in concentrations below the GC/FTIR detection limit. A large number of mass 226 and 252 peaks

appear as small peaks on the GC/FID, which has a much higher sensitivity than the GC/FTIR, but we can only speculate that ethynyl-pyrenes or ethynyl-cyclopenta(cd)pyrenes are present in the samples.

Some general trends for the relative concentrations of substituted aromatic species are observed. For the same type of substituent group, the relative concentrations roughly follow the same trend as the unsubstituted aromatic species. Except for methyl-substituted PAH, the relative abundance of substituted aromatics decreases with increasing degree of saturation. For example, the concentration of ethynyl-substituted benzene (phenylacetylene) is 2 orders of magnitude higher than vinyl-substituted benzene (styrene), and ethyl-benzene is just above detection limits. Substituent groups with more than 2 carbon atoms, such as butadynyl-benzene are very low in concentration and C4-substituted poly-aromatic species are not detected.

4.1.4 Species Containing a 5-membered Ring

Of the PAH with molecular weights between indene and benzo(ghi)perylene, species containing a 5-membered ring account for a significant fraction of the total PAH inventory. Of the total mass of PAH, including substituted PAH, approximately 60% of the species have a 5-membered ring, which can further be divided into 20% which contain a methylene group in the 5-membered ring, and the remaining 40% which do not contain a methylene group.

The 5-membered ring species which contain a methylene group would be indene, and its higher molecular weight analogs, fluorene and 4H-cyclopenta(def)phenanthrene. These species are always present, although in relatively low quantities. A possible formation mechanism for these species is from the oxidation of the corresponding species containing only 6-membered rings. For example, cyclopentadiene has been observed as an oxidation product of benzene in a flow reactor (Venkat, 1982), in a flat-flame (McKinnon, 1988b), and in the JSR from work done here at M.I.T. (Vaughn, 1988). A possible mechanism for benzene oxidation involves 1) OH addition to benzene to form phenol, followed by H-elimination to give phenoxy, or 2) H-abstraction from benzene by H or OH to give phenyl radical followed by O_2 addition to phenyl to give phenoxy, or 3) O atom addition to benzene followed by H elimination to give phenoxy, which rearranges to form a 5-membered ring and eliminates CO to form cyclopentadiene. This mechanism is illustrated in Figure 4.2. The reactions of the higher molecular weight analogues of benzene may yield 5-membered ring structures with a methylene group, and these are also shown in Figure 4.2. Table 4.1

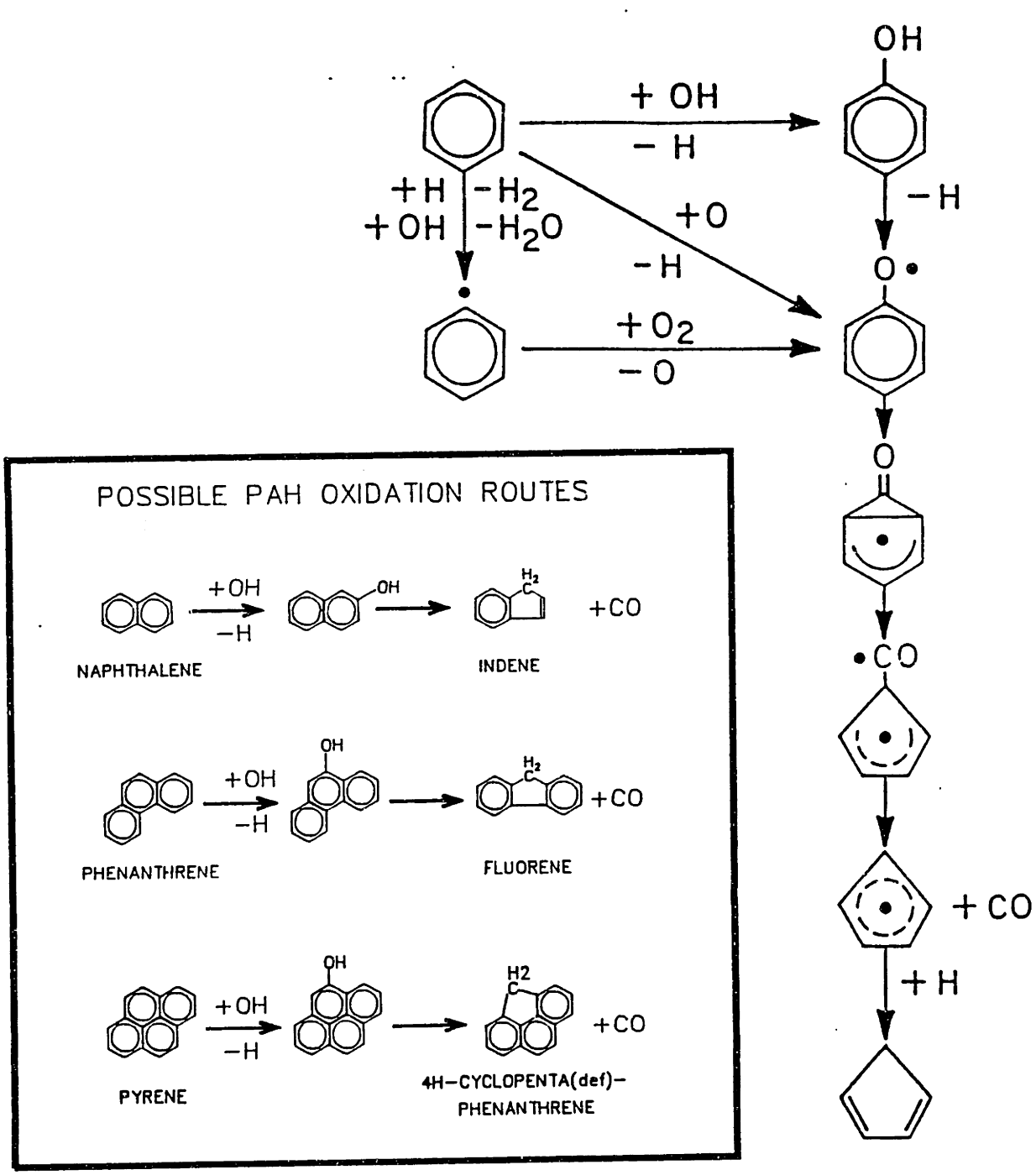

Figure 4.2 Oxidation Pathway for Benzene (proposed by Vaughn, 1988), and possible pathways for formation of 5-membered ring PAH by analogy.

Table 4.1 Possible 5-Membered Ring Oxidation Products

REACTANT	OXIDATION PRODUCT	MOLAR RATIO PRODUCT/REACTANT
		
BENZENE (C_6H_6)	CYCLOPENTADIENE (C_5H_6)	0.02-0.10
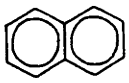	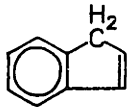	
NAPHTHALENE ($C_{10}H_8$)	INDENE (C_9H_8)	0.40-1.20
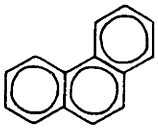	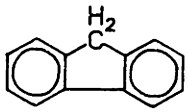	
PHENANTHRENE ($C_{14}H_{10}$)	FLUORENE ($C_{13}H_{10}$)	0.14-0.18
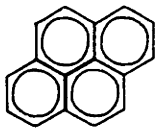	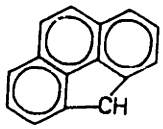	
PYRENE ($C_{16}H_{10}$)	4H-CYCLOPENTA(def)PHENANTHRENE ($C_{15}H_{10}$)	0.14-0.20

summarizes the 5-membered ring oxidation products and their ratio to the parent molecule.

The 5-membered ring species which do not contain a methylene group account for 40% of the total mass of PAH. These species have a 5-membered ring bridge structure, with the exception of fluoranthene. Acenaphthylene and cyclopenta(cd)pyrene are major species in the PAH inventory, and acephenanthrylene and aceanthrylene are usually detected. Fluoranthene is always observed.

These 5-membered ring structures are much different than those which contain methylene groups in the sense that they are probably products of the growth process. Acenaphthylene formation, for example, may be due to an addition reaction of C_2H_2 to 1-naphthalenyl followed by cyclization and H-elimination. Similarly, acephenanthrylene may be formed from phenanthrene, aceanthrylene from anthracene, and cyclopenta(cd)pyrene from pyrene. A possible formation mechanism for these 5-membered ring species is shown in Figure 4.3. The ratios of these 5-membered rings species to their parent 6-membered ring species is shown in Table 4.2. These ratios are sensitive to the PFR residence time, fuel equivalence ratio, injection species, but the typical ratio range is given in Table 4.4.

Table 4.2 Possible 5-Membered Ring Growth Products

REACTANT	GROWTH PRODUCT	MOLAR RATIO PRODUCT/REACTANT
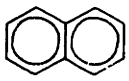	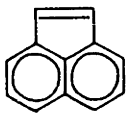	
NAPHTHALENE ($C_{10}H_8$)	ACENAPHTHYLENE ($C_{12}H_8$)	0.3 - 0.8
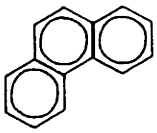	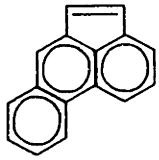	
PHENANTHRENE ($C_{14}H_{10}$)	ACEPHENANTHRYLENE ($C_{16}H_{10}$)	1.0 - 1.2
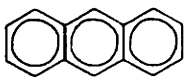	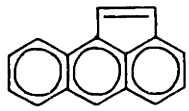	
ANTHRACENE ($C_{14}H_{10}$)	ACEANTHRYLENE ($C_{16}H_{10}$)	2.6 - 4.7
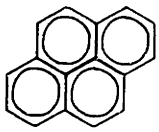	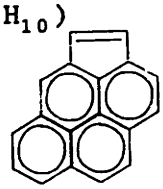	
PYRENE ($C_{16}H_{10}$)	CYCLOPENTA(cd)PYRENE ($C_{18}H_{10}$)	0.6 - 1.4

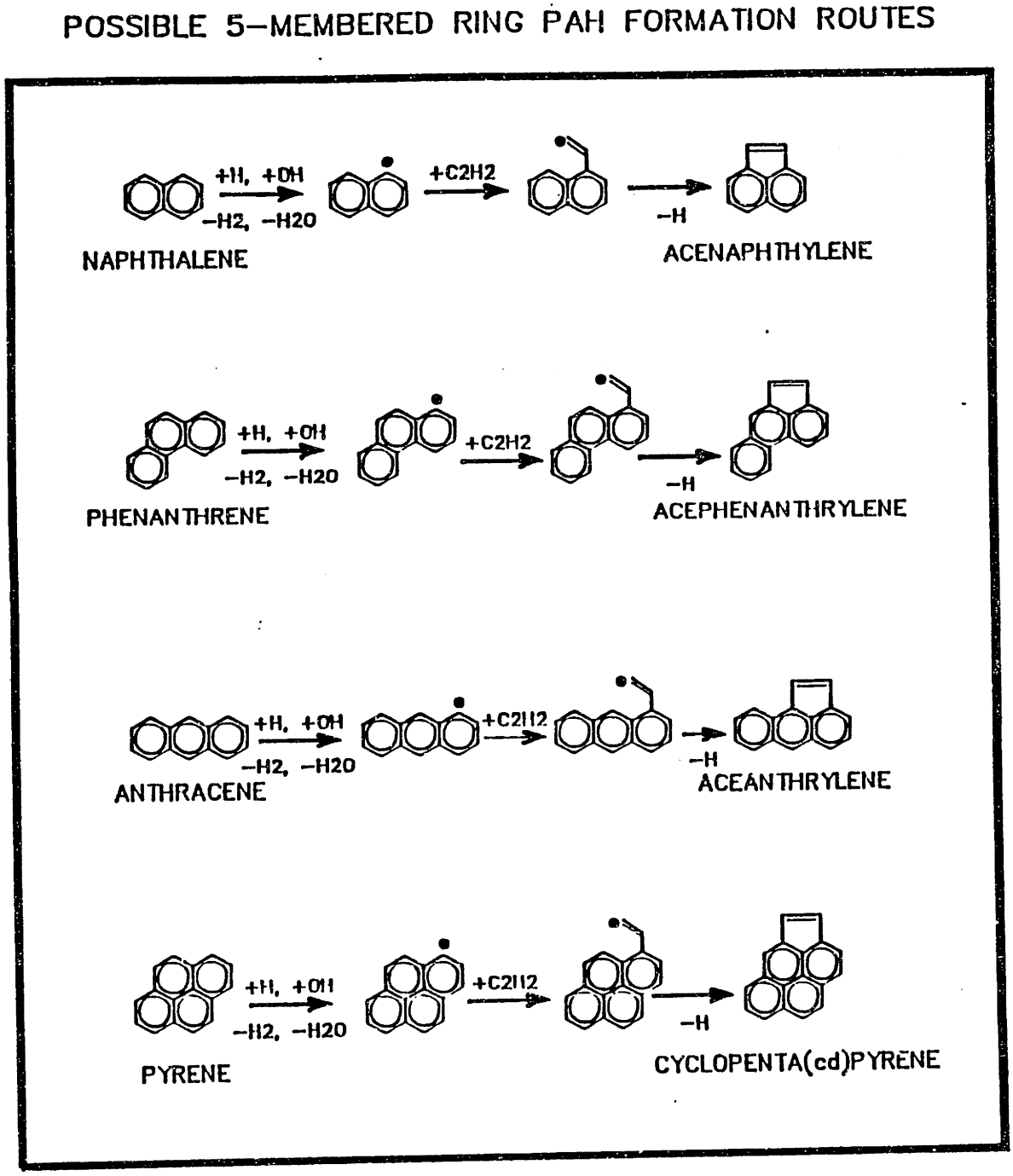

Figure 4.3 Possible pathways for formation of 5-membered ring PAH by free-radical C_2H_2 addition reactions.

Fluoranthene is the one 5-membered ring species whose formation mechanism has not yet been postulated. Fluoranthene may be formed from 2 sequential C_2H_2 additions to acenaphthylene. Of the 4 possible ethynyl-acenaphthylene isomers, ethynyl substitution at the acenaphthylene bridge structure, followed by a second C_2H_2 addition would lead to fluoranthene formation.

4.2 VERY HIGH-MOLECULAR WEIGHT MATERIAL

A limited number of High Performance Liquid Chromatography (HPLC) measurements were performed in order to extend the molecular weight range of the GC/FID measurements. This work was performed in collaboration with the Analytical Chemistry Group in the M.I.T. Center for Environmental Health Sciences.

Samples collected in CH_2Cl_2 were passed over a cyano gravity column (Analytichem) to remove highly polar compounds which might damage the HPLC column, and concentrated by nitrogen evaporation. The samples were injected onto 3 normal phase cyanopropyl columns (Alltech) in series. Each was 25 cm in length, with an internal diameter of 0.46 cm and packed with 5 μm cyanopropyl material having a 60 Å average pore diameter with a surface area of 400 m^2/g. The HPLC system consisted of a Hewlett-Packard Model 1090 ternary gradient pumping system with 190-600 nm diode-array detector.

The samples which were analyzed by HPLC were collected using a large version of the PAH sampling system developed for this work. Two large samples, one in the JSR and one near the end of the PFR, were obtained using 4 liquid nitrogen-cooled CH_2Cl_2 traps in series with a total liquid volume of 2 liters. Reactor conditions were the ϕ=2.37, JSR T=1630K, τ=5.8 ms, $C_2H_4/O_2/N_2$, and the PFR residence time was 9.4 ms. Figures 4.4 and 4.5 show the HPLC chromatograms for the JSR and PFR samples, respectively.

The HPLC and GC/FID techniques overlap, and peaks for species such as acenaphthylene (peak G), pyrene (peak I), fluoranthene (peak J) and cyclopenta-(cd)pyrene (peak L) are clearly visible on both HPLC

chromatograms. Species which are detected by HPLC and not by GC/FID include coronene (peak R) and naphthocoronene (peak Y). The main difference between the JSR and PFR samples is that the PFR sample has a higher proportion of the species with molecular weights greater than acenaphthylene than the JSR sample.

In order to quantify the results, a calibration curves for the total UV absorbance as a function of carbon number (Figure 4.6) and as a function of elution volume (Figure 4.7) were prepared using verified standard compounds up to and including naphthocoronene. Tables 4.3 and 4.4 show the identifications and calculated amounts for the two samples.

Calculation of the total mass of material which has molecular weight greater than CPEP for the PFR sample could not account for a significant fraction of the difference between the mass of CH_2Cl_2-soluble material as determined by the total tar weight measurements, and the mass of the ΣGC PAH as determined from GC/FID. It is possible that fractionation of the HPLC sample through the cyano-column may have removed some CH_2Cl_2-soluble material and thus not appear on the HPLC chromatogram. These species are probably polar in nature.

Further analysis of the material which is CH_2Cl_2-soluble, but not analyzable by GC techniques, should provide interesting information on the very high molecular weight PAH produced during combustion.

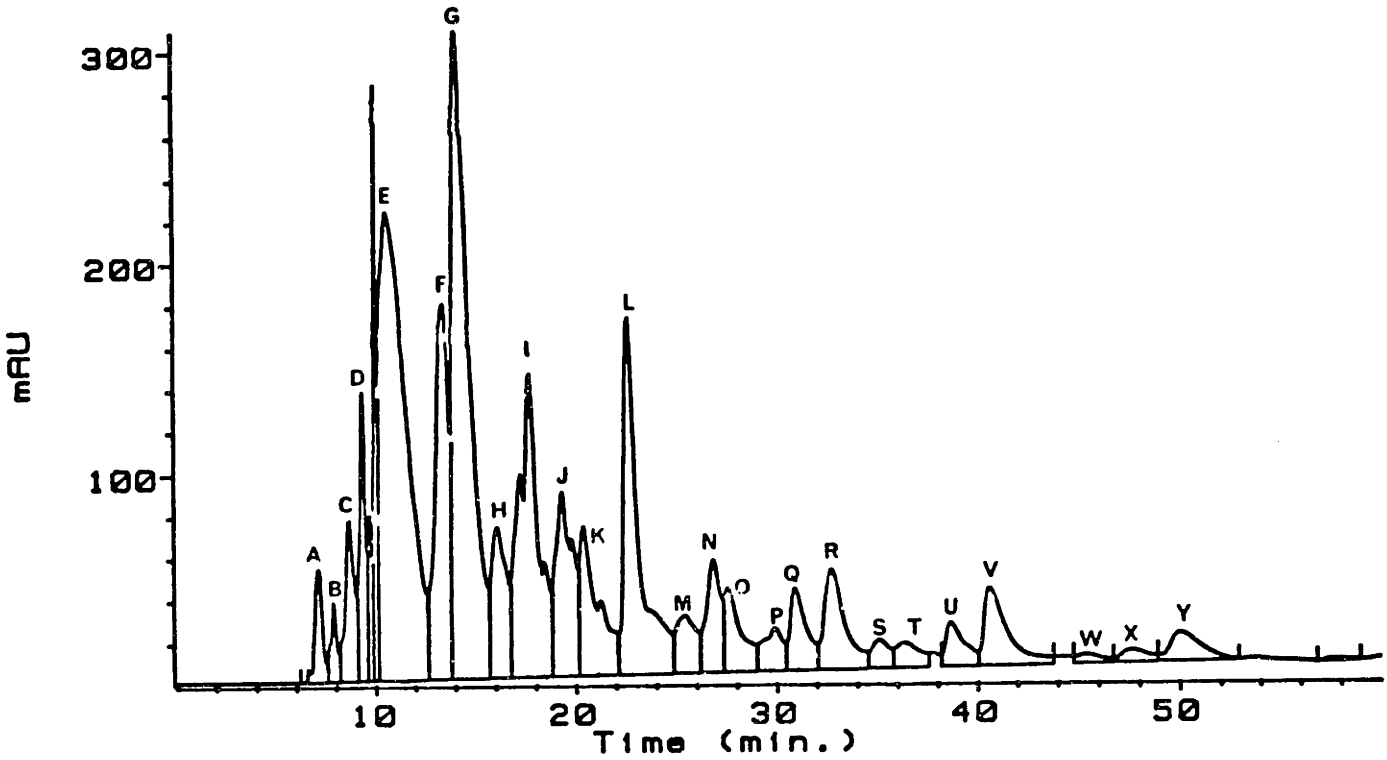

Figure 4.4 HPLC chromatogram of JSR sample obtained for combustion conditions: ϕ=2.37, JSR T=1630K, residence time=5.8 ms.

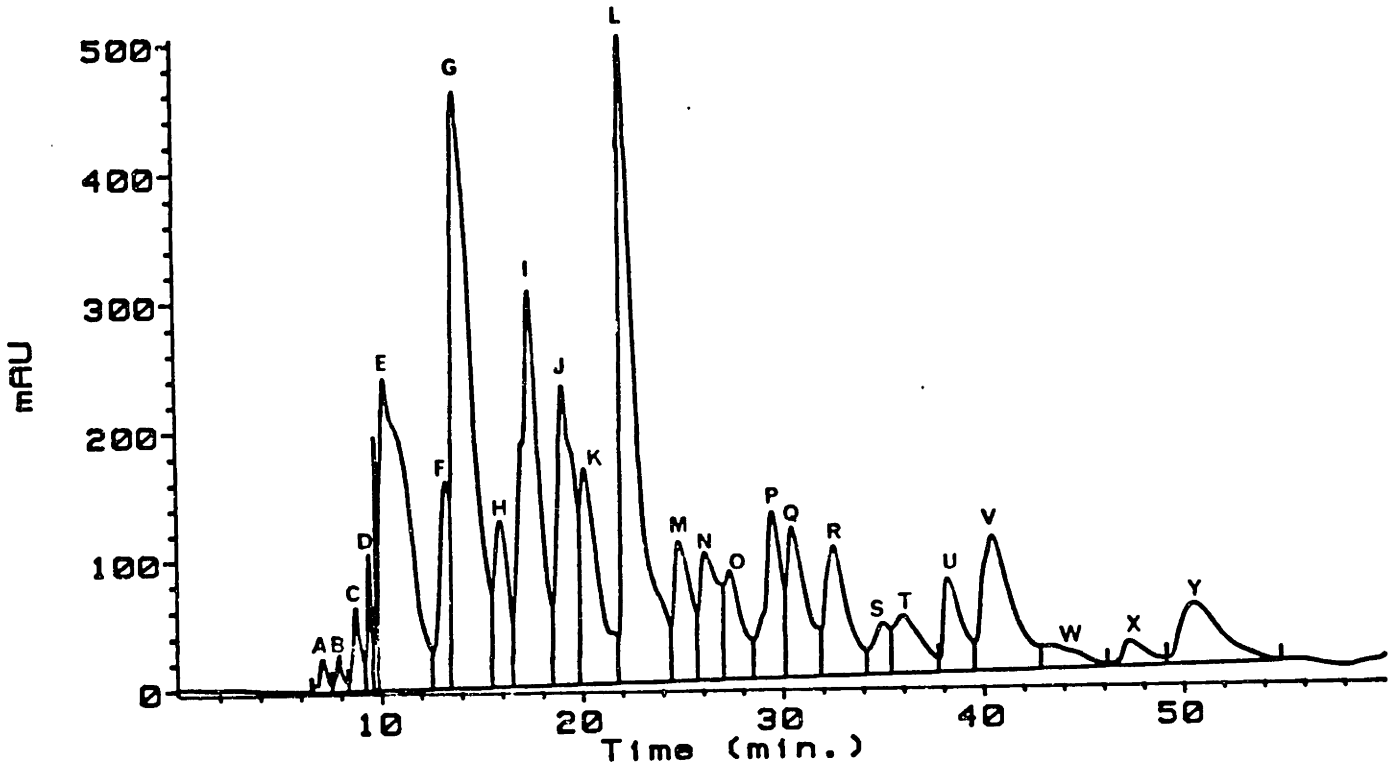

Figure 4.5 HPLC chromatogram of PFR sample obtained for combustion conditions: ϕ=2.37, JSR T=1630K, PFR residence time=9.4 ms.

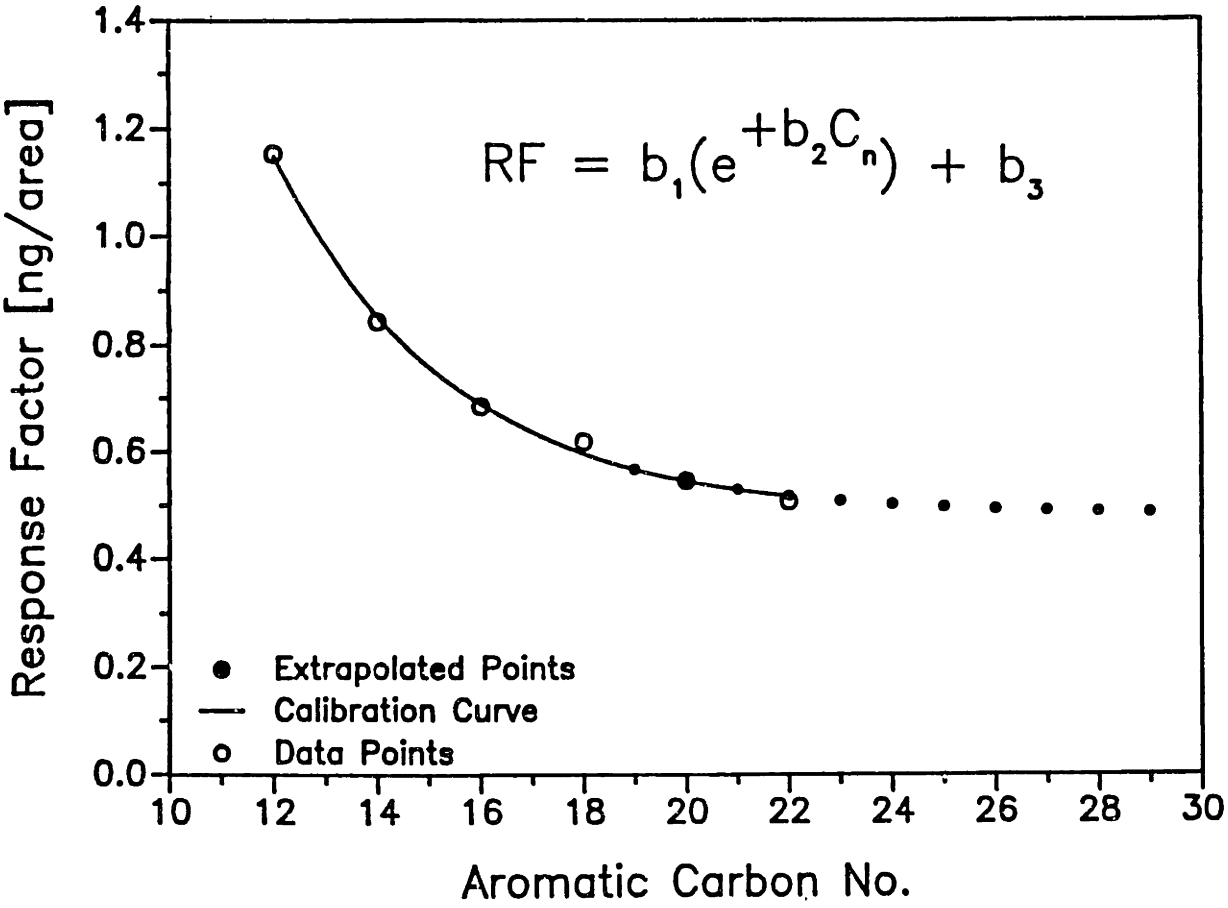

Figure 4.6 Calibration curve for HPLC total UV absorbance as a function of aromatic carbon number.

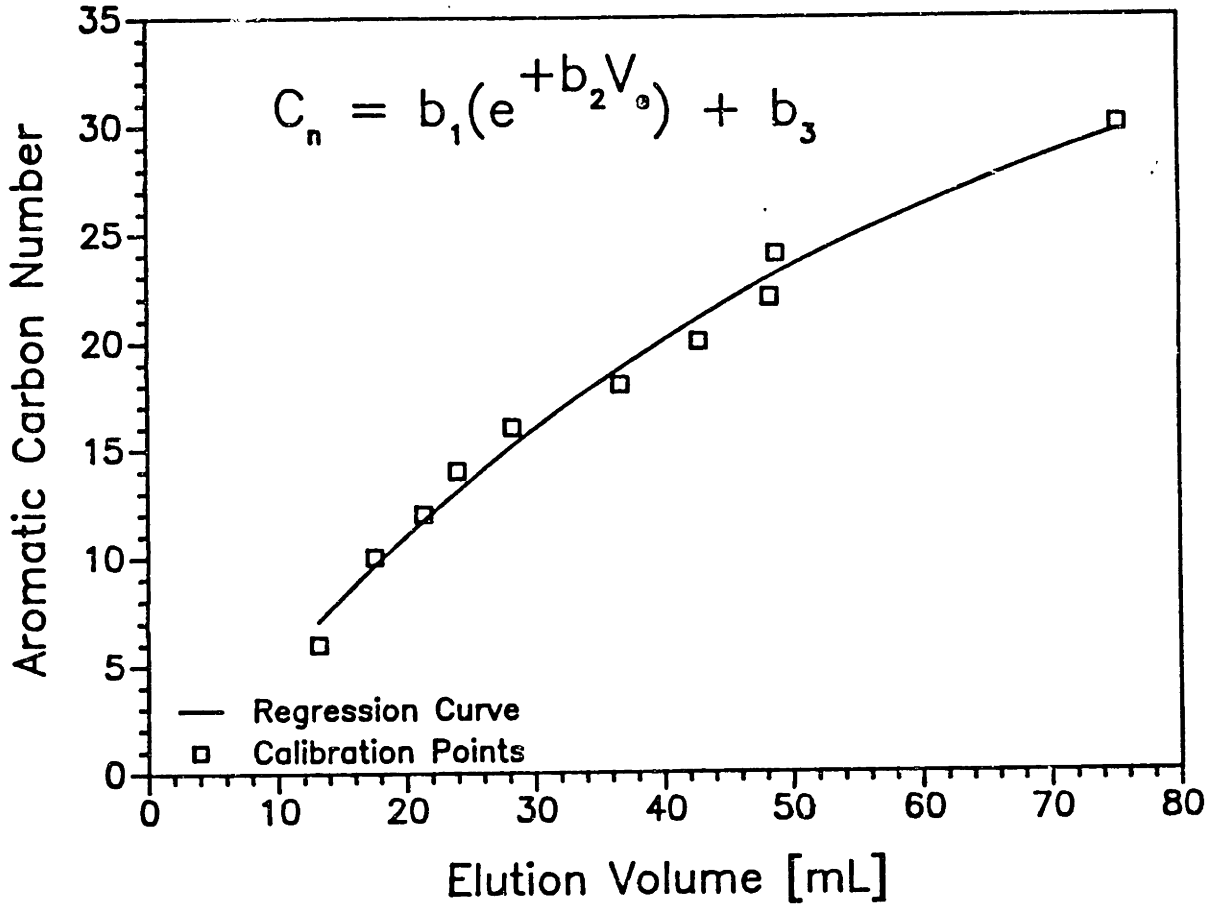

Figure 4.7 Calibration curve for HPLC total UV absorbance as a function of elution volume.

Peak	RT	S.D.	RSD	Area	SD	RSD	Ve Range (mL)	C-Number Range	R.F. [ng/A]	Amt (ng/ul)	Output [ug/Kg]
A)	7.19	0.02	0.32%	1166.3	204.1	17.5%	9.52--11.30	4.71--5.86	4.94	960.1	16.36
B)	7.92	0.04	0.47%	668.0	91.8	13.7%	11.30--12.20	5.86--6.44	4.11	457.8	7.80
C)	8.69	0.09	1.07%	2070.5	263.9	12.8%	12.20--13.56	6.44--7.27	3.42	1180.5	20.12
D)	9.55	0.13	1.35%	5444.3	1564.6	28.7%	13.65--15.04	7.33--8.17	2.81	2554.3	43.54
E)	10.16	0.66	6.52%	20345.3	918.7	4.5%	14.60--18.59	7.90--10.21	2.47	8381.6	142.86
F)	13.49	0.23	1.73%	9097.3	743.6	8.2%	18.59--20.71	10.21--11.37	1.35	2046.3	34.88
G)	14.15	0.23	1.61%	14673.5	4607.0	31.4%	20.32--23.00	11.37--12.83	1.22	3065.4	52.25
H)	16.31	0.14	0.85%	3245.7	843.9	26.0%	23.70--25.23	12.93--13.69	0.94	506.3	8.63
I)	17.80	0.16	0.88%	9329.7	2018.4	21.6%	25.23--28.33	13.69--15.17	0.81	1260.4	21.48
J)	19.54	0.17	0.87%	4966.0	1049.2	21.1%	28.33--30.43	15.17--16.12	0.71	588.3	10.03
K)	20.54	0.21	1.02%	4455.3	931.3	20.9%	30.43--33.36	16.12--17.40	0.67	496.8	8.47
L)	22.89	0.21	0.91%	8686.7	1790.3	20.6%	33.36--37.74	17.39--19.17	0.60	869.9	14.83
M)	25.23	0.84	3.32%	1733.7	381.6	22.0%	36.86--38.87	18.82--19.61	0.56	161.6	2.75
N)	26.83	0.56	2.07%	2677.5	303.3	11.3%	38.91--41.40	19.62--20.55	0.54	241.1	4.11
O)	28.02	0.33	1.17%	2224.7	489.6	22.0%	41.31--44.04	20.51--21.48	0.53	196.3	3.35
P)	30.22	0.24	0.80%	1400.0	283.3	20.2%	44.04--46.16	21.48--22.02	0.51	120.1	2.05
Q)	31.43	0.35	1.12%	2039.0	509.1	25.0%	46.16--48.56	22.20--22.98	0.51	172.9	2.95
R)	33.16	0.33	0.98%	3306.7	817.3	24.7%	48.56--52.73	22.98--24.26	0.50	276.8	4.72
S)	35.86	0.54	1.49%	789.5	116.9	14.8%	52.73--54.68	24.26--24.82	0.49	65.1	1.11
T)	36.96	0.44	1.18%	1147.2	376.2	32.8%	54.68--57.91	24.82--25.71	0.49	94.2	1.61
U)	39.42	0.54	1.37%	1351.2	307.6	22.8%	58.23--61.14	25.79--26.55	0.49	110.1	1.88
V)	41.51	0.69	1.65%	2954.0	732.8	24.8%	61.14--66.94	26.55--27.93	0.49	239.6	4.08
W)	45.97	0.44	0.96%	488.3	187.3	38.3%	67.43--71.07	28.04--28.82	0.48	39.4	0.67
X)	48.59	0.75	1.55%	626.1	229.9	36.7%	71.07--75.15	28.82--29.64	0.48	50.3	0.86
Y)	51.40	1.15	2.25%	1542.6	473.2	30.7%	75.55--83.50	29.72--31.14	0.48	123.8	2.11

Table 4.3 -- HPLC/UV Results from the JSR.

Peak	RT	S.D.	RSD	Area	SD	RSD	V_e Range (mL)	C-Number Range	R.F. [ng/A]	Amount [ng/ul]	Output [mg/Kg]
A)	7.15	0.03	0.44%	687.6	52.0	7.6%	9.64--11.31	4.79--5.87	4.98	571.15	16.25
B)	7.93	0.02	0.30%	519.4	145.6	28.0%	11.31--12.46	5.87--6.59	4.11	355.33	10.11
C)	8.75	0.05	0.59%	1674.0	106.0	6.3%	12.46--13.80	6.59--7.42	3.37	941.39	26.78
D)	9.41	0.08	0.83%	1303.7	36.2	2.8%	13.80--14.42	7.42--7.80	2.90	630.75	17.94
E)	10.45	0.48	4.57%	22409.9	2062.6	9.2%	14.55--18.91	7.88--10.39	2.33	8685.17	247.05
F)	13.35	0.10	0.72%	5570.3	109.5	2.0%	18.91--20.37	10.39--11.19	1.38	1278.98	36.41
G)	13.91	0.12	0.88%	30243.3	1462.1	4.8%	20.37--23.40	11.19--12.77	1.27	6379.64	181.47
H)	16.02	0.18	1.14%	5803.7	400.0	6.9%	23.40--24.94	12.77--13.54	0.97	933.88	26.56
I)	17.51	0.17	0.99%	18349.0	1061.3	5.8%	24.89--27.75	13.52--14.90	0.83	2542.50	72.32
J)	19.20	0.22	1.16%	13485.7	809.2	6.0%	27.75--29.99	14.90--15.93	0.73	1634.10	46.48
K)	20.25	0.24	1.18%	9717.0	815.0	8.4%	29.99--32.71	15.93--17.12	0.68	1101.70	31.34
L)	22.21	0.20	0.89%	25769.3	2088.8	8.1%	32.71--36.22	17.12--18.57	0.62	2651.06	75.41
M)	24.91	0.23	0.93%	5950.3	153.3	2.6%	36.79--38.76	18.80--19.56	0.56	559.25	15.91
N)	26.22	0.26	1.01%	5463.3	643.4	11.8%	38.76--40.51	19.56--20.22	0.55	497.86	14.16
O)	27.43	0.32	1.18%	5418.3	329.5	6.1%	40.50--43.04	20.22--21.13	0.53	482.66	13.73
P)	29.59	0.30	1.03%	6865.3	386.8	5.6%	43.04--45.33	21.13--21.93	0.52	593.10	16.87
Q)	30.56	0.31	1.01%	6985.3	473.4	6.8%	45.33--47.77	21.93--22.73	0.51	597.15	16.99
R)	32.49	0.13	0.40%	7492.0	55.9	0.8%	47.77--51.34	22.73--23.84	0.50	629.96	17.92
S)	35.03	0.40	1.15%	2381.7	102.3	4.3%	51.34--53.30	23.84--24.42	0.50	197.22	5.61
T)	36.07	0.32	0.89%	3980.3	149.4	3.8%	53.30--56.73	24.42--25.39	0.49	328.04	9.33
U)	38.28	0.40	1.06%	4488.7	61.7	1.4%	56.73--59.47	25.39--26.12	0.49	367.02	10.44
V)	40.31	0.40	1.00%	9954.0	628.5	6.3%	59.47--64.22	26.12--27.30	0.49	809.55	23.03
W)	43.47	0.40	0.91%	2409.2	225.0	9.4%	64.22--69.40	27.30--28.47	0.49	194.79	5.54
X)	47.13	0.49	1.05%	1872.0	236.1	12.6%	69.40--73.49	28.47--29.32	0.48	150.69	4.29
Y)	50.21	0.57	1.14%	6279.0	769.5	12.3%	73.49--80.60	29.32--30.65	0.48	504.20	14.34

Table 4.4 -- HPLC/UV Results from the PFR.

--Jet-Stirred Reactor/Toroid Section--					Major Component	Aromatic Carbon No.	----------Plug-Flow Section----------				
Peak I.D.	R.T. min.	C-Number Range	R.F. [ng/A]	Output [mg/Kg]			Peak ID	R.T. min.	C-Number Range	R.F. [ng/A]	Output [mg/Kg]
(A)	7.19	4.71--5.86	4.94	16.36			(A)	7.15	4.79--5.87	4.98	16.25
(B)	7.92	5.86--6.44	4.11	7.80			(B)	7.93	5.87--6.59	4.11	10.11
(C)	8.69	6.44--7.27	3.42	20.12	benzene.....[6]		(C)	8.75	6.59--7.42	3.37	26.78
(D)	9.55	7.33--8.17	2.81	43.54			(D)	9.41	7.42--7.80	2.90	17.94
(E)	10.16	7.90--10.21	2.47	142.86	naphthalene.....[10]		(E)	10.45	7.88--10.39	2.33	247.05
(F)	13.49	10.21--11.37	1.35	34.88			(F)	13.35	10.39--11.19	1.38	36.41
(G)	14.15	11.37--12.83	1.22	52.25	acenaphthylene.....[12]		(G)	13.91	11.19--12.77	1.27	181.47
(H)	16.31	12.93--13.69	0.94	8.63	phenanthrene.....[14]		(H)	16.02	12.77--13.54	0.97	26.56
(I)	17.80	13.69--15.17	0.81	21.48	pyrene.....[16]		(I)	17.51	13.52--14.90	0.83	72.32
(J)	19.54	15.17--16.12	0.71	10.03	fluoranthene.....[16]		(J)	19.20	14.90--15.93	0.73	46.48
(K)	20.54	16.12--17.40	0.67	8.47	acephenanthrylene.....[16]		(K)	20.25	15.93--17.12	0.68	31.34
(L)	22.89	17.39--19.17	0.60	14.83	cyclopenta[cd]pyrene.....[18]		(L)	22.21	17.12--18.57	0.62	75.41
(M)	25.23	18.82--19.61	0.56	2.75			(M)	24.91	18.80--19.56	0.56	15.91
(N)	26.83	19.62--20.55	0.54	4.11			(N)	26.22	19.56--20.22	0.55	14.16
(O)	28.02	20.51--21.48	0.53	3.35			(O)	27.43	20.22--21.13	0.53	13.73
(P)	30.22	21.48--22.02	0.51	2.05			(P)	29.59	21.13--21.93	0.52	16.87
(Q)	31.43	22.20--22.98	0.51	2.95	benzo[ghi]perylene.....[22]		(Q)	30.56	21.93--22.73	0.51	16.99
(R)	33.16	22.98--24.26	0.50	4.72	coronene.....[24]		(R)	32.49	22.73--23.84	0.50	17.92
(S)	35.86	24.26--24.82	0.49	1.11			(S)	35.03	23.84--24.42	0.50	5.61
(T)	36.96	24.82--25.71	0.49	1.61			(T)	36.07	24.42--25.39	0.49	9.33
(U)	39.42	25.79--26.55	0.49	1.88			(U)	38.28	25.39--26.12	0.49	10.44
(V)	41.51	26.55--27.93	0.49	4.08			(V)	40.31	26.12--27.30	0.49	23.03
(W)	45.97	28.04--28.82	0.48	0.67			(W)	42.47	27.30--28.47	0.49	5.54
(X)	48.59	28.82--29.64	0.48	0.86			(X)	47.13	28.47--29.32	0.48	4.29
(Y)	51.40	29.72--31.14	0.48	2.11	naphtho[8,1,2,abc]coronene [30]		(Y)	50.21	29.32--30.65	0.48	14.34

Table 4.5 -- Comparison of HPLC/UV Results from JSR and PFR.

5. DATA OVERVIEW

A complete set of stable species measurements of fixed gases, light hydrocarbons, aromatics, PAH, and soot for each of the 5 reactor conditions studied are presented. Two baseline cases for ethylene combustion in the JSR, fuel equivalence ratios (ϕ) of 2.18 and 2.37, and temperature of 1630 K were studied. These experimental conditions correspond to non-sooting and incipient sooting conditions, respectively, in the JSR. In both cases, soot which was defined as methylene chloride insoluble material, was observed at the end of the PFR.

Studies were also performed in which additional ethylene was injected into the PFR in order to test the effect of additional fuel introduced into the hydrocarbon-rich, hot pyrolysis zone in the PFR. The ethylene injection experiments were performed for both equivalence ratio cases. For the ϕ = 2.18 case, the amount of ethylene injected was equal to the difference in ethylene fuel fed to the JSR between ϕ = 2.18 and ϕ = 2.37. In this way we could examine the incremental effect of fuel added to the oxidation zone (JSR) versus the pyrolysis zone (PFR). Benzene was also injected into the PFR for the ϕ = 2.18 case. The effect of an intact aromatic ring on PAH and soot production was quite dramatic, as has been observed by others in the past. The role of intact aromatic rings in PAH and soot growth may be to provide "building blocks" by which the addition of aliphatic species to the intact aromatic ring can cause the molecular weight growth process to occur. Table 4.1 summarizes the experimental operating conditions for the 5 cases.

Table 5.1: Summary of Experimental Conditions

	Case 1	Case 2	Case 3	Case 4	Case 5
Feed to JSR Flow rates (moles/sec)					
C_2H_4	4.44×10^{-2}	4.44×10^{-2}	4.08×10^{-2}	4.08×10^{-2}	4.08×10^{-2}
O_2	5.60×10^{-2}	5.60×10^{-2}	5.60×10^{-2}	5.60×10^{-2}	5.60×10^{-2}
N_2	2.23×10^{-1}	2.23×10^{-1}	2.45×10^{-1}	2.45×10^{-1}	2.45×10^{-1}
Ar	2.29×10^{-3}	2.29×10^{-3}	2.29×10^{-3}	2.29×10^{-3}	2.29×10^{-3}
Injection Flow Rates (moles/sec)					
N_2	2.48×10^{-3}	0	2.48×10^{-3}	0	2.48×10^{-3}
C_2H_4	0	2.67×10^{-3}	0	3.61×10^{-3}	0
C_6H_6	0	0	0	0	7.08×10^{-4}
Experimental Conditions					
ϕ	2.37	2.37	2.18	2.18	2.18
JSR T(K)	1630	1630	1630	1630	1630
JSR τ(ms)	5.74	5.74	5.38	5.38	5.38

The temperature for Case 1 was 1630K in the JSR, 1580K at the first PFR point, and fell to 1540K by the end of the PFR. Additional ethylene (0.82% by mole of total flow, or 6.0% of fuel flow) was injected for Case 2, and temperature dropped by about 30K at the end of the PFR. The temperature at the end of the PFR for Case 3 was 1550K. For Cases 4 and 5, ethylene and benzene were injected into the PFR in amounts corresponding to 8.8% and 1.7% of the fuel ethylene, respectively (moles injected/mole fuel C_2H_4 fed to the JSR). These injection flows correspond to 1.0% and 0.2% by moles of the total flow, and it was expected that the temperature would not be changed greatly from the no injection case. In fact, the maximum temperature perturbation which was observed was for the injection of C_6H_6, which decreased the temperature by 20K at the end of the PFR from the no injection case. Thus, the injection of small amounts of hydrocarbons into the fuel-rich zone of the PFR did not drastically alter the temperature.

For each of the 5 experimental conditions studied, species concentration profiles for fixed gases, light hydrocarbons, aromatics, PAH, tar and soot data are presented in Figures 4.1 - 4.45. The data points at zero residence time correspond to samples obtained from the JSR. The rest of the data points were obtained in the PFR by positioning the PFR probe at varying elevations. The combustion gas leaving the JSR passes through 8 outlets ports and proceeds through the zirconia flow straightening section. Because the PFR probe cannot physically be positioned in the flow straightening section, the first data point sampled in the PFR corresponds to an additional residence

time of 1.7 msec. This 1.7 msec residence time was calculated assuming plug-flow behavior in the 8 exhaust ports and through the flow straightening section. The flow in this transition region is not well-characterized, and so the polynomial fits to the data do not include the JSR point. Consequently, the curves are not extrapolated back to the JSR data point.

In addition to the species concentration profiles, limited measurements of PAH species with molecular weights greater than cyclopenta(cd)pyrene were obtained using high-performance liquid chromatography (HPLC). These measurements identified species with molecular weights up to naphtho(8,1,2,abc)coronene ($C_{30}H_{14}$), including benzo(ghi)perylene ($C_{22}H_{12}$) and coronene ($C_{24}H_{12}$). The total mass of tar collected was determined using a microgravimetric technique, as discussed earlier. Finally, transmission electron microscopy (TEM) measurements were used to determine if solid particulates were present under our reactor conditions, and to estimate the size of the soot spherules found in the aggregates. This information was used in kinetics calculations involving soot particles.

5.1 Case 1: ϕ = 2.37, No Injection

The baseline case is ethylene combustion at an equivalence ratio of 2.37, JSR temperature of 1630K. Temperature in the PFR was 1580K at the first data point and fell to 1540K by the end of the PFR. This experimental condition corresponds to an incipient sooting condition in the JSR. Figures 5.1 through 5.9 summarize the chemical species measurements for Case 1.

Figure 5.1 shows the fixed gas species observed in the JSR/PFR. As is observed in the post-flame zone of flat-flames, the major species are CO, CO_2, H_2, H_2O, and O_2. The O_2 measurements, as discussed earlier, were not accurate at very low O_2 concentrations (less than 0.5%), and so measurements in the PFR are not presented. Water is not measured, but may be calculated from atom mass balances. Carbon monoxide is the major product, on a molar basis, and its concentration is increasing slightly in the PFR. The second most abundant species, hydrogen, also shows a gradually increasing profile in the PFR. Carbon dioxide concentration is almost constant, showing only a slight increase.

Figure 5.2 shows the C_1 and C_2 species: CH_4, C_2H_2, C_2H_4, and C_2H_6. Acetylene is the dominant species (about 3 mole percent), and its profile shows a slight decrease in the PFR. Although C_2H_2 has been proposed as a growth species in both PAH and soot formation, its concentration is so high compared to the total PAH and soot concentrations that even rapid growth rates in PAH and soot will not consume the bulk of the C_2H_2 present in the PFR. Methane is also produced, and decreases from 1 mole percent to 0.8 mole percent during

the 15 msec PFR residence time. Ethylene mole fraction in the JSR is quite high, $5x10^{-3}$, drops precipitously before measurement of the first PFR point to a value of $7x10^{-4}$, and declines to a final concentration of $3x10^{-4}$ at the end of the PFR. The ethane concentration shows an even more dramatic decrease, from $2x10^{-4}$ in the JSR, to $2x10^{-5}$ at the first PFR point, to a final mole fraction of $3x10^{-6}$. From elementary kinetic modeling studies, the radical concentrations are predicted to decrease dramatically in the flow straightening section before the first PFR data point. The effect of probe quenching in the JSR probe is also important, expecially for ethane, which is predominantly formed from methyl-methyl recombination. Species such as ethylene and ethane cannot be modelled in the JSR without taking these effects into consideration.

The C3 and C4 species are shown in Figure 5.3. Of the C3 species, methyl-acetylene (CH_3-C≡CH) is about twice as much as allene (CH_2=C=CH_2). Although the concentrations of these C3 species are relatively high, we do not detect any C3-substituted aromatics or PAH. Diacetylene is the most abundant C4 species, followed by vinylacetylene, 1,3-butadiene, and 1-butyne. Other C4 species which are just barely detectable include 2-butyne and 1-butene.

Figure 5.4 shows the major species which are determined from the C4-C8 analysis. The mole fractions of diacetylene, vinylacetylene and 1,3-butadiene are redundant measurements and are compared with the C3-C4 analysis to check for accuracy. Of the higher molecular weight material which can be analyzed in the gas phase, benzene is the dominant species. Its concentration is an order of magnitude higher

than the next most abundant species, triacetylene and phenylacetylene. A C5 species, cyclopentadiene, is observed and shows a decreasing profile in the PFR. Toluene is a factor of 3 lower than cyclopentadiene and also shows a decreasing profile. Styrene and tetra-acetylene were at the detection limit for obtaining a full profile, and their concentrations were approximately 1 ppm.

Figures 5.5 through 5.8 summarize the PAH species which were present in concentrations high enough to obtain a full profile. The two-ring aromatic species naphthalene and indene show an order of magnitude increase in the PFR. The larger species such as pyrene and cyclopenta(cd)pyrene show even larger increases in the PFR. For example, cyclopenta(cd)pyrene mole fraction increases from $1x10^{-7}$ to $3x10^{-6}$, or a factor of 30. The PAH data shows some scatter, but the general trend of a substantial increase in PAH concentration with increasing residence time is observed.

The total amount of high molecular weight tar material and soot is shown in Figure 5.9. The soot profile shows a very dramatic increase from essentially zero at the JSR to a concentration of $1x10^{-7}$ g/cm^3 by the end of the PFR. The tar concentration reaches a value of $4.2x10^{-8}$ g/cm^3. The total tar profile in the PFR is increasing, but the rate of increase declines at long residence times. At early residence times in the PFR, there is actually more tar than soot, based on mass concentration. The ratio of tar to soot decreases from 2 at the beginning of the PFR to 0.4 by the end of the PFR. The relative amounts of soot and tar reflect the fact that the conditions we are studying are very lightly sooting, compared with some of the

flat-flame studies. For example, in a study of atmospheric pressure, sooting (C/O=0.635) methane-oxygen laminar flat-flames, D'Alessio (1974) and co-workers found that the mass ratio of PAH to soot decreases from about 0.25 at a burner height of 7 mm to 0.013 at a height of 20 mm.

The shapes of the soot and total tar profiles are also quite different. The soot profile is increasing at an increasing rate, while the tar profile is increasing, but the rate of increase is decreasing. If one makes a simple hypothesis that the soot mass growth rate is directly proportional to the mass of tar and the only source of soot mass is from the tar, then we would expect the slope of the soot profile to be increasing, because the total mass of tar is increasing.

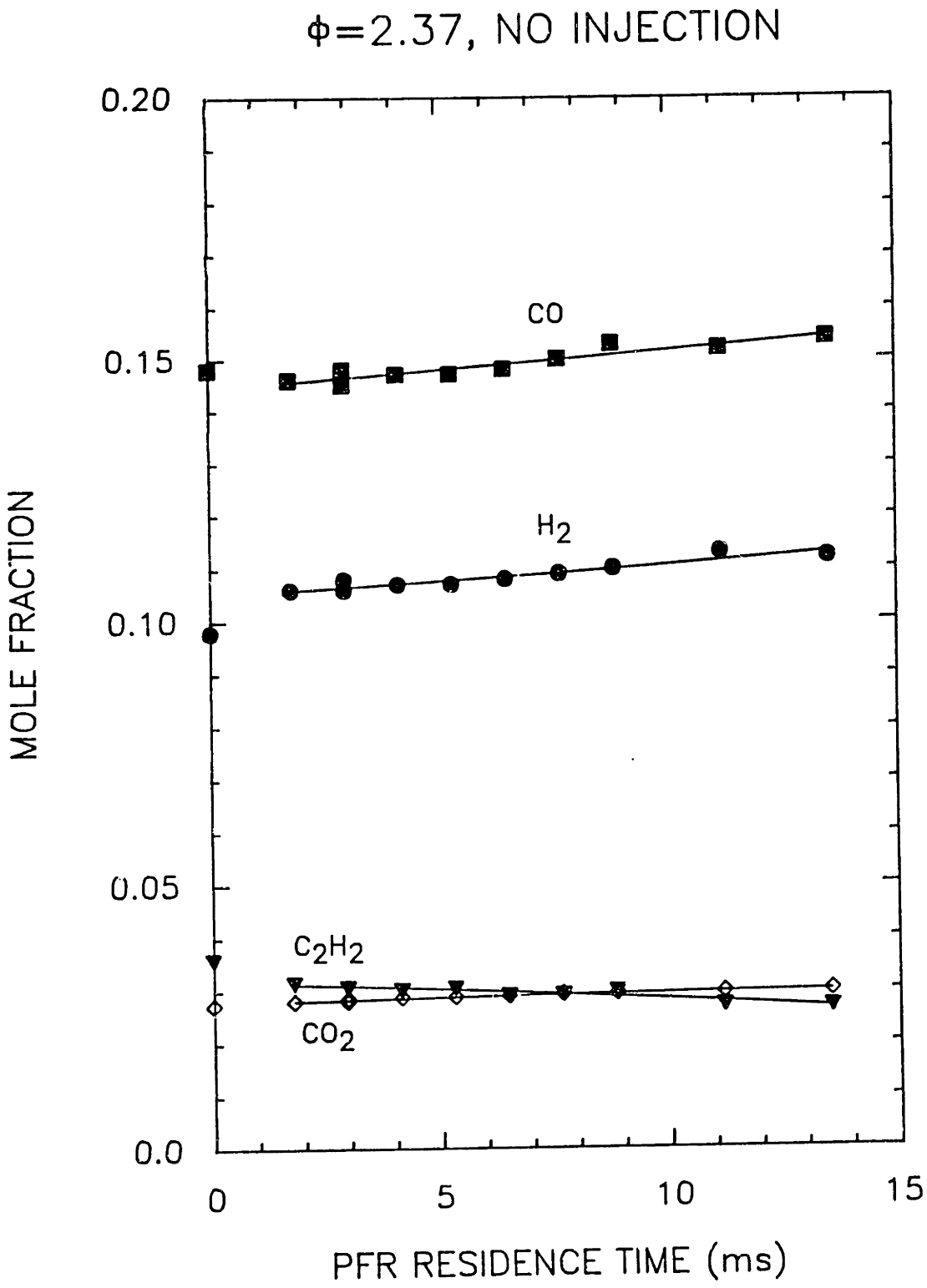

Figure 5.1 Mole Fraction Profiles for CO, CO_2, H_2, and C_2H_2 for Case 1: ϕ=2.37, $C_2H_4/O_2/N_2$ combustion in the JSR/PFR with no injection. Curves are polynomial fits to the data.

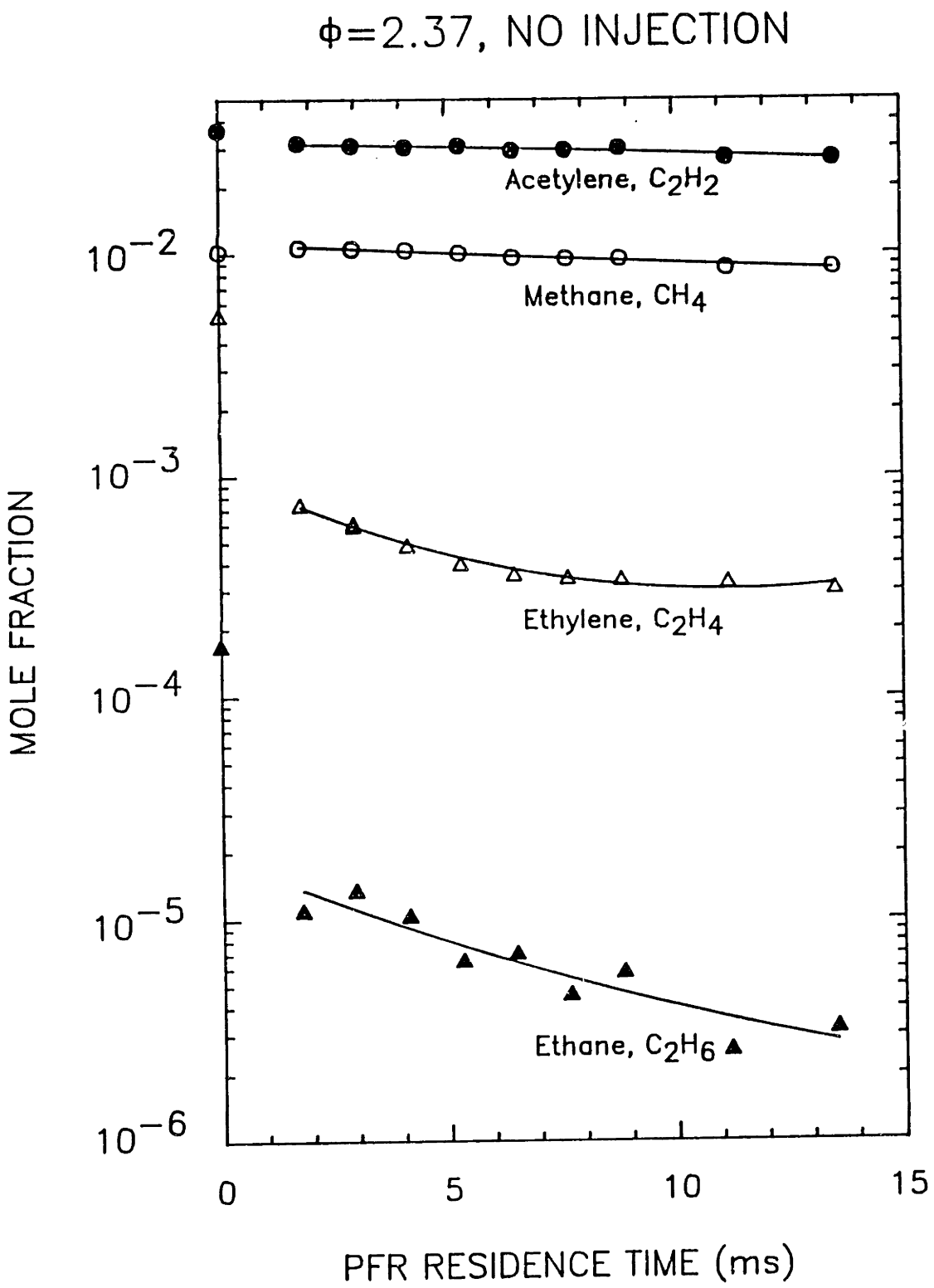

Figure 5.2 Mole Fraction Profiles for CH_4, C_2H_2, C_2H_4, and C_2H_6 for Case 1: ϕ=2.37, $C_2H_4/O_2/N_2$ combustion in the JSR/PFR with no injection. Curves are polynomial fits to the data.

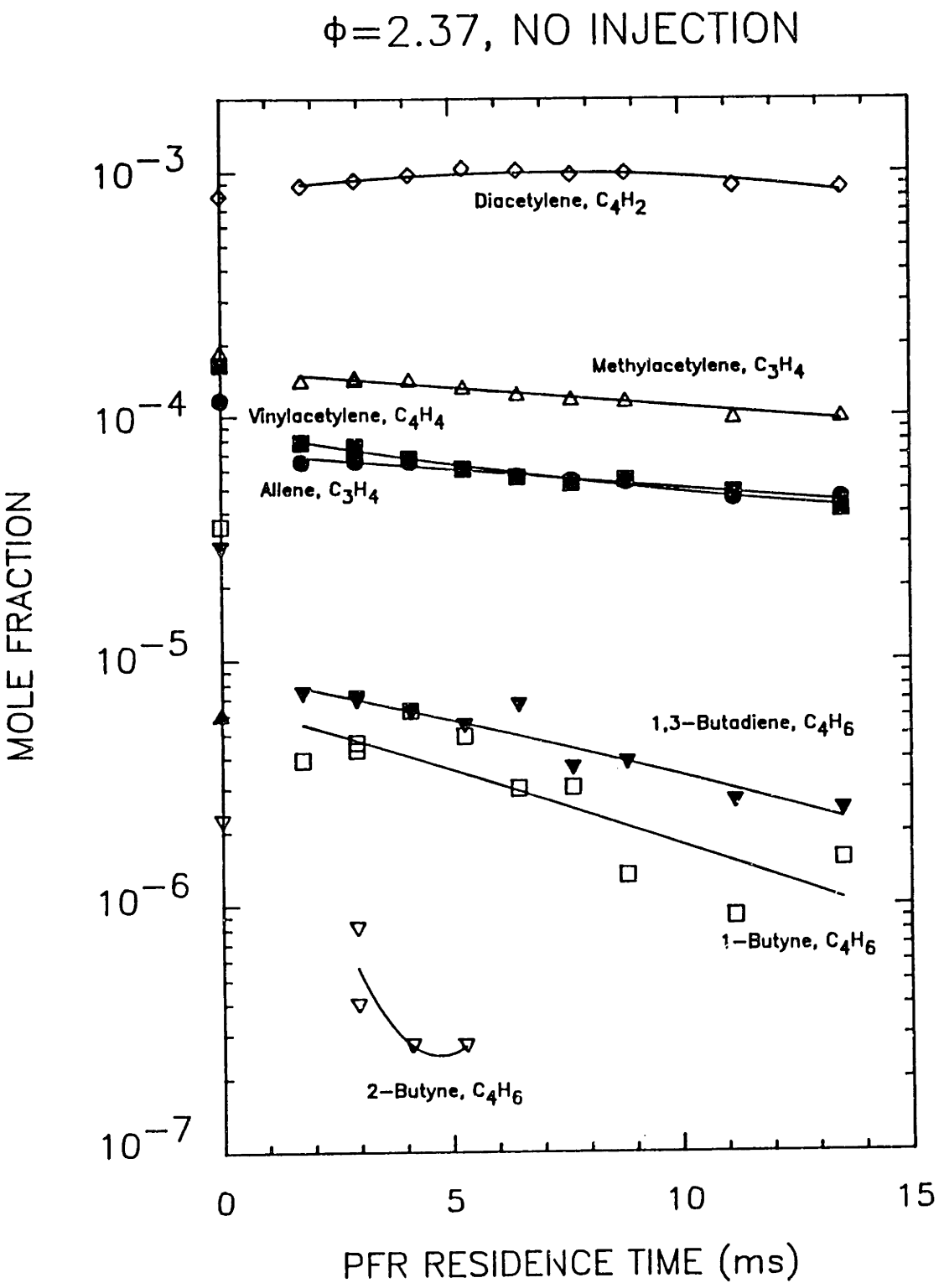

Figure 5.3 Mole Fraction Profiles for C_3 and C_4 species for Case 1: ϕ=2.37, $C_2H_4/O_2/N_2$ combustion in the JSR/PFR with no injection. Curves are polynomial fits to the data.

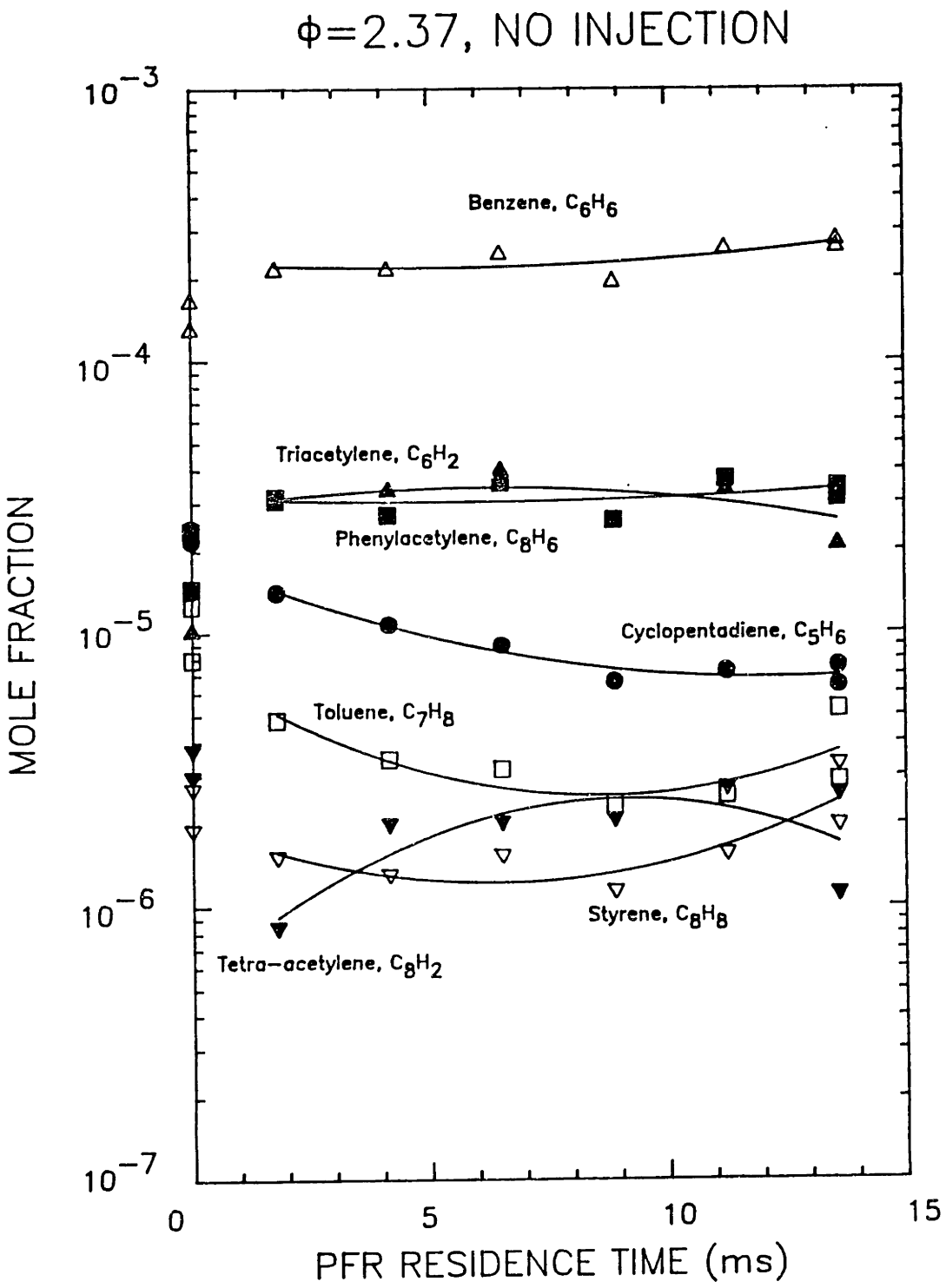

Figure 5.4 Mole Fraction Profiles for C_5 - C_8 species for Case 1: ϕ=2.37, $C_2H_4/O_2/N_2$ combustion in the JSR/PFR with no injection. Curves are polynomial fits to the data.

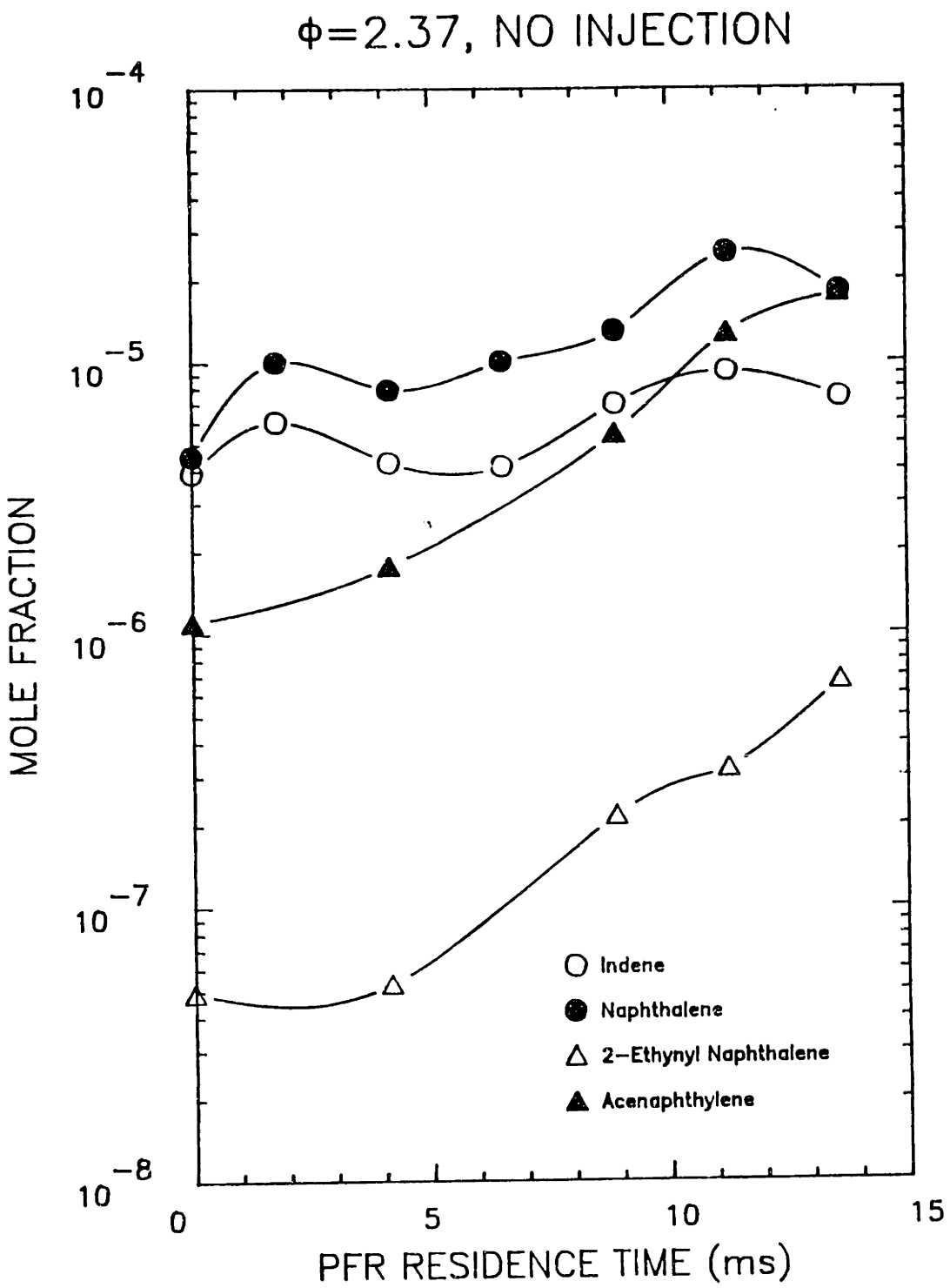

Figure 5.5 Mole Fraction Profiles for 116 - 152 amu species for Case 1: ϕ=2.37, $C_2H_4/O_2/N_2$ combustion in the JSR/PFR with no injection. Curves are visual fits to the data.

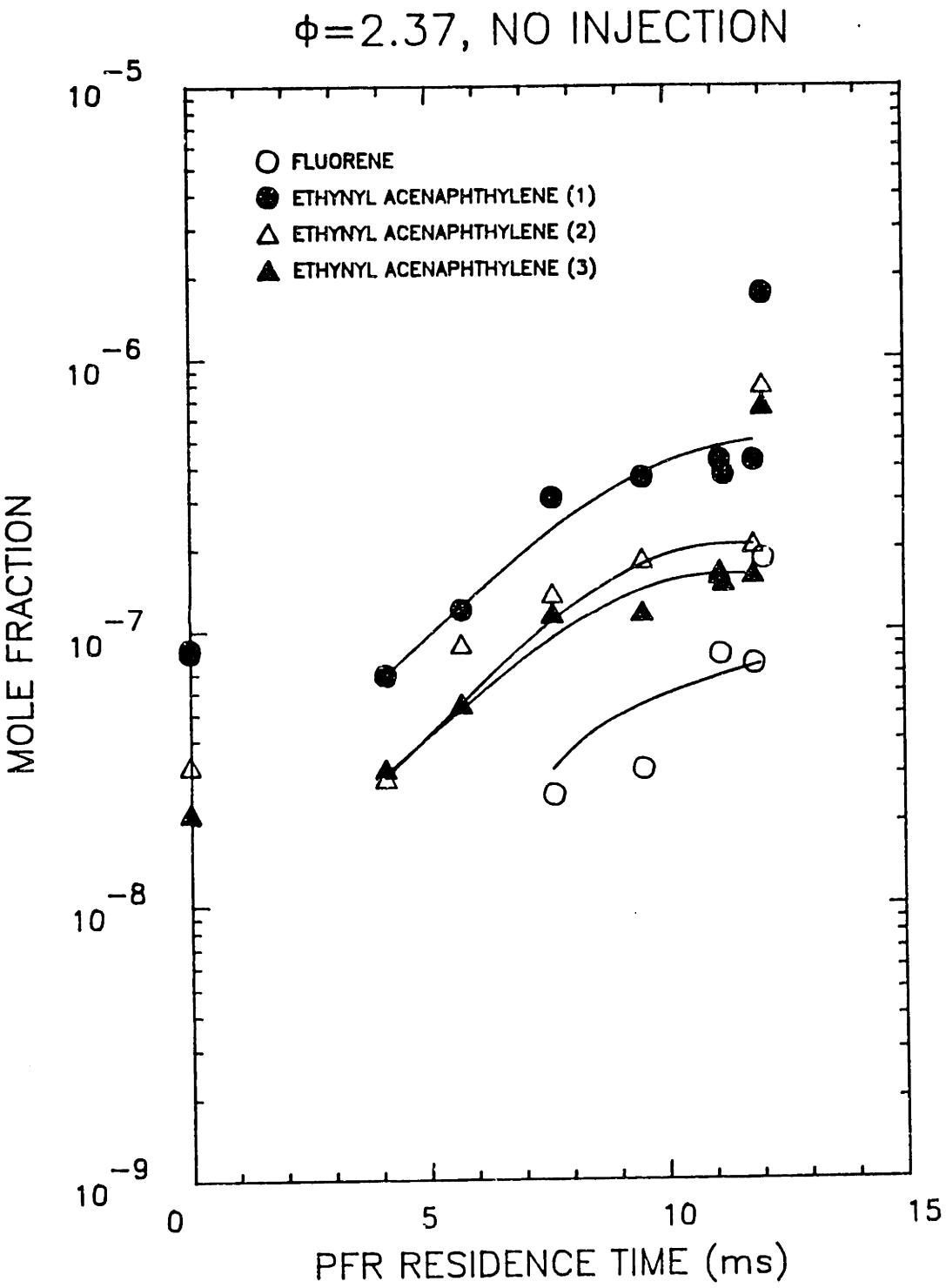

Figure 5.6 Mole Fraction Profiles for 166 - 176 amu species for Case 1: ϕ=2.37, $C_2H_4/O_2/N_2$ combustion in the JSR/PFR with no injection. Curves are visual fits to the data.

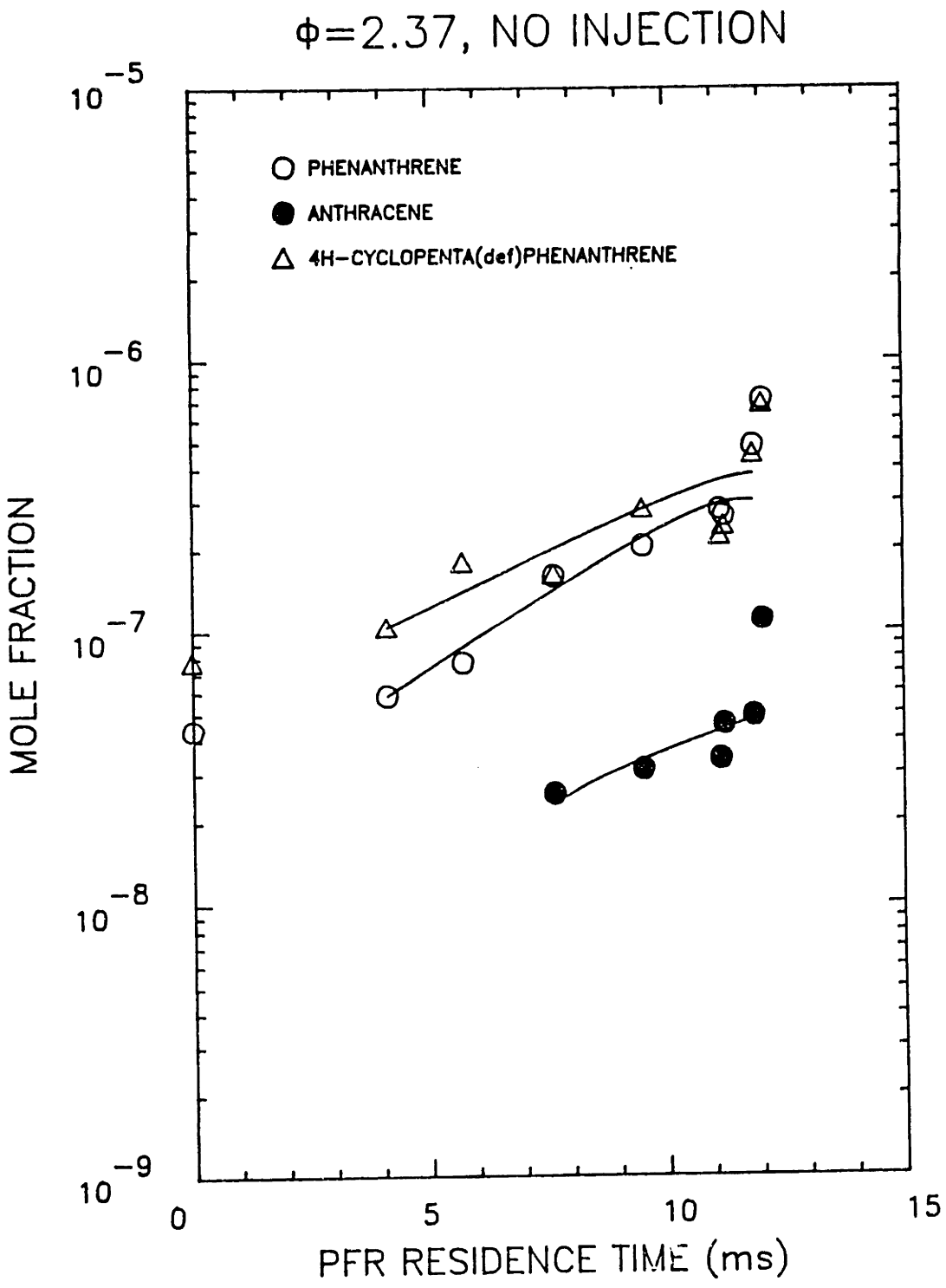

Figure 5.7 Mole Fraction Profiles for 178 - 190 amu species for Case 1: ϕ=2.37, $C_2H_4/O_2/N_2$ combustion in the JSR/PFR with no injection. Curves are visual fits to the data.

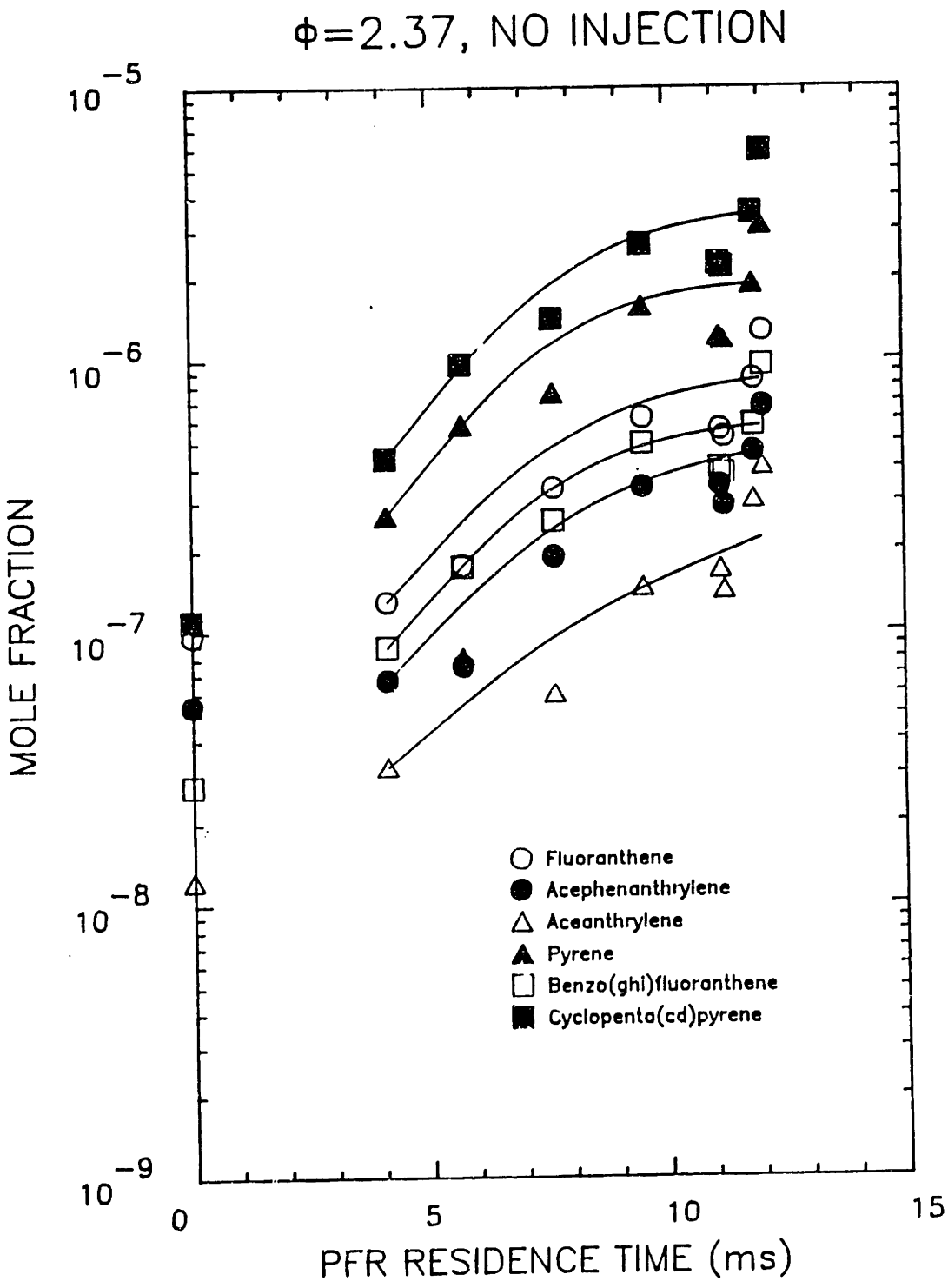

Figure 5.8 Mole Fraction Profiles for 202 - 226 amu species for Case 1: ϕ=2.37, $C_2H_4/O_2/N_2$ combustion in the JSR/PFR with no injection. Curves are visual fits to the data.

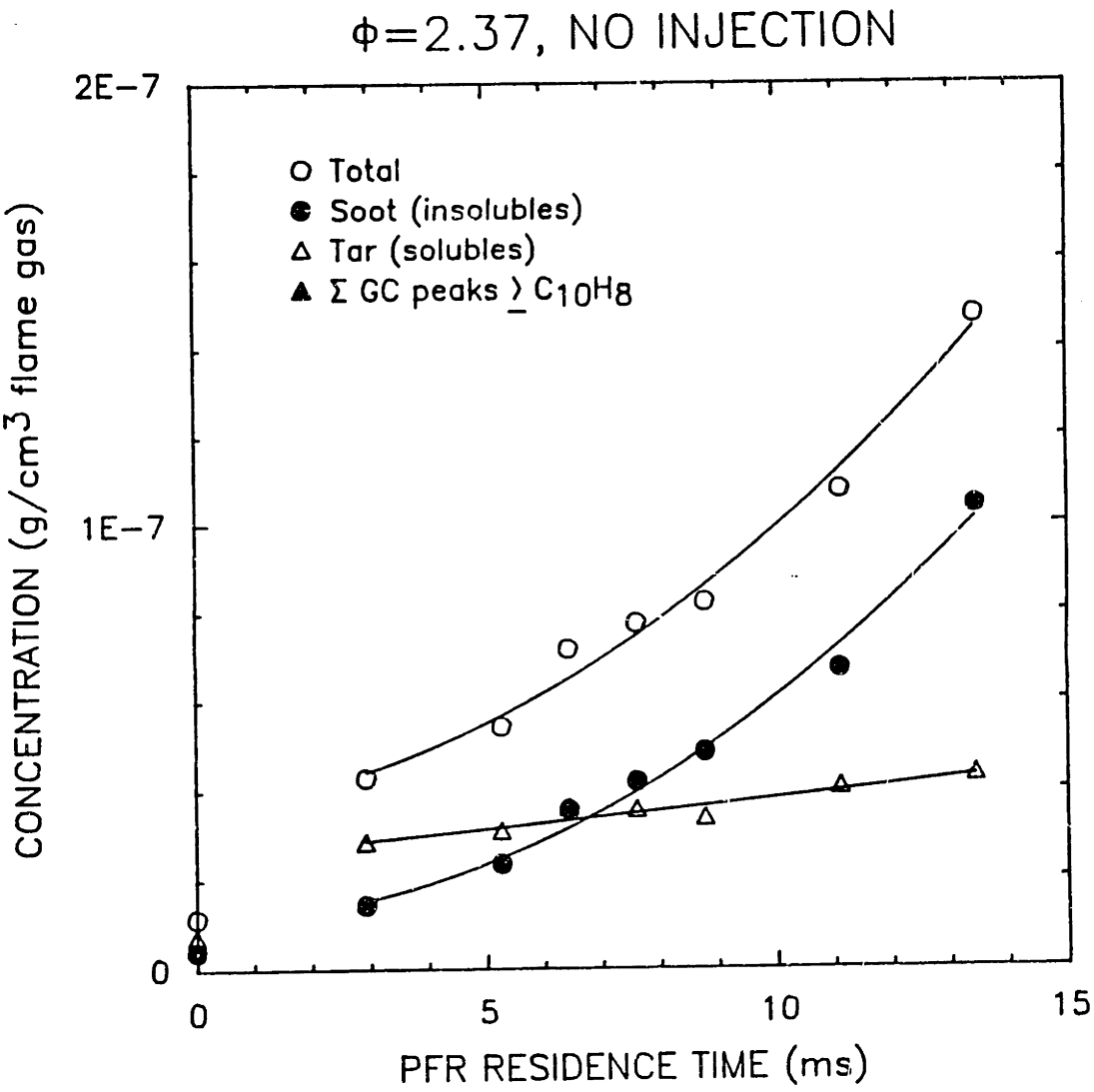

Figure 5.9 Mass Concentration Profiles for ΣGC PAH (128-226 amu), tar (CH_2Cl_2-soluble material), and soot (CH_2Cl_2-insoluble material) for Case 1: ϕ=2.37, $C_2H_4/O_2/N_2$ combustion in the JSR/PFR with no injection. Curves are polynomial fits to the data.

5.2 Case 2: ϕ = 2.37, C_2H_4 Injection

The injection of ethylene into the PFR tested the effect of additional aliphatic hydrocarbons on the production of higher molecular weight products. By injecting a small amount of C_2H_4 (0.8% by moles of the total flow), we tried to maintain the overall chemical and temperature environment of the baseline case. The goal was to see how the other species profiles respond to the perturbation of the injected C_2H_4 Figures 5.10 through 5.18 show a summary of the experimental data for Case 2.

The major fixed gases shown in Figure 5.10 are not affected by the injection of C_2H_4. In general, species which are present in concentrations much higher than the concentration of the injected species would not be expected to show a large perturbation. As a hypothetical example, if all of the injected C_2H_4 were oxidized to CO and no other species profiles were affected by the oxidation, the expected increase in the CO mole fraction profile would be 0.016 from a baseline mole fraction of 0.16, or a 10% increase. Since we are injecting the C_2H_4 into a pyrolysis environment, we expect considerably less than complete conversion of C_2H_4 to CO. Unfortunately, the experimental uncertainties in major species profiles, such as CO (±3%) and H_2 (±3%), are about the same as the expected perturbation from C_2H_4 injection. Thus we cannot determine with accuracy how much of the injected C_2H_4 is converted to CO or H_2.

Figure 5.11 shows the C1 and C2 species profiles. The ethylene profile is dramatically affected by the injection of ethylene. With ethylene injection, the ethylene concentration is an order of

magnitude higher at the first sampling point in the PFR, and declines sharply to a final value twice that of the no injection case. The curves do not extend back to the JSR because the mixing and flow in the transition region between the JSR and the PFR is not well characterized, as mentioned previously. Ethylene is probably converted to acetylene through the very fast reaction sequence

$$C_2H_4 + H = C_2H_3 + H_2 \qquad \text{Rxn (5.1)}$$
$$(+ OH) \qquad (+ H_2O) \qquad \text{Rxn (5.2)}$$

$$C_2H_3 (+M) = C_2H_2 + H \qquad \text{Rxn (5.3)}$$

These hydrocarbon reactions are very fast and compete with O_2 for the radical species. For example, the rate constant at 1600K for the main chain-branching combustion reaction $H + O_2 = O + OH$ is 6.7×10^{11} mol/cc•s, compared with a rate constant of 7.6×10^{12} mol/cc•s for the hydrocarbon reaction $C_2H_4 + H = C_2H_3 + H_2$ (Rxn. 5.1). The very fast rate constant for the hydrocarbon reaction explains why many hydrocarbon species may act as catalysts for H-atom recombination. For example, if the elementary reaction

$$C_2H_3 + H = C_2H_4 \qquad \text{Rxn (5.4)}$$

is added with Reaction 5.1, the overall reaction is

$$H + H = H_2 \qquad \text{Rxn (5.5)}$$

In fuel-rich flames with an abundance of hydrocarbon species, the H-

magnitude higher at the first sampling point in the PFR, and declines sharply to a final value twice that of the no injection case. The curves do not extend back to the JSR because the mixing and flow in the transition region between the JSR and the PFR is not well characterized, as mentioned previously. Ethylene is probably converted to acetylene through the very fast reaction sequence

$$C_2H_4 + H = C_2H_3 + H_2 \qquad \text{Rxn (5.1)}$$
$$(+ OH) \qquad (+ H_2O) \qquad \text{Rxn (5.2)}$$

$$C_2H_3 (+M) = C_2H_2 + H \qquad \text{Rxn (5.3)}$$

These hydrocarbon reactions are very fast and compete with O_2 for the radical species. For example, the rate constant at 1600K for the main chain-branching combustion reaction $H + O_2 = O + OH$ is 6.7×10^{11} mol/cc•s, compared with a rate constant of 7.6×10^{12} mol/cc•s for the hydrocarbon reaction $C_2H_4 + H = C_2H_3 + H_2$ (Rxn. 5.1). The very fast rate constant for the hydrocarbon reaction explains why many hydrocarbon species may act as catalysts for H-atom recombination. For example, if the elementary reaction

$$C_2H_3 + H = C_2H_4 \qquad \text{Rxn (5.4)}$$

is added with Reaction 5.1, the overall reaction is

$$H + H = H_2 \qquad \text{Rxn (5.5)}$$

In fuel-rich flames with an abundance of hydrocarbon species, the H-

atom recombination rate may be enhanced considerably by the hydrocarbon species such as C_2H_4.

Inspection of the acetylene profile reveals that the concentration of C_2H_2 is increased at the end of the PFR by about 20% from a mole fraction of 0.027 to 0.032. If all of the injected C_2H_4 were converted to C_2H_2, then the increase in C_2H_2 mole fraction would be 0.008 and the expected mole fraction of C_2H_2 would be 0.035. Thus the increase in the C_2H_2 concentration may be explained by 62% conversion of the injected C_2H_4 to C_2H_2.

A significant perturbation of the vinylacetylene profile (Figure 5.12) is observed for the C_2H_4 injection. The vinylacetylene concentration is approximately doubled from the no injection case. A plausible mechanism for vinylacetylene formation from ethylene injection is through the reaction sequence

$C_2H_4 + H = C_2H_4 + H_2$		Rxn (5.6)
$C_2H_3 + C_2H_2 = C_4H_5$		Rxn (5.7)
$C_4H_5 = C_4H_4 + H$		Rxn (5.8)

Thus we see that with our relatively high concentrations of C_2H_2, the vinyl radical can add C_2H_2 to form butadienyl radical which can decompose by β-scission of H-atom to form vinylacetylene.

The concentrations of the single-ring aromatic species, such as benzene, cyclopentadiene, and phenylacetylene (Figure 5.13) are also increased by the addition of C_2H_4. These increases are probably from the enhancement of reactions which form benzene, due to the increased

concentrations of the C2 and C4 hydrocarbons. Two of the proposed major routes to aromatics formation are

$$C_4H_3 + C_2H_2 = 1\text{-}C_6H_5 \qquad \text{Rxn (5.9)}$$

$$1\text{-}C_6H_5 = c\text{-}C_6H_5 \qquad \text{Rxn (5.10)}$$

$$c\text{-}C_6H_5 + H_2 = C_6H_6 + H \qquad \text{Rxn (5.11)}$$

and

$$C_4H_5 + C_2H_2 = 1\text{-}C_6H_7 \qquad \text{Rxn (5.12)}$$

$$1\text{-}C_6H_7 = c\text{-}C_6H_7 \qquad \text{Rxn (5.13)}$$

$$c\text{-}C_6H_7 = C_6H_6 + H \qquad \text{Rxn (5.14)}$$

For Reactions 5.12 - 5.13, Westmoreland (1986) has shown that a chemically activated route exists in which the linear C_6H_7 adduct undergoes a unimolecular cyclization rather than stabilization to the thermalized C_6H_7.

The PAH species profiles shown in Figures 5.14 - 5.17 show a general trend of increasing concentration with increasing residence time in the PFR. The ultimate concentrations at the end of the PFR are comparable to those for the no injection case. Differences in the starting concentrations from the JSR may be responsible for the differences between Case 1 and Case 2 at early PFR residence times. Part of the explanation for these differences may be due to the fact that the data for Case 1 were obtained using a different JSR than the data for Case 2. As has been observed by others (Vaughn, 1988), different jet-stirred reactors have slightly different operating characteristics, and the PAH concentrations may be quite sensitive to the particular JSR operating conditions.

Figure 5.18 shows the soot concentration increasing in the PFR from 1.7×10^{-8} g/cm^3 at the first data point in the PFR to 1.8×10^{-7} g/cm^3 at the end of the PFR. The total tar concentration shown in Figure 5.18 shows an increasing profile which starts at 1×10^{-8} g/cm^3 at a PFR residence time of 1.7 msec and reaches a value of 9.5×10^{-7} g/cm^3 at the end of the PFR (14 msec). As seen for Case 1, the ratio of tar to soot decreases from 2 at the first point in the PFR to about 0.4 by the end of the PFR. The absolute concentrations of tar and soot are higher for C_2H_4 injection. Tar is increased by C_2H_4 injection from 4×10^{-8} g/cm^3 to 9×10^{-8} g/cm^3 at the end of the PFR. The soot concentration at the end of the PFR is increased from 1×10^{-7} g/cm^3 for no injection to 1.8×10^{-7} g/cm^3 for the injection of C_2H_4. The observation that the total tar and soot concentrations are increased by C_2H_4 addition may be due to an increase in the single ring aromatics and the additional effect of a moderate (30%) increase in C_2H_2. These two factors, the amount of single-ring aromatics and the amount of C2 aliphatic species may play a key role in determining the total amount of high molecular weight material produced in combustion.

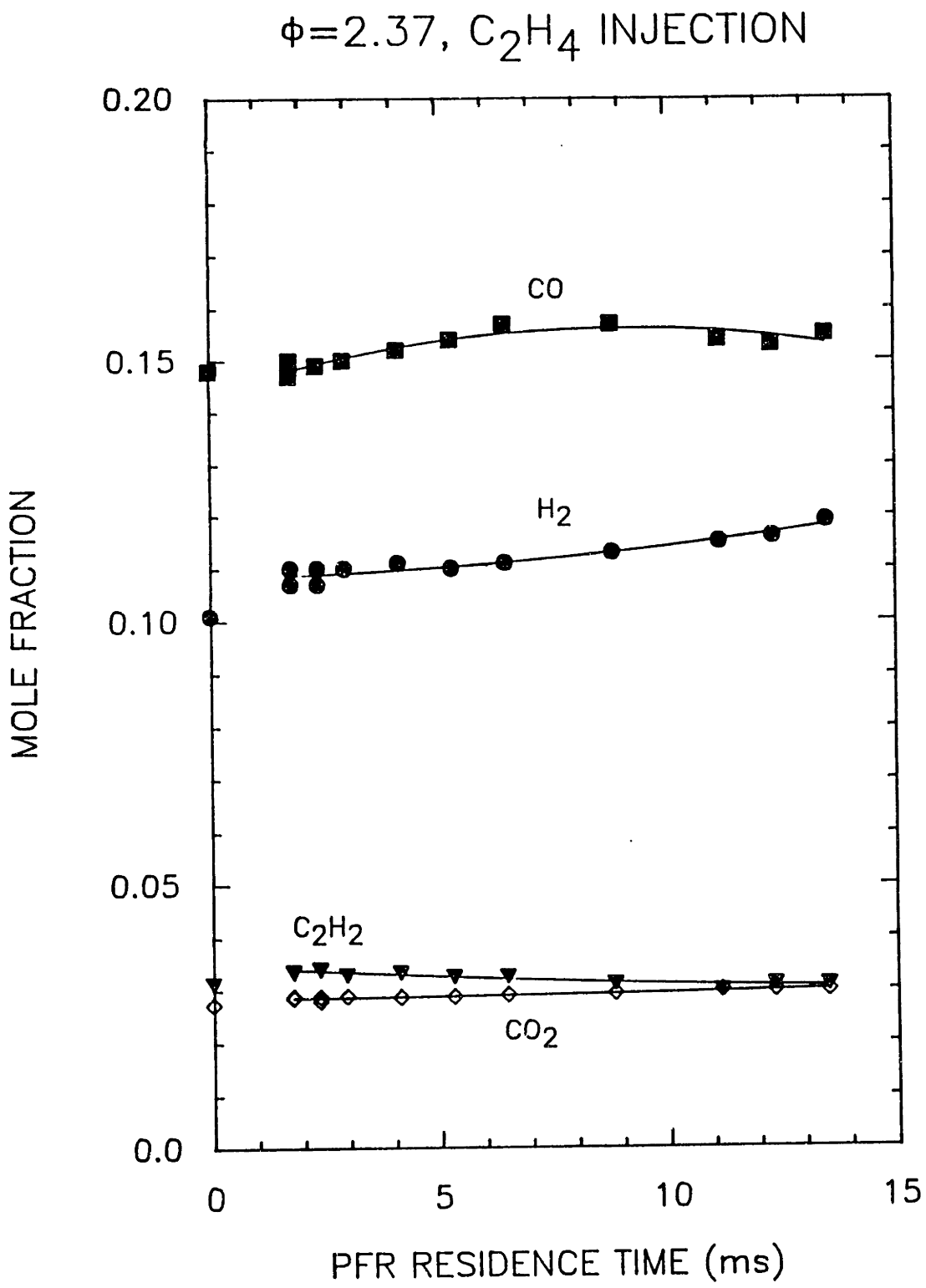

Figure 5.10 Mole Fraction Profiles for CO, CO_2, H_2, and C_2H_2 for $\alpha\psi^2$ ϕ=2.37, $C_2H_4/O_2/N_2$ combustion in the JSR/PFR with C_2H_4 injection. Curves are polynomial fits to the data.

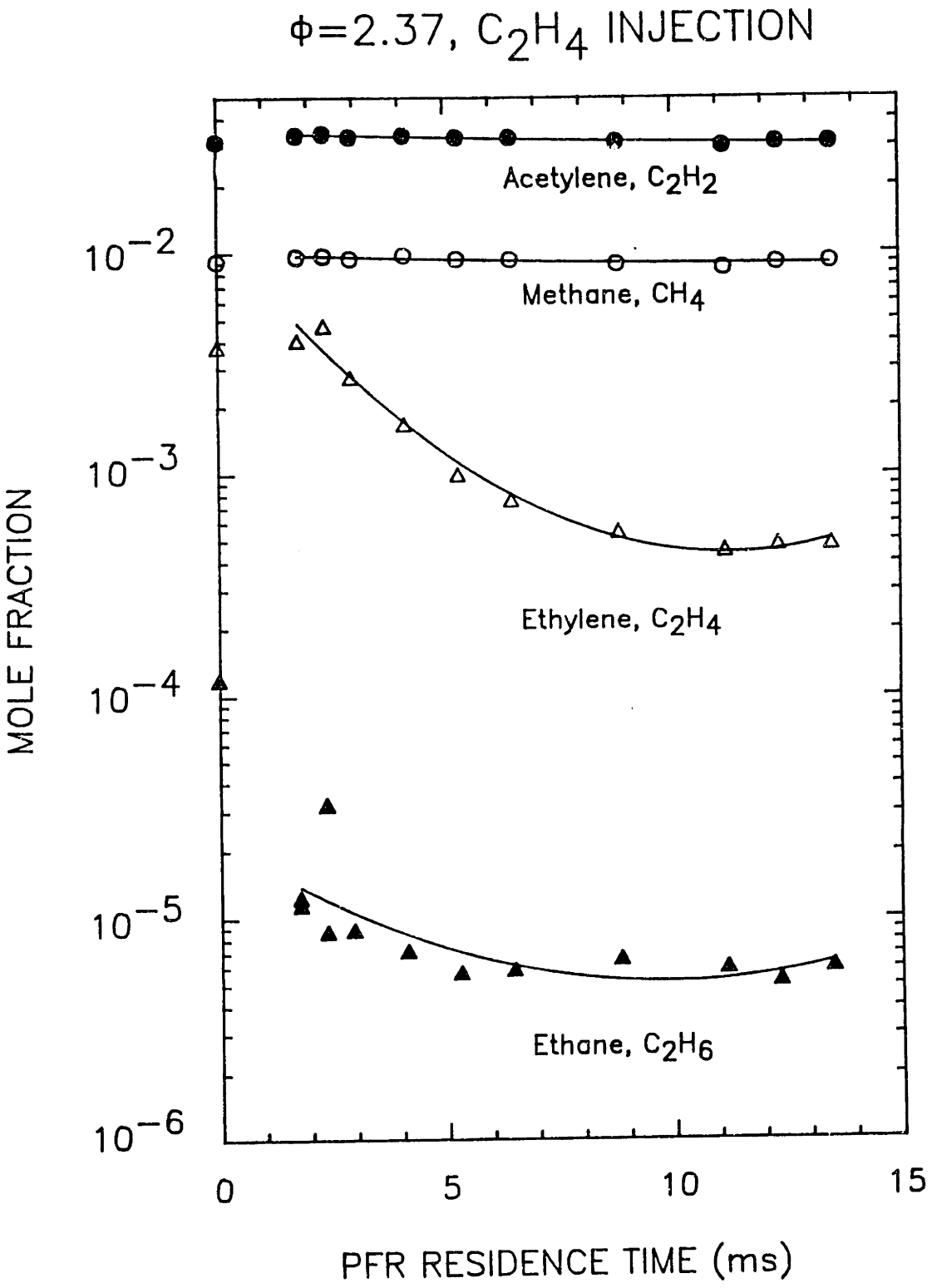

Figure 5.11 Mole Fraction Profiles for CH_4, C_2H_2, C_2H_4, and C_2H_6 for Case 2: ϕ=2.37, $C_2H_4/O_2/N_2$ combustion in the JSR/PFR with C_2H_4 injection. Curves are polynomial fits to the data.

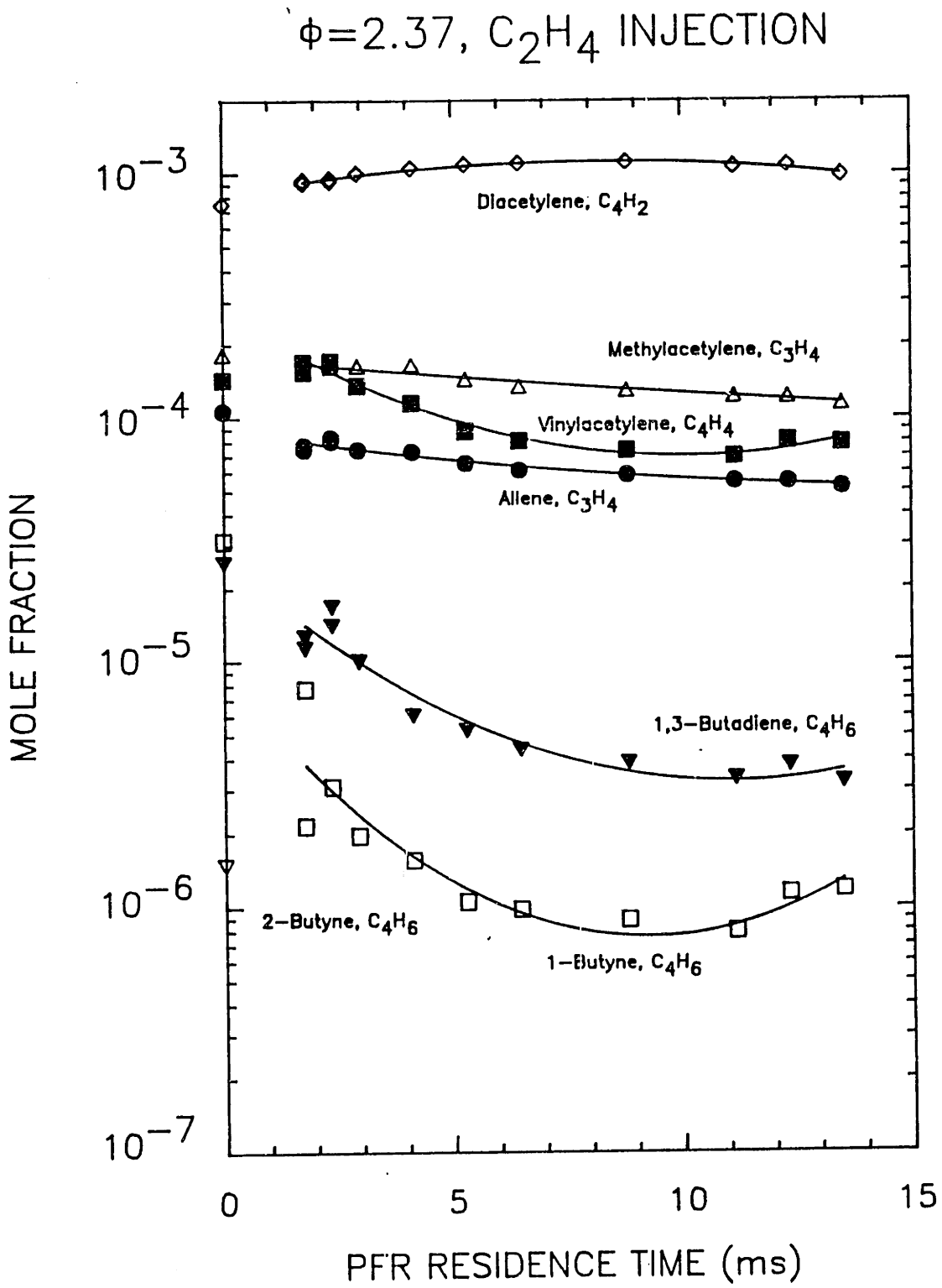

Figure 5.12 Mole Fraction Profiles for C_3 and C_4 species for Case 2: ϕ=2.37, $C_2H_4/O_2/N_2$ combustion in the JSR/PFR with C_2H_4 injection. Curves are polynomial fits to the data.

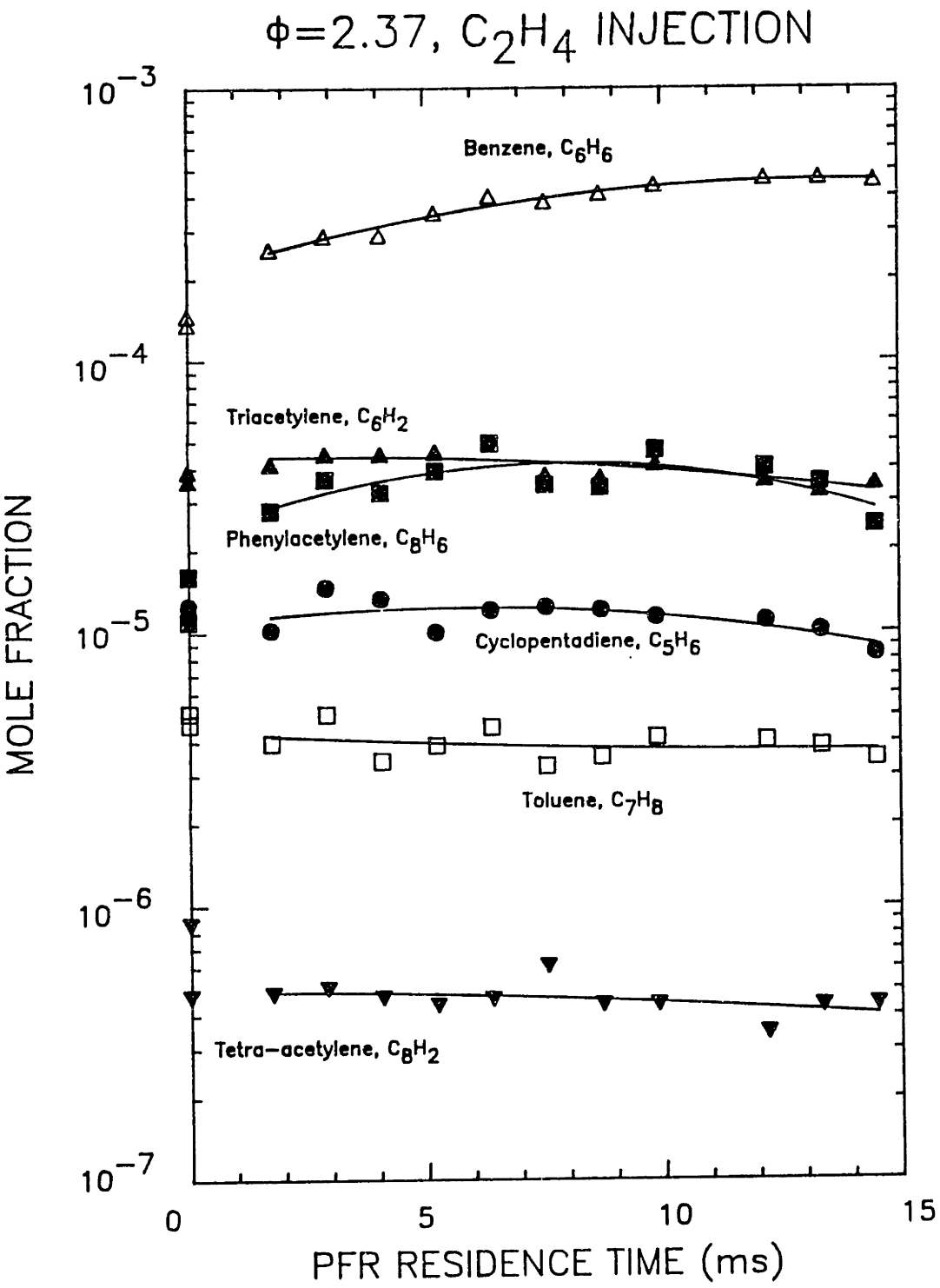

Figure 5.13 Mole Fraction Profiles for C_5 - C_8 species for Case 2: ϕ=2.37, $C_2H_4/O_2/N_2$ combustion in the JSR/PFR with C_2H_4 injection. Curves are polynomial fits to the data.

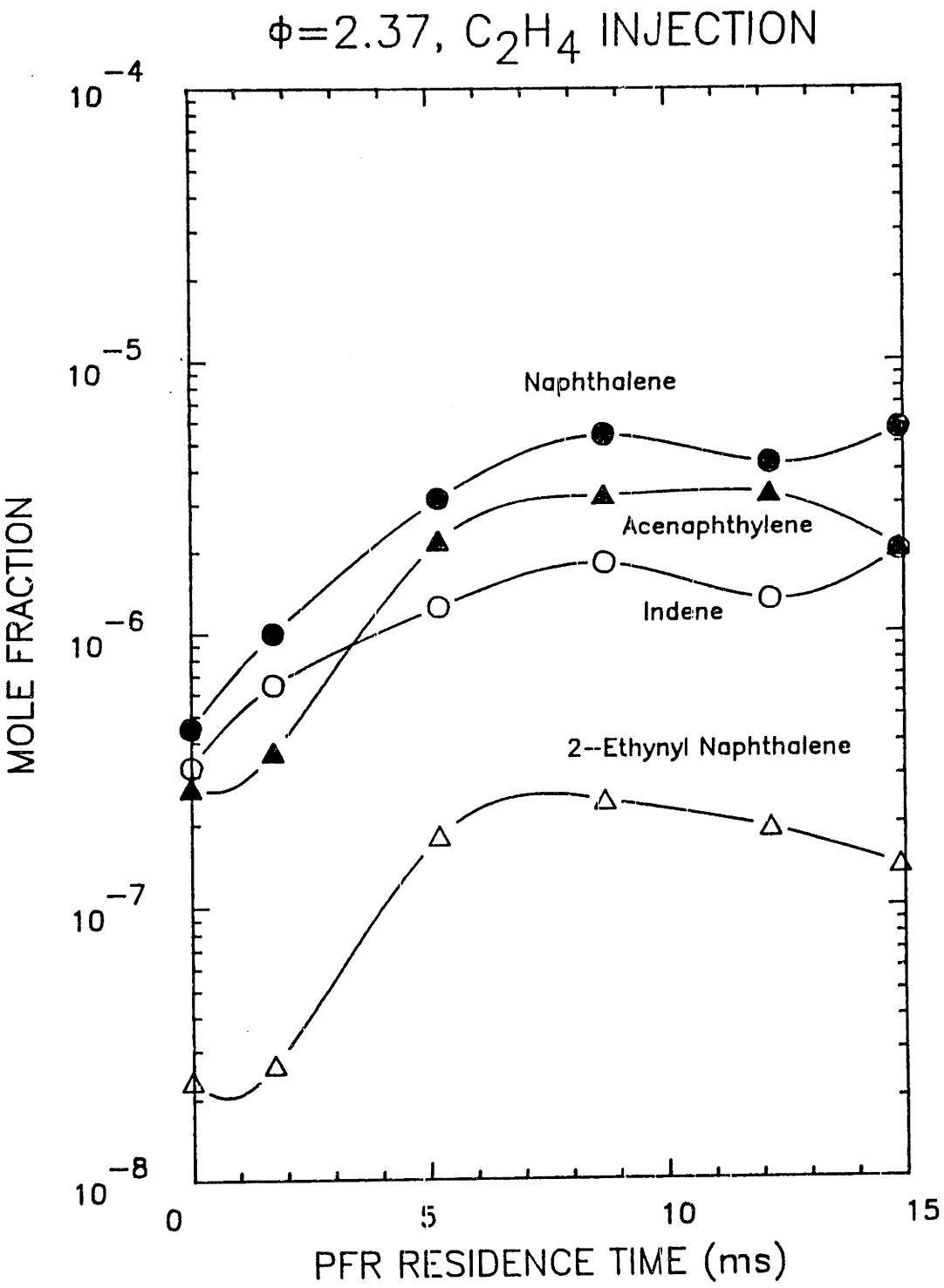

Figure 5.14 Mole Fraction Profiles for 116 - 152 amu species for Case 2: ϕ=2.37, $C_2H_4/O_2/N_2$ combustion in the JSR/PFR with C_2H_4 injection. Curves are visual fits to the data.

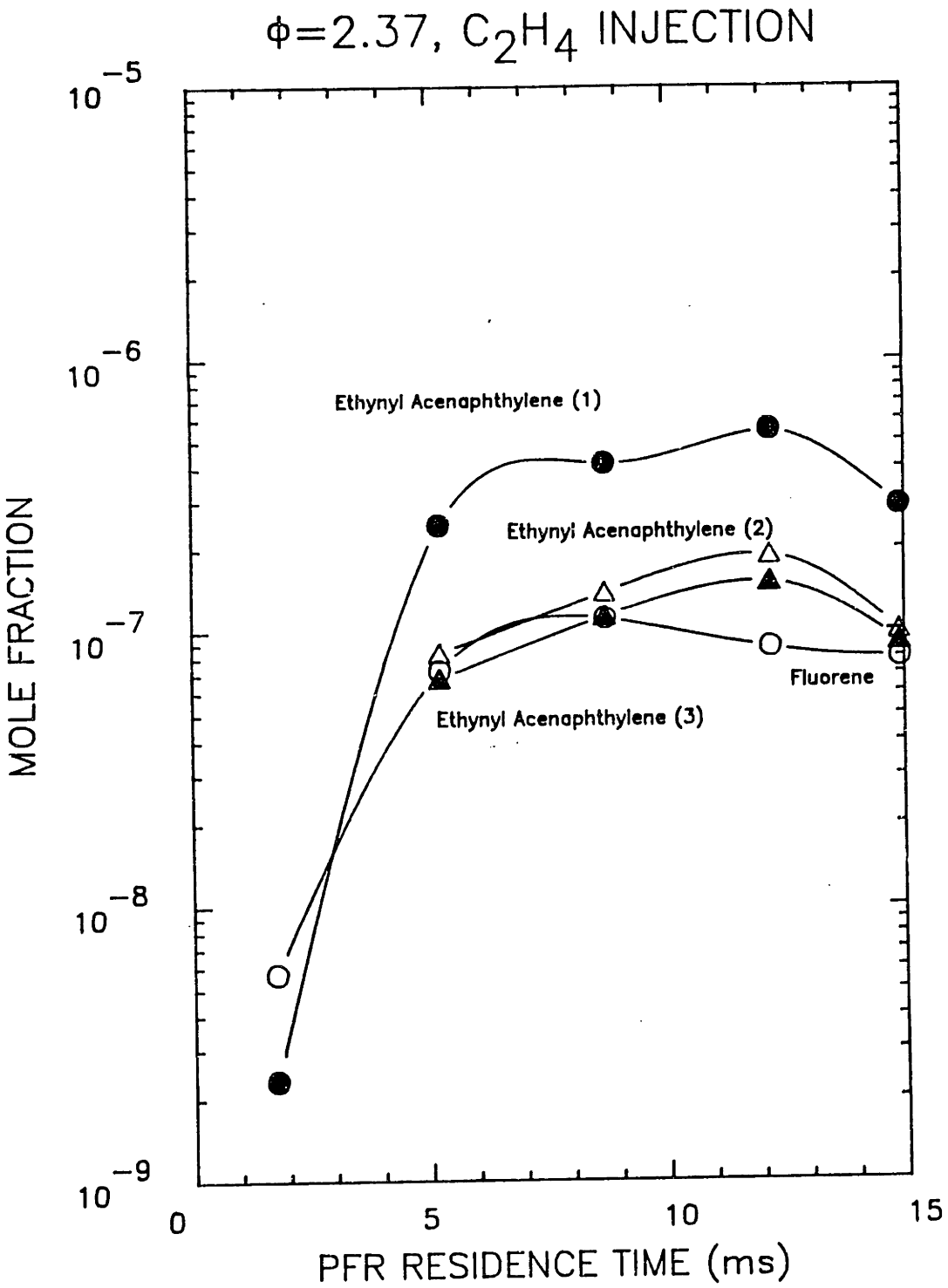

Figure 5.15 Mole Fraction Profiles for 166 - 176 amu species for Case 2: ϕ=2.37, $C_2H_4/O_2/N_2$ combustion in the JSR/PFR with C_2H_4 injection. Curves are visual fits to the data.

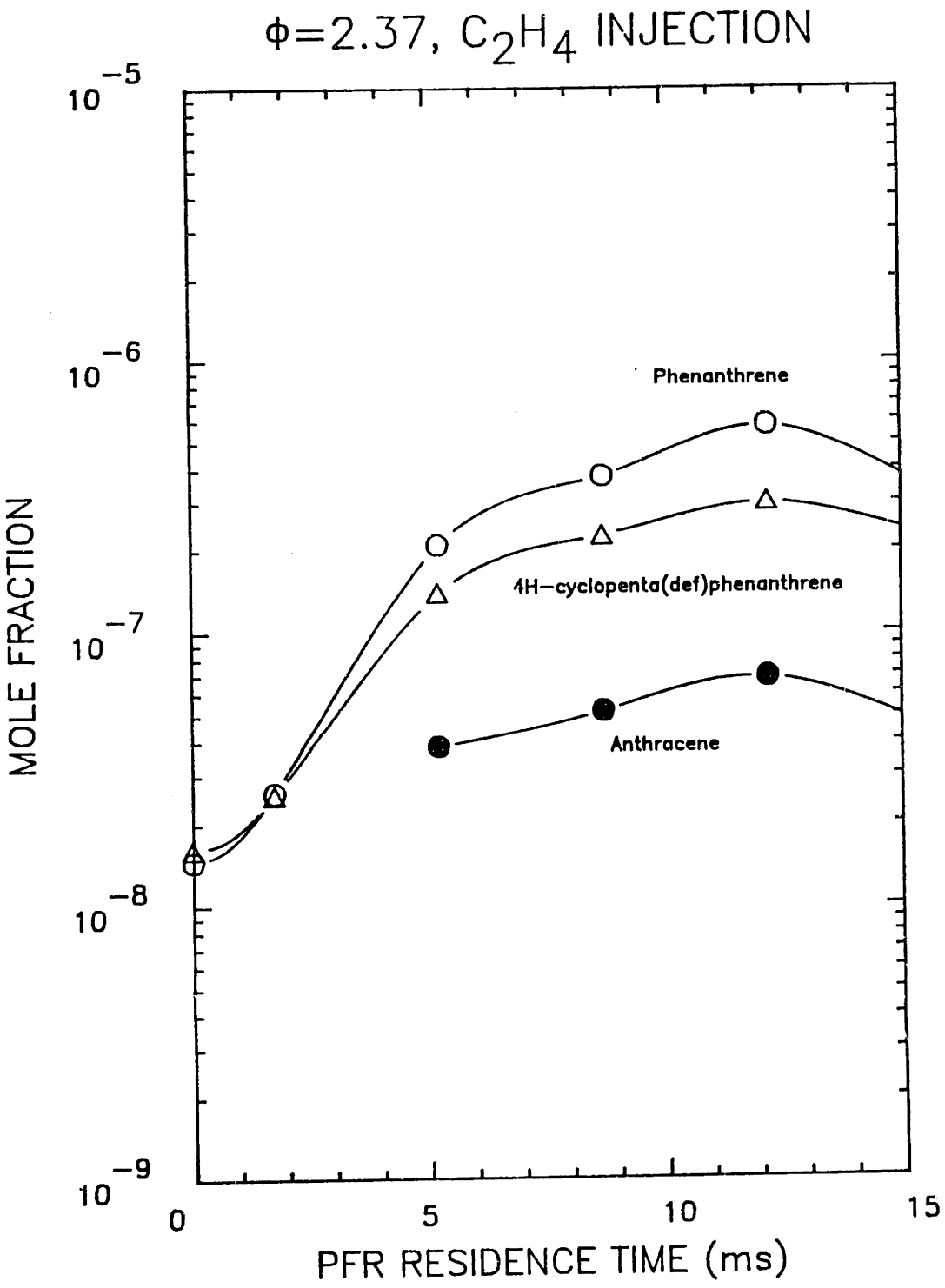

Figure 5.16 Mole Fraction Profiles for 178 - 190 amu species for Case 2: ϕ=2.37, $C_2H_4/O_2/N_2$ combustion in the JSR/PFR with C_2H_4 injection. Curves are visual fits to the data.

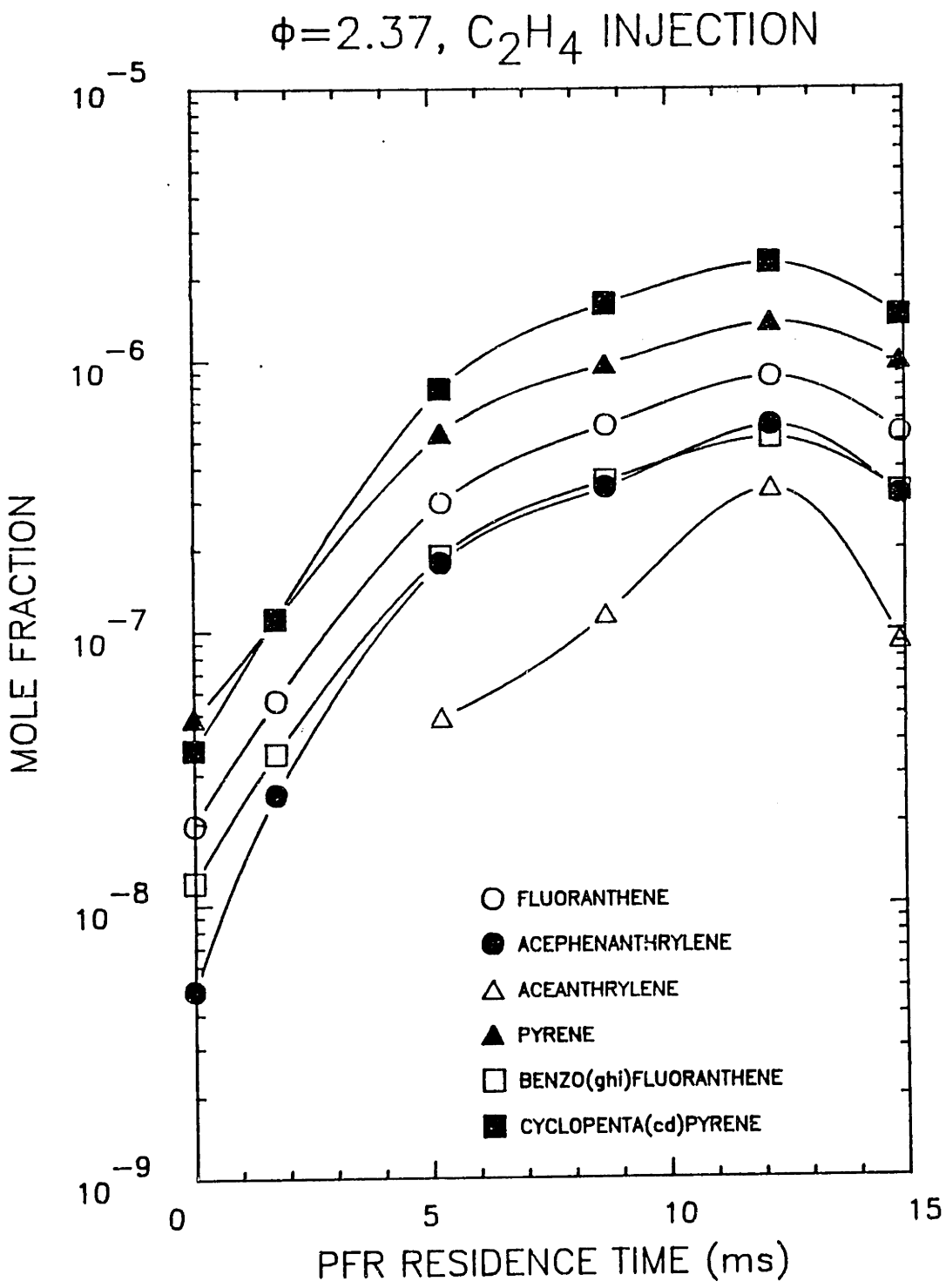

Figure 5.17 Mole Fraction Profiles for 202 - 226 amu species for Case 2: ϕ=2.37, $C_2H_4/O_2/N_2$ combustion in the JSR/PFR with C_2H_4 injection. Curves are visual fits to the data.

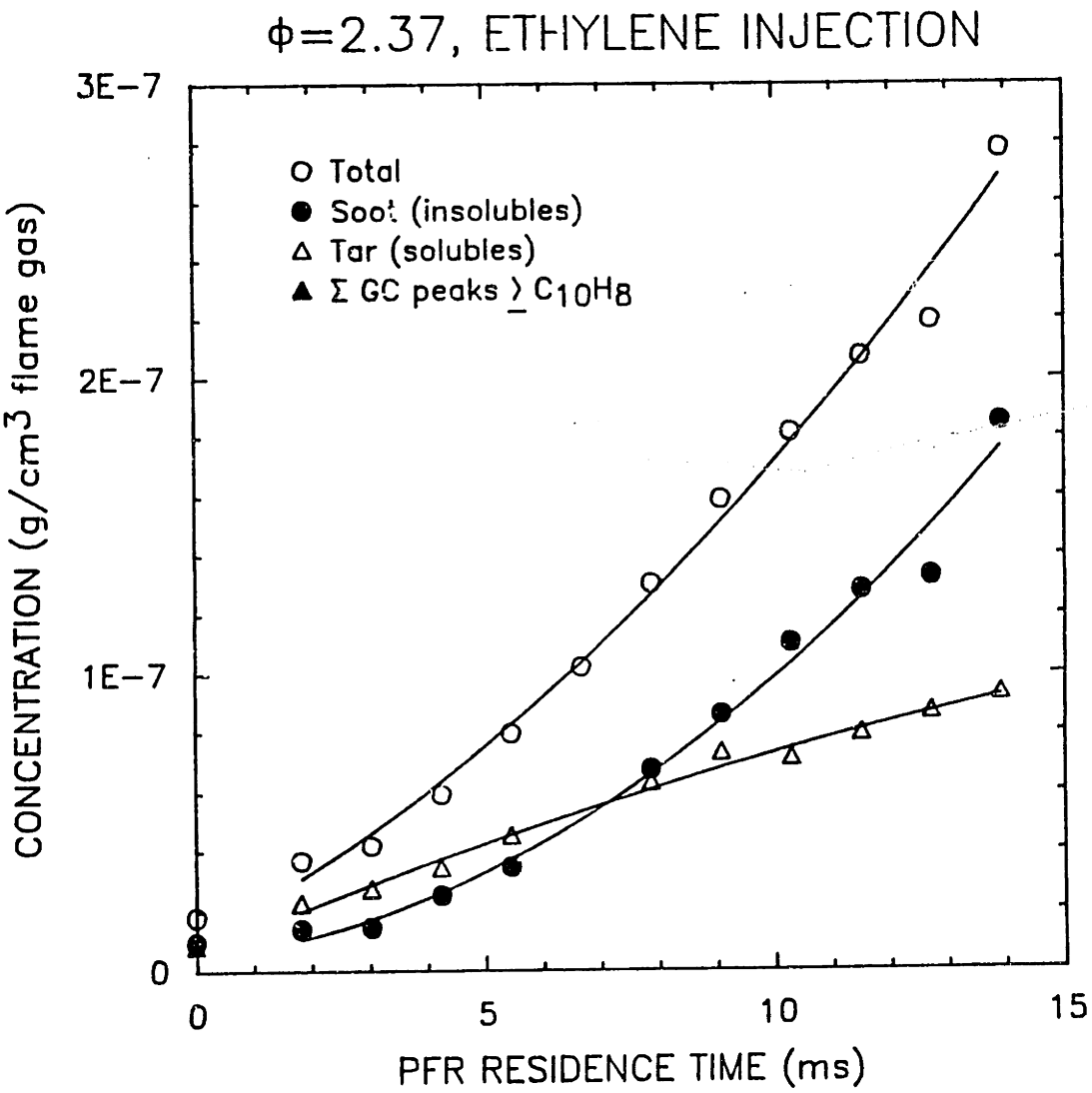

Figure 5.18 Mass Concentration Profiles for ΣGC PAH (128-226 amu), tar (CH_2Cl_2-soluble material), and soot (CH_2Cl_2-insoluble material) for Case 2: ϕ=2.37, $C_2H_4/O_2/N_2$ combustion in the JSR/PFR with C_2H_4 injection. Curves are polynomial fits to the data.

5.3 Case 3: ϕ = 2.18, No Injection

The soot samples obtained from the JSR at ϕ = 2.37 appeared as a yellowish-light tan stain on the filter, and the samples from the end of the PFR were black, fluffy and powdery. The material collected from the JSR is similar to the material collected from a height of 1.3 cm (insoluble peak at ≈3 cm) from a 20 mmHg acetylene-oxygen flat-flame studied by Tompkins and Long (1969). They describe the material as "Continous, smooth translucent film...yellow to medium brown in color--polymer-like." The CH_2Cl_2 insoluble material collected from the end of the PFR fits the description of the material collected at from burner heights of 6.4-15.2 cm by Tompkins and Long: "Progressively becoming more fluffy and of lower bulk density, black in color."

It was originally thought that the material from the JSR was tar, or heavy liquid hydrocarbons, and the material at the end of the PFR was soot. From our TEM studies, we determined that the yellowish substance observed on the soot filters for the ϕ = 2.37, JSR T = 1630K, experimental conditions actually consisted of solid particles, with individual spherule diameters of approximately 50Å, and not just liquid tar products as we had previously thought. We decided to operate the JSR at a non-sooting condition in order to study the formation of PAH and soot at an early stage. The fuel equivalence ratio was lowered, keeping the temperature constant by adjusting the N2/O2 ratio, until no observable deposit was collected on the filter. It was determined experimentally that ϕ = 2.18 was a non-sooting condition in the JSR. Soot was formed by the end of the PFR,

however, even for this ϕ = 2.18 case. The soot concentrations were an order of magnitude lower than the ϕ = 2.37 case, and showed the same profile shape. The PAH species also decreased by about an order of magnitude.

Figures 5.19 through 5.27 show the individual chemical species data, as well as total tar and soot measurements. As seen in Figure 5.19, the major gas species, CO, H_2, CO_2, CH_4 and C_2H_2 show relatively constant mole fraction profiles. Comparison with Case 1 shows that the concentrations of CO, H_2, CH_4, C_2H_2, C_2H_4 are lower, but the CO_2 concentration is higher. These are the expected trends for a more fuel-lean case, and indeed, our kinetic modeling of the major gaseous and hydrocarbon species predict the species profiles to shift in the direction observed experimentally.

The major C2-C4 hydrocarbons, such as C_2H_2, C_2H_4, C_4H_2, and C_4H_4, shown in Figures 5.20 - 5.21 are approximately 30% lower at the end of the PFR for Case 3 than for Case 1 shown in Figures 5.2 - 5.3. The profiles show similar trends, and the main difference is the starting concentration in the JSR. The minor C2-C4 species, such as ethane or 1,3-butadiene, appear within the scatter of the data to be the same for the ϕ = 2.18 and ϕ = 2.37 cases.

The most significant differences between Case 3 and Case 1 are that the aromatics, PAH and soot concentrations are much higher for the fuel-rich case (Case 1) as may be seen from comparision of Figures 5.4 - 5.9 and Figures 5.22 - 5.27. For example, comparison of Figures 5.4 and 5.22 shows that the benzene mole fraction for Case 1 is a factor of 2 higher than Case 3 in the JSR and at the end of the PFR.

The PAH species are even more sensitive to fuel equivalence ratio. The PAH profiles shown in Figures 5.23 - 5.26 for Case 3 show an increasing profile in the PFR, similar to that observed for Case 1, but their absolute concentrations are much lower than for Case 1. The higher molecular weight PAH species are decreased by more than the factor of 2 which was observed for benzene. For example, comparision of Figures 5.26 and 5.8 shows that cyclopenta(cd)pyrene is not detected in the JSR for Case 3, and its concentration at the end of the PFR is about a factor of 5 times lower than Case 1.

The soot, tar and ΣGC PAH profiles are plotted in Figure 5.27. They are similar in shape to the soot and tar profiles for the ϕ = 2.37 case, but the absolute concentrations are an order of magnitude lower. For example soot is a factor of 8 times lower for Case 3 than for Case 1.

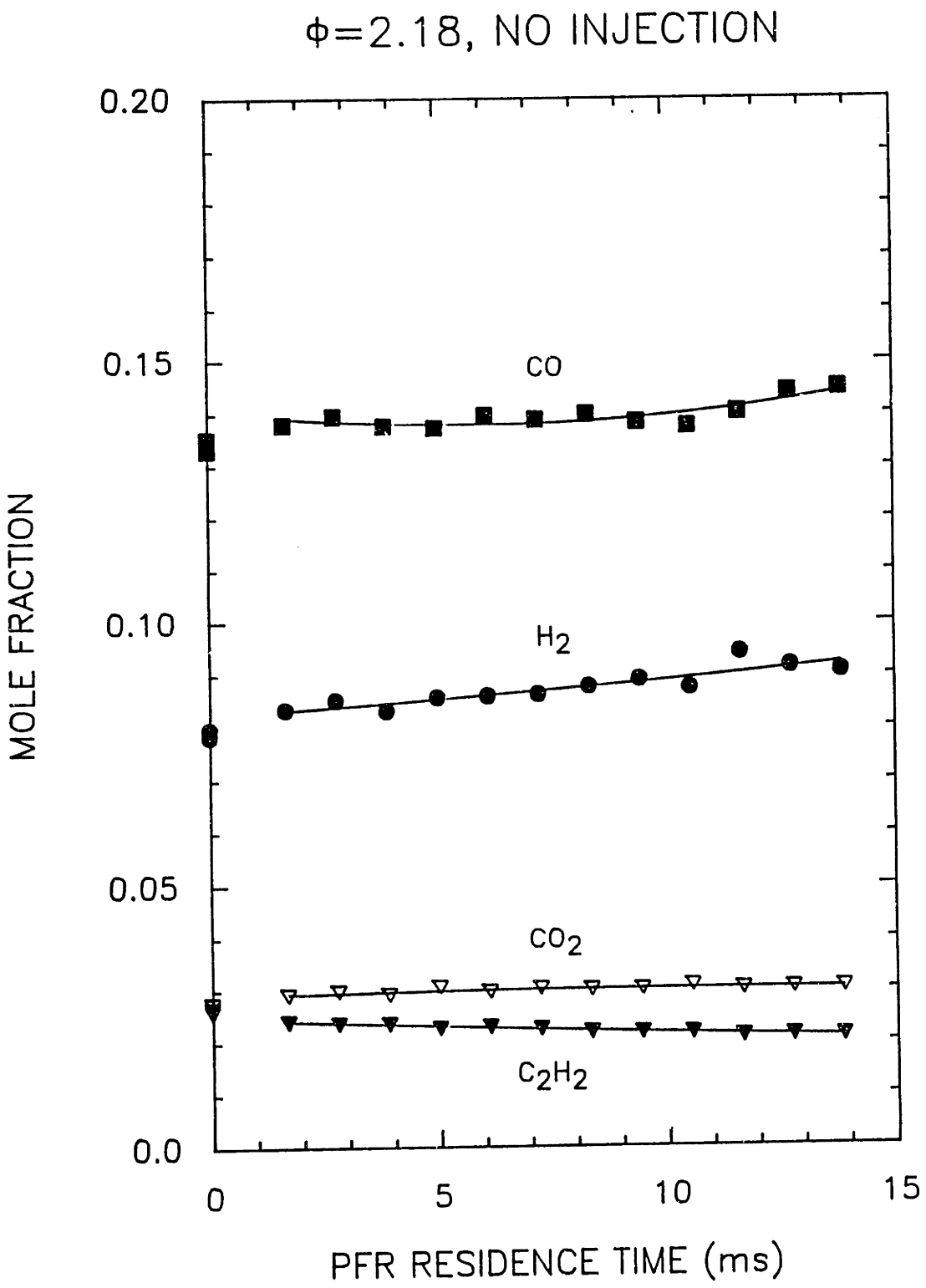

Figure 5.19 Mole Fraction Profiles for CO, CO_2, H_2, and C_2H_2 for Case 3: ϕ=2.18, $C_2H_4/O_2/N_2$ combustion in the JSR/PFR with no injection. Curves are polynomial fits to the data.

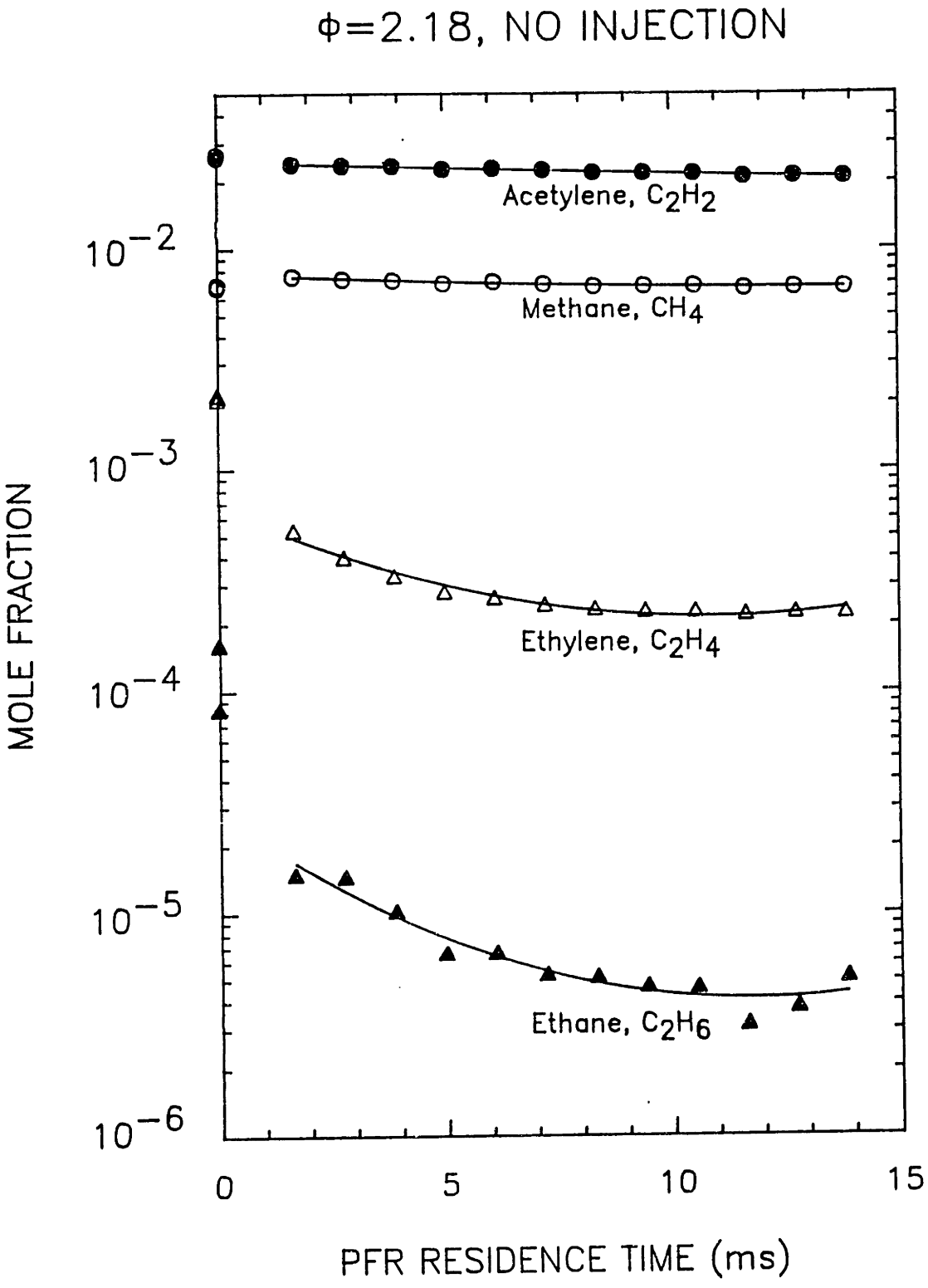

Figure 5.20 Mole Fraction Profiles for CH_4, C_2H_2, C_2H_4, and C_2H_6 for Case 3: ϕ=2.18, $C_2H_4/O_2/N_2$ combustion in the JSR/PFR with no injection. Curves are polynomial fits to the data.

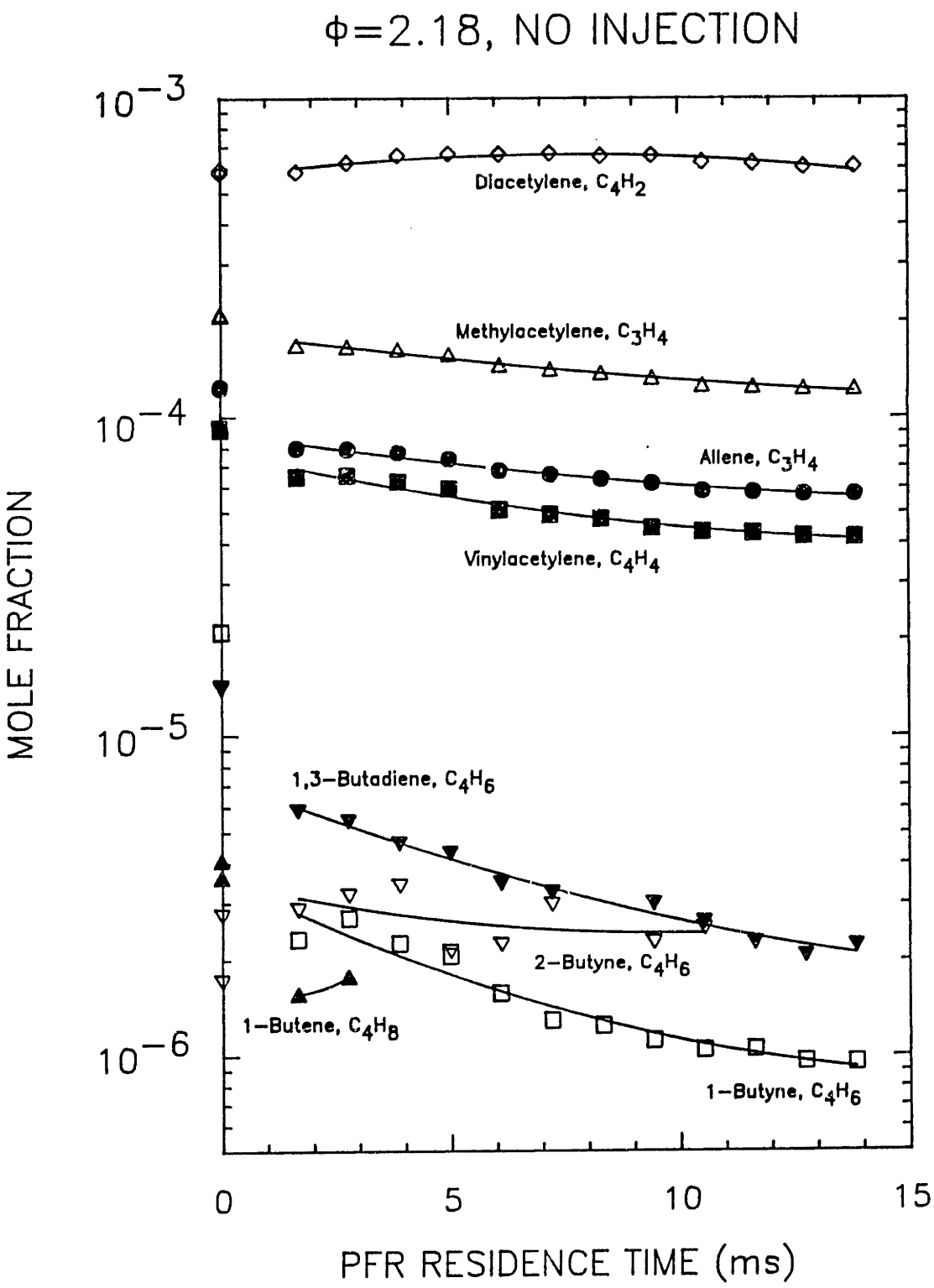

Figure 5.21 Mole Fraction Profiles for C_3 and C_4 species for Case 3: ϕ=2.18, $C_2H_4/O_2/N_2$ combustion in the JSR/PFR with no injection. Curves are polynomial fits to the data.

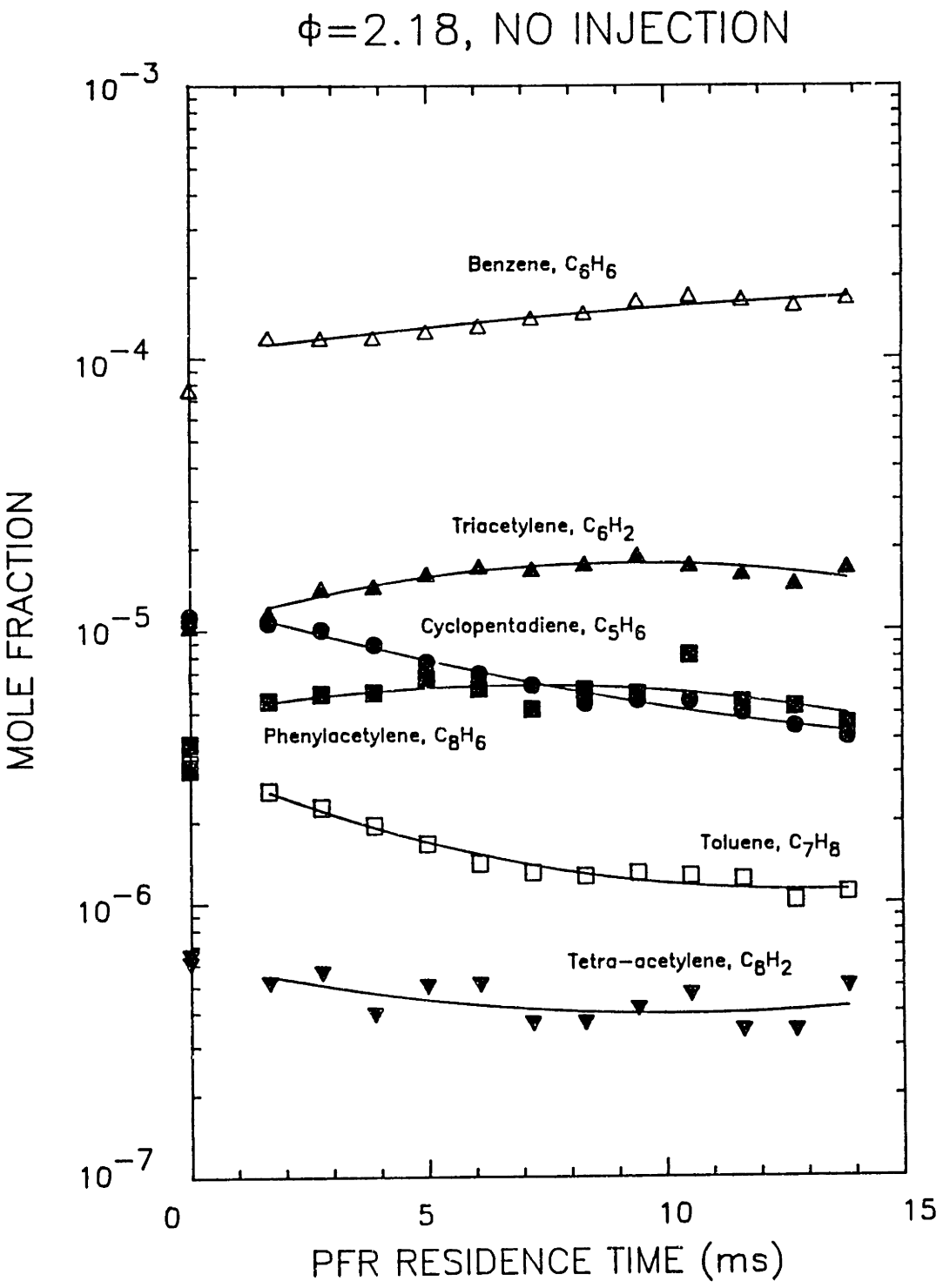

Figure 5.22 Mole Fraction Profiles for C_5 - C_8 species for Case 3: ϕ=2.18, $C_2H_4/O_2/N_2$ combustion in the JSR/PFR with no injection. Curves are polynomial fits to the data.

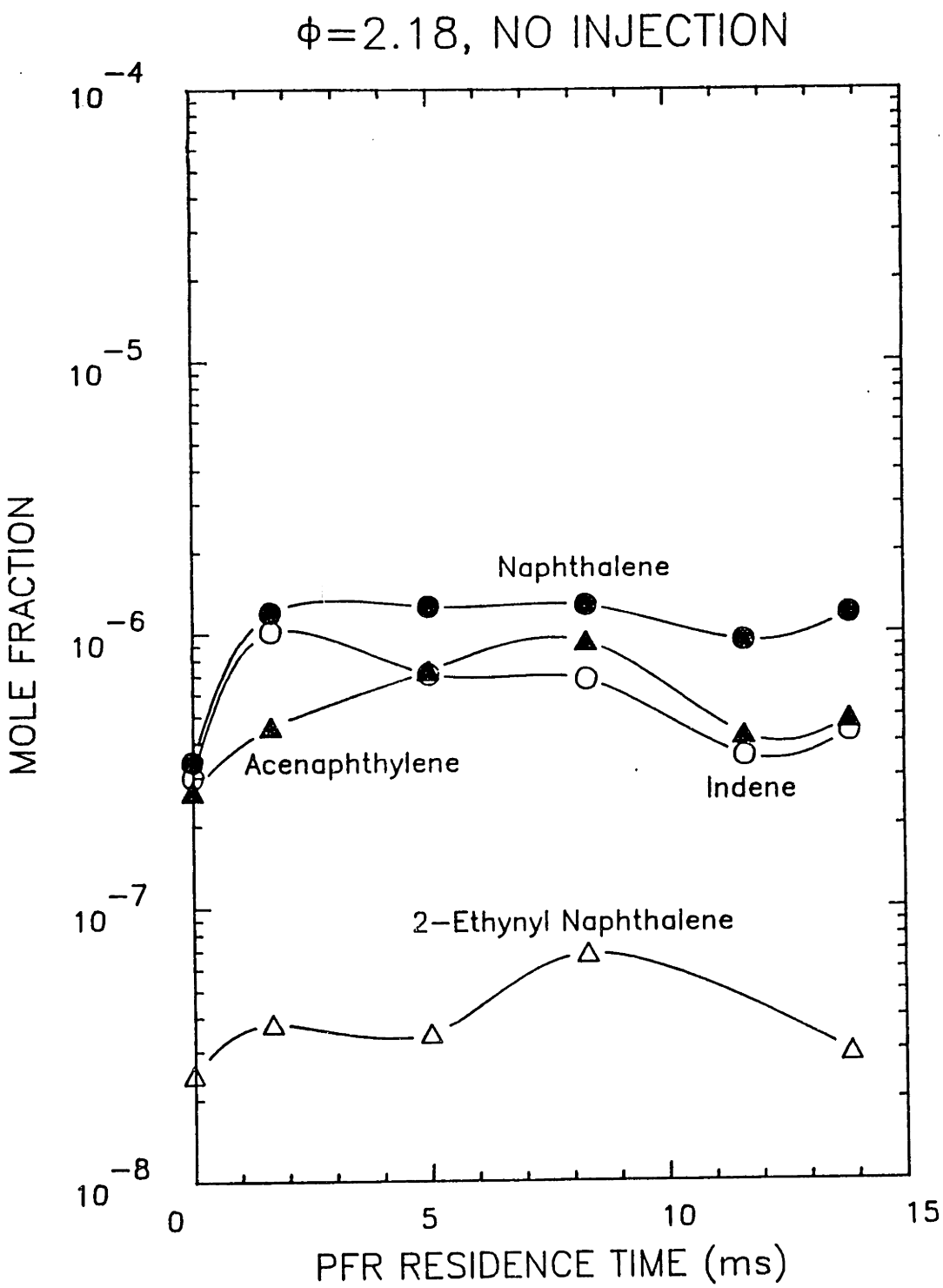

Figure 5.23 Mole Fraction Profiles for 116 - 152 amu species for Case 3: ϕ=2.18, $C_2H_4/O_2/N_2$ combustion in the JSR/PFR with no injection. Curves are visual fits to the data.

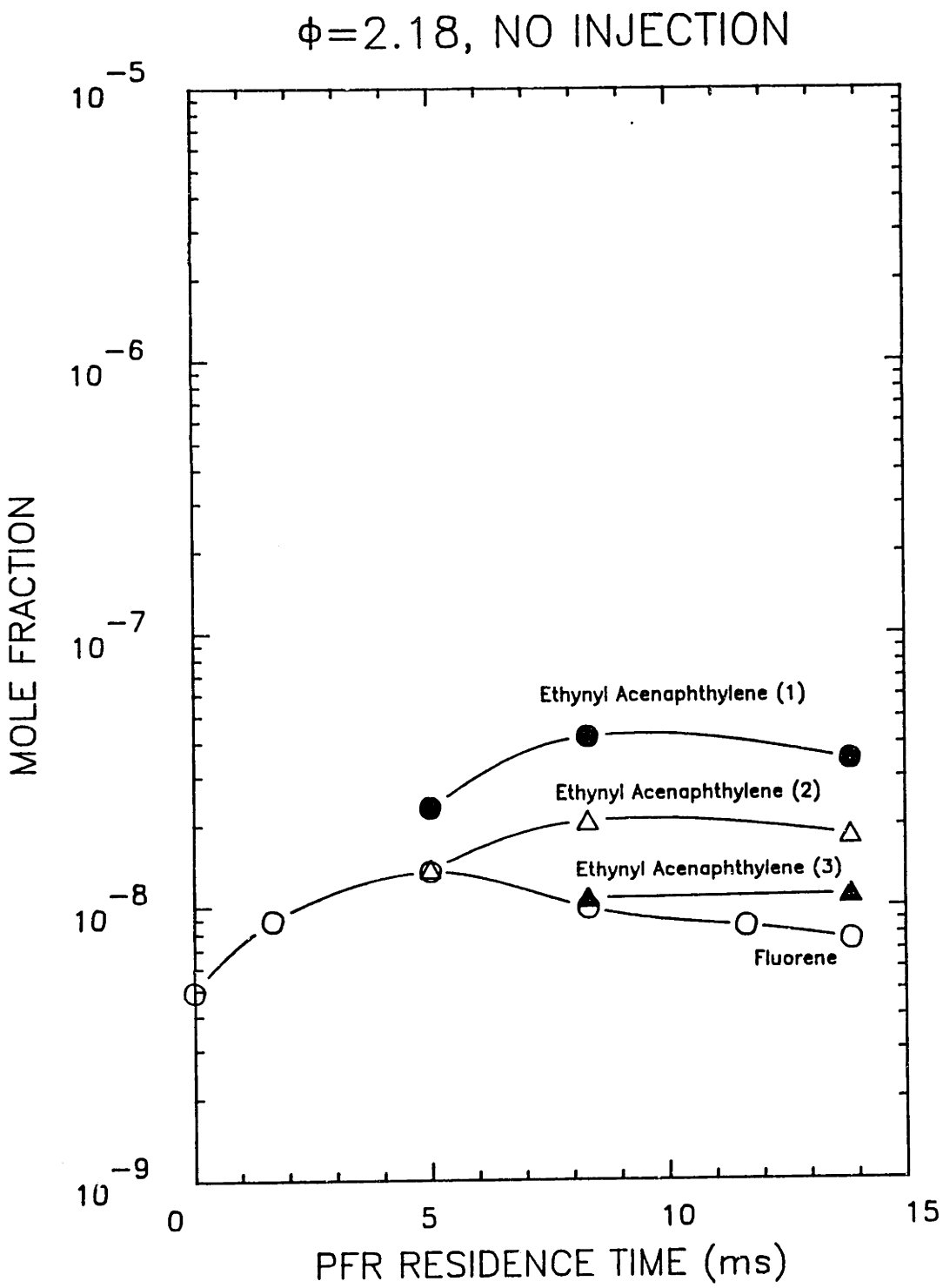

Figure 5.24 Mole Fraction Profiles for 166 - 176 amu species for Case 3: ϕ=2.18, $C_2H_4/O_2/N_2$ combustion in the JSR/PFR with no injection. Curves are visual fits to the data.

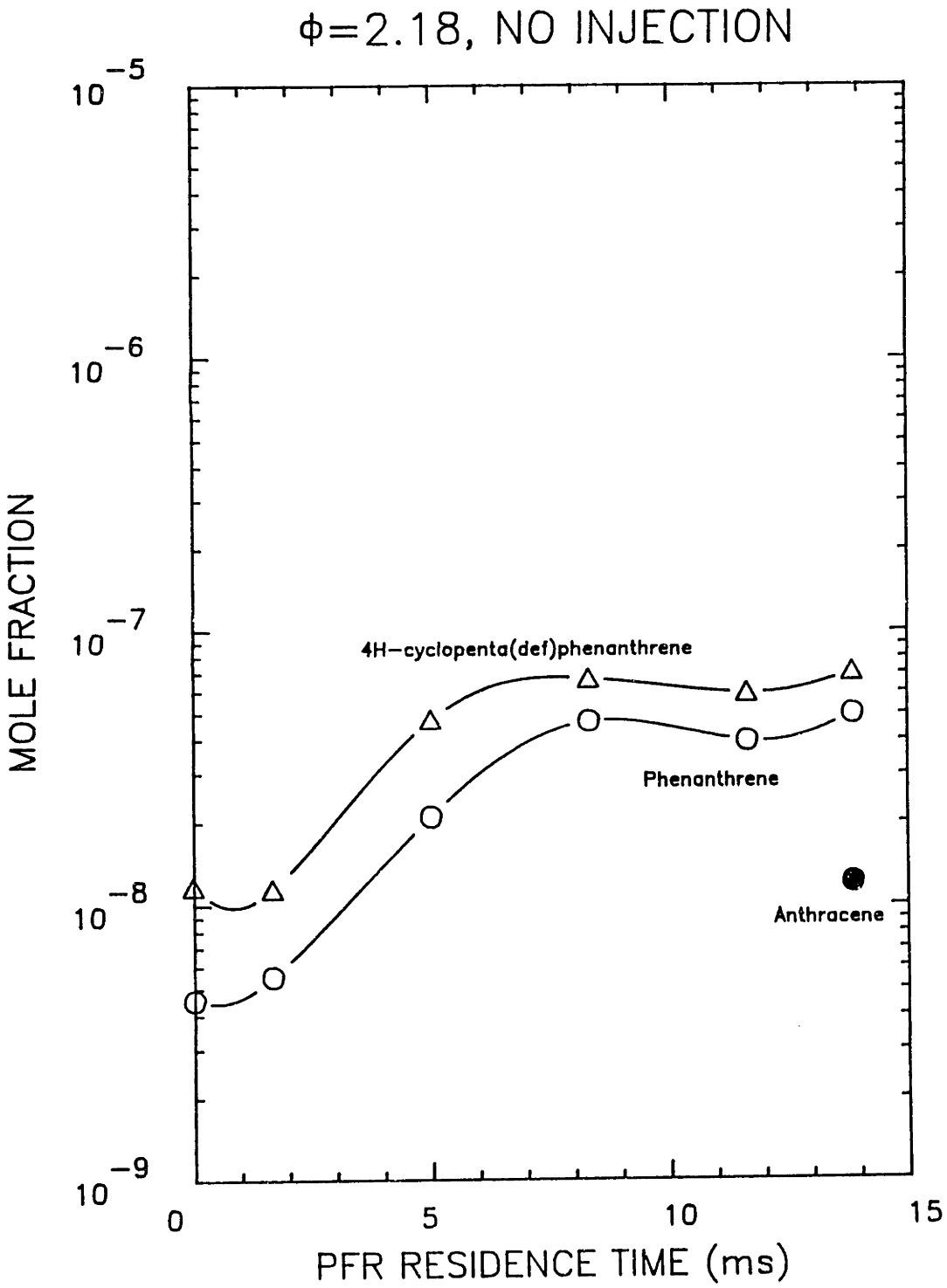

Figure 5.25 Mole Fraction Profiles for 178 - 190 amu species for Case 3: ϕ=2.18, $C_2H_4/O_2/N_2$ combustion in the JSR/PFR with no injection. Curves are visual fits to the data.

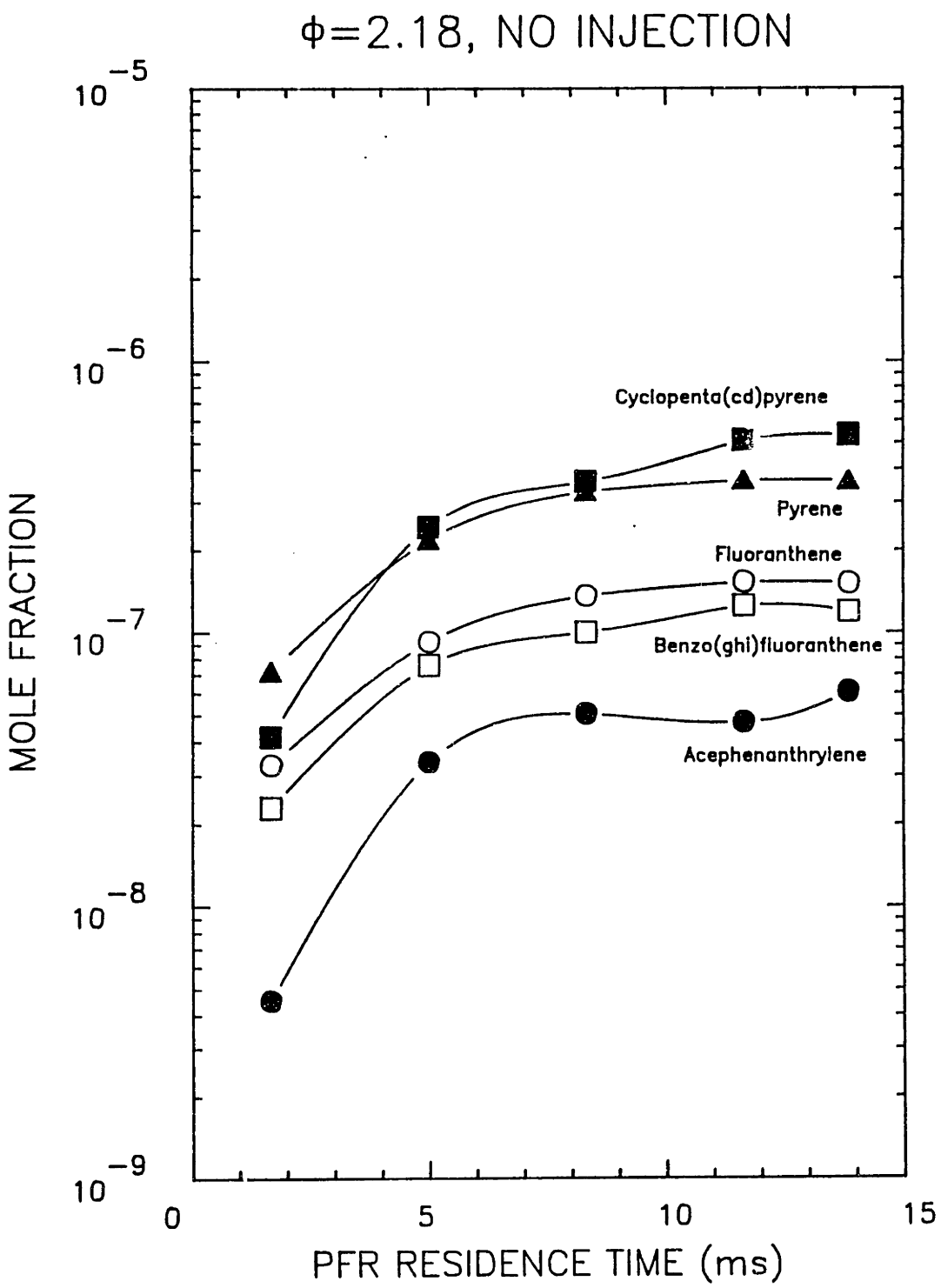

Figure 5.26 Mole Fraction Profiles for 202 - 226 amu species for Case 3: ϕ=2.18, $C_2H_4/O_2/N_2$ combustion in the JSR/PFR with no injection. Curves are visual fits to the data.

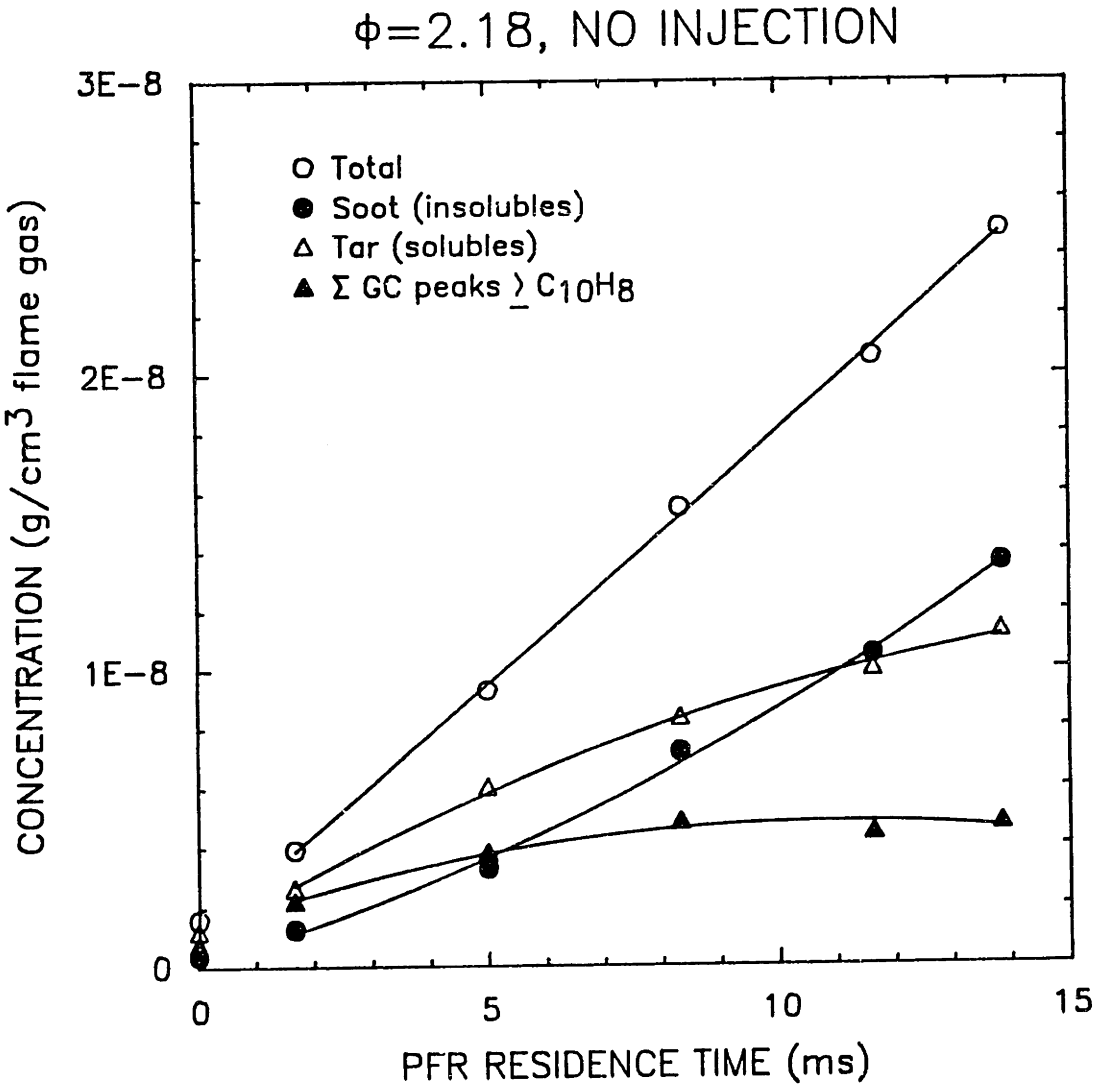

Figure 5.27 Mass Concentration Profiles for ΣGC PAH (128-226 amu), tar (CH_2Cl_2-soluble material), and soot (CH_2Cl_2-insoluble material) for Case 3: ϕ=2.18, $C_2H_4/O_2/N_2$ combustion in the JSR/PFR with no injection. Curves are polynomial fits to the data.

5.4 Case 4: ϕ = 2.18, C_2H_4 Injection

The effect of C_2H_4 injection on the C_2H_2 concentration is significant for ϕ = 2.18 as was observed for ϕ =2.37. Ethylene is predicted to decay very rapidly through the reaction sequence given by Rxns 5.1 - 5.3, resulting in an increase in the C_2H_2 concentration. By looking at the difference between the no injection and C_2H_4 injection profiles for C_2H_2, we conclude that 69% of the injected C_2H_4 is converted to C_2H_2, which is similar to the C_2H_4 to C_2H_2 conversion for ϕ = 2.37. The rest of the injected C_2H_4 is converted to CH_4(7%), C_4H_2(4%), C_6H_6(2%), two C_3H_4 isomers(1%), and tar(1%). The unaccounted fraction of the injected C_2H_4 (≈16%) is probably converted to CO and CO_2 near the entrance of the PFR, since the JSR has a small amount of oxygen remaining (≈0.5%). Other hydrocarbons show similar decreases near the entrance of the PFR, again, probably from oxidation by the remaining O_2 from the JSR.

The major fixed gases shown in Figure 5.28 are similar to the species profiles for the no injection case. Unfortunately, the experimental uncertainties in species profiles such as CO and H_2 are the same as the expected perturbation from C_2H_4 injection. Thus we cannot determine with accuracy how much of the injected C_2H_4 is converted to CO or H_2.

The C1-C2 species shown in Figure 5.29 are similar to those in Figure 5.2, with the exception of C_2H_4. The ethylene concentration is much higher at the first sampling point (mole fraction = 2.2×10^{-3}) and declines sharply to a mole fraction of 5×10^{-4}, as compared to a final mole fraction of 2×10^{-4} for Case 3.

The C3-C4 species for Case 4 are shown in Figure 5.30. The species show the same trend as for the no injection case, but we see that the concentrations of diactylene, vinylacetylene, methylacetylene, and allene are increased by the C_2H_4 injection.

The single ring-aromatic species for Case 4 are shown in Figure 5.31. The profiles are similar to Case 3, although the benzene profile is increased by almost a factor of 2 by the end of the PFR by the addition of C_2H_4.

The PAH species shown in Figures 5.32 - 5.35 show the same general trends as for Case 3 and are moderately increased by the additional C_2H_4. For example, the mole fraction of cyclopenta(cd)pyrene is increased by a factor of 2.5 at the end of the PFR for Case 4. The other PAH profiles show similar increases due to injection of C_2H_4.

The tar and soot profiles shown in Figure 5.36 are similar to the tar and soot profiles in Case 3. The concentration of the tar at the end of the PFR for Case 4 is a factor of 2.5 higher than Case 3, but the concentration of soot is nearly the same for Case 4 and Case 3. Although the uncertainty in the soot measurements is significant at these low soot concentrations, this observation suggests that C_2H_2 contributes preferentially to the tar inventory, rather than the soot inventory. The contribution of tar to soot growth may be delayed by a time-lag in order to build up the tar concentration. Although the tar concentration for Case 4 is 2.5 times higher than Case 3 at the end of the PFR, for most of the residence time in the PFR, the tar concentrations for the two cases are comparable. Figure 5.49 shows

that the most of the increase in tar concentration due to C_2H_4 injection does not occur until late in the PFR. Thus the soot concentration may not build up appreciably in the PFR residence time.

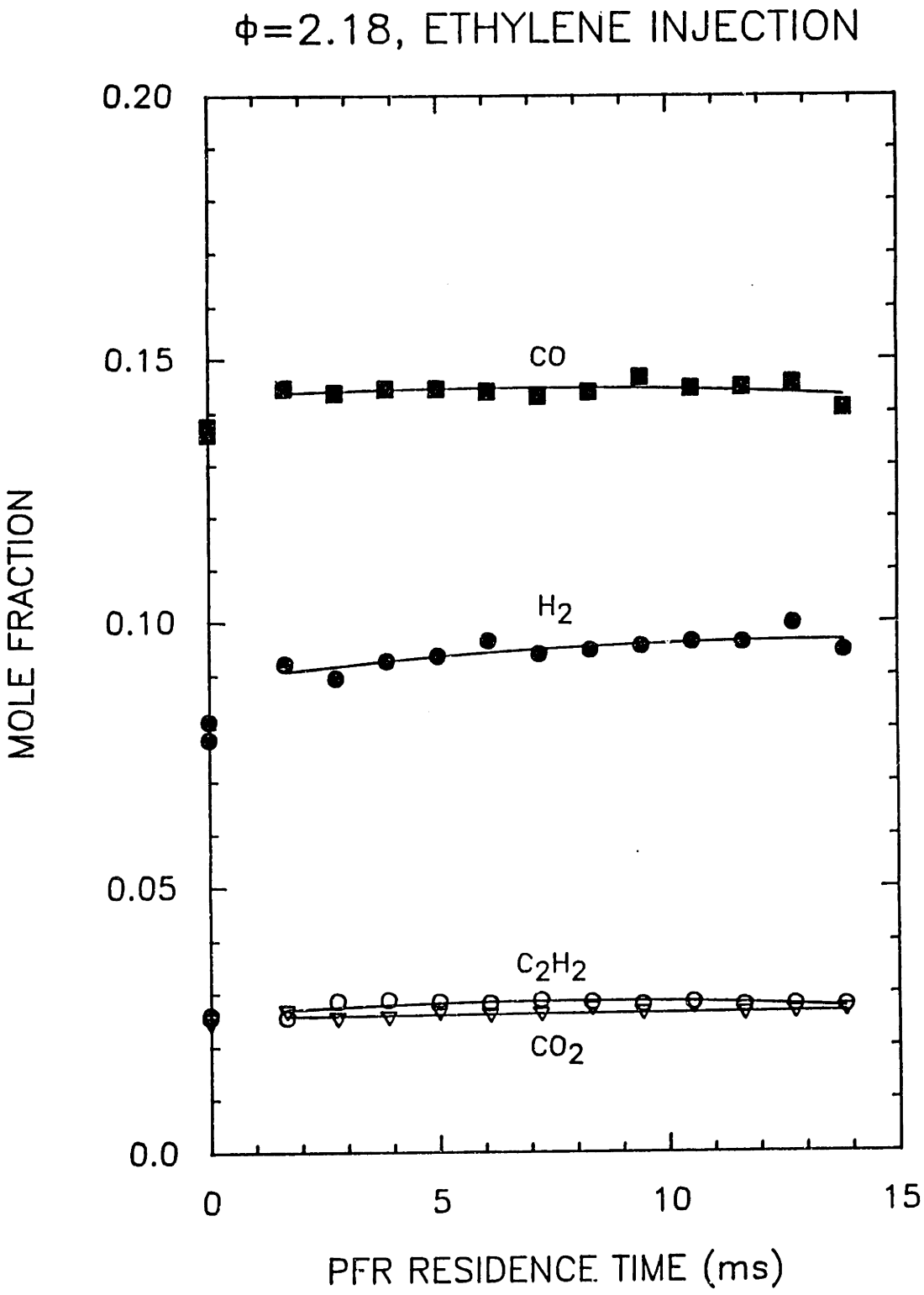

Figure 5.28 Mole Fraction Profiles for CO, CO_2, H_2, and C_2H_2 for Case 4: ϕ=2.18, $C_2H_4/O_2/N_2$ combustion in the JSR/PFR with C_2H_4 injection. Curves are polynomial fits to the data.

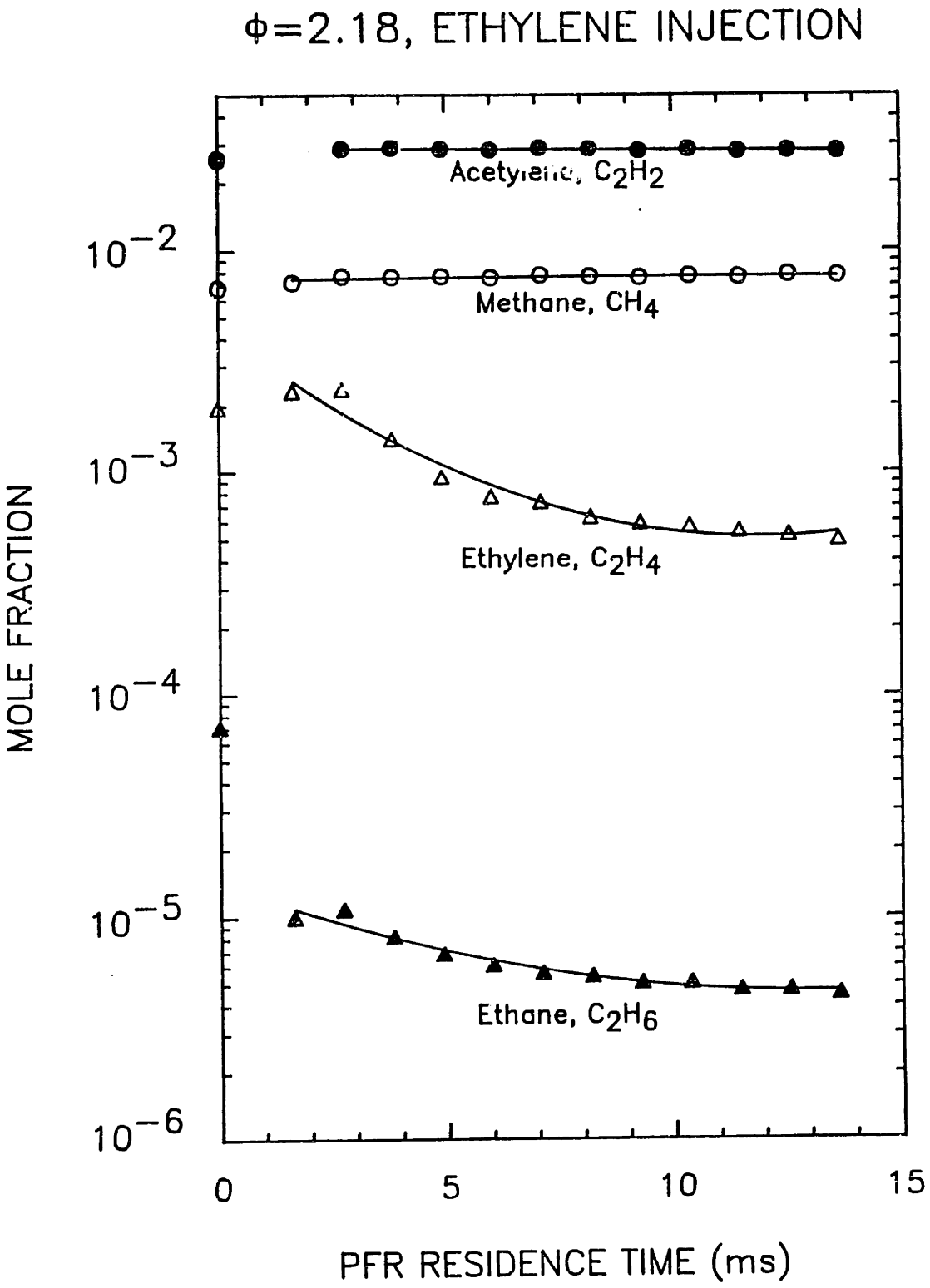

Figure 5.29 Mole Fraction Profiles for CH_4, C_2H_2, C_2H_4, and C_2H_6 for Case 4: ϕ=2.18, $C_2H_4/O_2/N_2$ combustion in the JSR/PFR with C_2H_4 injection. Curves are polynomial fits to the data.

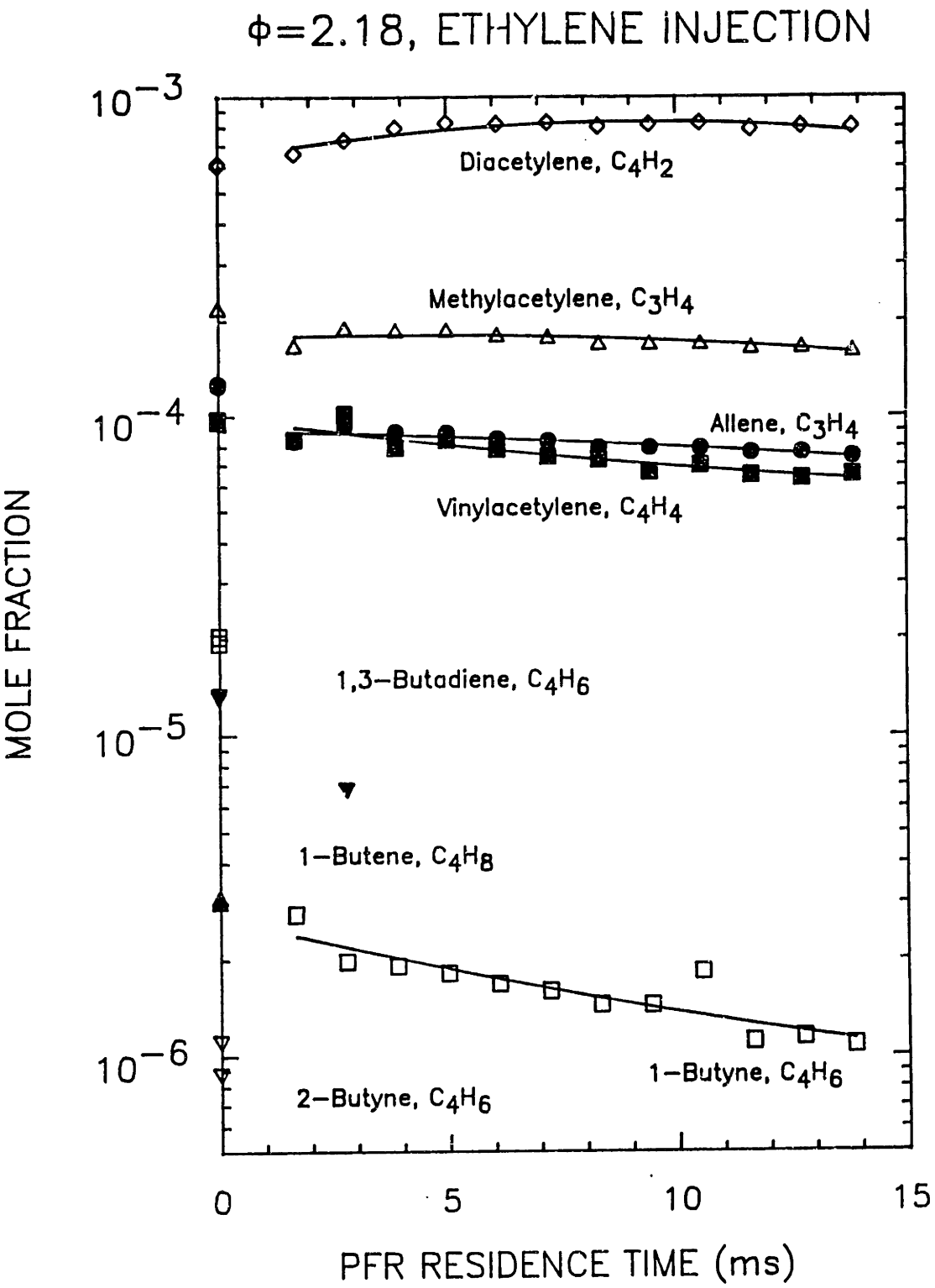

Figure 5.30 Mole Fraction Profiles for C_3 and C_4 species for Case 4: ϕ=2.18, $C_2H_4/O_2/N_2$ combustion in the JSR/PFR with C_2H_4 injection. Curves are polynomial fits to the data.

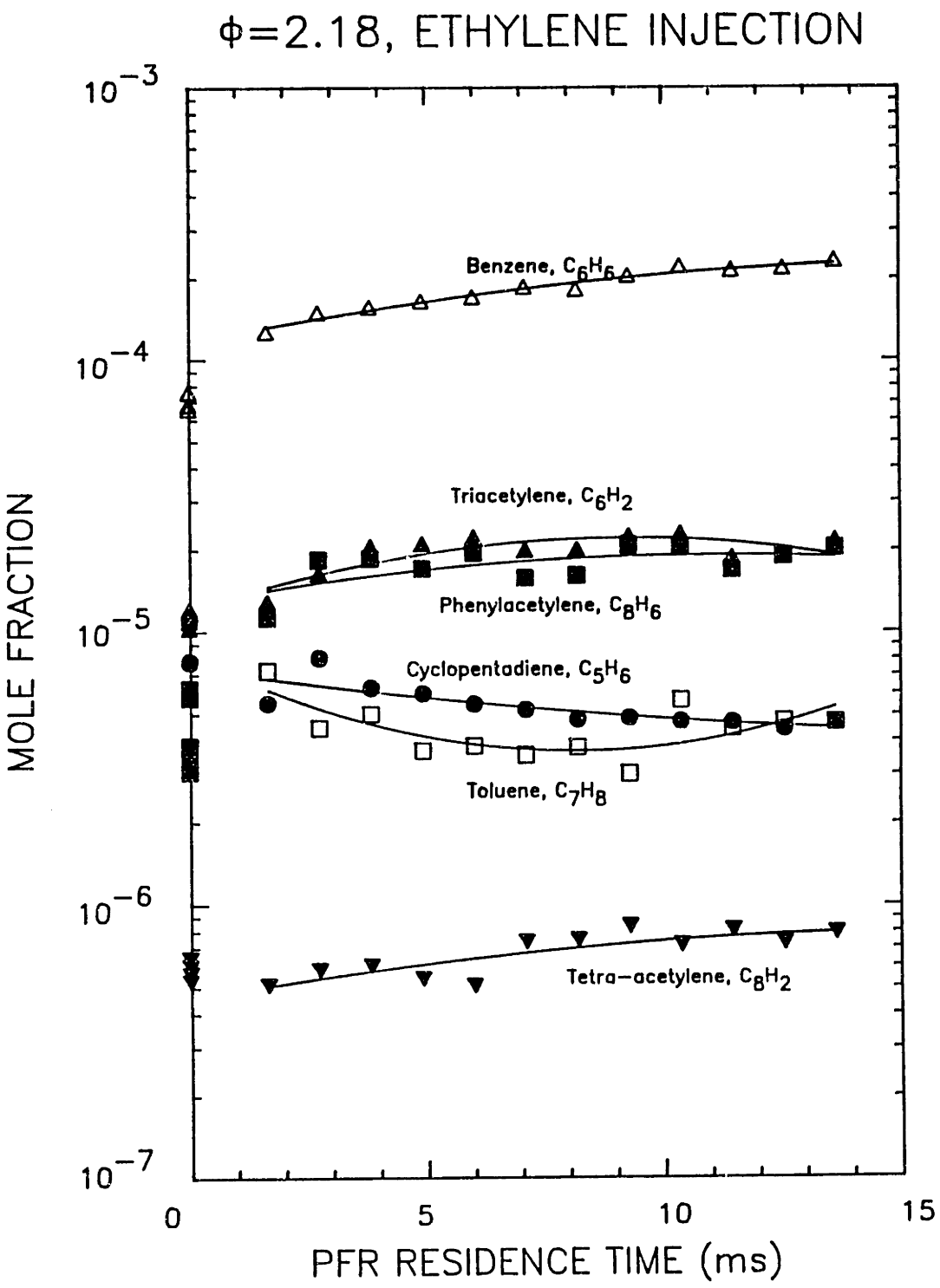

Figure 5.31 Mole Fraction Profiles for C_5 - C_8 species for Case 4: ϕ=2.18, $C_2H_4/O_2/N_2$ combustion in the JSR/PFR with C_2H_4 injection. Curves are polynomial fits to the data.

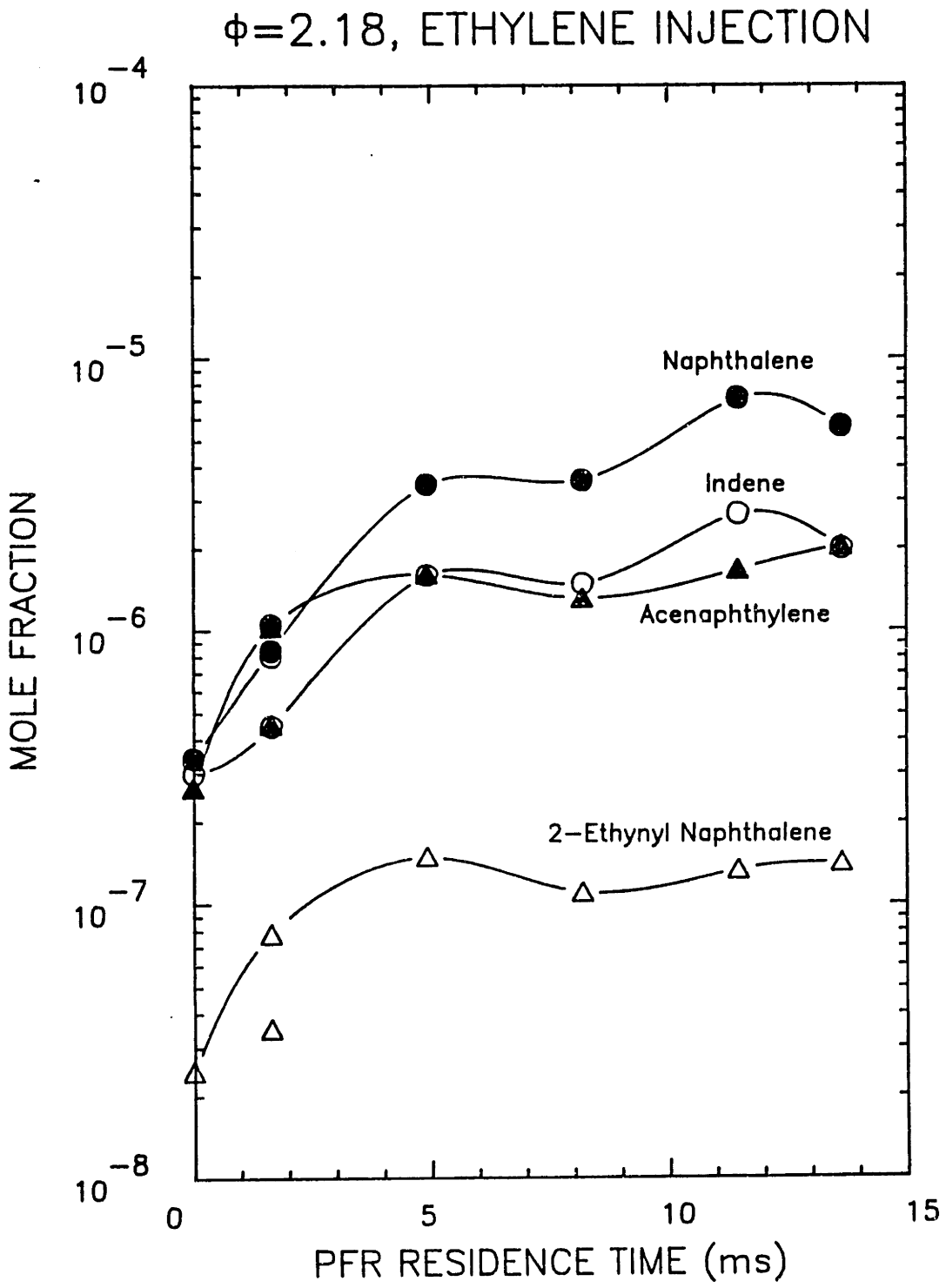

Figure 5.32 Mole Fraction Profiles for 116 - 152 amu species for Case 4: ϕ=2.18, $C_2H_4/O_2/N_2$ combustion in the JSR/PFR with C_2H_4 injection. Curves are visual fits to the data.

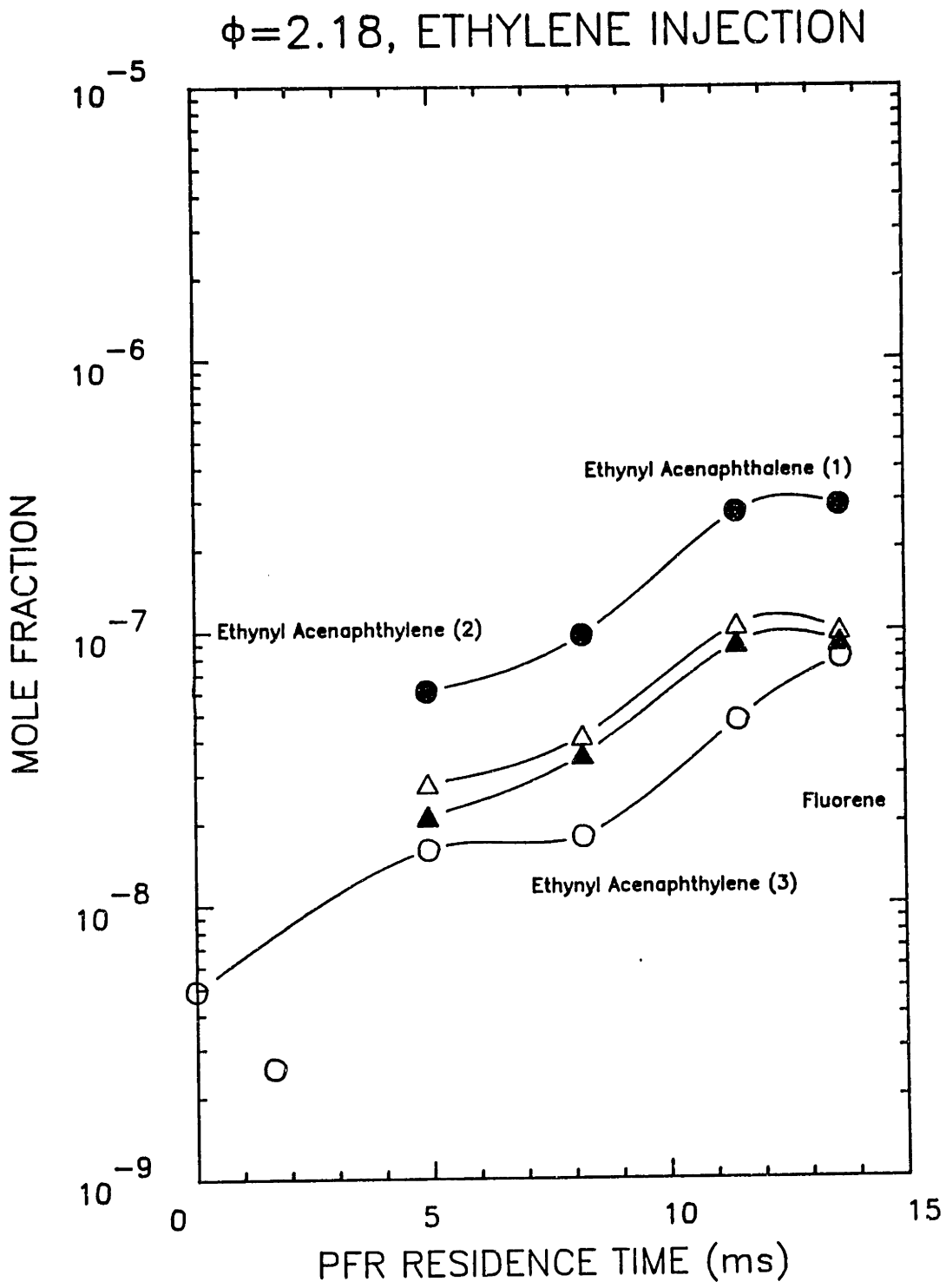

Figure 5.33 Mole Fraction Profiles for 166 - 176 amu species for Case 4: ϕ=2.18, $C_2H_4/O_2/N_2$ combustion in the JSR/PFR with C_2H_4 injection. Curves are visual fits to the data.

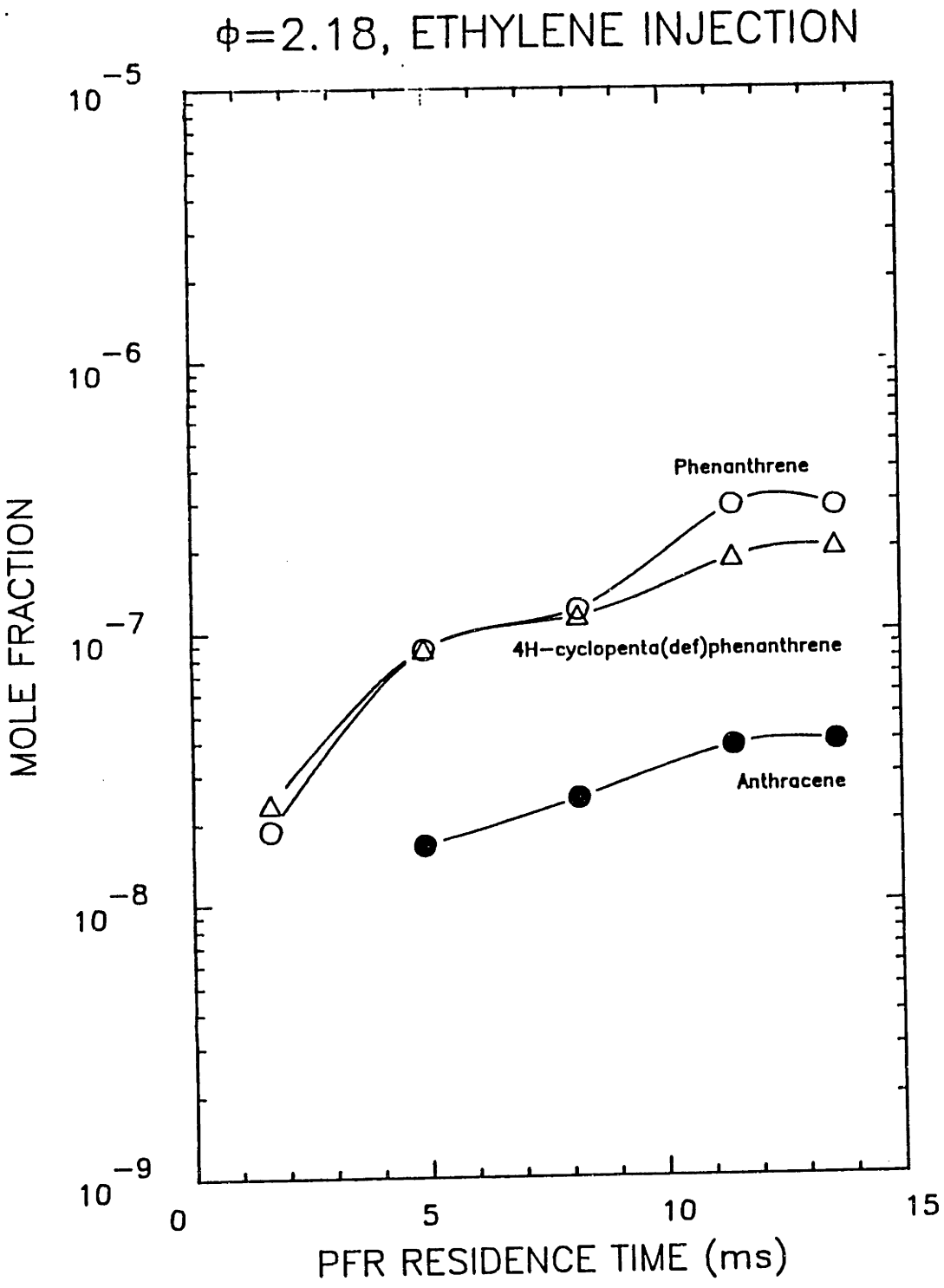

Figure 5.34 Mole Fraction Profiles for 178 - 190 amu species for Case 4: ϕ=2.18, $C_2H_4/O_2/N_2$ combustion in the JSR/PFR with C_2H_4 injection. Curves are visual fits to the data.

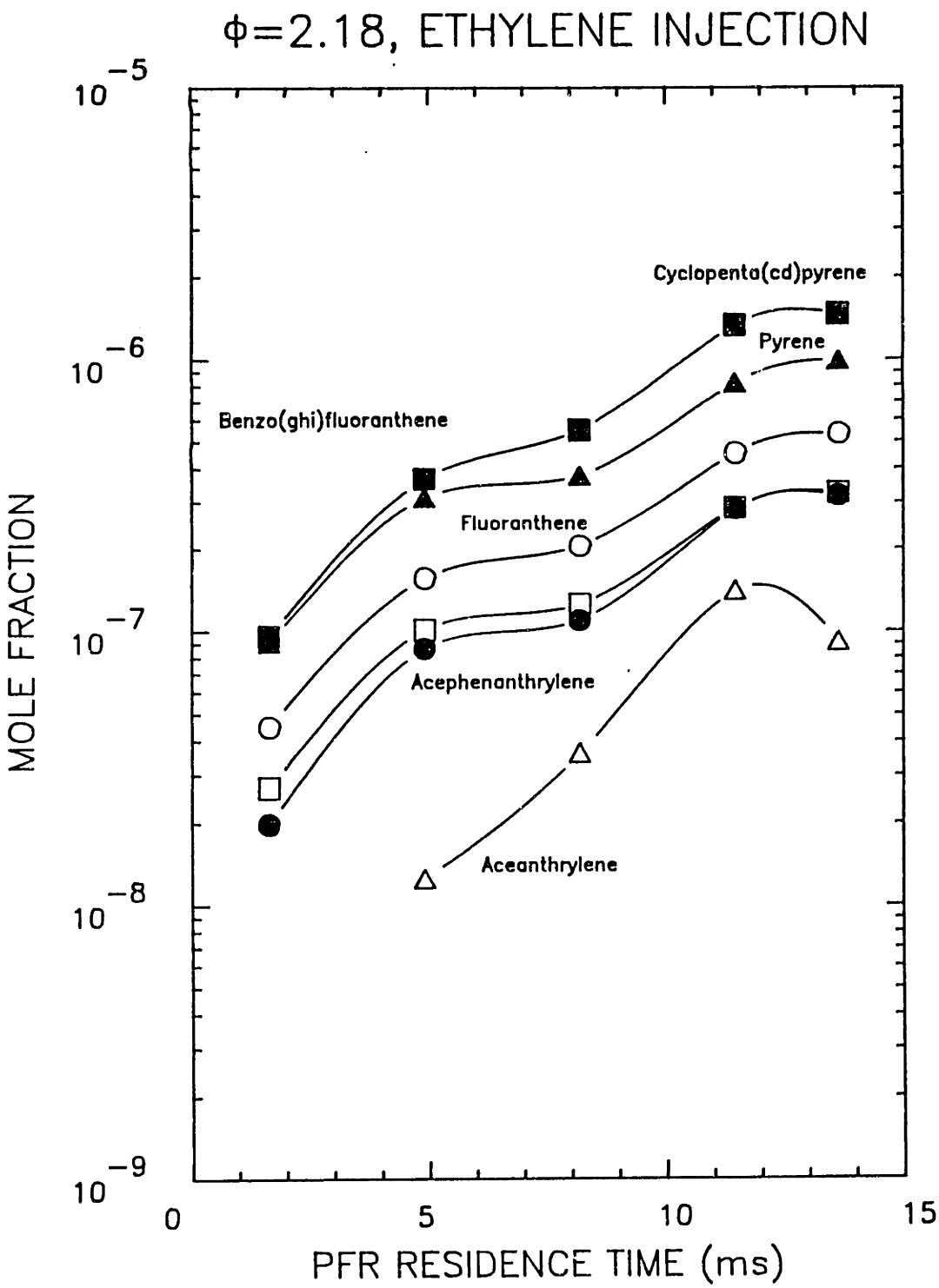

Figure 5.35 Mole Fraction Profiles for 202 - 226 amu species for Case 4: ø=2.18, $C_2H_4/O_2/N_2$ combustion in the JSR/PFR with C_2H_4 injection. Curves are visual fits to the data.

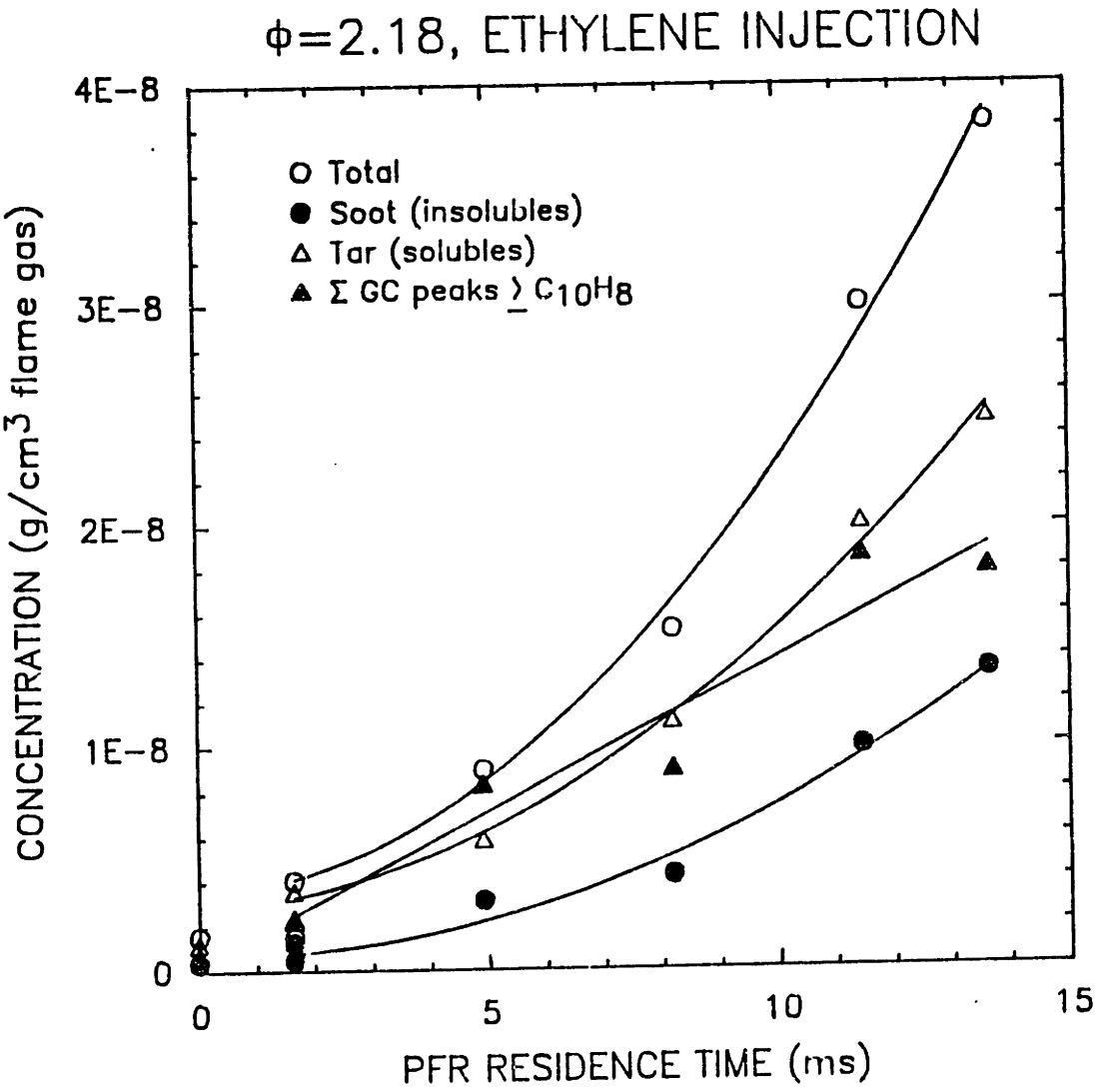

Figure 5.36 Mass Concentration Profiles for ΣGC PAH (128-226 amu), tar (CH_2Cl_2-soluble material), and soot (CH_2Cl_2-insoluble material) for Case 4: ϕ=2.18, $C_2H_4/O_2/N_2$ combustion in the JSR/PFR with C_2H_4 injection. Curves are polynomial fits to the data.

5.5 Case 5: ϕ = 2.18, C_6H_6 Injection

The injection of benzene was designed to test the effect of an intact aromatic ring on PAH and soot production. The total amount of benzene injected was very small, corresponding to a benzene mole fraction of 1800 ppm, or about 5% by moles of the total C_2H_4 fuel fed to the JSR. The amount of benzene was selected to be 10 times the amount of benzene which was present in the PFR for the no injection case, so that we could clearly see the perturbation of the injection on the benzene profile. Compared with the C_2H_4 injection for the ϕ = 2.18, the amount of benzene injected is less than the amount of ethylene injected in terms of either moles (mole C_6H_6/mole C_2H_4 = 0.2) or mass (gram C_6H_6 /gram C_2H_4 = 0.6).

From comparision of Figures 4.37 - 4.38 with Figures 5.19-5.20, we see that the fixed gases and C1-C2 species are not affected much by benzene addition. The C3-C4 species shown in Figure 5.39 are also not greatly affected by benzene injection, but as discussed earlier, this is primarily due to the very low concentration of C_6H_6 added to the system.

As shown in Figure 5.40, the concentrations of the single ring aromatic species are increased by benzene injection. Benzene and phenylacetylene both show decreasing profiles in the PFR, and the ratio of their mole fractions is approximately constant. Toluene is increased from Case 3 by injection of benzene by a factor of 4 at the end of the PFR.

A dramatic effect of benzene on the production of the individual PAH species is seen in Figures 4.41 - 4.44. Naphthalene is increased

by an order of magnitude and the other PAH species are affected similarly. For the PAH species with 4-5 rings shown in Figure 5.44, we see that the rate of increase is very high initially at early residence times in the PFR, and decreases at longer PFR residence times.

The total tar and soot concentrations are also greatly increased by the injection of benzene, as shown in Figure 5.45. An order of magnitude more soot is produced at the end of the PFR for the addition of benzene. The tar concentration is also increased by an order of magnitude, and it is even higher than for the more fuel-rich case (ϕ=2.37) with ethylene injection.

If all of the injected benzene were converted to C_2H_2 by the end of the PFR, and no other species profiles were affected, we would expect to see an increase in the C_2H_2 mole fraction at the end of the PFR of 0.005, from 2.1×10^{-2} for Case 3, to 2.6×10^{-2} for Case 5. If we assume that the destruction of C_2H_2 is not much faster than the destruction of benzene to C_2H_2, then the fact that the C_2H_2 profiles are nearly identical for Cases 3 and 5, suggests that benzene decomposition to C_2H_2 is not the dominant route of benzene destruction.

If all of the injected benzene were converted to CO by the end of the PFR, and no other species profiles were affected, we would expect to see an increase in the CO mole fraction at the end of the PFR of 0.015, which is close to the experimental uncertainty for CO. Since the mole fraction of O_2 is $\approx$0.005, there is enough O_2 to oxidize the remaining portion of the C_6H_6 to CO.

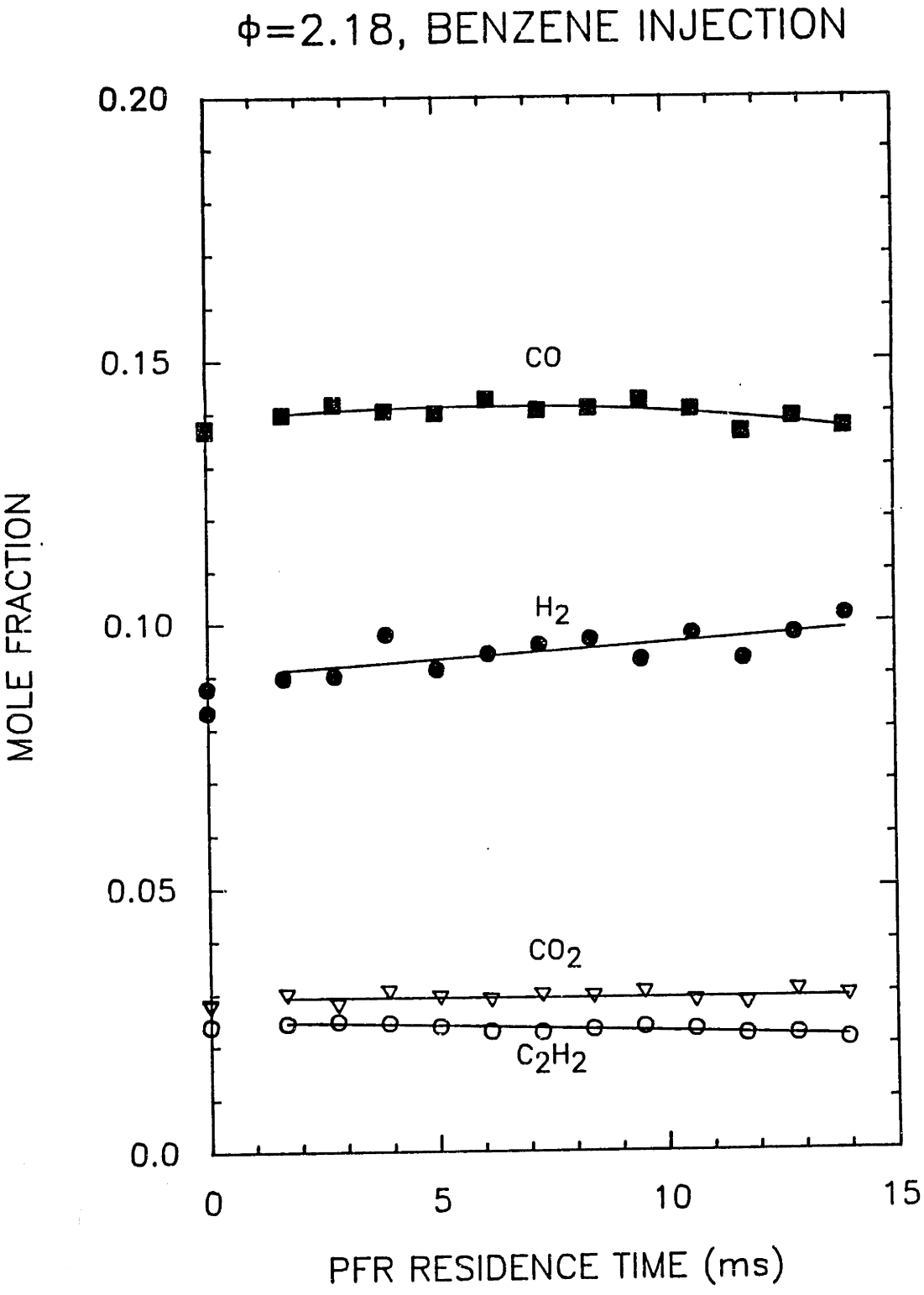

Figure 5.37 Mole Fraction Profiles for CO, CO_2, H_2, and C_2H_2 for Case 5: ϕ=2.18, $C_2H_4/O_2/N_2$ combustion in the JSR/PFR with C_6H_6 injection. Curves are polynomial fits to the data.

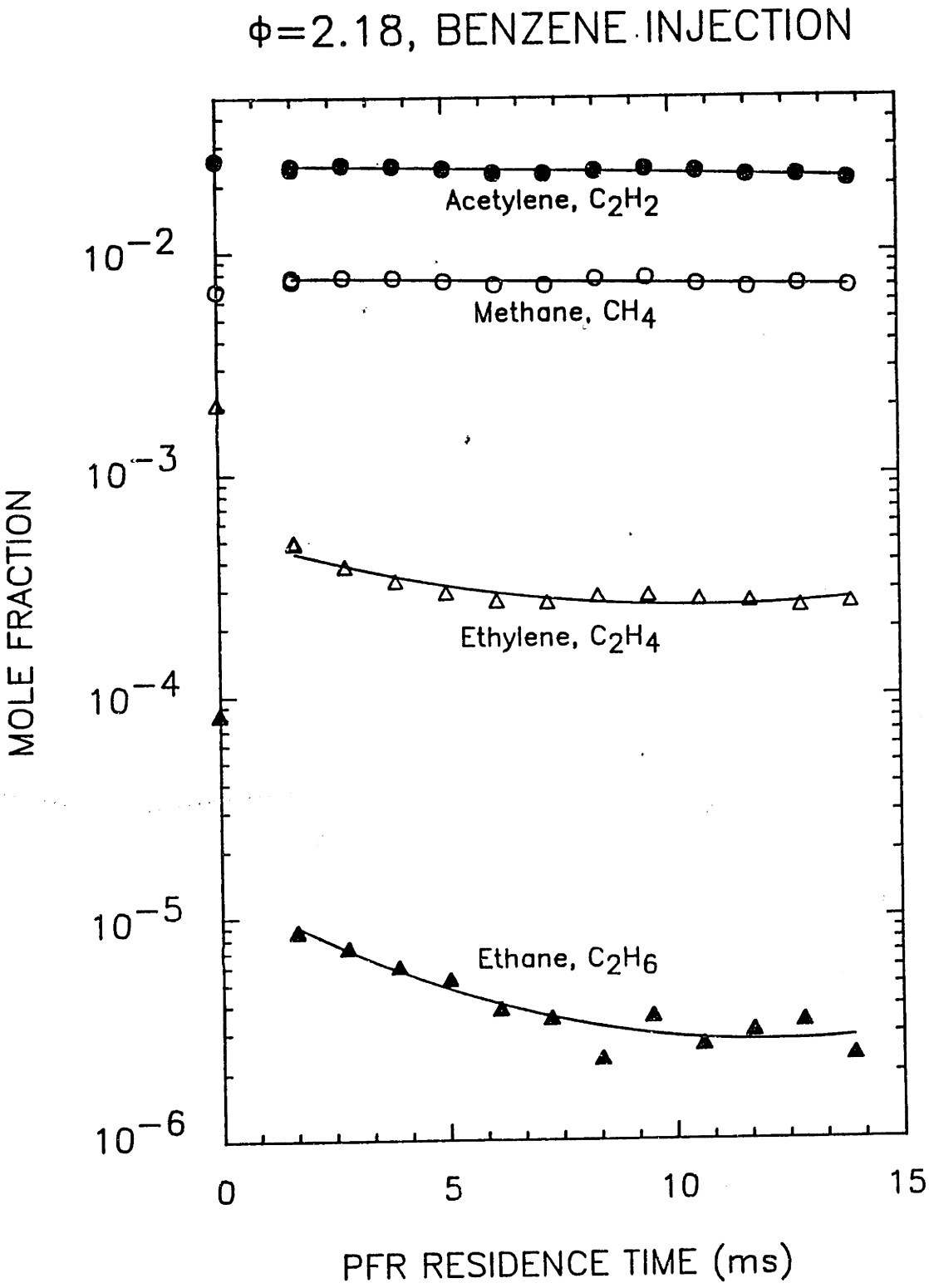

Figure 5.38 Mole Fraction Profiles for CH_4, C_2H_2, C_2H_4, and C_2H_6 for Case 5: ϕ=2.18, $C_2H_4/O_2/N_2$ combustion in the JSR/PFR with C_6H_6 injection. Curves are polynomial fits to the data.

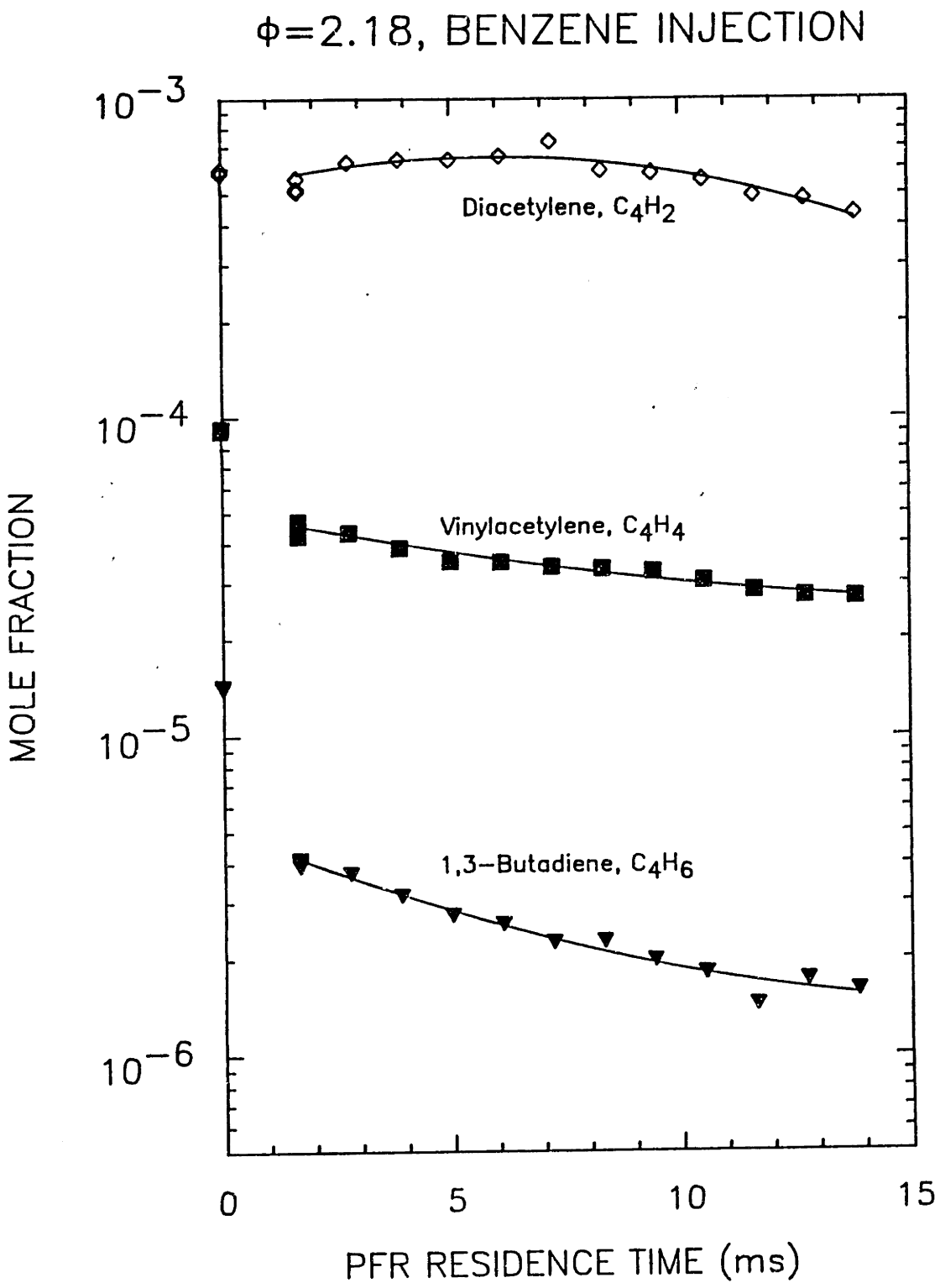

Figure 5.39 Mole Fraction Profiles for C_3 and C_4 species for Case 5: ϕ=2.18, $C_2H_4/O_2/N_2$ combustion in the JSR/PFR with C_6H_6 injection. Curves are polynomial fits to the data.

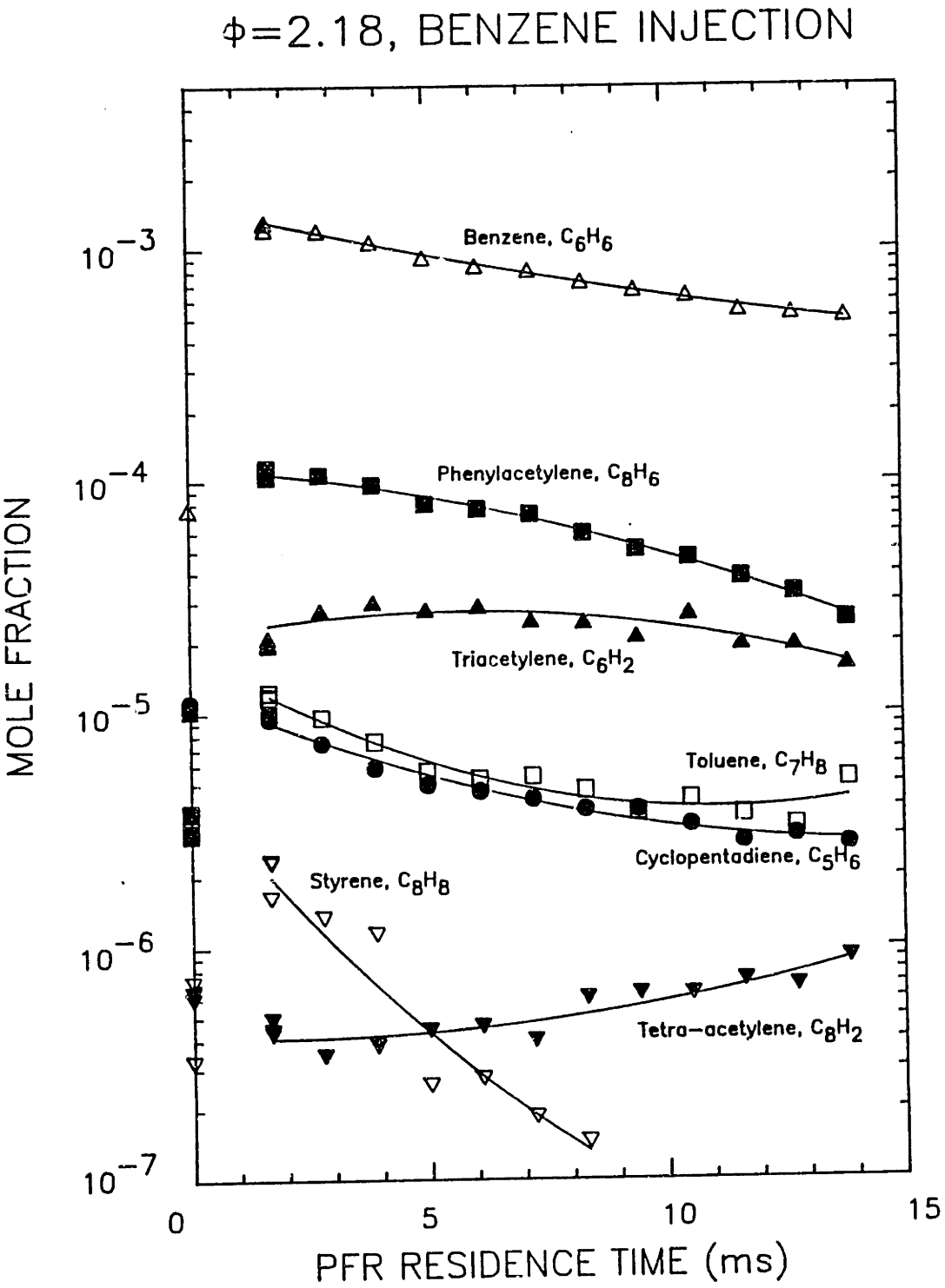

Figure 5.40 Mole Fraction Profiles for C_5 - C_8 species for Case 5: ϕ=2.18, $C_2H_4/O_2/N_2$ combustion in the JSR/PFR with C_6H_6 injection. Curves are polynomial fits to the data.

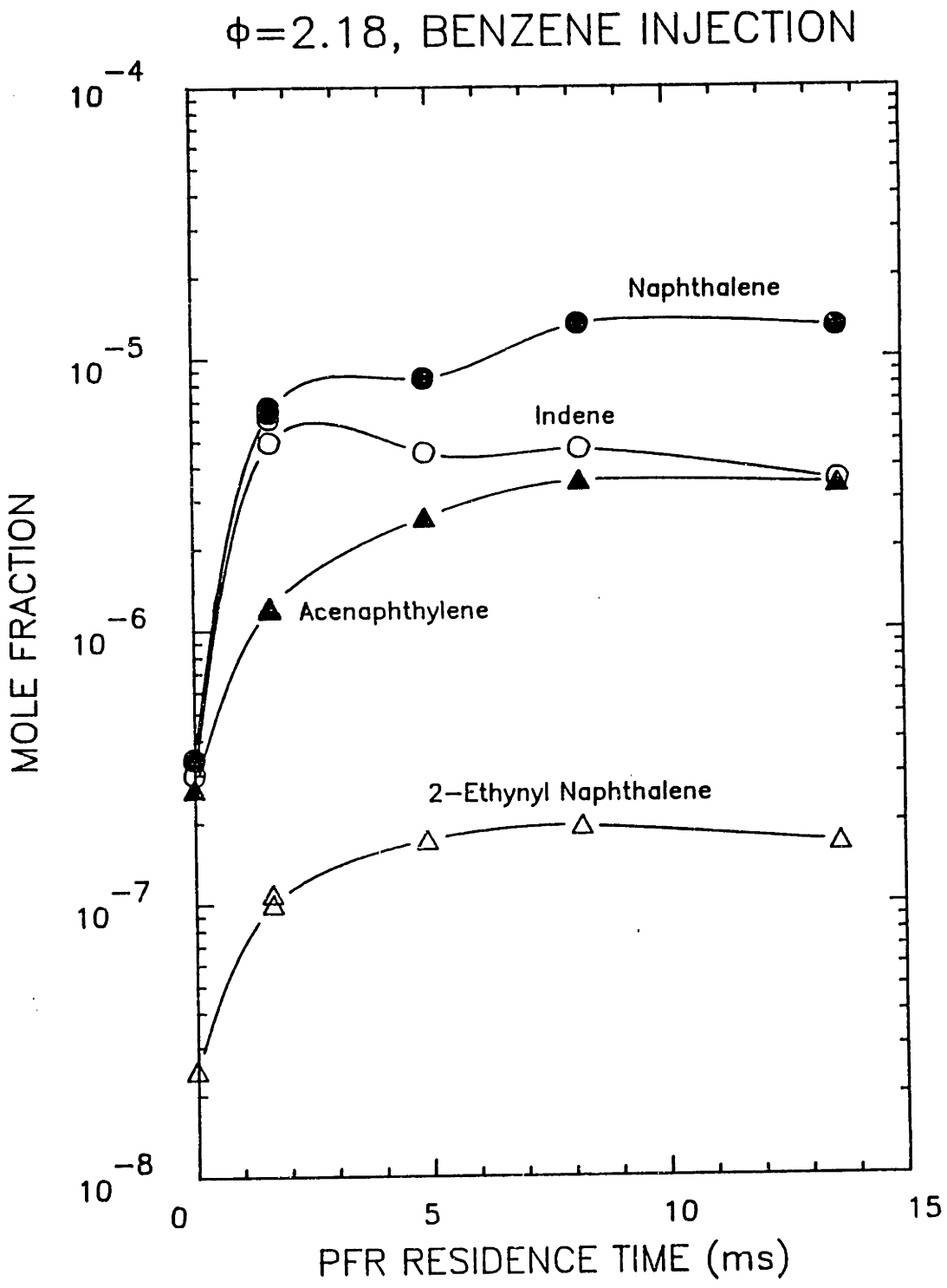

Figure 5.41 Mole Fraction Profiles for 116 - 152 amu species for Case 5: ϕ=2.18, $C_2H_4/O_2/N_2$ combustion in the JSR/PFR with C_6H_6 injection. Curves are visual fits to the data.

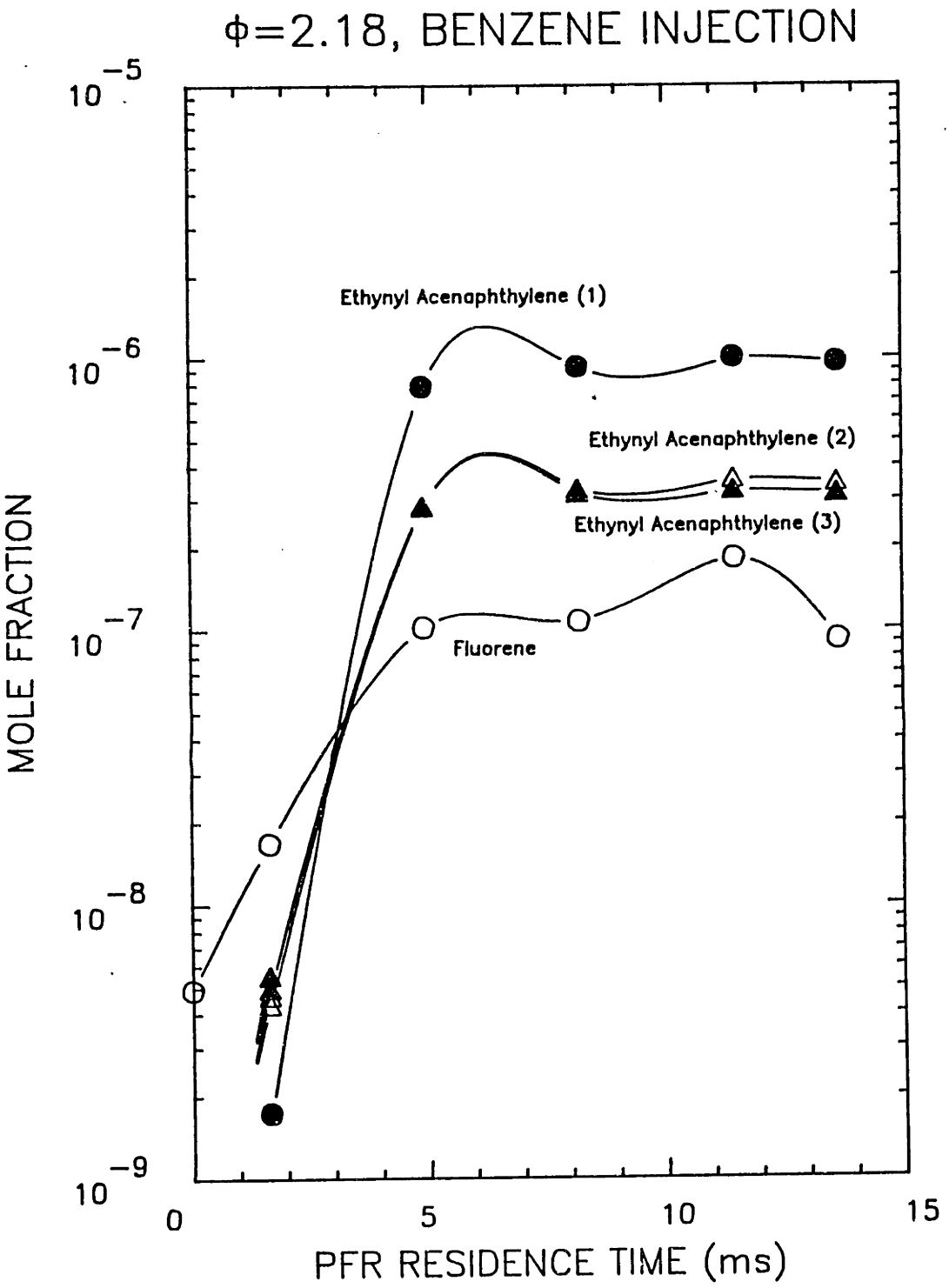

Figure 5.42 Mole Fraction Profiles for 166 - 176 amu species for Case 5: ϕ=2.18, $C_2H_4/O_2/N_2$ combustion in the JSR/PFR with C_6H_6 injection. Curves are visual fits to the data.

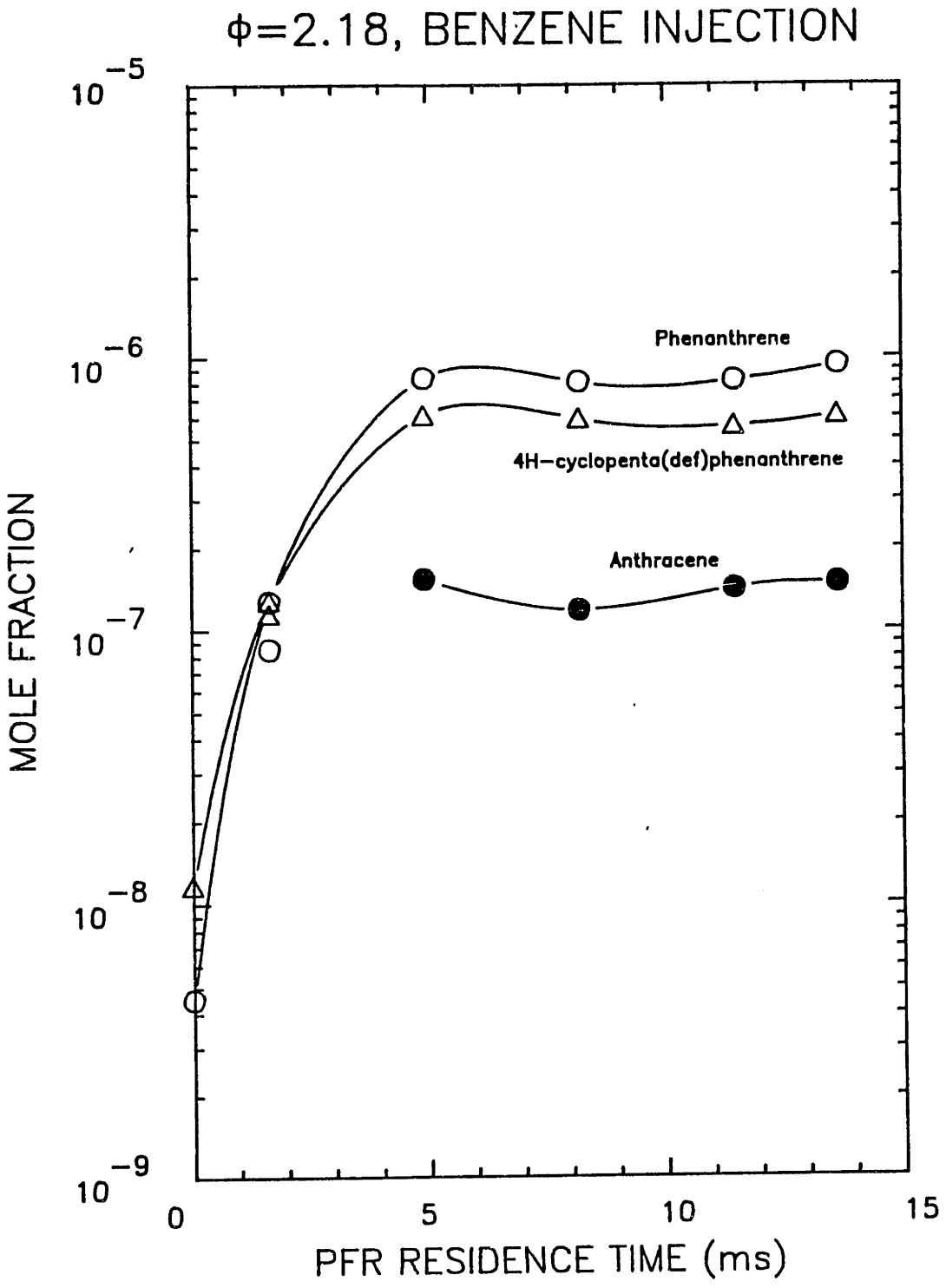

Figure 5.43 Mole Fraction Profiles for 178 - 190 amu species for Case 5: ϕ=2.18, $C_2H_4/O_2/N_2$ combustion in the JSR/PFR with C_6H_6 injection. Curves are visual fits to the data.

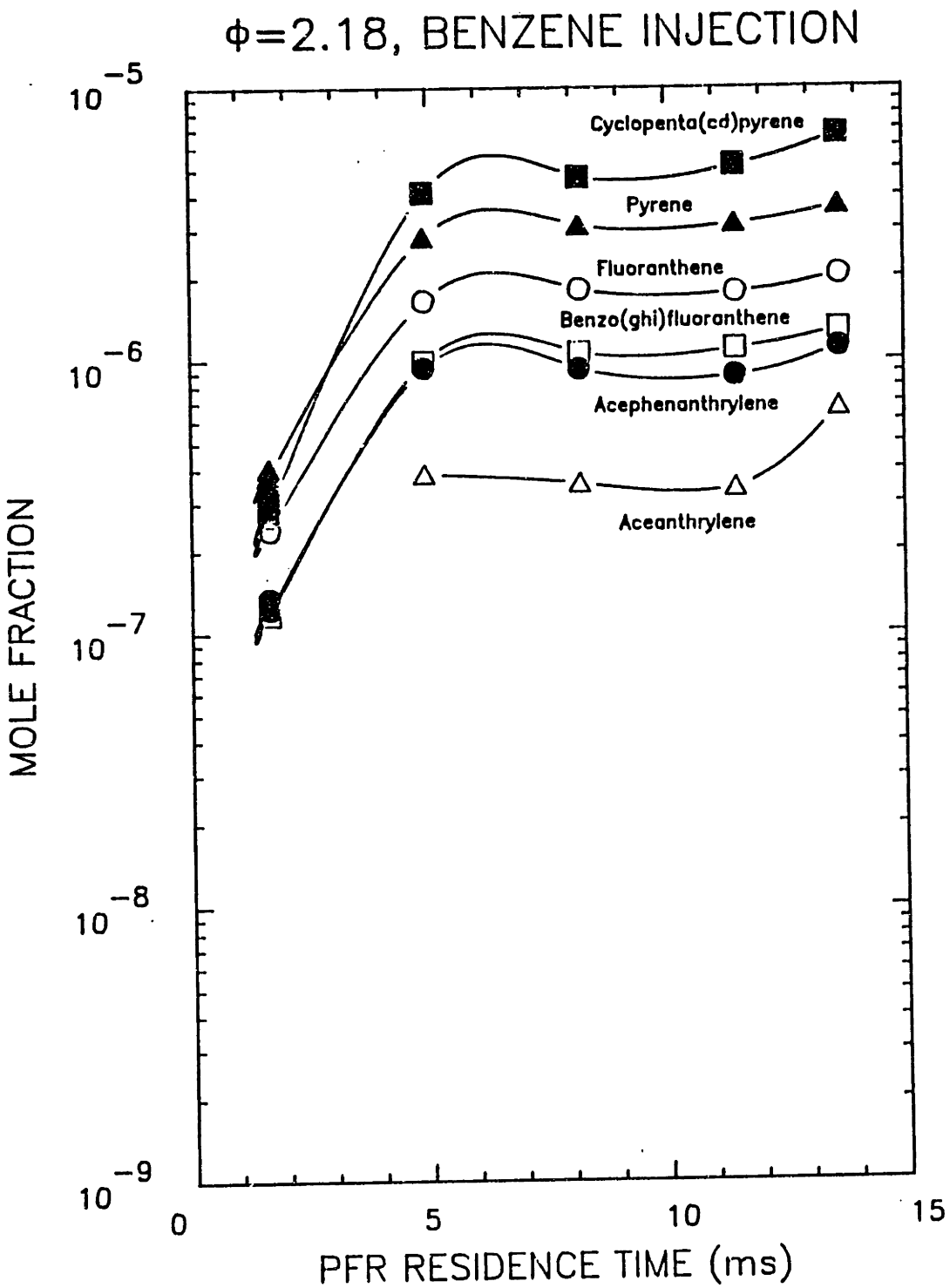

Figure 5.44 Mole Fraction Profiles for 202 - 226 amu species for $\alpha\psi$ [5] ϕ=2.18, $C_2H_4/O_2/N_2$ combustion in the JSR/PFR with C_6H_6 injection. Curves are visual fits to the data.

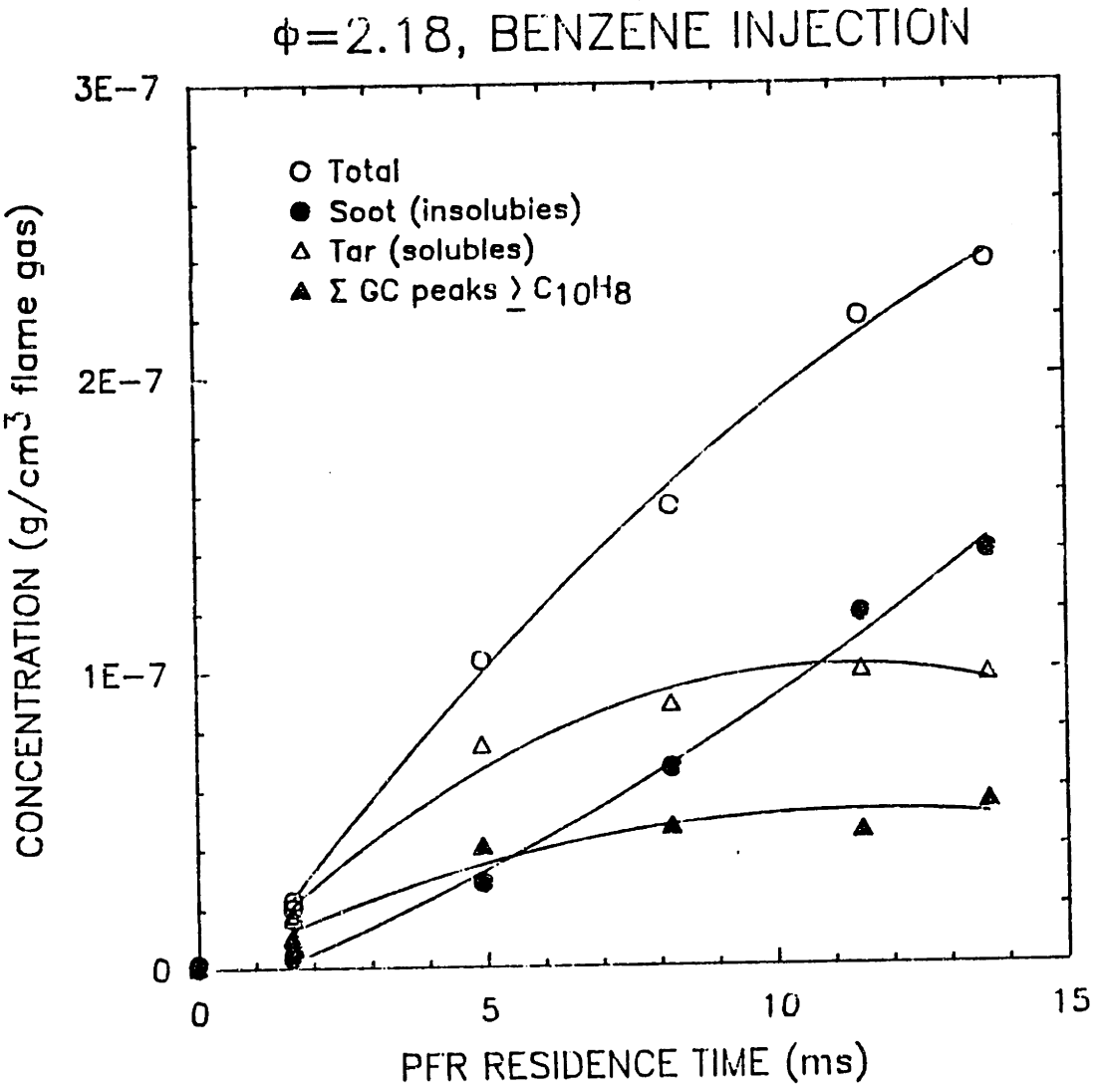

Figure 5.45 Mass Concentration Profiles for ΣGC PAH (128-226 amu), tar (CH_2Cl_2-soluble material), and soot (CH_2Cl_2-insoluble material) for Case 5: ϕ=2.18, $C_2H_4/O_2/N_2$ combustion in the JSR/PFR with C_6H_6 injection. Curves are polynomial fits to the data.

5.6 SUMMARY OF MAJOR EXPERIMENTAL OBSERVATIONS

5.6.1 Major Fixed Gases and Light Hydrocarbons

The concentrations of major species such as H_2, CO, C_2H_2, and CH_4 are increased by increasing ϕ from 2.18 to 2.37, in contrast to the concentration of CO_2 which is decreased. The addition of small amounts of C_2H_4 or C_6H_6 did not affect the fixed gas species concentrations significantly at either fuel equivalence ratio.

As shown in Figure 5.46, methane concentrations at ϕ=2.37 are about 30% higher than at ϕ=2.18, and methane is increased slightly by the addition of C_2H_4, but shows almost no effect from C_6H_6 addition. Acetylene at ϕ=2.37 is higher by about 30% than at ϕ=2.18, and its concentration is greatly affected by C_2H_4 injection. Almost 70% of the injected C_2H_4 is converted to C_2H_2 for both ϕ's, and this conversion occurs rapidly at the beginning of the PFR. The acetylene concentration for Case 4 is nearly equal to the acetylene concentration for Case 1, at the end of the PFR, indicating that most of ethylene fed to the reactor is converted to acetylene. Acetylene profiles for the 5 cases are shown in Figure 5.47.

5.6.2 Aromatics and PAH

The benzene concentrations for all 5 cases are shown in Figure 5.48. The effect of fuel equivalence ratio is to increase benzene by a factor of 2 which may be seen by comparision of Case 1 and Case 3 benzene profiles. The effect of C_2H_4 injection is to increase benzene for each of the two fuel equivalence ratios. The effect of C_6H_6 injection results in an initially high benzene mole fraction

(1.3×10^{-3}) which rapidly decays in the PFR. The concentration profiles of 4-5 ring PAH species, such as cyclopenta(cd)pyrene, have the same general shape--a sharp initial increase followed by a leveling out. The PAH concentrations are increased by increasing fuel equivalence ratio. The injection of C_2H_4 enhances slightly the production of individual PAH, and the injection of benzene greatly enhances the production of individual PAH.

5.6.3 Total Tar and Soot

The most significant effects of fuel equivalence ratio and injection of aliphatic and aromatic species, for our experimental conditions, appear in the perturbations to the total tar and soot concentration profiles. As shown in Figure 5.49, total tar is increased by a factor of 8 at the JSR and by a factor of 5 at the end of the PFR, by increasing ϕ from 2.18 to 2.37. Soot, shown in Figure 5.50, is increased by a factor of 10 at the end of the PFR for the 8.7% increase in fuel equivalence ratio from 2.18 to 2.37. The extreme sensitivity of soot yield to ϕ has been observed by many others.

The injection of C_2H_4 at $\phi = 2.18$ results in an increase in the total tar concentration, but the increased tar concentration is well below that of the ϕ=2.37 case with no injection. Although the total amount of ethylene is the same for Case 1 and Case 4, the tar yields are much less for Case 4, and implies that the tar production does not depend solely on the total amount of aliphatic fuel which is in the system. It appears that while the total amount of tar produced is

influenced by the amount of fuel, the manner in which the fuel is decomposed (ie. in the JSR vs. PFR environment) to produce intermediate growth species is an important factor.

The injection of a small amount of benzene (0.002 moles benzene/mole total flow) into the PFR increases tar production by a factor of 10 at the end of the PFR. Although 80% of the injected benzene is consumed by the end of the PFR, the concentrations of single ring aromatic species, in particular phenylacetylene, are increased and this suggests that the tar production is sensitive to the concentrations of single ring species.

The soot concentration profile is increased only slightly by C_2H_4 injection for the ϕ=2.37 case, and it is almost the same for the ϕ=2.18 case. The injection of benzene at ϕ=2.18, however, results in an increase in soot concentration of an order of magnitude, which gives a soot concentration comparable to that for the ϕ=2.37 case at the end of the PFR. The total amount of fuel for Case 1 is greater than Case 5, yet the amount of soot produced in the PFR is comparable. From this observation, we conclude that soot formation is promoted by high concentrations of intact aromatic rings, perhaps indirectly through production of tar species. This conclusion is limited to our experimental conditions, where we are studying the early stages of soot formation under lightly sooting conditions for a non-aromatic fuel.

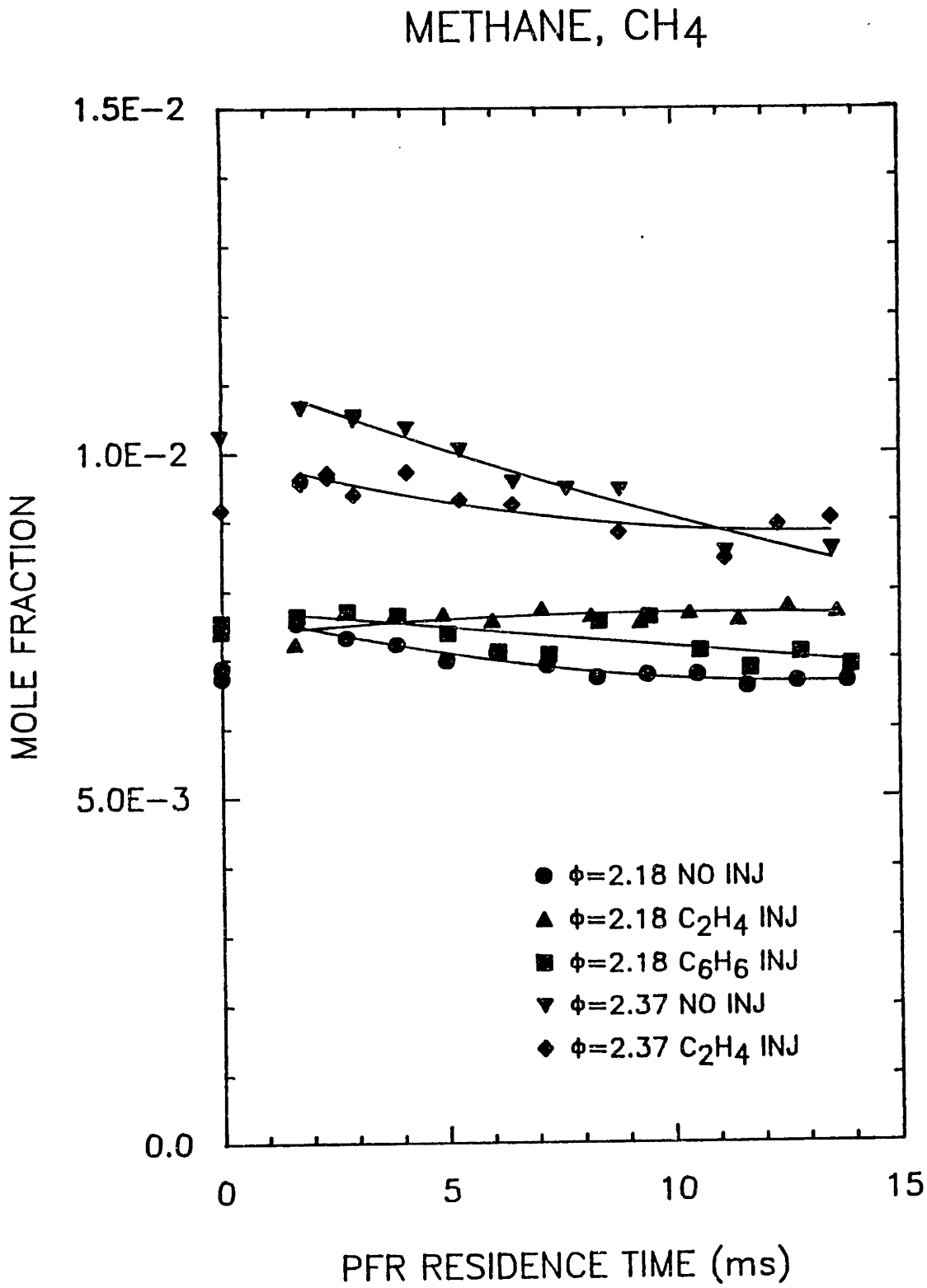

Figure 5.46 Mole Fraction Profiles for CH_4 for all 5 Cases as defined Table 5.1 for $C_2H_4/O_2/N_2$ combustion in the JSR/PFR. Curves are polynomial fits to the data.

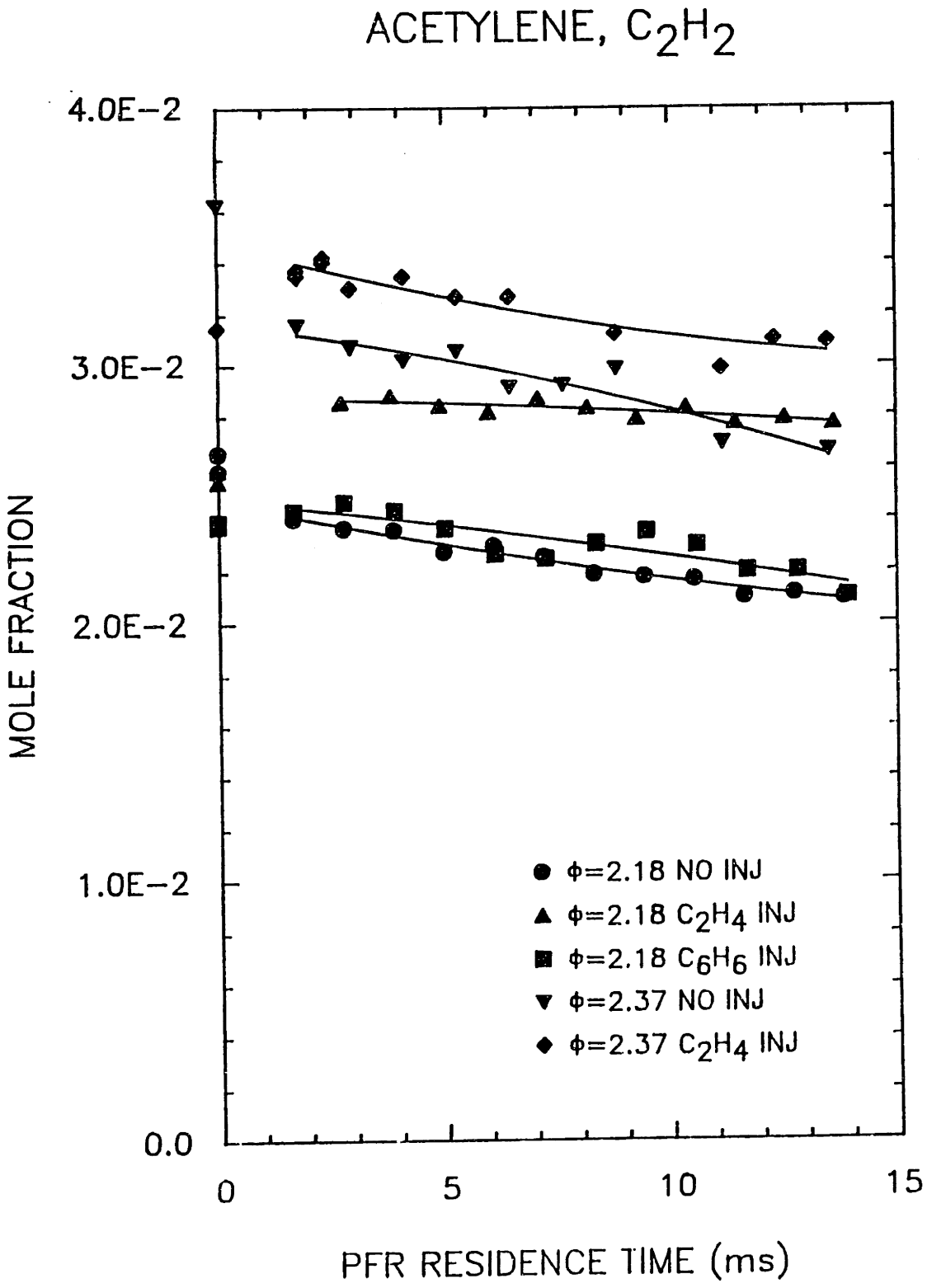

Figure 5.47 Mole Fraction Profiles for C_2H_2 for all 5 Cases as defined Table 5.1 for $C_2H_4/O_2/N_2$ combustion in the JSR/PFR. Curves are polynomial fits to the data.

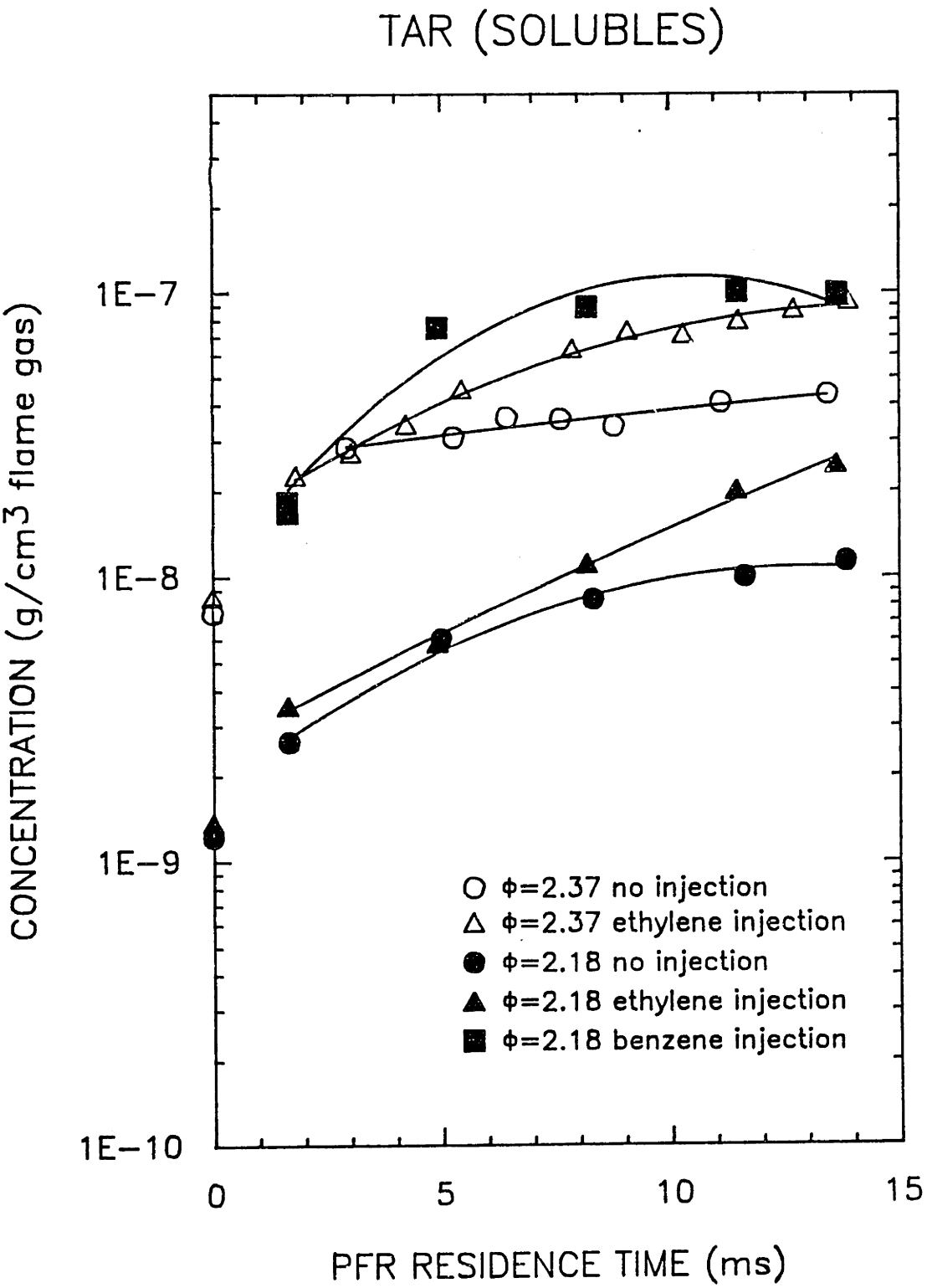

Figure 5.49 Mass Concentration Profiles for Tar (CH_2Cl_2-soluble material) for all 5 Cases as defined Table 5.1 for $C_2H_4/O_2/N_2$ combustion in the JSR/PFR. Curves are polynomial fits to the data.

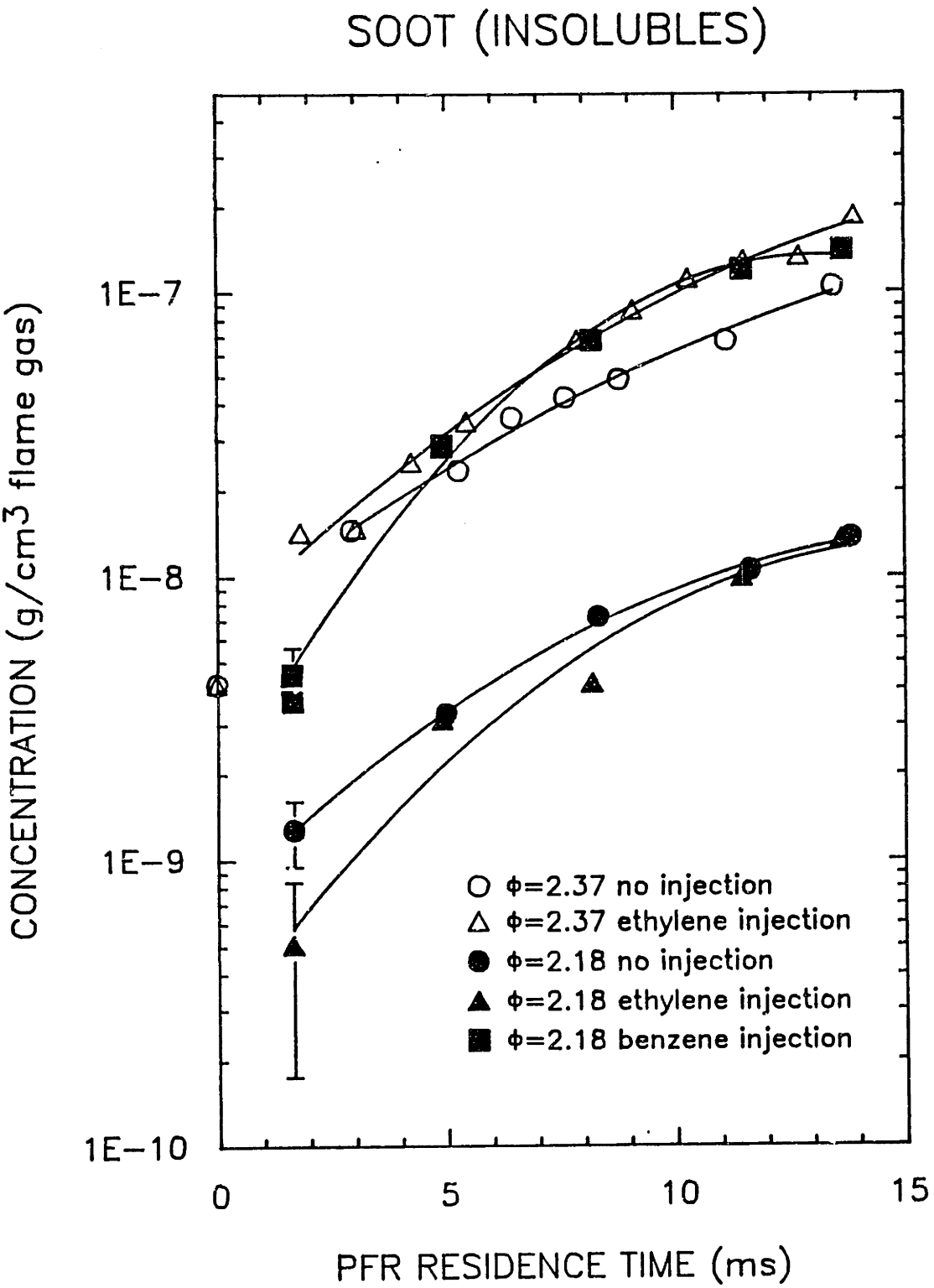

Figure 5.50 Mass Concentration Profiles for Soot (CH_2Cl_2-insoluble material) for all 5 Cases as defined Table 5.1 for $C_2H_4/O_2/N_2$ combustion in the JSR/PFR. Curves are polynomial fits to the data.

6 KINETIC MODELLING OF FIXED GASES AND LIGHT HYDROCARBONS

6.1 INTRODUCTION

Chemical mechanisms for fuel-rich combustion are much more complex than those for fuel-lean combustion because of the molecular weight growth process which forms species of higher mass than the fuel. Westmoreland (1986c) has critically tested combustion mechanisms for fuel-rich conditions proposed by Miller et al. (1983), Warnatz (1983), Westbrook et al. (1983a, 1983b), and Westbrook and Dryer (1984). The model predictions for stable and radical species were compared to data obtained by molecular beam/mass spectrometry (MB/MS) from Westmoreland's 20 torr acetylene-oxygen laminar flat flame, and the agreement for major stable species was usually within a factor of 2. The features of the species concentration profiles were generally predicted quite well and dominant reactions were analyzed using reaction path analysis.

Glarborg et al. (1986a) proposed a mechanism for nitrogen oxide formation in well-stirred reactors. This mechanism consisted 29 species with 134 hydrocarbon reactions and a subset of 75 nitrogen fixation reactions. Vaughn (1988) modelled the light hydrocarbon chemistry in the jet-stirred reactor, using the hydrocarbon set of the Glarborg mechanism with minor modifications to the reaction set, as well as adding a probe quench calculation.

Harris (1988a) has developed a model which includes species up to acenaphthylene (193 reactions, 49 species) in order to model the formation of single-ring aromatics in his ethylene-oxygen laminar flat-flame. His experimental conditions are similar to the ϕ =2.37,

T=1630K conditions in the JSR. Frenklach has used a very large mechanism (600 reactions, 180 species) to model soot formation from acetylene pyrolysis in shock tubes. In this work we use the Glarborg mechanism and the Harris mechanism to predict the fixed gases and light hydrocarbon profiles in the PFR. Computation time for the Frenklach mechanism on the VAX 11/785 would have been prohibitive, since computation time is roughly proportional to the number of species squared.

Besides being able to model fixed gases and major stable species, an important feature of extending these elementary chemical mechanisms to our sooting conditions is that we can use the predictions for important radical species concentrations, such as H, OH, and O. Since we do not have any way of experimentally determining the radical concentrations, this modeling approach allows us to make an estimation of the radical concentrations. We do not try to extend the model predictions for hydrocarbon radical species, because Westmoreland (1986c) has shown that hydrocarbon mechanisms do not predict these hydrocarbon radical species with the same accuracy as the H, OH, and O radicals for fuel-rich conditions.

6.2 DEVELOPMENT OF MODEL EQUATIONS

The problem is modelled assuming a completely-stirred tank reactor (CSTR) condition applies in the JSR, and perfect plug flow behavior is assumed for the PFR. The governing equations are simply the CSTR and PFR equations for energy and mass conservation. Because the measured reactor temperature is used as an input parameter, the energy conservation equations are decoupled from the species conservation equations, and only the mass balance for each species needs to be solved. In the PFR, the measured temperature profile was initially used. The assumption of an isothermal temperature did not change the model predictions and so a temperature of 1600K was used. In the JSR, a mass balance on each chemical species k gives

$$\dot{m} \cdot (Y_k - Y_k^{in}) = w_k \cdot W_k \cdot V \qquad \text{(Eq. 6.1)}$$

where $\dot{m}$ = the mass flow rate
Y_k = the mass fraction of the kth species in the JSR
Y_k^{in} = the mass fraction of the kth species input into the JSR
W_k = the molecular weight of the kth species
V = the volume of the reactor
w_k = the molar production rate of the kth species per unit volume.

The w_k term is dependent upon the reaction mechanism chosen for the problem. Solving the resulting set of k algebraic equations yields the solution vector $[Y_k]$, the mass fractions of each species in the WSR. The solution is used as the starting point for the PFR problem.

In the PFR, the concentration of each species will change as a function of residence time. The mass fraction of each species k is

obtained by solving the expression

$$(1/\tau)\ (Yk^{t2} - Yk^{t1}) = (wkWk/\rho) \qquad \text{(Eq. 6.2)}$$

where the residence time, τ, is given by

$$\tau = (\rho V/m) \qquad \text{(Eq. 6.3)}$$

and the mass density, ρ, is calculated from the ideal gas equation of state,

$$\rho = PW_{mean}/RT \qquad \text{(Eq. 6.4)}$$

Modelling work was facilitated by use of the computer program CHEMKIN (Kee et al. 1980), which is a FORTRAN transportable chemical kinetics computer code package. The CSTR problem was solved using code (PSR) written by Glarborg et al. (1986b) which uses a hybrid Newton/time-integration procedure. The governing differential equations for the PFR problem were solved using the Livermore Solver for Ordinary Differential Equations, LSODE, (Hindmarsh, 1983), an efficient numerical integration routine which is based on Gear and Gearb packages. LSODE is especially efficient at solving the initial value problem for systems of first order ordinary differential equations for combustion problems. The computations were performed on a VAX 11/785.

The experimental reactor conditions dictated the temperature,

residence time, and fuel-equivalence ratio for the computations. These were the only experimental values which were used in the model.

The solution vector of species concentrations for the CSTR problem was used as the initial value for the PFR problem. It should be emphasized that for the kinetic modelling of light hydrocarbons, no adjustable parameters were used. The rate constants from the literature mechanisms were used, except for the reactions which have been noted.

6.3 MODEL RESULTS

The Glarborg mechanism is shown in Appendix A.1 with the appropriate modifications. Some of the reactions in the set had undefined products such as reaction #78 CH + C_2H_4 --> "PRODUCTS" and reaction #79 CH + C_2H_6 --> "PRODUCTS". The CHEMKIN code is not equipped to handle undefined chemical species because of the mass balance requirement, and so for reaction #78, methyne was assumed to add to C_2H_4 to form C_3H_2 + H, and for reaction #79, methyne was assumed to abstract H from C_2H_6 to give CH_2 + C_2H_5. Actually from the reaction path analysis, neither of these two reactions were very important in determining the fixed gases and light hydrocarbon species profiles.

The Harris mechanism is shown in Appendix A.2, and the modifications to the published mechanism are also noted. Some of the modifications were merely corrections of typographical errors in the published mechanism, and others were modifications to accommodate computation on the VAX 11/785. For example, Reactions K07 (C_4H_4+M = C_2H_2+C_2H_2+M) and K11 (C_4H_4+M = C_4H_2+H_2+M) had large A-factors ($\approx 10^{93}$) because of their highly non-Arhenius temperature dependence. The VAX 11/785 cannot handle numbers larger than $\approx 10^{38}$, and so these rate constants were computed at 1600K and a non-activated rate constant was used. Because the JSR/PFR is nearly isothermal, we do not expect the errors from this approximation to be large.

The two baseline cases (ϕ = 2.18 and ϕ = 2.37) were modelled using the Glarborg and Harris mechanisms and the comparison of the model predictions to the experimental data for fixed gases and

acetylene are shown in Figures 6.1 and 6.2. The differences in major species concentrations between the two fuel equivalence ratios are not large. Both models predict the species profiles quite well, although the Harris mechanism under-predicts C_2H_2 by about a factor of 2 at the end of the PFR for ϕ=2.18.

If we look at the individual species profiles, we see that the agreement between the Glarborg predictions and experiment for H_2, shown in Figure 6.3, are quite good. The model correctly predicts the profile shapes which are slightly increasing and the relative amounts of H_2 to within 10% for the two fuel equivalence ratios. The model correctly predicts that more H_2 is produced in the more fuel-rich case. The difference between the experimental data for the two equivalence ratios is slightly larger than the difference predicted by the model. The model predicts an increase in H_2 mole fraction at the end of the PFR from 0.092 to 0.104. The data shows an increase at the end of the PFR from 0.090 to 0.112.

The Glarborg prediction for CO is also quite good, as shown in Figure 6.4. The mole fraction of CO for the ϕ = 2.18 case is predicted to be less than for the ϕ = 2.37 case, as is experimentally observed.

Figure 6.5 shows that carbon dioxide is also well predicted by the Glarborg mechanism. For the ϕ = 2.18 case we would expect more CO_2 to be produced by the end of the PFR than for the ϕ = 2.37 case. The model predicts this trend, and the data seems to also show this trend, although not without some uncertainty due to experimental error.

The agreement between the Glarborg mechanism and experimental data for methane, as shown in Figure 6.6, is not as good as the fixed gases. For the both ϕ = 2.18 and ϕ = 2.37, CH_4 is underpredicted at the end of the PFR by a factor of about 2. Also the trend is not correctly predicted. The experimental data show a slight decrease in the PFR after an initial increase from the JSR, and model predicts an increasing CH_4 profile in the PFR.

Acetylene, as shown in Figure 6.7, is underpredicted in the JSR by 25% for both equivalences ratios. This discrepancy is much less, however, by the end of the PFR, where C_2H_2 is only underpredicted by ≈10%. The predicted C_2H_2 profile is almost flat, but the experimental profiles show a decrease over the length of the PFR. A possible explanation for the difference in C_2H_2 profiles is if reactions which consume C_2H_2 are occurring in the reactor involve species which are not included in the mechanism. Since aromatics, PAH and soot are all present in the PFR, but are not included in the mechanism, they may have an effect on the C_2H_2 profile.

Ethylene, as shown in Figure 6.8, is predicted to decrease very sharply after leaving the JSR. The experimental profiles do not show such as drastic decline. The final concentrations of C_2H_4 at the end of the PFR are close to that predicted by the mechanism. For ϕ = 2.18 the predicted and experimental values at the end of the PFR are within 10%, and for ϕ = 2.37, they are within 33%. As discussed earlier, the transition region between the JSR and PFR is not well characterized, and makes modelling difficult for some species. Ethylene is one such species.

One of the main reasons for modeling the fixed gases and light hydrocarbon chemistry is to obtain predictions for the species which we cannot experimentally measure. Oxygen is present in the PFR in concentration too low to detect, and radicals such as H, OH, O, CH_3, C_2H, and C_2H_3 may play an important role in the formation of PAH. It is necessary to estimate the concentrations of these species in the PFR. By using the combustion mechanisms we can obtain predictions for oxygen and the radical species, and these model predictions are shown in Figures 6.9 - 6.13.

Figure 6.9 shows the model predictions for oxygen for both fuel equivalence ratios. Oxygen is predicted to decay very rapidly (almost 3 orders of magnitude in 15 msec) by both models for both fuel equivalence ratios. The Glarborg mechanism gives similar predictions for O_2 for the two equivalence ratios and predicts more O_2 to be present throughout the PFR for the more fuel-lean case. The Harris mechanism predicts the opposite trend, that is, more oxygen for ϕ=2.37 than ϕ=2.18. The differences between the two mechanisms are largest in the flow transition region before 2 msec where the Harris mechanism predict 3 times more oxygen than the Glarborg mechanism for ϕ=2.37. Otherwise, the models are in close agreement.

We see from Figure 6.10 that the models give very similar predictions for H atoms, especially at long residence times in the PFR. For the Glarborg prediction at ϕ=2.37, the H atom concentration is predicted to drop sharply from a JSR mole fraction of $5x10^{-4}$ to $3x10^{-5}$ by the end of the PFR. Similar profiles are predicted by the Harris mechanism and for both equivalence ratios. The Harris

mechanism predicted higher oxygen mole fraction profiles than the Glarborg mechanism, because the Harris predictions for H atom are slightly lower than the Glarborg predictions, and oxygen destruction is directly linked to H atom concentration through the important chain-branching combustion reaction $H+O_2 = OH+O$. This reaction accounts for most of the oxygen destruction in the PFR. The H atom mole fraction for most of the PFR residence time is predicted by both models to not be sensitive to ϕ over this narrow range of equivalence ratios.

The mole fraction profiles of OH, as shown in Figure 6.11 show a similar behavior to the H atom profiles. For ϕ=2.37, the Glarborg mechanism predicts OH mole fraction to drop rapidly from $2x10^{-5}$ to $1x10^{-6}$. The Harris mechanism predicts OH to be a factor of 2 less in the JSR than the Glarborg mechanism and to decay rapidly to a similar mole fraction of about $9.5x10^{-7}$.

Oxygen atom, as shown in Figure 6.12, is predicted by the Glarborg mechanism to be at a much lower concentration than OH in the JSR for ϕ=2.37 by a factor of 10, and O decays more rapidly to a very low final mole fraction of $1x10^{-10}$. The Harris mechanism predicts almost identical O mole fractions for both ϕ=2.18 and ϕ=2.37, and these predictions are higher than the Glarborg predictions by a factor of 5-10.

Methyl radical predictions are different for the two mechanisms by a factor of 3 at the end of the PFR for both ϕ's, as shown in Figure 6.13. The profiles have similar shapes, however, and CH_3 approaches a constant mole fraction of $1x10^{-4}$ as predicted by the

Harris mechanism for both ϕ's, and a constant mole fraction of $3x10^{-5}$ for ϕ=2.37, ($2x10^{-5}$ for ϕ=2.18) as predicted by the Glarborg mechanism. Reaction path analysis reveals that the reaction $CH_4+H = CH_3+H_2$ is predicted to be near partial equilibrium throughout the PFR for both mechanisms.

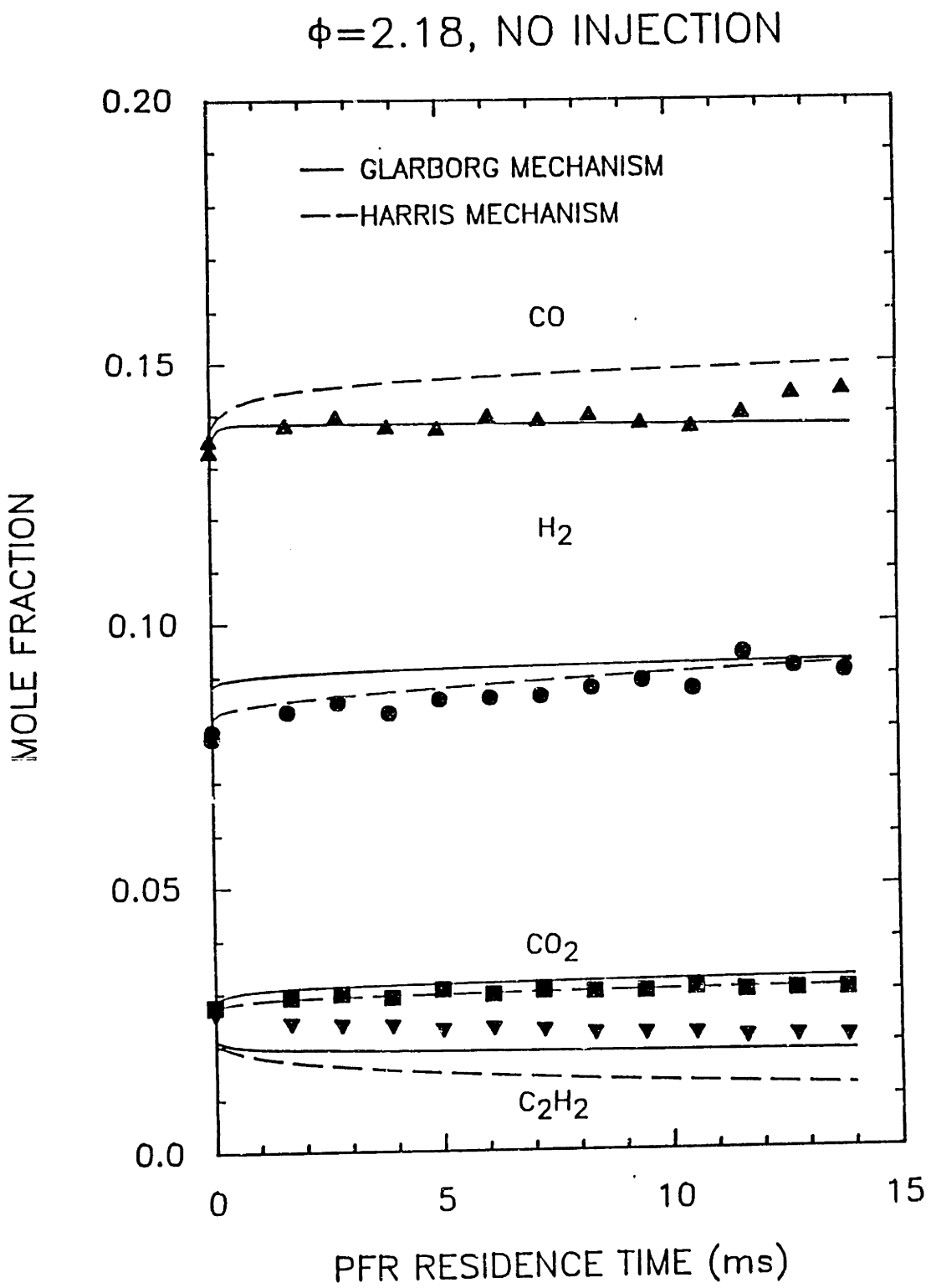

Figure 6.1 Comparison of Glarborg mechanism and Harris mechanism predictions with experimental concentration profiles for CO, H_2, CO_2, and C_2H_2 in JSR/PFR at ϕ=2.18.

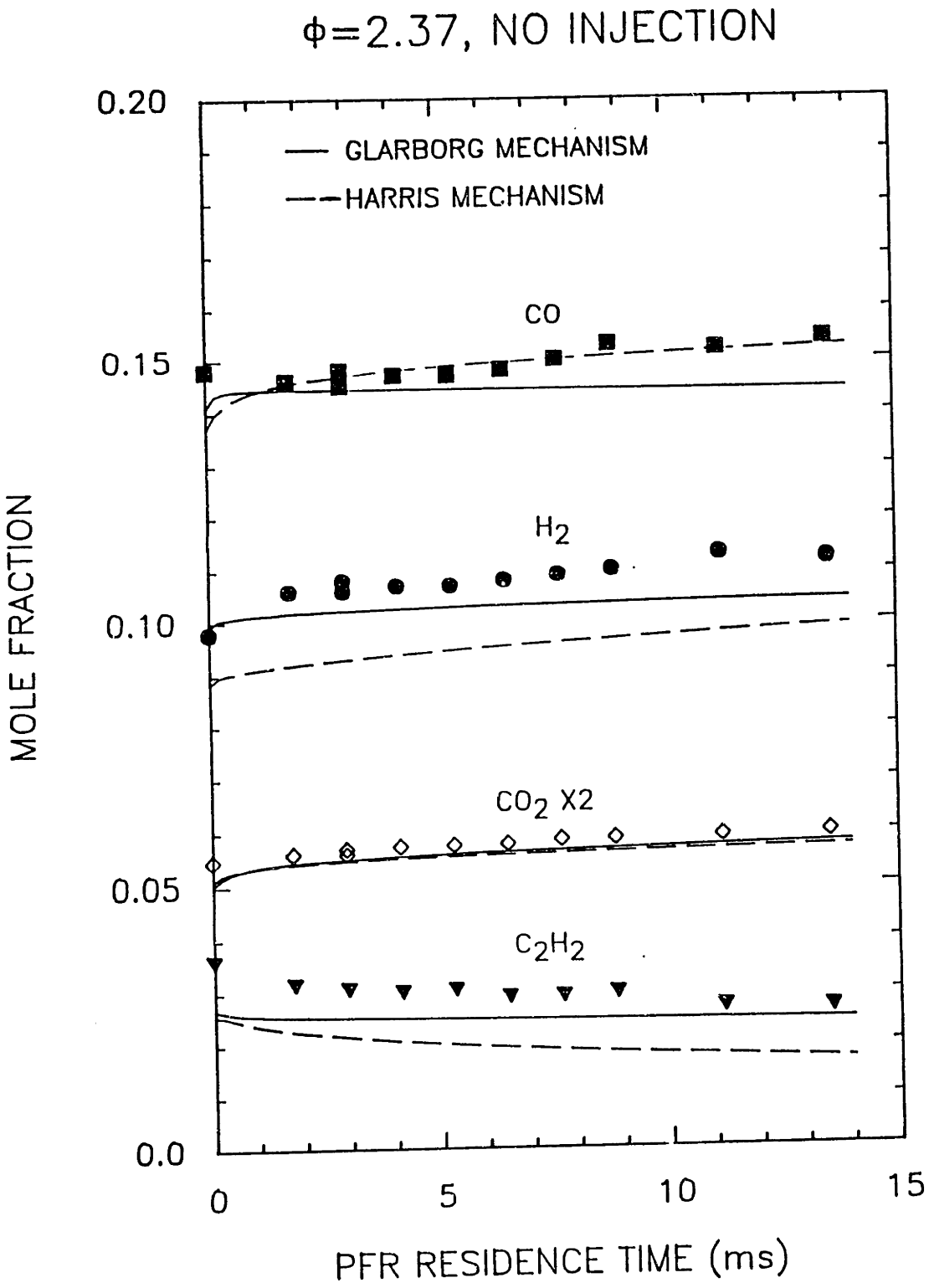

Figure 6.2 Comparison of Glarborg mechanism and Harris mechanism predictions with experimental concentration profiles for CO, H_2, CO_2, and C_2H_2 in JSR/PFR at ϕ=2.37.

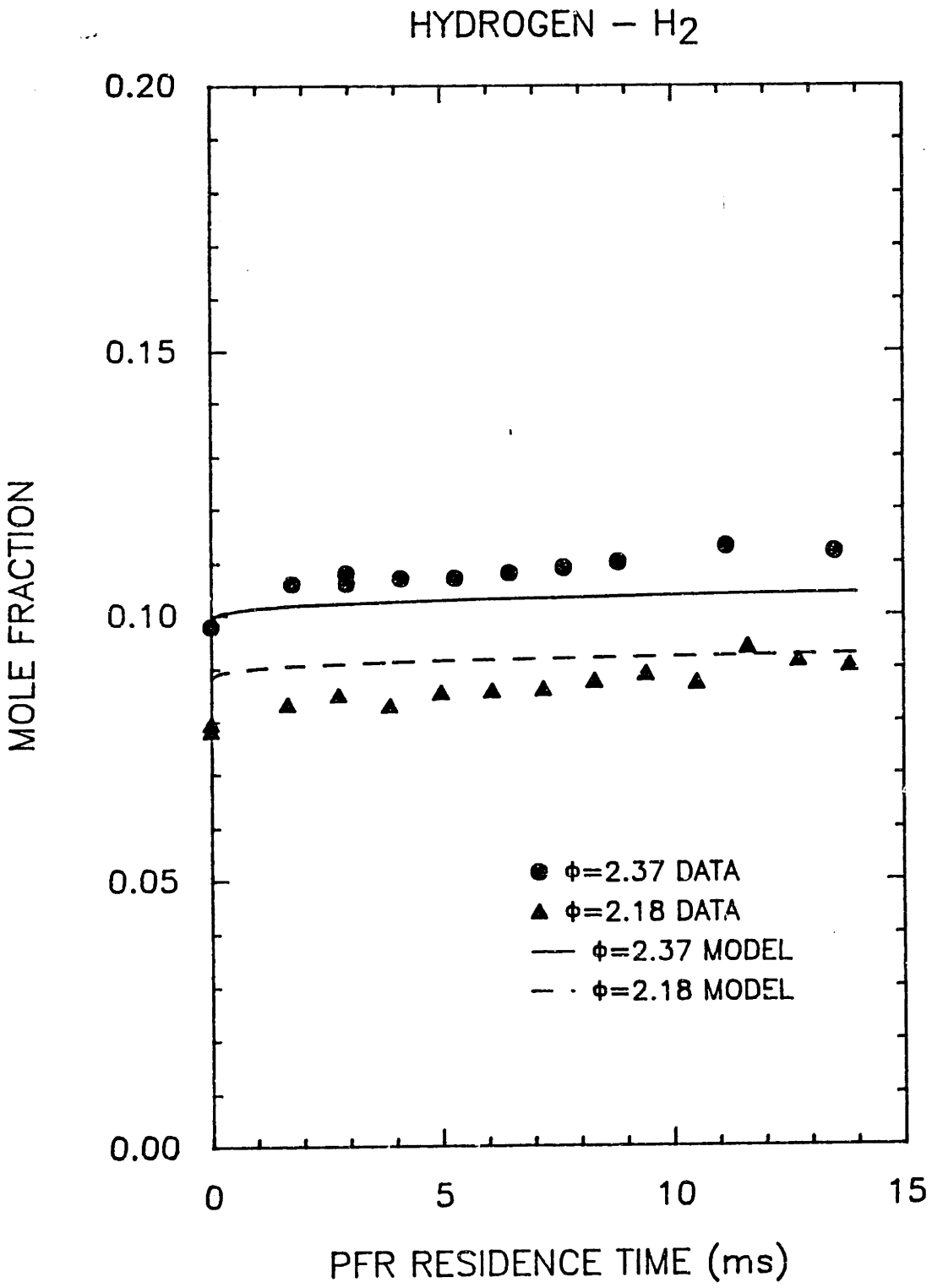

Figure 6.3 Comparison of Glarborg mechanism and Harris mechanism predictions with experimental concentration profiles for H_2 in JSR/PFR at ϕ=2.18 and ϕ=2.37.

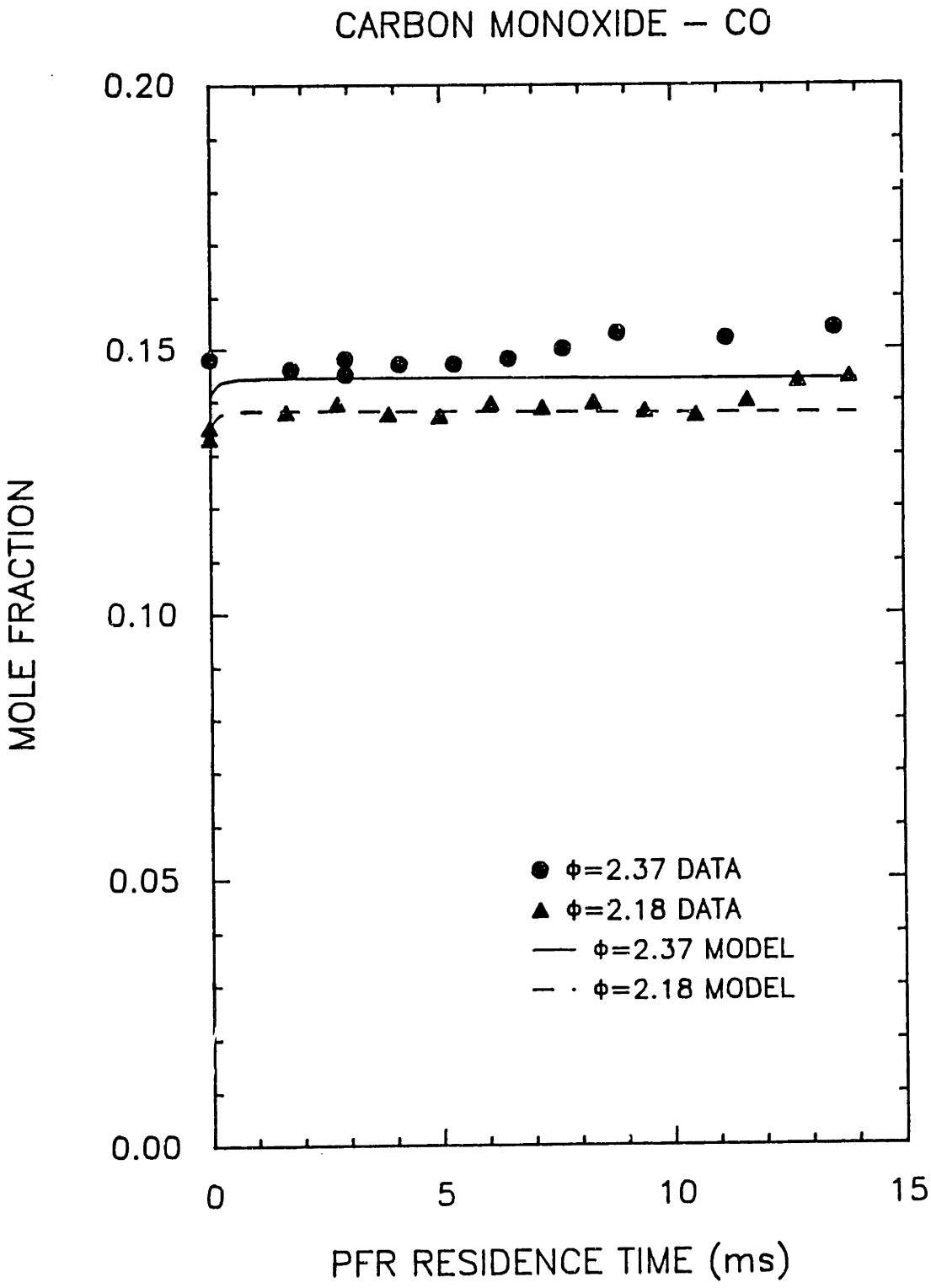

Figure 6.4 Comparison of Glarborg mechanism and Harris mechanism predictions with experimental concentration profiles for CO in JSR/PFR at ϕ=2.18 and ϕ=2.37.

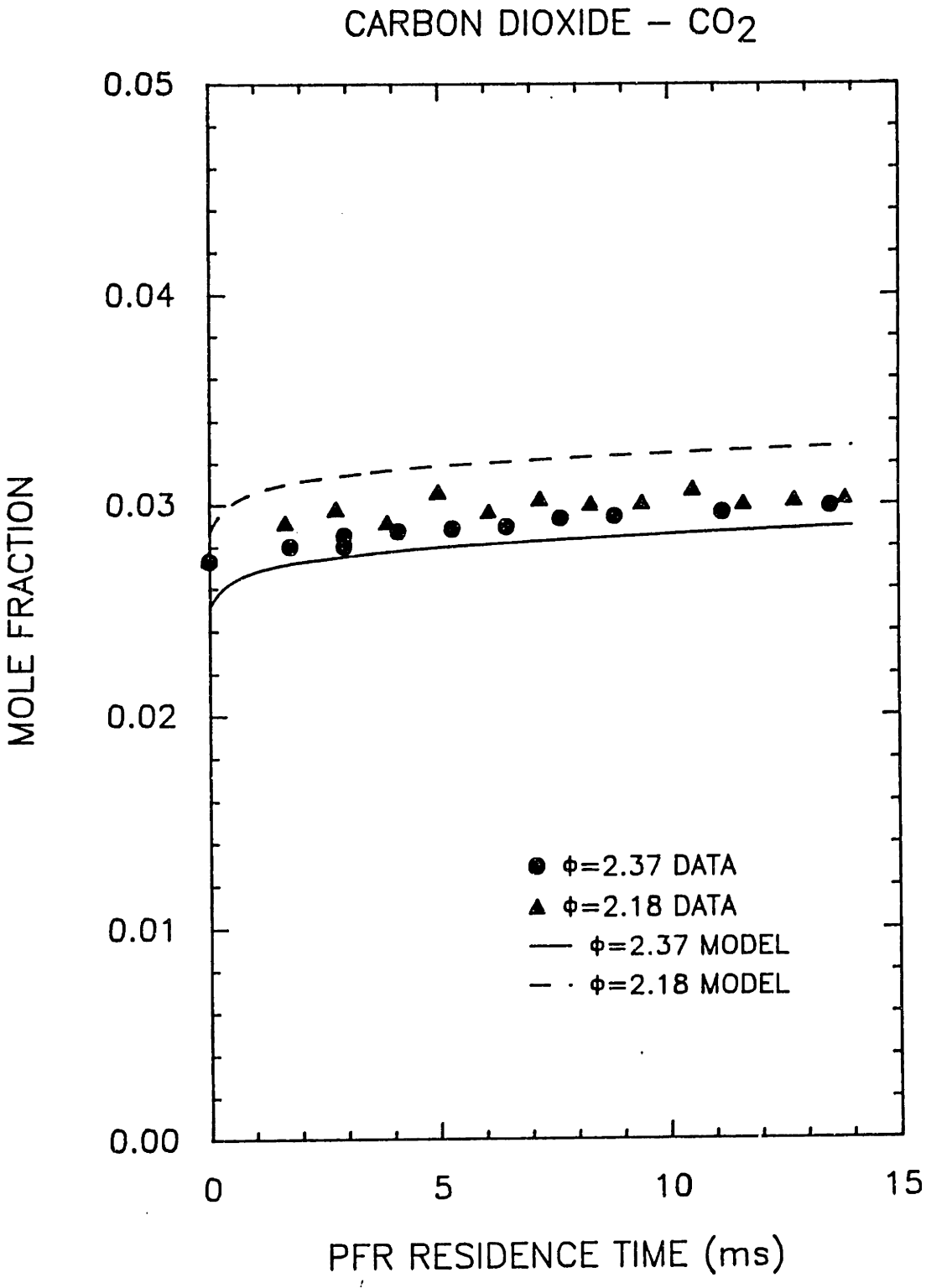

Figure 6.5 Comparison of Glarborg mechanism and Harris mechanism predictions with experimental concentration profiles for CO_2 in JSR/PFR at ϕ=2.18 and ϕ=2.37.

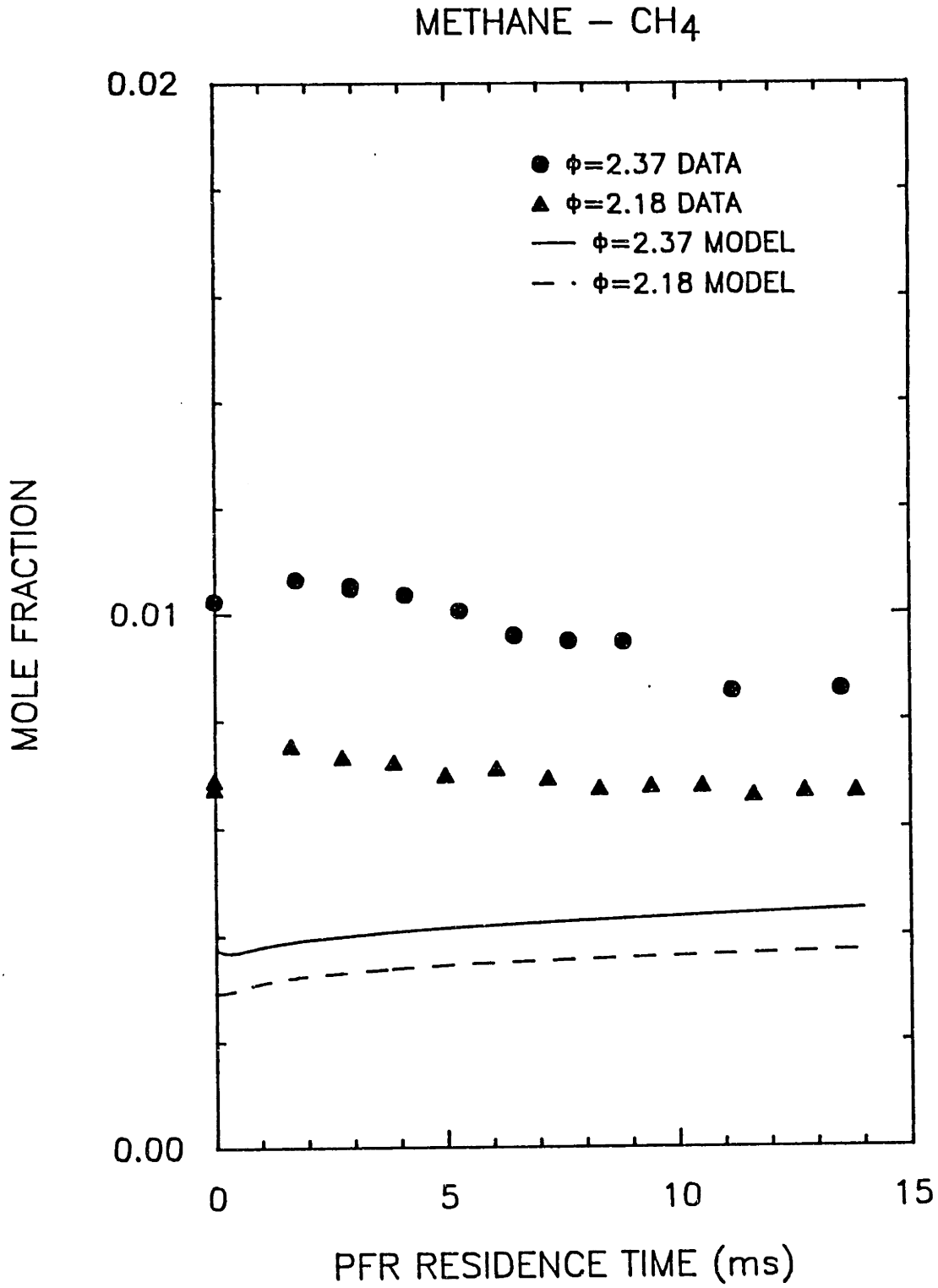

Figure 6.6 Comparison of Glarborg mechanism and Harris mechanism predictions with experimental concentration profiles for CH_4 in JSR/PFR at ϕ=2.18 and ϕ=2.37.

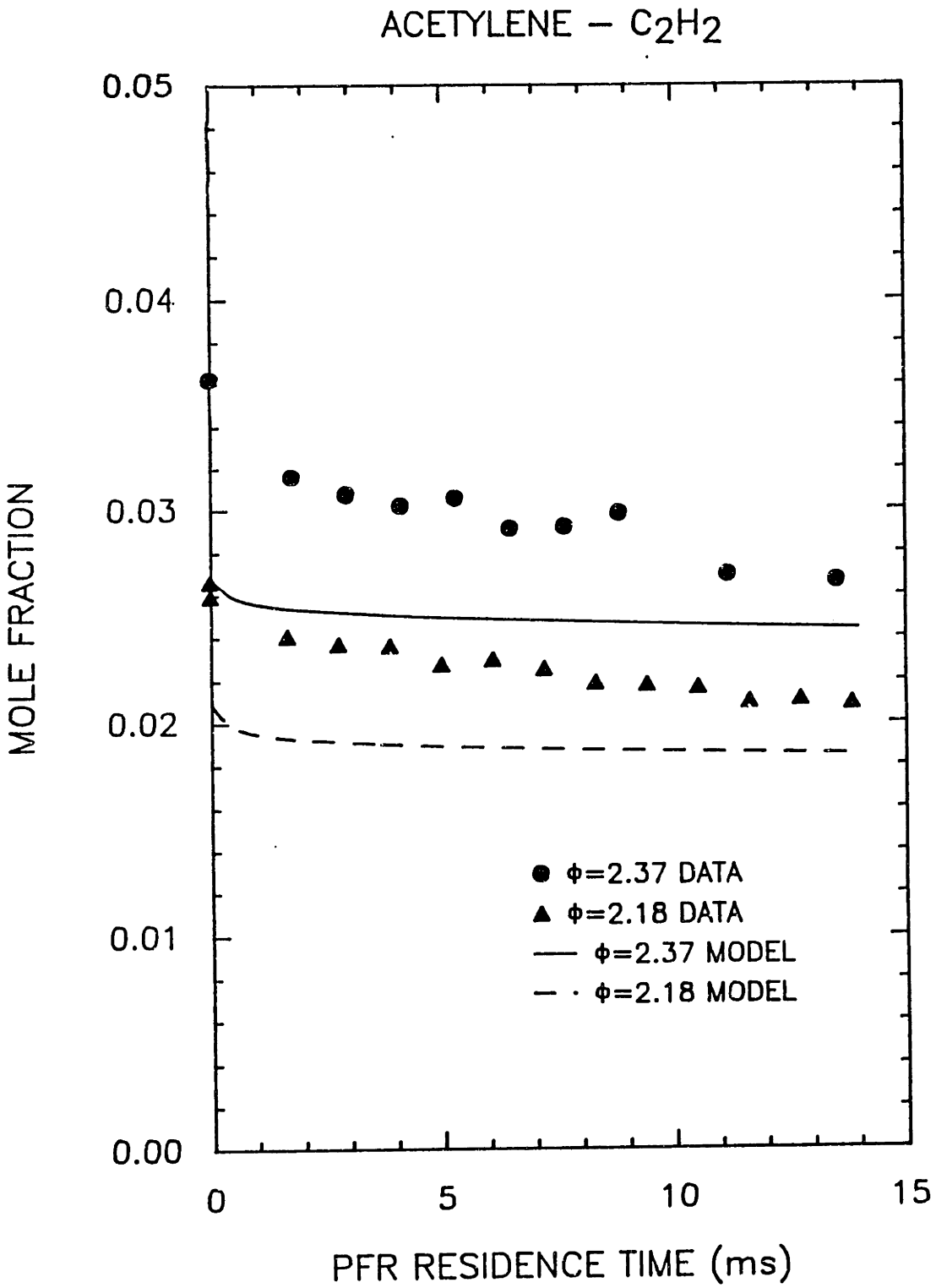

Figure 6.7 Comparison of Glarborg mechanism and Harris mechanism predictions with experimental concentration profiles for C_2H_2 in JSR/PFR at ϕ=2.18 and ϕ=2.37.

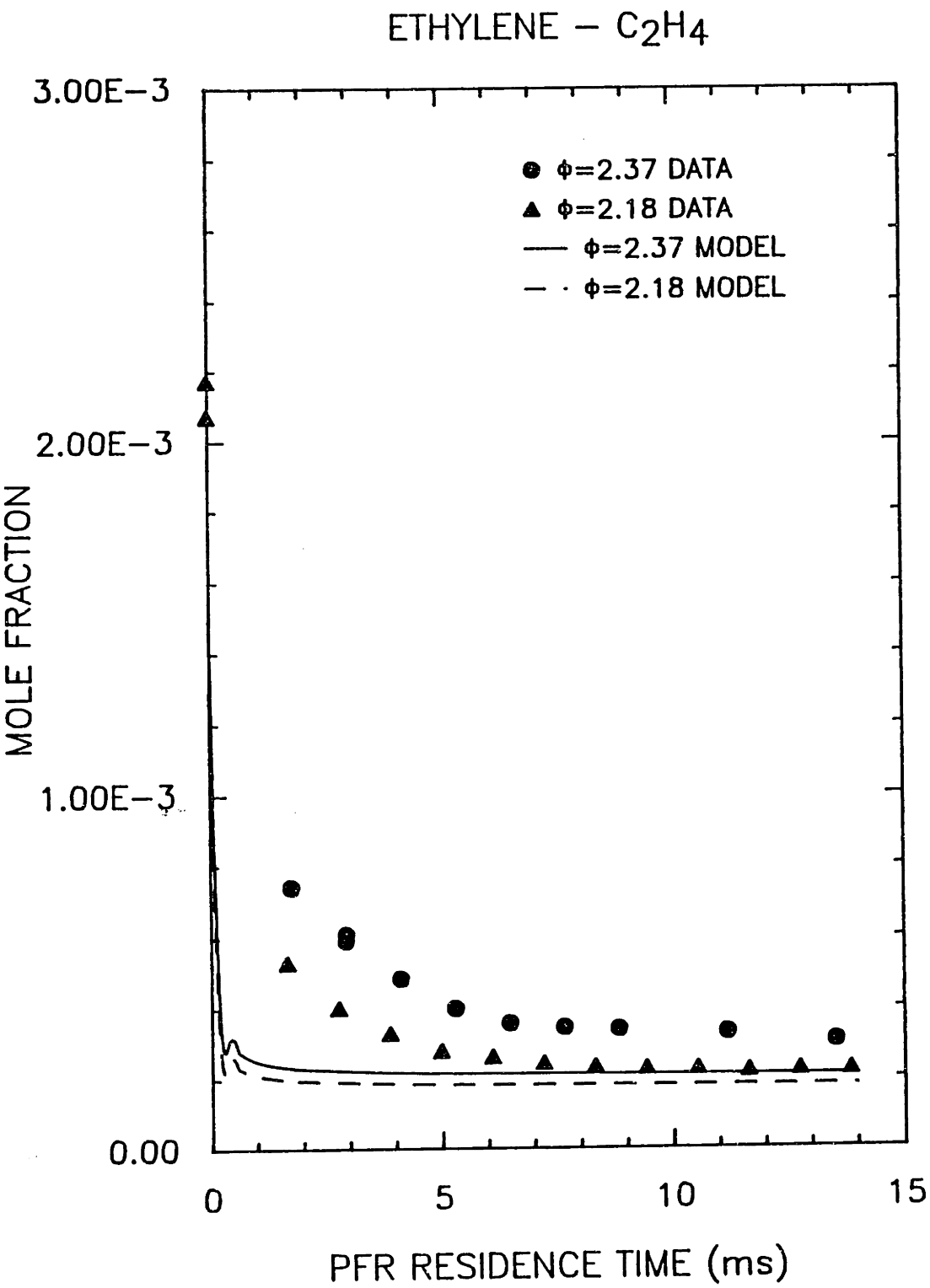

Figure 6.8 Comparison of Glarborg mechanism and Harris mechanism predictions with experimental concentration profiles for C_2H_4 in JSR/PFR at ϕ=2.18 and ϕ=2.37.

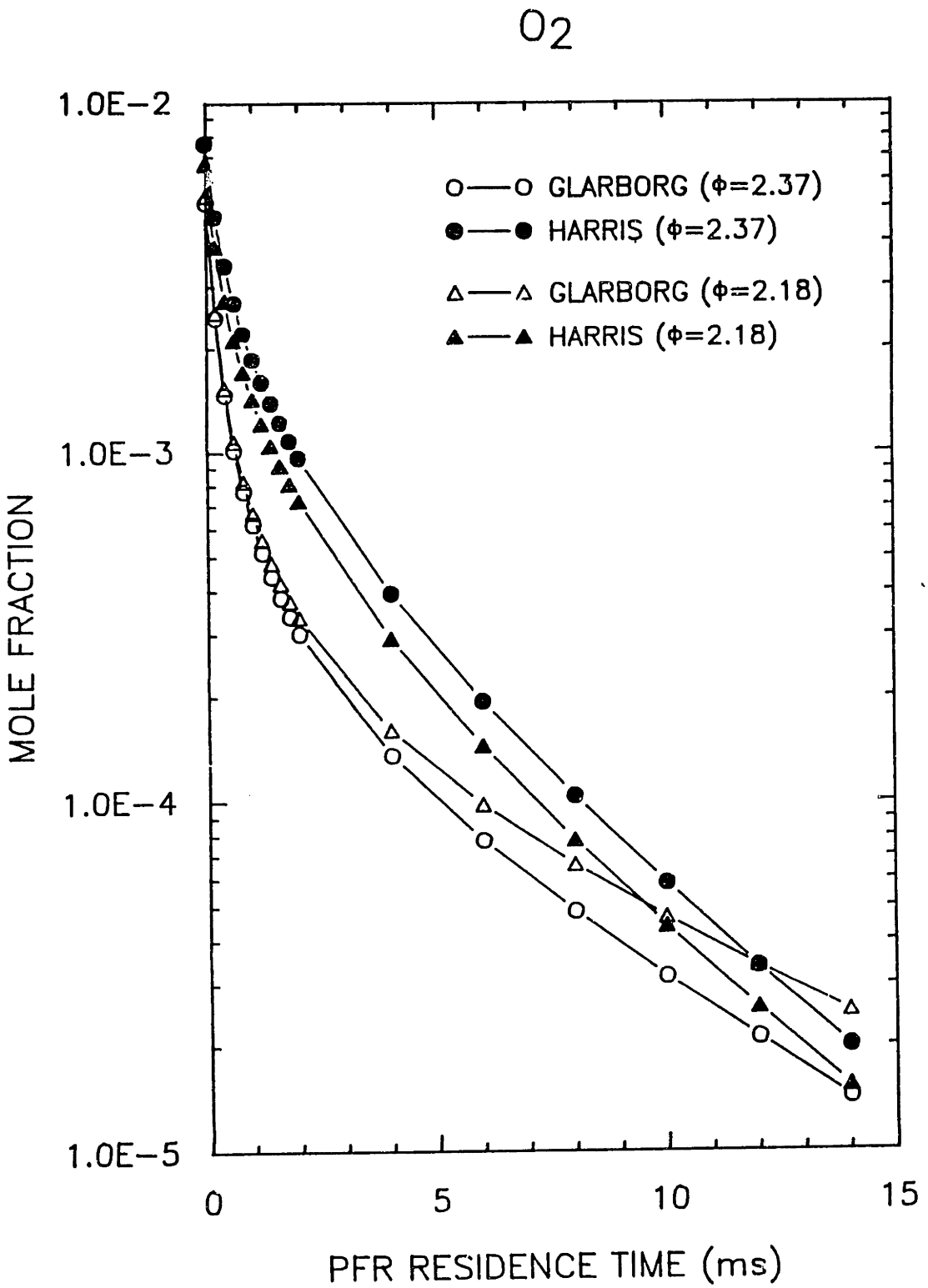

Figure 6.9 Comparison of Glarborg mechanism and Harris mechanism predictions for O_2 in JSR/PFR at ϕ=2.18 and ϕ=2.37.

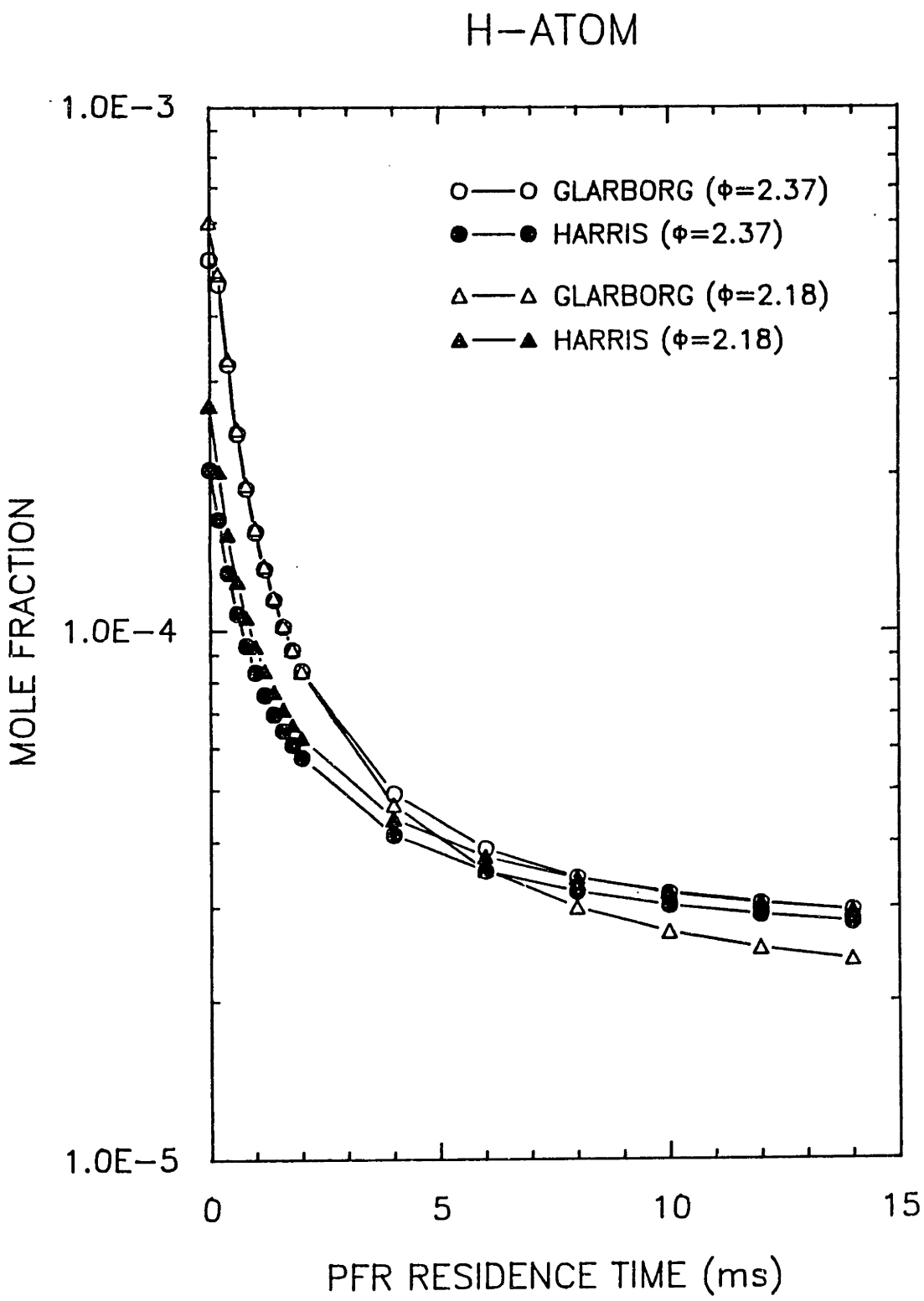

Figure 6.10 Comparison of Glarborg mechanism and Harris mechanism predictions for H atom in JSR/PFR at ϕ=2.18 and ϕ=2.37.

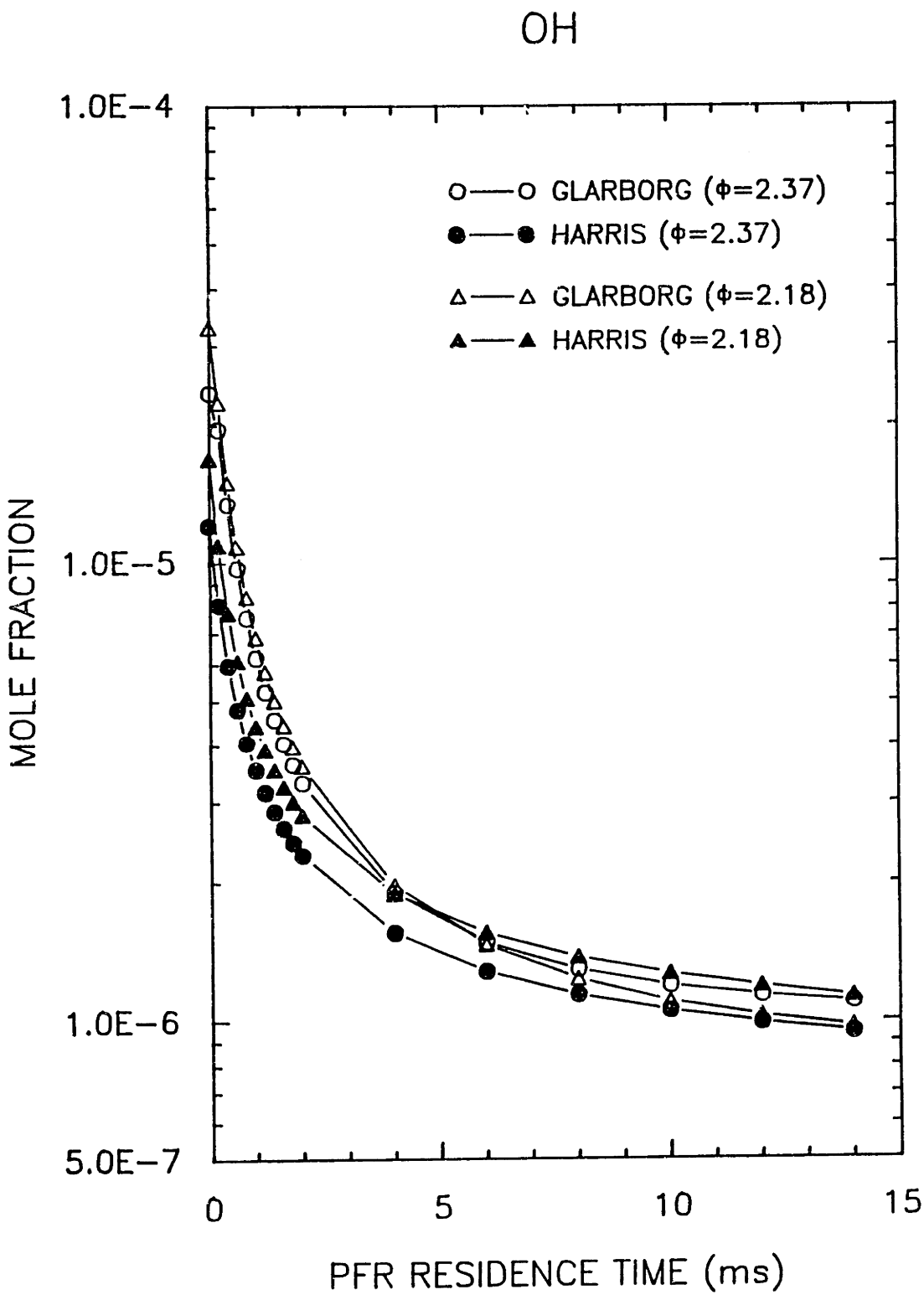

Figure 6.11 Comparison of Glarborg mechanism and Harris mechanism predictions for OH in JSR/PFR at ϕ=2.18 and ϕ=2.37.

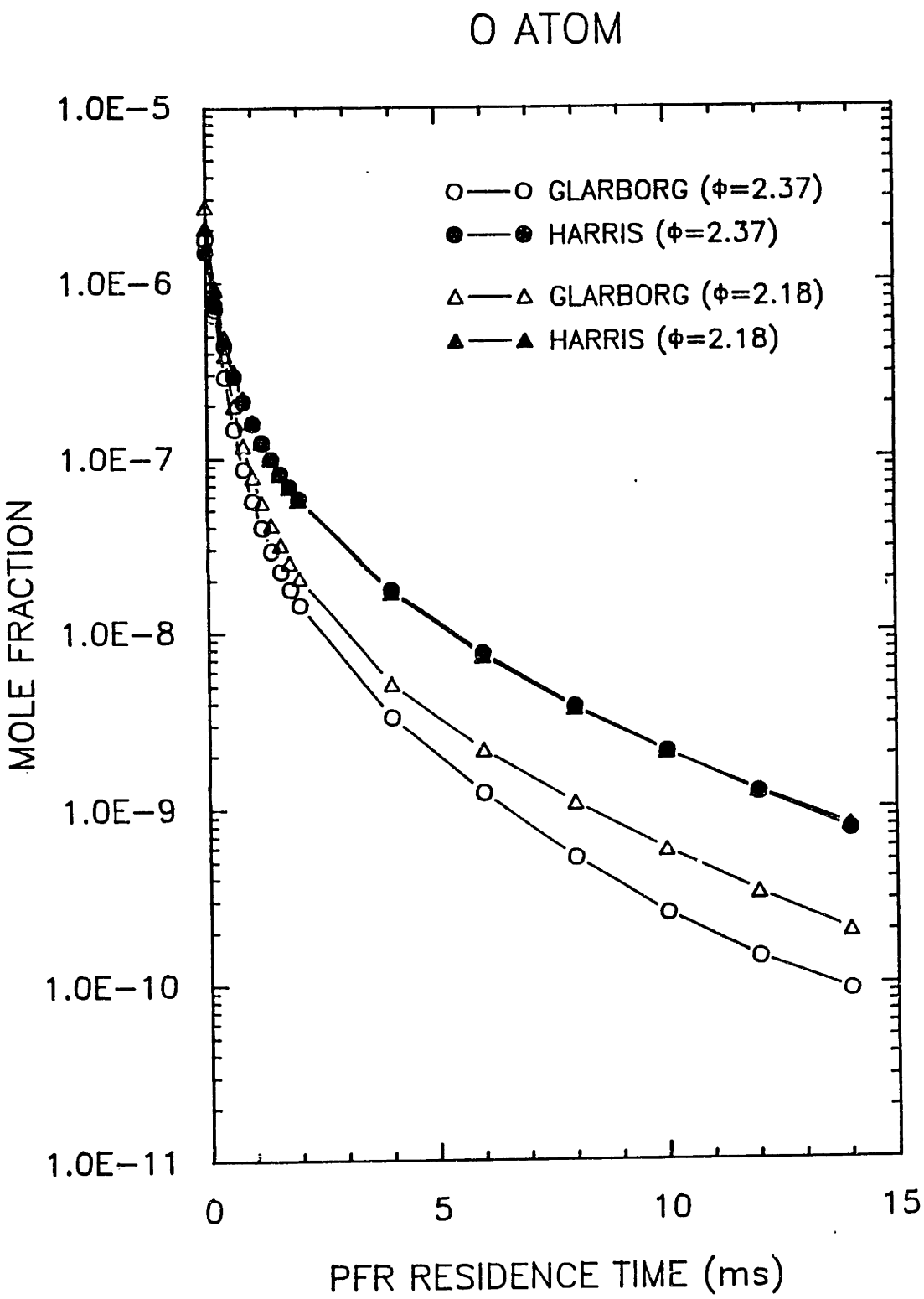

Figure 6.12 Comparison of Glarborg mechanism and Harris mechanism predictions for O atom in JSR/PFR at ϕ-2.18 and ϕ-2.37.

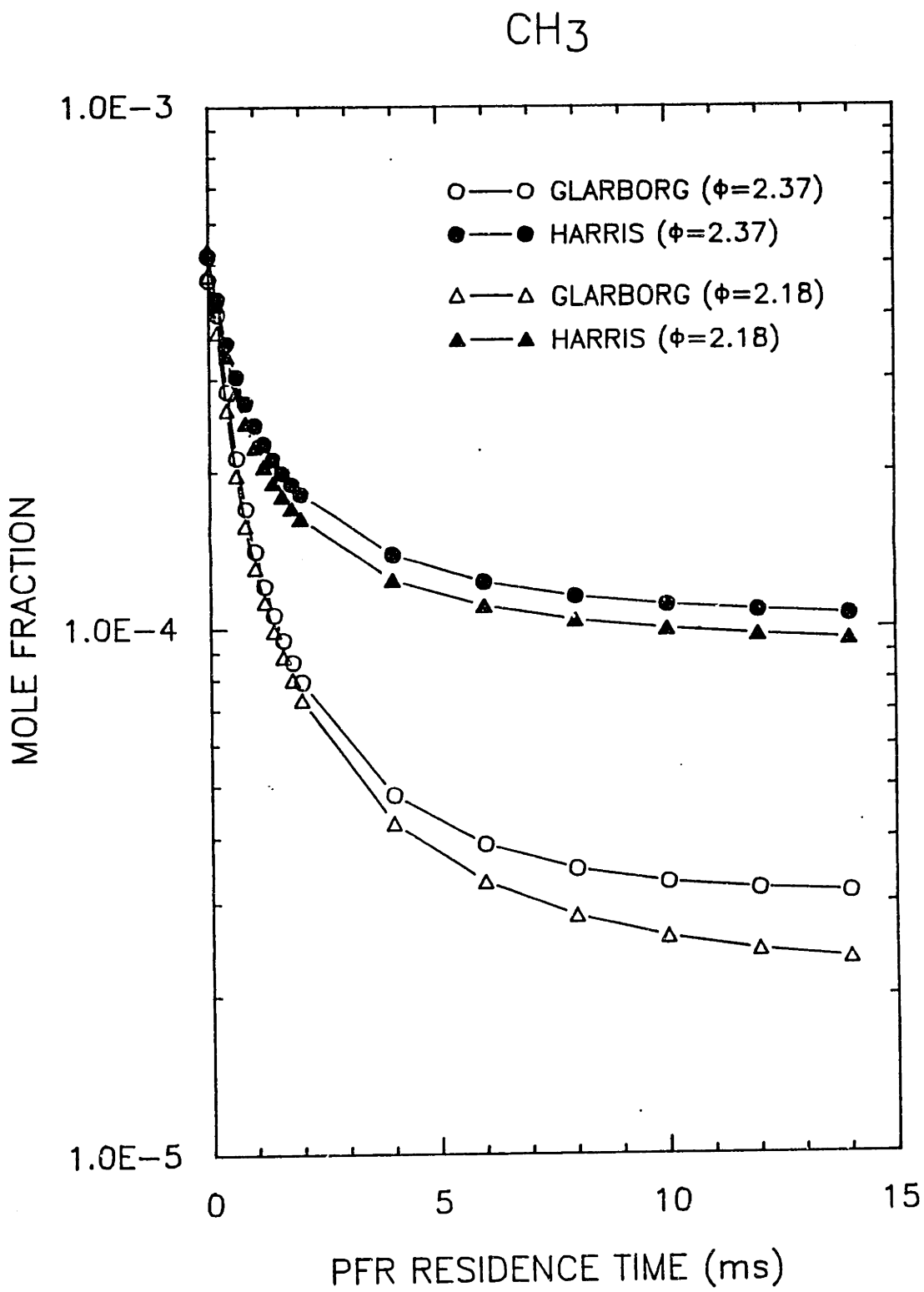

Figure 6.13 Comparison of Glarborg mechanism and Harris mechanism predictions for CH_3 in JSR/PFR at ϕ=2.18 and ϕ=2.37.

6.4 MODEL LIMITATIONS

The obvious shortcoming of the Glarborg reaction set is the lack of species with molecular weights higher than C_3H_4. As a result, only species containing up to 2 carbon atoms could be well modelled. Further development of kinetic mechanisms which include the C4 species and eventually aromatics formation may eventually enable modelling of PAH species to be done at the elementary reaction level. The mechanism development for C4 and aromatics formation is an active area of research at present. The PFR data set provides the modeler with an excellent opportunity to test proposed mechanisms and identify reaction pathways because the fluid dynamics simplifies computational effort, (diffusion is unimportant), and the relatively isothermal temperature field minimizes effort in rate parameter estimation (no steep temperature gradients so rate constants do not need to be extrapolated over a very wide range of temperatures). The data set obtained in the PFR should be used to test mechanisms which involve higher hydrocarbon species.

The Harris mechanism does contain species with high molecular weights up to acenaphthylene. Although the predictions for these higher molecular weight species were not in close agreement to our experimental data, implying that the mechanism for formation of aromatics and PAH needs refinement, we tested the effect of inclusion of high molecular weight species on the predictions for the major species and radical species concentrations. The species concentration predictions for a subset of the mechanism which eliminated the reactions involving aromatic species was compared to the full Harris

mechanism. As seen in Figures 5.11 - 5.14, major species and radical concentrations were not predicted to be much affected by the inclusion or exclusion of reactions involving higher molecular weight species. From reaction path analysis, the mass fluxes which form and destroy species in the high molecular weight inventory are small compared to the fluxes of formation and destruction of the major species. The implication is that the PAH formation mechanism may be "decoupled" from the main hydrocarbon chemistry. A similar conclusion was reached by Frenklach (1987) in which the PAH formation mechanism was superimposed on top of a hydrocarbon mechanism developed by Warnatz in the modelling of an acetylene laminar flat-flame.

Another limitation of this kinetic modelling approach is the assumption that the flow exiting the JSR may be described by Plug flow behavior. While this assumption may be valid for some species, other species will be very sensitive to the flow field (eg. C_2H_4). An alternative approach to this modelling work is to solve only the PFR problem, by using measured concentrations at the first data point in the PFR.

7. THERMODYNAMIC MODELLING

7.1 GLOBAL EQUILIBRIUM

Complete global equilibrium for hydrocarbon mixtures at typical combustion temperatures (1000-2500K) would predict decomposition to the elements and very low concentrations of gaseous hydrocarbons. Solid carbon is predicted to form only if the C/O ratio is greater than unity. Global thermodynamic calculations involve determination of the composition of the mixture which minimizes the Gibbs free energy of the system. Various mathematical algorithms have been used. A relatively efficient equilibrium solver, STANJAN (Reynolds, 1986), uses the method of element potentials, and a modified version of STANJAN is incorporated into the CHEMKIN PSR (Glarborg, 1986b) code solver which was used for the hydrocarbon kinetic modelling. Table 7.1 shows the computed global equilibrium mole fractions for ethylene combustion at 1630K, for both equivalence ratios studied, ϕ = 2.18 and ϕ = 2.37. These experimental conditions correspond to molar C/H/O ratios of 0.73/1.46/1.00 and 0.79/1.58/1.00, respectively.

The thermodynamic database used in these equilibrium calculations, and also for the kinetic modelling work of Chapter 6, was compiled from a variety of sources. Thermodynamic data for the aliphatic species were obtained from Burcat (1984), and data for the aromatic and poly-aromatic species were obtained from Stein (1987b). Thermodynamics for the PAH species were estimated using group additivity predictive methods (Benson, 1976; Stein et al., 1977, 1981). The data are in the form of the seven-constant NASA-form (Gordon-McBride), and the complete data set of coefficients is shown

Table 7.1 - Predicted Species Mole Fractions at Global Equilibrium

Species	ϕ=2.37, T=1630K	ϕ=2.18, T=1630K
H	3.09E-05	2.88E-05
H2	1.76E-01	1.52E-01
O	4.57E-11	7.02E-11
OH	3.26E-07	4.65E-07
H2O	4.22E-02	5.60E-02
O2	5.01E-12	1.18E-11
HO2	3.77E-15	8.27E-15
H2O2	3.88E-14	7.90E-14
C	1.03E-18	6.17E-19
CH	1.64E-17	9.10E-18
CH2	2.70E-14	1.39E-14
CH3	1.14E-18	5.45E-11
CH4	2.63E-08	1.17E-08
C2H	9.47E-19	3.14E-19
C2H2	2.88E-12	8.88E-13
C2H3	5.71E-17	1.64E-17
C2H4	3.91E-14	1.04E-14
C2H5	1.14E-18	2.81E-19
C2H6	2.38E-17	5.48E-18
CO	2.02E-01	1.86E-01
HCO	5.97E-09	5.09E-09
CH2O	2.69E-08	2.13E-08
CH3O	4.73E-16	3.48E-16
C3H4	2.95E-21	4.69E-22
C3H2	6.22E-21	1.15E-21
HCCO	5.71E-15	2.91E-15
CH2CO	2.14E-12	1.01E-12
CO2	1.56E-02	2.20E-02
N2	5.64E-01	5.85E-01

in Appendix A.3.

As seen in Table 7.1, the major stable species predicted at equilibrium are CO, CO_2, H_2 and H_2O for both equivalence ratios. For the ϕ = 2.37 case, the most abundant hydrocarbon species is predicted to be CH_4 at a mole fraction of about 2.6×10^{-8}. Acetylene and ethylene, the next most abundant hydrocarbon species, are predicted to have mole fractions of 2.9×10^{-12} and 3.9×10^{-14}, respectively. From the experimental data, we know that the C_2H_2 and C_2H_4 are found in concentrations much higher than predicted by equilibrium, by a factor of 10^{10}. Aromatic and polyaromatic species were predicted to be present in mole fractions less than 1×10^{-38}, which is the smallest non-zero number the VAX 11/785 can handle.

For ϕ=2.37, the major radical species at equilibrium are predicted to be H atom (mole fraction 3×10^{-5}) and OH (mole fraction 3×10^{-7}). Comparison of the H atom global equilibrium value and the calculated profile using the Glarborg (1986a) and Harris (1988a) mechanisms, shows that the H-atom mole fraction profile in the PFR decreases to values very close to values predicted by global equilibrium for both ϕ=2.18 and ϕ=2.37. It appears that the reactions which control the concentration of H are fast enough to allow the H atom to reach equilibrium concentration over the 15 msec residence time in the PFR.

To test this hypothesis, kinetic and equilibrium calculations were performed for a number of equivalence ratios and temperatures. Three equivalence ratios (ϕ = 2.0, 2.37, and 2.8) and 5 different temperatures (1400, 1500, 1600, 1700 and 1800K) were selected to see

if H atom decays to its equilibrium value in 15 msec. The Glarborg mechanism as discussed in Chapter 6 was used for the kinetic calculations, and the STANJAN equilibrium program gave the predicted equilibrium results. Table 7.2 shows the calculated equilibrium concentrations of H and OH, and Figures 7.1-7.3 show the comparison between the kinetics and equilibrium results.

Table 7.2 Predicted H and OH equilibrium concentrations as a function of temperature for ϕ=2.37, $C_2H_4/O_2/N_2$ combustion.

Temperature (K)	H mole fraction	OH mole fraction
1400	2.05E-06	8.69E-09
1500	7.37E-06	4.78E-08
1600	2.27E-05	2.12E-07
1700	6.12E-05	7.88E-07
1800	1.48E-04	2.50E-06

We see from Figure 7.1 that the temperature determines if the H atom profile will reach equilibrium in the PFR. At low temperatures such as 1400K, the 15 msec residence time in the PFR is not long enough for the H atom to decay to its equilbrium value. At 1600K, H-atom is at its global equilibrium concentration at a PFR residence time of ≈15 ms, and at 1800K, H atom decays very quickly to equilibrium, and is actually slightly below its equilibrium value for most of the residence time in the PFR. The H atom decay is kinetically controlled by reactions with hydrocarbons which are present in high concentrations in the PFR. As temperature is increased, these reactions become faster and allow for the relaxation

of H atom towards it equilibrium value.

But then, why does H-atom concentration for 1800K, as well as 1700K, fall below its global equilibrium value? From reaction path analysis, the H-atom recombination reaction

$$H + H = H_2 \qquad \text{Rxn (7.1)}$$

is partially equilibrated at 1800K, and because H_2 (mole fraction = 0.09) is below its global equilibrium value (mole fraction = 0.18), the H atom concentration is also below its equilibrium value. The equilibrium constant, K_p, for Rxn 7.1 at 1800K is equal to 7.87×10^6, which gives a value for $[H] = ([H_2]/K_p)^{\frac{1}{2}} = 1.1 \times 10^{-4}$, which is the final constant value reached by H-atom in the PFR. The H atom concentration is predicted to decay towards its equilibrium value as predicted by the equilibration of Rxn 7.1, and the observation that at 1600K, the H-atom profile reaches its global equilibrium value is coincidental.

Figure 7.2 shows that OH decays in a similar manner as H, and OH has a higher final concentration in the PFR for higher temperatures. The OH concentration is always above its equilbrium concentration in the PFR for the temperature range 1400-1800K.

The effect of ϕ on the predicted H-atom profile is small, and Figure 7.3 shows the comparison of the predictions from the Glarborg mechanism with the computed equilbrium values at 1600K. Although the concentrations in the JSR differ by a factor of 10% for each 100K increment in temperature, the concentrations at the end of the PFR are quite similar.

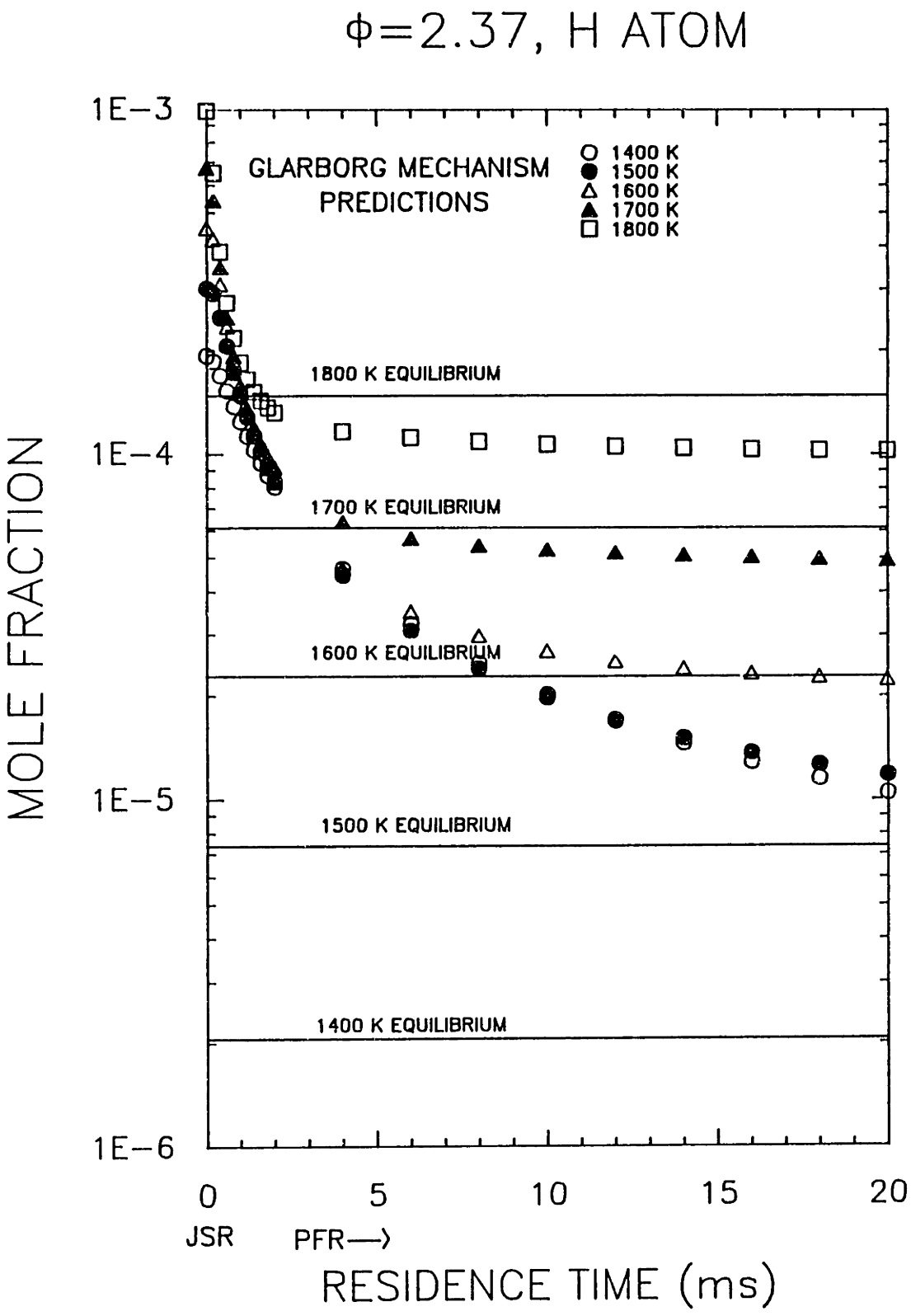

Figure 7.1 Mole fraction profiles for H atom as predicted by Glarborg mechanism (1986a) and Harris mechanism (1988a) compared with global equilibrium for ϕ=2.37 $C_2H_4/O_2/N_2$ combustion.

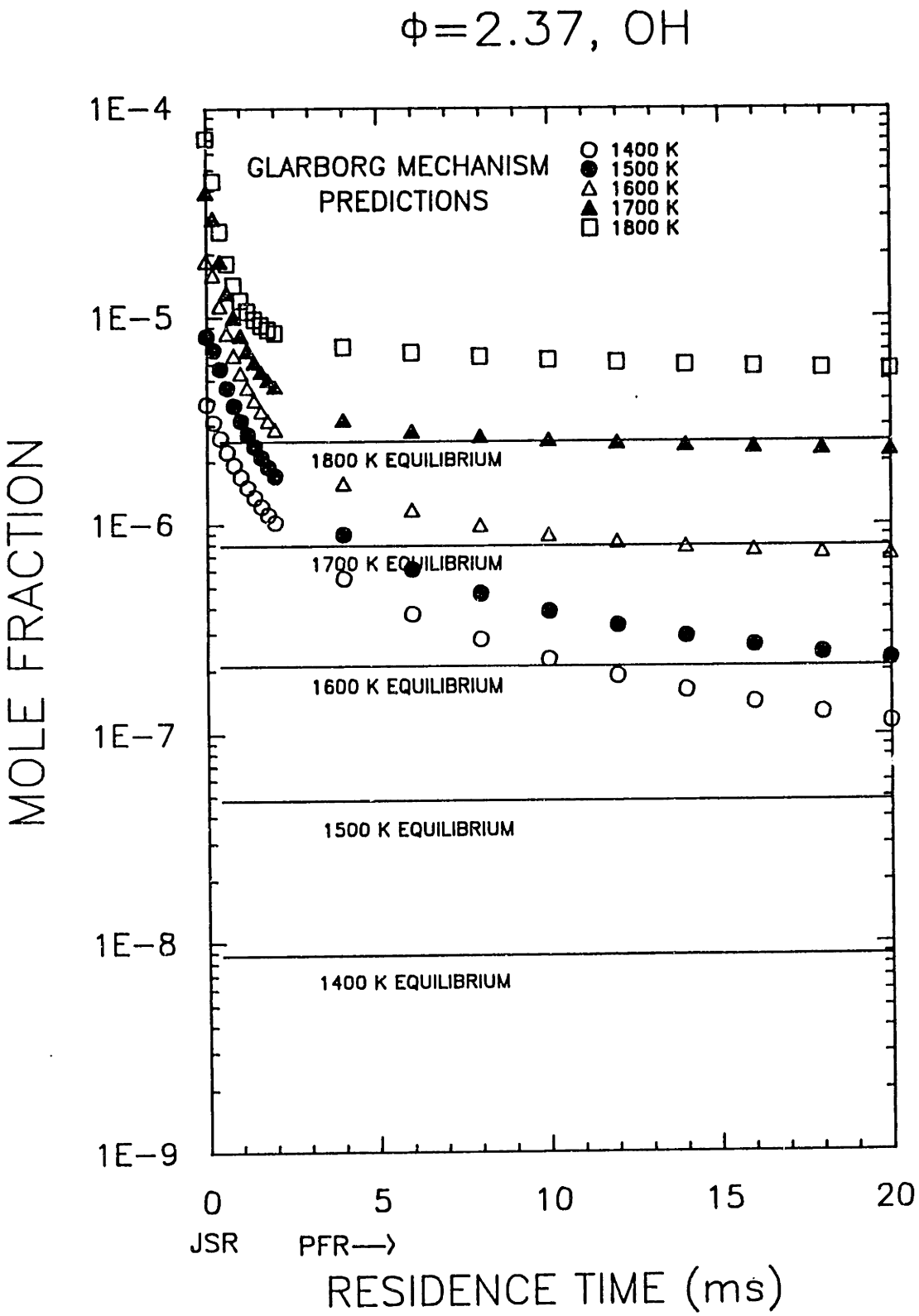

Figure 7.2 Mole fraction profiles for OH as predicted by Glarborg mechanism (1986a) and Harris mechanism (1988a) compared with global equilibrium for ϕ=2.37 $C_2H_4/O_2/N_2$ combustion.

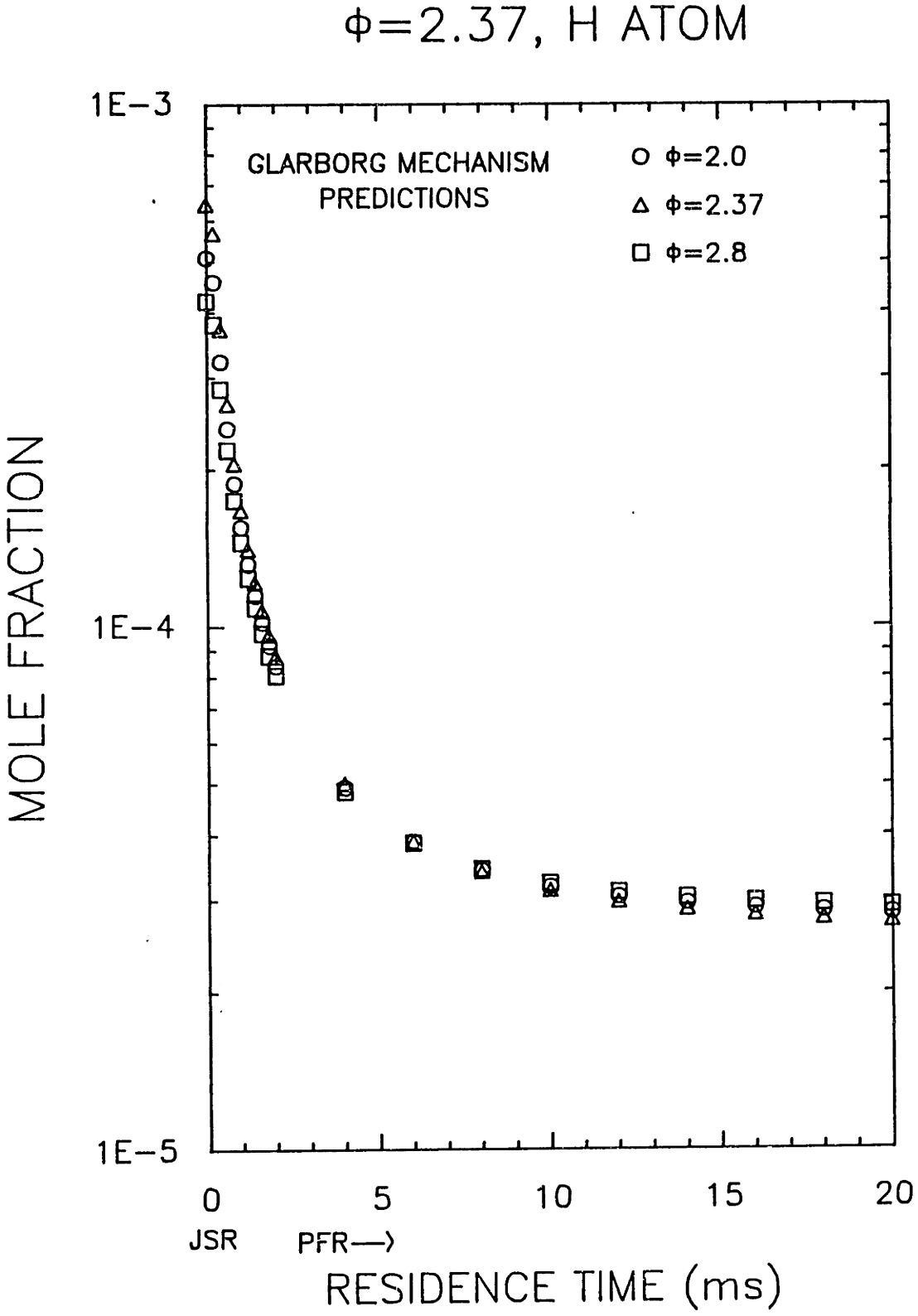

Figure 7.3 Mole fraction profiles for H atom as predicted by Glarborg mechanism (1986a) for ϕ=2.0, 2.37, 2.8 for T=1600K, $C_2H_4/O_2/N_2$ combustion.

7.2 PARTIAL EQUILIBRIUM

Since we observe the light hydrocarbons and aromatic species in concentrations much greater than that predicted by global equilibrium, the formation and destruction of these hydrocarbon species must be kinetically controlled. Although the entire hydrocarbon mixture is clearly not at equilibrium, subsets of species may be chemically converted through reactions which are rapid relative to the characteristic time of observation in the flame, and these species will exhibit a "rapid equilibrium" or partial equilibrium behavior. The relative concentrations of species may be calculated from knowledge of the equilibrium constant for a reaction which is partially equilibrated. For example, although methane is present in flames at a concentration far above its global equilibrium concentration, the elementary reaction

$$CH_4 + H = CH_3 + H_2 \qquad \text{Rxn (7.2)}$$

was partially equilibrated in the post-flame zone of a ϕ=1.8, 20 torr, C_6H_6-O_2-Ar laminar flat-flame studied by Bittner (1981c). Bittner has shown that the ratio $[CH_3][H_2]/[CH_4][H]$ is equal to the equilibrium constant for Rxn 7.2 throughout post flame zone by independent measurement of the 4 species in Rxn 7.2. Similar relationships may hold for other hydrocarbon species.

7.2.1 Partial Equilibria of the Polyacetylenes

Bittner (1981c) has shown that in the post-flame zone of a ϕ=1.8 C_6H_6-O_2-Ar laminar flat-flame, the polyacetylene reactions

$$2\ C_2H_2 = C_4H_2 + H_2 \qquad \text{Rxn (7.3)}$$

$$3\ C_2H_2 = C_6H_2 + 2\ H_2 \qquad \text{Rxn (7.4)}$$

$$4\ C_2H_2 = C_8H_2 + 3\ H_2 \qquad \text{Rxn (7.5)}$$

were found to be equilibrated throughout the post-flame zone, although Reaction 7.5 was equilibrated only within a factor of 2. A similar equilibrium relationship for the polyacetylenes was observed by Bonne et al. (1965) in studying C_2H_2 laminar flat-flames. The elementary reactions which are responsible for the overall equilibration were not positively identified.

Figure 7.4 shows experimentally determined H_2, C_2H_2, and polyacetylene mole fraction profiles. The polyacetylene concentrations show little change with residence time, and the concentrations decrease by about a factor of 30 for each additional C2 increment. Figure 7.5 shows the equilibrium constant and experimental equilibrium ratios for the polyacetylenes as measured in the PFR for ϕ = 2.18. We see that in our system the polyacetylenes are not equilibrated as observed in Bittner's flame, although the experimental ratios appear to be increasing toward the predicted equilibrium ratio. A similar situation is observed for the ϕ=2.37 case.

Uncertainties in the thermodynamic properties of the polyacetylenes may be a reason for the disagreement between our

experimental data and equilibrium predictions. The equilibrium constants in Figure 7.5 were calculated using the same equilibrium constants which Bittner used, and these equilibrium constants are given by

$$Kp_{Rxn\ (7.3)} = 0.425 \cdot \exp(-1130/T) \qquad \text{Eq. (7.1)}$$

$$Kp_{Rxn\ (7.4)} = 0.221 \cdot \exp(-2220/T) \qquad \text{Eq. (7.2)}$$

$$Kp_{Rxn\ (7.5)} = 0.075 \cdot \exp(-3200/T) \qquad \text{Eq. (7.3)}$$

where T is in degrees Kelvin. The heat of formation of diacetylene was estimated by Bittner to be 109 kcal/mol, and group additivity was used to obtain the heats of formation of triacetylene ($\Delta H_{f,298K}$ = 164 kcal/mol) and tetra-acetylene ($\Delta H_{f,298K}$ = 219 kcal/mol). Use of Stein's thermodynamic group value of 25.6 kcal/mol for [Ct-(C_t)] results in $\Delta H_{f,298K}$ = 105.1 kcal/mol for diacetylene. This value is significantly lower than Bittner's value and other published values of 112.3 kcal/mol (Stull et al., 1969) and 112.6 kcal/mol (Cowperthwaite et al., 1962, and Duff et al., 1962). Stein has recommended using a value of 27.3 kcal/mol for [Ct-(C_t)] in order to match the equilibrium presumed in flames.

Another possibility for why the polyacetylenes are not partially equilibrated in our system may be because the temperature is too low. Our temperature is much lower than in Bittner's flame (1540K vs 1835K), and the kinetics for polyacetylene formation may not be fast enough at 1540K for Reactions 7.3 -7.5 to be partially equilibrated. Because Reactions 7.3-7.5 are almost thermal-neutral, the equilibrium

constants are not sensitive to temperature, but the elementary reactions may be strongly temperature dependent.

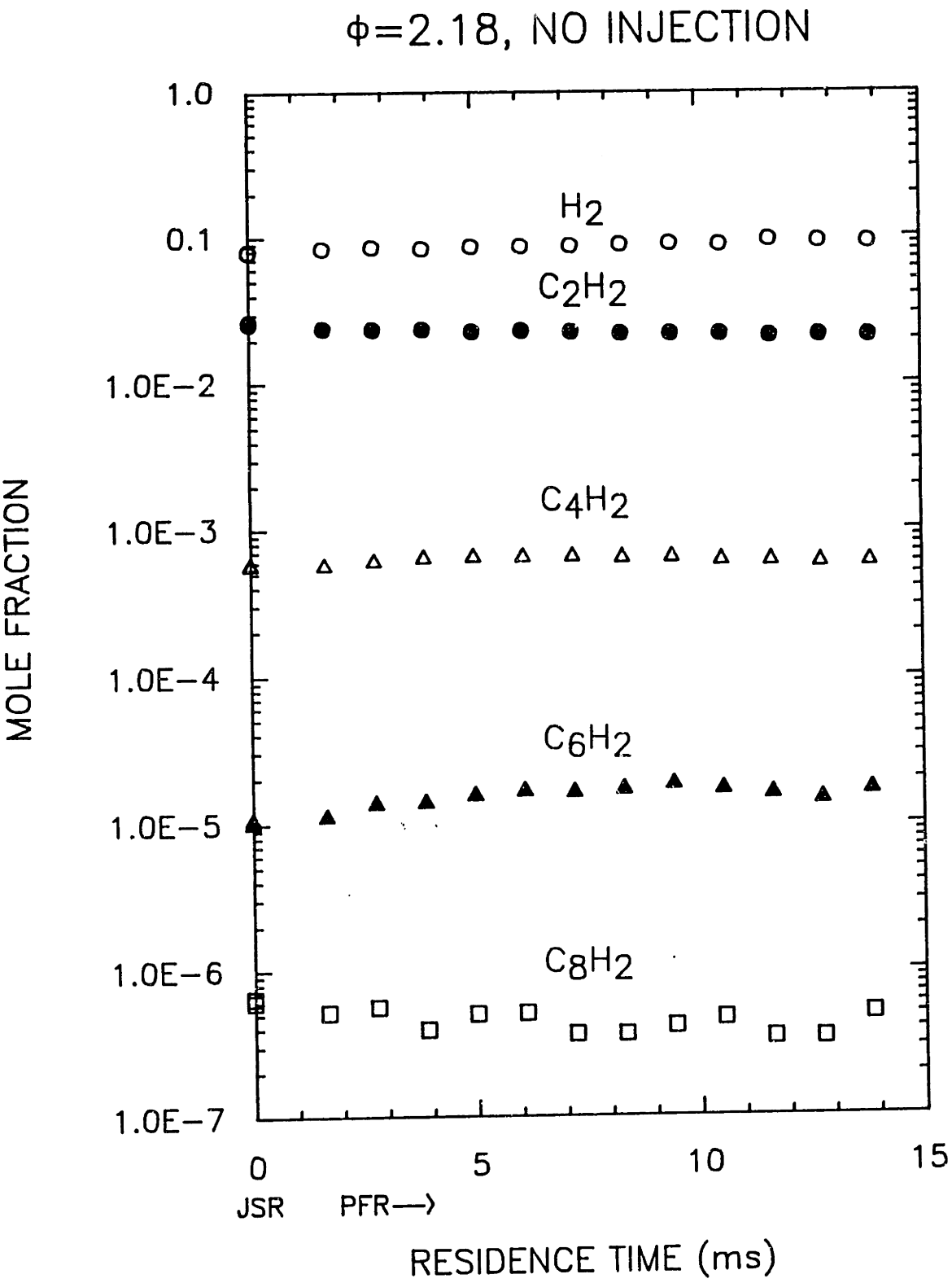

Figure 7.4 Measured H_2, C_2H_2, and polyacetylene concentrations for ϕ=2.18, 1630K, $C_2H_4/O_2/N_2$ combustion in the JSR/PFR.

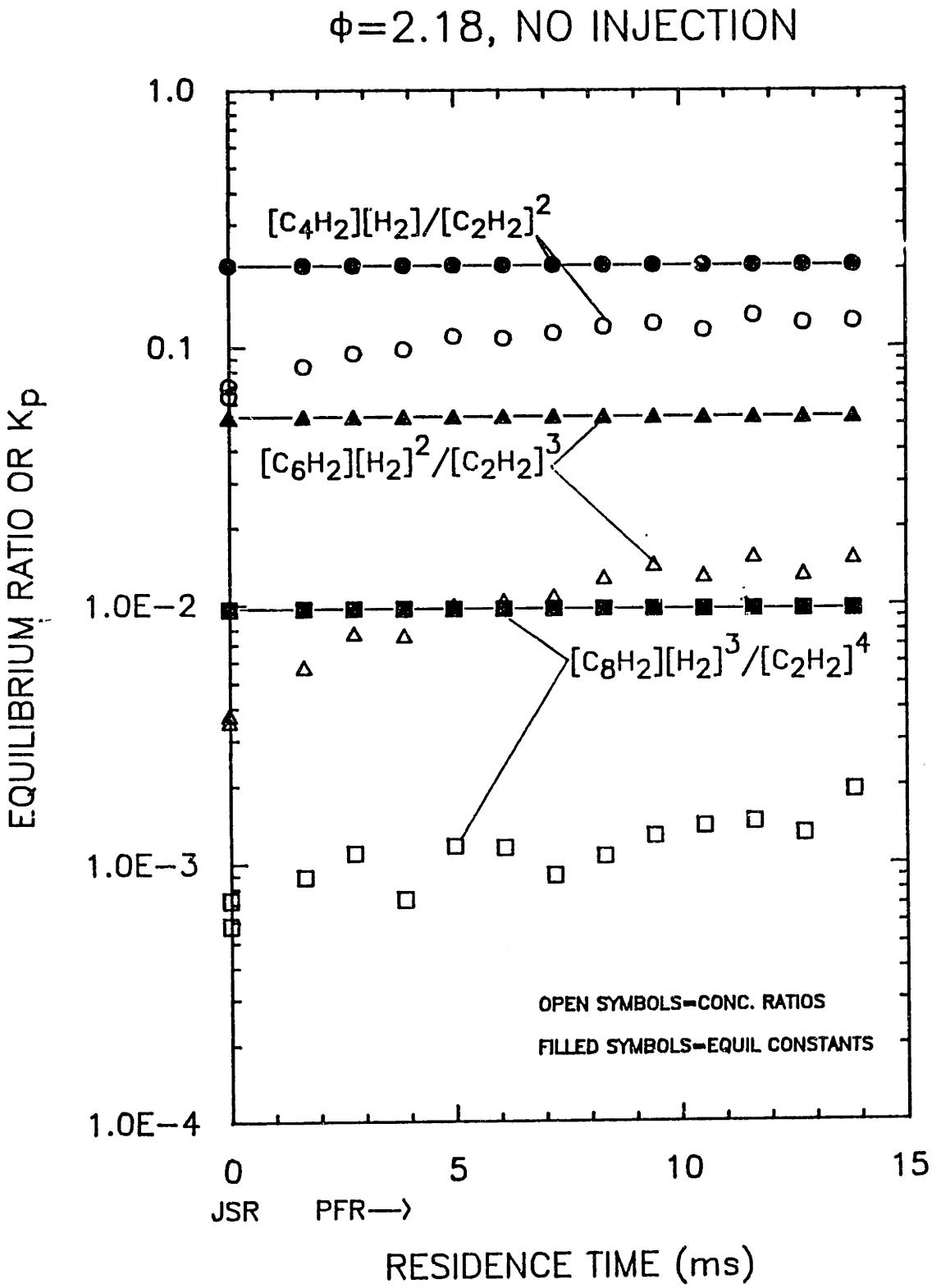

Figure 7.5 Comparison of measured and predicted equilbrium concentrations of polyacetylenes for ϕ=2.18, 1630K, $C_2H_4/O_2/N_2$ combustion in the JSR/PFR.

7.2.2 PAH Stabilomers

The equilibrium distribution of PAH isomers of the same number of carbon and hydrogen atoms will favor the PAH isomer with the lowest ΔG_f. These have been defined as "stabilomers" (Godleski, 1981). Alberty (1988) has identified the most stable isomers in each class of the benzenoid series up to 5 aromatic rings and has calculated the equilibrium distribution among the PAH isomers at flame temperatures. Based on theoretical considerations, Stein et al. (1985) has predicted the most stable isomer for each $C_{2n}H_{2m}$ class of species up to $C_{42}H_{16}$ at 1500K.

It is important to note that at high temperatures entropy plays a critical role in determining thermodynamic stability, as defined by the Gibbs free energy, $\Delta G = \Delta H - T\Delta S$. Because of the potentially large contribution of the entropic term at high temperatures, one's chemical "intuition" may be misleading. For example, at room temperature polyacetylenes are explosively unstable, but at high temperatures polyacetylenes are more thermodynamically stable than alkanes.

The stabilomers up to cyclopenta(cd)pyrene ($C_{18}H_{10}$) are shown in Figure 7.6, and Figure 7.7 shows the structures of the most abundant PAH observed experimentally in each $C_{2n}H_{2m}$ class for our experimental conditions. Comparision of Figures 7.6 and 7.7 shows that, with the exception of the ethynyl-acenaphthylenes, ($C_{14}H_8$), all of the experimentally abundant PAH species are the stabilomers which have been predicted by Stein. Pyracylene is the predicted $C_{14}H_8$ stabilomer.

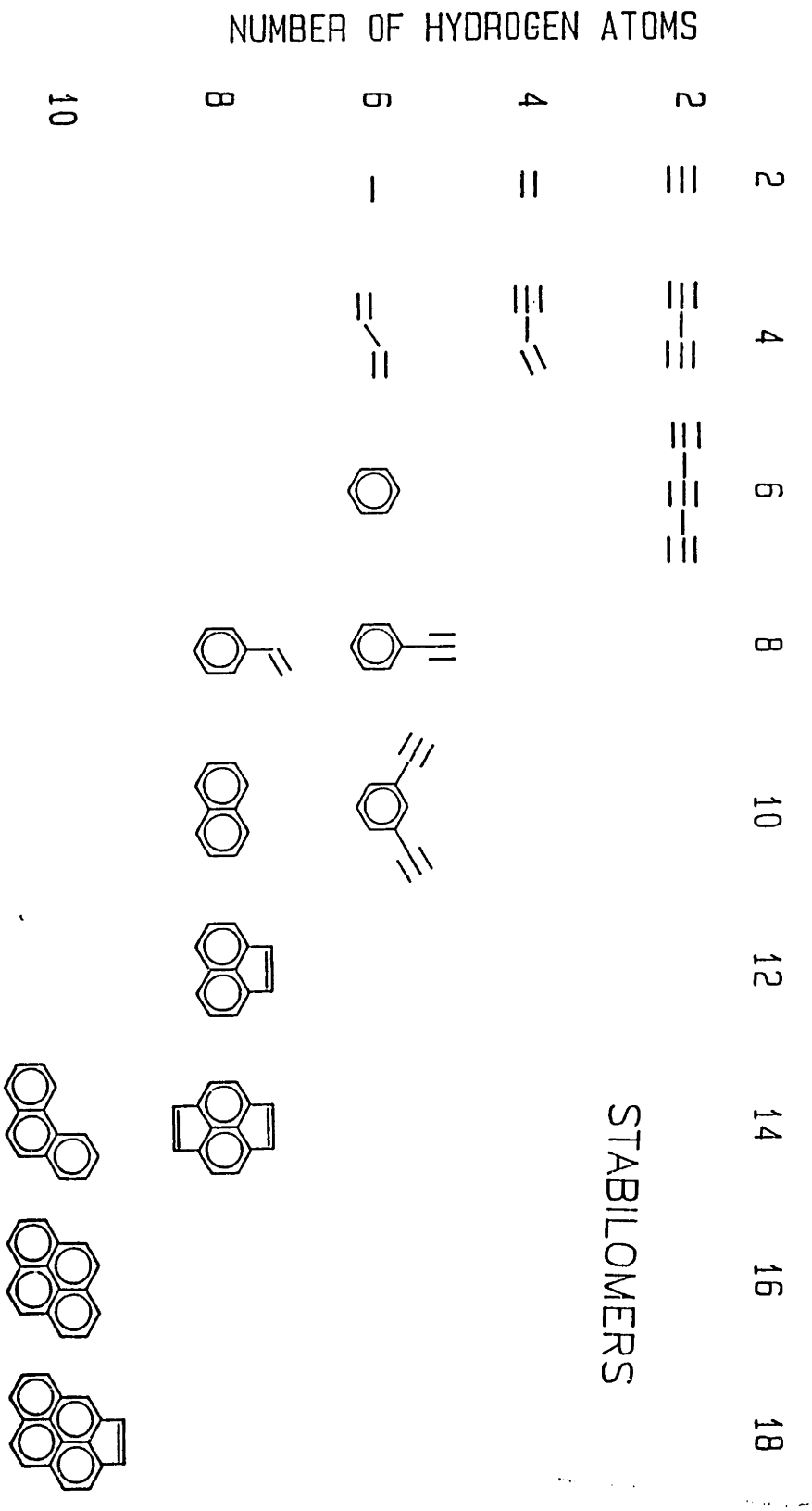

Figure 7.6 Stabilomers predicted by Stein (1985) for 1500K.

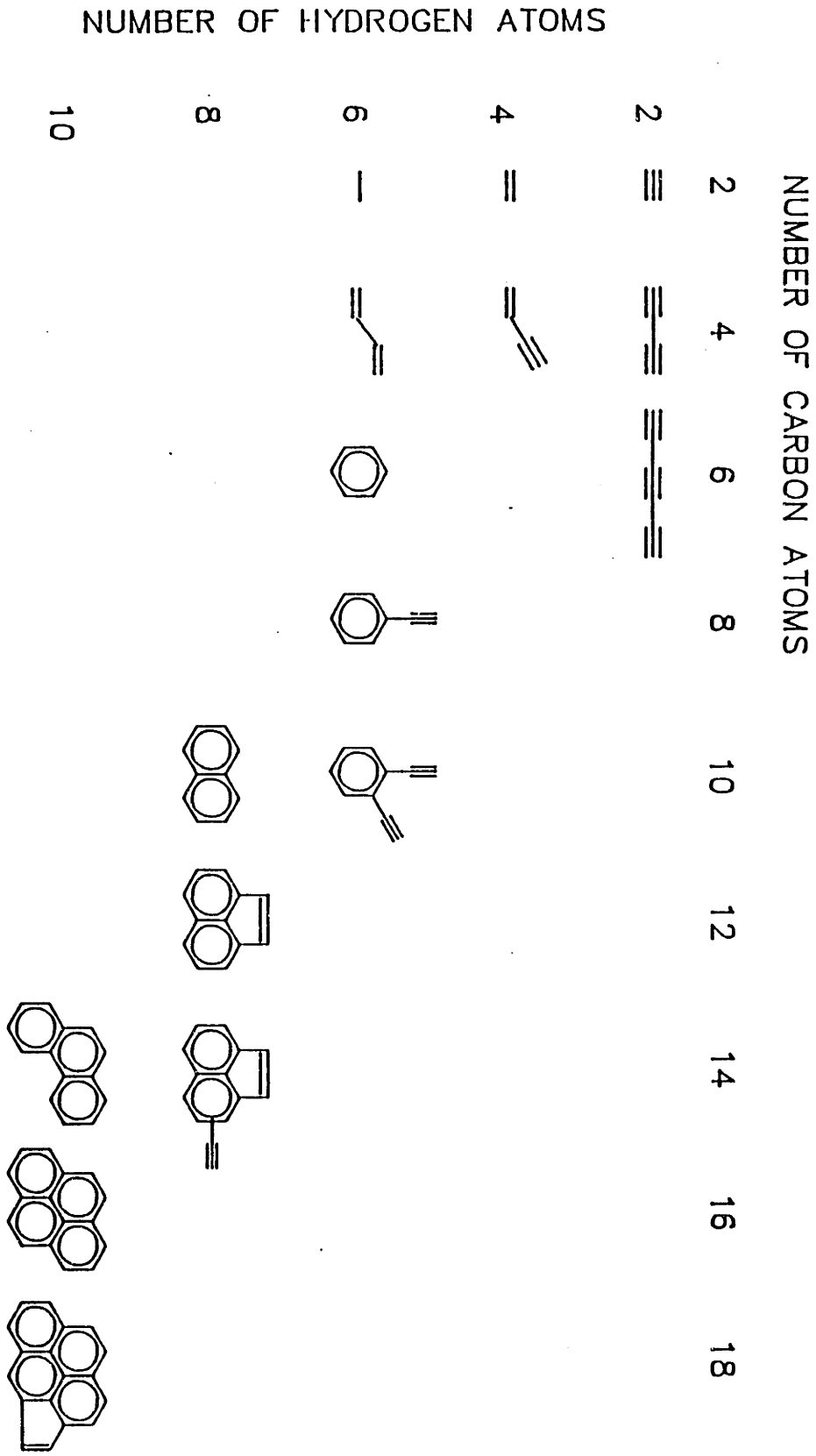

Figure 7.7 Most abundant experimentally observed $C_{2n}H_{2m}$ species in the JSR/PFR.

Pyracylene has an interesting structure because of its strained carbon framework due to the presence of the two 5-membered rings. Pyracylene has been synthesized by a variety of methods. (Schaden, 1983; Trost, 1971). Interestingly, one of the methods of synthesis (Schaden, 1983) involved the oxidation of pyrene to a di-carbonyl, followed by pyrolysis at 1100°C in a flow tube to produce pyracylene. Although at a lower temperature, these synthesis conditions are similar to those found in the PFR. Bridging the both peri positions of naphthalene by short carbon bonds inhibits the normal strain releasing mechanism of naphthalene, and Dauben (1956) has estimated the strain energy of pyracylene to be 48 kcal/mol. It is not known to this author if the ring strain energy for 2 5-membered rings was incoporated into the estimation of pyracylene. The most abundant experimentally observed $C_{2n}H_{2m}$ class of species was ethynyl-acenaphthylene, of which at least 3 different isomers were observed to be produced in the PFR.

7.2.3 Partial Equilibrium of the C_2H_2-H_2-PAH System

Following the development of Stein, if we assume partial equilibration of the C_2H_2-H_2-PAH system, then the equilibrium concentration of an individual PAH species could be predicted by finding K_p for the reaction

$$nC_2H_2 = C_{2n}H_{2m} + (n-m)H_2 \qquad n,m = 1,2,3... \qquad \text{(Rxn. 7.6)}$$

and so

$$[C_{2n}H_{2m}] = K_p \cdot [C_2H_2]^n \cdot [H_2]^{(m-n)} \qquad \text{(Eq. 7.4)}$$

Thus we see that the equilibrium concentration of PAH species will be a function of temperature, C_2H_2 concentration, and H_2 concentration. For $n/m > 1$, which is the case for the most stable PAH species, increasing H_2 inhibits PAH formation. Increasing C_2H_2 favors PAH formation. Table 7.3 shows the computed equilibrium constants, K_p, at 1600K for the most experimentally abundant PAH species shown in Figure 7.7.

The aliphatic light hydrocarbon species, except diacetylene, are produced in the JSR in super-equilibrium quantities, and then decay in the PFR towards their equilibrium limits, as calculated by Eq. 7.4, and shown in Figure 7.8. The diacetylene concentration increases slightly towards its equilibrium limit.

Table 7.3 - Equilibrium Constants (Kp) for $nC_2H_2 = C_{2n}H_{2m} + (n-m)H_2$

C	H	SPECIES	Kp(1600K)
2	2	ACETYLENE	1.00E+00
2	4	ETHYLENE	1.02E-01
2	6	ETHANE	4.44E-04
4	2	DIACETYLENE	2.13E-01
4	4	VINYLACETYLENE	2.72E-02
4	6	1,3-BUTADIENE	1.70E-03
6	2	TRIACETYLENE	4.22E-02
6	4	HEXENE-DIYNE	1.51E-02
6	6	BENZENE	1.34E+01
8	6	PHENYLACETYLENE	3.09E+00
8	8	STYRENE	8.01E-01
10	6	DI-ETHYNLBENZENE	1.21E-01
10	8	NAPHTHALENE	9.84E+02
12	8	ACENAPHTHYLENE	1.69E+05
14	8	ETHYNYL-ACENAPHTHYLENE	1.32E+04
14	10	PHENANTHRENE	9.51E+04
16	10	PYRENE	5.93E+08
18	10	CYCLOPENTA(cd)PYRENE	2.15E+11

In contrast to the aliphatic species, the aromatic species (Figure 7.9) are far below their equilibrium concentrations in the JSR, but are increasing rapidly in the PFR towards their thermodynamic limits. Similar trends were observed for the sooting ϕ=2.37 conditions (Lam, 1988). The equilbrium limits shown in Figures 7.8 and 7.9 change as a function of residence time because the concentrations of C_2H_2 and H_2 are not quite constant and also the temperature is decreasing slightly. Clearly the formation of PAH species is kinetically controlled.

Equilibration of the C_2H_2-H_2-PAH system implies that all stoichiometric reactions involving species in the C_2H_2-H_2-PAH system will obey equilibrium, (ie. the equilbrium ratio of products over reactants will equal the equilibrium constant for the overall reaction). The fact that naphthalene for example, is not at its equilibrium concentration relative to C_2H_2 and H_2 implies the C_2H_2-H_2-$C_{2n}H_{2m}$ system is not fully equilibrated.

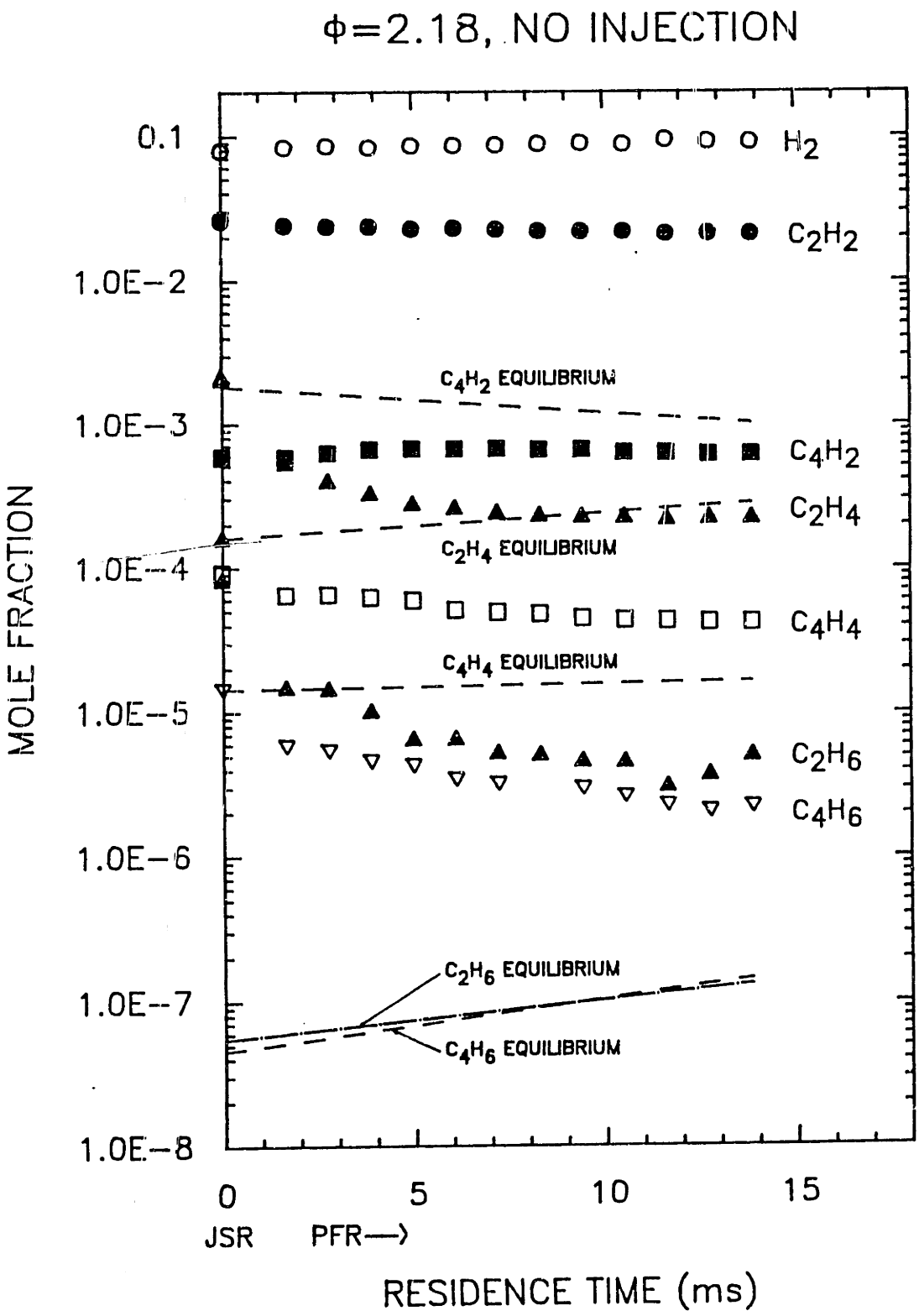

Figure 7.8 Aliphatic $C_{2n}H_{2m}$ species concentrations and equilibrium concentrations predicted from equilibration of the C_2H_2-H_2-$C_{2n}H_{2m}$ system, using measured C_2H_2 and H_2 concentrations.

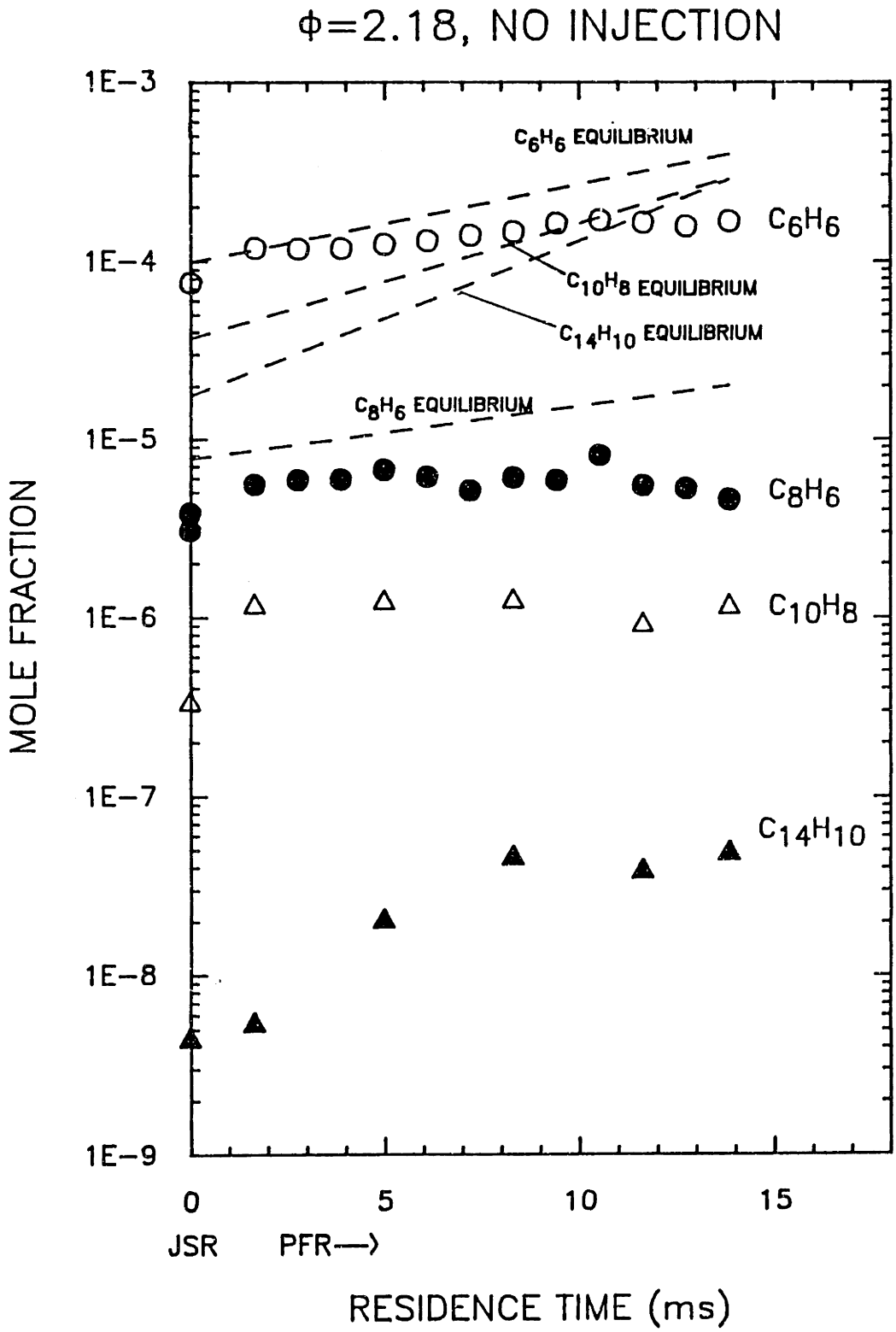

Figure 7.9 Aromatic $C_{2n}H_{2m}$ species concentrations and equilibrium concentrations predicted from equilibration of the C_2H_2-H_2-$C_{2n}H_{2m}$ system, using measured C_2H_2 and H_2 concentrations.

7.3 THERMODYNAMICALLY FAVORED PATH FOR PAH FORMATION

Figure 7.10 shows the most favored thermodynamic path (in bold arrows) which leads from C_2H_2 to large PAH for our experimental conditions of ϕ=2.18, T=1600K, with C_2H_2 and H_2 mole fractions of $2x10^{-3}$ and $9x10^{-2}$, respectively. Polymerization along this path occurs by a logical series of steps, each involving addition of H_2 (vertical step), addition of C_2H_2 (diagonal step), or addition of C_2H_2 and loss of H_2 (horizontal step). The number associated with each step is the ratio of product to reactant, R, for the 3 different steps and is given by

$$[C_{2n}H_{2m+2}]/[C_{2n}H_{2m}] = K_p \cdot [H_2] \qquad \text{(vertical step)} \qquad \text{(Eq. 7.5)}$$

$$[C_{2n+2}H_{2m+2}]/[C_{2n}H_{2m}] = K_p \cdot [C_2H_2] \qquad \text{(diagonal step)} \qquad \text{(Eq. 7.6)}$$

$$[C_{2n+2}H_{2m}]/[C_{2n}H_{2m}] = K_p \cdot [C_2H_2]/[H_2] \qquad \text{(horizontal step)} \qquad \text{(Eq. 7.7)}$$

Although the path indicated by the bold arrows in Figure 7.10 represents a thermodynamic path and not a kinetic path, we can imagine a polymerization starting from only acetylene consisting of chemical reactions with the overall stoichiometry given by Equations 7.5 -7.7 along the most favored thermodynamic path. For R values greater than 1, the formation of the higher molecular weight species is favored. These reactions usually involve ring closure, and until the ratio of product to reactant becomes greater than R, they may be considered irreversible. For R less than 1, product formation is inhibited, and if R is much less than 1, the reverse reaction may be the most favored pathway. For example, the most favored pathway for benzene to grow to

a larger species is to add C_2H_2 and lose H_2 to form phenylacetylene (R = $5.7x10^{-2}$). The most favored pathway for phenylacetylene to grow to a larger species is to add C_2H_2 to form naphthalene (R = 8.5), but the reaction of phenylacetylene back to benzene would actually be more slightly thermodynamically favorable (R_{-1} = $1/5.7x10^{-2}$ = 17.5). If the rate of formation of benzene from phenylacetylene is much greater than, or comparable to, the rate of formation of naphthalene from phenylacetylene, then phenylacetylene and benzene will be partially equilibrated by the overall reaction

$$C_6H_6 + C_2H_2 = C_8H_6 + H_2 \qquad \text{(Rxn.7.7)}$$

Using the experimentally measured C_6H_6, C_2H_2, and H_2 concentrations and equilibrium constants calculated for our temperature profile in the PFR, we find that Reaction 7.7 is nearly partially equilibrated for the ϕ=2.18, no injection case, as well as for the C_6H_6 injection case, as shown in Figure 7.11. For benzene injection, the phenylacetylene profile shows a similar decay as the benzene profile. Although the benzene profile is quite different for the two cases, the fact that the phenylacetylene/benzene ratio is given by $K_{p(Rxn\ 7.7)} \cdot [H_2]/[C_2H_2]$ for both cases is strong evidence for partial equilibration.

The two-ring analog of the benzene/phenylacetylene partial equilibrium is the ethynyl-naphthalene/naphthalene equilbrium and the ethynyl-naphthalene concentration is nearly the same as that predicted from partial equilibration of the reaction

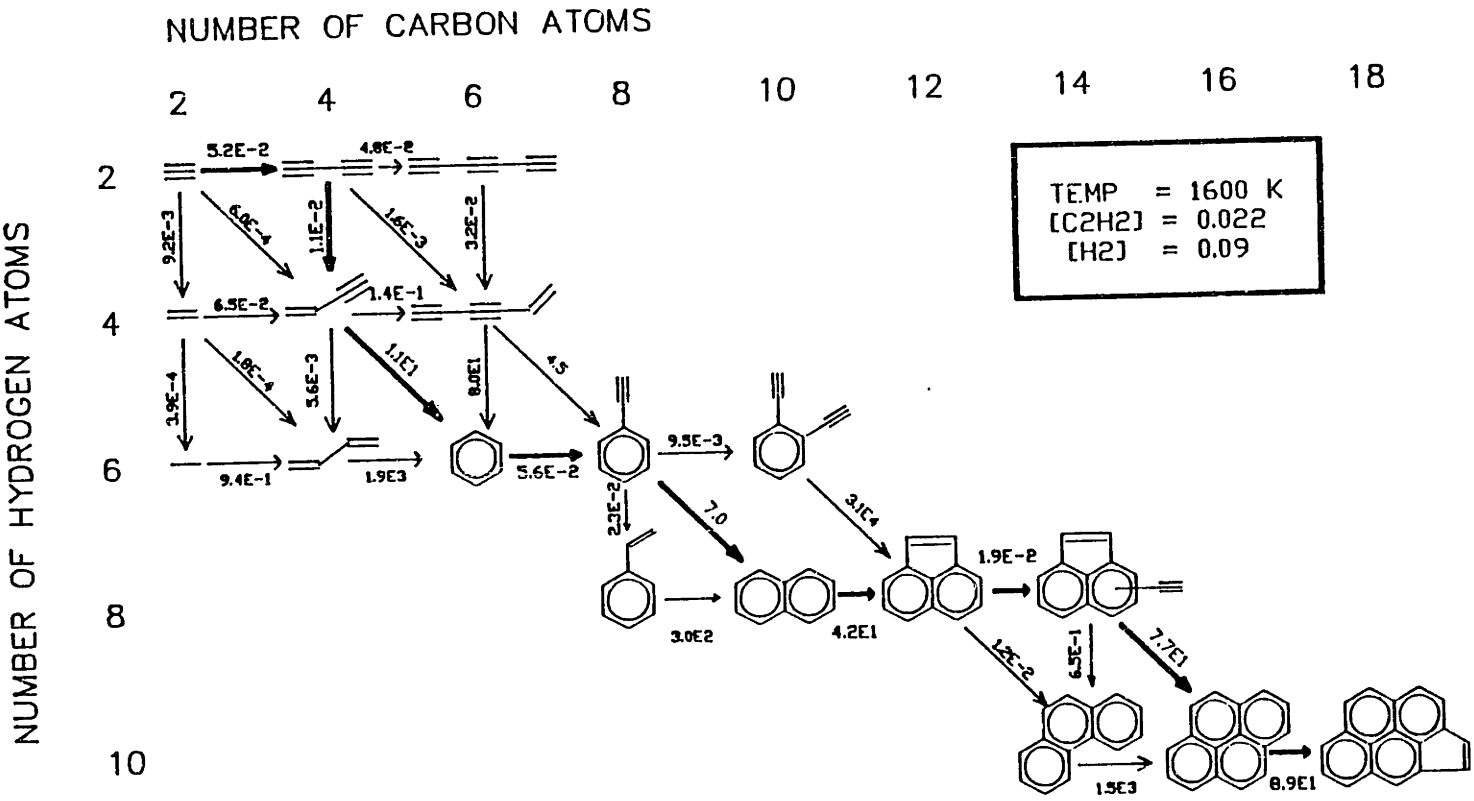

Figure 7.10 Most abundant experimentally observed PAH species in the PFR, and most favored thermodynamic pathway. Numbers are the ratio of product to reactant, assuming equilibration of the C_2H_2-H_2-$C_{2n}H_{2m}$ system. See text for discussion.

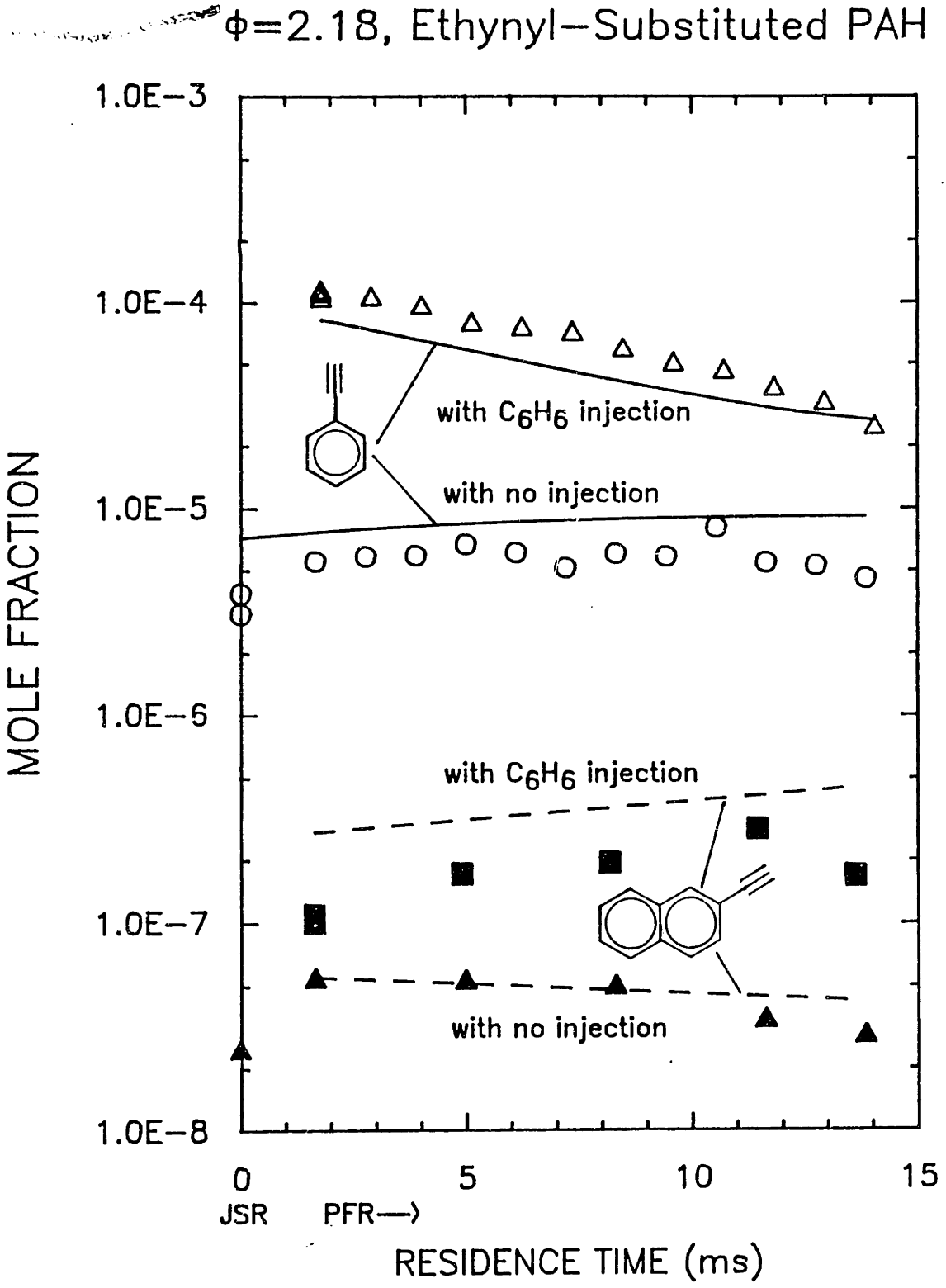

Figure 7.11 Ethynyl-aromatic $C_{2n}H_{2m}$ species concentrations and equilibrium concentrations predicted from equilibration of the reactions $C_6H_6+C_2H_2=C_8H_5+H_2$ and $C_{10}H_8+C_2H_2=C_{12}H_8+H_2$, using measured $C_{10}H_8$, C_6H_6, C_2H_2, H_2 concentrations.

$$C_{10}H_8 + C_2H_2 = C_{10}H_7C_2H + H_2 \qquad \text{Rxn (7.8)}$$

Figure 7.11 also shows the partial equilibration of the ethynyl naphthalene with naphthalene for both the no injection and benzene injection cases. Naphthalene is <u>not</u> equilibrated with phenylacetylene, and naphthalene is substantially below its equilibrium concentration.

A possible free radical mechanism for the formation of two-ring PAH involving cyclization across a triple bond (Fig. 7.12), as proposed by Frenklach (1985b), includes phenylacetylene as an intermediate. Although the C_2H_2 addition reactions to form ethynyl-substituted PAH appear to be partially equilibrated, C_2H_2 addition reactions which result in ring closure are not. This experimental finding is consistent with the conclusion determined from kinetic modelling studies (Frenklach, 1985b) that ring cyclization reactions to form fused ring PAH are essentially irreversible and provide the driving force for molecular weight growth by "pulling" chains of reversible reactions.

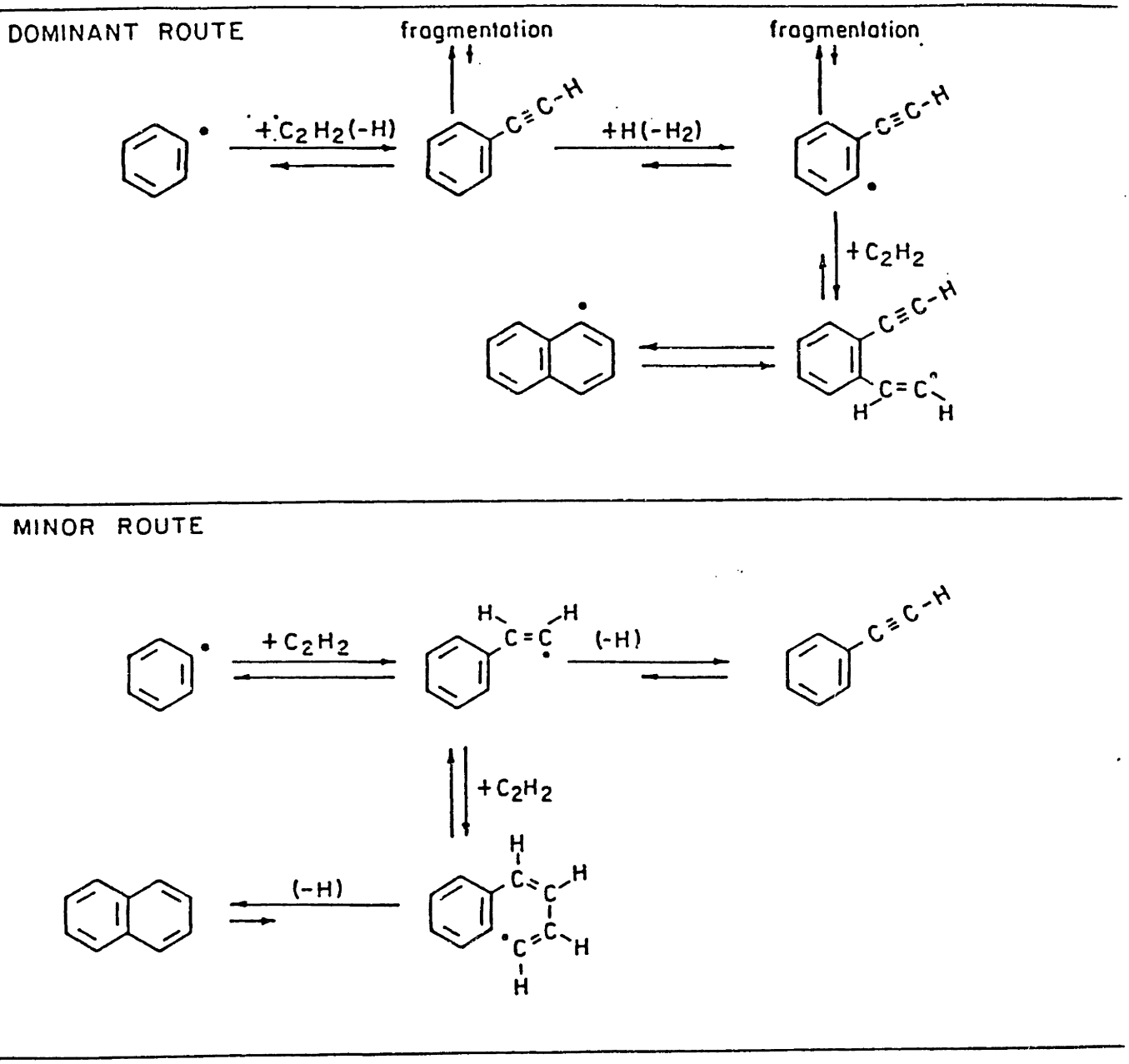

Figure 7.12 Possible mechanism for formation of two-ring aromatics. Dominant route was determined from computer simulations (taken from Frenklach, 1985b).

8. PAH KINETICS MODELLING

8.1 SUMMARY OF ϕ=2.18 EXPERIMENTAL DATA

Although the experimental data has been presented in Chapter 5, the effect of ethylene and benzene addition for the ϕ=2.18 experimental conditions is summarized in this chapter. The injection of small amounts of C_2H_4 and C_6H_6 would be expected to perturb the baseline species profiles. Figures 8.1 through 8.8 show the effects of C_2H_4 and C_6H_6 injection on the concentration profiles for methane (CH_4), acetylene (C_2H_2), ethylene (C_2H_4), benzene (C_6H_6), phenylacetylene (C_8H_6), naphthalene ($C_{10}H_8$), cyclopenta(cd)pyrene ($C_{18}H_{10}$), tar, and soot. Complete conversion of the injected C_2H_4 would increase the carbon atom mole fraction by $1.9x10^{-2}$ mole C-atom/mole flame gas, or mass concentration by $1.7x10^{-6}$ gram C-atom/cm^3 flame gas. Complete conversion of the injected C_6H_6 would increase mole fraction by $1.1x10^{-2}$ mole C-atom/mole flame gas, or $1.0x10^{-6}$ gram C-atom/cm^3 flame gas. On either a mass or mole basis, the amount of C_6H_6 injected was less than injected C_2H_4.

From elementary kinetic modeling calculations, C_2H_4 under these conditions would be expected to be converted very rapidly to C_2H_2 by H-abstraction to give vinyl radical, followed by decomposition of vinyl to acetylene. Complete conversion of the injected ethylene to acetylene at the beginning of the PFR would result in a 40% increase in acetylene mole fraction, from $2.5x10^{-2}$ to $3.5x10^{-2}$. The acetylene profile shown in Fig. 8.1 is indeed increased by 33% by the end of the PFR for the C_2H_4 injection case, while it is almost the same for the no injection and C_6H_6 injection case. Figure 8.3 shows that C_2H_4

injection increases benzene concentration by about 33% by the end of the PFR.

The ethylene mole fraction (Fig. 8.2) drops very rapidly from $1.0x10^{-2}$ at the injection point to $2.3x10^{-3}$ at the first PFR data point. Almost 70% of the injected C_2H_4 is converted to C_2H_2, by the end of the PFR, and most of this conversion occurs before the first PFR data point.

Figure 8.3 shows that the injection of C_6H_6 results in an initially high benzene mole fraction ($1.3x10^{-3}$) at the first PFR data point, which rapidly decays to $5.0x10^{-4}$ by the end of the PFR. The amount of benzene injected is about 14 times the amount of benzene present at the first PFR data point for the no injection case. Figure 8.4 shows that the profile of phenylacetylene (C_8H_6) has a decay similar to benzene, indicating that conversion of benzene to phenylacetylene is very rapid. The concentration of naphthalene at the end of the PFR, as shown in Fig. 8.5, is increased by a factor of 2 for C_2H_4 injection, and a factor of 10 for C_6H_6 injection. Large PAH species, such as cyclopenta(cd)-pyrene in Fig. 8.6, show increasing profiles in the PFR and the final concentration is increased by a factor of 20 for the injection of C_6H_6.

The tar fraction shown in Fig. 8.7 is doubled by the C_2H_4 injection and increased by an order of magnitude by the C_6H_6 injection. Figure 8.8 shows that soot production is nearly the same for the no injection and C_2H_4 injection case, but is 10 times higher for the addition of benzene.

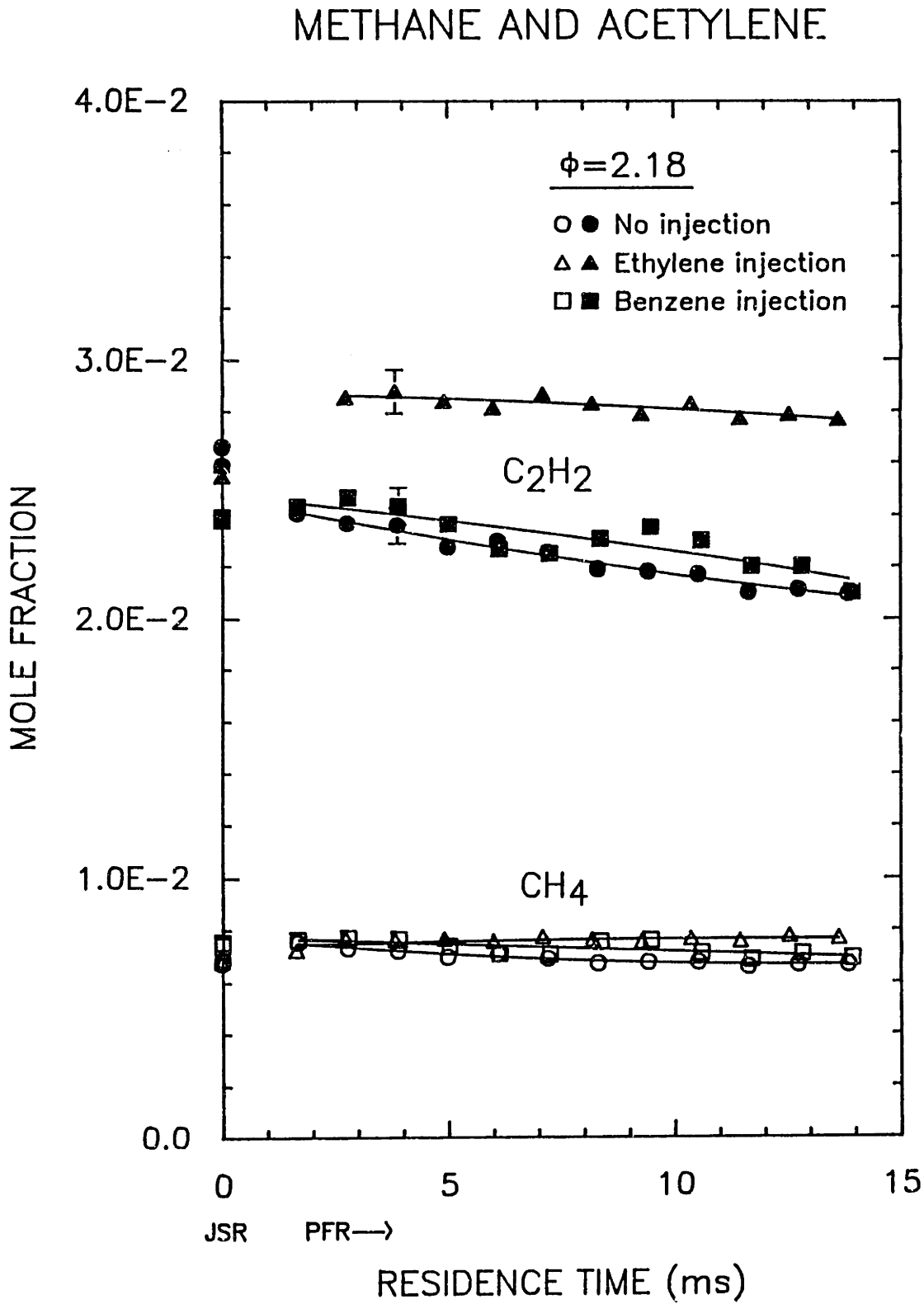

Figure 8.1 Concentration profiles for methane (CH_4) and acetylene (C_2H_2) in JSR/PFR for ϕ=2.18, for no injection, C_2H_4 injection and C_6H_6 injection cases.

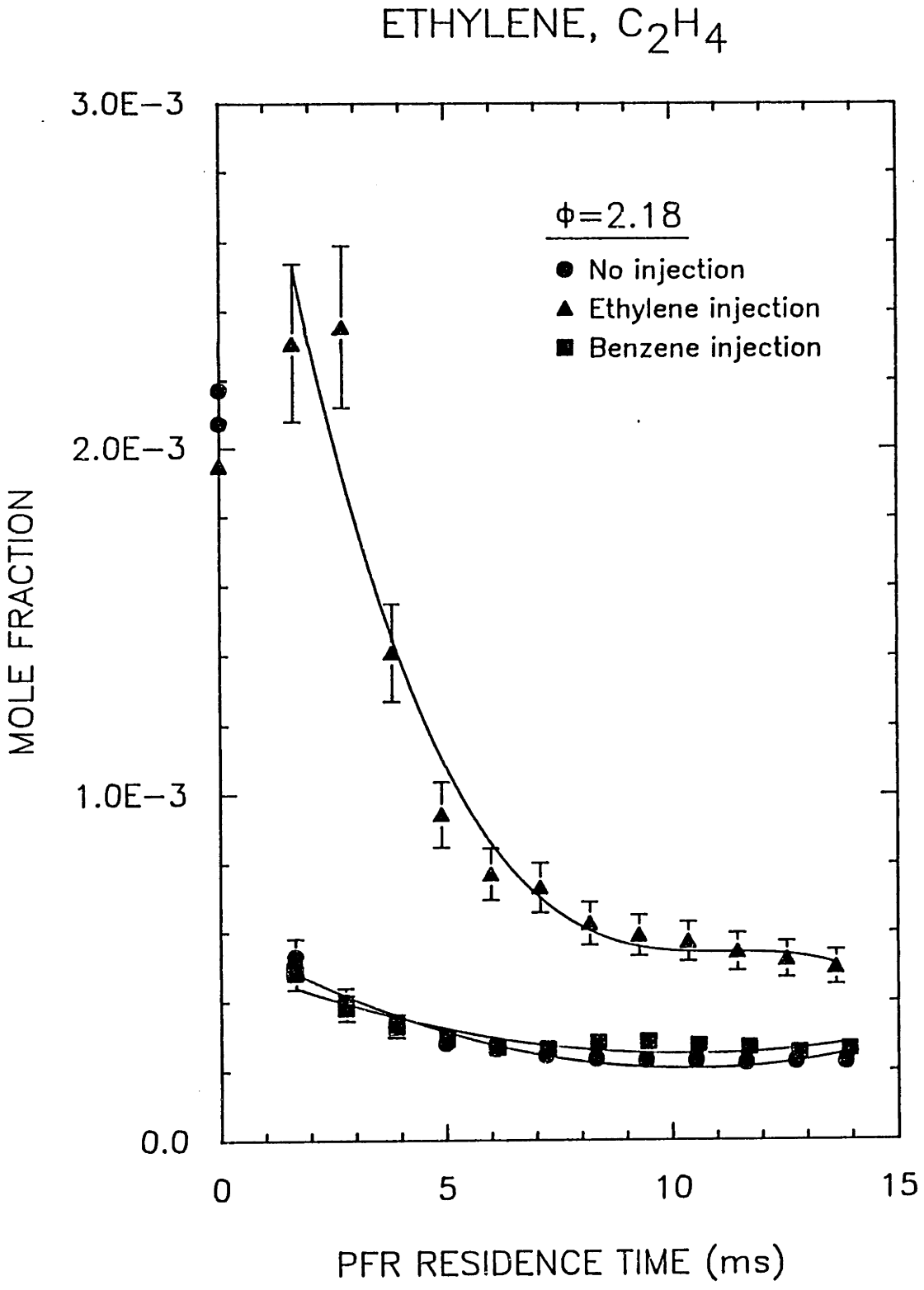

Figure 8.2 Concentration profiles for ethylene (C_2H_4) in JSR/PFR for ϕ=2.18, for no injection, C_2H_4 injection and C_6H_6 injection cases.

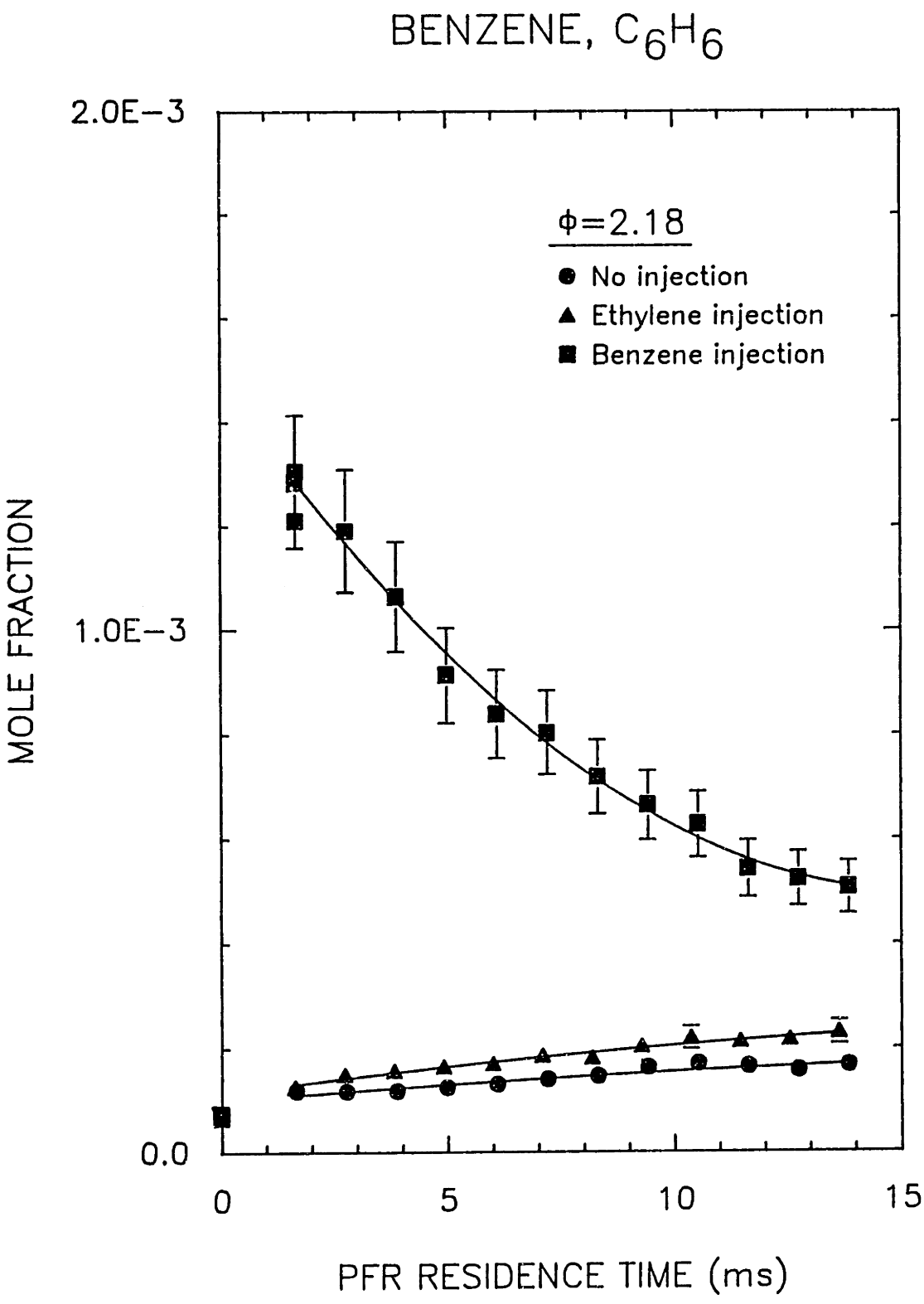

Figure 8.3 Concentration profiles for benzene (C_6H_6) in JSR/PFR for ϕ=2.18, for no injection, C_2H_4 injection and C_6H_6 injection cases.

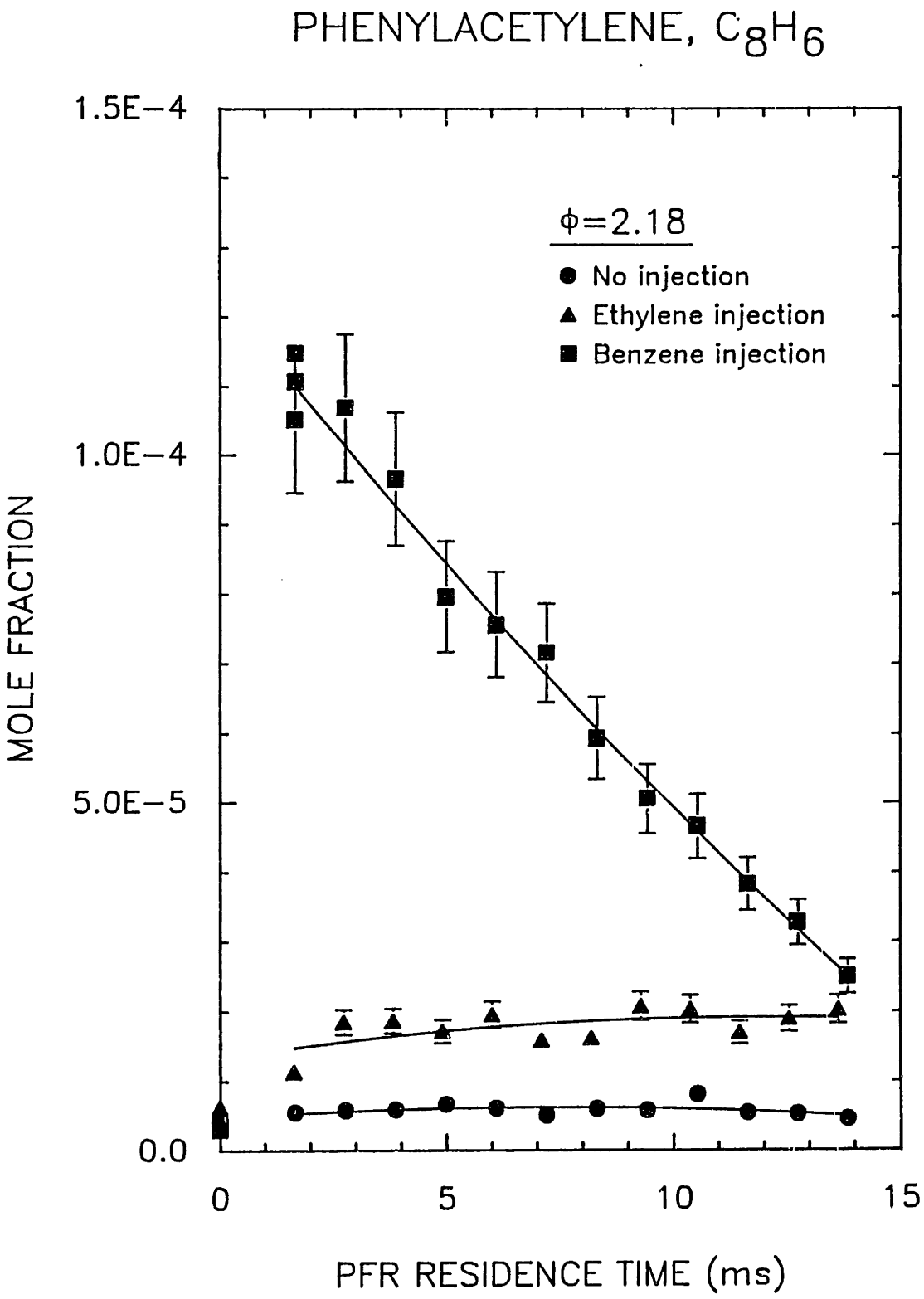

Figure 8.4 Concentration profiles for phenylacetylene (C_8H_6) in JSR/PFR for ϕ=2.18, for no injection, C_2H_4 injection and C_6H_6 injection cases.

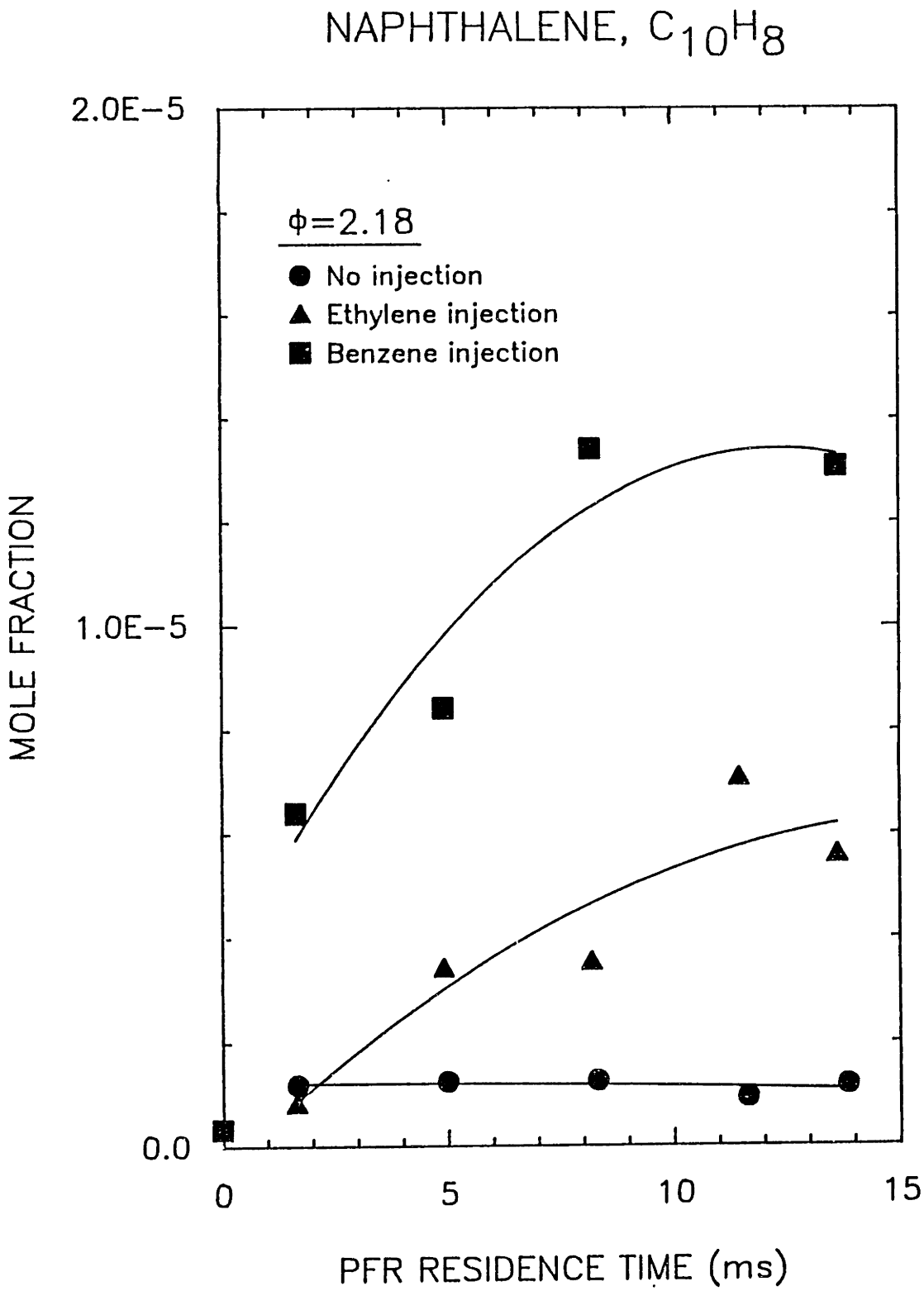

Figure 8.5 Concentration profiles for naphthalene ($C_{10}H_8$) in JSR/PFR for ϕ=2.18, for no injection, C_2H_4 injection and C_6H_6 injection cases.

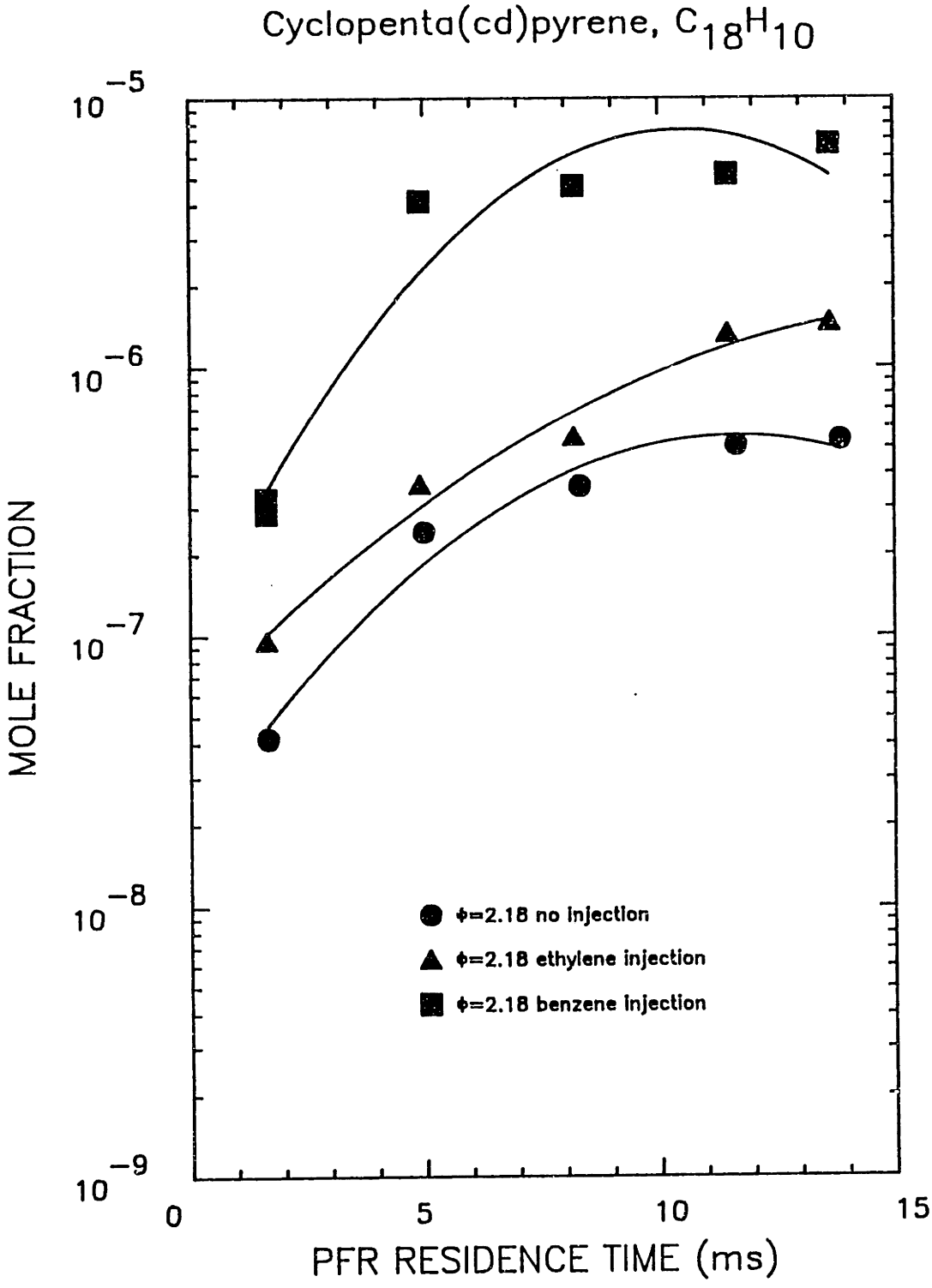

Figure 8.6 Concentration profiles for cyclopenta(cd)pyrene in JSR/PFR for ϕ=2.18, for no injection, C_2H_4 injection and C_6H_6 injection cases.

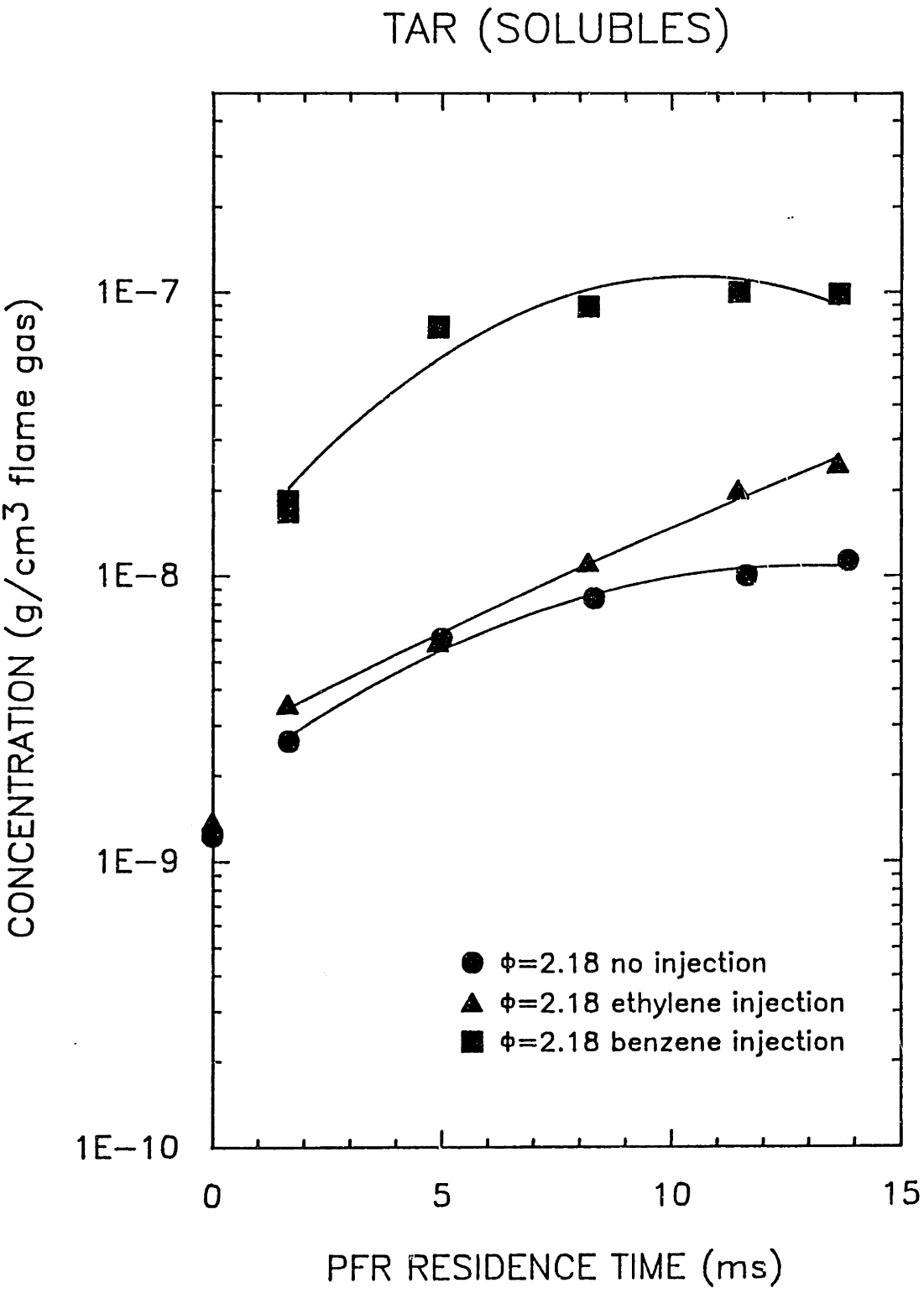

Figure 8.7 Concentration profiles for tar (defined as CH_2Cl_2-soluble material with mass ≥ naphthalene) in JSR/PFR for ϕ=2.18, for no injection, C_2H_4 injection and C_6H_6 injection cases.

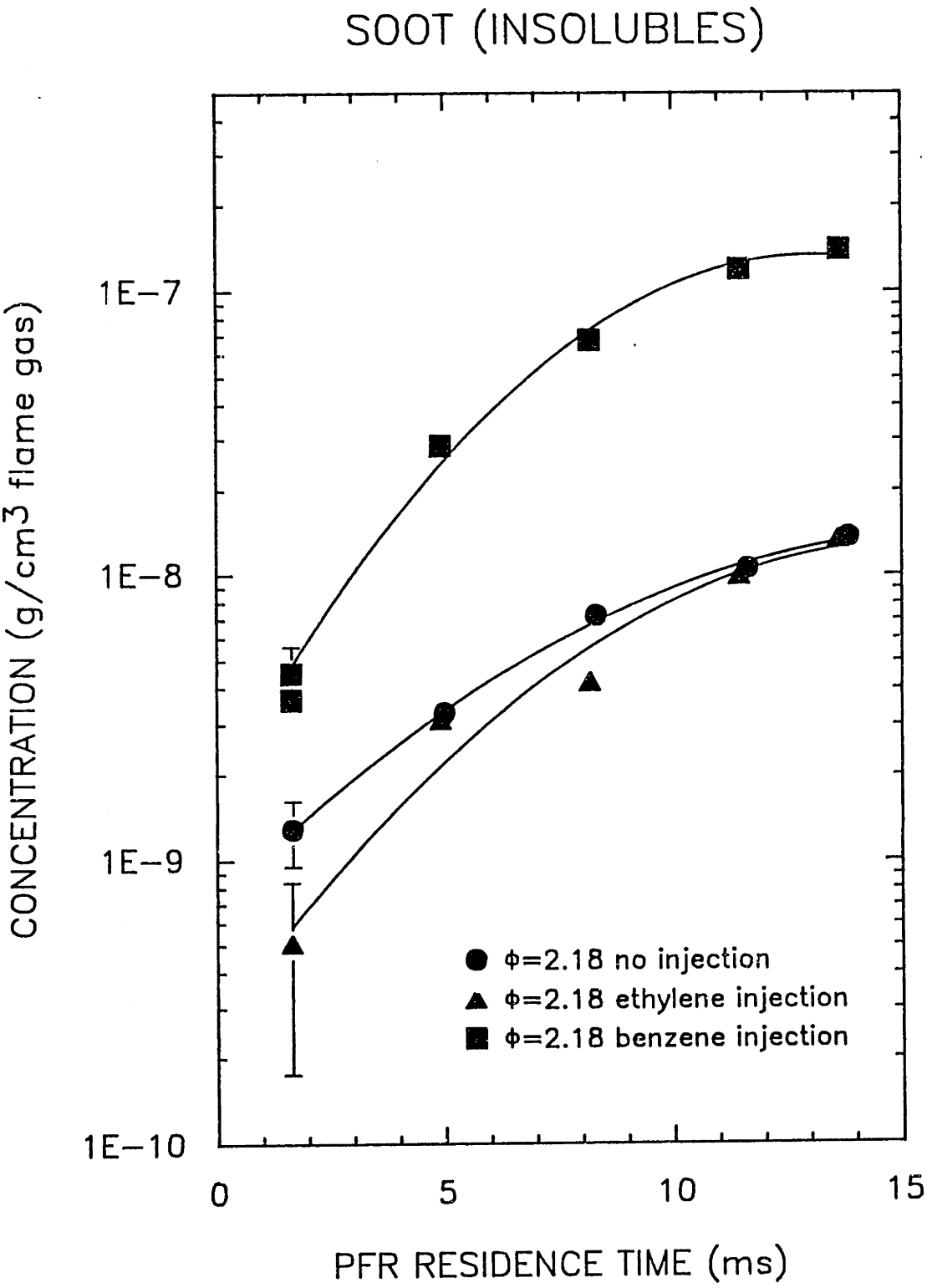

Figure 8.8 Concentration profiles for soot (defined as CH_2Cl_2-insoluble material) in JSR/PFR for ϕ=2.18, for no injection, C_2H_4 injection and C_6H_6 injection cases.

The ΣGC PAH inventory includes species between 2 and 5 aromatic rings, and the molar concentration, mass concentration, average molecular weight profiles are shown in Figures 8.9 through 8.11. Three overall trends are observed for the ΣGC PAH. The first is that the total mass of species in the ΣGC PAH inventory is increasing as a function of residence time in the PFR. The mass is further increased by addition of either ethylene or benzene, but much more so for the benzene addition. The second observation is that the total number of moles of ΣGC PAH species is generally increasing. The third trend is that the average molecular weight of the PAH inventory is increasing. These three observations indicate that smaller PAH structures are being transformed into larger PAH structures. This trend is observed for both the addition of C_2H_4 or C_6H_6. For the C_2H_4 injection, the ΣGC PAH rate of formation is doubled. For the C_6H_6 injection, the ΣGC PAH formation rate is fast at the beginning of the PFR and decreases as residence time increases. We see that the ΣGC PAH concentration is increased by an order of magnitude by the end of the PFR for the benzene injection case.

The molar concentration of the ΣGC PAH is almost constant for the no injection case, but the mass concentration increases, indicating a molecular weight shift to larger PAH species. For the C_2H_4 injection case, both the molar concentration and the mass concentration are increasing, and they are increasing in such a way so that the average molecular weight is increasing. The same observation is made for the C_6H_6 injection case.

If we calculate the fractional conversion of the injected species by the end of the PFR, we find that for ethylene (C_2H_4) injection, 97% of the injected C_2H_4 is converted to other species. If increases in the other species are attributed to the injected material, then the observed increases would imply that most of the carbon mass of the injected C_2H_4 is converted to C_2H_2 (69%), and to a lesser extent CH_4(7%), C_4H_2(4%), C_6H_6(2%), two C_3H_4 isomers(1%), and tar(1%). The unaccounted fraction of the injected C_2H_4 (≈16%) is probably converted to CO and CO_2 near the entrance of the PFR, since the JSR has a small amount of oxygen remaining (≈1%). By stoichiometry, oxidation of 16% of the injected C_2H_4 to CO and CO_2 would require only an O_2 mole fraction of $1.6x10^{-3}$. Unfortunately, the exact amount of injected C_2H_4 converted to CO and CO_2 cannot be determined because oxidation of 16% of the injected C_2H_4 is less than our experimental uncertainty for the CO and CO_2.

Of the initial amount of C_6H_6 injected, 30% is consumed prior to the first sampling point in the PFR, and by the end of the PFR, 16% is converted to tar, 11% is converted to soot, and 18% remains as benzene, assuming these increases over the no injection case are due to the benzene injection. The rest of the benzene consumption is probably oxidation to CO and perhaps decomposition to C_2H_2, although we cannot accurately determine the small expected increases in CO and C_2H_2 concentrations. The stoichiometric amount of O_2 required to account for oxidation of 55% of the injected C_6H_6 to CO is a mole fraction of $3.1x10^{-3}$, and there is more than enough O_2 exiting from the JSR to account for the benzene oxidation.

Although we have calculated where most of the mass of the injected species goes, it is perhaps more instructive to look at the rates of formation and destruction of species which are greatly affected by the injected species. These species are usually present in small quantities compared to the injected species and may be involved in chemical reactions with the injected species.

At early residence times in the PFR ($1.7<t<5$ ms), the net rate of benzene destruction is 6.3×10^{-5} g/cm^3·s, while the net rate of formation of tar is 1.8×10^{-5} g/cm^3·s, and soot is 7.5×10^{-6} g/cm^3·s. Therefore, the net rates of tar and soot formation are equal to 29% and 12%, respectively, of the benzene net destruction rate. If we assume that the remaining 59% of the benzene destruction rate is due to oxidation by OH to form CO and cyclopentadiene (C_5H_6), then the required rate constant is 2.1×10^{12} cm^3/mol·s. This rate constant is comparable to the literature rate constant of 2.5×10^{12} cm^3/mol·s from direct high temperature measurements of the reaction $C_6H_6 + OH = C_6H_5OH + H$ by He et al. (1988b). Phenol (C_6H_5OH) may undergo further decomposition to cyclopentadiene (C_5H_6) and CO. The OH mole fraction at 2.0 ms is calculated to be 3.0×10^{-6} from elementary kinetics modelling. Additional experimental support for benzene oxidation comes from the prompt CO and C_5H_6 formation experimentally observed by Bittner (1981c) in the pre-flame zone of his rich benzene flat-flames. Thus, besides growth to larger species, a large fraction of the benzene consumption in the PFR is probably oxidation to CO and C_5H_6.

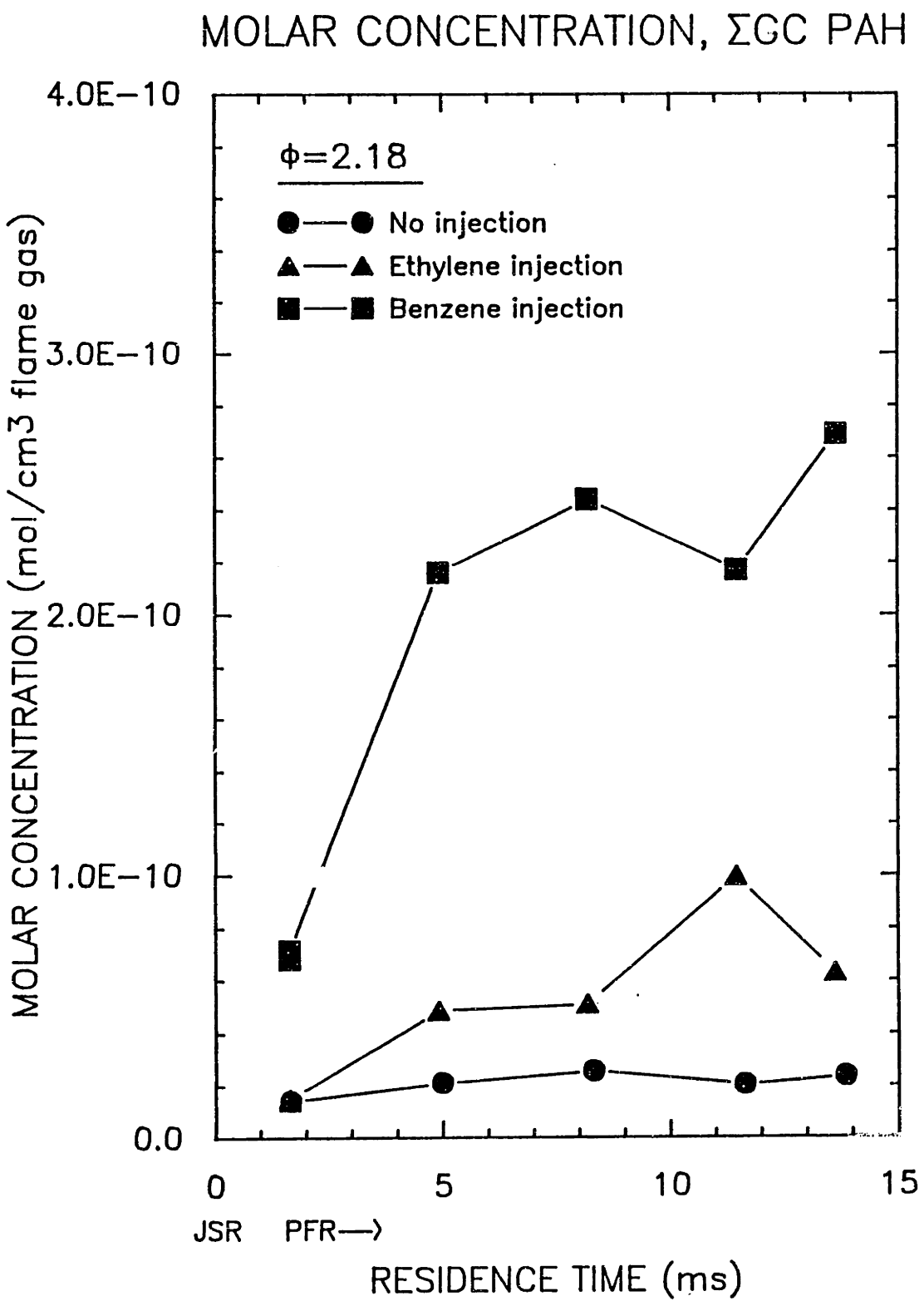

Figure 8.9 Molar Concentration of ΣGC PAH in JSR/PFR for ϕ=2.18, for no injection, C_2H_4 injection and C_6H_6 injection cases.

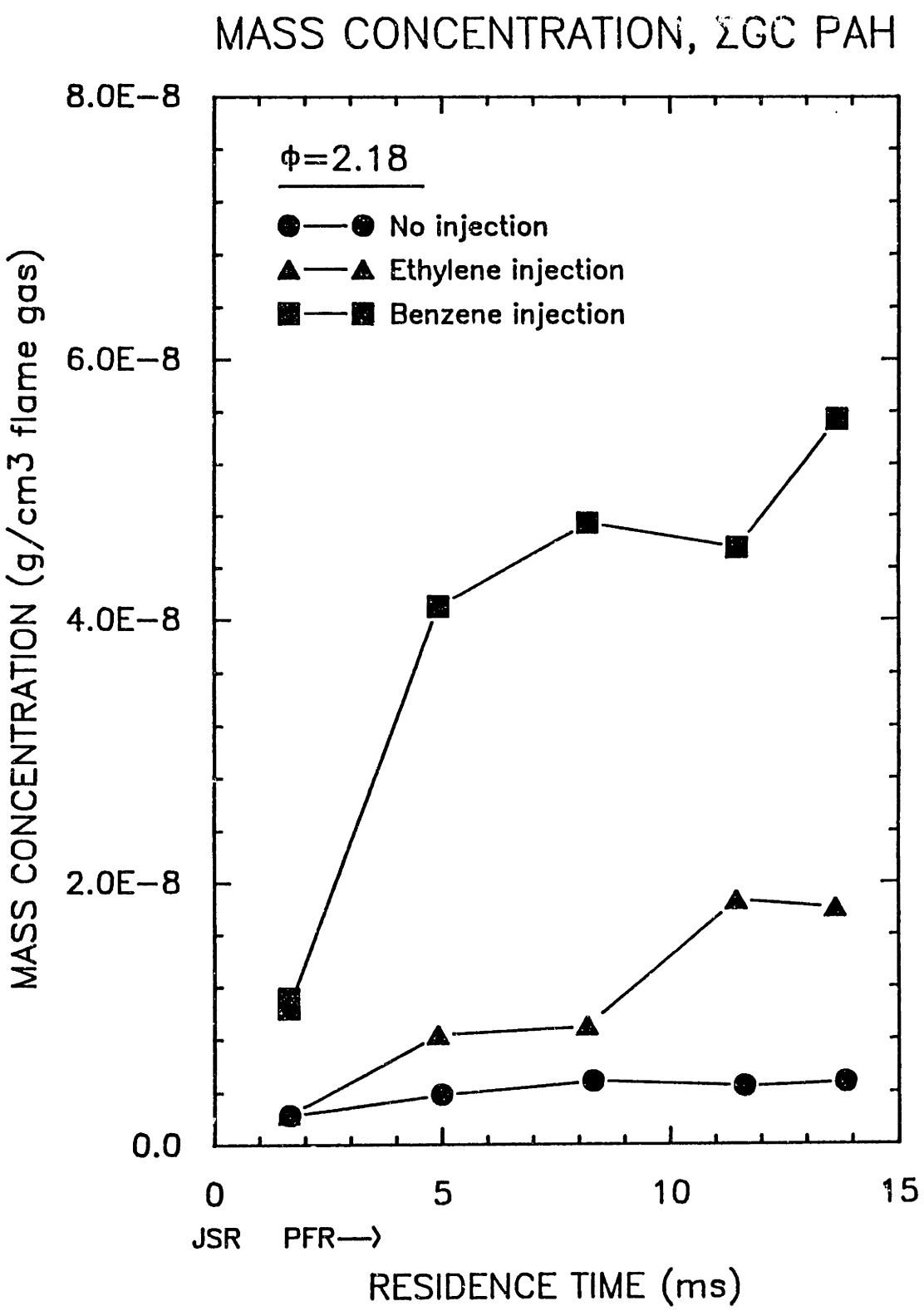

Figure 8.10 Mass Concentration of ΣGC PAH in JSR/PFR for ϕ=2.18, for no injection, C_2H_4 injection and C_6H_6 injection cases.

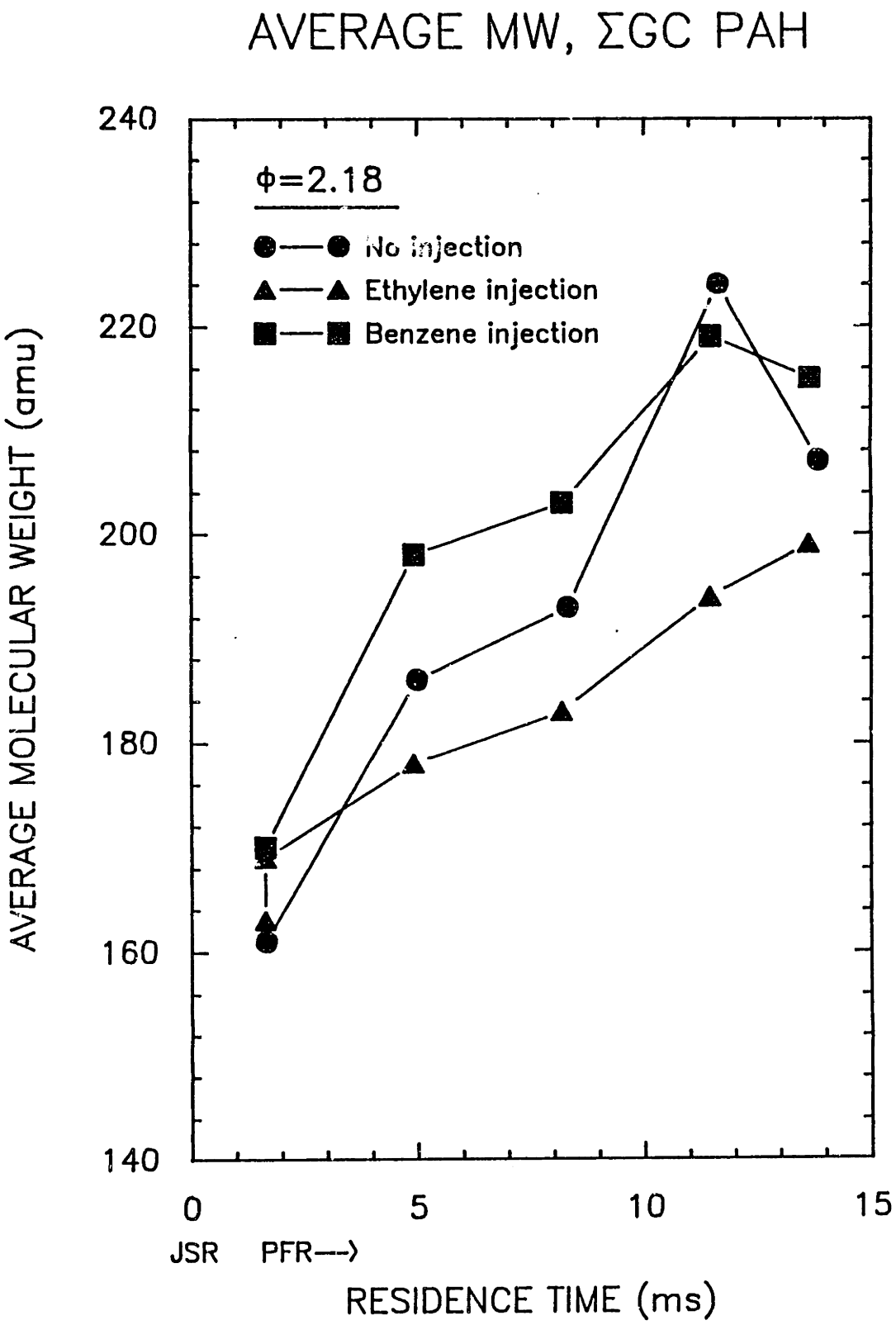

Figure 8.11 Average Molecular Weight of ΣGC PAH in JSR/PFR for ϕ=2.18, for no injection, C_2H_4 injection and C_6H_6 injection cases.

8.2 PAH MODELLING BACKGROUND

8.2.1 Acetylene Addition Mechanism

Attempts at PAH modeling have involved extensions of the elementary chemical kinetics mechanisms which have been successful at modeling the C_2 hydrocarbon chemistry. Frenklach et al. (1987) have proposed a free-radical mechanism, which includes PAH species up to 7 aromatic rings (coronene), to model an $C_2H_2/O_2/Ar$ laminar flat flame. The mechanism was developed based on shock tube soot measurements for C_2H_2 and C_2H_2/O_2 mixtures (Frenklach et al. 1985b; Frenklach et al. 1986). The model predictions for individual PAH species profiles had the same general shape as the experimental data, but the mechanism over-estimated the decline of PAH species by factors of 10^3 - 10^4. Most notable was the misprediction of the benzene profile, since the formation of single ring aromatic species is often assumed to be an important step in the PAH growth process. Harris' (1988a) mechanism includes species up to acenaphthylene and was moderately successful at modeling benzene and phenylacetylene formation in his C_2H_4 laminar flat-flame. Unfortunately, lack of knowledge of rate constants for aromatic and polyaromatic species at combustion temperatures and uncertainties in the thermochemical properties of large PAH present the elementary chemical kinetics modeler with serious challenges. PAH oxidation rate constants in Frenklach's mechanism were all assigned the value $1x10^{13}$ $cm^3/mol \cdot s$, and Harris' mechanism did not include PAH oxidation reactions.

Bittner (1978) has proposed that the role of the aromatic ring is to provide a structure which can undergo substitution reactions

with non-aromatic species, such as CH_3, C_2H_2, C_4H_2, and C_4H_4. Internal substitution reactions, which result in ring closure, stabilize the growing PAH structure through H-elimination and aromatization. From a thermodynamic analysis of the heats of reactions of possible growth pathways, Bittner concluded that only vinylacetylene (C_4H_4) addition to phenyl (C_6H_5), or allene (C_3H_3) addition to benzyl (C_7H_7) had a unimolecular cyclization pathway to form fused ring aromatics which was favored over the decomposition channel. Bittner also concluded, however, that aromatic species with polyacetylenic side chains could form fused ring aromatic structures through a bimolecular pathway.

Both the Frenklach and Harris mechanisms propose that PAH growth takes place through a bimolecular acetylene addition mechanism. The first aromatic ring, benzene, is formed through C_2H_2 addition to either C_4H_3 or C_4H_5 followed by cyclization. The addition of C_2H_2 to the phenyl radical is followed by a second C_2H_2 addition which leads to the formation of two ring aromatic, naphthalene. The dominant route for PAH growth was proposed to be stabilization of the adduct formed from C_2H_2 addition to C_6H_5 to phenylacetylene (C_6H_6), reactivation of the species by H-abstraction at a position ortho to the ethynyl side chain, a second C_2H_2 addition to the radical site, followed by cyclization across the triple bond to form 1-naphthalenyl ($C_{10}H_7\bullet$), which can be stabilized by H addition. This route was shown to be faster than a second C_2H_2 addition directly to the vinylic side chain of the styrene radical, followed by cyclization of the butadienyl moiety to form naphthalene. The evidence for these

pathways is based on an analysis of the reaction fluxes as predicted by the computational model. Figure 8.12 shows the mechanism proposed by Frenklach (1985b).

8.2.2 Coagulation of PAH

Badger and co-workers (1958-1967) have proposed a PAH growth mechanism based on a series of low temperature aromatic and polyaromatic hydrocarbon pyrolysis experiments. In these experiments benzene, naphthalene, phenanthrene, anthracene and their substituted derivatives were pyrolized at temperatures around 700°C and residence times of about 30 minutes. The proposed mechanism involves formation of an aryl radical by H-atom dissociation or thermal cleavage of the substituted group, condensation of intact aromatic ring structures followed by eventual cyclization. The major products observed were the dimers of the reactant aromatic ring structures. It was proposed that formation of the aryl radical was the rate limiting step.

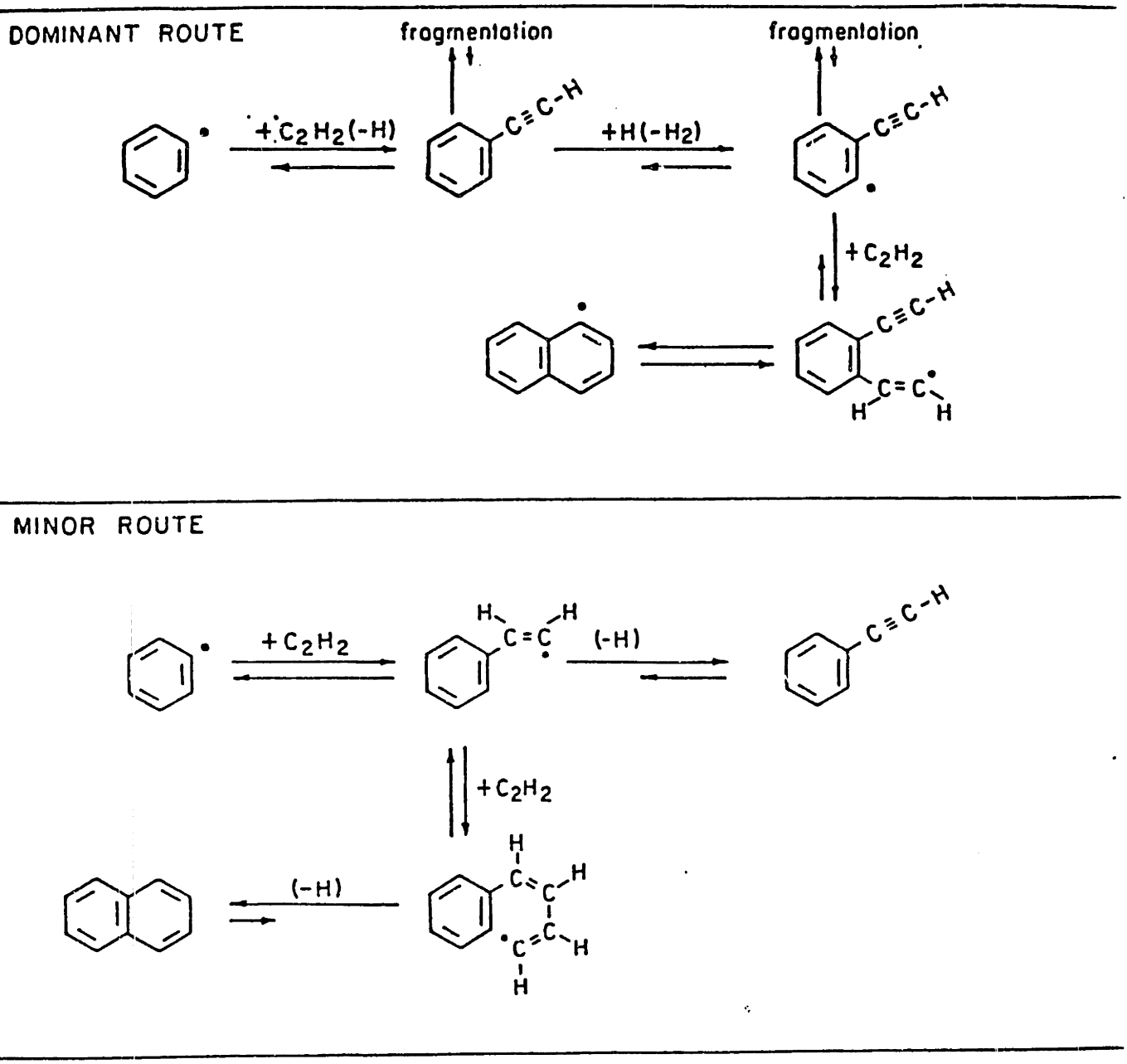

Figure 8.12 Possible mechanism for formation of two-ring aromatics. Dominant route was determined from computer simulations (taken from Frenklach, 1985b).

8.3 EXPERIMENTAL OBSERVATIONS OF PAH STRUCTURES

From our detailed experimental characterization of the PAH which are amenable to GC analysis, mechanisms for the formation and destruction of PAH are suggested by the structures of the different types of species which are present, and those which are not present. These different structural types include PAH with acetylenic substituent groups, PAH with 5-membered rings, PAH with condensed ring structures, and PAH with non-condensed ring structures.

8.3.1 Acetylenic-Substituted PAH

Acetylenic-substituted PAH species were positively identified by GC/FTIR and include phenylacetylene, 2-ethynyl-naphthalene, and three ethynyl-acenaphthylene isomers. All 3 di-substituted (1,2-, 1,3-, 1,4-) ethynyl-benzene isomers were also observed to be present. Ethynyl groups show a very strong absorbance at 3330 cm^{-1}, which corresponds to the ≡C-H stretching frequency. We were unable to observe higher molecular weight species such as the ethynyl-pyrenes or ethynyl-cyclopenta(cd)pyrenes due to detectability limits for the GC-FTIR, but we expect these species to be present. The ethynyl-PAH species have been postulated to explain the fragmentation patterns observed in GC-MS data in flat-flames (Wenz, 1983).

Acetylenic-substituted PAH have been proposed as important intermediates for molecular weight growth, and the fact that we observe the di-substituted ethynyl-benzenes seems to support the dominant kinetic mechanism proposed by Frenklach (1985b). Figure 8.12 shows the formation mechanism for the two-ring aromatics proposed by

Frenklach (1985b).

The ethynyl-acenaphthylene structures suggest acetylene addition to different acenaphthylenyl radicals. Stein (1987) has found that since the unpaired electrons are localized, to a first approximation, aryl radicals such as naphthylenyl and phenanthrenyl should behave like phenyl. Since the H-abstraction reactions at the different positions for acenaphthylene should proceed at comparable rates, we would expect to get a mix of ethynyl-substituted acenaphthylene isomers.

8.3.2 PAH With 5-Membered Rings

PAH species which contain 5-membered ring structures account for more than half of the total PAH inventory from indene (C_9H_8) to benzo(ghi)perylene ($C_{22}H_{12}$). These PAH species with 5-membered ring structures consisted of 2 types: 1) 5-membered rings containing a methylene group, such as indene, fluorene, and 4H-cyclopenta-(def)phenanthrene, and 2) "acenaphthylene bridge" structures, such as acenaphthylene, acephenanthrylene, aceanthrylene, and cyclopenta-(cd)pyrene.

The first class of PAH, containing a 5-membered ring with a methylene group, may be oxidation products of 6-membered ring PAH. Vaughn (1988) has proposed benzene oxidation mechanisms which lead to cyclopentadiene formation through phenoxy, similar to that proposed by Venkat (1982). Cyclopentadiene (C_5H_6) has been positively identified for our experimental conditions, and it is proposed that analogous oxidation reactions of the 6-membered ring PAH species may yield the

observed 5-membered ring species. Thus, indene may be the oxidation product of naphthalene, fluorene may be the oxidation product of phenanthrene, and 4H-cyclopenta(def)phenanthrene may be the oxidation product of pyrene. Figure 8.13 shows the proposed benzene oxidation mechanism (Vaughn, 1988), as well as the proposed analogous PAH oxidation reactions. Rate constants at high temperatures for these PAH oxidation reactions are unknown.

The second class of PAH species with 5-membered rings, which have an acenaphthylene bridge group, are different from the first class in the sense that they may be growth products from acetylene addition reactions. As an example, acenaphthylene may be formed by acetylene addition to 1-naphthalenyl, followed by cyclization across the peri-positions of naphthalene. Similarly, acephenanthrylene may be formed from acetylene addition to phenanthrenyl, and aceanthrylene from acetylene addition to anthracenyl, and cyclopenta(cd)pyrene may be formed from acetylene addition to pyrene. Fluoranthene is also found in relatively high concentrations, ≈50% of the pyrene concentration, and it may be formed from two acetylene additions to acenaphthylene. Figure 8.14 shows the proposed formation routes for the second class of 5-membered ring PAH.

8.3.3 PAH With Condensed/Non-Condensed Structures

The possibility exists for both types of PAH growth mechanisms (acetylene addition and PAH coagulation) to be occurring in the PFR. For a closed system of PAH molecules, if coagulation is the only process, the PAH distribution will shift to higher molecular weights.

Coagulation does not change the mass and decreases the number of moles. If C_2H_2 addition were the only mechanism, the PAH and the average molecular weight would increase, but the number of moles would remain constant. If we allow new moles of PAH to be introduced at the low molecular weight limit, number of moles will increase for the C_2H_2 addition mechanism, and will increase for the coagulation mechanism, if the rate at which new moles are being added is greater than the rate at which moles are being lost through coagulation.

From the data in Figures 8.9-8.11 we see that for the no injection case, the number of moles in the ΣGC PAH inventory is essentially constant, while the mass concentration and hence the average molecular weight is increasing. Unless the increase in the number of moles of naphthalene added compensates for the number of moles lost through coagulation reactions, coagulation alone cannot explain the increase in molecular weight. As seen in Figure 8.4, the mole fraction profile of naphthalene for the no injection case is constant, so we conclude that coagulation is not the major pathway for molecular weight growth. For the C_2H_4 and C_6H_6 injection cases, the increase in the number of moles due to naphthalene formation is not greater than the increase in the number of moles in the ΣGC PAH, and we reach the same conclusion.

Additional evidence against coagulation as the dominant PAH formation mechanism in our system is that even for the C_6H_6 injection case, we do not see the expected intermediates of the coagulation mechanism, namely the non-condensed PAH structures such as biphenyl, terphenyl, or condensed structures such as triphenylene. Finally,

coagulation between aryl species and aromatics alone cannot explain the formation of PAH structures such as phenyl-acetylene, naphthalene and acenaphthylene. There must be some other pathway for molecular weight growth, and we conclude that C_2H_2 addition is the most probable mechanism.

From our thermodynamic modelling, we saw that, with the exception of the pyracylene, the stabilomers were the most abundant experimentally observed PAH species. These stabilomers may be formed through an acetylene addition mechanism. Reactions along the most favored thermodynamic pathway which involves these stabilomers are highly reversible, as evidenced by the partial equilibria of the ethynyl-substituted species, and the irreversibility of the ring-closure reactions may provide the driving force for polymerization along the path.

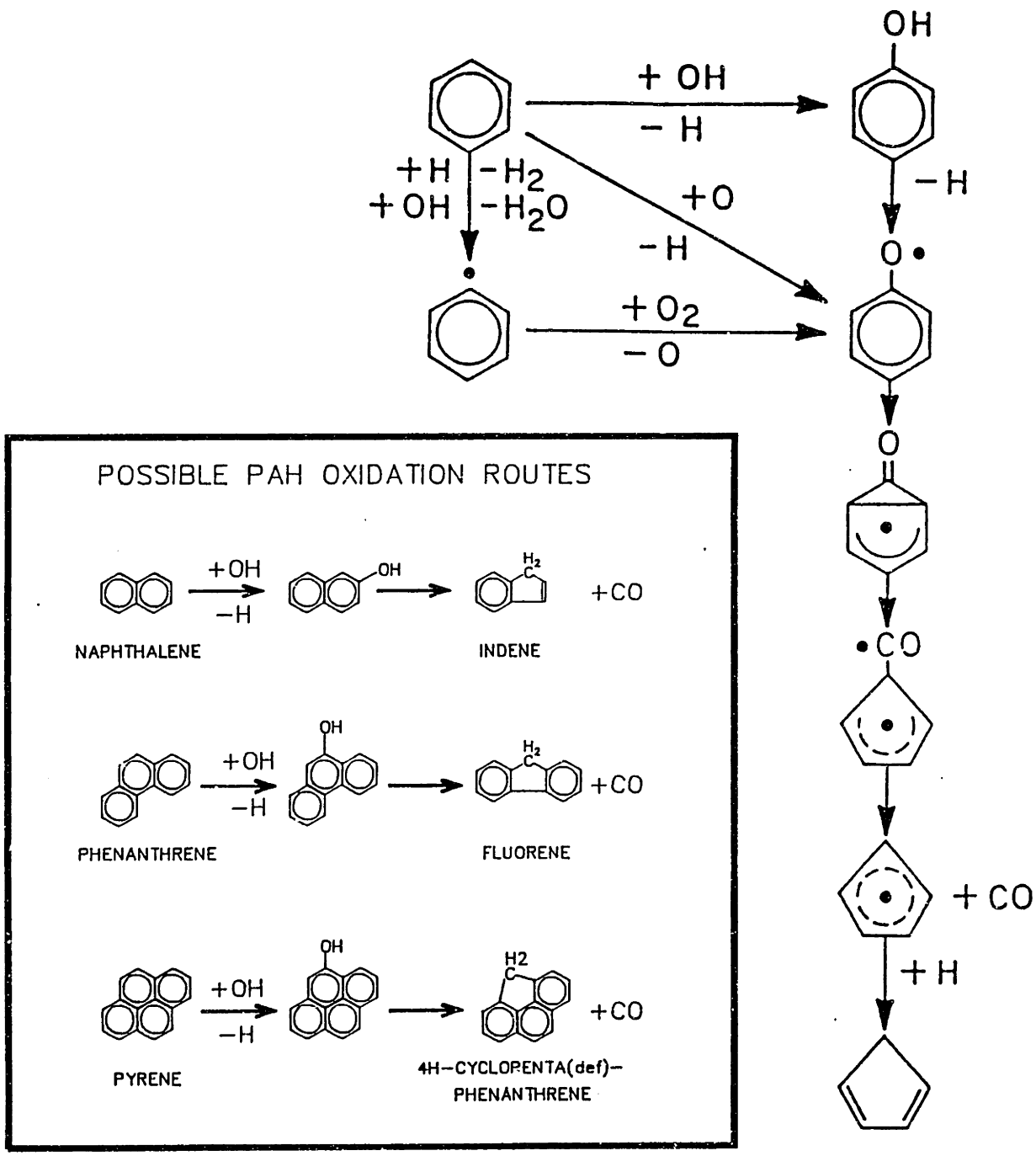

Figure 8.13 Possible formation mechanism of PAH containing 5-membered ring structures with methylene groups based on the oxidation of benzene (benzene oxidation mechanism taken from Vaughn, 1988).

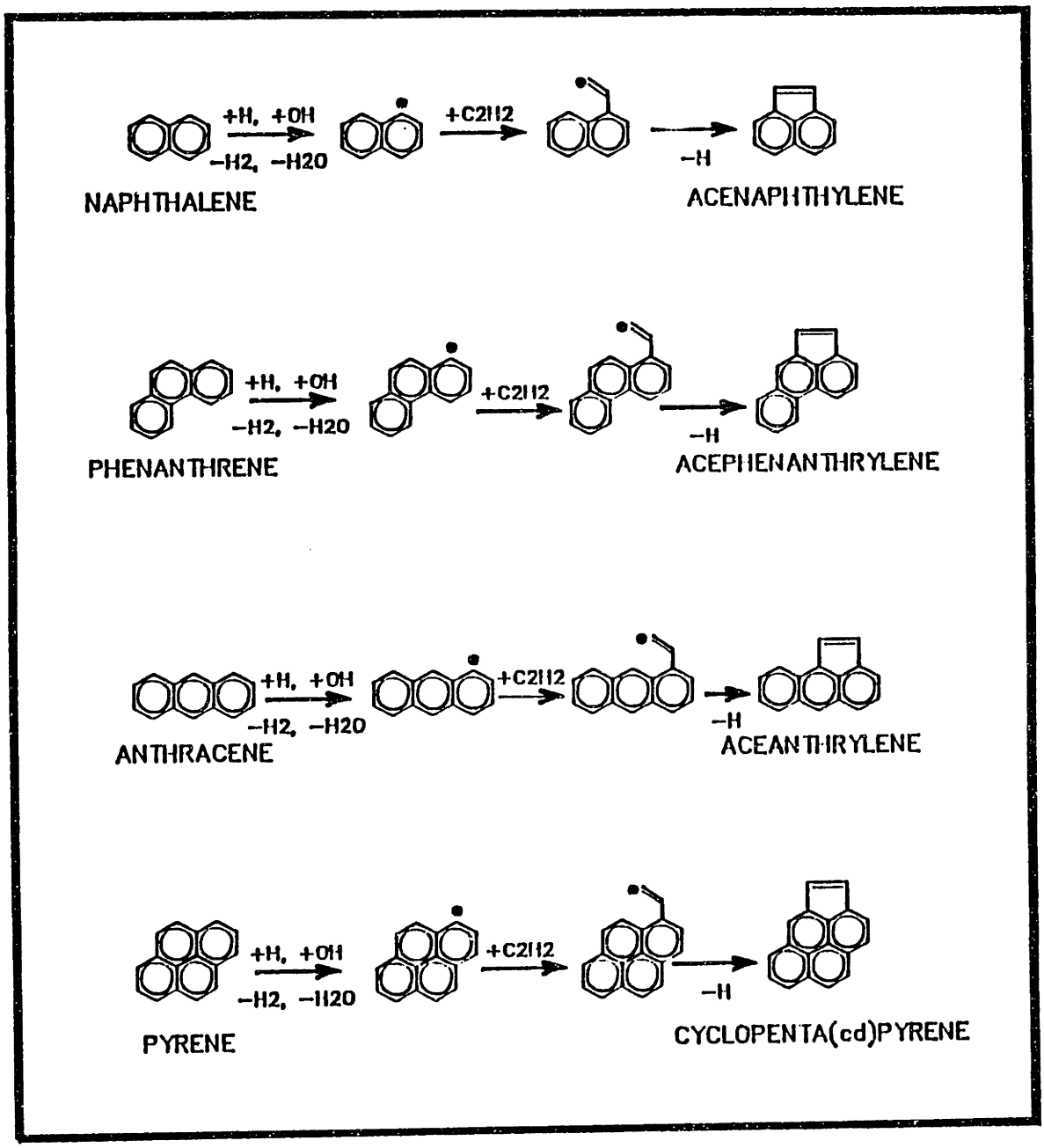

Figure 8.14 Possible formation mechanism of PAH containing 5-membered ring "acenaphthylene bridge" structures.

8.4 MODEL FORMULATION

With the insights gained from the detailed PAH chemical characterization and thermodynamics modelling, we now attempt to model the kinetics of PAH formation. The type of model is "global" in the sense that PAH formation is not modeled at the elementary reaction level. It was felt that without adequate knowledge of rate constants, the modelling of individual PAH species (ala Frenklach, Harris) would only be semi-quantitative at best.

In order to model the formation of PAH, we must first realize that PAH are intermediates in the molecular weight growth process. Since it is necessary to form PAH structures between the fuel and the formation of the first soot nuclei, the PAH inventory is being simultaneously formed from fuel decomposition and consumed through soot forming reactions. The PAH inventory is by definition bounded at both ends of the molecular weight scale, and species may enter through the lower bound and exit through the upper bound, so that at any position in the PFR the rate of change in the mass concentration of PAH is determined by the net of these rates. Figure 8.15 shows a representation of these rates for the ΣGC PAH inventory.

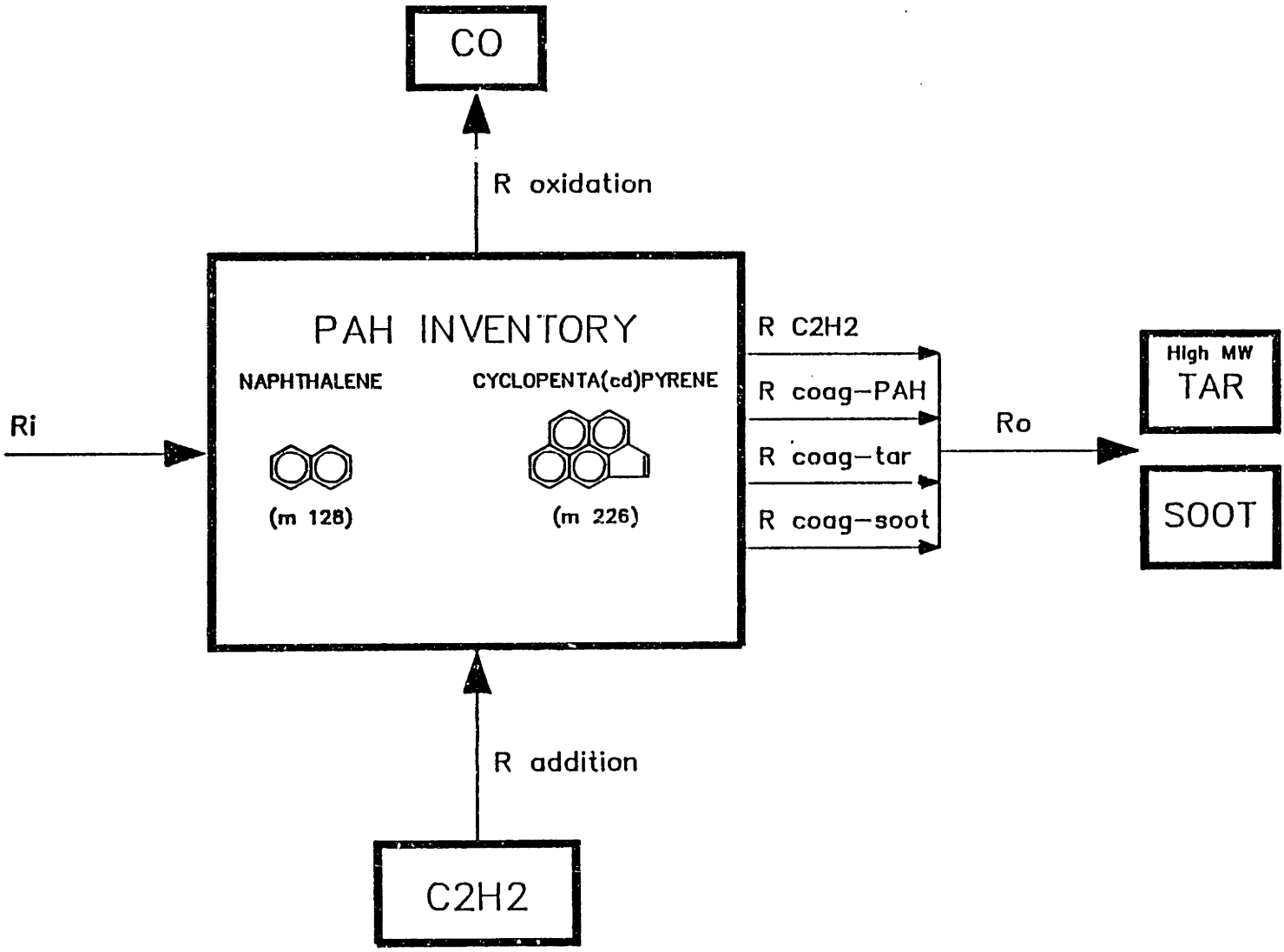

Figure 8.15 Representation of ΣGC PAH formation and destruction pathways.

The change in the mass concentration of the ΣGC PAH inventory with respect to time is given by

$$dC/dt = R_i + R_{add} - R_{ox} - R_o \qquad \text{Eq. (8.1)}$$

where R_i is the initiation rate ($g/cm^3 \cdot s$) for the formation of species at the low molecular weight limit (ie. naphthalene, the smallest species in the ΣGC PAH inventory); R_{add} is the net rate of addition of aliphatic species (assumed to be primarily C_2H_2) to the PAH inventory; R_{ox} is the rate of oxidation of species to form CO (OH is assumed to be the primary oxidizing species); and R_o is the net rate at which mass is lost through the high molecular weight limit of the ΣGC PAH inventory. This last term, R_o, is comprised of 4 different components as given by

$$R_o = R_{C_2H_2} + R_{coag\text{-}PAH} + R_{coag\text{-}tar} + R_{coag\text{-}soot} \qquad \text{Eq. (8.2)}$$

where $R_{C_2H_2}$ is the rate at which a 5 ring PAH species (mostly cyclopenta(cd)pyrene) adds C_2H_2 and leaves the ΣGC PAH pool through the high MW limit, $R_{coag\text{-}PAH}$ is the rate at which two small PAH (2-5 rings) coagulate to form a PAH species larger than 5 rings, $R_{coag\text{-}tar}$ is the rate at which PAH coagulate with high MW tar species (≥ 6 rings) and are removed from the ΣGC PAH inventory, and $R_{coag\text{-}soot}$ is the rate at which soot particles scavenge PAH molecules.

For each of the rate terms given in Equations 1 and 2, we can write expressions in terms of a rate constant (or collision efficiency

times collision frequency), molar concentrations of species, and mass transferred in or out of the PAH inventory. These expressions are given in Equations 8.3 through 8.9,

$$R_i = k_i \cdot [C_8H_6] \cdot [C_2H_2] \cdot 128 \quad \text{Eq. (8.3)}$$

$$R_{add} = k_{add} \cdot [\Sigma GC\ PAH] \cdot [C_2H_2] \cdot 24 \quad \text{Eq. (8.4)}$$

$$R_{ox} = k_{ox} \cdot [\Sigma GC\ PAH] \cdot [OH] \cdot 12 \quad \text{Eq. (8.5)}$$

$$Rc_2H_2 = kc_2H_2 \cdot [\Sigma GC\ PAH] \cdot [C_2H_2] \cdot 226 \quad \text{Eq. (8.6)}$$

$$R_{coag\text{-}PAH} = \gamma_{PAH} \cdot (Z_{PAH}/N_{av}) \cdot [\Sigma GC\ PAH] \cdot [\Sigma GC\ PAH] \cdot MW_{PAH} \quad \text{Eq. (8.7)}$$

$$R_{coag\text{-}tar} = \gamma_{tar} \cdot (Z_{tar}/N_{av}) \cdot [tar] \cdot [\Sigma GC\ PAH] \cdot MW_{PAH} \quad \text{Eq. (8.8)}$$

$$R_{coag\text{-}soot} = \gamma_{soot} \cdot (Z_{soot}/N_{av}) \cdot [soot] \cdot [\Sigma GC\ PAH] \cdot MW_{PAH} \quad \text{Eq. (8.9)}$$

where k's are rate constants, γ's are collision efficiencies, and Z's are collision frequencies for the coagulation-type reactions. If we can find or calculate the rate constants (or equivalently $\gamma \cdot Z$), we will be able to model the formation of PAH because we measure or calculate the species concentrations given in Equations 8.3-8.9. The method used to determine the different kinetic rate constants is detailed in the following sections.

8.4.1 Initiation Rate, R_i

The initiation rate, R_i ($g/cm^3 \cdot s$), is the rate at which mass is introduced into the ΣGC PAH inventory at the lower molecular weight limit. We assume that the initiation rate is given by the reactions which form naphthalene from single-ring aromatic species, specifically from the addition of acetylene to phenylacetylene, and is given by

$$R_i = k_i \cdot [C_8H_6] \cdot [C_2H_2] \cdot 128 \text{ g/mol} \qquad \text{Eq. (8.3)}$$

where k_i is the initiation rate constant, and 128 reflects the mass added to the PAH inventory by formation of naphthalene. This rate is NOT equal to the slope of the naphthalene concentration profile, because naphthalene itself is an intermediate. The slope of the naphthalene curve gives us the NET rate of naphthalene formation. Thus, Ri must be at least as great as the slope of the naphthalene profile.

Since we assume that molecular weight growth for the ΣGC PAH inventory occurs through sequential C_2H_2 addition reactions, we may write a possible overall reaction sequence for two-ring formation from a single-ring aromatic species starting with benzene:

C_6H_6	+ H	=	$C_6H_5\cdot$	+ H_2	Rxn (8.1)
$C_6H_5\cdot$	+ C_2H_2	=	$C_6H_5C_2H_2\cdot$		Rxn (8.2)
$C_6H_5C_2H_2\cdot$		=	C_8H_6	+ H	Rxn (8.3)
C_8H_6	+ H	=	$C_8H_5\cdot$	+ H_2	Rxn (8.4)
$C_8H_5\cdot$	+ C_2H_2	=	1-$C_{10}H_7\cdot$		Rxn (8.5)
1-$C_{10}H_7\cdot$		=	c-$C_{10}H_7\cdot$		Rxn (8.6)
c-$C_{10}H_7\cdot$	+ H_2	=	$C_{10}H_8$	+ H$\cdot$	Rxn (8.7)
C_6H_6	+2 C_2H_2	=	$C_{10}H_8$	+ H_2	Rxn (8.8)

This mechanism is the same as the one Frenklach et al. (1985b) proposed to explain soot formation for C_2H_2 shock tube pyrolysis and is shown in Figure 8.12. From our thermodynamic modelling studies, Reactions 8.1 through 8.3 are nearly at partial equilibrium, and since we measure the phenylacetylene concentration, it is only necessary to use Reactions 8.4 through 8.7, which have the overall reaction stoichiometry

C_8H_6	+ C_2H_2	=	$C_{10}H_8$	Rxn (overall)

From reactions 8.4-8.7, we can express the initiation rate in terms of elementary reaction rate constants and equilibrium constants given by

$$R_i = \frac{K_{overall}\cdot[H]\cdot[C_2H_2]\cdot[C_8H_6] - [H]\cdot[C_{10}H_8]}{\frac{K_6\cdot K_7}{k_{-5}}[H_2] + \frac{K_5\cdot K_6\cdot K_7}{k_{-4}}[C_2H_2] + \frac{K_7}{k_{-6}}[H_2] + \frac{1}{k_{-7}}}\cdot 128 \qquad \text{Eq. (8.10)}$$

The expression for R_i in Eq. (8.10) was derived by solving the algebraic equations and assuming that the rates of change of the hydrocarbon radical species ($C_8H_5\cdot$, 1-$C_{10}H_7\cdot$, and c-$C_{10}H_7\cdot$) were small enough to allow the steady-state approximation to be applied to these species. The expression for $d[C_{10}H_8]/dt$ would of course include terms for the oxidation of $C_{10}H_8$, further growth reactions of $C_{10}H_8$, as well as other possible formation and destruction paths for $C_{10}H_8$. Using literature rate constants given in Table 8.1, calculated equilibrium constants, and our experimentally determined concentrations of C_2H_2 and H_2, the first term in the denominator on the right hand side of Eq. (8.10) is much greater than the other terms, so we can write for R_i

$$R_i = \frac{k_{-5}\ [H]}{K_6 \cdot K_7\ [H_2]} \cdot (K_{overall} \cdot [C_2H_2] \cdot [C_8H_6] - [C_{10}H_8]) \cdot 128 \qquad \text{Eq. (8.11)}$$

From our thermodynamic modelling we know that $C_{10}H_8$ is not partially equilibrated with C_2H_2 and C_8H_6 and is far below it partial equilibrium value, (ie. $[C_{10}H_8] \ll K_{overall} \cdot [C_2H_2] \cdot [C_8H_6]$), so Eq. 8.11 reduces to

$$R_i = \frac{k_{-5}\ [H]}{K_6 \cdot K_7\ [H_2]} \cdot (K_{overall} \cdot [C_2H_2] \cdot [C_8H_6]) \cdot 128 \qquad \text{Eq. (8.12)}$$

and by comparison of Eq. 8.3 with 8.12, we see that k_i is equal to

$$k_i = (k_{-5}/K_6 \cdot K_7) \cdot ([H]/[H_2]) \cdot K_{overall} \qquad \text{Eq. (8.13)}$$

Equation 8.13 may be simplified by noting that $K_{overall}$ is equal to $K_4 \cdot K_5 \cdot K_6 \cdot K_7$ and so

$$k_i = k_5 \cdot K_4 \cdot ([H]/[H_2]) \qquad \text{Eq. (8.14)}$$

Thus the initiation rate constant, k_i, depends on the rate constant for acetylene addition to phenylacetylene radical (with the radical site ortho to the ethynyl group), the equilibrium constant for the H-abstraction reaction aromatic + H = aryl + H_2, and the ratio of $[H]/[H_2]$. We see that the initiation rate, R_i, is independent of the amount of PAH, and will change as a function of time, depending upon how phenylacetylene, acetylene, and k_i change with time.

Table 8.1. Rate Constants and Equilibrium Constants For the Formation of Naphthalene.

	Reaction	$\log_{10}A$	n	E	Kc	Ref.
1	$C_6H_6 + H = C_6H_5\cdot + H_2$	14.4	0	16	$67.3\cdot\exp(-6.2/RT)$	a
2	$C_6H_5\cdot + C_2H_2 = C_6H_5C_2H_2\cdot$	12.6	0	6.8	$0.02\cdot\exp(39.8/RT)$	b
-3	$C_8H_6 + H = C_6H_5C_2H_2\cdot$	12.8	0	17.5	$2.7\cdot\exp(36.1/RT)$	c
4	$C_8H_6 + H = C_8H_5\cdot + H_2$	14.4	0	16	$22.5\cdot\exp(-6.2/RT)$	d
5	$C_8H_5\cdot + C_2H_2 = 1\text{-}C_{10}H_7\cdot$	12.6	0	6.8	$0.02\cdot\exp(39.8/RT)$	e
6	$1\text{-}C_{10}H_7\cdot = c\text{-}C_{10}H_7\cdot$	10.0	0	0	$8.4E\text{-}4\cdot\exp(53.1/RT)$	f
-7	$C_{10}H_8 + H = c\text{-}C_{10}H_7\cdot + H_2$	14.4	0	16	$44.9\cdot\exp(-6.2/RT)$	g

$k=A\cdot T^n\cdot\exp(-E/RT)$, Kc used to calculate reverse rate constants
Units are kcal, mole, cm^3, s

Notes:

All equilibrium constants are thermodynamics from Stein (1987b).

Rate constants are from the following sources:

a) From Kiefer, J. H., Mizerka, L. J., Patel, M. R., and Wei, H. C., Journal of Physical Chemistry, 89, p. 2013, (1985).

b) From fit to data in Fahr, A., Mallard, W. G., and Stein, S. E., 21st Symposium (International) on Combustion, (1986), p.825, as presented by McKinnon, J. T., Poster # , 22nd Symposium (International) on Combustion, (1988).

c) By analogy to $C_4H_2 + H = C_4H_3$ from Warnatz recommendation in Combustion Chemistry, Gardiner, W.C. Ed. (1984).

d) Assumed same as Reaction 1.

e) Assumed same as Reaction 2.

f) Frenklach, M., and Warnatz, J., Combustion Science and Technology, 51, p. 265, (1987).

g) Assumed same as Reaction 1.

8.4.2 Addition Rate, Raddition

The equation for the rate of addition of aliphatic hydrocarbon species into the PAH inventory is given by

$$R_{addition} = k_{add} \cdot [\Sigma GC\ PAH] \cdot [C_2H_2] \cdot 24 \qquad \text{Eq. (8.4)}$$

where k_{add} is the rate constant for the addition of C_2H_2 to a PAH molecule, and 24 represents the addition of 2 C atoms to the ΣGC PAH mass for every successful reaction.

Mass is assumed to be added to the PAH inventory through the addition of C_2H_2 to the polycyclic aryl radicals. We assume that C_2H_2 can add to naphthylenyl radical as well as pyrenyl radical, and also that the addition rate per carbon site is the same. The rate constant for the addition of C_2H_2 to aryl species was obtained from high temperature (1030°C) gas-phase measurements by Fahr et al. (1986) for C_2H_2 addition to phenyl. If C_4 species add to aryl radicals with the same rate constant as C_2H_2, although the mass added is twice as much per successful collision, the concentration of C_2H_2 for our conditions is 30 times greater than C_4H_2. The contribution of C_4 species to Radd, therefore, will be less than 10% of the C_2H_2 contribution.

From the steady-state analysis for Ri, we found that Rxn 8.4 was partially equilibrated, and so we assume partial equilibration of the reaction

$$\text{Aromatic} + H = \text{Aryl} + H_2 \qquad \text{Rxn (8.9)}$$

so that

$$[\Sigma GC\ PAH\cdot]/[\Sigma GC\ PAH] = [H]\cdot K_p/[H_2] \qquad \text{Eq. (8.15)}$$

where K_p is the equilibrium constant for Rxn 8.9. The molar concentration of PAH radicals, denoted [ΣGC PAH·], represents <u>all</u> of the aryl radicals which may be formed from H-abstraction reactions. Table 8.2 shows the computed equilibrium constants for several aryl/aromatic reactions.

Since the equilibrium constant, K_p, reflects the symmetry of the aryl radical, if we divide K_p by the number of possible aryl isomers, we obtain an equilibrium constant per aryl isomer of 1.58 at 1600K, which is independent of number of H atoms which can react in the H-abstraction reactions. Since in the ΣGC PAH inventory the total number of H atoms which can be abstracted per molecule only varies from 8 to 10, an average value of 9 was chosen which gives a value for K_p of 14.2 to be used in Eq. 8.15. For our reactor temperature and H_2 and H concentrations, this results in an aryl/aromatic ratio of about 0.004, implying that only 0.4% of the [ΣGC PAH] is in the aryl radical form.

Since we assume that C_2H_2 can add to the aryl radicals, we can write for R_{add}

$$R_{add} = k_2\cdot[\Sigma GC\ PAH\cdot]\cdot[C_2H_2]\cdot 24 \qquad \text{Eq. (8.16)}$$

where k_2 is the rate constant for acetylene addition to phenyl from

Fahr et al. (1986). From the partial equilibrium of the aromatic + H = aryl + H_2 reaction, we can rearrange and substitute Eq. 8.15 into Eq. 8.16, and we find that

$$R_{add} = k_2 \cdot K_p \cdot ([H]/[H_2]) \cdot [\Sigma GC\ PAH] \cdot [C_2H_2] \cdot 24 \qquad \text{Eq. (8.17)}$$

Since the mass concentration of ΣGC PAH, C, is equal to [ΣGC PAH]/MW_{PAH}, in terms of measurable or calculable quantities Eq. 8.17 becomes

$$R_{add} = k_2 \cdot K_p \cdot ([H]/[H_2]) \cdot [C_2H_2] \cdot 24 \cdot (1/MW_{PAH}) \cdot C \qquad \text{Eq. (8.18)}$$

and from comparison of Eq. 8.17 with Eq. 8.4, we see that the addition rate constant, k_{add}, is equal to

$$k_{add} = k_2 \cdot K_p \cdot [H]/[H_2] \qquad \text{Eq. (8.19)}$$

The expression for k_{add} in Eq. 8.19 is similar that in Eq. 8.14 for the initiation rate constant, k_i. Since we have assumed $k_2 = k_5$, the difference between K_4 and K_p reflects the fact that PAH have more sites available per mole for H-abstraction reactions and subsequent C_2H_2 addition reactions.

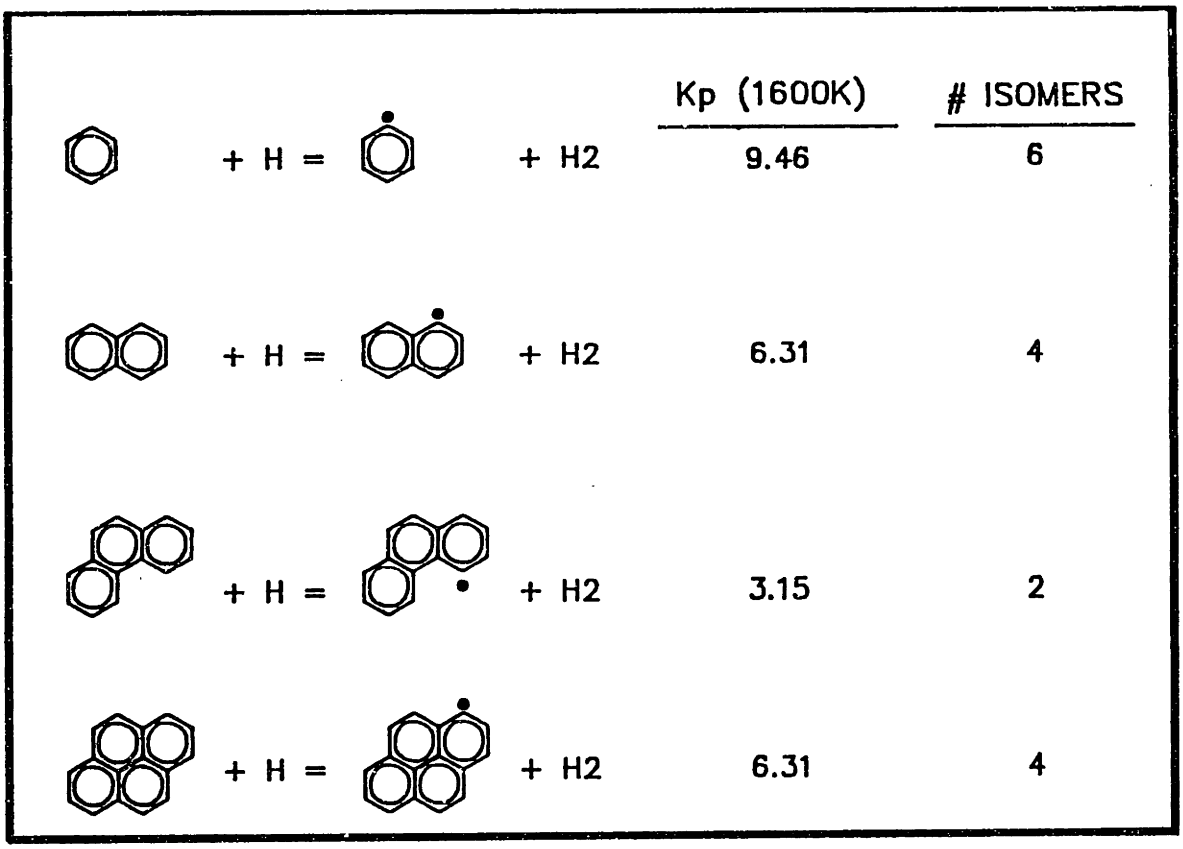

Table 8.2 - Equilibrium Constants for Aryl + H = Aromatic + H_2.

8.4.3 Oxidation Rate, Rox

The rate at which mass is lost from the ΣGC PAH system through oxidation is given by the expression

$$R_{ox} = k_{ox} \cdot [\Sigma GC\ PAH] \cdot [OH] \cdot (12\ g/mol) \qquad Eq.\ (8.20)$$

where the factor of 12 g/mol reflects the loss of one C atom from the PAH inventory as CO, and the PAH species is assumed to be converted to a 5-membered ring species containing a methylene group. We assume that oxidation, like C_2H_2 addition, occurs for all PAH species with between 2-5 rings. As mentioned previously, naphthalene ($C_{10}H_8$) may be oxidized to indene (C_9H_8), phenanthrene ($C_{14}H_{10}$) could be converted to fluorene ($C_{13}H_{10}$), and the oxidation product of pyrene ($C_{16}H_{10}$) may be 4H-cyclopenta(def)phenanthrene ($C_{17}H_{10}$). The detailed GC chromatogram shows that these species are formed in the PFR, and their formation mechanism is probably similar to the formation of cyclopentadiene from benzene oxidation.

The rate constant, k_{ox}, for oxidation of polyaromatic molecules by OH is not well known, but we can use a value for soot oxidation by OH obtained by Neoh (1980). In Neoh's formulation the rate constant would be a collision efficiency times the collision frequency given in cc/mol·s, and the value for the collision efficiency was determined to be 0.2. Assuming collision efficiency is constant, extrapolation of Neoh's oxidation rate to benzene corresponds to a rate constant of 9.5×10^{13} $cm^3/mol \cdot s$ at 1600K.

8.4.4 Rate of Growth out of PAH inventory at High MW Limit, R_o

Of the 4 terms which comprise R_o, Rc_2H_2 is of the same form as $R_{addition}$, and the other three, $R_{coag-PAH}$, $R_{coag-tar}$ and $R_{coag-soot}$, are coagulation reactions. Rc_2H_2 is equal to $R_{addition}$ times the fraction of 5 ring aromatic species in the PAH inventory, and is given by

$$Rc_2H_2 = f_{5\ rings} \cdot R_i. \qquad \text{Eq. (8.21)}$$

We experimentally measure $f_{5\ rings}$, the fraction of the ΣGC PAH inventory which has 5 rings, and as seen from the increase in average MW, the larger PAH species, such as cyclopenta(cd)pyrene and benzo(ghi)fluoranthene, are preferentially formed in the PFR. For example, cyclopenta(cd)pyrene accounts for less than 1% by mass of the PAH inventory at early residence times in the PFR, but accounts for 10% at the end of the PFR. Thus we expect Rc_2H_2 to increase as a function of time in the PFR.

The other three pathways for mass to leave to PAH inventory at the high molecular weight limit are through coagulation reactions of the PAH with soot particles, large tar molecules, or among themselves to form species larger than 5 aromatic rings. For example, a sticking collision between 2 naphthalene molecules would not cause a change in the mass of the PAH inventory, but a sticking collision between naphthalene and pyrene would decrease the PAH inventory by 330 g/mol. From kinetic collision theory, the number of collisions between molecules A and B in 1 cm^3 in 1 second is given by

$$Z_{AB} = \left[\frac{\sigma_A + \sigma_B}{2}\right]^2 \cdot \left[\frac{8\pi RT}{\mu_{AB}}\right]^{1/2} \cdot N_A \cdot N_B \qquad \text{Eq. (8.22)}$$

where σ_A, σ_B are the collision radii (cm) for molecules A and B, which are equivalent to the molecular diameters of A and B; R is the universal gas constant ($=8.31 \times 10^7$ g·cm^2/s^2·mole·K); T is the gas temperature (K); μ_{AB} is the reduced mass of A and B in g/mol, not atomic mass units; and N_A and N_B are the number of molecules A and B per cm^3. If we wish to use moles instead of molecules, we can divide both sides of Eq. (8.22) by N_{av}^2, (N_{av} = Avogadro's number = 6.023×10^{23} molecules/mole), to get

$$\frac{Z_{AB}}{N_{av}} = \left[\frac{\sigma_A + \sigma_B}{2}\right]^2 \cdot \left[\frac{8\pi RT}{\mu_{AB}}\right]^{1/2} \cdot N_{av} \cdot [A] \cdot [B] \qquad \text{Eq. (8.23)}$$

where Z_{AB}/N_{av} has the units moles/cm^3·s. For the PAH-PAH and PAH-tar coagulation reactions, it was assumed that the aryl PAH collide with stable PAH or tar molecules. Equation 8.15 was used to estimate the concentration of aryl PAH. For the PAH-soot coagulation reactions, it was assumed that stable PAH molecules could stick to the soot particles directly.

Using Eq. 8.23, we can then write the coagulation reactions the expressions given in Equations 8.7-8.9. We do not know the collision efficiency, γ, for each of the 3 coagulation reactions, but we can establish an upper limit at the kinetic collision frequency by setting γ equal to 1.

8.5 MATHEMATICAL FORMULATION

The expression for dC/dt can be rearranged to give an equation of the form

$$dC/dt = a(t) + b(t)\cdot C + c(t)\cdot C^2 \qquad \text{Eq. (8.24)}$$

where

$a(t) = R_i$
$b(t) = F_{add} - F_{ox} - F_{C_2H_2} - F_{coag\text{-}tar} - F_{coag\text{-}soot}$
$c(t) = F_{coag\text{-}PAH}$

and

$F_{add} = k_{add} \cdot [C_2H_2] \cdot 24 / MW_{PAH}$
$F_{ox} = k_{ox} \cdot [OH] \cdot 12 / MW_{PAH}$
$F_{C_2H_2} = f_{5\ rings} \cdot k_{add} \cdot [C_2H_2] \cdot 226 / MW_{PAH}$
$F_{coag\text{-}tar} = \gamma_{tar} \cdot Z_{tar} \cdot [tar]$
$F_{coag\text{-}soot} = \gamma_{soot} \cdot Z_{soot} \cdot [soot]$
$F_{coag\text{-}PAH} = \gamma_{PAH} \cdot Z_{PAH} \cdot (PAH+PAH \geq 6 rings)$

which is a first-order, non-linear ordinary differential equation. Since the functions a(t), b(t) and c(t) are obtained from experimental data as well as literature rate constants and estimated radical concentrations, we can solve this equation numerically using a fourth-order Runga-Kutta integration technique. The initial value is the measured concentration of the ΣGC PAH inventory at the first PFR data point. A constant time-step size of 1.5×10^{-5} s was used, and when we doubled the step size, we observed no change in the predicted concentration profile. Thus our predictions are not sensitive to the particular time-step size we selected.

8.6 MODEL RESULTS

Figure 8.16 shows the experimental data and the predictions from our model for ϕ=2.18 with no injection, C_2H_4 injection and C_6H_6 injection. It was found that the shape of the curves was best predicted assuming low collision efficiencies (<1%) for the ΣGC PAH with the soot particles and tar molecules. The coagulation of PAH molecules to form species larger than 5 aromatic rings was not important, and so $R_{coag-PAH}$ was equal to zero. The rate at which C_2H_2 adds to the 5 ring aromatic species, Rc_{2H_2}, does contribute to the net rate, especially at long residence times in the PFR when the fraction of 5 ring aromatic species approaches 10% of the total ΣGC PAH.

The most successful feature of the model is that it is able to predict the changes in the ΣGC PAH inventory due to the addition of either aliphatic or aromatic species. We expect the injection of ethylene to increase the C_2H_2 concentration and thus increase R_i and R_{add}. If we increase the C_2H_2 addition rate we will also increase the rate at which mass is lost through the high molecular weight limit through Rc_{2H_2}. A secondary effect of the ethylene addition is an increased phenylacetylene profile, which increases Ri. These factors result in a higher rate of ΣGC PAH mass production, and consequently higher concentrations. The injection of benzene should have a large effect on the initiation rate, R_i, because the phenylacetylene mole fraction is increased dramatically by the benzene injection. From our phenylacetylene profile we know that R_i is high at early PFR residence times, and decreases at later times, so we expect the PAH concentration profile to be increasing steeply at early times in the

PFR, and then leveling out at later times.

Figures 8.17 - 8.19 show the rates and net rate (dC/dt) for no injection, ethylene injection and benzene injection. We can see for the no injection case at early residence times the model predicts that the major contributor to the mass of the PAH inventory is R_i, and at later residence times, once the mass of PAH has built up, the major contributor is R_{add}. Oxidation is the major consumption route for PAH, and R_{ox} nearly balances R_{add}. The net rate, R_{net}, is always positive and the mass concentration of PAH is always increasing in the PFR, although the rate of increase is leveling off. For the ethylene injection case, the model predicts a similar balance of rate contributions, but each component has a higher rate than the corresponding component for the no injection case. For the benzene injection case, the model predicts R_i to be dominant at early residence times, but is overtaken at later residence times by R_{add}, primarily because the concentration of single-ring aromatics has decreased substantially. The net rate is predicted to be high initially, then levels off at later residence times, and although the net rate becomes slightly negative at long residence times, this trend is close to that of the experimental data for the benzene injection case.

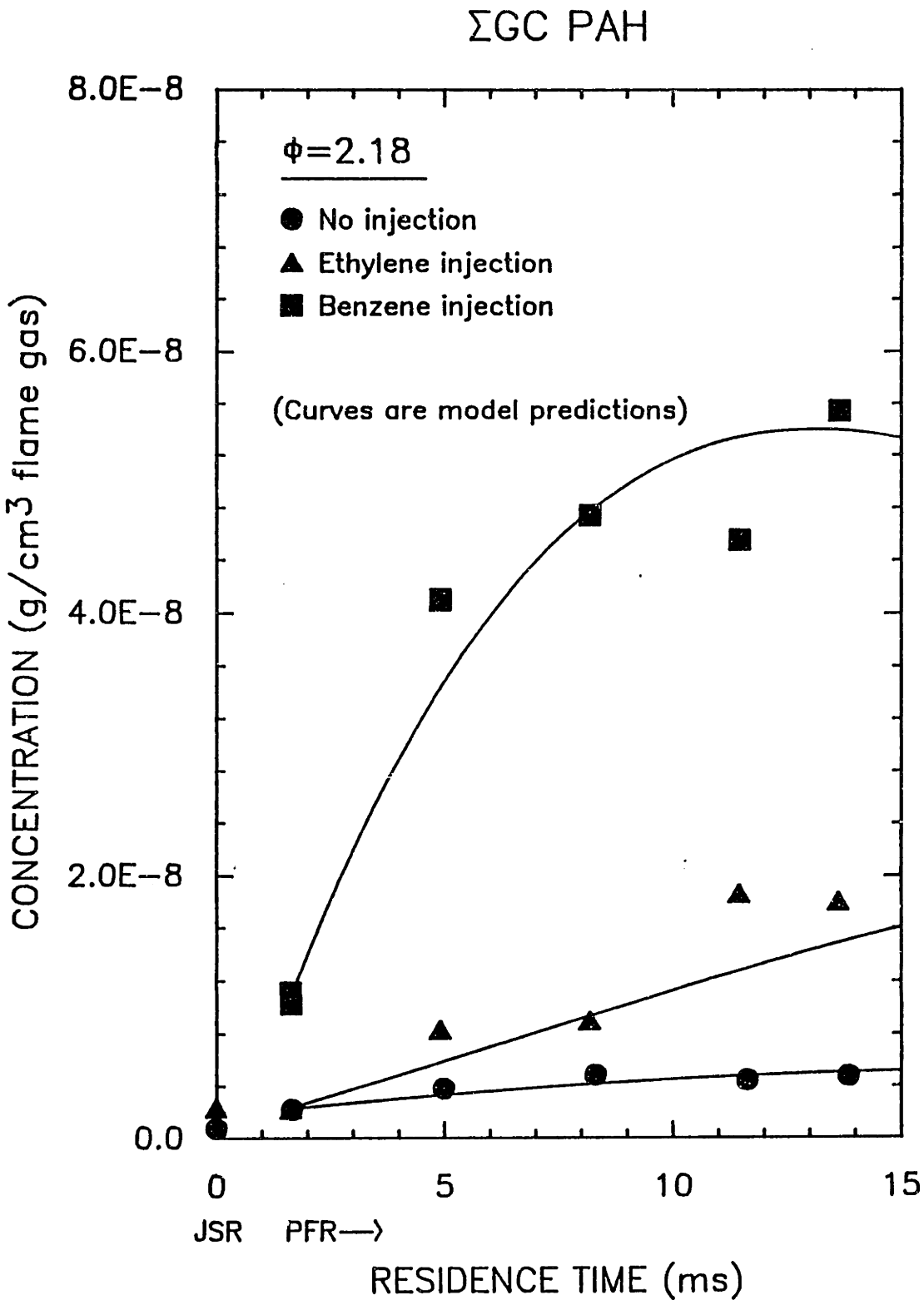

Figure 8.16 Comparison of global PAH kinetic model predictions with experimental data for ΣGC PAH species for ϕ=2.18, no injection, C_2H_4 injection and C_6H_6 injection cases.

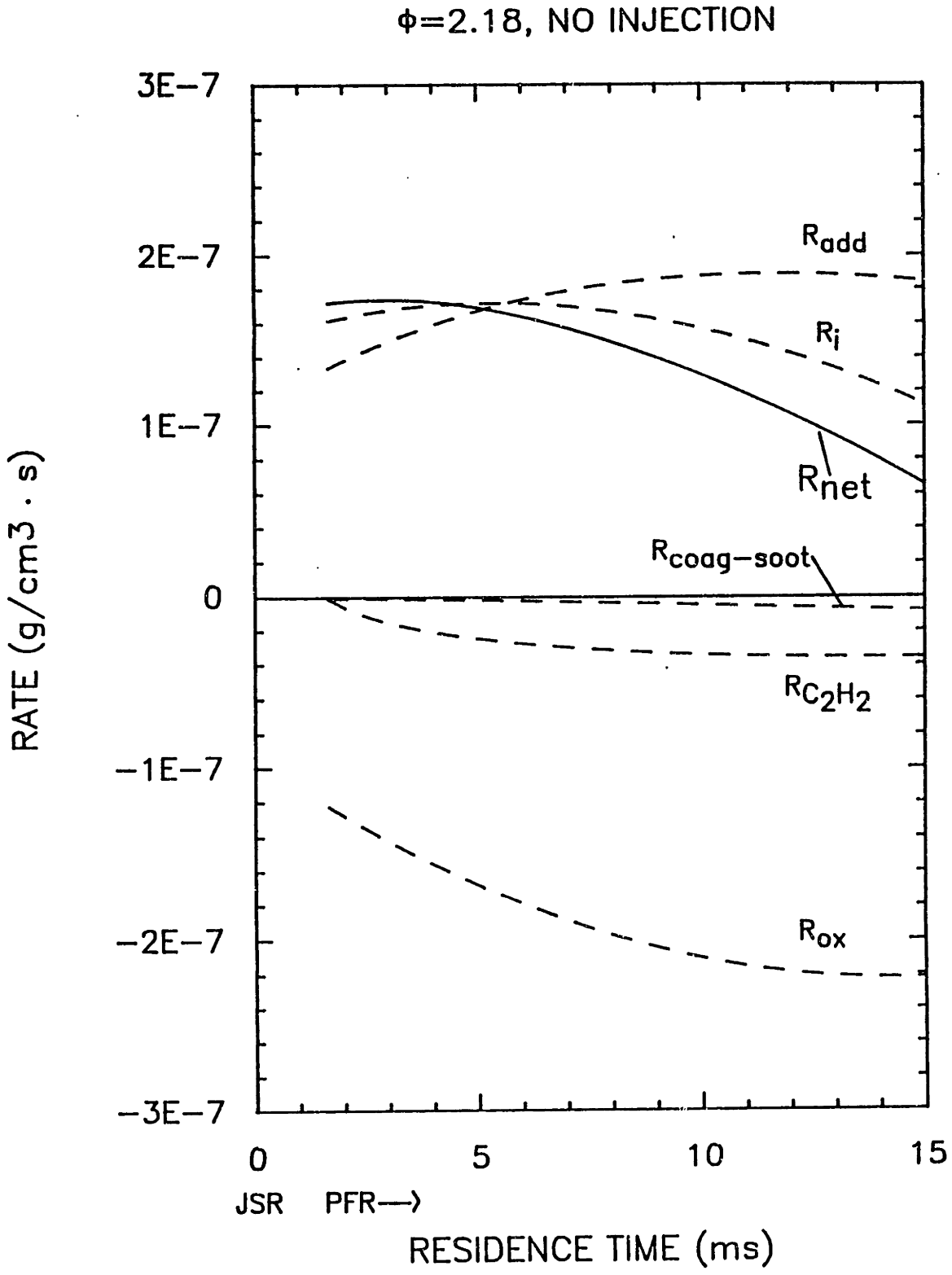

Figure 8.17 Rates of formation and destruction of ΣGC PAH inventory for ϕ=2.18, no injection.

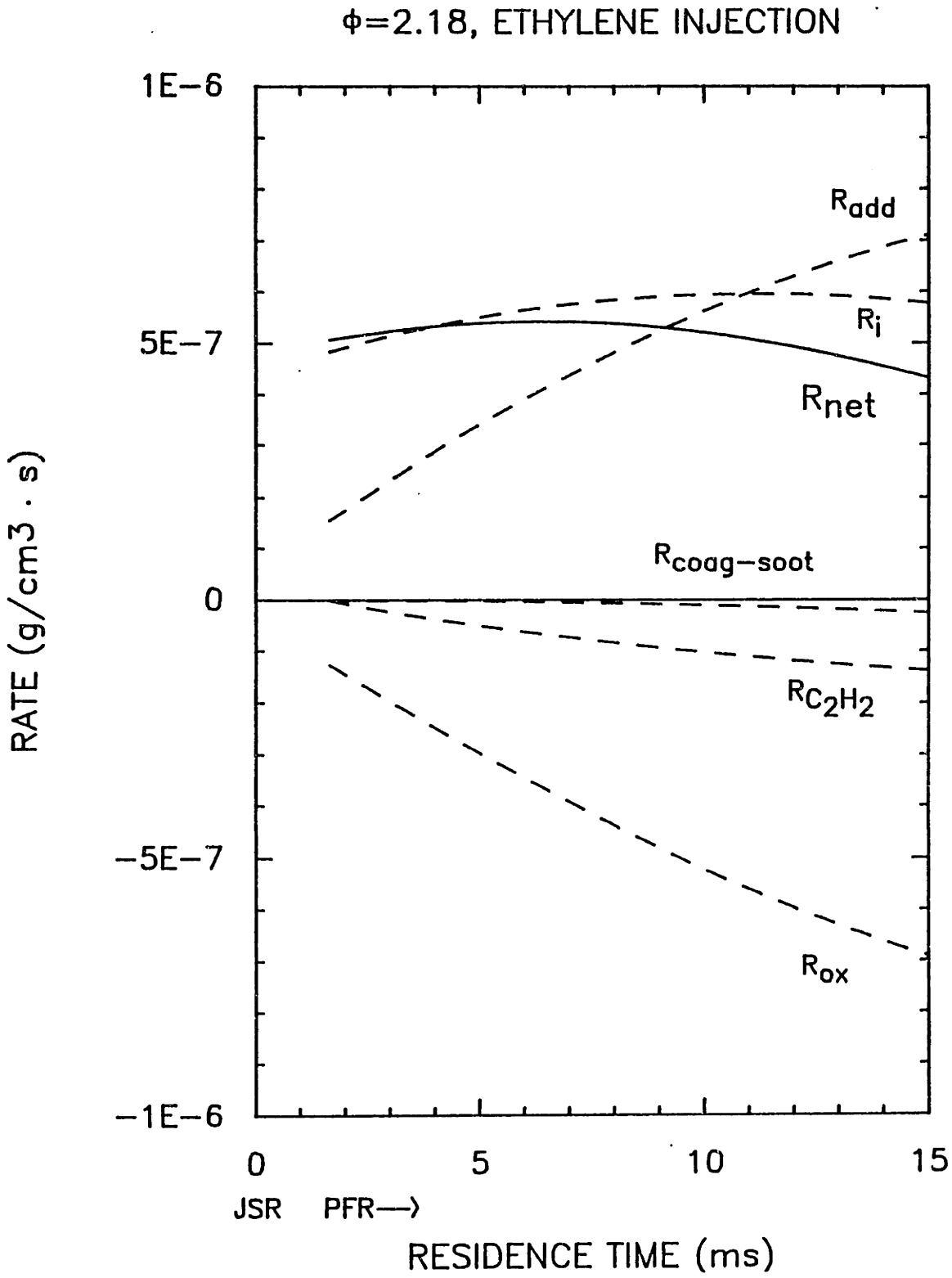

Figure 8.18 Rates of formation and destruction of ΣGC PAH inventory for ϕ=2.18, C_2H_4 injection.

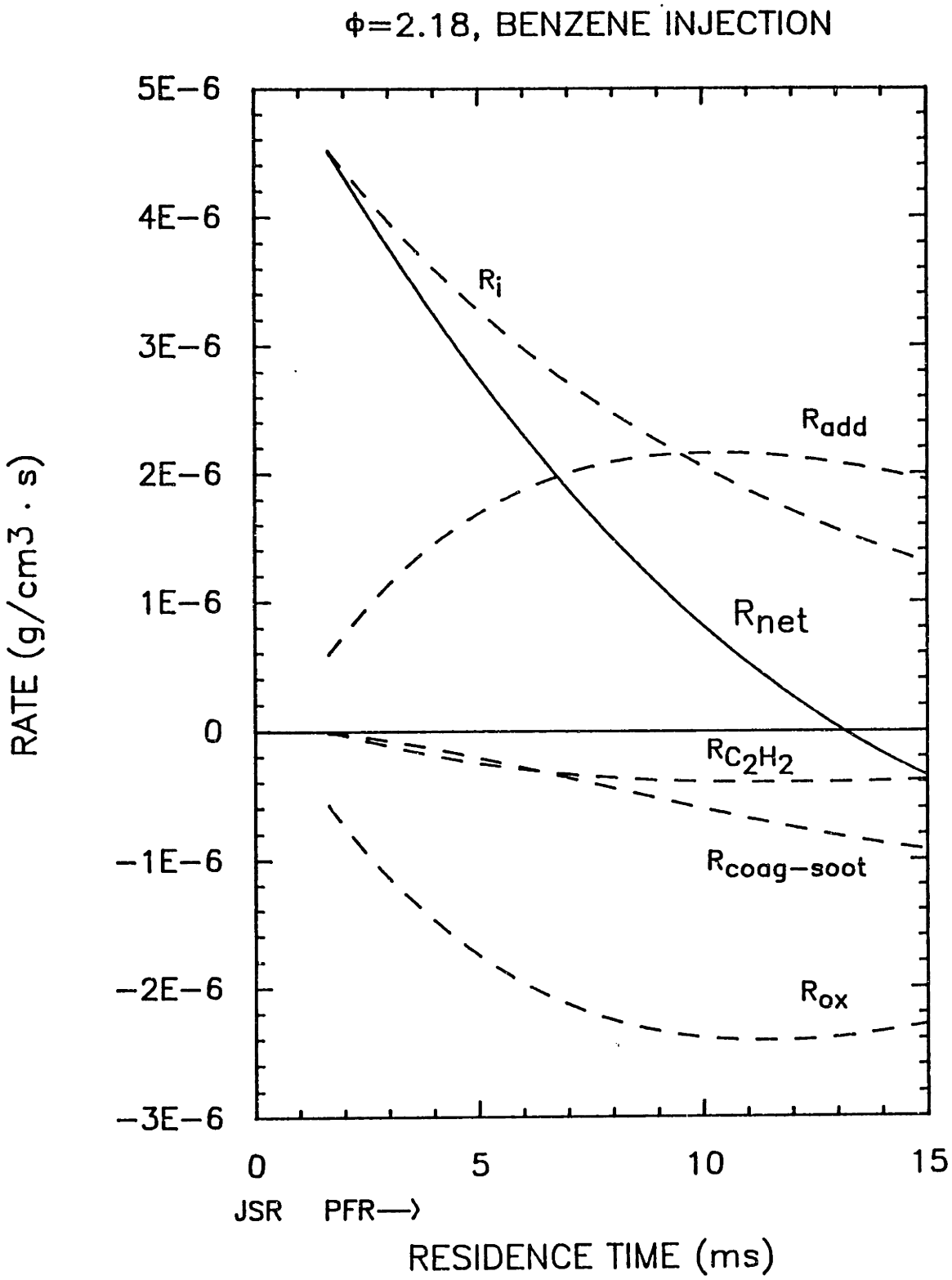

Figure 8.19 Rates of formation and destruction of ΣGC PAH inventory for ϕ=2.18, C_6H_6 injection.

8.7 SENSITIVITY ANALYSIS OF MODEL

8.7.1 Effect of Oxidation

An important result from the modelling study is that the oxidation rate is comparable to the addition rate for the ΣGC PAH inventory. From our previous analysis of the rate of benzene decay for the C_6H_6 injection case, we found that a significant fraction (≈60%) of the benzene consumption could be attributed to oxidation of benzene to cyclopentadiene and CO. Since we observe PAH species with 5-membered rings which may be oxidation products of 6-membered ring PAH, we would expect oxidation of PAH to occur, perhaps through a mechanism analogous to that for benzene oxidation. The rate constant for benzene oxidation, ($k=2.5x10^{12}$ $cm^3/mol \cdot s$), however, is a factor of 40 lower than that used for the ΣGC PAH oxidation rate constant ($k=9.5x10^{13}$ $cm^3/mol \cdot s$).

Assuming the kinetics for the growth reactions, (ie. R_i and R_{add}) are correctly predicted from Fahr et al.'s (1986) rate constant for the addition of C_2H_2 to phenyl, if we do not include oxidation in the model, we can try to predict the data by increasing the coagulation rates of ΣGC PAH with tar and soot. Figures 8.20-8.22 show the results for the benzene injection case if we do not include oxidation and try to match the data by varying the coagulation efficiencies for ΣGC PAH reactions with tar and soot.

We see from Fig. 8.20 for the $\phi=2.18$, C_6H_6 injection case, that if we turn off the oxidation pathway by setting $k_{ox}=0$, with $\gamma_{soot}=0$, even unity collision efficiency for ΣGC PAH reacting with tar results in an over-prediction of the ΣGC PAH concentration. Figure 8.21 shows

that with k_{ox}=0 and γ_{tar}=0, a high collision efficiency with soot results in the wrong profile shape. Since γ_{tar}=1 predicts a profile which levels out at long residence times, we can vary γ_{soot} to try to fit the data. Fig 8.22 shows that a value of 0.01 for γ_{soot} results in the best fit, although it over-predicts the ΣGC PAH concentration at early residence times. However, the same set of parameters (γ_{soot}=0.01 and γ_{tar} =1) does not predict the no injection case, and over-predicts the ΣGC PAH concentration. It appears that oxidation is required as a destruction route for species in the ΣGC PAH inventory.

If we set $k_{ox}=2.5\times10^{12}$ $cm^3/mol\cdot s$, which is the value for benzene oxidation, Fig. 8.23 shows that for the no injection case, with γ_{soot}=1 and γ_{tar}=0.01, results in an over-prediction of the concentration profile which is the same as the with k_{ox} = 0. With γ_{soot} = 1, the model over-predicts the data at early residence times, and shows a sharp decline at longer residence times. Figure 8.24 shows that for benzene injection, $k_{ox}=2.5\times10^{12}$ $cm^3/mol\cdot s$ is not high enough to cause an appreciable difference in the concentration profiles, as can be seen by comparison with Fig. 8.22.

With γ_{tar}=1, and γ_{soot}=0, as we vary k_{ox} from 2.5×10^{12} to 9.5×10^{13} $cm^3/mol\cdot s$, we see from Fig. 8.25 that a value of 3.0×10^{13} $cm^3/mol\cdot s$ seems to correctly predict the experimental data. This value of k_{ox} would correspond to a collision efficiency of 0.06 for reaction of OH with benzene and is a factor of 12 higher than the value obtained by He et al. (1988b). If we try to apply the same parameters ($k_{ox}=3.0\times10^{13}$ $cc/mol\cdot s$, γ_{tar}=1, γ_{soot}=0) to the no injection case, however, the predicted concentration profile is much

too high (Fig. 8.26).

Thus, it appears that oxidation is necessary to correctly model the ΣGC PAH concentration profiles. Furthermore the value of the oxidation rate constant must be higher than that for C_6H_6 + OH = C_6H_5OH + H, as determined by He et al. (1988b). The best value for our experimental conditions is comparable to that determined by Neoh (1980) for soot oxidation by OH.

Although we have assumed a single rate for the entire ΣGC PAH inventory, the oxidation rate may be a sensitive function of molecular size. It is reasonable to expect that the oxidation of naphthalene would be faster than benzene. Since the oxidation reactions involve OH substitution reactions to the aromatic structure, the addition reaction may be the key step in determining the overall rate. Since naphthalene has more sites than benzene, and the reactivity per site for naphthalene is higher than that for benzene, it seems plausible that oxidation of naphthalene would be faster than oxidation of benzene. The oxidation of cyclopenta(cd)pyrene will probably be even faster than naphthalene. How much faster is a question for which we do not have an adequate answer. More work needs to be done to establish the kinetics of oxidation of large PAH molecules.

8.7.2 Effect of H and OH

We used the H and OH mole fraction predictions from the Harris mechanism, and it is of some interest to determine the sensitivity of the model to the predicted H and OH concentrations. From our kinetic modeling, both the Harris and Glarborg mechanisms gave very similar H

and OH predictions. The H and OH concentrations were predicted to decrease sharply at the JSR exit, and then more slowly in the PFR. Figures 8.27 and 8.28 show the differences in the model predictions for three different H and OH profiles: Harris mechanism, Glarborg mechanism, and an equilibrium value for H if the reaction $H + H = H_2$ is partially equilibrated throughout the PFR. There is some difference in the profiles, but all three predict the data fairly well.

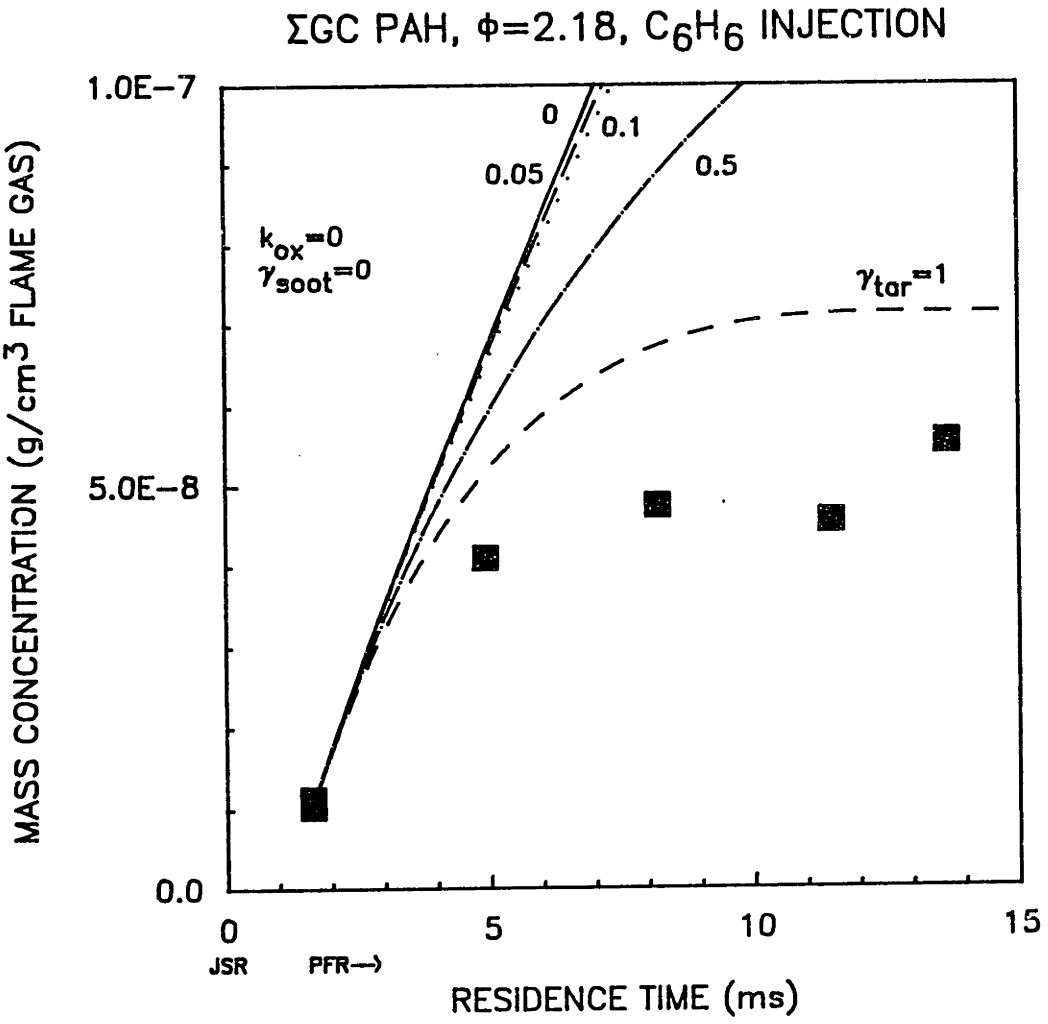

Figure 8.20 Comparison of PAH Model Predictions and Experimental Data for ϕ=2.18, C_6H_6 injection.

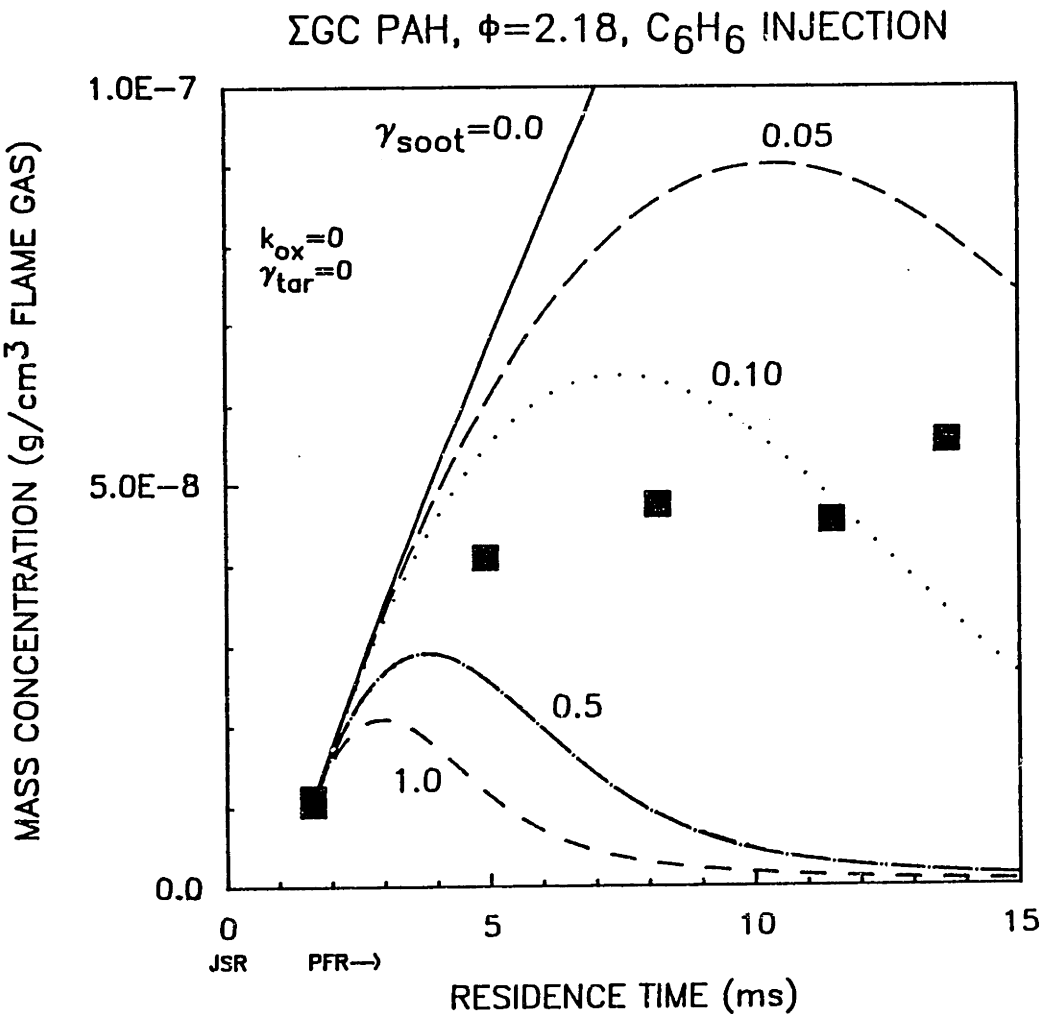

Figure 8.21 Comparison of PAH Model Predictions and Experimental Data for ϕ=2.18, C_6H_6 injection.

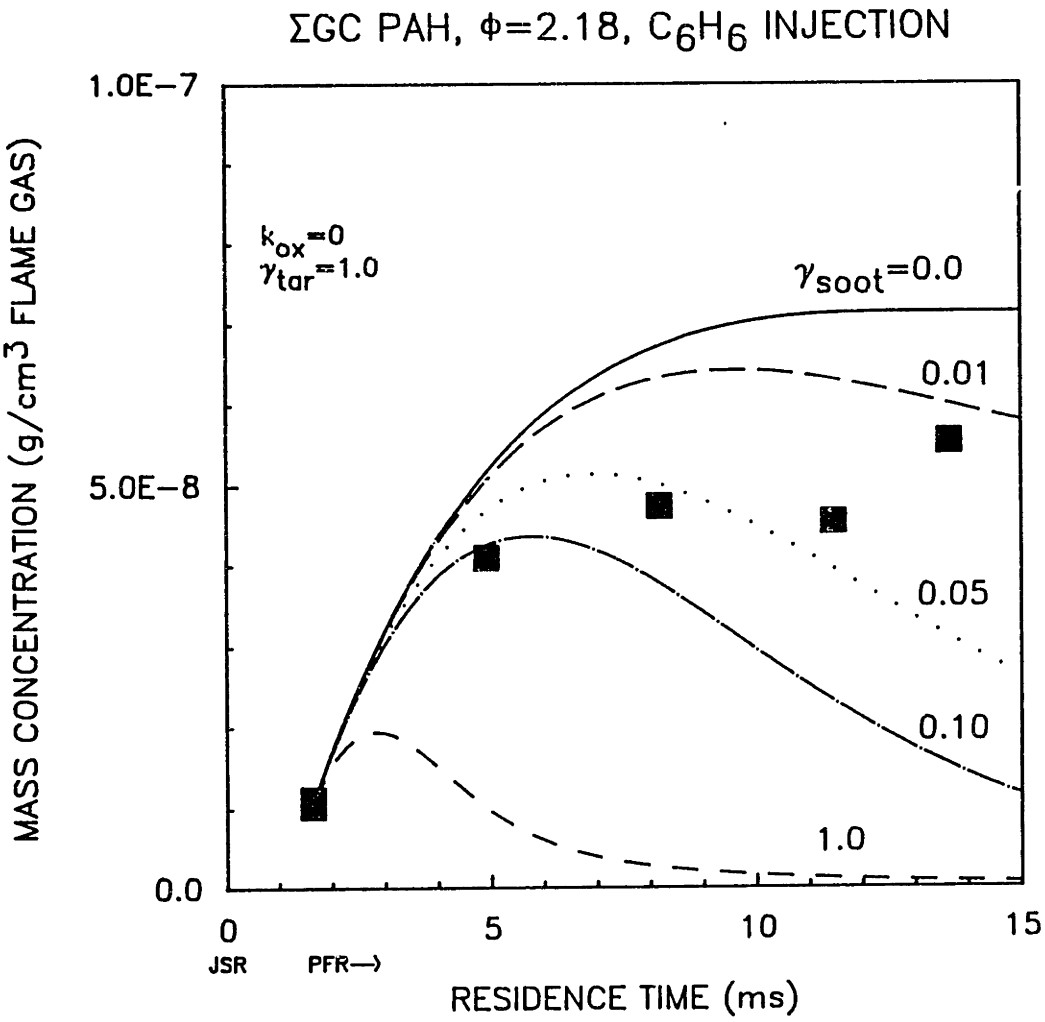

Figure 8.22 Comparison of PAH Model Predictions and Experimental Data for ϕ=2.18, C_6H_6 injection.

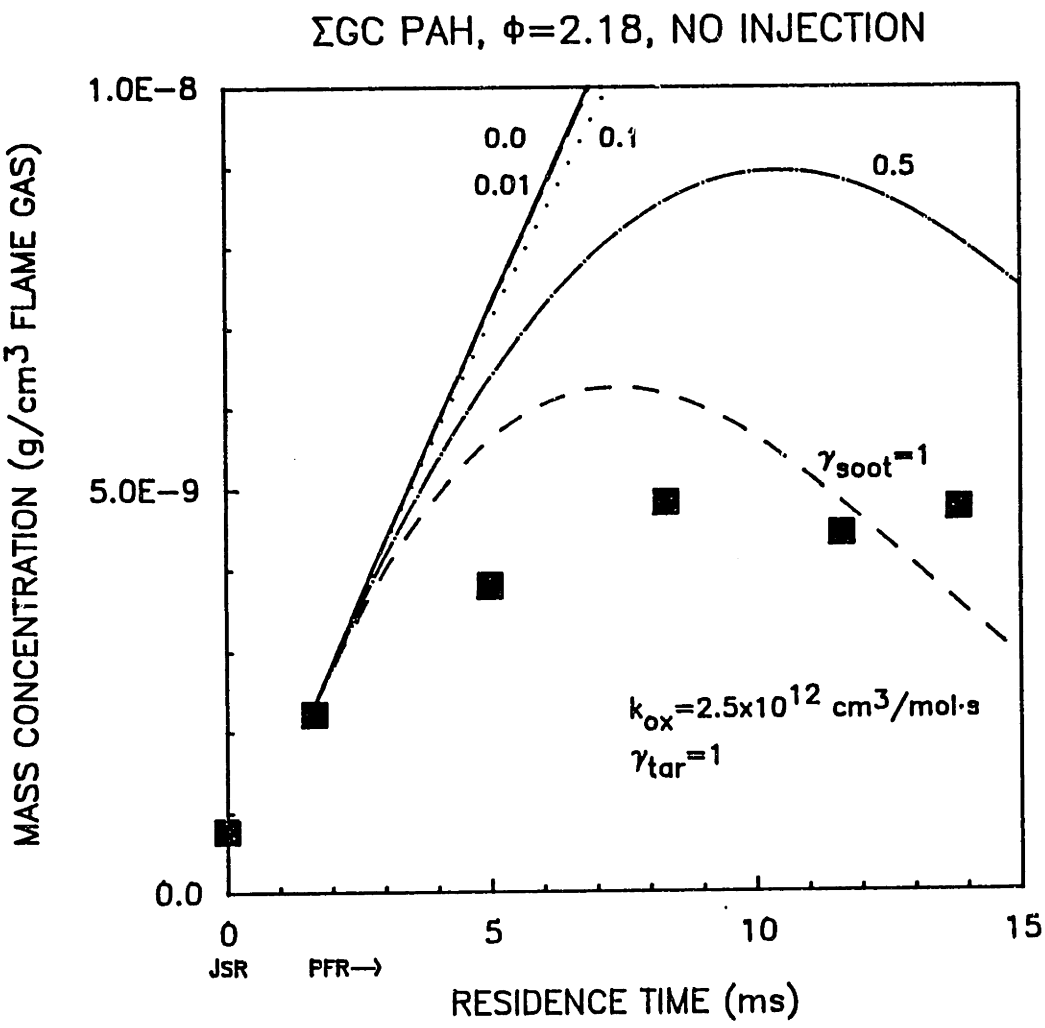

Figure 8.23 Comparison of PAH Model Predictions and Experimental Data for ϕ=2.18, no injection.

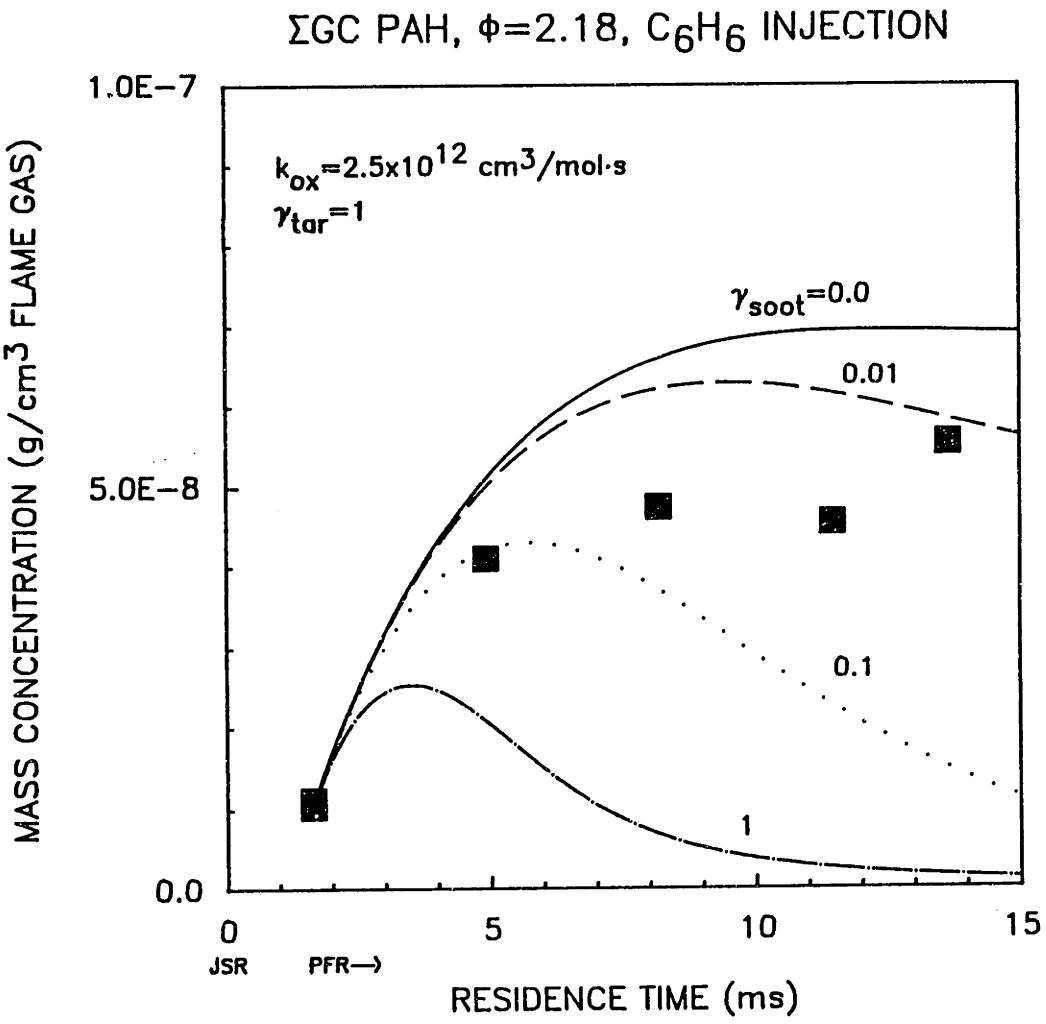

Figure 8.24 Comparison of PAH Model Predictions and Experimental Data for ϕ=2.18, C_6H_6 injection.

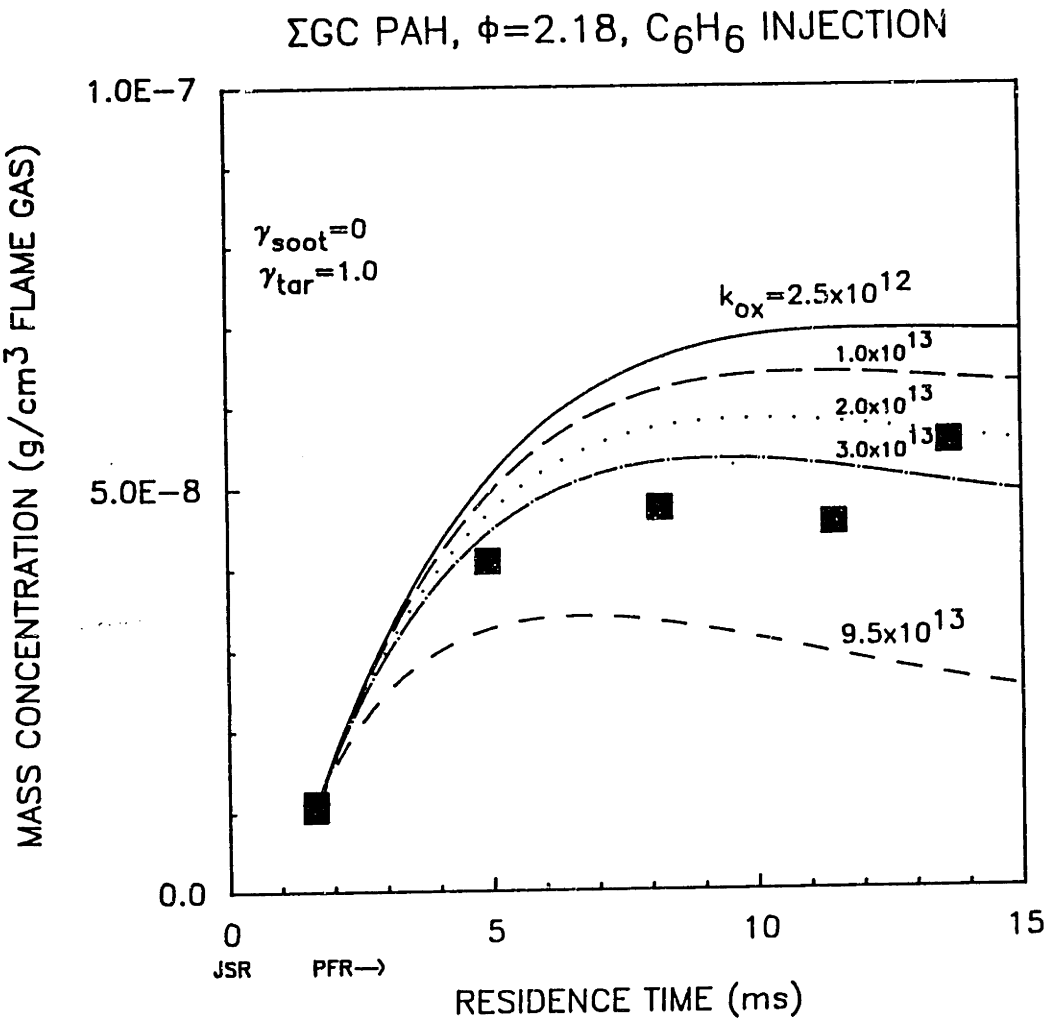

Figure 8.25 Comparison of PAH Model Predictions and Experimental Data for ϕ=2.18, C_6H_6 injection.

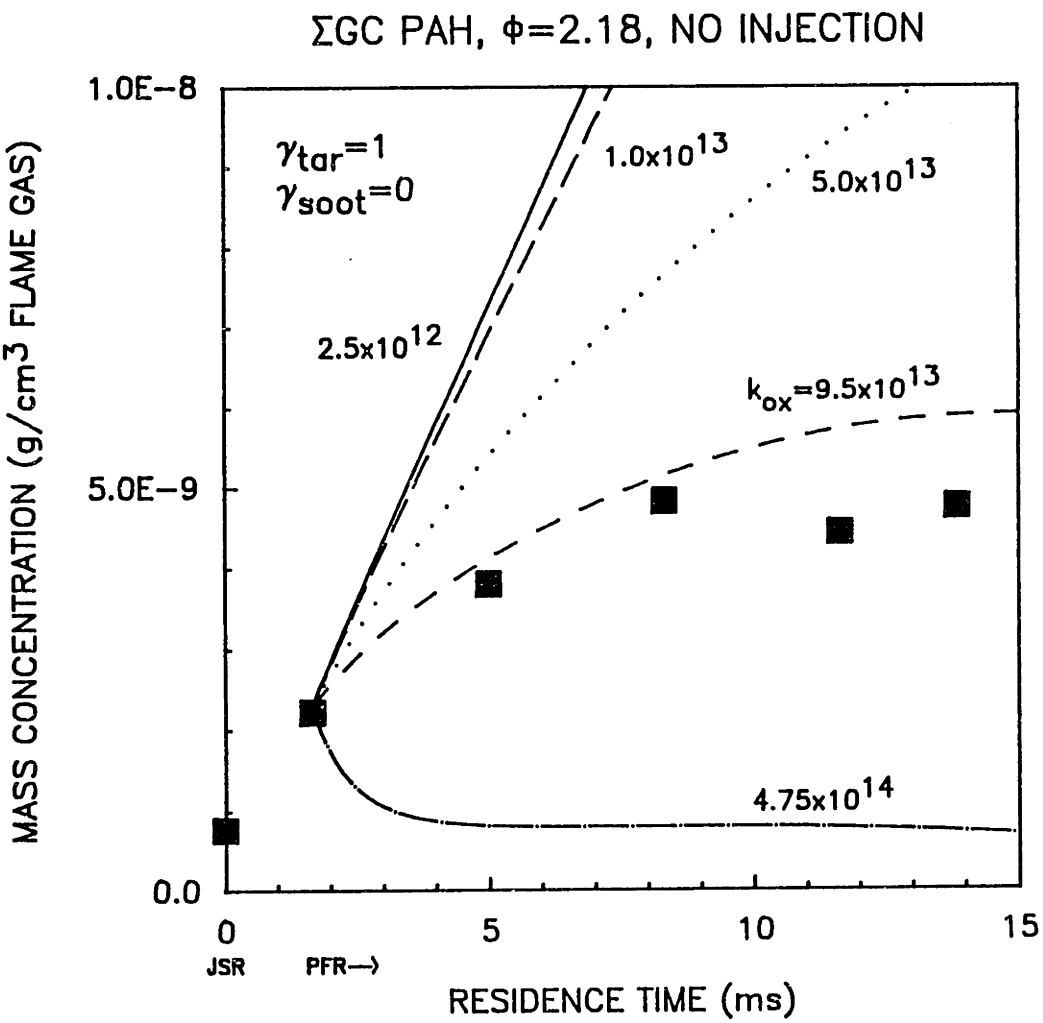

Figure 8.26 Comparison of PAH Model Predictions and Experimental Data for ϕ=2.18, no injection.

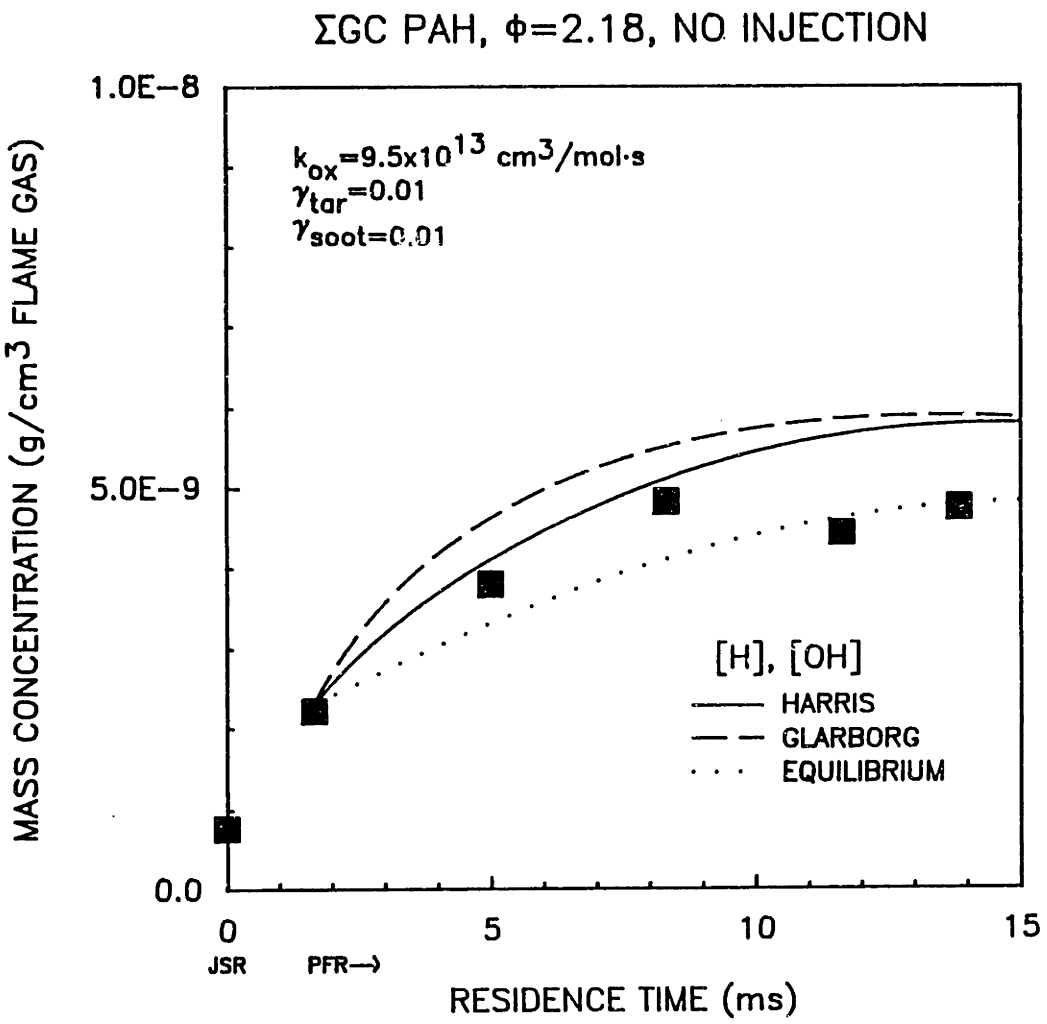

Figure 8.27 Comparison of PAH Model Predictions and Experimental Data for ϕ=2.18, no injection.

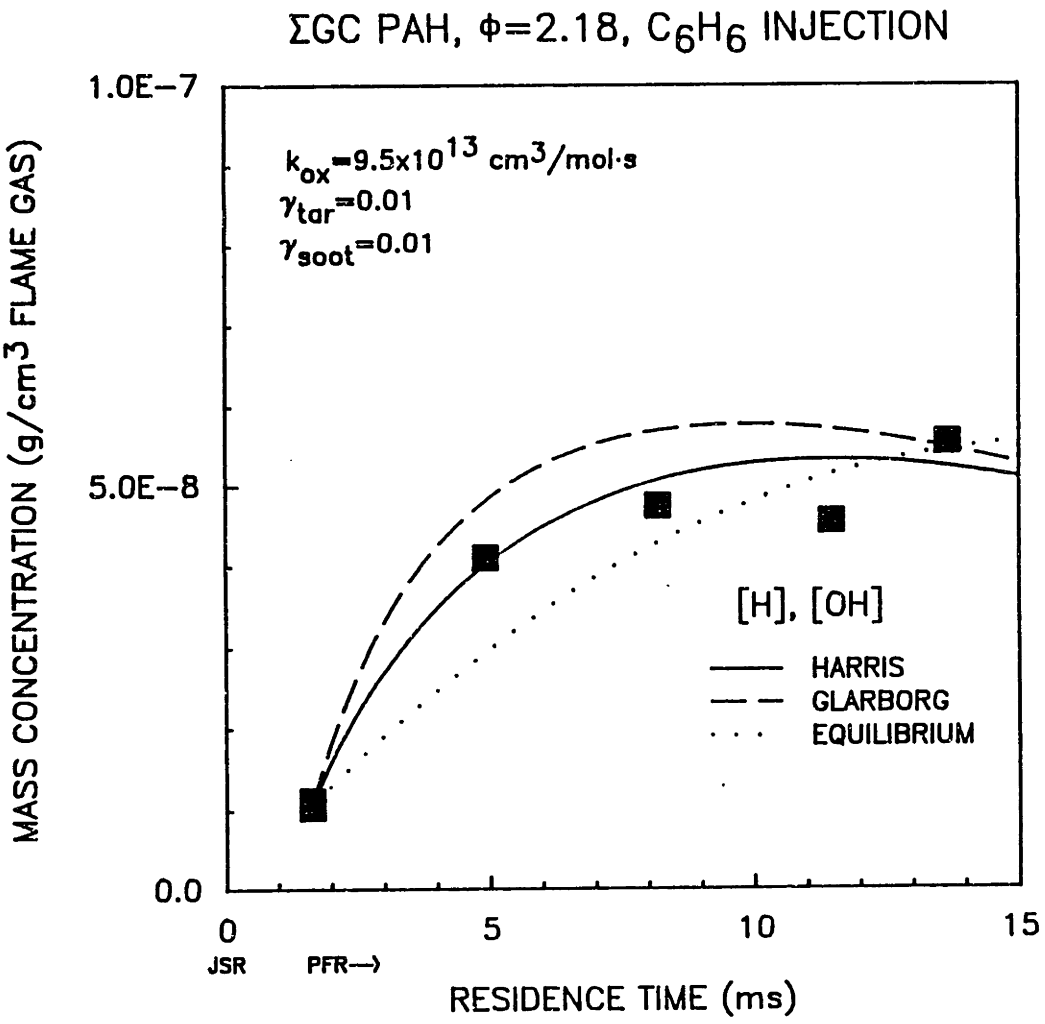

Figure 8.28 Comparison of PAH Model Predictions and Experimental Data for ϕ=2.18, C_6H_6 injection.

8.8 CONCLUSIONS

A global kinetics model of the PAH inventory (2-5 rings species) successfully predicted the concentration profile of the PAH inventory in the PFR at ϕ=2.18, as well as the perturbation to the PAH profiles from the injection of additional ethylene and benzene. The model includes pathways for mass flux into the PAH inventory due to 1) C_2H_2 addition reactions with single-ring aromatics and 2) C_2H_2 addition reactions with PAH; and pathways for mass flux out of the PAH inventory by 3) C_2H_2 addition reactions with 5-ring PAH, 4) coagulation reactions between PAH, 5) coagulation of PAH with high molecular weight tar, 6) coagulation of PAH with soot, and 7) oxidation reactions of PAH with OH.

An aromatic coagulation mechanism for PAH formation, consisting of bimolecular reactions of aryl species reacting with intact aromatic rings, is NOT the dominant mechanism of PAH formation for our experimental conditions. This conclusion is based on the following three facts: 1) the expected products of such a mechanism, namely biphenyl, terphenyl and triphenylene, are not observed; 2) a coagulation mechanism of aryl radicals with aromatics cannot explain formation of PAH structures such as phenylacetylene, naphthalene and acenaphthylene which are observed in the JSR/PFR; and 3) coagulation of aromatics alone cannct explain the observed increase in molar concentration of the PAH inventory in the PFR.

Mostly acetylene, and possibly diacetylene (<10%) addition is the major growth route for PAH. Acetylene provides most of the mass for the ΣGC PAH inventory. The rate constant for C_2H_2 addition to

aryl species is based on the value determined from an interpretation (McKinnon, 1988a) of Fahr and Stein's (1986) rate constant for the addition of C_2H_2 to phenyl ($k=4.4x10^{12}\cdot\exp(-3400/T)$, $cm^3/mol\cdot s$, T[K]). Aryl species concentrations were calculated by assuming partial equilibrium of the reaction Aromatic + H = Aryl + H_2.

Oxidation of the ΣGC PAH inventory was required to successfully model the experimental data. A collision efficiency, γ, of 0.2 for OH with PAH (based on Neoh's (1980) observation of γ = 0.2 for OH reaction with soot) was necessary in order to successfully predict the experimental trends. This rate is ≈40 times higher than the rate of benzene oxidation by reaction with OH.

Coagulation of PAH with soot and tar was predicted to have low collision efficiencies (≈ 1%). PAH species with 2-5 rings do not stick to soot particles, or stick with very low efficiencies (≈1%).

9. BIOLOGICAL TESTING OF PAH SAMPLES

9.1 INTRODUCTION

Polycyclic aromatic hydrocarbons (PAH) and soot are undesirable products of fuel-rich combustion that pose biological and environmental hazards. Certain PAH are known to be mutagenic to bacterial cells and human cells and may adsorb onto soot particles and be transported into the human body by inhalation. Practical combustors, such as large industrial furnaces, do not have control strategies to minimize PAH formation, and may actually enhance the production of PAH. For example, in large furnaces staged combustion is used to control NO_x emissions, and soot is allowed to form in the primary chamber under fuel-rich conditions. Soot enhances radiative heat transfer to the walls of the furnace, but PAH are also formed under fuel rich conditions, and PAH destruction in the secondary chamber is not certain.

A great deal of research has been directed at the mutagenicity of PAH because of their known existence in the combustion products of fuels. Although individual PAH generally comprise only a small fraction by mass of the original fuel, the environmental hazards to the general population must be investigated due to the high mutagenicity of certain PAH species. It is important to realize that the overall mutagenicity of an individual PAH is the product of its specific mutagenicity and the concentration at which it is present. Although the combustion byproduct benzo(a)pyrene has received widespread attention because of its long-known carcinogenicity in mice, researchers at M.I.T. (Kaden, 1979, Thilly, 1986, Longwell,

1983) have found that cyclopenta(cd)pyrene (CPEP) and fluoranthene (FLUOR) have specific mutagenicities comparable to that of benzo(a)pyrene, but are responsible for most of the mutagenicity observed in bacterial cells because of their high concentrations relative to benzo(a)pyrene.

Collaborative efforts with researchers in the Department of Applied Biology have involved biological testing of the samples produced in the JSR/PFR. In this work, we try to address the following three questions:

1) Can CPEP and FLUOR account for the observed mutagenicity of samples obtained from the PFR?

2) How is the mutagenicity of samples collected from the PFR changing as a function of residence time in the PFR? Can we attribute these changes, if any, to changes in the chemical composition of the samples?

3) Are there other PAH compounds, besides CPEP and FLUOR, which may be responsible for significant portions of the mutagenicities of the samples?

The approach involves determination of the amount of CPEP and FLUOR present in the samples, biological testing of the samples and reconstituted mixtures containing only CPEP and FLUOR, and calculation of the relative contributions of CPEP and FLUOR to the whole mixture.

This chapter gives a brief description of the biological assay used to test the PAH samples; presents chemical composition and biological experimental data for the PAH samples; and describes calculations to answer the 3 questions posed.

9.2 BIOLOGICAL ASSAYS

9.2.1 Bacterial Cell Assays

In his pioneering work at the University of California, Berkeley, Ames (1971) developed special mutant strains of the bacteria, *Salmonella Typhimurium*, to be used to detect mutagenicity of chemicals. Each strain of *Salmonella Typhimurium* has a specific type of base mutation, and all mutant strains require histidine for growth. A mutagen will cause a reverse mutation of the bacteria to normal form, enabling it to grow on a histidine-free medium. In order to increase test sensitivity, all strains have been deprived of DNA repair mechanisms and have increased permeability due to a very thin cell wall caused by a "deep rough" mutation.

The Ames reverse mutation assay allows rapid screening of potentially mutagenic compounds. Since the type of mutation is generally unknown, 4 or 5 different strains should be used to properly test a suspected mutagen. Results are usually reported as the number of revertants per weight of test species, after subtracting spontaneous revertants. The best and most complete representation, however, is a dose-response curve, in which revertant concentration is plotted as a function of mutagen concentration.

At M.I.T., Thilly has developed a variation of the Ames test

which involves a forward mutation of the *Salmonella Typhimurium*, and this is the assay which we use. The Ames reverse mutation assay allows rapid screening of potentially mutagenic compounds, but since the type of mutation is generally unknown, 4 or 5 different bacteria strains are required to properly test a suspected mutagen. The forward mutation assay allows for even more rapid testing by eliminating the repetition of using different strains, but the assay does not distinguish the type of mutation.

For the forward mutation assay, healthy normal bacteria are treated for 2 hours with the suspected mutagen dissolved in a small volume of dimethyl sulfoxide (DMSO). Surviving bacteria are then treated with a poison, 8-azaguanine. The remaining living bacteria are 8-azaguanine resistant, and these bacteria are the mutants. The mutagen has altered the metabolic process of the *Salmonella Typhimurium* so that the bacteria is no longer susceptible to 8-azaguanine poisoning. The mutant fraction is defined as the number of 8-azaguanine resistant cells divided by the number of cells surviving mutagen treatment, and this quantity is a measure of the mutagenicity of the test substance. The number of dead cells is a measure of the toxicity of the test substance.

Even in the absence of a mutagen, some bacterial cells will be resistant to 8-azaguanine because of random mutations, which may be analyzed using statistics. The concentration at which the dose-response curve crosses the 99% upper confidence limit (99% UCL) is defined as the Minimum Detectable Mutagen Concentration (MDMC) and is inversely proportional to the biological activity of the sample.

9.2.2 Enzymatic Activation

Many PAH species are not active, unless converted to their metabolic product. Metabolic activation in the assays is provided by the S-9 homogenate of rat liver, extracted from male rats which have been induced with a polychlorinated biphenyl mixture to elevate microsomal enzymatic activity. The S-9 homogenate is also known as postmitochondrial supernatant (PMS), and we classify the PAH as -PMS (direct, no activation) and +PMS (indirect, with activation) mutagens. Many of the +PMS mutagens are PAH containing only C and H atoms, such as CPEP, FLUOR, and benzo(a)pyrene, and we will concentrate on the +PMS mutagenicity of our PFR samples. It is suspected that polar, or hetero-atom containing PAH may be responsible for the -PMS activity observed in our samples. Even if a PAH species shows slight mutagenic activity without activation, in many cases its metabolic product is more potent. It should be noted, however, that in some cases, the metabolic product is less active.

Toxicity affects the mutagenicity studies because "dead cells don't mutate" (Thilly, 1987). At doses where the death rate is very high, the reliability of the mutagenicity is not as great because of the increase in statistical variation. In the assays, plate counts for toxicity are also taken, so the uncertainties could be estimated.

9.2.3 Sample Preparation

Samples were injected into the GC for PAH analysis, and then concentrated to approximately 3 ml for biological testing preparation.

The tar weight was determined using the microgravimetric evaporation technique developed by Lafleur (1986). A 100 μl aliquot was drawn from the sample using a 500 μl syringe, and then squirted onto an aluminum foil cup which had been previously weighed for tare. After the methylene chloride evaporated (usually within the first couple of minutes) the foil cup was spread flat to allow liquid trapped in the creases to evaporate. At 4 and 1/2 minutes the foil sample was transferred to a microbalance and the weight was measured at 5 minutes exactly. This procedure was used to determine the total extract weight.

The next step was to get the PAH sample into DMSO (dimethylsulfoxide) which is used as the solvent for the bacterial assay. It was required to measure out using a dispensing pipette a volume of DMSO such that the concentration of extract in DMSO was equal to 30 mg/ml. The PAH sample in the methylene chloride solution was added to the DMSO and shaken and blown down to the original level of DMSO before DCM was added. A data sheet was filled out and the samples were turned into the toxicology group about two hours after the work-up.

9.3 CHEMICAL AND BIOLOGICAL RESULTS

Table 9.1 shows the yields of tar, CPEP, and FLUOR in 5 different PAH samples obtained from the PFR at varying residence times for combustion conditions of ϕ=2.18, JSR T=1630K, with no injection. Although the total amount of PAH material is increasing, this fact will not be reflected in the bioassays, since only the specific

mutagenicity of the sample (ie. $MFx10^5/g$ tar) is determined. Differences in mutagenicity between the 5 samples will be due to differences in the chemical composition of the samples as a result of additional reaction time in the PFR. Note that the CPEP fraction of the tar is approaching 10% by the end of the PFR. The concentrations of the samples in DMSO were calculated for the sample submitted for biological testing, and to prevent ambiguity between the engineering and biology groups, the amount of CPEP and FLUOR in the samples for the successive dilutions required for the forward mutation assay were also calculated.

To test the hypothesis that a substantial part of the mutagenicity of the samples can be accounted for by the mutagenicities of CPEP and FLUOR, mixtures of CPEP and FLUOR in the same ratio as those found in the samples were biologically tested. If CPEP and FLUOR are the only active direct mutagens, and the rest of the sample is biologically inert, then ideally the dose response curve of a physically reconstituted mixture should match the sample dose response curve. For samples obtained from the JSR, it was found that CPEP and FLUOR could not account for the total mutagenicity of the JSR samples (Vaughn, 1988). The physically reconstituted mixture gave responses much lower than the samples. Recently, it was discovered that problems with the pure CPEP standard used in the bacterial assay precipitating out of solution may have been responsible for this conclusion.

Table 9.1 -- Yields of CPEP, FLUOR, and tar for ϕ=2.18, JSR T=1630K, no injection, at varying PFR residence times.

SAMPLE ID	54PAH1	54PAH2	54PAH3	54PAH4	54PAH5
HEIGHT (cm)	31.8	26.7	19.1	11.4	3.8
RES TIME (ms)	13.9	11.6	12.0	8.7	1.7
TAR YIELD (μg/g)	504	449	372	269	117
FLUOR (μg/g)	10.6	7.1	9.3	3.9	2.24
CPEP (μg/g)	41.9	26.4	27.6	11.6	3.21
%FLUOR	2.1%	1.6%	2.5%	1.5%	1.9%
%CPEP	8.3%	5.9%	7.4%	4.3%	2.7%
CPEP/FLUOR RATIO	4.0	3.7	3.0	3.0	1.4
TOTAL TAR (mg)	1.5197	0.611	1.3317	1.1437	0.517

DOSES and AMOUNTS OF FLUOR AND CPEP IN SAMPLE GIVEN TO BIOLOGY

	54PAH1	54PAH2	54PAH3	54PAH4	54PAH5
Sample (μg tar/ml DMSO)	152	61	133	114	52
FLUOR (μg/ml DMSO)	3.19	0.96	3.33	1.67	0.99
CPEP (μg/ml DMSO)	12.64	3.59	9.87	4.94	1.42
Sample (μg tar/ml DMSO)	51	20	44	38	17
FLUOR (μg/ml DMSO)	1.06	0.32	1.11	0.56	0.33
CPEP (μg/ml DMSO)	4.21	1.20	3.29	1.65	0.47
Sample (μg tar/ml DMSO)	16.9	6.8	14.8	12.7	5.7
FLUOR (μg/ml DMSO)	0.35	0.11	0.37	0.19	0.11
CPEP (μg/ml DMSO)	1.40	0.40	1.10	0.55	0.16

An important point to be made is that the testing of the pure standards should be done at concentrations comparable to that in the samples. Dose response curves are notoriously non-linear, and usually exhibit a "hockey stick" behavior. At low doses, the slope of the dose response curve may be close to zero, and then increase sharply at higher doses. Problems with the MDMC approach are that the curves may cross the 99%UCL during this non-linear portion. When calculating the additive mutagenicities, one assumes that the dose response curve is linear between zero and the MDMC, and this may cause large errors. The best approach is to prepare reconstituted mixtures and test a wide range of concentrations to produce a full dose-response curve. Use of this approach eliminates the calculational problems caused by non-linearities in the dose-response curves.

Individual assays were performed for pure CPEP and pure FLUOR and Table 9.2 shows the MF and the induced MF. Care was taken to ensure that the pure CPEP standard was accurate. Figures 9.1 and 9.2 show the dose response curves for CPEP and FLUOR. The amount of CPEP and FLUOR in our samples is near the linear portion of the curve at the lower doses. Consequently additional assays were performed at these low doses. Because of the statistical background mutant fraction, we subtract the observed mutant fraction from the negative control mutant fraction to determine the induced mutant fraction. Figures 9.3 and 9.4 show the induced mutant fractions for CPEP and FLUOR, respectively.

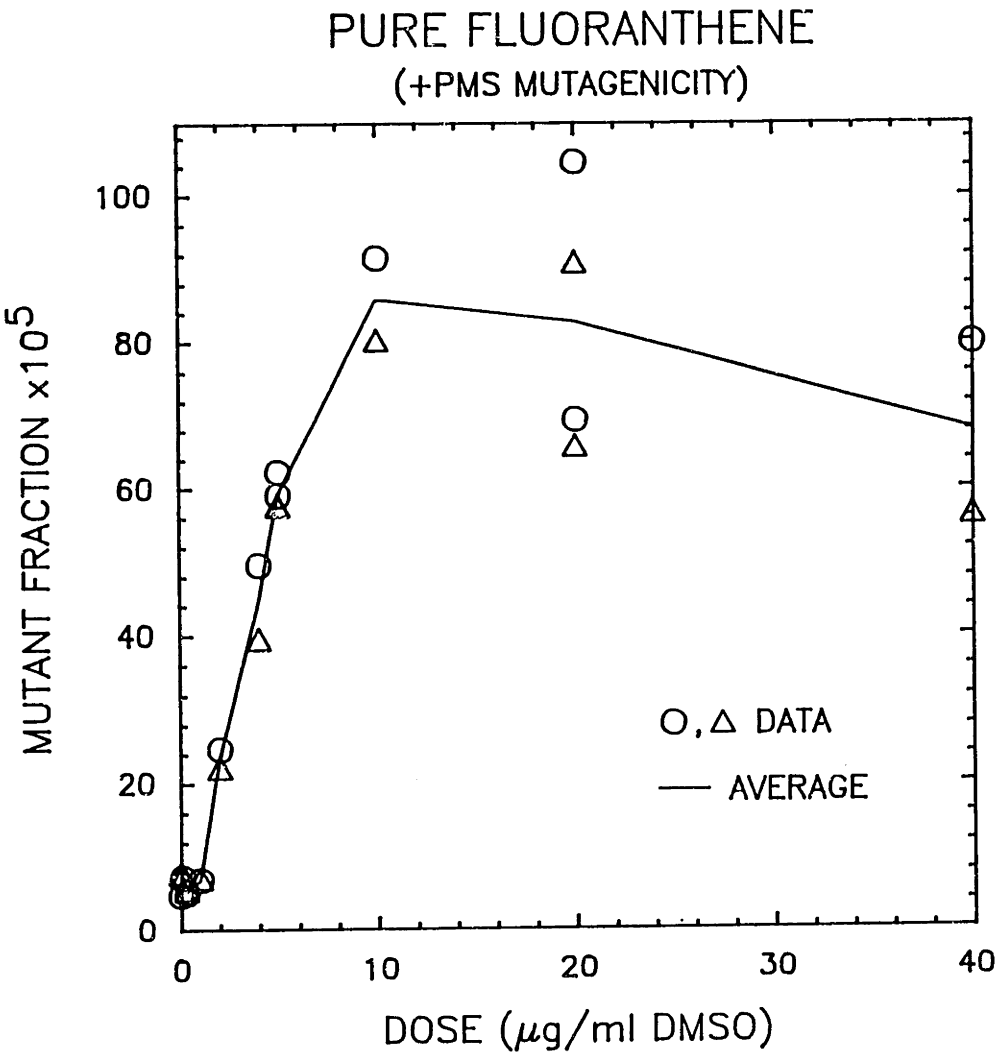

Figure 9.1 Dose response curve (+PMS) for pure Fluoranthene standard. Data points are results of individual assays, and the curve is a line connecting the averages of the data.

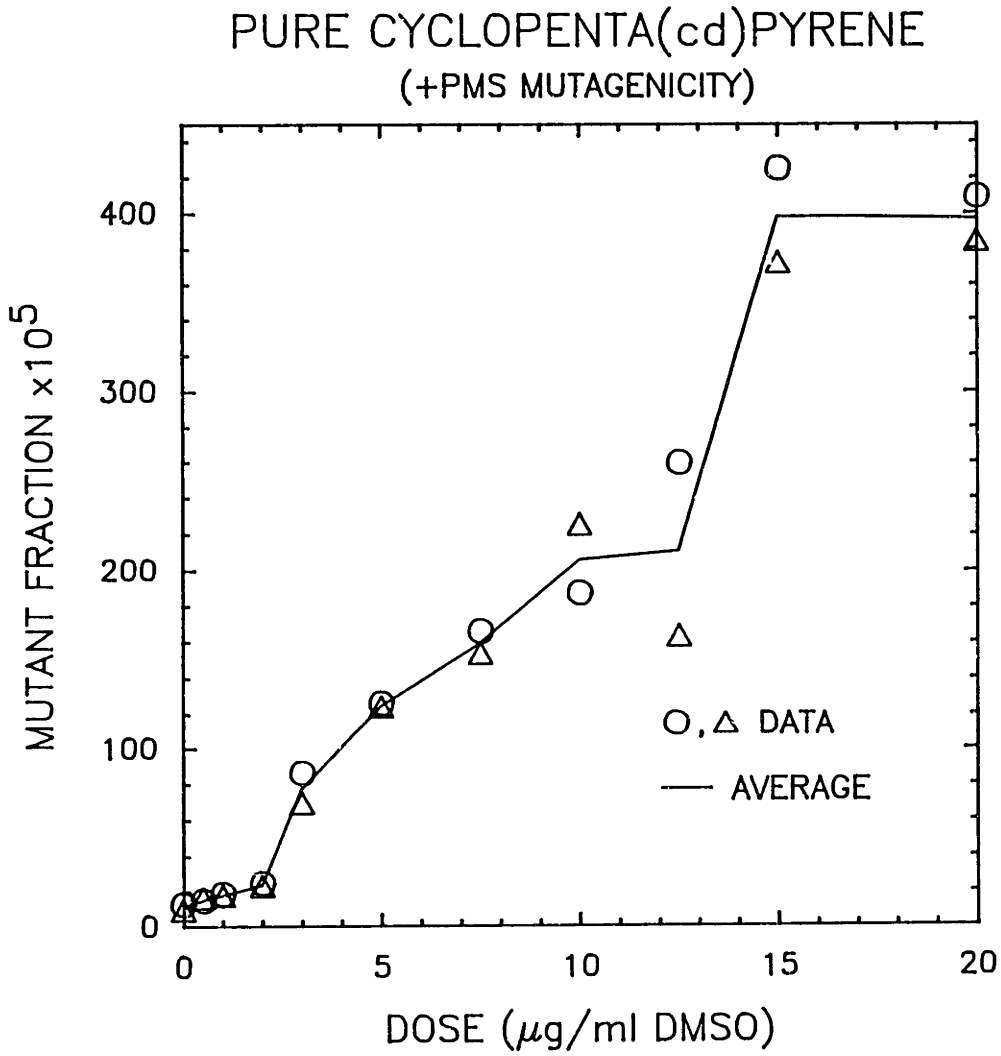

Figure 9.2 Dose response curve (+PMS) for pure Cyclopenta(cd)pyrene standard. Data points are results of individual assays, and the curve is a line connecting the averages of the data.

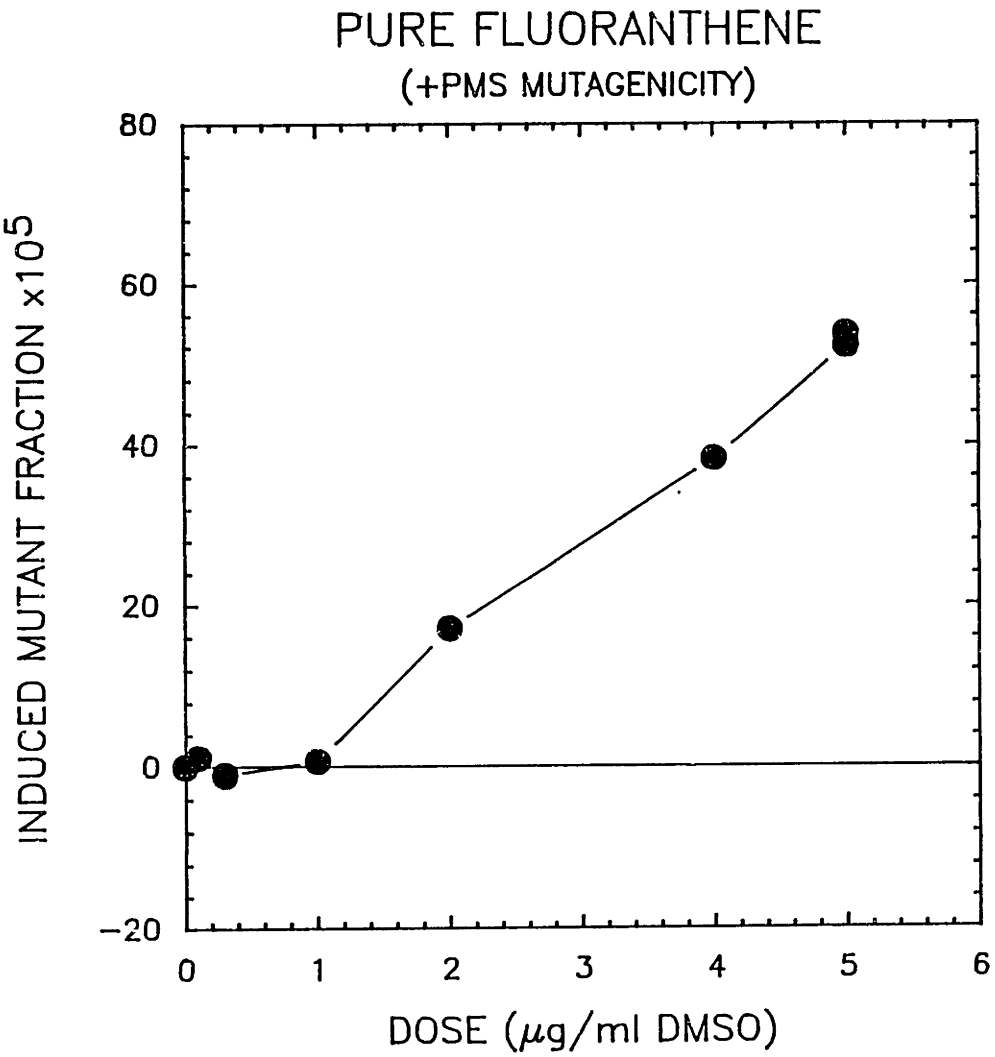

Figure 9.3 Induced mutant fraction dose response curve (+PMS) for pure Fluoranthene standard Data points are averages of individual assays and the curve is a line connecting the averages of the data.

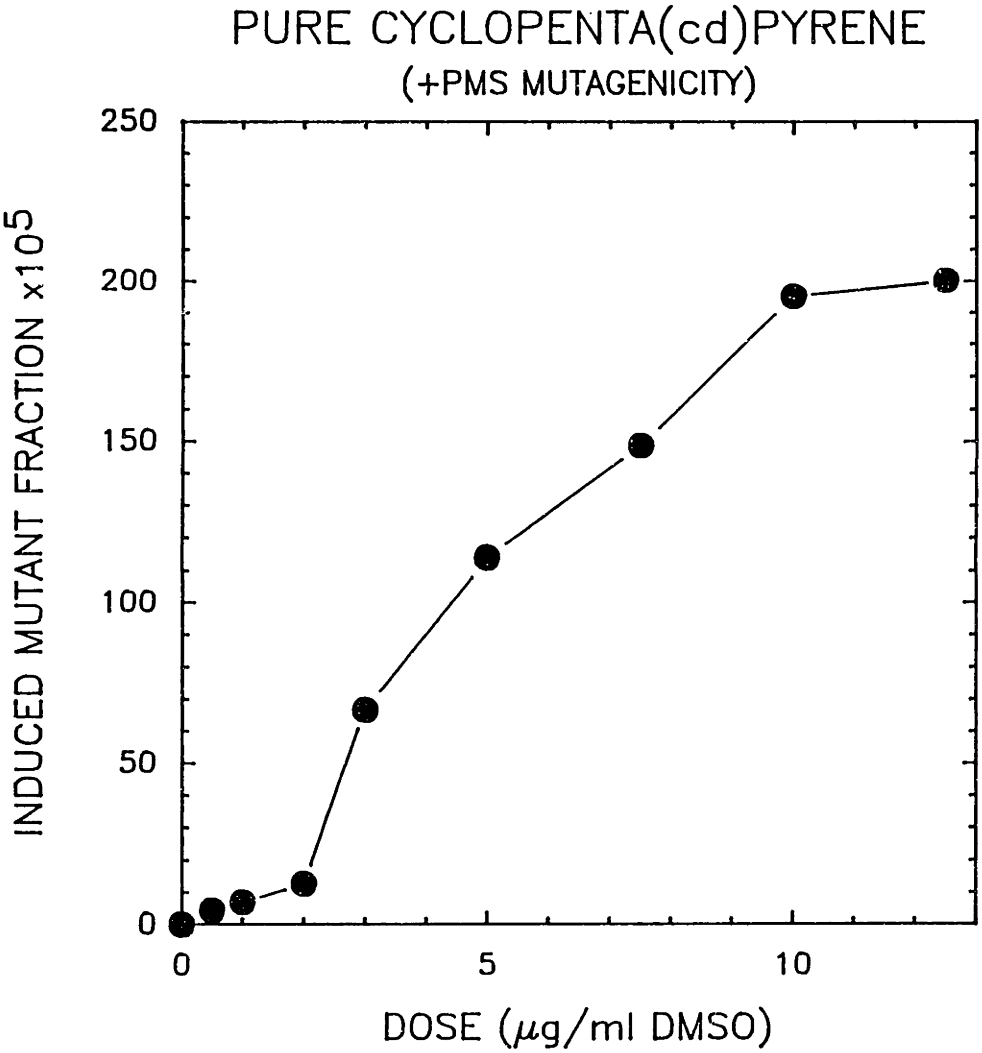

Figure 9.4 Induced mutant fraction dose response curve (+PMS) for pure Cyclopenta(cd)pyrene standard. Data points are averages of individual assays, and the curve is a line connecting the averages of the data.

The results of the +PMS mutagenicity assays for the PFR samples and the reconstituted mixtures are shown in Table 9.3, and the results of -PMS assays are shown in Table 9.4. Duplicate assays were performed, and the average induced mutant fractions (MF) for each are presented. The induced MF is the average value of the MF minus the average MF value for the negative control assay. Occasionally negative induced MF are encountered, but these are not meaningful. The induced MF's for the reconstituted mixtures are calculated in a similar manner.

The induced MF for all 5 PFR samples are shown in Figure 9.5. The general trend seems to be that higher mutagenicities are observed for the PAH samples obtained at longer residence times. Recall that the concentrations of fluoranthene and cyclopenta(cd)pyrene increase as a function of residence time in the PFR, both in absolute and relative concentration of the sample. It appears that qualitatively, the correct trend is observed, if the total mutagenicity of the sample is attributable in large part to cyclopenta(cd)pyrene and fluoranthene.

Comparison of the induced MF's for the PFR samples and the reconstituted mixtures for all 5 samples are shown in Figures 9.6-9.10. The abscissa shows the sample dose, as well as the CPEP and FLUOR dose for each sample. Figure 9.6 shows remarkable agreement for 54PAH1 at a sample dose of 152 μg/ml DMSO, and at this dose, CPEP and FLUOR account for 77% of the total mutagenicity. Therefore, CPEP and FLUOR are certainly major contributors to the overall mutagenicity. At lower doses, however, the CPEP and FLUOR do not account for a major

fraction of the total induced MF. At a dose of 17.1 μg/ml DMSO, CPEP and FLUOR only account for 5% of the total. A similar situation exists for 54PAH2 and 54PAH3 as shown in Figures 9.7 and 9.8. Thus, at the highest doses tested, CPEP and FLUOR account for 71% and 60% of the total induced MF for 54PAH2 and 54PAH3, respectively, but only 21% and 19% at the lowest doses. This trend is not observed for samples 54PAH4 and 54PAH5 shown in Figures 9.9 and 9.10; in fact for 54PAH4, the reconstituted mixture gave a nearly identical dose-response curve to the sample at low doses.

The difference between the reconstituted mixture and the sample must be due to biological activity of at least one species which is present in the sample, but not in the reconstituted mixture. Furthermore, since the differences between the reconstituted mixtures and the samples was largest at low doses, this species must have a high activity relative to CPEP and FLUOR at low doses, and a somewhat lower activity at high doses. A species with a dose response curve which is very steep at low doses and then plateaus quickly would be a possible suspect.

Another clue to the identity of the missing biologicall active species is that the difference is not large at low doses for the 54PAH4 and 54PAH5 samples. These samples were taken at short residence times in the PFR, where the concentration of species with molecular weights greater than CPEP are quite low. Only at later PFR residence times do we see appreciable quantities of these species for our experimental conditions of ϕ=2.18. It is possible that the missing biologically active species has a molecular weight greater

than CPEP. Although speculative at this time, perylene has the required shape of dose-response curve and it would be expected to be produced in greater quantities at late PFR residence times. If not perylene, then another species with high molecular weight would be the most likely candidate to explain the discrepancies between reconstituted mixtures and sample dose response curves.

Table 9.2 - Pure Compound (+PMS) Mutagenicities

FLUORANTHENE

DOSE (ug/ml DMSO)	MF	MF	AVG MF	INDUCED AVG MF
0	4.8	7.8	6.3	0.0
0.1	7.3	7.6	7.5	1.2
0.3	5.1	5.5	5.3	-1.0
1	6.9	7.1	7.0	0.7
2	24.7	22.1	23.4	17.1
4	49.6	39.5	44.6	38.3
5	59.1	57.7	58.4	52.1
5	62.3	57.6	60.0	53.7
10	91.5	80.2	85.9	79.6
20	104.5	90.8	97.7	91.4
20	69.4	65.7	67.6	61.3
40	79.7	56.2	68.0	61.7

CYCLOPENTA(cd)PYRENE

DOSE (ug/ml DMSO)	MF	MF	AVG MF	INDUCED AVG MF
0	12.9	9.4	11.2	0.0
0.5	14.8	16.2	15.5	4.4
1	18.6	17.5	18.1	6.9
2	24.7	22.9	23.8	12.7
3	86.2	69.3	77.8	66.6
5	126.1	123.9	125.0	113.9
7.5	165.9	153.4	159.7	148.5
10	187.2	225.2	206.2	195.0
12.5	259.5	163.0	211.3	200.1
15	425.0	372.0	398.5	387.4
20	409.0	384.0	396.5	385.4

Table 9.3 -- Results of Biological Assays for PAH samples (+PMS)

PAH Samples					Reconstituted Mixtures					
TAR DOSE	MF	MF	AVG MF	INDUCED AVG MF	INDUCED AVG MF	AVG MF	MF	MF	CPEP DOSE	FLUOR DOSE
54PAH1										
0.0	7.7	7.1	7.4	0.0	0.0	8.6	8.9	8.3	0.00	0.00
1.5	9.0	9.4	9.2	1.8						
5.7	15.8	10.9	13.4	6.0						
17.2	32.1	38.6	35.4	28.0	1.4	10.0	8.9	11.1	1.43	0.36
51.0	65.9	38.4	52.2	44.8	30.9	39.5	35.5	43.5	4.24	1.07
152.0	92.5	61.3	76.9	69.5	53.6	62.2	56.3	68.0	12.64	3.19
54PAH2										
0.0	7.8	7.2	7.5	0.0	0.0	10.4	11.2	9.6	0.00	0.00
0.7	5.7	6.2	6.0	-1.5						
2.2	14.8	13.1	14.0	6.5						
6.6	27.3	23.5	25.4	17.9	3.8	14.2	15.1	13.2	0.44	0.12
20.0	51.4	43.6	47.5	40.0	7.5	17.9	17.7	18.1	1.30	0.35
61.0	93.2	63.2	78.2	70.7	50.2	60.6	61.4	59.7	3.98	1.07
					149.1	159.5	163.6	155.4	11.90	3.20
					306.6	317.0	281.6	352.4	35.90	9.60
54PAH3										
0.0	6.9	7.2	7.1	0.0	0.0	8.6	8.3	8.9	0.00	0.00
1.6	9.8	9	9.4	2.3						
4.7	14.2	16.3	15.3	8.2						
14.0	31.8	25.3	28.6	21.5	4.1	12.7	12.1	13.3	1.04	0.35
42.0	86.7	76.6	81.7	74.6	22.6	31.2	34.4	28.0	3.11	1.05
133.0	126.1	98.0	112.1	105.0	62.5	71.1	67.6	74.6	9.86	3.33
54PAH4										
0.0	2.5	3.7	3.1	0.0	0.0	7.5	7.8	7.1	0.00	0.00
13.0	10.2	8.2	9.2	5.3	5.7	13.2	13.9	12.4	0.55	0.18
38.0	19.5	28.1	23.8	21.3	21.9	29.3	28.7	29.9	1.65	0.55
76.0					34.0	41.5	42.9	40.0	3.30	1.10
114.0	27.7	39.2	33.5	30.4						
54PAH5										
0.0	2.5	3.7	3.1	0.0	0.0	7.5	7.8	7.1	0.00	0.00
6.0	3.2	3.9	3.6	0.4						
17.0	11.7	8.2	10.0	6.9	3.4	10.9	11.4	10.3	0.47	0.33
52.0	26.8	22.4	24.6	21.5						
102.0					18.7	26.1	29.9	22.3	2.84	1.98

Table 9.4 -- Results of Biological Assays for PAH samples (-PMS)

PAH Samples

TAR DOSE	MF	MF	AVG MF	INDUCED AVG MF
54PAH1				
0.0	6.6	6.1	6.4	0.0
17.2	16.6	14.1	15.4	9.0
19.0	20.9	19.1	20.0	13.7
38.0	43.1	39.8	41.5	35.1
51.0	25.8	25.4	25.6	19.3
76.0	101.8	68.3	85.1	78.7
54PAH2				
0.0	9.5	6.8	8.2	0.0
0.7	14.3	11.7	13.0	4.9
2.2	14.1	16.8	15.5	7.3
6.6	20.0	16.8	18.4	10.3
20.0	33.9	28.1	31.0	22.9
30.0	103.4	84.0	93.7	85.6
60.0	42.4	13.3	27.9	19.7
54PAH3				
0.0	8.1	6.8	7.5	0.0
1.6	13.9	10.9	12.4	5.0
4.7	18.9	13.7	16.3	8.9
14.0	14.7	35.9	25.3	17.9
33.0	50.2	76.3	63.3	55.8
42.0	130.1	75.0	102.6	95.1
66.5	0	53	26.5	19.1
133	15.9	53	34.5	27.0
54PAH4				
0.0	5.7	4.6	5.2	0.0
13.0	7.3	9.4	8.4	3.2
28.5	50.6	14.7	32.7	27.5
38.0	20.9	31.8	26.4	21.2
57.0	114.4	61.5	88.0	82.8
114.0	0.0	0.0	0.0	-5.2
54PAH5				
0.0	5.7	4.7	5.2	0.0
6.0	3.2	3.9	3.6	-1.7
17.0	19.3	14.1	16.7	11.5
25.8	55.2	22.2	38.7	33.5
52.0	26.9	22.4	24.7	19.5

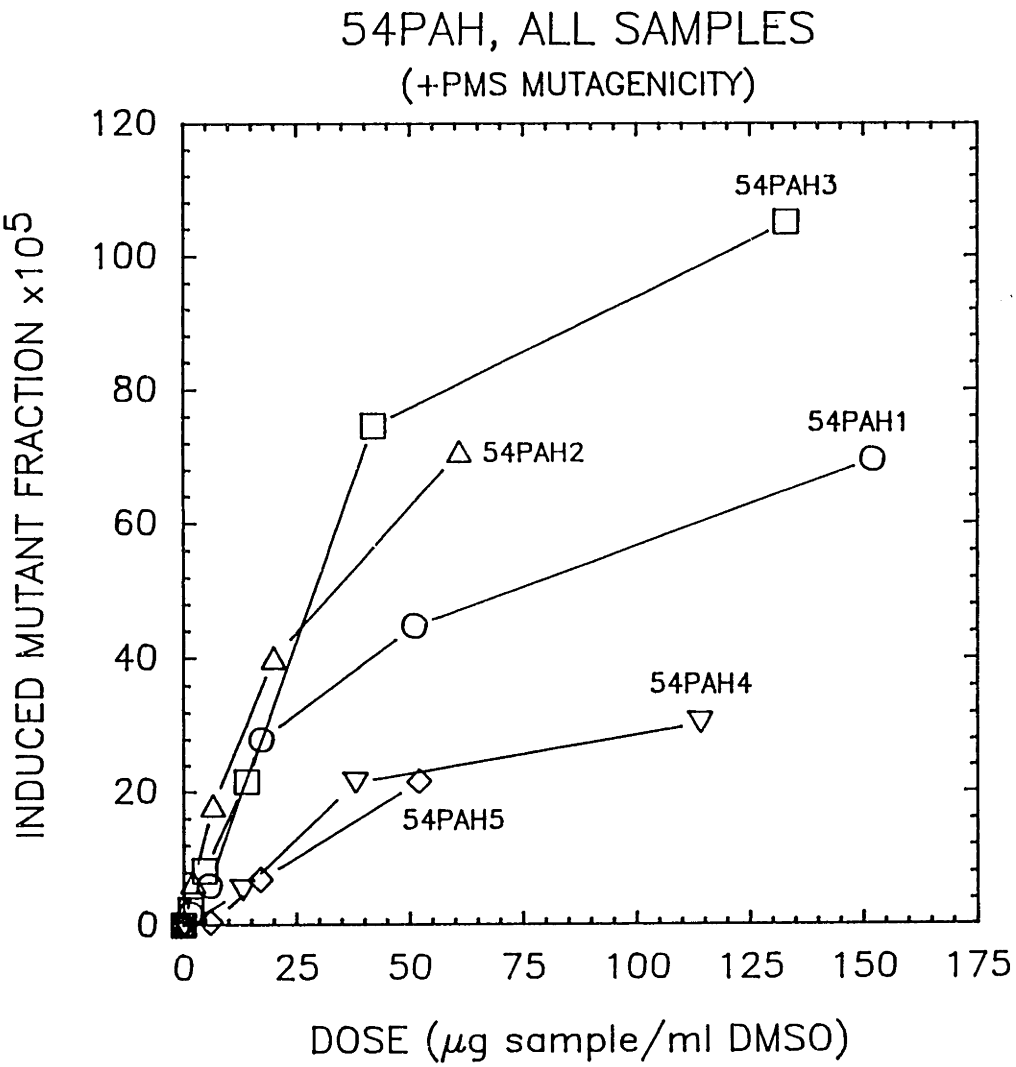

Figure 9.5 Induced mutant fraction dose response curve for all 5 PFR samples for combustion conditions given in Table 9.1.

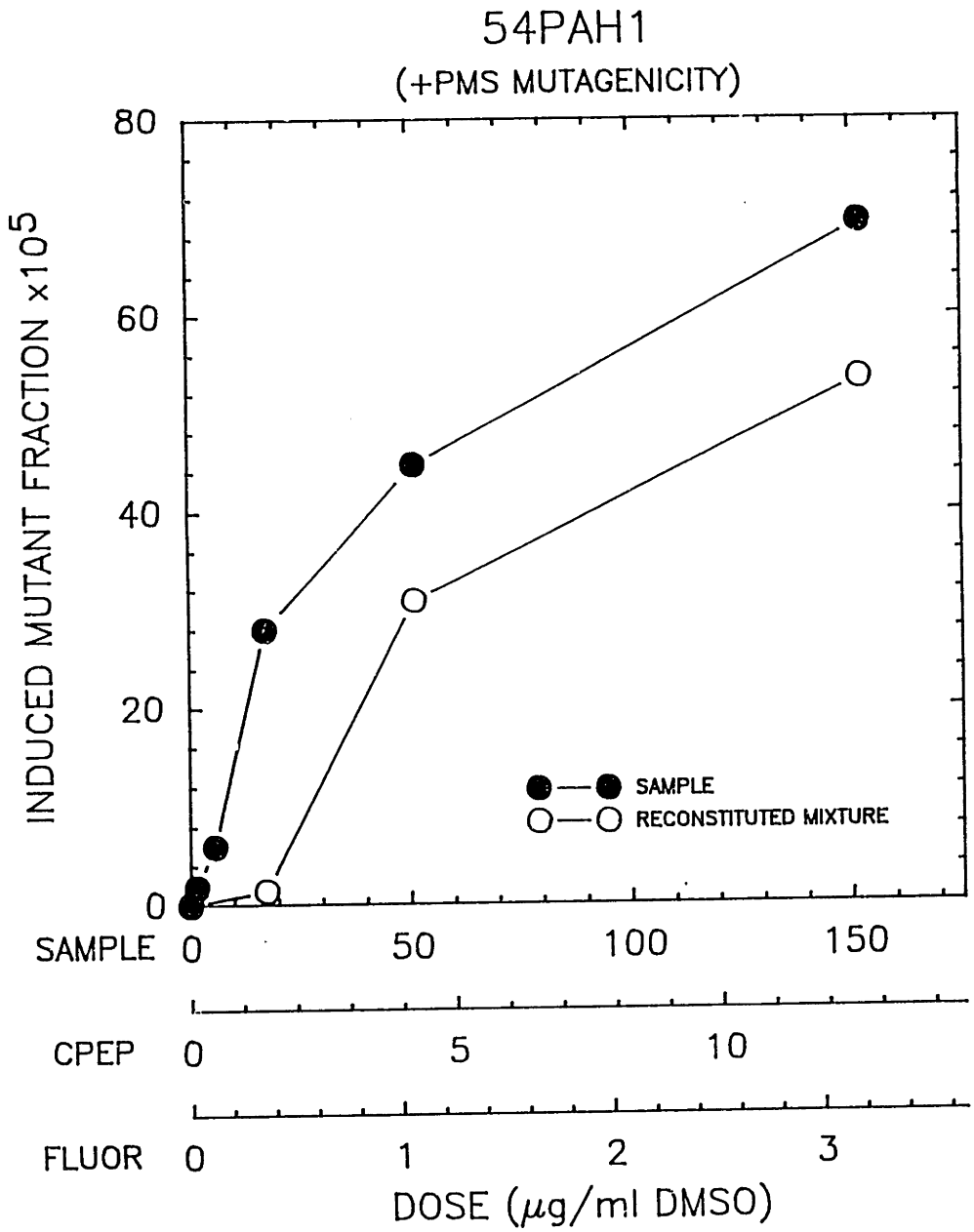

Figure 9.6 Induced mutant fraction dose response curve for 54PAH1 for combustion conditions given in Table 9.1 and reconstituted mixture consisting of cyclopenta(cd)pyrene and fluoranthene in amounts given in Table 9.3.

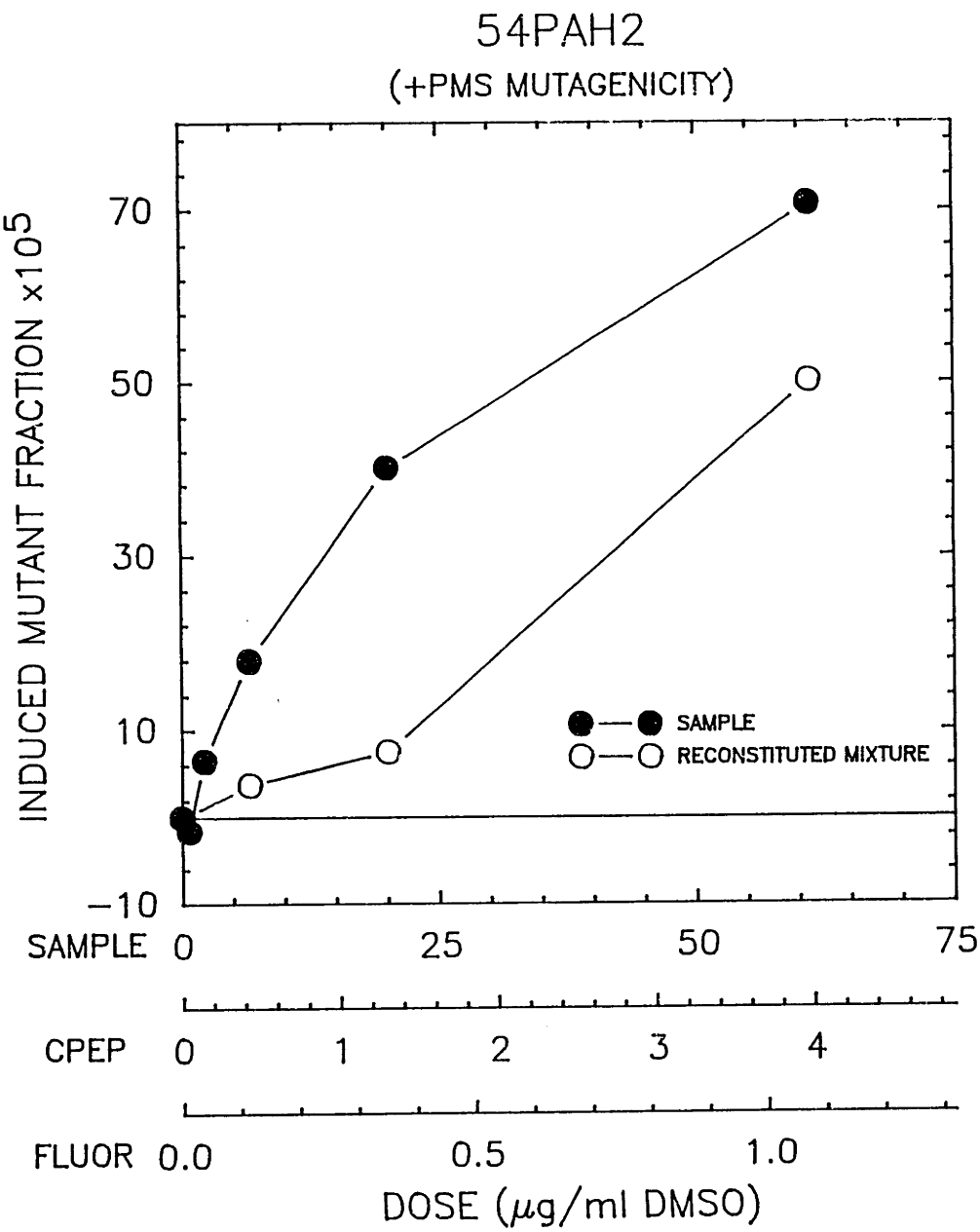

Figure 9.7 Induced mutant fraction dose response curve for 54PAH2 for combustion conditions given in Table 9.1 and reconstituted mixture consisting of cyclopenta(cd)pyrene and fluoranthene in amounts given in Table 9.3.

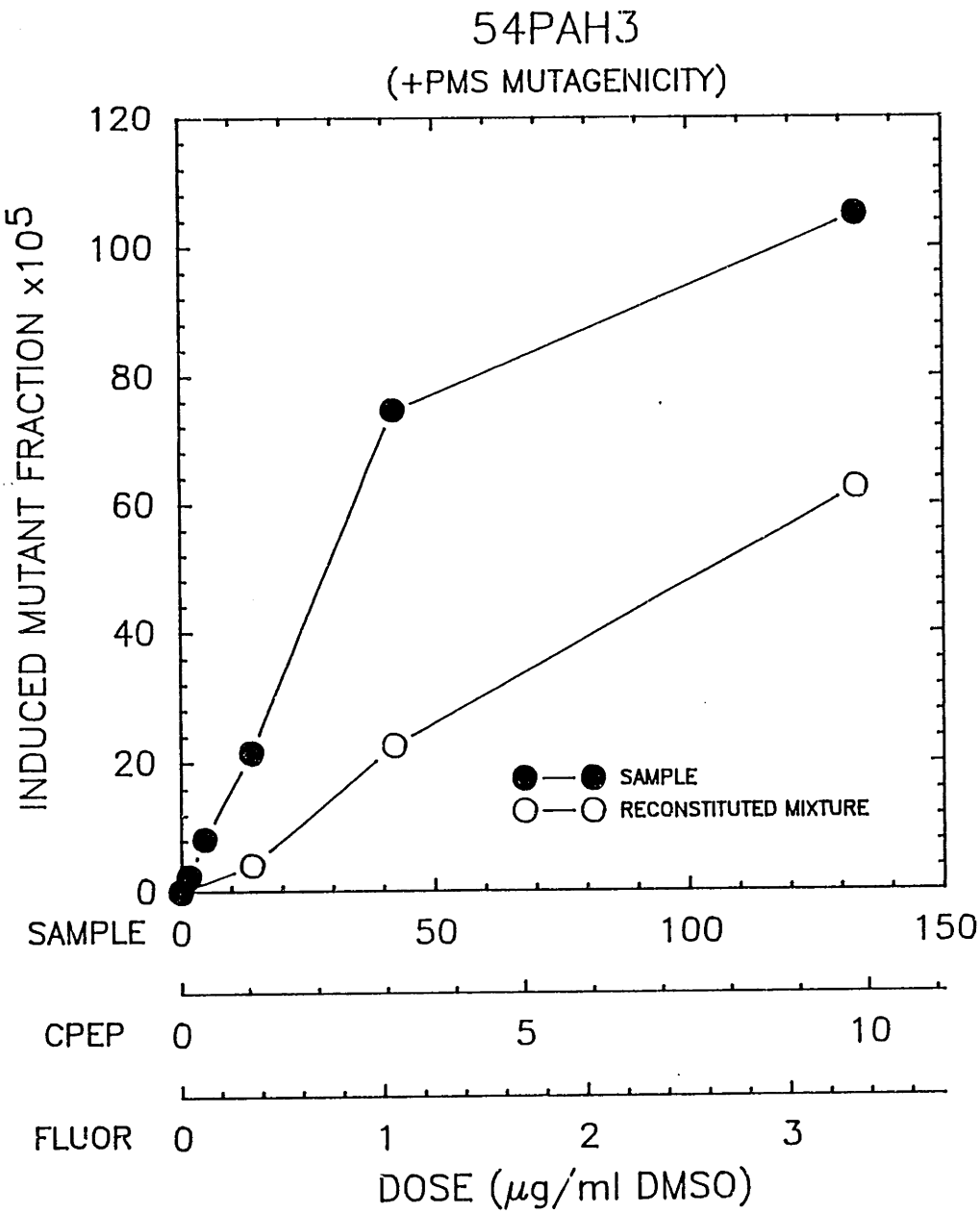

Figure 9.8 Induced mutant fraction dose response curve for 54PAH2 for combustion conditions given in Table 9.1 and reconstituted mixture consisting of cyclopenta(cd)pyrene and fluoranthene in amounts given in Table 9.3.

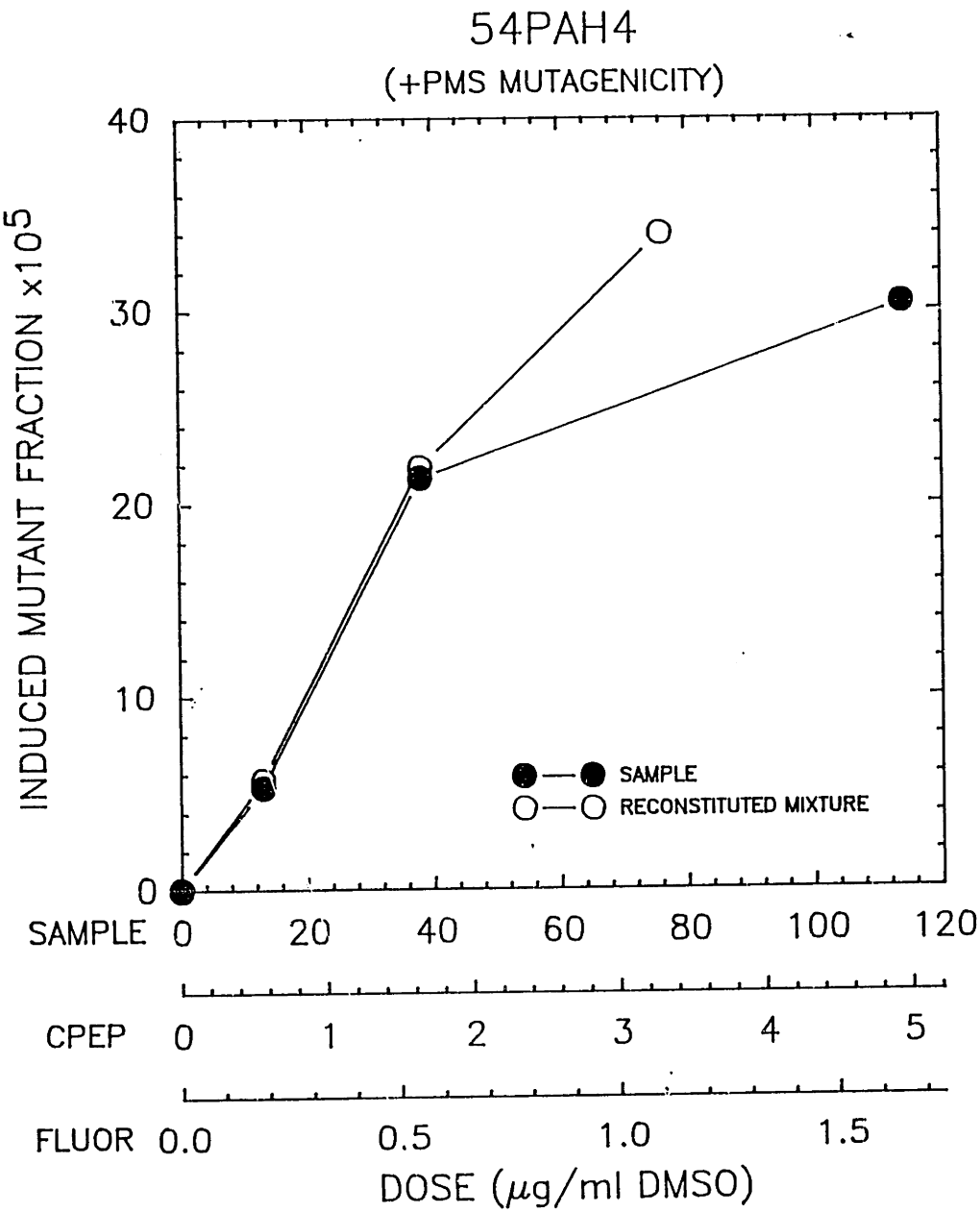

Figure 9.9 Induced mutant fraction dose response curve for 54PAH4 for combustion conditions given in Table 9.1 and reconstituted mixture consisting of cyclopenta(cd)pyrene and fluoranthene in amounts given in Table 9.3.

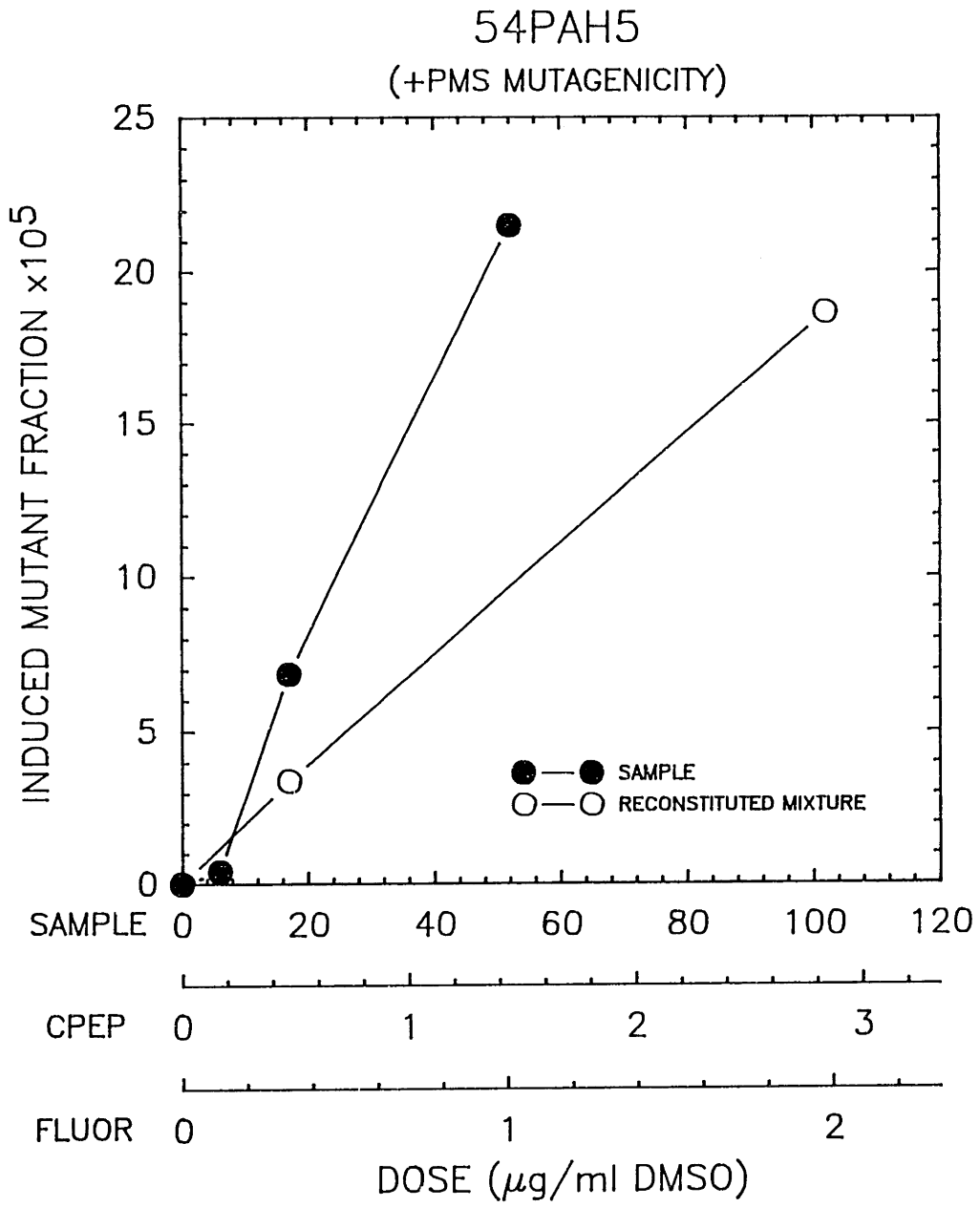

Figure 9.10 Induced mutant fraction dose response curve for 54PAH5 for combustion conditions given in Table 9.1 and reconstituted mixture consisting of cyclopenta(cd)pyrene and fluoranthene in amounts given in Table 9.3.

If we assume additivity of the CPEP and FLUOR, then the sum of the induced MF for the individual pure standards should match those of reconstituted mixtures. Figure 9.11 shows that the dose response curve for CPEP and FLUOR plotted on the same graph as 54PAH1 sample and its reconstituted mixture. The mutant fraction for CPEP at the highest dose tested (152 μg sample/ml DMSO, 12.64 μg CPEP/ml DMSO, 3.19 μg FLUOR/ml DMSO) is a factor of 3 higher than for the 54PAH1 sample and a factor of 4 higher than the reconstituted mixture. Fluoranthene's contribution is quite small. If we had calculated the expected contribution from CPEP and FLUOR based on additivity of their individual mutagenicities, then either CPEP alone or their sum would exceed that of the sample. The sample 54PAH4 is much less mutagenic than 54PAH1, yet a similar trend is observed as shown in Figure 9.12. The expected contribution from CPEP and FLUOR based on additivity of their individual mutagenicities, would over predict the sample mutagenicity at high doses, but not at low doses.

The difference in mutagenicities between the reconstituted mixture and the sum of the pure PAH standards, reflects the degree of non-additivity of the individual mutagenicities for CPEP and FLUOR.

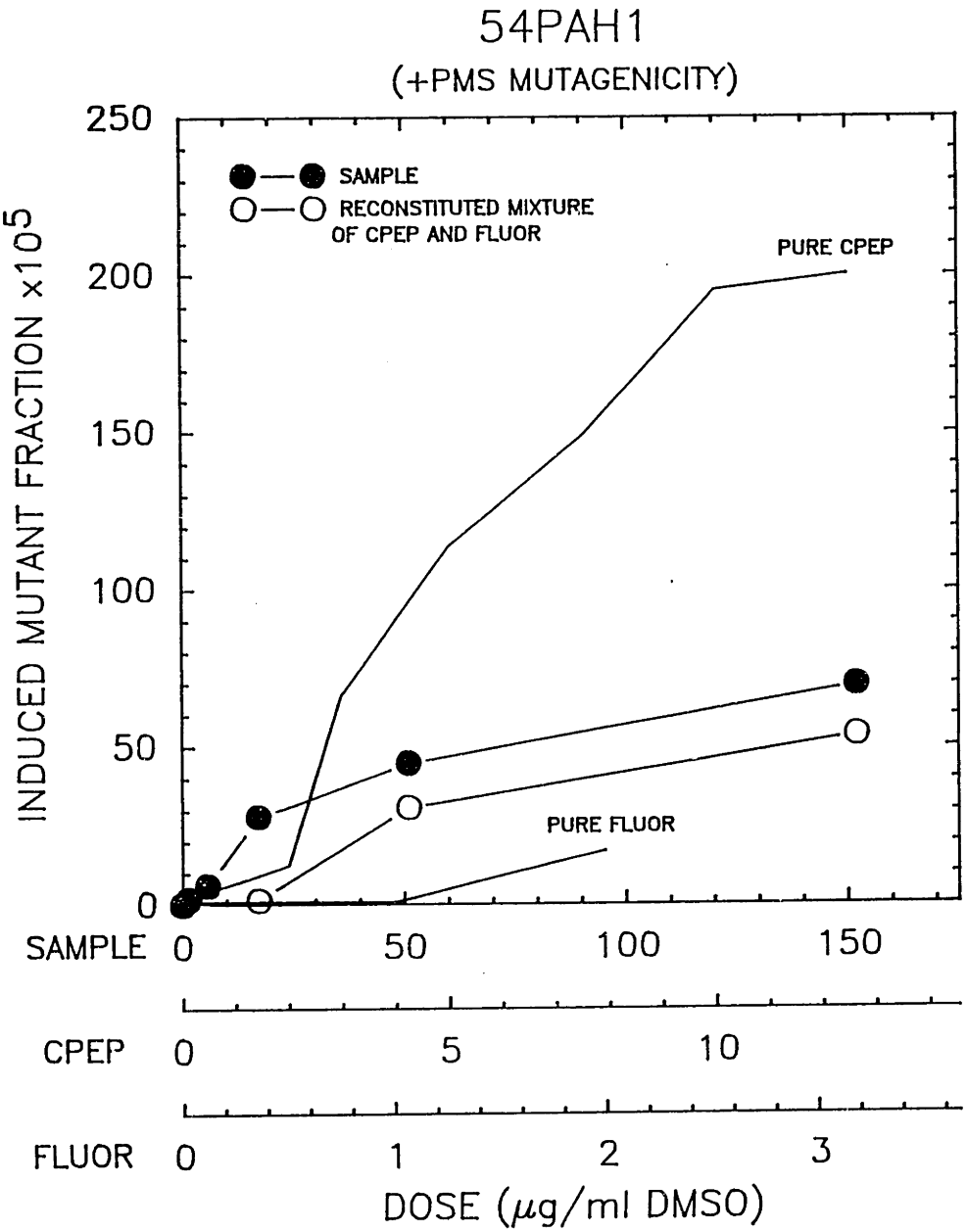

Figure 9.11 Dose response curve for 54PAH1, reconstituted mixture, pure cyclopenta(cd)pyrene, and pure fluoranthene. Combustion conditions are given in Table 9.1.

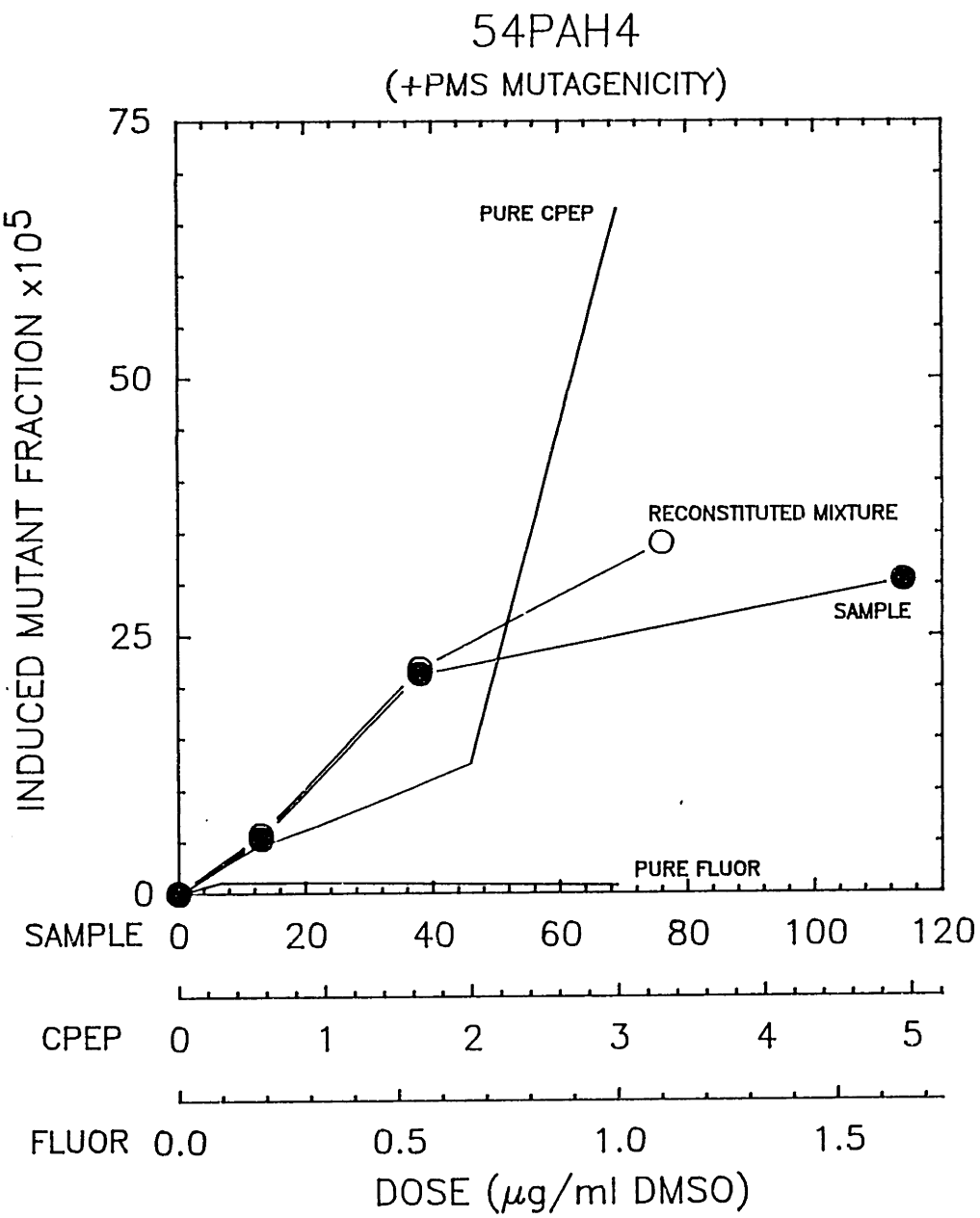

Figure 9.12 Dose response curve for 54PAH4, reconstituted mixture, pure cyclopenta(cd)pyrene, and pure fluoranthene. Combustion conditions are given in Table 9.1.

9.4 CONCLUSIONS

S.8 SUMMARY AND CONCLUSIONS

From our experimental observations of PAH and soot formation for fuel-rich (ϕ=2.18, 2.37) combustion of $C_2H_4/O_2/N_2$ in a JSR/PFR, we reach the following conclusions:

(1) The concentration profiles of fixed gases and major light hydrocarbon species change little in the PFR as equivalence ratio is increased from non-sooting to incipient sooting conditions in the JSR, but for the sooting condition, the tar concentrations are 5 times higher, and soot concentration is 10 times higher.

(2) At the end of the PFR, the combined mass concentration of PAH species with 2-5 rings is comparable that of the high molecular weight tar material (≥6 rings and CH_2Cl_2-soluble).

(3) Injection of C_2H_4 (8.2×10^{-3} moles/mole total flow at ϕ=2.37, 1.0×10^{-2} moles/mole total flow at ϕ=2.18) into the PFR results predominantly in conversion to C_2H_2, but also increases the concentrations of benzene and PAH. An incremental amount of C_2H_4 injected into the PFR is not as effective in enhancing PAH and soot production as the same incremental amount of C_2H_4 fed to the JSR.

(4) Injection of a small amount of C_6H_6 (≈1800 ppm) into the PFR caused a 10-fold increase in the PAH and soot concentrations in the

PFR for the ϕ = 2.18 condition studied. Assuming the 10-fold increase in tar and soot concentration comes from benzene, then these data indicate that 16% of the injected benzene is converted to tar and 11% to soot. Oxidation of C_6H_6 to CO and C_2H_2 is also occurring. Benzene promotes tar and soot formation by causing a 10-fold increase in the benzene concentration at the beginning of the PFR. This observation is consistent with the hypothesis that the number concentration of single-ring aromatics in a combustion environment with high C_2H_2 concentrations controls the growth of higher aromatics. An increase in benzene concentration increases the production of 2-ring aromatics, and is the major source of new moles of PAH material.

(5) Acetylenic-substituted PAH species, which have been proposed as important intermediates in PAH formation, were positively identified by the use of Gas Chromatography/Fourier Transform Infrared Spectroscopy (GC/FTIR).

(6) PAH species which contain 5-membered ring structures account for more than half of the total PAH inventory from indene (C_9H_8) to benzo(ghi)perylene ($C_{22}H_{12}$) on either a mass or mole basis. These PAH species with 5-membered ring structures consisted of 2 types: 1) 5-membered rings containing a methylene group, which may be oxidation products of 6-membered ring PAH, and 2) "acenaphthylene bridge" structures, which may be growth products from acetylene addition reactions.

(7) Phenylacetylene formation from the injected benzene is rapid, and the ratio of phenylacetylene to benzene is near that predicted from equilibration of the reaction $C_6H_6 + C_2H_2 = C_8H_6 + H_2$.

For the fixed gases and light hydrocarbons, kinetics modeling was done at the elementary reaction level; and for PAH both thermodynamics and global kinetics modelling efforts proved insightful. The major conclusions from the modelling work are:

(8) Fixed gases and major hydrocarbon species (CO, CO_2, H_2, CH_4, C_2H_2, C_2H_4) can be modelled assuming a perfectly-stirred/plug-flow reactor system using an elementary reaction mechanism proposed by Glarborg (1986a), which contains 134 reactions, and 29 chemical species, or by a mechanism proposed by Harris (1988a) consisting of 193 reactions and 49 species.

(9) Thermodynamics analysis of the PAH reveals that, with the exception of the ethynyl-acenaphthylenes, the most abundant PAH species observed experimentally are the stabilomers predicted by Stein, which are the most thermodynamically stable species for a given carbon and hydrogen number.

(10) Aliphatic hydrocarbons with the general formula $C_{2n}H_{2m}$ are produced in excess concentrations in the JSR for equilibration of the C_2H_2-H_2-$C_{2n}H_{2m}$ system, and these species decay towards their equilibrium limits in the PFR. Aromatic species, including PAH, with the

general formula $C_{2n}H_{2m}$ are far below their equilibrium limit, but are increasing towards their predicted thermodynamic limits in the PFR.

(11) An aromatic coagulation mechanism for PAH formation, consisting of bimolecular reactions of aryl species reacting with intact aromatic rings, is not the dominant mechanism of PAH formation for our experimental conditions.

(12) A global kinetics model of the PAH inventory (2-5 rings species) successfully predicted the concentration profile of the PAH inventory in the PFR at ϕ=2.18, as well as the perturbation to the PAH profiles from the injection of additional ethylene and benzene. The model includes pathways for mass flux into the PAH inventory due to 1) C_2H_2 addition reactions with single-ring aromatics and 2) C_2H_2 addition reactions with PAH; and pathways for mass flux out of the PAH inventory by 3) C_2H_2 addition reactions with 5-ring PAH, 4) coagulation reactions between PAH, 5) coagulation of PAH with high molecular weight tar, 6) coagulation of PAH with soot, and 7) oxidation reactions of PAH with OH. Acetylene addition to aromatic species provided the major source of mass flux into the PAH inventory, while oxidation was the main route of mass loss from the PAH inventory. Coagulation of PAH with soot was predicted to have low collision efficiencies ($\approx$ 1%). A collision efficiency, γ, of 0.2 for OH with PAH (based on γ = 0.2 for OH reaction with soot) was necessary in order to successfully predict the experimental trends. This rate is $\approx$40 times higher than the rate of benzene oxidation by reaction with

OH.

13) The fraction of CPEP and FLUOR in the tar sample increases as PFR residence time increases, and the mutagenicities of the samples also increase. Comparison of mutagenicities observed for reconstituted mixtures showed that CPEP and FLUOR could account for 60-80% of the total mutagenicity at high doses, but a much smaller fraction at low doses. It is possible that a high molecular weight PAH species may be responsible for the difference between the sample and the reconstituted mixtures.

S.9 RECOMMENDATIONS FOR FUTURE WORK

The use of the injection system along with the unique capabilities of the JSR/PFR should enable further progress to be made in the acquisition of experimental data in order to better understand PAH formation. Specific areas for further research include:

(1) Further injection studies on the effect of multi-ring aromatics on the formation of PAH would be useful in identifying pathways for PAH (as well as soot) formation and destruction. Since PAH are destroyed as well as formed, the destruction of large PAH to smaller PAH needs to be investigated.

(2) The effect of temperature on PAH formation should be investigated further by obtaining experimental data at higher temperatures closer to those found in typical laminar flat-flames.

(3) The measurement of radical species, especially aromatic radicals, by molecular beam-mass spectrometry would be very valuable in evaluating elementary kinetic models for PAH formation.

(4) The modelling of PAH at the elementary reaction level is not possible until more rate constants become available from isolated kinetic studies at high temperatures. In particular, kinetics experiments to determine the high temperature rate parameters for PAH oxidation reactions, as well as further studies on aliphatic addition reactions to PAH, should be performed. Chemically activated pathways

for PAH formation should be considered.

(5) Hydrocarbon combustion mechanisms for formation of C_4 species and aromatic species should be tested against this data set.

(6) Additional characterization of the high molecular weight tar material which is soluble in CH_2Cl_2 but not amenable to GC analysis, should provide information necessary to obtain a better understanding of soot formation.

APPENDICES

APPENDIX A.1 - GLARBORG MECHANISM

```
ELEMENTS
  H   O   N   C
END
SPECIES
H       H2
O       OH      H2O
O2      HO2     H2O2
C       CH      CH2     CH3     CH4
C2H     C2H2    C2H3    C2H4    C2H5    C2H6
CO      HCO     CH2O    CH3O
C3H4    C3H2
HCCO    CH2CO   CO2
N2
END
```

REACTIONS

								A	n	Ea
1	H + O2			= OH + O			(M #1)	5.1E16	-0.82	16510.
2	O + H2			= OH + H			(M #2)	1.8E10	1.0	8830.
3	OH + H2			= H2O + H			(M #3)	1.2E09	1.3	3630.
4	OH + OH			= H2O + O			(M #4)	6.0E08	1.3	0.
5	O2 + M			= O + O	+ M		(M #6)	1.9E11	0.5	95560.
6	H + H	+ M		= H2		+ M	(M #7)	1.0E18	-1.0	0.
7	H + H	+ H2		= H2	+ H2		(M #8)	9.2E16	-0.6	0.
8	H + H	+ H2O		= H2	+ H2O		(M #9)	6.0E19	-1.25	0.
9	H + H	+ CO2		= H2	+ CO2		(M #10)	5.5E20	-2.0	0.
10	H + OH	+ M		= H2O		+ M	(M #5)	7.5E23	-2.6	0.
11	H + O2	+ M		= HO2		+ M	(M #12)	2.1E18	-1.0	0.
12	H + O2	+ O2		= HO2	+ O2		(M #13)	6.7E19	-1.42	0.
13	H + O2	+ N2		= HO2	+ N2		(M #14)	6.7E19	-1.42	0.
14	H2 + O2			= OH	+ OH		(M #11)	1.7E13	0.0	47780.
15	H + HO2			= OH	+ OH		(M #16)	2.5E14	0.0	1900.
16	H + HO2			= H2	+ O2		(M #15)	2.5E13	0.0	700.
17	O + HO2			= OH	+ O2		(M #17)	4.8E13	0.0	1000.
18	OH + HO2			= H2O	+ O2		(M #18)	5.0E13	0.0	100.
19	HO2 + HO2			= H2O2	+ O2		(M #19)	2.0E12	0.0	0.
20	H2O2	+ M		= OH	+ OH	+ M	(M #20)	1.2E17	0.0	45500.
21	H2O2 + H			= HO2	+ H2		(M #21)	1.7E12	0.0	3750.
22	H2O2 + OH			= H2O	+ HO2		(M #22)	1.0E13	0.0	1800.
23	CO + OH			= CO2	+ H		(M #25)	1.5E07	1.3	-760.
24	CO + O	+ M		= CO2		+ M	(M #23)	3.2E13	0.0	-4200.
25	CO + O2			= CO2	+ O		(M #24)	2.5E12	0.0	47700.
26	CO + HO2			= CO2	+ OH		(M #26)	5.8E13	0.0	22930.
27	CH4 + M			= CH3	+ H	+ M	(M #27)	1.0E17	0.0	88000.
28	CH4 + H			= CH3	+ H2		(M #28)	2.2E04	3.0	8750.
29	CH4 + O			= CH3	+ OH		(M #29)	1.2E07	2.08	7630.
30	CH4 + OH			= CH3	+ H2O		(M #30)	3.5E03	3.08	2000.
31	CH4 + CH2			= CH3	+ CH3		(M #31)	1.3E13	0.0	9500.
32	CH3 + O			= CH2O	+ H		(M #34)	6.8E13	0.0	0.
33	CH3 + OH			= CH2	+ H2O		(M #36)	1.5E13	0.0	5000.

34	CH3	+ O	= CH2 + OH	(M #35)	5.0E13	0.0	12000.
35	CH3	+ H	= CH2 + H2	(M #33)	9.0E13	0.0	15100.
36	CH3	+ M	= CH2 + H + M	(M #32)	1.9E16	0.0	91600.
37	CH3	+ OH	= CH2O + H2	(M #37)	1.0E12	0.0	0.
38	CH3	+ O2	= CH2O + OH	(M #38)	5.2E13	0.0	34570.
39	CH3	+ O2	= CH3O + O	(M #39)	7.0E12	0.0	25650.
40	CH3O	+ M	= CH2O + H + M	(M #40)	1.0E14	0.0	25000.
41	CH3O	+ H	= CH2O + H2	(M #41)	2.0E13	0.0	0.
42	CH3O	+ O	= CH2O + OH	(M #42)	1.0E13	0.0	0.
43	CH3O	+ OH	= CH2O + H2O	(M #43)	1.0E13	0.0	0.
44	CH3O	+ O2	= CH2O + HO2	(M #44)	6.3E10	0.0	2600.
45	CH2O	+ M	= HCO + H + M	(M #45)	3.3E16	0.0	81000.
46	CH2O	+ H	= HCO + H2	(M #46)	2.2E08	1.77	10500.
47	CH2O	+ O	= HCO + OH	(M #47)	1.8E13	0.0	3080.
48	CH2O	+ OH	= HCO + H2O	(M #48)	3.4E09	1.18	-447.
49	HCO	+ M	= CO + H + M	(M #49)	1.6E14	0.0	14700.
50	HCO	+ H	= CO + H2	(M #50)	4.0E13	0.0	0.
51	HCO	+ O	= CO + OH	(M #51)	3.0E13	0.0	0.
52	HCO	+ O	= CO2 + H	(M #52)	3.0E13	0.0	0.
53	HCO	+ OH	= CO + H2O	(M #53)	5.0E12	0.0	0.
54	HCO	+ O2	= CO + HO2	(M #54)	3.3E13	-0.4	0.
55	CH2	+ H	= CH + H2	(M #55)	7.3E17	-1.56	0.
56	CH2	+ OH	= CH + H2O	(M #60)	4.5E13	0.0	3000.
57	CH2	+ OH	= CH2O + H	(M #59)	3.0E13	0.0	0.
58	CH	+ OH	= HCO + H	(M #72)	3.0E13	0.0	0.
59	CH2	+ O	= CO + H + H	(M #56)	3.0E13	0.0	0.
60	CH2	+ O	= CO + H2	(M #57)	5.0E13	0.0	0.
61	CH2	+ O	= CH + OH	(M #58)	5.0E13	0.0	12000.
62	CH2	+ O2	= CO2 + H + H	(M #61)	1.6E12	0.0	1000.
63	CH2	+ O2	= CO2 + H2	(M #62)	6.9E11	0.0	500.
64	CH2	+ O2	= CO + H2O	(M #63)	1.9E10	0.0	-1000.
65	CH2	+ O2	= CO + OH + H	(M #64)	8.6E10	0.0	-500.
66	CH2	+ O2	= HCO + OH	(M #65)	4.3E10	0.0	-500.
67	CH2	+ O2	= CH2O + O	(M #66)	2.0E13	0.0	9000.
68	CH2	+ CO2	= CO + CH2O	(M #67)	1.1E11	0.0	1000.
69	CH2	+ CH	= C2H2 + H	(M #68)	4.0E13	0.0	0.
70	CH2	+ CH2	= C2H2 + H2	(M #69)	3.2E13	0.0	0.
71	CH	+ O	= CO + H	(M #71)	5.7E13	0.0	0.
72	CH	+ O2	= HCO + O	(M #73)	3.3E13	0.0	0.
73	CH	+ H	= C + H2	(M #70)	1.5E14	0.0	0.
74	CH	+ CO2	= HCO + CO	(M #74)	3.4E12	0.0	690.
75	CH	+ CH3	= C2H3 + H	(M #75)	3.0E13	0.0	0.
76	CH	+ CH4	= C2H4 + H	(M #76)	6.0E13	0.0	0.
77	CH	+ C2H2	= C3H2 + H	(M #77)	1.3E14	0.0	0.
78	CH	+ C2H4	= C3H4 + H	(M #78*)	1.3E14	0.0	0.
79	CH	+ C2H6	= CH2 + C2H5	(M #79*)	2.4E14	0.0	0.
80	C	+ OH	= CO + H	(M #80)	5.0E13	0.0	0.
81	C	+ O2	= CO + O	(M #81)	2.0E13	0.0	0.
82	C	+ CO2	= CO + CO	(M #82)	6.0E08	0.0	0.
83	C	+ CH4	= CH + CH3	(M #83)	5.0E13	0.0	24000.
84	C	+ CH3	= C2H2 + H	(M #84)	5.0E13	0.0	0.
85	C	+ CH2	= C2H + H	(M #85)	5.0E13	0.0	0.

```
 86 CH3    +  CH3        = C2H6              (M #86P*)   7.5E11   0.0    -306.
 87 CH3    +  CH3        = C2H4 + H2         (M #88)     2.1E14   0.0   19200.
 88 CH3    +  CH2        = C2H4 + H          (M #89)     3.0E13   0.0       0.
 89 C2H6   +  H          = C2H5 + H2         (M #90)     5.4E02   3.5    5200.
 90 C2H6   +  O          = C2H5 + OH         (M #91)     2.5E13   2.0    6360.
 91 C2H6   +  OH         = C2H5 + H2O        (M #92)     8.7E09   1.05   1810.
 92 C2H6   +  CH3        = C2H5 + CH4        (M #93)     5.5E-1   4.0    8280.
 93 C2H6   +  CH2        = CH3  + C2H5       (M #94)     2.2E13   0.0    8660.
 94 C2H5   +  H          = CH3  + CH3        (M #87)     4.0E13   0.0       0.
 95 C2H5   +  O2         = C2H4 + HO2        (M #96)     3.2E12   0.0    5020.
 96 C2H5   +  M          = C2H4 + H  + M     (M #95)     1.0E17   0.0   31000.
 97 C2H4   +  O          = CH3  + HCO        (M #100)    1.6E09   1.2     746.
 98 C2H4   +  OH         = C2H3 + H2O        (M #101)    4.8E12   0.0    1230.
 99 C2H4   +  H          = C2H3 + H2         (M #99)     1.1E14   0.0    8500.
100 C2H4   +  M          = C2H2 + H2 + M     (M #97)     2.6E17   0.0   79350.
101 C2H4   +  M          = C2H3 + H  + M     (M #98)     2.6E17   0.0   96900.
102 C2H4   +  OH         = CH2O + CH3        (M #102)    2.0E12   0.0     960.
103 C2H3   +  H          = C2H2 + H2         (M #104)    4.0E13   0.0       0.
104 C2H3   +  O          = CH2CO + H         (M #105)    3.3E13   0.0       0.
105 C2H3   +  OH         = C2H2 + H2O        (M #106)    5.0E12   0.0       0.
106 C2H3   +  O2         = HCO  + CH2O       (M #107)    4.0E12   0.0    -250.
107 C2H3   +  CH2        = C2H2 + CH3        (M #108)    3.0E13   0.0       0.
108 C2H3   +  C2H        = C2H2 + C2H2       (M #109)    3.0E13   0.0       0.
109 C2H3   +  M          = C2H2 + H  + M     (M #103)    8.0E14   0.0   31500.
110 C2H2   +  M          = C2H  + H  + M     (M #110)    4.2E16   0.0  107000.
111 C2H    +  H2         = C2H2 + H          (M #111)    4.1E05   2.39    860.
112 C2H2   +  O          = CH2  + CO         (M #112)    2.2E10   1.0    2580.
113 C2H2   +  O          = HCCO + H          (M #113)    3.6E04   2.7    1390.
114 C2H2   +  O          = C2H  +  OH        (M #114)    3.2E15  -0.6   15000.
115 C2H2   +  OH         = CH2CO + H         (M #115)    3.2E11   0.0     200.
116 C2H2   +  OH         = C2H   + H2O       (M #116)    6.0E12   0.0    7000.
117 CH2CO  +  H          = CH3  + CO         (M #118)    1.1E13   0.0    3430.
118 CH2CO  +  H          = HCCO + H2         (M #119)    7.5E13   0.0    8000.
119 CH2CO  +  O          = CH2O + CO         (M #120)    2.0E13   0.0       0.
120 CH2CO  +  O          = HCCO + OH         (M #121)    5.0E13   0.0    8000.
121 CH2CO  +  OH         = CH2O + HCO        (M #122)    2.8E13   0.0       0.
122 CH2CO  +  M          = CH2  + CO + M     (M #117)    3.6E15   0.0   59300.
123 CH2CO  +  OH         = HCCO + H2O        (M #123)    7.5E12   0.0    3000.
124 HCCO   +  H          = CH2  + CO         (M #124)    1.1E14   0.0       0.
125 HCCO   +  O          = CO   + CO + H     (M #125)    1.1E14   0.0       0.
126 HCCO   +  OH         = HCO  + CO + H     (M #126)    1.0E13   0.0       0.
127 HCCO   +  O2         = CO   + CO + OH    (M #127)    1.5E12   0.0    2500.
128 HCCO   +  CH2        = C2H  + CH2O       (M #128)    1.0E13   0.0    2000.
129 HCCO   +  CH2        = C2H3 + CO         (M #129)    3.0E13   0.0       0.
130 HCCO   +  HCCO       = C2H2 + CO + CO    (M #130)    1.0E13   0.0       0.
131 C2H    +  O          = CO   + CH         (M #131)    5.0E13   0.0       0.
132 C2H    +  OH         = HCCO + H          (M #132)    2.0E13   0.0       0.
133 C2H    +  O2         = CO   + HCO        (M #133)    2.4E12   0.0       0.
134 C2H    +  O2         = HCCO + O          (M #134)    6.0E11   0.0       0.
    END
```

where $k = A \cdot T^{n} \cdot \exp(-Ea/RT)$
Units are moles, cm^3, cal, K.

Glarborg et al. mechanism from COMBUSTION AND FLAME, vol 65, number 2, August 1986.

Reactions 78* and 79* went to "products" as published so assumed rxn products were used in this rxn set.

Rxn 78 CH + C2H4 = C3H4 + H based on CH + C2H2 = C3H2 + H
Rxn 79 CH + C2H6 = CH2 + C2H5 assume that methyne abstracts from C2H6

APPENDIX A.2 - HARRIS MECHANISM

```
ELEMENTS
  H   O   N   C
END
SPECIES
H       H2
O       OH      H2O
O2      HO2     H2O2
CH2     CH3     CH4
C2H     C2H2    C2H3    C2H4    C2H5    C2H6
CO      HCO     CH2O
HCCO    CH2CO   CO2
C3H2    C3H3    C3H4    C3H5    C3H6    C3H7U   C3H7S
C4H     C4H2    C4H3U   C4H3S   C4H4    C4H5U   C4H6    C4H7U   C4H8
C6H5U
C8H5SX
A1      A1-
A1C2H   A1C2H-  A1C2H*  A1C2H3  A1C2HC2H2
A2      A2-X
A2R5    A2R5-
N2
END
```

REACTIONS							A	n	Ea
1	H2	+OH	=	H2O	+H		(A01) 1.2E+09	1.3	3630
2	H2	+O	=	H	+OH		(A02) 1.5E+07	2.0	7550
3	H	+O2	=	O	+OH		(A03) 1.2E+17	-0.9	16620
4	H	+H	+M =	H2		+M	(A04) 9.0E+16	-0.6	0
5	H	+OH	+M =	H2O		+M	(A05) 2.2E+22	-2.0	0
6	H	+HO2	=	OH	+OH		(A06) 1.5E+14	0.0	1000
7	H	+HO2	=	H2	+O2		(A07) 2.5E+13	0.0	690
8	H	+HO2	=	H2O	+O		(A08) 1.0E+13	0.0	1073
9	H	+O2	+M =	HO2		+M	(A09) 2.3E+18	-0.8	0
10	HO2	+OH	=	H2O	+O2		(A10) 1.5E+13	0.0	0
11	HO2	+O	=	O2	+OH		(A11) 2.0E+13	0.0	0
12	HO2	+HO2	=	H2O2	+O2		(A12) 2.0E+12	0.0	0
13	H2O2	+H	=	HO2	+H2		(A13) 1.7E+12	0.0	3750
14	H2O2	+OH	=	H2O	+HO2		(A14) 1.0E+13	0.0	1800
15	H2O2		+M =	OH	+OH	+M	(A15) 1.2E+17	0.0	45500
16	OH	+OH	=	H2O	+O		(A16) 1.5E+09	1.1	0
17	CO	+OH	=	CO2	+H		(B01) 1.5E+07	1.3	-770
18	CO	+HO2	=	CO2	+OH		(B02) 1.5E+14	0.0	23650
19	CO2	+O	=	CO	+O2		(B03) 2.8E+12	0.0	43830
20	C2H3	+O2	=	HCO	+CH2O		(C01) 4.0E+12	0.0	-250
21	CH2O	+H	=	HCO	+H2		(C02) 1.0E+14	0.0	4950
22	CH2O	+OH	=	HCO	+H2O		(C03) 1.8E+13	0.0	440
23	CH2O	+O	=	HCO	+OH		(C04) 6.0E+13	0.0	3800

24	CH2O	+HO2	=	HCO	+H2O2		(C05)	1.0E+09	0.0	0
25	CH2O	+CH3	=	HCO	+CH4		(C06)	1.0E+11	0.0	6000
26	CH2O		+M =	HCO	+H	+M	(C07)	5.0E+16	0.0	76480
27	HCO		+M =	H	+CO	+M	(C08)	2.5E+13	0.0	16800
28	HCO	+H	=	CO	+H2		(C09)	7.2E+13	0.0	0
29	HCO	+OH	=	CO	+H2O		(C10)	5.0E+13	0.0	0
30	HCO	+O2	=	CO	+HO2		(C11)	5.0E+11	0.5	835
31	HCO	+O	=	CO	+OH		(C12)	3.0E+13	0.0	0
32	HCO	+O	=	CO2	+H		(C13)	3.0E+13	0.0	0
33	HCO	+CH3	=	CO	+CH4		(C14)	3.0E+11	0.5	0
34	CH2CO	+OH	=	CH2O	+HCO		(C15)	1.0E+13	0.0	0
35	CH2CO	+H	=	CH3	+CO		(C16)	7.0E+12	0.0	3010
36	CH2CO	+O	=	HCO	+HCO		(C17)	2.0E+13	0.0	2290
37	CH2CO		+M =	CH2	+CO	+M	(C18)	3.6E+15	0.0	59300
38	CH4		=	CH3	+H		(D01)	1.1E+33	-5.9	105150
39	CH4	+H	=	CH3	+H2		(D02)	7.2E+14	0.0	15100
40	CH4	+O	=	CH3	+OH		(D03)	6.9E+08	1.6	8540
41	CH4	+OH	=	CH3	+H2O		(D04)	5.7E+06	2.0	2640
42	CH4	+CH2	=	CH3	+CH3		(D05)	1.0E+13	0.0	0
43	CH4	+HO2	=	CH3	+H2O2		(D06)	2.0E+13	0.0	18000
44	CH3	+CH3	=	C2H5	+H		(D07)	7.8E+11	0.0	13039
45	CH3	+O2	=	CH2O	+OH		(D08)	1.5E+13	0.0	28700
46	CH3	+H	=	CH2	+H2		(D09)	7.2E+14	0.0	15100
47	CH3	+O	=	CH2O	+H		(D10)	8.4E+13	0.0	0
48	CH3	+CH3	=	C2H4	+H2		(D11)	1.0E+16	0.0	31792
49	CH3	+CH2	=	C2H4	+H		(D12)	2.0E+13	0.0	0
50	CH2	+O2	=	CO	+OH	+H	(D13)	1.3E+13	0.0	1450
51	C2H6	+H	=	C2H5	+H2		(E01)	1.3E+14	0.0	9370
52	C2H6	+O	=	C2H5	+OH		(E02)	1.8E+13	0.0	6100
53	C2H6	+OH	=	C2H5	+H2O		(E03)	6.3E+13	0.0	3600
54	C2H6	+CH3	=	C2H5	+CH4		(E04)	5.5E+14	0.0	21500
55	C2H6	+O2	=	C2H5	+HO2		(E05)	1.0E+13	0.0	51000
56	C2H6	+HO2	=	C2H5	+H2O2		(E06)	3.0E+11	0.0	11500
57	C2H6		=	CH3	+CH3		(E07)	2.0E+32	-5.0	92225
58	C2H5		=	C2H4	+H		(F01)	7.0E+25	-4.1	42984
59	C2H5	+O2	=	C2H4	+HO2		(F02)	1.5E+12	0.0	4860
60	C2H5	+CH3	=	C2H4	+CH4		(F03)	7.9E+11	0.0	0
61	C2H4		+M =	C2H2	+H2	+M	(F04)	3.0E+17	0.0	79280
62	C2H4		+M =	C2H3	+H	+M	(F05)	3.1E+17	0.0	98160
63	C2H4	+H	=	C2H3	+H2		(F06)	1.5E+14	0.0	10200
64	C2H4	+O	=	CH3	+HCO		(F07)	1.6E+09	1.2	740
65	C2H4	+OH	=	C2H3	+H2O		(F08)	1.0E+13	0.0	0
66	C2H4	+CH3	=	CH4	+C2H3		(F09)	4.2E+11	0.0	11200
67	C2H4	+O2	=	C2H3	+HO2		(F10)	4.0E+13	0.0	61500
68	C2H3	+H	=	C2H2	+H2		(G01)	1.0E+13	0.0	0
69	C2H3		=	C2H2	+H		(G02)	6.6E+19	-2.8	36130
70	C2H3	+CH3	=	C2H2	+CH4		(G03)	7.9E+11	0.0	0
71	C2H2		+M =	C2H	+H	+M	(G04)	4.1E+16	0.0	107000

72	C2H2	+H	=	C2H	+H2		(G05)	6.0E+13	0.0	23700
73	C2H2	+O	=	CH2	+CO		(G06)	7.0E+03	2.8	500
74	C2H2	+O	=	HCCO	+H		(G07)	1.4E+04	2.8	500
75	C2H2	+OH	=	CH2CO	+H		(G08)	1.0E+14	0.0	11500
76	C2H2	+OH	=	C2H	+H2O		(G09)	2.7E+14	0.0	15100
77	C2H	+O2	=	HCO	+CO		(G10)	2.4E+12	0.0	0
78	C2H	+O2	=	HCCO	+O		(G11)	6.0E+11	0.0	0
79	HCCO	+H	=	CH2	+CO		(G12)	1.5E+13	0.0	0
80	HCCO	+O	=	HCO	+CO		(G13)	1.2E+12	0.0	0
81	C3H7S		=	C3H5	+H2		(H01)	1.0E+13	0.0	30000
82	C3H7U		=	C3H6	+H		(H02)	1.0E+14	0.0	37280
83	C3H7S		=	C3H6	+H		(H03)	2.0E+14	0.0	38720
84	C3H7S	+O2	=	C3H6	+HO2		(H04)	1.0E+12	0.0	5000
85	C3H7U	+O2	=	C3H6	+HO2		(H05)	1.0E+12	0.0	5000
86	C3H6		+M =	C2H3	+CH3	+M	(H06)	1.0E+18	0.0	74000
87	C3H6		=	C3H5	+H		(H07)	1.0E+13	0.0	78000
88	C3H6	+H	=	C3H5	+H2		(H08)	5.0E+13	0.0	3500
89	C3H6	+OH	=	C3H5	+H2O		(H09)	2.0E+13	0.0	3060
90	C3H6	+O2	=	C3H5	+HO2		(H10)	1.0E+14	0.0	39000
91	C3H5		=	C3H4	+H		(H11)	4.0E+13	0.0	70000
92	C3H5	+CH3	=	C4H8			(H12)	1.3E+13	0.0	0
93	C3H5	+O2	=	C3H4	+HO2		(H13)	6.0E+11	0.0	10000
94	C3H5	+H	=	C3H4	+H2		(H14)	1.0E+13	0.0	0
95	C3H5	+C4H8	=	C4H7U	+C3H6		(H15)	7.9E+10	0.0	13500
96	C3H5	+C2H4	=	C3H6	+C2H3		(H16)	3.2E+12	0.0	18000
97	C3H4	+OH	=	CO	+C2H5		(H17)	5.0E+12	0.0	1291
98	C3H4	+H	=	CH3	+C2H2		(H18)	2.0E+13	0.0	2411
99	C3H4	+OH	=	HCO	+C2H4		(H19)	1.0E+12	0.0	0
100	C3H4	+O	=	CO	+C2H4		(H20)	1.5E+13	0.0	2103
101	C3H3	+H	=	C3H4			(H21)	2.0E+13	0.0	0
102	C3H3	+O	=	C3H2	+OH		(H22)	3.2E+12	0.0	0
103	C3H3	+O2	=	CH2CO	+HCO		(H23)	3.0E+10	0.0	2868
104	C3H2	+H	=	C3H3			(H24)	6.0E+12	0.0	0
105	C3H2	+O	=	C2H	+HCO		(H25)	6.8E+13	0.0	0
106	C3H2	+OH	=	C2H2	+HCO		(H26)	6.8E+13	0.0	0
107	C2H2	+CH2	=	C3H3	+H		(H27)	2.0E+12	0.0	0
108	C4H8		=	C4H7U	+H		(I01)	1.0E+19	0	90000
109	C4H8	+H	=	C4H7U	+H2		(I02)	5.0E+13	0	3900
110	C4H8	+CH3	=	C4H7U	+CH4		(I03)	1.0E+11	0	7300
111	C4H8	+OH	=	C3H7U	+CH2O		(I04)	1.5E+12	0	0
112	C4H8	+OH	=	C4H7U	+H2O		(I05)	1.4E+13	0	3060
113	C4H8	+O2	=	C4H7U	+HO2		(I06)	2.5E+13	0	49000
114	C2H5	+C2H3	=	C4H8			(I07)	8.9E+12	0	0
115	C2H5	+C2H2	=	C4H7U			(I08)	2.5E+10	0	7000
116	C4H7U		=	C4H6	+H		(J01)	1.2E+14	0	49300
117	C4H7U	+O2	=	C4H6	+HO2		(J02)	1.0E+11	0	0
118	C4H7U		=	C2H4	+C2H3		(J03)	1.0E+11	0	37000
119	C4H7U	+H	=	C4H6	+H2		(J04)	3.2E+13	0	0
120	C4H6	+OH	=	C2H5	+CH2CO		(J05)	1.0E+12	0	0

121	C4H6	+OH		= C3H5	+CH2O		(J06)	1.0E+12	0	0
122	C4H6	+O		= C2H4	+CH2CO		(J07)	1.0E+12	0	0
123	C4H6	+O		= C3H4	+CH2O		(J08)	1.0E+12	0	0
124	C4H6	+H		= C2H4	+C2H3		(J09)	5.0E+11	0	0
125	C4H6	+C2H3		= C2H4	+C2H3	+C2H2	(J10)	6.3E+13	0	14500
126	C4H5U	+H2		= C4H6	+H		(J11)	3.2E+12	0	19200
127	C2H3	+C2H3		= C4H6			(J12)	8.9E+12	0	0
128	C4H6	+H		= C4H4	+H2	+H	(K01)	1.0E+14	0	14500
129	C4H6	+C2H3		= C4H4	+C2H4	+H	(K02)	6.3E+13	0	14500
130	C4H5U			= C4H4	+H		(K03)	1.0E+14	0	41400
131	C4H4	+H		= C4H3U	+H2		(K04)	7.9E+13	0	14500
132	C4H4	+C2H		= C4H3U	+C2H2		(K05)	4.0E+13	0	0
133	C4H4	+C2H3		= C4H3U	+C2H4		(K06)	5.0E+11	0	16300
134	C4H4		+M	= C2H2	+C2H2	+M	(K07)	5.5E+08	0	0
135	C2H2	+C2H		= C4H3U			(K08)	3.9E+07	1.66	-1600
136	C2H3	+C2H2		= C4H4	+H		(K09)	1.6E+13	0	25060
137	C2H3	+C2H2		= C4H5U			(K10)	1.0E+13	0	8000
138	C4H4		+M	= C4H2	+H2	+M	(K11)	1.8E+08	0	0
139	C4H4	+H		= C4H3S	+H2		(K12)	3.1E+14	0	14500
140	C4H4	+C2H		= C4H3S	+C2H2		(K13)	4.0E+13	0	0
141	C4H4	+C2H3		= C4H3S	+C2H4		(K14)	5.0E+11	0	16300
142	C4H3S			= C4H3U			(K15)	1.0E+13	0	64000
143	C4H3U	+H		= C4H2	+H2		(L01)	1.0E+13	0	0
144	C4H3U		+M	= C4H2	+H	+M	(L02)	8.5E+15	0	60000
145	C4H2		+M	= C4H	+H	+M	(L03)	3.5E+17	0	80000
146	C4H2	+OH		= C3H2	+HCO		(L04)	6.7E+13	0	410
147	C4H2	+O		= C3H2	+CO		(L05)	7.9E+12	0	1350
148	C4H	+H2		= C4H2	+H		(L06)	4.0E+13	0	0
149	C2H2	+C2H		= C4H2	+H		(L07)	4.0E+13	0	0
150	C4H3S	+H		= C4H2	+H2		(L08)	1.0E+13	0	0
151	A1			= A1-	+H		(M01)	5.0E+15	0.0	108600
152	A1	+OH		= A1-	+H2O		(M02)	2.1E+13	0.0	4600
153	A1	+H		= A1-	+H2		(M03)	2.5E+14	0.0	16000
154	A1	+C2H		= A1-	+C2H2		(M04)	5.0E+13	0.0	16000
155	A1	+C2H3		= A1-	+C2H4		(M05)	5.0E+13	0.0	16000
156	C6H5U			= A1-			(M06)	1.0E+10	0.0	0
157	C4H5U	+C2H2		= A1	+H		(M07)	3.2E+11	0.0	3700
158	C4H3U	+C2H2		= C6H5U			(M08)	7.0E+11	0.0	0
159	A1C2H			= A1C2H*	+H		(N01)	5.0E+15	0.0	108600
160	A1C2H	+H		= A1C2H*	+H2		(N02)	2.5E+14	0.0	16000
161	A1C2H	+OH		= A1C2H*	+H2O		(N03)	1.2E+13	0.0	4600
162	A1C2H	+C2H3		= A1C2H*	+C2H4		(N04)	5.0E+13	0.0	16000
163	A1C2H	+C2H		= A1C2H*	+C2H2		(N05)	5.0E+13	0.0	16000
164	A1C2H			= A1C2H-	+H		(N06)	5.0E+15	0.0	108600
165	A1C2H	+H		= A1C2H-	+H2		(N07)	2.5E+14	0.0	16000
166	A1C2H	+OH		= A1C2H-	+H2O		(N08)	2.1E+13	0.0	4600
167	A1C2H	+C2H3		= A1C2H-	+C2H4		(N09)	5.0E+13	0.0	16000
168	A1C2H	+C2H		= A1C2H-	+C2H2		(N10)	5.0E+13	0.0	16000

169	A1	+C2H	= A1C2H	+H	(N11)	1.0E+12	0.0	0
170	A1	+C2H3	= A1C2H3	+H	(N12)	1.0E+12	0.0	0
171	A1-	+C2H	= A1C2H		(N13)	1.0E+13	0.0	0
172	A1-	+C2H3	= A1C2H3		(N14)	1.0E+13	0.0	0
173	A1-	+C2H2	= A1C2H	+H	(N15)	3.2E+11	0.0	1350
174	A1-	+C4H2	= A1C2H	+C2H	(N16)	3.2E+11	0.0	1350
175	A1-	+C4H4	= A1C2H	+C2H3	(N17)	3.2E+11	0.0	1350
176	A1-	+C2H4	= A1C2H3	+H	(N18)	3.2E+11	0.0	1900
177	A1-	+C4H4	= A1C2H3	+C2H	(N19)	3.2E+11	0.0	1900
178	A1-	+C4H6	= A1C2H3	+C2H3	(N20)	3.2E+11	0.0	1900
179	C8H5SX		= A1C2H-		(N21)	1.0E+10	0.0	0
180	C4H3U	+C4H2	= C8H5SX		(N22)	7.0E+11	0.0	0
181	A2R5		= A2R5-	+H	(O01)	5.0E+15	0.0	108600
182	A2R5	+H	= A2R5-	+H2	(O02)	2.5E+14	0.0	16000
183	A2R5	+OH	= A2R5-	+H2O	(O03)	2.1E+13	0.0	4600
184	A2R5	+C2H	= A2R5-	+C2H2	(O04)	5.0E+13	0.0	16000
185	A2R5	+C2H3	= A2R5-	+C2H4	(O05)	5.0E+13	0.0	16000
186	A2		= A2-X	+H	(O06)	5.0E+15	0.0	108600
187	A2	+OH	= A2-X	+H2O	(O07)	2.1E+13	0.0	4600
188	A2	+C2H3	= A2-X	+C2H4	(O08)	5.0E+13	0.0	16000
189	A2	+C2H	= A2-X	+C2H2	(O09)	5.0E+13	0.0	16000
190	A2-X	+C2H2	= A2R5	+H	(O10)	3.2E+11	0.0	1350
191	A2	+H	= A2-X	+H2	(O11)	2.5E+14	0.0	16000
192	A1C2HC2H2		= A2-X		(O12)	1.0E+10	0.0	0
193	A1C2H*	+C2H2	= A1C2HC2H2		(O13)	1.0E+13	0.0	0

END

where $k = A \cdot T^{n} \cdot \exp(-Ea/RT)$

Units are moles, cm^3, cal, K.

Mechanism taken from "Formation of Small Aromatic Molecules in a Sooting Ethylene Flame", Stephen J. Harris, Anita M. Weiner, and Richard J. Blint, Combustion and Flame 72:91-109 (1988).

The following are changes made to the published mechanism:

Errors:

- Rxn (H06) A-factor 1.0F18 entered as 1.0E+18.
- Rxn (H08) A-factor 5.01E+13 entered as 5.0E+13.
- Rxn (H09) Reactant C6 entered as C3H6.
- Rxn (H15) A-factor 7.9F10 entered as 7.9E+10.
- Rxn (J08) Product C3H3 entered as C3H4 to satisfy atom balance.
- Rxn (J10) Products C2H4+C2H2+C2H2 entered as C2H4+C2H3+C2H2.
- Rxn (K10) A-factor 1.0E-13 entered as 1.0E+13.
- Rxn (K15) Product H deleted from reaction to satisfy atom balance.

Other changes:

- Rxn (K06) replaced rate parameters 1.7E+93 -20.5 139000 with rate constant evaluated at 1630K = 5.5E+08. (intpreter couldn't handle E+93).
- Rxn (K11) same as (K06), replaced 5.6E+92 -20.5 139000 with 1.8E+08.

APPENDIX A.3 - THERMODYNAMIC DATABASE

```
   300.000  1000.000  5000.000
C                 121086C   1               G  0300.00   5000.00  1000.00      1
 2.60208750E+00-1.78708127E-04 9.08704081E-08-1.14993327E-11 3.31084400E-16    2
 8.54215391E+04 4.19517708E+00 2.49858475E+00 8.08577679E-05-2.69769714E-07    3
 3.04072934E-10-1.10665180E-13 8.54587813E+04 4.75345898E+00                   4
C(S)              121286C   1               S  0300.00   5000.00  1000.00      1
 1.49016643E+00 1.66212558E-03-6.68720418E-07 1.29087963E-10-9.20533384E-15    2
-7.07401856E+02-8.71778488E+00-6.70566082E-01 7.18149962E-03-5.63292133E-06    3
 2.14229878E-09-4.16856220E-13-7.33949814E+01 2.60159564E+00                   4
C+                120186C   1E  -1          G  0300.00   5000.00  1000.00      1
 2.51182747E+00-1.73597837E-05 9.50426760E-09-2.21885184E-12 1.86218923E-16    2
 2.16677203E+05 4.28612995E+00 2.59538388E+00-4.06866457E-04 6.89236686E-07    3
-5.26648780E-10 1.50833773E-13 2.16662813E+05 3.89572978E+00                   4
C-                121686C   1E   1          G  0300.00   5000.00  1000.00      1
 2.99022126E+00-9.18459613E-04 5.05556045E-07-7.70341013E-11 3.16327144E-15    2
 6.98393125E+04 1.25945330E+00 2.78390265E+00-1.77428755E-03 3.69676059E-06    3
-3.06669334E-09 8.63762187E-13 6.99851094E+04 2.72628117E+00                   4
C2                121286C   2               G  0300.00   5000.00  1000.00      1
 4.13597870E+00 6.53161842E-05 1.83709915E-07-5.29508520E-11 4.71213704E-15    2
 9.96727188E+04 7.47292280E-01 6.99604511E+00-7.40060164E-03 3.23470385E-06    3
 4.80253481E-09-3.29591758E-12 9.89748672E+04-1.38622685E+01                   4
C2-               121286C   2E   1          G  0300.00   5000.00  1000.00      1
 3.79689145E+00 2.53004982E-04 9.70911813E-08-1.61480378E-11-3.21289325E-17    2
 5.20798086E+04 1.65814674E+00 3.46801186E+00-2.35287458E-04 1.24391227E-06    3
 4.70596062E-10-8.16427384E-13 5.23121523E+04 3.88669920E+00                   4
C2H                20387C   2H   1          G  0300.00   5000.00  1000.00      1
 4.42768812E+00 2.21626856E-03-6.04895263E-07 9.88251703E-11-7.35117957E-15    2
 6.59041484E+04-1.19944179E+00 3.05066776E+00 6.05167449E-03-4.95663426E-06    3
 2.80415913E-09-8.19333208E-13 6.63001094E+04 5.95436096E+00                   4
C2H2              121386C   2H   2          G  0300.00   5000.00  1000.00      1
 4.43677044E+00 5.37603907E-03-1.91281674E-06 3.28637895E-10-2.15670953E-14    2
 2.56676641E+04-2.80033827E+00 2.01356220E+00 1.51904458E-02-1.61631888E-05    3
 9.07899178E-09-1.91274600E-12 2.61244434E+04 8.80537796E+00                   4
C2H3               12787C   2H   3          G  0300.00   5000.00  1000.00      1
 5.93346787E+00 4.01774561E-03-3.96673954E-07-1.44126655E-10 2.37864351E-14    2
 3.18543457E+04-8.53031254E+00 2.45927644E+00 7.37147639E-03 2.10987287E-06    3
-1.32164213E-09-1.18478383E-12 3.33522500E+04 1.15562019E+01                   4
C2H4              121286C   2H   4          G  0300.00   5000.00  1000.00      1
 3.52841878E+00 1.14851845E-02-4.41838529E-06 7.84460053E-10-5.26684849E-14    2
 4.42828857E+03 2.23038912E+00-8.61487985E-01 2.79616285E-02-3.38867721E-05    3
 2.78515220E-08-9.73787891E-12 5.57304590E+03 2.42114868E+01                   4
C2H5               12387C   2H   5          G  0300.00   5000.00  1000.00      1
 7.19048023E+00 6.48407731E-03-6.42806469E-07-2.34787939E-10 3.88087728E-14    2
 1.06745488E+04-1.47808924E+01 2.69070172E+00 8.71913321E-03 4.41983866E-06    3
 9.33870314E-10-3.92777347E-12 1.28704043E+04 1.21381950E+01                   4
C2H6              121686C   2H   6          G  0300.00   4000.00  1000.00      1
 4.82593823E+00 1.38404286E-02-4.55725876E-06 6.72496725E-10-3.59816140E-14    2
-1.27177930E+04-5.23950672E+00 1.46253872E+00 1.54946670E-02 5.78050731E-06    3
-1.25783188E-08 4.58626713E-12-1.12391758E+04 1.44322949E+01                   4
C2N               121286C   2N   1          G  0300.00   5000.00  1000.00      1
```

```
 6.15156126E+00 1.51164969E-03-6.62936202E-07 1.28614841E-10-9.16082988E-15    2
 6.48431797E+04-8.17784977E+00 3.49854446E+00 8.55443254E-03-6.28869702E-06    3
 8.63847771E-10 4.91599600E-13 6.55661094E+04 5.54837418E+00                   4
C2N2             121286C   2N   2          G  0300.00   5000.00  1000.00     1
 6.54800272E+00 3.98470741E-03-1.63421635E-06 3.03859660E-10-2.11106902E-14    2
 3.49071641E+04-9.73579025E+00 4.26545906E+00 1.19225690E-02-1.34201418E-05    3
 9.19229670E-09-2.77894179E-12 3.54788750E+04 1.71321237E+00                   4
C2O              121286C   2O   1          G  0300.00   5000.00  1000.00     1
 4.84980917E+00 2.94758519E-03-1.09072869E-06 1.79256235E-10-1.11575847E-14    2
 3.28205547E+04-6.45322561E-01 3.36885071E+00 8.24180339E-03-8.76514514E-06    3
 5.56926194E-09-1.54000868E-12 3.31708125E+04 6.71331406E+00                   4
C3               121286C   3            G  0300.00   5000.00  1000.00     1
 3.80370951E+00 2.25356664E-03-7.70453482E-07 1.31629388E-10-8.69426381E-15    2
 9.73613516E+04 6.12806273E+00 4.34552765E+00 1.26446609E-03-4.65255698E-06    3
 8.69585559E-09-4.24353564E-12 9.73140313E+04 3.51943731E+00                   4
C3H2             121686C   3H   2          G  0300.00   5000.00  1000.00     1
 6.53085327E+00 5.87031618E-03-1.72077671E-06 2.12749790E-10-8.29191045E-15    2
 5.11521367E+04-1.12272778E+01 2.69107723E+00 1.48036638E-02-3.25055135E-06    3
-8.64436345E-09 5.28487757E-12 5.21907188E+04 8.75739098E+00                   4
C3H3             121686C   3H   3          G  0300.00   3000.00  1000.00     1
 8.09162521E+00 3.73728504E-03 1.38866471E-06-1.22986044E-09 2.06815847E-13    2
 3.54377930E+04-1.82044678E+01 2.50973225E+00 1.71038657E-02-4.57108581E-06    3
-8.28415736E-09 5.43622872E-12 3.70406797E+04 1.10112639E+01                   4
C3H4              40687C   3H   4          G  0300.00   5000.00  1000.00     1
 5.72914410E+00 1.23680448E-02-4.80562676E-06 8.60136407E-10-5.81280223E-14    2
 2.01298418E+04-9.44866753E+00-2.13196874E-01 3.35871354E-02-3.80487036E-05    3
 2.74583787E-08-8.69004434E-12 2.16204844E+04 2.02939262E+01                   4
C3H4C            121686C   3H   4          G  0300.00   5000.00  1000.00     1
 6.69999313E+00 1.03573725E-02-3.45511671E-06 5.06529485E-10-2.66822765E-14    2
 3.01990508E+04-1.33919334E+01-2.46210471E-02 2.31972151E-02-1.84743567E-06    3
-1.59275935E-08 8.68461553E-12 3.23341367E+04 2.27165985E+01                   4
C3H4P             40687C   3H   4          G  0300.00   5000.00  1000.00     1
 5.51103449E+00 1.24695618E-02-4.81416464E-06 8.57376947E-10-5.77156121E-14    2
 1.96196738E+04-1.07947483E+01 6.27144694E-01 3.11617889E-02-3.74766387E-05    3
 2.96411784E-08-9.98738158E-12 2.08349277E+04 1.34687958E+01                   4
C3H5             120186C   3H   5          G  0300.00   5000.00  1000.00     1
 7.90919781E+00 1.21152550E-02-4.11758629E-06 6.15667961E-10-3.32357331E-14    2
 1.23541563E+04-1.96723328E+01-5.41004002E-01 2.72841007E-02-9.63653292E-07    3
-1.91294625E-08 9.83941748E-12 1.51303945E+04 2.60673370E+01                   4
C3H6             120186C   3H   6          G  0300.00   5000.00  1000.00     1
 6.73225689E+00 1.49083361E-02-4.94989945E-06 7.21202209E-10-3.76620427E-14    2
-9.23570313E+02-1.33133478E+01 1.49330711E+00 2.09251754E-02 4.48679384E-06    3
-1.66891212E-08 7.15814647E-12 1.07482642E+03 1.61453400E+01                   4
C3H7U            BCT 81C   3H   7    0    0G    300.000  5000.000             1
 0.79782906E+01 0.15761133E-01-0.51732432E-05 0.74438922E-09-0.38249782E-13    2
 0.75794023E+04-0.19356110E+02 0.19225368E+01 0.24789274E-01 0.18102492E-05    3
-0.17832658E-07 0.85829963E-11 0.97132812E+04 0.13992715E+02                   4
C3H7S            BCT 81C   3H   7    0    0G    300.000  5000.000             1
 0.80633688E+01 0.15744876E-01-0.51823918E-05 0.74772455E-09-0.38544221E-13    2
 0.53138711E+04-0.21926468E+02 0.17132998E+01 0.25426164E-01 0.15808082E-05    3
-0.18212862E-07 0.88277103E-11 0.75358086E+04 0.12979008E+02                   4
C3H8             120186C   3H   8          G  0300.00   5000.00  1000.00     1
```

```
 7.52521706E+00 1.88903399E-02-6.28392445E-06 9.17937282E-10-4.81240990E-14    2
-1.64645469E+04-1.78439026E+01 8.96920800E-01 2.66898610E-02 5.43142505E-06    3
-2.12600071E-08 9.24333006E-12-1.39549180E+04 1.93553314E+01                   4
C3O2              121286C   3O   2          G  0300.00   5000.00  1000.00     1
 8.09889698E+00 5.56003954E-03-2.31226477E-06 4.34070946E-10-3.03638747E-14    2
-1.42143525E+04-1.52197447E+01 4.01812744E+00 1.83666069E-02-1.90714800E-05    3
 1.18558710E-08-3.41874771E-12-1.31282363E+04 5.58208370E+00                   4
C4                121286C   4              G  0300.00   5000.00  1000.00     1
 6.50018025E+00 4.22863197E-03-1.79071765E-06 3.40481254E-10-2.40397844E-14    2
 1.14340078E+05-1.14888945E+01 2.34302807E+00 1.64298117E-02-1.52798584E-05    3
 7.34382644E-09-1.58227424E-12 1.15453844E+05 9.82620430E+00                   4
C4H               121686C   4H   1          G  0300.00   5000.00  1000.00     1
 6.24288178E+00 6.19368255E-03-2.08593156E-06 3.08220338E-10-1.63648256E-14    2
 7.56801875E+04-7.21080589E+00 5.02324677E+00 7.09237531E-03-6.07376194E-09    3
-2.27575225E-09 8.08699407E-13 7.62381250E+04-6.94259405E-02                   4
C4H2              121686C   4H   2          G  0300.00   5000.00  1000.00     1
 9.03140736E+00 6.04725257E-03-1.94878885E-06 2.75486300E-10-1.38560801E-14    2
 5.29473555E+04-2.38506775E+01 4.00519180E+00 1.98100023E-02-9.86587747E-06    3
-6.63515820E-09 6.07741288E-12 5.42406484E+04 1.84573650E+00                   4
C4H3U             121686C   4H   3          G  0300.00   5000.00  1000.00     1
 8.48742008E+00 8.69089365E-03-2.85444367E-06 4.12007983E-10-2.13010931E-14    2
 4.79705547E+04-1.90185089E+01 3.55397129E+00 1.94619857E-02-4.81024836E-06    3
-9.73012249E-09 6.23905355E-12 4.94538633E+04 7.08298683E+00                   4
C4H3S             DUPC4 C   4H   3          G  0300.00   5000.00  1000.00     1
 8.48742008E+00 8.69089365E-03-2.85444367E-06 4.12007983E-10-2.13010931E-14    2
 4.79705547E+04-1.90185089E+01 3.55397129E+00 1.94619857E-02-4.81024836E-06    3
-9.73012249E-09 6.23905355E-12 4.94538633E+04 7.08298683E+00                   4
C4H4              121686C   4H   4          G  0300.00   5000.00  1000.00     1
 8.89214897E+00 1.09088495E-02-3.59495971E-06 5.19341903E-10-2.68089214E-14    2
 3.32843477E+04-2.17269440E+01 2.14033699E+00 2.46050470E-02-3.63916570E-06    3
-1.53040141E-08 8.89646083E-12 3.53740000E+04 1.42824774E+01                   4
C4H5U             PW8/85C   4H   5          G 300.      5000.                   1
+6.34900000D+00+1.88400003D-02-8.10899980D-06+1.32399999D-09+0.00000000D+00    2
+3.94400000D+04-7.50400000D+00-2.25500000D+00+5.50700008D-02-6.53099984D-05    3
+4.13900005D-08-1.04900001D-11+4.10900000D+04+3.35600000D+01                   4
C4H6              120186C   4H   6          G  0300.00   5000.00  1000.00     1
 8.04658318E+00 1.64852515E-02-5.52222718E-06 8.12359291E-10-4.29507843E-14    2
 1.37013047E+04-1.80045776E+01 3.19710827E+00 2.02559158E-02 6.51019218E-06    3
-1.65844227E-08 6.40028221E-12 1.57152031E+04 9.89566040E+00                   4
C4H7U             PW8/85C   4H   7          G 300.      5000.                   1
+3.20300000D+00+2.93500004D-02-1.29499997D-05+2.06999999D-09+0.00000000D+00    2
+2.68600000D+04+1.10800000D+01+9.36200000D-01+3.67800005D-02-2.06199995D-05    3
+4.55599997D-09+0.00000000D+00+2.73400000D+04+2.23000000D+01                   4
C4H8              120386C   4H   8          G  0300.00   5000.00  1000.00     1
 2.05358410E+00 3.43505070E-02-1.58831972E-05 3.30896621E-09-2.53610447E-13    2
-2.13972315E+03 1.55432015E+01 1.18113804E+00 3.08533795E-02 5.08652465E-06    3
-2.46548879E-08 1.11101926E-11-1.79040039E+03 2.10624695E+01                   4
C5                121286C   5              G  0300.00   5000.00  1000.00     1
 8.07808113E+00 5.74346446E-03-2.43640534E-06 4.63891592E-10-3.27890960E-14    2
 1.14702156E+05-1.95302391E+01 2.11527371E+00 2.32633166E-02-2.10949893E-05    3
 9.07273368E-09-1.54009260E-12 1.16273813E+05 1.09760265E+01                   4
C5H                20387C   5H   1          G  0300.00   5000.00  1000.00     1
```

```
 8.69574928E+00 6.05430082E-03-2.01601051E-06 2.89289259E-10-1.47009954E-14    2
 9.03106875E+04-2.10159454E+01 1.63482475E+00 2.50953808E-02-1.20663644E-05    3
-1.04651106E-08 8.80998833E-12 9.21248750E+04 1.51219368E+01                   4
C5H12              20387C   5H  12          G  0300.00   4000.00  1000.00     1
 1.66779785E+01 2.11448297E-02-3.53332143E-06-5.74220227E-10 1.51594828E-13    2
-2.55366992E+04-6.37294006E+01 1.87790775E+00 4.12164554E-02 1.25323368E-05    3
-3.70153686E-08 1.52556856E-11-2.00381563E+04 1.87725678E+01                   4
C5H2               20587C   5H   2          G  0300.00   5000.00  1000.00     1
 1.13291750E+01 7.42405653E-03-2.62818867E-06 4.08254097E-10-2.30133261E-14    2
 7.87870625E+04-3.61711731E+01 3.06232166E+00 2.70999819E-02-1.00916968E-05    3
-1.27274511E-08 9.16721907E-12 8.11496875E+04 7.07107830E+00                   4
C5H3               20387C   5H   3          G  0300.00   5000.00  1000.00     1
 1.07876225E+01 9.53961909E-03-3.20674462E-06 4.73332262E-10-2.51213540E-14    2
 6.39290430E+04-3.00544434E+01 4.32872009E+00 2.35248022E-02-5.85672296E-06    3
-1.21544943E-08 7.72647831E-12 6.58853125E+04 4.17325878E+00                   4
C5H6               20387C   5H   6          G  0300.00   5000.00  1000.00     1
 9.68981457E+00 1.83826201E-02-6.26488418E-06 9.39337719E-10-5.08770814E-14    2
 1.10212422E+04-3.12290802E+01-3.19673920E+00 4.08136100E-02 6.81650533E-07    3
-3.13745900E-08 1.57722307E-11 1.52906758E+04 3.86993866E+01                   4
C6H                121686C   6H   1          G  0300.00   5000.00  1000.00     1
 1.15873518E+01 7.29536265E-03-2.46600848E-06 3.40704576E-10-1.49818546E-14    2
 1.03144813E+05-3.17257843E+01 4.76984787E+00 2.45727897E-02-7.56125246E-06    3
-1.48069077E-08 9.76805355E-12 1.04852313E+05 3.24153042E+00                   4
C6H10              20387C   6H  10          G  0300.00   5000.00  1000.00     1
 1.59277706E+01 2.37441287E-02-6.90867182E-06 8.10977729E-10-2.68312255E-14    2
-8.64265625E+03-6.52518616E+01-1.39422798E+00 4.72069308E-02 1.19604192E-05    3
-4.16289581E-08 1.74033565E-11-2.21779004E+03 3.12960358E+01                   4
C6H14              20387C   6H  14          G  0300.00   4000.00  1000.00     1
 2.28047180E+01 2.09798925E-02-3.53067389E-06-5.46624523E-10 1.47894988E-13    2
-3.07375664E+04-9.58316193E+01 1.83617401E+00 5.09846136E-02 1.25958568E-05    3
-4.42836239E-08 1.87223709E-11-2.29274961E+04 2.08814545E+01                   4
C6H2               121686C   6H   2          G  0300.00   5000.00  1000.00     1
 1.27565193E+01 8.03438108E-03-2.61821515E-06 3.72506026E-10-1.87885088E-14    2
 8.07546875E+04-4.04126282E+01 5.75108528E+00 2.63671987E-02-1.16675956E-05    3
-1.07144977E-08 8.79029748E-12 8.26201250E+04-4.33553219E+00                   4
C6H3               20387C   6H   3          G  0300.00   5000.00  1000.00     1
 1.27611809E+01 1.03855729E-02-3.47919286E-06 5.10973264E-10-2.69096506E-14    2
 7.47770625E+04-3.89174500E+01 5.00708962E+00 2.69285180E-02-5.91986554E-06    3
-1.52723345E-08 9.40831007E-12 7.71320000E+04 2.22562122E+00                   4
C6H4               20387C   6H   4          G  0300.00   5000.00  1000.00     1
 1.00627413E+01 1.69030428E-02-6.47304569E-06 1.12408061E-09-7.30756601E-14    2
 5.64537305E+04-2.96931000E+01-1.30048466E+00 3.86647657E-02-3.64394418E-06    3
-2.66858073E-08 1.45093573E-11 6.00290742E+04 3.12493897E+01                   4
C6H6               20387C   6H   6          G  0300.00   5000.00  1000.00     1
 1.29107399E+01 1.72329657E-02-5.02421062E-06 5.89349680E-10-1.94752119E-14    2
 3.66451172E+03-5.00269928E+01-3.13801193E+00 4.72310297E-02-2.96220787E-06    3
-3.26281899E-08 1.71869186E-11 8.89003125E+03 3.65757294E+01                   4
C8H                121686C   8H   1          G  0300.00   5000.00  1000.00     1
 1.47499065E+01 9.93150100E-03-3.37484107E-06 4.68759254E-10-2.07353598E-14    2
 1.39944813E+05-4.89268951E+01 4.48950768E+00 3.52152102E-02-1.01938977E-05    3
-2.19702478E-08 1.42141646E-11 1.42599188E+05 3.99622536E+00                   4
C8H2               121686C   8H   2          G  0300.00   5000.00  1000.00     1
```

```
 1.56802130E+01 1.11546144E-02-3.72437262E-06 5.19789101E-10-2.37555032E-14    2
 1.08112250E+05-5.57143707E+01 4.63042736E+00 3.93708013E-02-1.14803479E-05    3
-2.56221355E-08 1.67079128E-11 1.10828500E+05 8.07742477E-01                   4
CH                121286C   1H   1          G  0300.00   5000.00  1000.00     1
 2.19622326E+00 2.34038103E-03-7.05820128E-07 9.00758218E-11-3.85504007E-15    2
 7.08672344E+04 9.17837334E+00 3.20020247E+00 2.07287562E-03-5.13443138E-06    3
 5.73389025E-09-1.95553318E-12 7.04525938E+04 3.33158779E+00                   4
CH+               121286C   1H   1E -1     G  0300.00   5000.00  1000.00     1
 2.75335789E+00 1.55289972E-03-5.36845334E-07 8.92177235E-11-5.41680069E-15    2
 1.94846703E+05 4.65489197E+00 3.32720709E+00 1.34705054E-03-3.89586148E-06    3
 5.12939025E-09-2.05457591E-12 1.94645234E+05 1.40847373E+00                   4
CH2               120186C   1H   2          G  0250.00   4000.00  1000.00     1
 3.63640785E+00 1.93305663E-03-1.68701632E-07-1.00989939E-10 1.80825576E-14    2
 4.53413398E+04 2.15656066E+00 3.76223707E+00 1.15981908E-03 2.48958543E-07    3
 8.80083562E-10-7.33243544E-13 4.53679063E+04 1.71257758E+00                   4
CH2(S)             31287C   1H   2          G  0300.00   4000.00  1000.00     1
 3.55288863E+00 2.06678826E-03-1.91411601E-07-1.10467337E-10 2.02134960E-14    2
 4.98497539E+04 1.68657005E+00 3.97126508E+00-1.69908875E-04 1.02536887E-06    3
 2.49255083E-09-1.98126628E-12 4.98936758E+04 5.75320721E-02                   4
CH2CO             121686C   2H   2O   1     G  0300.00   5000.00  1000.00     1
 6.03881741E+00 5.80484048E-03-1.92095376E-06 2.79448464E-10-1.45886755E-14    2
-8.58340234E+03-7.65758133E+00 2.97497082E+00 1.21187121E-02-2.34504569E-06    3
-6.46668497E-09 3.90564924E-12-7.63263672E+03 8.67355251E+00                   4
CH2HCO            120186O   1H   3C   2     G  0300.00   5000.00  1000.00     1
 5.97566986E+00 8.13059136E-03-2.74362446E-06 4.07030409E-10-2.17601714E-14    2
 4.90321777E+02-5.04525089E+00 3.40906239E+00 1.07385740E-02 1.89149250E-06    3
-7.15858306E-09 2.86738515E-12 1.52147656E+03 9.55829048E+00                   4
CH2O              121286C   1H   2O   1     G  0300.00   5000.00  1000.00     1
 2.99560618E+00 6.68132119E-03-2.62895469E-06 4.73715289E-10-3.21251747E-14    2
-1.53203691E+04 6.91257238E+00 1.65273118E+00 1.26314387E-02-1.88816848E-05    3
 2.05003143E-08-8.41323712E-12-1.48654043E+04 1.37848196E+01                   4
CH2OH             120186H   3C   1O   1     G  0250.00   4000.00  1000.00     1
 6.32752037E+00 3.60827078E-03-3.20154726E-07-1.93874999E-10 3.50970473E-14    2
-4.47450928E+03-8.32936573E+00 2.86262846E+00 1.00152725E-02-5.28543581E-07    3
-5.13853982E-09 2.24604103E-12-3.34967871E+03 1.03979378E+01                   4
CH3               121286C   1H   3          G  0300.00   5000.00  1000.00     1
 2.84405160E+00 6.13797410E-03-2.23034522E-06 3.78516080E-10-2.45215903E-14    2
 1.64378086E+04 5.45269728E+00 2.43044281E+00 1.11240987E-02-1.68022034E-05    3
 1.62182872E-08-5.86495262E-12 1.64237813E+04 6.78979397E+00                   4
CH3CO             120186C   2H   3O   1     G  0300.00   5000.00  1000.00     1
 5.61227894E+00 8.44988599E-03-2.85414717E-06 4.23837632E-10-2.26840370E-14    2
-5.18786328E+03-3.27494907E+00 3.12527847E+00 9.77822021E-03 4.52144832E-06    3
-9.00946162E-09 3.19371786E-12-4.10850781E+03 1.12288542E+01                   4
CH3HCO            120186C   2O   1H   4     G  0300.00   5000.00  1000.00     1
 5.86865044E+00 1.07942410E-02-3.64553034E-06 5.41291234E-10-2.89684421E-14    2
-2.26456875E+04-6.01294613E+00 2.50569534E+00 1.33699067E-02 4.67195332E-06    3
-1.12814007E-08 4.26356606E-12-2.12458867E+04 1.33508873E+01                   4
CH3O              121686C   1H   3O   1     G  0300.00   3000.00  1000.00     1
 3.77079964E+00 7.87149742E-03-2.65638391E-06 3.94443145E-10-2.11261638E-14    2
 1.27832520E+02 2.92957497E+00 2.10620403E+00 7.21659511E-03 5.33847197E-06    3
-7.37763628E-09 2.07561052E-12 9.78601074E+02 1.31521769E+01                   4
CH3OH             121686C   1H   4O   1     G  0300.00   5000.00  1000.00     1
```

```
 4.02906132E+00 9.37659293E-03-3.05025424E-06 4.35879333E-10-2.22472323E-14    2
-2.61579102E+04 2.37819576E+00 2.66011524E+00 7.34150782E-03 7.17005059E-06    3
-8.79319373E-09 2.39057038E-12-2.53534844E+04 1.12326307E+01                   4
CH4               121286C   1H   4          G  0300.00   5000.00  1000.00     1
 1.68347883E+00 1.02372356E-02-3.87512864E-06 6.78558487E-10-4.50342312E-14    2
-1.00807871E+04 9.62339497E+00 7.78741479E-01 1.74766835E-02-2.78340904E-05    3
 3.04970804E-08-1.22393068E-11-9.82522852E+03 1.37221947E+01                   4
CN                121286C   1N   1          G  0300.00   5000.00  1000.00     1
 3.72011972E+00 1.51835062E-04 1.98738107E-07-3.79837134E-11 1.32822961E-15    2
 5.11162617E+04 2.88859725E+00 3.66320419E+00-1.15652906E-03 2.16340891E-06    3
 1.85420818E-10-8.21469520E-13 5.12811797E+04 3.73901558E+00                   4
CN+               121286C   1N   1E  -1     G  0300.00   5000.00  1000.00     1
 3.70146298E+00 7.48293125E-04-1.79017306E-07 2.36636839E-11-1.43703671E-15    2
 2.15596641E+05 4.10867834E+00 3.11865711E+00 1.55325816E-03-9.48776403E-07    3
 1.47950052E-09-9.09676306E-13 2.15851234E+05 7.45625448E+00                   4
CN-               121286C   1N   1E   1     G  0300.00   5000.00  1000.00     1
 2.98127675E+00 1.46477274E-03-5.67273730E-07 1.01762258E-10-6.87093052E-15    2
 6.34609815E+03 6.17169285E+00 3.27899528E+00 1.46419159E-03-3.92589936E-06    3
 5.62987479E-09-2.47349667E-12 6.27950879E+03 4.56897211E+00                   4
CN2               121686C   1N   2          G  0300.00   5000.00  1000.00     1
 5.56706429E+00 2.10050144E-03-9.01051749E-07 1.71857167E-10-1.20625513E-14    2
 5.48996836E+04-5.63005400E+00 3.03996372E+00 8.81210528E-03-7.60550847E-06    3
 3.55435748E-09-8.74609955E-13 5.56326836E+04 7.55529785E+00                   4
CNN               121286C   1N   2          G  0300.00   5000.00  1000.00     1
 4.78593016E+00 2.55955383E-03-1.00313264E-06 1.80714888E-10-1.22738267E-14    2
 6.87041094E+04-2.95395702E-01 3.52443600E+00 7.27192313E-03-8.27269832E-06    3
 5.62870461E-09-1.64157587E-12 6.89964688E+04 5.93244457E+00                   4
CO                121286C   1O   1          G  0300.00   5000.00  1000.00     1
 3.02507806E+00 1.44268852E-03-5.63082779E-07 1.01858133E-10-6.91095156E-15    2
-1.42683496E+04 6.10821772E+00 3.26245165E+00 1.51194085E-03-3.88175522E-06    3
 5.58194424E-09-2.47495123E-12-1.43105391E+04 4.84889698E+00                   4
CO2               121286C   1O   2          G  0300.00   5000.00  1000.00     1
 4.45362282E+00 3.14016873E-03-1.27841054E-06 2.39399667E-10-1.66903319E-14    2
-4.89669609E+04-9.55395877E-01 2.27572465E+00 9.92207229E-03-1.04091132E-05    3
 6.86668678E-09-2.11728009E-12-4.83731406E+04 1.01884880E+01                   4
CO2-              121286C   1O   2E   1     G  0300.00   5000.00  1000.00     1
 4.61057377E+00 2.53296224E-03-1.07016524E-06 2.02677084E-10-1.42495811E-14    2
-5.47988164E+04 1.44962955E+00 2.63707733E+00 7.80323008E-03-8.19618708E-06    3
 6.53789689E-09-2.52021993E-12-5.41677266E+04 1.18895493E+01                   4
E                 120186E   1          G  0300.00   5000.00  1000.00     1
 2.50000000E+00 0.00000000E+00 0.00000000E+00 0.00000000E+00 0.00000000E+00    2
-7.45374939E+02-1.17340260E+01 2.50000000E+00 0.00000000E+00 0.00000000E+00    3
 0.00000000E+00 0.00000000E+00-7.45375000E+02-1.17340260E+01                   4
H                 120186H   1          G  0300.00   5000.00  1000.00     1
 2.50000000E+00 0.00000000E+00 0.00000000E+00 0.00000000E+00 0.00000000E+00    2
 2.54716270E+04-4.60117638E-01 2.50000000E+00 0.00000000E+00 0.00000000E+00    3
 0.00000000E+00 0.00000000E+00 2.54716270E+04-4.60117608E-01                   4
H+                120186H   1E  -1          G  0300.00   5000.00  1000.00     1
 2.50000000E+00 0.00000000E+00 0.00000000E+00 0.00000000E+00 0.00000000E+00    2
 1.84033438E+05-1.15386200E+00 2.50000000E+00 0.00000000E+00 0.00000000E+00    3
 0.00000000E+00 0.00000000E+00 1.84033438E+05-1.15386212E+00                   4
H-                120186H   1E   1          G  0300.00   5000.00  1000.00     1
```

```
 2.50000000E+00 0.00000000E+00 0.00000000E+00 0.00000000E+00 0.00000000E+00    2
 1.59610449E+04-1.15244877E+00 2.50000000E+00 0.00000000E+00 0.00000000E+00    3
 0.00000000E+00 0.00000000E+00 1.59610449E+04-1.15244865E+00                   4
H2                121286H   2               G  0300.00   5000.00  1000.00     1
 2.99142337E+00 7.00064411E-04-5.63382869E-08-9.23157818E-12 1.58275179E-15    2
-8.35033997E+02-1.35511017E+00 3.29812431E+00 8.24944174E-04-8.14301529E-07    3
-9.47543433E-11 4.13487224E-13-1.01252087E+03-3.29409409E+00                   4
H2CN               41687H   2C   1N   1     G  0300.00   4000.00  1000.00     1
 5.20970345E+00 2.96929106E-03-2.85558912E-07-1.63555031E-10 3.04325928E-14    2
 2.76771094E+04-4.44447804E+00 2.85166097E+00 5.69523312E-03 1.07114022E-06    3
-1.62261205E-09-2.35110840E-13 2.86378203E+04 8.99275112E+00                   4
H2CNH              41687C   1H   3N   1     G  0300.00   4000.00  1000.00     1
 5.22158909E+00 4.74852556E-03-4.17915885E-07-2.60661187E-10 4.70313994E-14    2
 8.65721875E+03-4.50077581E+00 2.36587882E+00 6.78057037E-03 2.42299961E-06    3
-6.15782370E-10-1.61509716E-12 9.97114063E+03 1.23071756E+01                   4
H2CNNO2            41687H   2C   1N   2O   2G  0300.00   4000.00  1000.00     1
 1.14079418E+01 4.56454186E-03-4.60030407E-07-2.51353854E-10 4.78221114E-14    2
 1.24214219E+04-3.16523762E+01 3.53431654E+00 1.81127172E-02 2.39401771E-07    3
-1.08002398E-08 4.22272503E-12 1.50900566E+04 1.13113775E+01                   4
H2O                20387H   2O   1           G  0300.00   5000.00  1000.00     1
 2.67214561E+00 3.05629289E-03-8.73026011E-07 1.20099639E-10-6.39161787E-15    2
-2.98992090E+04 6.86281681E+00 3.38684249E+00 3.47498246E-03-6.35469633E-06    3
 6.96858127E-09-2.50658847E-12-3.02081133E+04 2.59023285E+00                   4
H2O(L)             120186H   2O   1           L  0273.15   1000.00  1000.00     1
 0.00000000E+00 0.00000000E+00 0.00000000E+00 0.00000000E+00 0.00000000E+00    2
 0.00000000E+00 0.00000000E+00 1.27127819E+01-1.76627897E-02-2.25566619E-05    3
 2.08209073E-07-2.40786141E-10-3.74831992E+04-5.91153450E+01                   4
H2O(S)             120186H   2O   1           S  0200.00   0273.15  1000.00     1
 0.00000000E+00 0.00000000E+00 0.00000000E+00 0.00000000E+00 0.00000000E+00    2
 0.00000000E+00 0.00000000E+00-3.92693318E-02 1.69204194E-02 0.00000000E+00    3
 0.00000000E+00 0.00000000E+00-3.59495820E+04 5.69337845E-01                   4
H2O2               120186H   2O   2           G  0300.00   5000.00  1000.00     1
 4.57316685E+00 4.33613639E-03-1.47468882E-06 2.34890357E-10-1.43165356E-14    2
-1.80069609E+04 5.01136959E-01 3.38875365E+00 6.56922581E-03-1.48501258E-07    3
-4.62580552E-09 2.47151475E-12-1.76631465E+04 6.78536320E+00                   4
HCCO               32387H   1C   2O   1     G  0300.00   4000.00  1000.00     1
 6.75807285E+00 2.00040033E-03-2.02760731E-07-1.04113183E-10 1.96516472E-14    2
 1.90151328E+04-9.07126236E+00 5.04796505E+00 4.45347792E-03 2.26828277E-07    3
-1.48209456E-09 2.25074150E-13 1.96589180E+04 4.81843948E-01                   4
HCCOH              32387H   2C   2O   1     G  0300.00   4000.00  1000.00     1
 7.32832432E+00 3.33641609E-03-3.02470511E-07-1.78110637E-10 3.24516787E-14    2
 7.59825781E+03-1.40121403E+01 3.89946532E+00 9.70107503E-03-3.11930933E-07    3
-5.53773250E-09 2.46573248E-12 8.70119043E+03 4.49187470E+00                   4
HCN               121286H   1C   1N   1     G  0300.00   5000.00  1000.00     1
 3.65007782E+00 3.46099795E-03-1.27427870E-06 2.21765564E-10-1.47717735E-14    2
 1.49839160E+04 2.39322043E+00 2.49046230E+00 8.61128047E-03-1.03103421E-05    3
 7.48149809E-09-2.22910948E-12 1.52083438E+04 7.90498161E+00                   4
HCNH               41687C   1H   2N   1     G  0300.00   4000.00  1000.00     1
 4.92329264E+00 3.33289709E-03-3.37089659E-07-1.90161900E-10 3.53182483E-14    2
 3.13266934E+04-1.63250876E+00 2.75945616E+00 6.10338664E-03 7.71314944E-07    3
-2.06309370E-09 1.93191993E-13 3.21724746E+04 1.05748949E+01                   4
HCNO              120186H   1C   1N   1O   1G  0250.00   4000.00  1000.00     1
```

```
 6.69241238E+00 2.36836029E-03-2.37151014E-07-1.27550318E-10 2.40713685E-14    2
 1.69473652E+04-1.24543448E+01 3.18485880E+00 9.75231640E-03-1.28020281E-06    3
-6.16310425E-09 3.22627493E-12 1.79790723E+04 6.12384367E+00                    4
HCO               121286H   1C   1O   1     G  0300.00   5000.00  1000.00     1
 3.55727124E+00 3.34557286E-03-1.33500600E-06 2.47057264E-10-1.71385089E-14    2
 3.91632446E+03 5.55229950E+00 2.89832974E+00 6.19914662E-03-9.62308423E-06    3
 1.08982494E-08-4.57488518E-12 4.15992188E+03 8.98361397E+00                    4
HCO+              121286H   1C   1O   1E  -1G  0300.00   5000.00  1000.00     1
 3.69207430E+00 3.45473248E-03-1.31652439E-06 2.32355094E-10-1.55413216E-14    2
 9.89094141E+04 2.33072233E+00 2.49648333E+00 8.69065803E-03-1.06044527E-05    3
 7.88279131E-09-2.41838537E-12 9.91509688E+04 8.04817772E+00                    4
HE                120186HE  1              G  0300.00   5000.00  1000.00     1
 2.50000000E+00 0.00000000E+00 0.00000000E+00 0.00000000E+00 0.00000000E+00    2
-7.45375000E+02 9.15348887E-01 2.50000000E+00 0.00000000E+00 0.00000000E+00    3
 0.00000000E+00 0.00000000E+00-7.45375000E+02 9.15348828E-01                    4
HE+               120186HE  1E  -1           G  0300.00   5000.00  1000.00     1
 2.50000000E+00 0.00000000E+00 0.00000000E+00 0.00000000E+00 0.00000000E+00    2
 2.85342656E+05 1.60840452E+00 2.50000000E+00 0.00000000E+00 0.00000000E+00    3
 0.00000000E+00 0.00000000E+00 2.85342656E+05 1.60840464E+00                    4
HN3                82687H   1N   3           G  0300.00   4000.00  1000.00     1
 6.02301550E+00 2.45436234E-03-2.40427937E-07-1.32297257E-10 2.47414631E-14    2
 3.39405117E+04-7.01553679E+00 3.62100339E+00 6.03078539E-03 4.05446031E-07    3
-2.54527088E-09 6.17427984E-13 3.48237305E+04 6.33376885E+00                    4
HNCO               31287H   1N   1C   1O   1G  0300.00   4000.00  1000.00     1
 6.21186686E+00 2.29713717E-03-2.21612879E-07-1.22204372E-10 2.27240610E-14    2
-1.47707246E+04-8.01663303E+00 3.69405913E+00 6.65723626E-03-5.05446813E-08    3
-3.47341156E-09 1.36056943E-12-1.39197578E+04 5.71274185E+00                    4
HNO               121286H   1N   1O   1     G  0300.00   5000.00  1000.00     1
 3.61514401E+00 3.21248570E-03-1.26033694E-06 2.26729760E-10-1.53623570E-14    2
 1.06619111E+04 4.81026363E+00 2.78440261E+00 6.60964614E-03-9.30022270E-06    3
 9.43798018E-09-3.75314623E-12 1.09187793E+04 9.03562927E+00                    4
HNO3              121286H   1N   1O   3     G  0300.00   5000.00  1000.00     1
 7.00384474E+00 5.81149338E-03-2.33378887E-06 4.28881375E-10-2.95938506E-14    2
-1.88995234E+04-1.04786282E+01 1.35318494E+00 2.22002473E-02-1.97881182E-05    3
 8.77390782E-09-1.65838437E-12-1.73856289E+04 1.85186844E+01                    4
HO2                20387H   1O   2           G  0300.00   5000.00  1000.00     1
 4.07219124E+00 2.13129632E-03-5.30814532E-07 6.11226902E-11-2.84116471E-15    2
-1.57972702E+02 3.47602940E+00 2.97996306E+00 4.99669695E-03-3.79099697E-06    3
 2.35419240E-09-8.08902424E-13 1.76227387E+02 9.22272396E+00                    4
HOCN              120186H   1O   1C   1N   1G  0250.00   4000.00  1000.00     1
 5.64560747E+00 2.29820656E-03-2.16262919E-07-1.21480132E-10 2.23863625E-14    2
-3.17810986E+03-3.59026313E+00 3.62829232E+00 5.66418422E-03-1.17020562E-07    3
-2.34863862E-09 8.01640221E-13-2.47592554E+03 7.47682524E+00                    4
HONO               31787H   1N   1O   2     G  0300.00   5000.00  1000.00     1
 5.48689270E+00 4.21806471E-03-1.64914263E-06 2.97187663E-10-2.02114801E-14    2
-1.12686465E+04-2.99700189E+00 2.29041290E+00 1.40992226E-02-1.36787176E-05    3
 7.49878026E-09-1.87690532E-12-1.04319453E+04 1.32807694E+01                    4
N                 120186N   1              G  0300.00   5000.00  1000.00     1
 2.45026827E+00 1.06614578E-04-7.46533715E-08 1.87965234E-11-1.02598390E-15    2
 5.61160391E+04 4.44875813E+00 2.50307131E+00-2.18001806E-05 5.42052874E-08    3
-5.64756020E-11 2.09990445E-14 5.60989023E+04 4.16756630E+00                    4
N2                121286N   2              G  0300.00   5000.00  1000.00     1
```

```
 2.92664003E+00 1.48797676E-03-5.68476082E-07 1.00970378E-10-6.75335134E-15    2
-9.22797669E+02 5.98052788E+00 3.29867697E+00 1.40824041E-03-3.96322230E-06    3
 5.64151526E-09-2.44485487E-12-1.02089990E+03 3.95037222E+00                   4
N2H2             121286N   2H   2          G  0300.00   5000.00  1000.00      1
 3.37118530E+00 6.03996823E-03-2.30385354E-06 4.06278899E-10-2.71314445E-14    2
 2.41817188E+04 4.98058510E+00 1.61799944E+00 1.30631216E-02-1.71571155E-05    3
 1.60560791E-08-6.09363862E-12 2.46752637E+04 1.37946701E+01                   4
N2H3             120186N   2H   3          G  0300.00   5000.00  1000.00      1
 4.44184589E+00 7.21427053E-03-2.49568439E-06 3.92056471E-10-2.29894957E-14    2
 1.66422109E+04-4.27520454E-01 3.17420363E+00 4.71590692E-03 1.33486710E-05    3
-1.91968468E-08 7.48756352E-12 1.72726992E+04 7.55722380E+00                   4
N2H4             121286N   2H   4          G  0300.00   5000.00  1000.00      1
 4.97731686E+00 9.59551893E-03-3.54763893E-06 6.12429940E-10-4.02979482E-14    2
 9.34121875E+03-2.96298981E+00 6.44260570E-02 2.74972972E-02-2.89945128E-05    3
 1.74523986E-08-4.42228199E-12 1.04519170E+04 2.12778931E+01                   4
N2O              121286N   2O   1          G  0300.00   5000.00  1000.00      1
 4.71897698E+00 2.87371385E-03-1.19749575E-06 2.25055155E-10-1.57533695E-14    2
 8.16581104E+03-1.65725040E+00 2.54305768E+00 9.49219335E-03-9.79277502E-06    3
 6.26384455E-09-1.90182592E-12 8.76509961E+03 9.51122189E+00                   4
N2O+             121286N   2O   1E -1      G  0300.00   5000.00  1000.00      1
 5.39851618E+00 2.24947790E-03-9.57705652E-07 1.82319271E-10-1.28442221E-14    2
 1.58485125E+05-3.73314619E+00 3.18722820E+00 8.35071411E-03-7.89454862E-06    3
 4.59744465E-09-1.38107473E-12 1.59127938E+05 7.77942562E+00                   4
N2O4             121286N   2O   4          G  0300.00   5000.00  1000.00      1
 1.04822006E+01 5.97227225E-03-2.56404360E-06 4.91688523E-10-3.49096938E-14    2
-2.84998853E+03-2.61228905E+01 3.62459254E+00 2.47470811E-02-2.17287488E-05    3
 9.92710358E-09-2.22281698E-12-9.12824097E+02 9.45717430E+00                   4
N3               121286N   3          G  0300.00   5000.00  1000.00      1
 5.20850515E+00 2.44450709E-03-1.03894149E-06 1.97741684E-10-1.39564357E-14    2
 4.79617813E+04-3.61275554E+00 2.88221884E+00 8.93033762E-03-8.53903839E-06    3
 5.04558484E-09-1.52124797E-12 4.86346836E+04 8.48175716E+00                   4
NCO              121286N   1C   1O   1     G  0300.00   5000.00  1000.00      1
 5.01204538E+00 2.62677320E-03-1.10824328E-06 2.09386022E-10-1.46034697E-14    2
 1.73718574E+04-1.83007526E+00 2.83032036E+00 8.87149014E-03-8.94563618E-06    3
 5.87691851E-09-1.90773460E-12 1.80054297E+04 9.49883080E+00                   4
NH                31387H   1N   1          G  0300.00   5000.00  1000.00      1
 2.76024914E+00 1.37534621E-03-4.45191432E-07 7.69279154E-11-5.01759236E-15    2
 4.20782813E+04 5.85719919E+00 3.33975792E+00 1.25300861E-03-3.49164588E-06    3
 4.21881197E-09-1.55761786E-12 4.18504727E+04 2.50718069E+00                   4
NH2              121686N   1H   2          G  0300.00   5000.00  1000.00      1
 2.96131110E+00 2.93269893E-03-9.06360015E-07 1.61725744E-10-1.20420023E-14    2
 2.19197676E+04 5.77787781E+00 3.43249297E+00 3.29953991E-03-6.61360036E-06    3
 8.59094662E-09-3.57204674E-12 2.17722773E+04 3.09011054E+00                   4
NH3              121386N   1H   3          G  0300.00   5000.00  1000.00      1
 2.46190405E+00 6.05916604E-03-2.00497652E-06 3.13600312E-10-1.93831699E-14    2
-6.49326953E+03 7.47209692E+00 2.20435166E+00 1.01147648E-02-1.46526481E-05    3
 1.44723504E-08-5.32850890E-12-6.52548828E+03 8.12713814E+00                   4
NNH              120186N   2H   1          G  0250.00   4000.00  1000.00      1
 4.41534233E+00 1.61438785E-03-1.63289428E-07-8.55984589E-11 1.61479090E-14    2
 2.78802930E+04 9.04288828E-01 3.50134444E+00 2.05358653E-03 7.17040962E-07    3
 4.92134777E-10-9.67117012E-13 2.83334688E+04 6.39183712E+00                   4
NO               121286N   1O   1          G  0300.00   5000.00  1000.00      1
```

```
 3.24543548E+00 1.26913830E-03-5.01589000E-07 9.16928339E-11-6.27541935E-15    2
 9.80083984E+03 6.41729355E+00 3.37654162E+00 1.25306333E-03-3.30275066E-06    3
 5.21781018E-09-2.44626281E-12 9.81796094E+03 5.82958984E+00                   4
NO+              121286N   1O   1E  -1     G  0300.00   5000.00  1000.00     1
 2.91488862E+00 1.49933482E-03-5.72797205E-07 1.01777670E-10-6.82538980E-15    2
 1.18186883E+05 6.84434605E+00 3.29734898E+00 1.42288988E-03-4.00744102E-06    3
 5.67055114E-09-2.44697188E-12 1.18083383E+05 4.74994803E+00                   4
NO2              121286N   1O   2          G  0300.00   5000.00  1000.00     1
 4.68285894E+00 2.46242900E-03-1.04225853E-06 1.97690239E-10-1.39171681E-14    2
 2.26129224E+03 9.88598466E-01 2.67060041E+00 7.83850066E-03-8.06386470E-06    3
 6.16171469E-09-2.32015015E-12 2.89629053E+03 1.16120710E+01                   4
NO2-             121286N   1O   2E   1     G  0300.00   5000.00  1000.00     1
 5.04311419E+00 2.16642767E-03-9.45545367E-07 1.81631363E-10-1.23839444E-14    2
-2.62155371E+04-1.44590509E+00 2.44858599E+00 8.98250658E-03-7.85343127E-06    3
 3.92727673E-09-1.07169384E-12-2.54509688E+04 1.21306000E+01                   4
NO3              121286N   1O   3          G  0300.00   5000.00  1000.00     1
 7.12030745E+00 3.24622821E-03-1.43161333E-06 2.79705342E-10-2.01300785E-14    2
 5.86447949E+03-1.21373015E+01 1.22107625E+00 1.87879708E-02-1.34432121E-05    3
 1.27460131E-09 1.35406009E-12 7.47314404E+03 1.84020271E+01                   4
O                120186O   1          G  0300.00   5000.00  1000.00     1
 2.54205966E+00-2.75506191E-05-3.10280335E-09 4.55106742E-12-4.36805150E-16    2
 2.92308027E+04 4.92030811E+00 2.94642878E+00-1.63816649E-03 2.42103170E-06    3
-1.60284319E-09 3.89069636E-13 2.91476445E+04 2.96399498E+00                   4
O+               1212860   1E  -1          G  0300.00   5000.00  1000.00     1
 2.50186944E+00-6.10726238E-06 7.32430738E-09-3.43835312E-12 5.50640767E-16    2
 1.87955266E+05 4.37282658E+00 2.49927282E+00 5.82059829E-06-1.12092193E-08    3
 8.23210857E-12-1.91637795E-15 1.87955656E+05 4.38482571E+00                   4
O-               120186O   1E   1          G  0300.00   5000.00  1000.00     1
 2.54371738E+00-5.32587001E-05 2.51196166E-08-5.18514658E-12 3.90115423E-16    2
 1.14805156E+04 4.52025366E+00 2.81157970E+00-1.19056972E-03 1.87105525E-06    3
-1.34791778E-09 3.66635541E-13 1.14284307E+04 3.24028540E+00                   4
O2               1213860   2          G  0300.00   5000.00  1000.00     1
 3.69757819E+00 6.13519689E-04-1.25884199E-07 1.77528148E-11-1.13643531E-15    2
-1.23393018E+03 3.18916559E+00 3.21293640E+00 1.12748635E-03-5.75615047E-07    3
 1.31387723E-09-8.76855392E-13-1.00524902E+03 6.03473759E+00                   4
O2-              1212860   2E   1          G  0300.00   5000.00  1000.00     1
 3.88301301E+00 7.40787247E-04-2.96177632E-07 5.72430471E-11-4.08654772E-15    2
-7.12164404E+03 2.65821171E+00 2.87229157E+00 3.35971639E-03-2.66488632E-06    3
 9.80752368E-10-1.67095707E-13-6.82909375E+03 7.93837261E+00                   4
O3               1212860   3          G  0300.00   5000.00  1000.00     1
 5.42937088E+00 1.82037999E-03-7.70560689E-07 1.49929277E-10-1.07556286E-14    2
 1.52352666E+04-3.26638675E+00 2.46260858E+00 9.58278123E-03-7.08735934E-06    3
 1.36336831E-09 2.96964710E-13 1.60615225E+04 1.21418696E+01                   4
OH               1212860   1H   1          G  0300.00   5000.00  1000.00     1
 2.88273048E+00 1.01397431E-03-2.27687707E-07 2.17468370E-11-5.12630534E-16    2
 3.88688794E+03 5.59571219E+00 3.63726592E+00 1.85091049E-04-1.67616463E-06    3
 2.38720266E-09-8.43144185E-13 3.60678174E+03 1.35886049E+00                   4
OH+              1212860   1H   1E  -1     G  0300.00   5000.00  1000.00     1
 2.71905875E+00 1.50857132E-03-5.02936928E-07 8.26195154E-11-4.94745253E-15    2
 1.57634141E+05 6.23453617E+00 3.32697868E+00 1.34578592E-03-3.77716765E-06    3
 4.68774974E-09-1.78098215E-12 1.57402938E+05 2.74404216E+00                   4
OH-              1212860   1H   1E   1     G  0300.00   5000.00  1000.00     1
```

```
 2.84620452E+00 1.04183471E-03-2.41685058E-07 2.48321502E-11-7.77560523E-16    2
-1.80728027E+04 4.42271185E+00 3.39003754E+00 7.92238105E-04-1.94342965E-06    3
 2.00176964E-09-5.70208702E-13-1.83049375E+04 1.24989224E+00                   4
C4H5UU                    C   4H   5           G    300.00   3000.00          1
 0.61854200E+01 0.19993940E-01-0.96838190E-05 0.22852970E-08-0.21323580E-12    2
 0.38220340E+05-0.61870070E+01-0.11198990E+01 0.46743060E-01-0.47681130E-04    3
 0.26836040E-07-0.62185890E-11 0.39880260E+05 0.29843660E+02 0.00000000E+00    4
C6H5U                     C   6H   5           G    300.00   3000.00          1
 0.10117390E+02 0.22362990E-01-0.10888710E-04 0.25813830E-08-0.24171140E-12    2
 0.64833360E+05-0.23740230E+02-0.25086790E+01 0.75179060E-01-0.98104560E-04    3
 0.68939800E-07-0.19584990E-10 0.67402400E+05 0.36985790E+02 0.00000000E+00    4
C8H5U                     C   8H   5           G    300.00   3000.00          1
 0.13344890E+02 0.25868720E-01-0.12790200E-04 0.30696010E-08-0.29016780E-12    2
 0.91124840E+05-0.37374440E+02-0.24904980E+01 0.94544690E-01-0.13049070E-03    3
 0.95835240E-07-0.28210010E-10 0.94248300E+05 0.38244920E+02 0.00000000E+00    4
C8H5SX             DUPU   C   8H   5           G    300.00   3000.00          1
 0.13344890E+02 0.25868720E-01-0.12790200E-04 0.30696010E-08-0.29016780E-12    2
 0.91124840E+05-0.37374440E+02-0.24904980E+01 0.94544690E-01-0.13049070E-03    3
 0.95835240E-07-0.28210010E-10 0.94248300E+05 0.38244920E+02 0.00000000E+00    4
A1                        C   6H   6    0    0G    300.00   3000.00          1
 0.48775230E+01 0.34219620E-01-0.17681320E-04 0.43957540E-08-0.42703370E-12    2
 0.64238160E+04-0.66024580E+01-0.51544750E+01 0.60945050E-01-0.36347410E-04    3
 0.67090380E-09 0.52607980E-11 0.91087750E+04 0.45123400E+02 0.00000000E+00    4
A1C2H                     C   8H   6    0    0G    300.00   3000.00          1
 0.90922390E+01 0.36139920E-01-0.18604620E-04 0.46116410E-08-0.44688480E-12    2
 0.32885900E+05-0.25323960E+02-0.55735650E+01 0.86730960E-01-0.84119110E-04    3
 0.41847040E-07-0.81056020E-11 0.36317230E+05 0.47652910E+02 0.00000000E+00    4
A1C4H                     C  10H   6    0    0G    300.00   3000.00          1
 0.12319740E+02 0.39645650E-01-0.20506100E-04 0.50998580E-08-0.49534120E-12    2
 0.57466480E+05-0.38958160E+02-0.55553840E+01 0.10609660E+00-0.11650520E-03    3
 0.68742480E-07-0.16730620E-10 0.61452240E+05 0.48912040E+02 0.00000000E+00    4
A1C6H                     C  12H   6    0    0G    300.00   3000.00          1
 0.15547240E+02 0.43151380E-01-0.22407590E-04 0.55880770E-08-0.54379770E-12    2
 0.82047080E+05-0.52592360E+02-0.55372030E+01 0.12546230E+00-0.14889140E-03    3
 0.95637920E-07-0.25355640E-10 0.86587250E+05 0.50171160E+02 0.00000000E+00    4
A1C8H                     C  14H   6    0    0G    300.00   3000.00          1
 0.18774740E+02 0.46657110E-01-0.24309070E-04 0.60762940E-08-0.59225420E-12    2
 0.10662770E+06-0.66226560E+02-0.55190220E+01 0.14482790E+00-0.18127750E-03    3
 0.12253340E-06-0.33980660E-10 0.11172220E+06 0.51430290E+02 0.00000000E+00    4
A1C2H3                    C   8H   8    0    0G    300.00   3000.00          1
 0.76453740E+01 0.44108350E-01-0.22623680E-04 0.55889800E-08-0.54000450E-12    2
 0.12859910E+05-0.16172810E+02-0.34679400E+01 0.73239010E-01-0.42173830E-04    3
 0.59402790E-09 0.59755760E-11 0.15870220E+05 0.41275750E+02 0.00000000E+00    4
A1C4H3                    C  10H   8    0    0G    300.00   3000.00          1
 0.11577340E+02 0.46477400E-01-0.23828570E-04 0.58850660E-08-0.56848000E-12    2
 0.39472930E+05-0.33726030E+02-0.48567200E+01 0.10167500E+00-0.92597270E-04    3
 0.42697800E-07-0.73908280E-11 0.43392380E+05 0.48417880E+02 0.00000000E+00    4
A1C6H3                    C  12H   8    0    0G    300.00   3000.00          1
 0.14804840E+02 0.49983130E-01-0.25730050E-04 0.63732830E-08-0.61693650E-12    2
 0.64053520E+05-0.47360230E+02-0.48385390E+01 0.12104070E+00-0.12498340E-03    3
 0.69593240E-07-0.16015840E-10 0.68527380E+05 0.49677010E+02 0.00000000E+00    4
A1C8H3                    C  14H   8    0    0G    300.00   3000.00          1
```

```
 0.18032340E+02 0.53488860E-01-0.27631540E-04 0.68615020E-08-0.66539300E-12   2
 0.88634110E+05-0.60994430E+02-0.48203570E+01 0.14040630E+00-0.15736950E-03   3
 0.96488680E-07-0.24640860E-10 0.93662390E+05 0.50936130E+02 0.00000000E+00   4
A1C10H3                  C  16H   8    0    0G    300.00   3000.00           1
 0.21259840E+02 0.56994580E-01-0.29533020E-04 0.73497190E-08-0.71384940E-12   2
 0.11321470E+06-0.74628630E+02-0.48021760E+01 0.15977200E+00-0.18975570E-03   3
 0.12338410E-06-0.33265880E-10 0.11879740E+06 0.52195260E+02 0.00000000E+00   4
A1C4H5                   C  10H  10    0    0G    300.00   3000.00           1
 0.11966940E+02 0.51907820E-01-0.26373780E-04 0.64701300E-08-0.62216840E-12   2
 0.17757360E+05-0.37308720E+02-0.70175280E+01 0.11397360E+00-0.10058640E-03   3
 0.43374120E-07-0.64139550E-11 0.22378850E+05 0.58018530E+02 0.00000000E+00   4
A1C6H5                   C  12H  10    0    0G    300.00   3000.00           1
 0.15898910E+02 0.54276870E-01-0.27578680E-04 0.67662160E-08-0.65064400E-12   2
 0.44370380E+05-0.54861940E+02-0.84063060E+01 0.14240960E+00-0.15100990E-03   3
 0.85477890E-07-0.19780360E-10 0.49901000E+05 0.65160660E+02 0.00000000E+00   4
A1C8H5                   C  14H  10    0    0G    300.00   3000.00           1
 0.19126410E+02 0.57782600E-01-0.29480160E-04 0.72544340E-08-0.69910050E-12   2
 0.68950970E+05-0.68496150E+02-0.83881250E+01 0.16177520E+00-0.18339600E-03   3
 0.11237330E-06-0.28405380E-10 0.75036010E+05 0.66419790E+02 0.00000000E+00   4
A1C10H5                  C  16H  10    0    0G    300.00   3000.00           1
 0.22353910E+02 0.61288330E-01-0.31381640E-04 0.77426520E-08-0.74755700E-12   2
 0.93531560E+05-0.82130350E+02-0.83699450E+01 0.18114090E+00-0.21578220E-03   3
 0.13926880E-06-0.37030390E-10 0.10017100E+06 0.67678920E+02 0.00000000E+00   4
A1C2H)2/M                C  10H   6    0    0G    300.00   3000.00           1
 0.13306960E+02 0.38060230E-01-0.19527920E-04 0.48275260E-08-0.46673580E-12   2
 0.59347980E+05-0.45837210E+02-0.59926560E+01 0.11251690E+00-0.13189080E-03   3
 0.83023170E-07-0.21472000E-10 0.63525690E+05 0.48390660E+02 0.00000000E+00   4
A1C2HC4H                 C  12H   6    0    0G    300.00   3000.00           1
 0.16534460E+02 0.41565960E-01-0.21429410E-04 0.53157440E-08-0.51519230E-12   2
 0.83928560E+05-0.58778260E+02-0.59744750E+01 0.13188250E+00-0.16427690E-03   3
 0.10991860E-06-0.30097020E-10 0.88660700E+05 0.50342930E+02 0.00000000E+00   4
A1C2HC6H                 C  14H   6    0    0G    300.00   3000.00           1
 0.19761960E+02 0.45071680E-01-0.23330890E-04 0.58039620E-08-0.56364870E-12   2
 0.10850920E+06-0.72412470E+02-0.59562940E+01 0.15124820E+00-0.19666310E-03   3
 0.13681400E-06-0.38722040E-10 0.11379570E+06 0.51602060E+02 0.00000000E+00   4
A1C4H)2                  C  14H   6    0    0G    300.00   3000.00           1
 0.19761960E+02 0.45071680E-01-0.23330890E-04 0.58039620E-08-0.56364870E-12   2
 0.10850920E+06-0.73105610E+02-0.59562940E+01 0.15124820E+00-0.19666310E-03   3
 0.13681400E-06-0.38722040E-10 0.11379570E+06 0.50908910E+02 0.00000000E+00   4
A1C2HC2H3                C  10H   8    0    0G    300.00   3000.00           1
 0.11860090E+02 0.46028650E-01-0.23546980E-04 0.58048650E-08-0.55985550E-12   2
 0.39321990E+05-0.35992920E+02-0.38870310E+01 0.99024930E-01-0.89945520E-04   3
 0.41770160E-07-0.73908220E-11 0.43078680E+05 0.42706650E+02 0.00000000E+00   4
A1C4HC2H3                C  12H   8    0    0G    300.00   3000.00           1
 0.15087590E+02 0.49534380E-01-0.25448460E-04 0.62930830E-08-0.60831200E-12   2
 0.63902580E+05-0.49627120E+02-0.38688500E+01 0.11839060E+00-0.12233160E-03   3
 0.68665610E-07-0.16015840E-10 0.68213690E+05 0.43965780E+02 0.00000000E+00   4
A1C2HC4H3                C  12H   8    0    0G    300.00   3000.00           1
 0.15792060E+02 0.48397700E-01-0.24751880E-04 0.61009510E-08-0.58833110E-12   2
 0.65935010E+05-0.54239280E+02-0.52758100E+01 0.12746090E+00-0.14036900E-03   3
 0.83873930E-07-0.20757230E-10 0.70600830E+05 0.49155620E+02 0.00000000E+00   4
A1C2H)3/SY               C  12H   6    0    0G    300.00   3000.00           1
```

```
 0.17521670E+02 0.39980530E-01-0.20451230E-04 0.50434130E-08-0.48658680E-12    2
 0.85810060E+05-0.67449080E+02-0.64117460E+01 0.13830280E+00-0.17966250E-03    3
 0.12419930E-06-0.34838400E-10 0.90734160E+05 0.48029800E+02 0.00000000E+00    4
A1C2H)3/UN              C  12H   6    0    0G    300.00   3000.00              1
 0.17521670E+02 0.39980530E-01-0.20451230E-04 0.50434130E-08-0.48658680E-12    2
 0.85810060E+05-0.65657330E+02-0.64117460E+01 0.13830280E+00-0.17966250E-03    3
 0.12419930E-06-0.34838400E-10 0.90734160E+05 0.49821560E+02 0.00000000E+00    4
AC2H)2C2H3/S            C  12H   8    0    0G    300.00   3000.00              1
 0.16074810E+02 0.47948950E-01-0.24470280E-04 0.60207520E-08-0.57970650E-12    2
 0.65784060E+05-0.57199320E+02-0.43061210E+01 0.12481080E+00-0.13771720E-03    3
 0.82946290E-07-0.20757220E-10 0.70287150E+05 0.42751240E+02 0.00000000E+00    4
AC2H)2C2H3/U            C  12H   8    0    0G    300.00   3000.00              1
 0.16074810E+02 0.47948950E-01-0.24470280E-04 0.60207520E-08-0.57970650E-12    2
 0.65784060E+05-0.56506170E+02-0.43061210E+01 0.12481080E+00-0.13771720E-03    3
 0.82946290E-07-0.20757220E-10 0.70287150E+05 0.43444390E+02 0.00000000E+00    4
A1C2H)2C4H/S            C  14H   6    0    0G    300.00   3000.00              1
 0.20749170E+02 0.43486260E-01-0.22352710E-04 0.55316300E-08-0.53504330E-12    2
 0.11039060E+06-0.79984670E+02-0.63935650E+01 0.15766840E+00-0.21204860E-03    3
 0.15109480E-06-0.43463420E-10 0.11586920E+06 0.50387540E+02 0.00000000E+00    4
A1C2H)2C4H/U            C  14H   6    0    0G    300.00   3000.00              1
 0.20749170E+02 0.43486260E-01-0.22352710E-04 0.55316300E-08-0.53504330E-12    2
 0.11039060E+06-0.79291530E+02-0.63935650E+01 0.15766840E+00-0.21204860E-03    3
 0.15109480E-06-0.43463420E-10 0.11586920E+06 0.51080680E+02 0.00000000E+00    4
AC2H)2C4H3/S            C  14H   8    0    0G    300.00   3000.00              1
 0.20006780E+02 0.50318010E-01-0.25675180E-04 0.63168380E-08-0.60818210E-12    2
 0.92397090E+05-0.74752550E+02-0.56949000E+01 0.15324680E+00-0.18814070E-03    3
 0.12505010E-06-0.34123630E-10 0.97809300E+05 0.49893380E+02 0.00000000E+00    4
AC2H)2C4H3/U            C  14H   8    0    0G    300.00   3000.00              1
 0.20006780E+02 0.50318010E-01-0.25675180E-04 0.63168380E-08-0.60818210E-12    2
 0.92397090E+05-0.74059400E+02-0.56949000E+01 0.15324680E+00-0.18814070E-03    3
 0.12505010E-06-0.34123630E-10 0.97809300E+05 0.50586520E+02 0.00000000E+00    4
A1C2H)4                 C  14H   6    0    0G    300.00   3000.00              1
 0.21736390E+02 0.41900840E-01-0.21374530E-04 0.52592990E-08-0.50643790E-12    2
 0.11227210E+06-0.86863720E+02-0.68308350E+01 0.16408870E+00-0.22743420E-03    3
 0.16537540E-06-0.48204800E-10 0.11794260E+06 0.49866160E+02 0.00000000E+00    4
A1-                     C   6H   5    0    0G    300.00   3000.00              1
 0.52173050E+01 0.30612620E-01-0.15947700E-04 0.39900570E-08-0.38954940E-12    2
 0.35895550E+05-0.50435590E+01-0.41420590E+01 0.55518760E-01-0.33564580E-04    3
 0.10244800E-08 0.46365570E-11 0.38410310E+05 0.43242940E+02 0.00000000E+00    4
A1C2H-                  C   8H   5    0    0G    300.00   3000.00              1
 0.94320210E+01 0.32532930E-01-0.16871000E-04 0.42059430E-08-0.40940050E-12    2
 0.62357620E+05-0.24863670E+02-0.45611490E+01 0.81304680E-01-0.81336270E-04    3
 0.42200620E-07-0.87298430E-11 0.65618770E+05 0.44673840E+02 0.00000000E+00    4
A1C2H*               DUP-  C   8H   5    0    0G    300.00   3000.00              1
 0.94320210E+01 0.32532930E-01-0.16871000E-04 0.42059430E-08-0.40940050E-12    2
 0.62357620E+05-0.24863670E+02-0.45611490E+01 0.81304680E-01-0.81336270E-04    3
 0.42200620E-07-0.87298430E-11 0.65618770E+05 0.44673840E+02 0.00000000E+00    4
A1C4H-                  C  10H   5    0    0G    300.00   3000.00              1
 0.12659520E+02 0.36038660E-01-0.18772480E-04 0.46941610E-08-0.45785700E-12    2
 0.86938220E+05-0.38497870E+02-0.45429680E+01 0.10067030E+00-0.11372240E-03    3
 0.69096050E-07-0.17354860E-10 0.90753780E+05 0.45932960E+02 0.00000000E+00    4
A1C6H-                  C  12H   5    0    0G    300.00   3000.00              1
```

```
 0.15887020E+02 0.39544380E-01-0.20673960E-04 0.51823790E-08-0.50631340E-12    2
 0.11151880E+06-0.52132080E+02-0.45247860E+01 0.12003600E+00-0.14610850E-03    3
 0.95991500E-07-0.25979880E-10 0.11588880E+06 0.47192090E+02 0.00000000E+00    4
A1C8H-                  C  14H   5    0    0G    300.00   3000.00              1
 0.19114520E+02 0.43050110E-01-0.22575450E-04 0.56705960E-08-0.55476990E-12    2
 0.13609940E+06-0.65766280E+02-0.45066060E+01 0.13940160E+00-0.17849460E-03    3
 0.12288700E-06-0.34604900E-10 0.14102380E+06 0.48451220E+02 0.00000000E+00    4
A1C2H)2-/S              C  10H   5    0    0G    300.00   3000.00              1
 0.13646740E+02 0.34453240E-01-0.17794300E-04 0.44218290E-08-0.42925150E-12    2
 0.88819710E+05-0.46070070E+02-0.49802390E+01 0.10709060E+00-0.12910800E-03    3
 0.83376740E-07-0.22096240E-10 0.92827230E+05 0.44718440E+02 0.00000000E+00    4
A1C2H)2-/U              C  10H   5    0    0G    300.00   3000.00              1
 0.13646740E+02 0.34453240E-01-0.17794300E-04 0.44218290E-08-0.42925150E-12    2
 0.88819710E+05-0.45376920E+02-0.49802390E+01 0.10709060E+00-0.12910800E-03    3
 0.83376740E-07-0.22096240E-10 0.92827230E+05 0.45411580E+02 0.00000000E+00    4
A1C2H2U                 C   8H   7    0    0G    300.00   3000.00              1
 0.79851560E+01 0.40501350E-01-0.20890050E-04 0.51832820E-08-0.50252020E-12    2
 0.41073620E+05-0.15712520E+02-0.24555240E+01 0.67812730E-01-0.39390990E-04    3
 0.94760440E-09 0.53513350E-11 0.43913750E+05 0.38296670E+02 0.00000000E+00    4
A1C4H2U                 C  10H   7    0    0G    300.00   3000.00              1
 0.11917130E+02 0.42870410E-01-0.22094950E-04 0.54793680E-08-0.53099580E-12    2
 0.67686650E+05-0.33265740E+02-0.38443030E+01 0.96248730E-01-0.89814440E-04    3
 0.43051380E-07-0.80150690E-11 0.71435900E+05 0.45438800E+02 0.00000000E+00    4
A1C6H2U                 C  12H   7    0    0G    300.00   3000.00              1
 0.15144630E+02 0.46376140E-01-0.23996430E-04 0.59675860E-08-0.57945220E-12    2
 0.92267230E+05-0.46899940E+02-0.38261220E+01 0.11561440E+00-0.12220060E-03    3
 0.69946820E-07-0.16640080E-10 0.96570910E+05 0.46697930E+02 0.00000000E+00    4
A1C8H2U                 C  14H   7    0    0G    300.00   3000.00              1
 0.18372130E+02 0.49881860E-01-0.25897910E-04 0.64558040E-08-0.62790870E-12    2
 0.11684780E+06-0.60534140E+02-0.38079410E+01 0.13498000E+00-0.15458670E-03    3
 0.96842260E-07-0.25265100E-10 0.12170590E+06 0.47957050E+02 0.00000000E+00    4
A1C4H4U                 C  10H   9    0    0G    300.00   3000.00              1
 0.12306730E+02 0.48300820E-01-0.24640160E-04 0.60644320E-08-0.58468420E-12    2
 0.45971070E+05-0.36848430E+02-0.60051110E+01 0.10854730E+00-0.97803610E-04    3
 0.43727700E-07-0.70381960E-11 0.50422380E+05 0.55039460E+02 0.00000000E+00    4
A1C6H4U                 C  12H   9    0    0G    300.00   3000.00              1
 0.13205000E+02 0.55021980E-01-0.28416570E-04 0.70561580E-08-0.68434330E-12    2
 0.73826810E+05-0.35659260E+02-0.44599360E+01 0.11143050E+00-0.93312890E-04    3
 0.37180960E-07-0.46746600E-11 0.78186470E+05 0.53361420E+02 0.00000000E+00    4
A1C2H2S                 C   8H   7    0    0G    300.00   3000.00              1
 0.79851560E+01 0.40501350E-01-0.20890050E-04 0.51832820E-08-0.50252020E-12    2
 0.37047980E+05-0.16405670E+02-0.24555240E+01 0.67812730E-01-0.39390990E-04    3
 0.94760440E-09 0.53513350E-11 0.39888100E+05 0.37603530E+02 0.00000000E+00    4
A1C4H2S                 C  10H   7    0    0G    300.00   3000.00              1
 0.11917130E+02 0.42870410E-01-0.22094950E-04 0.54793680E-08-0.53099580E-12    2
 0.63661000E+05-0.33958890E+02-0.38443030E+01 0.96248730E-01-0.89814440E-04    3
 0.43051380E-07-0.80150690E-11 0.67410250E+05 0.44745660E+02 0.00000000E+00    4
A1C6H2S                 C  12H   7    0    0G    300.00   3000.00              1
 0.15144630E+02 0.46376140E-01-0.23996430E-04 0.59675860E-08-0.57945220E-12    2
 0.88241590E+05-0.47593090E+02-0.38261220E+01 0.11561440E+00-0.12220060E-03    3
 0.69946820E-07-0.16640080E-10 0.92545270E+05 0.46004780E+02 0.00000000E+00    4
A1C8H2S                 C  14H   7    0    0G    300.00   3000.00              1
```

```
 0.18372130E+02 0.49881860E-01-0.25897910E-04 0.64558040E-08-0.62790870E-12    2
 0.11282220E+06-0.61227290E+02-0.38079410E+01 0.13498000E+00-0.15458670E-03    3
 0.96842260E-07-0.25265100E-10 0.11768030E+06 0.47263910E+02 0.00000000E+00    4
A1C4H4S                 C  10H   9    0    0G    300.00   3000.00               1
 0.12306730E+02 0.48300820E-01-0.24640160E-04 0.60644320E-08-0.58468420E-12    2
 0.41945430E+05-0.37541580E+02-0.60051110E+01 0.10854730E+00-0.97803610E-04    3
 0.43727700E-07-0.70381960E-11 0.46396730E+05 0.54346310E+02 0.00000000E+00    4
A1C6H4S                 C  12H   9    0    0G    300.00   3000.00               1
 0.16238700E+02 0.50669880E-01-0.25845050E-04 0.63605180E-08-0.61315980E-12    2
 0.68558450E+05-0.55094800E+02-0.73938900E+01 0.13698330E+00-0.14822710E-03    3
 0.85831470E-07-0.20404600E-10 0.73918880E+05 0.61488440E+02 0.00000000E+00    4
A1C8H4S                 C  14H   9    0    0G    300.00   3000.00               1
 0.19466190E+02 0.54175610E-01-0.27746540E-04 0.68487370E-08-0.66161620E-12    2
 0.93139050E+05-0.68729010E+02-0.73757090E+01 0.15634900E+00-0.18061320E-03    3
 0.11272690E-06-0.29029620E-10 0.99053890E+05 0.62747570E+02 0.00000000E+00    4
A1C10H4S                C  16H   9    0    0G    300.00   3000.00               1
 0.22693700E+02 0.57681330E-01-0.29648020E-04 0.73369540E-08-0.71007270E-12    2
 0.11771960E+06-0.82363210E+02-0.73575280E+01 0.17571460E+00-0.21299930E-03    3
 0.13962240E-06-0.37654630E-10 0.12418890E+06 0.64006690E+02 0.00000000E+00    4
A1C6H6S                 C  12H  11    0    0G    300.00   3000.00               1
 0.16628290E+02 0.56100300E-01-0.28390260E-04 0.69455830E-08-0.66684810E-12    2
 0.46842880E+05-0.58677500E+02-0.95546990E+01 0.14928190E+00-0.15621620E-03    3
 0.86507790E-07-0.19427730E-10 0.52905360E+05 0.71089100E+02 0.00000000E+00    4
A1C8H6S                 C  14H  11    0    0G    300.00   3000.00               1
 0.20560260E+02 0.58469350E-01-0.29595160E-04 0.72416700E-08-0.69532370E-12    2
 0.73455900E+05-0.76230730E+02-0.10943480E+02 0.17771790E+00-0.20663970E-03    3
 0.12861160E-06-0.32794130E-10 0.80427520E+05 0.78231220E+02 0.00000000E+00    4
A1C10H6S                C  16H  11    0    0G    300.00   3000.00               1
 0.23787760E+02 0.61975080E-01-0.31496650E-04 0.77298870E-08-0.74378020E-12    2
 0.98036480E+05-0.89864930E+02-0.10925300E+02 0.19708360E+00-0.23902580E-03    3
 0.15550700E-06-0.41419150E-10 0.10556250E+06 0.79490350E+02 0.00000000E+00    4
A1C12H6S                C  18H  11    0    0G    300.00   3000.00               1
 0.27015260E+02 0.65480810E-01-0.33398130E-04 0.82181040E-08-0.79223670E-12    2
 0.12261710E+06-0.10349910E+03-0.10907120E+02 0.21644920E+00-0.27141200E-03    3
 0.18240240E-06-0.50044160E-10 0.13069750E+06 0.80749480E+02 0.00000000E+00    4
A1C14H6S                C  20H  11    0    0G    300.00   3000.00               1
 0.30242760E+02 0.68986540E-01-0.35299610E-04 0.87063230E-08-0.84069310E-12    2
 0.14719770E+06-0.11713330E+03-0.10888930E+02 0.23581480E+00-0.30379810E-03    3
 0.20929790E-06-0.58669180E-10 0.15583250E+06 0.82008610E+02 0.00000000E+00    4
A1C8H8S                 C  14H  13    0    0G    300.00   3000.00               1
 0.20949860E+02 0.63899770E-01-0.32140370E-04 0.78267340E-08-0.74901210E-12    2
 0.51740330E+05-0.79813420E+02-0.13104290E+02 0.19001650E+00-0.21462890E-03    3
 0.12928790E-06-0.31817260E-10 0.59414000E+05 0.87831890E+02 0.00000000E+00    4
A1C10H8S                C  16H  13    0    0G    300.00   3000.00               1
 0.24881830E+02 0.66268820E-01-0.33345270E-04 0.81228200E-08-0.77748770E-12    2
 0.78353340E+05-0.97366650E+02-0.14493070E+02 0.21845250E+00-0.26505230E-03    3
 0.17139170E-06-0.45183660E-10 0.86936140E+05 0.94974010E+02 0.00000000E+00    4
A1C12H8S                C  18H  13    0    0G    300.00   3000.00               1
 0.28109330E+02 0.69774550E-01-0.35246750E-04 0.86110370E-08-0.82594420E-12    2
 0.10293390E+06-0.11100080E+03-0.14474890E+02 0.23781810E+00-0.29743850E-03    3
 0.19828710E-06-0.53808680E-10 0.11207120E+06 0.96233140E+02 0.00000000E+00    4
AC2H)3C2H3              C  14H   8    0    0G    300.00   3000.00               1
```

```
 0.20289520E+02 0.49869260E-01-0.25393580E-04 0.62366370E-08-0.59955760E-12    2
 0.92246150E+05-0.77712570E+02-0.47252110E+01 0.15059680E+00-0.18548890E-03    3
 0.12412240E-06-0.34123620E-10 0.97495610E+05 0.43488990E+02 0.00000000E+00    4
AC2H)3C4H3               C  16H   8    0    0G    300.00   3000.00           1
 0.24221490E+02 0.52238320E-01-0.26598480E-04 0.65327240E-08-0.62803320E-12    2
 0.11885920E+06-0.95265790E+02-0.61139900E+01 0.17903280E+00-0.23591240E-03    3
 0.16622620E-06-0.47490030E-10 0.12501780E+06 0.50631120E+02 0.00000000E+00    4
A1C2HC4H2S               C  12H   7    0    0G    300.00   3000.00           1
 0.16131840E+02 0.44790710E-01-0.23018250E-04 0.56952540E-08-0.55084680E-12    2
 0.90123080E+05-0.54472140E+02-0.42633930E+01 0.12203460E+00-0.13758610E-03    3
 0.84227500E-07-0.21381470E-10 0.94618720E+05 0.45483400E+02 0.00000000E+00    4
A1C2HC2H2                C  10H   7    0    0G    300.00   3000.00           1
 0.12199870E+02 0.42421660E-01-0.21813360E-04 0.53991680E-08-0.52237120E-12    2
 0.67535700E+05-0.35532640E+02-0.28746140E+01 0.93598640E-01-0.87162680E-04    3
 0.42123740E-07-0.80150640E-11 0.71122210E+05 0.39727570E+02 0.00000000E+00    4
A1C4H3-                  C  10H   7    0    0G    300.00   3000.00           1
 0.13753590E+02 0.40332400E-01-0.20621100E-04 0.50870930E-08-0.49156450E-12    2
 0.67255080E+05-0.43483560E+02-0.81107350E+01 0.12203930E+00-0.13974890E-03    3
 0.84980700E-07-0.21119370E-10 0.72127410E+05 0.63932650E+02 0.00000000E+00    4
A2                       C  10H   8    0    0G    300.00   3000.00           1
 0.88073940E+01 0.51665230E-01-0.27048340E-04 0.67886190E-08-0.66399420E-12    2
 0.12300800E+05-0.27077850E+02-0.70329820E+01 0.95826610E-01-0.64412250E-04    3
 0.11022810E-07 0.41266860E-11 0.16498430E+05 0.54255090E+02 0.00000000E+00    4
A2C2H                    C  12H   8    0    0G    300.00   3000.00           1
 0.13022110E+02 0.53585540E-01-0.27971650E-04 0.70045040E-08-0.68384520E-12    2
 0.38762880E+05-0.46204820E+02-0.74520720E+01 0.12161250E+00-0.11218400E-03    3
 0.52198950E-07-0.92397140E-11 0.43706890E+05 0.56379130E+02 0.00000000E+00    4
A2C4H                    C  14H   8    0    0G    300.00   3000.00           1
 0.16249610E+02 0.57091270E-01-0.29873130E-04 0.74927230E-08-0.73230170E-12    2
 0.63343460E+05-0.59839020E+02-0.74338910E+01 0.14097820E+00-0.14457010E-03    3
 0.79094390E-07-0.17864730E-10 0.68841900E+05 0.57638260E+02 0.00000000E+00    4
A2C6H                    C  16H   8    0    0G    300.00   3000.00           1
 0.19477110E+02 0.60597000E-01-0.31774610E-04 0.79809400E-08-0.78075820E-12    2
 0.87924060E+05-0.73473220E+02-0.74157100E+01 0.16034380E+00-0.17695620E-03    3
 0.10598980E-06-0.26489750E-10 0.93976910E+05 0.58897380E+02 0.00000000E+00    4
A2C2H3                   C  12H  10    0    0G    300.00   3000.00           1
 0.11575250E+02 0.61553960E-01-0.31990700E-04 0.79818440E-08-0.77696490E-12    2
 0.18736890E+05-0.37053660E+02-0.53464470E+01 0.10812060E+00-0.70238660E-04    3
 0.10945940E-07 0.48414640E-11 0.23259880E+05 0.50001970E+02 0.00000000E+00    4
A2C4H3                   C  14H  10    0    0G    300.00   3000.00           1
 0.15507220E+02 0.63923010E-01-0.33195590E-04 0.82779300E-08-0.80544050E-12    2
 0.45349910E+05-0.54606890E+02-0.67352260E+01 0.13655660E+00-0.12066210E-03    3
 0.53049710E-07-0.85249390E-11 0.50782030E+05 0.57144100E+02 0.00000000E+00    4
A2C6H3                   C  16H  10    0    0G    300.00   3000.00           1
 0.18734720E+02 0.67428740E-01-0.35097080E-04 0.87661470E-08-0.85389690E-12    2
 0.69930500E+05-0.68241090E+02-0.67170450E+01 0.15592220E+00-0.15304820E-03    3
 0.79945150E-07-0.17149960E-10 0.75917040E+05 0.58403220E+02 0.00000000E+00    4
A2C2H)2                  C  14H   8    0    0G    300.00   3000.00           1
 0.17236830E+02 0.55505840E-01-0.28894950E-04 0.72205910E-08-0.70369630E-12    2
 0.65224950E+05-0.66718070E+02-0.78711620E+01 0.14739840E+00-0.15995560E-03    3
 0.93375080E-07-0.22606110E-10 0.70915350E+05 0.57116880E+02 0.00000000E+00    4
A2-                      C  10H   7    0    0G    300.00   3000.00           1
```

```
 0.91471760E+01 0.48058240E-01-0.25314720E-04 0.63829210E-08-0.62650990E-12    2
 0.41772530E+05-0.25924420E+02-0.60205660E+01 0.90400320E-01-0.61629410E-04    3
 0.11376390E-07 0.35024450E-11 0.45799970E+05 0.51969160E+02 0.00000000E+00    4
A2-X              DUP-  C  10H   7    0    0G    300.00   3000.00               1
 0.91471760E+01 0.48058240E-01-0.25314720E-04 0.63829210E-08-0.62650990E-12    2
 0.41772530E+05-0.25924420E+02-0.60205660E+01 0.90400320E-01-0.61629410E-04    3
 0.11376390E-07 0.35024450E-11 0.45799970E+05 0.51969160E+02 0.00000000E+00    4
A2C2H-                  C  12H   7    0    0G    300.00   3000.00               1
 0.13361890E+02 0.49978540E-01-0.26238020E-04 0.65988070E-08-0.64636100E-12    2
 0.68234610E+05-0.46437680E+02-0.64396550E+01 0.11618620E+00-0.10940110E-03    3
 0.52552530E-07-0.98639550E-11 0.73008420E+05 0.52706910E+02 0.00000000E+00    4
A2C4H-                  C  14H   7    0    0G    300.00   3000.00               1
 0.16589390E+02 0.53484270E-01-0.28139510E-04 0.70870250E-08-0.69481740E-12    2
 0.92815200E+05-0.60071880E+02-0.64214740E+01 0.13555190E+00-0.14178720E-03    3
 0.79447960E-07-0.18488970E-10 0.98143440E+05 0.53966040E+02 0.00000000E+00    4
A2C2H2U                 C  12H   9    0    0G    300.00   3000.00               1
 0.11915030E+02 0.57946960E-01-0.30257080E-04 0.75761460E-08-0.73948060E-12    2
 0.46950610E+05-0.36593380E+02-0.43340310E+01 0.10269430E+00-0.67455820E-04    3
 0.11299520E-07 0.42172230E-11 0.51303410E+05 0.47022890E+02 0.00000000E+00    4
A2C4H2U                 C  14H   9    0    0G    300.00   3000.00               1
 0.15847000E+02 0.60316020E-01-0.31461970E-04 0.78722320E-08-0.76795620E-12    2
 0.73563620E+05-0.54146600E+02-0.57228100E+01 0.13113030E+00-0.11787930E-03    3
 0.53403290E-07-0.91491800E-11 0.78825560E+05 0.54165020E+02 0.00000000E+00    4
A2C6H2U                 C  16H   9    0    0G    300.00   3000.00               1
 0.19074500E+02 0.63821750E-01-0.33363460E-04 0.83604490E-08-0.81641260E-12    2
 0.98144220E+05-0.67780810E+02-0.57046290E+01 0.15049600E+00-0.15026540E-03    3
 0.80298730E-07-0.17774200E-10 0.10396060E+06 0.55424150E+02 0.00000000E+00    4
A2C2H2S                 C  12H   9    0    0G    300.00   3000.00               1
 0.11915030E+02 0.57946960E-01-0.30257080E-04 0.75761460E-08-0.73948060E-12    2
 0.42924960E+05-0.37286530E+02-0.43340310E+01 0.10269430E+00-0.67455820E-04    3
 0.11299520E-07 0.42172230E-11 0.47277760E+05 0.46329750E+02 0.00000000E+00    4
A2C4H2S                 C  14H   9    0    0G    300.00   3000.00               1
 0.15847000E+02 0.60316020E-01-0.31461970E-04 0.78722320E-08-0.76795620E-12    2
 0.69537980E+05-0.54839750E+02-0.57228100E+01 0.13113030E+00-0.11787930E-03    3
 0.53403290E-07-0.91491800E-11 0.74799910E+05 0.53471870E+02 0.00000000E+00    4
A2C6H2S                 C  16H   9    0    0G    300.00   3000.00               1
 0.19074500E+02 0.63821750E-01-0.33363460E-04 0.83604490E-08-0.81641260E-12    2
 0.94118580E+05-0.68473950E+02-0.57046290E+01 0.15049600E+00-0.15026540E-03    3
 0.80298730E-07-0.17774200E-10 0.99934920E+05 0.54731000E+02 0.00000000E+00    4
A2C2HC2H2-              C  14H   9    0    0G    300.00   3000.00               1
 0.16129740E+02 0.59867270E-01-0.31180380E-04 0.77920310E-08-0.75933160E-12    2
 0.74670700E+05-0.57799780E+02-0.47531210E+01 0.12848020E+00-0.11522750E-03    3
 0.52475650E-07-0.91491760E-11 0.79769880E+05 0.47067490E+02 0.00000000E+00    4
A2C2HC2H2U              C  14H   9    0    0G    300.00   3000.00               1
 0.16129740E+02 0.59867270E-01-0.31180380E-04 0.77920310E-08-0.75933160E-12    2
 0.73412690E+05-0.57106640E+02-0.47531210E+01 0.12848020E+00-0.11522750E-03    3
 0.52475650E-07-0.91491760E-11 0.78511870E+05 0.47760640E+02 0.00000000E+00    4
A2R5                    C  12H   8    0    0G    300.00   3000.00               1
 0.11624110E+02 0.55962240E-01-0.29406290E-04 0.73843210E-08-0.72157950E-12    2
 0.24015660E+05-0.40911420E+02-0.85554170E+01 0.11897360E+00-0.10044480E-03    3
 0.40630590E-07-0.57849300E-11 0.29070110E+05 0.61175440E+02 0.00000000E+00    4
A2R5C2H                 C  14H   8    0    0G    300.00   3000.00               1
```

```
 0.15838820E+02 0.57882540E-01-0.30329590E-04 0.76002070E-08-0.74143050E-12    2
 0.50477740E+05-0.60731530E+02-0.89745070E+01 0.14475950E+00-0.14821650E-03    3
 0.81806730E-07-0.19151330E-10 0.56278570E+05 0.62606340E+02 0.00000000E+00    4
A2R5C2H)2                C  16H   8    0    0G    300.00   3000.00           1
 0.20053540E+02 0.59802840E-01-0.31252890E-04 0.78160930E-08-0.76128160E-12    2
 0.76939810E+05-0.81244790E+02-0.93935980E+01 0.17054540E+00-0.19598820E-03    3
 0.12298290E-06-0.32517730E-10 0.83487030E+05 0.63344080E+02 0.00000000E+00    4
A2R5-                    C  12H   7    0    0G    300.00   3000.00           1
 0.11963890E+02 0.52355240E-01-0.27672660E-04 0.69786240E-08-0.68409520E-12    2
 0.53487390E+05-0.40451140E+02-0.75430010E+01 0.11354730E+00-0.97661960E-04    3
 0.40984170E-07-0.64091710E-11 0.58371640E+05 0.58196360E+02 0.00000000E+00    4
A2R5C2H-                 C  14H   7    0    0G    300.00   3000.00           1
 0.16178600E+02 0.54275550E-01-0.28595970E-04 0.71945100E-08-0.70394620E-12    2
 0.79949470E+05-0.60964390E+02-0.79620900E+01 0.13933320E+00-0.14543360E-03    3
 0.82160300E-07-0.19775570E-10 0.85580110E+05 0.58934110E+02 0.00000000E+00    4
ANC2HC2H2U               C  16H   9    0    0G    300.00   3000.00           1
 0.18946460E+02 0.64164270E-01-0.33538320E-04 0.83877340E-08-0.81691690E-12    2
 0.85127550E+05-0.71633350E+02-0.62755570E+01 0.15162720E+00-0.15126010E-03    3
 0.82083420E-07-0.19060790E-10 0.91083550E+05 0.53987840E+02 0.00000000E+00    4
A3                       C  14H  10    0    0G    300.00   3000.00           1
 0.12737260E+02 0.69110850E-01-0.36415370E-04 0.91814820E-08-0.90095470E-12    2
 0.17070730E+05-0.47958710E+02-0.89114900E+01 0.13070820E+00-0.92477070E-04    3
 0.21374720E-07 0.29925740E-11 0.22781040E+05 0.62981310E+02 0.00000000E+00    4
A3C2H                    C  16H  10    0    0G    300.00   3000.00           1
 0.16951980E+02 0.71031150E-01-0.37338670E-04 0.93973680E-08-0.92080560E-12    2
 0.43532810E+05-0.67778820E+02-0.93305790E+01 0.15649410E+00-0.14024880E-03    3
 0.62550860E-07-0.10373820E-10 0.49989500E+05 0.64412200E+02 0.00000000E+00    4
A3C2H)2                  C  18H  10    0    0G    300.00   3000.00           1
 0.21166700E+02 0.72951460E-01-0.38261970E-04 0.96132540E-08-0.94065670E-12    2
 0.69994880E+05-0.88292080E+02-0.97496690E+01 0.18228000E+00-0.18802050E-03    3
 0.10372700E-06-0.23740220E-10 0.77197950E+05 0.65149960E+02 0.00000000E+00    4
A3R5                     C  16H  10    0    0G    300.00   3000.00           1
 0.15553980E+02 0.73407850E-01-0.38773310E-04 0.97771840E-08-0.95853990E-12    2
 0.28785590E+05-0.61792280E+02-0.10433920E+02 0.15385510E+00-0.12850960E-03    3
 0.50982500E-07-0.69190420E-11 0.35352710E+05 0.69901660E+02 0.00000000E+00    4
A3R5C2H                  C  18H  10    0    0G    300.00   3000.00           1
 0.19768690E+02 0.75328160E-01-0.39696620E-04 0.99930700E-08-0.97839100E-12    2
 0.55247670E+05-0.82305540E+02-0.10853010E+02 0.17964110E+00-0.17628130E-03    3
 0.92158640E-07-0.20285440E-10 0.62561170E+05 0.70639400E+02 0.00000000E+00    4
A3-                      C  14H   9    0    0G    300.00   3000.00           1
 0.13077050E+02 0.65503860E-01-0.34681750E-04 0.87757840E-08-0.86347040E-12    2
 0.46542460E+05-0.47498420E+02-0.78990730E+01 0.12528190E+00-0.89694240E-04    3
 0.21728300E-07 0.23683330E-11 0.52082570E+05 0.60002240E+02 0.00000000E+00    4
A3C2H-                   C  16H   9    0    0G    300.00   3000.00           1
 0.17291760E+02 0.67424160E-01-0.35605050E-04 0.89916700E-08-0.88332140E-12    2
 0.73004540E+05-0.68011690E+02-0.83181630E+01 0.15106780E+00-0.13746600E-03    3
 0.62904430E-07-0.10998070E-10 0.79291030E+05 0.60739980E+02 0.00000000E+00    4
A3C2H2U                  C  16H  11    0    0G    300.00   3000.00           1
 0.15844900E+02 0.75392590E-01-0.39624110E-04 0.99690100E-08-0.97644100E-12    2
 0.51720540E+05-0.58167380E+02-0.62125380E+01 0.13757580E+00-0.95520660E-04    3
 0.21651420E-07 0.30831120E-11 0.57586010E+05 0.55055960E+02 0.00000000E+00    4
A3C2HC2H2U               C  18H  11    0    0G    300.00   3000.00           1
```

```
 0.20059610E+02 0.77312890E-01-0.40547410E-04 0.10184900E-07-0.99629200E-12    2
 0.78182610E+05-0.78680630E+02-0.66316280E+01 0.16336180E+00-0.14329240E-03    3
 0.62827550E-07-0.10283290E-10 0.84794480E+05 0.55793720E+02 0.00000000E+00    4
A3R5-                  C  16H   9    0    0G    300.00   3000.00               1
 0.15893760E+02 0.69800860E-01-0.37039690E-04 0.93714870E-08-0.92105570E-12    2
 0.58257320E+05-0.62025140E+02-0.94215090E+01 0.14842890E+00-0.12572680E-03    3
 0.51336080E-07-0.75432830E-11 0.64654250E+05 0.66229440E+02 0.00000000E+00    4
A3R5C2H2U              C  18H  11    0    0G    300.00   3000.00               1
 0.18661610E+02 0.79689590E-01-0.41982050E-04 0.10564710E-07-0.10340260E-11    2
 0.63435400E+05-0.72694100E+02-0.77349730E+01 0.16072280E+00-0.13155320E-03    3
 0.51259200E-07-0.68285040E-11 0.70157690E+05 0.61283170E+02 0.00000000E+00    4
A4                     C  16H  10    0    0G    300.00   3000.00               1
 0.15818180E+02 0.73304150E-01-0.38914010E-04 0.98695600E-08-0.97300760E-12    2
 0.18185970E+05-0.66400860E+02-0.12772970E+02 0.15862650E+00-0.12476260E-03    3
 0.37927120E-07 0.57212260E-13 0.25511720E+05 0.79091690E+02 0.00000000E+00    4
A4C2H                  C  18H  10    0    0G    300.00   3000.00               1
 0.20032900E+02 0.75224450E-01-0.39837310E-04 0.10085450E-07-0.99285860E-12    2
 0.44648040E+05-0.85527830E+02-0.13192060E+02 0.18441240E+00-0.17253440E-03    3
 0.79103260E-07-0.13309190E-10 0.52720180E+05 0.81215720E+02 0.00000000E+00    4
A4C2H)2                C  20H  10    0    0G    300.00   3000.00               1
 0.24247610E+02 0.77144760E-01-0.40760610E-04 0.10301330E-07-0.10127100E-11    2
 0.71110120E+05-0.10604110E+03-0.13611150E+02 0.21019830E+00-0.22030610E-03    3
 0.12027940E-06-0.26675590E-10 0.79928640E+05 0.81953480E+02 0.00000000E+00    4
A4R5                   C  18H  10    0    0G    300.00   3000.00               1
 0.18634890E+02 0.77601150E-01-0.41271950E-04 0.10465260E-07-0.10305930E-11    2
 0.29900820E+05-0.79541290E+02-0.14295400E+02 0.18177350E+00-0.16079520E-03    3
 0.67534900E-07-0.98544040E-11 0.38083400E+05 0.86705180E+02 0.00000000E+00    4
A4-                    C  16H   9    0    0G    300.00   3000.00               1
 0.16157960E+02 0.69697160E-01-0.37180390E-04 0.94638630E-08-0.93552340E-12    2
 0.47657700E+05-0.65247440E+02-0.11760550E+02 0.15320020E+00-0.12197980E-03    3
 0.38280700E-07-0.56702870E-12 0.54813250E+05 0.76805760E+02 0.00000000E+00    4
A4C2H-                 C  18H   9    0    0G    300.00   3000.00               1
 0.20372680E+02 0.71617460E-01-0.38103690E-04 0.96797490E-08-0.95537430E-12    2
 0.74119770E+05-0.85760700E+02-0.12179640E+02 0.17898620E+00-0.16975150E-03    3
 0.79456830E-07-0.13933430E-10 0.82021720E+05 0.77543500E+02 0.00000000E+00    4
A4C2HC2H2U             C  20H  11    0    0G    300.00   3000.00               1
 0.23140530E+02 0.81506190E-01-0.43046050E-04 0.10872980E-07-0.10683450E-11    2
 0.79297860E+05-0.96429640E+02-0.10493100E+02 0.19128010E+00-0.17557790E-03    3
 0.79379950E-07-0.13218650E-10 0.87525160E+05 0.72597230E+02 0.00000000E+00    4
A5                     C  20H  12    0    0G    300.00   3000.00               1
 0.19748050E+02 0.90749760E-01-0.48281030E-04 0.12262420E-07-0.12099680E-11    2
 0.21848850E+05-0.87281720E+02-0.14651470E+02 0.19350810E+00-0.15282750E-03    3
 0.48279030E-07-0.10769000E-11 0.30687270E+05 0.87817900E+02 0.00000000E+00    4
A5C2H                  C  22H  12    0    0G    300.00   3000.00               1
 0.23962760E+02 0.92670080E-01-0.49204340E-04 0.12478310E-07-0.12298190E-11    2
 0.48310920E+05-0.10710180E+03-0.15070560E+02 0.21929400E+00-0.20059920E-03    3
 0.89455170E-07-0.14443300E-10 0.57895730E+05 0.89248800E+02 0.00000000E+00    4
A5-                    C  20H  11    0    0G    300.00   3000.00               1
 0.20087830E+02 0.87142770E-01-0.46547410E-04 0.11856730E-07-0.11724840E-11    2
 0.51320580E+05-0.86821440E+02-0.13639060E+02 0.18808180E+00-0.15004470E-03    3
 0.48632610E-07-0.17011400E-11 0.59988810E+05 0.84838820E+02 0.00000000E+00    4
A5C2H2U                C  22H  13    0    0G    300.00   3000.00               1
```

```
 0.22855680E+02 0.97031510E-01-0.51489770E-04 0.13049950E-07-0.12854540E-11    2
 0.56498660E+05-0.97490400E+02-0.11952520E+02 0.20037580E+00-0.15587110E-03    3
 0.48555740E-07-0.98636180E-12 0.65492250E+05 0.79892560E+02 0.00000000E+00    4
A6                      C  22H  12    0    0G    300.00   3000.00             1
 0.22828970E+02 0.94943070E-01-0.50779670E-04 0.12950500E-07-0.12820210E-11    2
 0.22964080E+05-0.10503070E+03-0.18512950E+02 0.22142640E+00-0.18511310E-03    3
 0.64831430E-07-0.40122620E-11 0.33417950E+05 0.10462140E+03 0.00000000E+00    4
A6C2H                   C  24H  12    0    0G    300.00   3000.00             1
 0.27043680E+02 0.96863370E-01-0.51702980E-04 0.13166390E-07-0.13018720E-11    2
 0.49426160E+05-0.12485080E+03-0.18932040E+02 0.24721230E+00-0.23288480E-03    3
 0.10600760E-06-0.17378660E-10 0.60626410E+05 0.10605230E+03 0.00000000E+00    4
A6-                     C  22H  11    0    0G    300.00   3000.00             1
 0.23168750E+02 0.91336080E-01-0.49046050E-04 0.12544810E-07-0.12445370E-11    2
 0.52435810E+05-0.10457040E+03-0.17500540E+02 0.21600010E+00-0.18233020E-03    3
 0.65185010E-07-0.46365030E-11 0.62719490E+05 0.10164240E+03 0.00000000E+00    4
A6C2H2U                 C  22H  13    0    0G    300.00   3000.00             1
 0.22855680E+02 0.97031500E-01-0.51489770E-04 0.13049950E-07-0.12854540E-11    2
 0.57605710E+05-0.97490400E+02-0.11952520E+02 0.20037580E+00-0.15587110E-03    3
 0.48555740E-07-0.98636180E-12 0.66599300E+05 0.79892550E+02 0.00000000E+00    4
A7                      C  24H  12    0    0G    300.00   3000.00             1
 0.25909880E+02 0.99136370E-01-0.53278310E-04 0.13638580E-07-0.13540740E-11    2
 0.24079320E+05-0.12457150E+03-0.22374430E+02 0.24934470E+00-0.21739870E-03    3
 0.81383830E-07-0.69476240E-11 0.36148640E+05 0.11963320E+03 0.00000000E+00    4
A7C2H                   C  26H  12    0    0G    300.00   3000.00             1
 0.30124600E+02 0.10105670E+00-0.54201610E-04 0.13854470E-07-0.13739250E-11    2
 0.50541400E+05-0.14259980E+03-0.22793520E+02 0.27513060E+00-0.26517040E-03    3
 0.12256000E-06-0.20314020E-10 0.63357090E+05 0.12285580E+03 0.00000000E+00    4
A7C2H)2                 C  28H  12    0    0G    300.00   3000.00             1
 0.34339320E+02 0.10297700E+00-0.55124910E-04 0.14070350E-07-0.13937760E-11    2
 0.77003480E+05-0.16380620E+03-0.23212610E+02 0.30091660E+00-0.31294200E-03    3
 0.16373610E-06-0.33680420E-10 0.90565550E+05 0.12290040E+03 0.00000000E+00    4
A7-                     C  24H  11    0    0G    300.00   3000.00             1
 0.26249660E+02 0.95529380E-01-0.51544690E-04 0.13232880E-07-0.13165900E-11    2
 0.53551050E+05-0.12231940E+03-0.21362010E+02 0.24391840E+00-0.21461580E-03    3
 0.81737400E-07-0.75718650E-11 0.65450170E+05 0.11844590E+03 0.00000000E+00    4
A7C2H-                  C  26H  11    0    0G    300.00   3000.00             1
 0.30464380E+02 0.97449690E-01-0.52467990E-04 0.13448770E-07-0.13364410E-11    2
 0.80013130E+05-0.14283270E+03-0.21781100E+02 0.26970430E+00-0.26238750E-03    3
 0.12291360E-06-0.20938260E-10 0.92658620E+05 0.11918360E+03 0.00000000E+00    4
A7C2HC2H2U              C  28H  13    0    0G    300.00   3000.00             1
 0.33232230E+02 0.10733840E+00-0.57410350E-04 0.14642000E-07-0.14494110E-11    2
 0.85191200E+05-0.15350170E+03-0.20094570E+02 0.28199830E+00-0.26821390E-03    3
 0.12283670E-06-0.20223490E-10 0.98162070E+05 0.11423730E+03 0.00000000E+00    4
A8                      C  28H  14    0    0G    300.00   3000.00             1
 0.29839750E+02 0.11658200E+00-0.62645330E-04 0.16031450E-07-0.15910340E-11    2
 0.27742200E+05-0.14435370E+03-0.24252940E+02 0.28422630E+00-0.24546350E-03    3
 0.91735740E-07-0.80817350E-11 0.41324190E+05 0.12945800E+03 0.00000000E+00    4
A8C2H                   C  30H  14    0    0G    300.00   3000.00             1
 0.34054470E+02 0.11850230E+00-0.63568640E-04 0.16247330E-07-0.16108850E-11    2
 0.54204280E+05-0.16417380E+03-0.24672030E+02 0.31001220E+00-0.29323520E-03    3
 0.13291190E-06-0.21448140E-10 0.68532650E+05 0.13088890E+03 0.00000000E+00    4
A8-                     C  28H  13    0    0G    300.00   3000.00             1
```

```
 0.30179540E+02 0.11297500E+00-0.60911710E-04 0.15625750E-07-0.15535500E-11    2
 0.57213930E+05-0.14389340E+03-0.23240520E+02 0.27880000E+00-0.24268060E-03    3
 0.92089320E-07-0.87059760E-11 0.70625720E+05 0.12647890E+03 0.00000000E+00    4
A9                      C  30H  14    0    0G    300.00   3000.00             1
 0.32920670E+02 0.12077530E+00-0.65143980E-04 0.16719520E-07-0.16630870E-11    2
 0.28857430E+05-0.16140960E+03-0.28114410E+02 0.31214460E+00-0.27774910E-03    3
 0.10828820E-06-0.11017100E-10 0.44054870E+05 0.14695470E+03 0.00000000E+00    4
A9-                     C  30H  13    0    0G    300.00   3000.00             1
 0.33260450E+02 0.11716830E+00-0.63410360E-04 0.16313830E-07-0.16256030E-11    2
 0.58329160E+05-0.16164250E+03-0.27102000E+02 0.30671830E+00-0.27496620E-03    3
 0.10864170E-06-0.11641340E-10 0.73356410E+05 0.14328250E+03 0.00000000E+00    4
A9C2H                   C  32H  14    0    0G    300.00   3000.00             1
 0.37135380E+02 0.12269560E+00-0.66067280E-04 0.16935410E-07-0.16829380E-11    2
 0.55319510E+05-0.18192280E+03-0.28533510E+02 0.33793060E+00-0.32552080E-03    3
 0.14946430E-06-0.24383500E-10 0.71263330E+05 0.14769240E+03 0.00000000E+00    4
A10                     C  32H  14    0    0G    300.00   3000.00             1
 0.36001580E+02 0.12496860E+00-0.67642610E-04 0.17407600E-07-0.17351400E-11    2
 0.29972670E+05-0.18054490E+03-0.31975890E+02 0.34006290E+00-0.31003460E-03    3
 0.12484050E-06-0.13952460E-10 0.46785550E+05 0.16237190E+03 0.00000000E+00    4
END
```

REFERENCES

Alberty, R.A., Journal of Physical and Chemical Reference Data, in press, (1988).

Alberty, R.A., personal communication, May, (1985).

Ames, B.N., McCann, J., Yamasaki, E., Mutation Research, 31, pp. 347-364, (1971).

Asaba, T., Fujii, N., Thirteenth Symposium (International) on Combustion, p. 155, The Combustion Institute, Pittsburgh, PA (1971).

Badger, G.M., Jolad, S.D., and Spotswood, T.M., "The Formation of Aromatic Hydrocarbons at High Temperatures: part XXIX", Australian Journal of Chemistry, (1967). [plus 28 previously published papers by Badger starting in 1958.]

Barat, B.B., Longwell, J.P., and Sarofim, A.F., Poster Session presented at Twenty-Second Symposium (International) on Combustion, The Combustion Institute, (1988).

Bauer, S.H., and Jeffers, P.M., Energy and Fuels, 2, pp. 446-453, (1988).

Bauer, S.H., and Jeffers, P.M., "Pyrolysis of Di and Tri-cyclic Aromatics: I. A Minimal Mechanism of Soot Precursor Production", paper presented at the poster session of the Twentieth Symposium (International) on Combustion, The Combustion Institute, (1984).

Bauer, S.H., and Zhang, L.M., 14th International Symposium on Shock Tubes and Waves, New South Wales University Press, pp. 654-661, (1983).

Benson, S.W. "Thermochemical Kinetics", Second edition, John Wiley and Sons, New York, (1976).

Bittner, J.D., "A Molecular Beam Mass Spectrometer Study of Fuel-Rich and Sooting Benzene-Oxygen Flames", Ph.D. Thesis, Massachusetts Institute of Technology, (1981c).

Bittner, J.D., and Howard, J.B., "Composition Profiles and Reaction Mechanisms in a Near-sooting Premixed Benzene/Oxygen/Argon Flame", Eighteenth Symposium (International) on Combustion, p. 1105, The Combustion Institute, (1981b).

Bittner, J.D., and Howard, J.B., "Pre-Particle Chemistry in Soot Formation", paper presented at the General Motors Research Symposium, Particulate Carbon -- Formation During Combustion, Warren, Michigan, October 14-16, (1981a).

Bittner, J.D., and Howard, J.B., "Role of Aromatics in Soot Formation", in Alternative Hydrocarbon Fuels: Combustion and Chemical Kinetics (C.T. Bowman and J. Birkeland, Eds.), Progress in Astro. and Aero., Vol. 62, p. 335, AIAA (1978).

Blazowski, W.S., Combustion Science and Technology, 21, pp. 87-96, (1980).

Bockhorn, H., Fetting, F., and Wenz, H., Ber. Bunsenges Phys. Chem., 87, p. 1067, (1983).

Bonne, U., Homann, K.H., and Wagner, H.Gg., "Carbon Formation in Pre-mixed Flames", Tenth Symposium (International) on Combustion, p. 503, The Combustion Institute, (1965).

Burcat, A., Appendix C, "Table of Coefficient Sets for NASA Polynomials," in Combustion Chemistry, Gardiner, W.C. eds., Springer-Verlag, New York, (1984).

Calcote, H.F., "Ionic Mechanisms of Soot Formation in Flames", paper presented at Fall Technical Meeting of Eastern States Section of the Combustion Institute, Miami, Florida, November (1978).

Chakraborty, B.B., and Long, R., "The Formation of Soot and Polycyclic Aromatic Hydrocarbons in Diffusion Flames -- Part Two", Combustion and Flame 12, p. 237, (1968).

Cole, J.A., Bittner, J.D., Longwell, J.P., and Howard, J.B., Combustion and Flame, 56, pp. 51-70, (1984).

Cole, J.A., "A Molecular-Beam Mass-Spectrometric Study of Stoichiometric and Fuel-Rich 1,3-Butadiene Flames", M.S. thesis, Department of Chemical Engineering, Massachusetts Institute of Technology, Cambridge, MA, (1981).

Colket, III, M.B., Twenty-first Symposium (International) on Combustion, pp. 851-864, The Combustion Institute, (1986).

Cowperthwaite, M., and Bauer, S.H., Journal of Chemical Physics, 36, p. 1743, (1962).

Crittenden, B.D., and Long, R., "The Mechanisms of Formation of Polynuclear Aromatic Compounds in Combustion Systems", in Carcinogenesis, Vol 1., Polynuclear Aromatic Hydrocarbons: Chemistry, Metabolism, and Carcinogenesis, (R.I. Freudenthal and P.W. Jones, Eds.), Raven Press, New York, (1976).

D'Alessio, A., Di Lorenzo, A., Borghese, A., Beretta, F., and Masi, S., "Study of the Soot Nucleation Zone of Rich Methane-Oxygen Flames", Sixteenth Symposium (International) on Combustion, p. 695, The Combustion Institute, (1976).

D'Alessio, A., Di Lorenzo, A., Sarofim, A.F., Beretta, F., Masi, S., and Venitozzi, C., "Soot Formation in Methane-Oxygen Flames", Fifteenth Symposium (International) on Combustion, p. 1427, The Combustion Institute, (1974).

Dauben Jr., H.J., and Osborne, A.G., Abstracts of the 130th National Meeting of the American Chemical Society, Atlantic City, N.J., p 370, (1956).

Davies, R.A., and Scully, D.B., "Carbon Formation from Aromatic Hydrocarbons II", Combustion and Flame, 10, p. 165, (1965).

Duff, R.E., and Bauer, S.H., Journal of Chemical Physics, 36, p 1754, (1962).

Fahr, A., Mallard, W.G., and Stein, S.E., Twenty-First Symposium (International) on Combustion, pp. 825-831, The Combustion Institute, (1986).

Frenklach, M., Twenty-Second Symposium (International) on Combustion, in press, The Combustion Institute, (1988).

Frenklach, M., and Warnatz, Combustion Science and Technology, 51, pp. 265-283, (1987).

Frenklach, M., Clary, D.W., and Yuan, T., Combustion Science and Technology, 50, p. 79, (1986).

Frenklach, M., Clary, D.W., Gardiner, W.C., and Stein, S.E., Twentieth Symposium (International) on Combustion, p. 887, The Combustion Institute, (1985b).

Frenklach, M., Ramachandra, M.K., and Matula, R.A., Twentieth Symposium (International) on Combustion, p. 871, The Combustion Institute, (1985a).

Frenklach, M., Taki, S., Durgaprasad, M.B., and Matula, R.A., Combustion and Flame, 54, pp. 81-101, (1983).

Fujii, N., and Asaba, T., "Shock-Tube Study of the Reaction of Rich Mixtures of Benzene and Oxygen", Fourteenth Symposium (International) on Combustion, p. 433, The Combustion Institute, (1973).

Glarborg, P., Kee, R.J., Grcar, J.F., and Miller, J.A., Sandia Report, SAND86-8209, Sandia National Laboratories, Albuquerque, New Mexico and Livermore, California, February, (1986b).

Glarborg, P., Miller J.A., and Kee R.J., Combustion and Flame, 65, pp. 177-202, (1986a).

Godleski, S.A., Progress in Physical and Organic Chemistry 13, p. 63, (1981).

Goldstein, S., Modern Developments in Fluid Mechanics, Oxford Press, (1938).

Graham, S.C., Homer, J.B., and Rosenfeld, J.L.J., "The Formation and Coagulation of Soot Aerosols Generated by the Pyrolysis of Aromatic Hydrocarbons", Proceedings of the Royal Society of London, 344, p. 259, (1975).

Harris, S.J., Twenty-Second Symposium (International) on Combustion, in press, The Combustion Institute (1988b).

Harris, S.J., Weiner, A.M., and Blint, R.J., Combustion and Flame, 72, pp. 91-109, (1988a).

Harris, S.J. and Weiner A.M., Twentieth Symposium (International) on Combustion, The Combustion Institute, Pittsburgh, pp. 969-978, (1984).

Haynes, B.S., and Wagner, H.Gg., "Soot Formation", Progress in Energy and Combustion Science, 7, pp. 229-273, (1980).

He, Y.Z., Mallard, W.G., and Tsang, W., Journal of Physical Chemistry, 92, p. 2196, (1988b).

He, Y.Z., Cui, J.P., Mallard, W.G., and Tsang, W., Journal of Physical Chemistry, 92, p. 1510 (1988a)

Hindmarsh, A.C., Scientific Computing, R.S. Stepleman et al. eds., Vol. 1 of "IMACS Transactions on Scientific Computation," North Holland, Amsterdam, (1983).

Homann, K.H., Twentieth Symposium (International) on Combustion, p. 857, The Combustion Institute, (1984).

Homann, K.H., and Wagner, H.Gg., "Some New Aspects of the Mechanism of Carbon Formation in Premixed Flames", Eleventh Symposium (International) on Combustion, p. 371, The Combustion Institute (1967).

Hou, K.C., and Palmer, H.B., "The Kinetics of Thermal Decomposition of Benzene in a Flow System", Journal of Physical Chemistry, Vol 69, Number 3, p. 863, (1965b).

Hou, K.C., and Palmer, H.B., "The Kinetics of Thermal Decomposition of Diacetylene in a Flow System", Journal of Physical Chemistry, Vol 69, Number 3, p. 858, (1965a).

Hou, K.C., and Anderson, R.C., "Comparative Studies of Pyrolysis of Acetylene, Vinylacetylene, and Diacetylene", Journal of Physical Chemistry, 67, p. 1579, (1963).

Howard, J.B. and Longwell, J.P., Seventh International Symposium on Polynuclear Aromatic Hydrocarbons, Battelle Press, Columbus, OH, (1982).

Hsu, D.S.Y., Lin, C.Y., and Lin, M.C., Twentieth Symposium (International) on Combustion, p. 623, The Combustion Institute, (1984).

Kaden, D.A., Hites, R.A. and Thilly, W.G., Cancer Research, 39, pp. 4152-4159, (1979).

Kee, R.J., Miller, J.A., and Jefferson, T.H., Sandia Report, SAND80-8003, (1980).

Kern, R.D., Wu, C.H., Skinner, G.B., Rao, V.S., Kiefer, J.H, Towers, J.A., and Mizerka, L.J., Twentieth Symposium (International) on Combustion, The Combustion Institute, (1985).

Kern, R.D., and Singh, H.J., paper presented at the 183rd National Meeting of the American Chemical Society, Las Vegas, Nevada, (1982b).

Kern, R.D., Singh, H.J., Esslinger, M.A., and Winkeler, P.W., "Product Profiles Observed During the Pyrolyses of Toluene, Benzene, Butadiene, and Acetylene", Nineteenth Symposium (International) on Combustion, p. 1351, The Combustion Institute, (1982a).

Kiefer, J.H., Mizerka, L.J., Patel, M.R., and Wei, H.C., Journal of Physical Chemistry, 89, pp. 2013-2019, (1985).

Kinney, C.R., and Slysh, R.S., Proc. Conf. Carbon, 4th, Buffalo, p. 301, (1960).

Kridiotis, A.C., "The Effect of Imperfect Micromixing On Chemical Reaction In the CO/H_2 - Air System", Ph.D. thesis, Department of Chemical Engineering, Massachusetts Institute of Technology, Cambridge, MA, (1986).

LaFleur, A.L., Monchamp, P.A., Chang, N.S., Plummer, E.F., and Wornat, M.J., Journal of Chromatographic Science, in press, (1988b).

Lafleur, A.L., Gagel, J.J., Longwell, J.P., and Monchamp, P.A., Energy and Fuels, 2, pp. 709-716, (1988a).

LaFleur, A.L., Monchamp, P.A., Plummer, E.F., and Kruzel, E.L., Analytical Letters, 19, p. 2013, (1986).

Lahaye, J., and Prado, G., "Mechanisms of Carbon Black Formation", Chemistry and Physics of Carbon, Vol. 14, (P.L. Walker and P.A. Thrower, eds.), p. 168, Marcel Dekker, New York, (1978).

Lam, F.W., Howard, J.B., and Longwell, J.P., Twenty-Second Symposium (International) on Combustion, in press, (1988).

Lam, F.W., in the Sixth Annual Report of Progress to NIEHS, (1987).

Lee, M.L. and Wright, B.W., Journal of Chromatographic Science, 18, p. 345, (1980).

Lee, M.L., Vassilaros, D.L., White, C.M., and Novotny, M., Analytical Chemistry, 51, p. 788, (1979).

Levenspiel, O., Chemical Reaction Engineering, Second Edition, John Wiley and Sons, (1962).

Levenspiel, O., and Bischoff, K.B., "Backmixing in the Design of Chemical Reactors", Industrial and Engineering Chemistry, Vol. 51, no. 12, (1959).

Longwell, J.P., "Polycyclic Aromatic Hydrocarbons and Soot from Practical Combustion Systems", in Soot in Combustion Systems and its Toxic Properties, (J. Lahaye and G. Prado eds.) Plenum Publishing Corp., (1983).

Longwell, J.P., "The Formation of Polycyclic Aromatic Hydrocarbons by Combustion", Nineteenth Symposium (International) on Combustion, p. 1339, The Combustion Institute, (1982).

Longwell, J.P. and Weiss, M.A., Industrial Engineering Chemistry, 47, p. 1634, (1955).

McKinnon, J.T., Personal communication, (1988b).

McKinnon, J.T., and Howard, J.B., From Poster session presented at Twenty-Second Symposium (International) on Combustion, (1988a).

Miller, J.A., Mitchell, R.E., Smooke, M.B., and Kee, R.J., Nineteenth Symposium (International) on Combustion, The Combustion Institute, (1983).

Nenniger, J.E., Kridiotis, A., Chomiak, J., Longwell, J.P., and Sarofim, A.F., Twentieth Symposium (International) on Combustion, p. 473, The Combustion Institute, (1985).

Nenniger, J.E., "Polycyclic Aromatic Hydrocarbon Production in a Jet Stirred Combustor", Ph.D. Thesis, Massachusetts Institute of Technology, (1983).

Neoh, K.G., " Soot Burnout in Flames", Ph.D. Thesis, Massachusetts Institute of Technology, (1980).

Olson, K.L., Harris, S.J., and Weiner, A.M., Combustion Science and Technology, 51, p. 97, (1987).

Palmer, H.B., and Cullis, C.F., "The Formation of Carbon from Gases",

in Chemistry and Physics of Carbon, Vol. 1, (P.L. Walker, ed.), p. 265, Marcel Dekker, NY, (1965).

Patrick, M.A., Sheffield Univ. Fuel Soc. J., 16, pp. 46-61, (1965).

Pope, C.J., "Fluxes and Net Reaction Rates of High Molecular Weight Material in a Near-Sooting Benzene-Oxygen Flame", M.S. Thesis, Massachusetts Institute of Technology, (1988).

Reynolds, W.C., STANJAN Program V.3.60, (on disk), June 27, (1986).

Schaden, G., Journal of Organic Chemistry, 48, pp. 5385-5386, (1983).

Scully, D.B., and Davies, R.A., "Carbon Formation from Aromatic Hydrocarbons", Combustion and Flame 9, p. 185, (1964).

Smith, E.C.W., Proceedings on the Royal Society of London, Ser. A, 174, 110, (1940).

Smith, R.D. and Johnson, A.L., Combustion and Flame, 51, pp. 1-22, (1983).

Smith, R.D., "A Direct Mass Spectrometric Study of the Mechanism of Toluene Pyrolysis at High Temperatures", Journal of Physical Chemistry Vol. 83, No. 12, p. 1553, (1979b).

Smith, R.D., "Formation of Radicals and Complex Organic Compounds by High-Temperature Pyrolysis: The Pyrolysis of Toluene", Combustion and Flame 35, p. 179, (1979a).

Stehling, F.C., Frazee, J.D., and Anderson, R.C., "Mechanisms of Nucleation in Carbon Formation", Eighth Symposium (International) on Combustion, p. 774, The Combustion Institute, (1962).

Stein, S.E., personal communication, (1987b).

Stein, S.E., Golden, D.M., Benson, S.W., Journal of Physical Chemistry, 81, No. 4, p. 314, (1987a).

Stein, S.E., and Fahr, A., Journal of Physical Chemistry, 89, pp. 3714-3725, (1985).

Stein, S.E., Barton, B.D., Thermochimica Acta, 44, pp. 265-251, (1981).

Stein, S.E., Journal of Physical Chemistry, 82:5, (1978).

Street, J.C., and Thomas, A., "Carbon Formation in Premixed Flames", Fuel 34, p. 4, (1955).

Stull, D.R., Westrum, E.F., and Sinke, G.C., The Chemical Thermodynamics of Organic Compounds, Wiley, New York, (1969).

Sun, W.H., "Reactions of Nitrogen Compounds during Back-mixed, Fuel Rich Hydrocarbon Combustion", Ph.D. Thesis, Massachusetts Institute of Technology, (1985).

Szekely, J. "Reaction Rate Constant May Modify the Effects of Backmixing", Industrial and Engineering Chemistry, Vol 53, No. 4, (1961).

Tanzawa, T., and Gardiner, W.C. Jr., Journal of Physical Chemistry, 84, p. 236, (1980).

Taylor, G.I., "Conditions Under Which Dispersion of a Solute in a Stream of Solvent can be used to Measure Molecular Diffusion", Proceedings of the Royal Society (London), 225A, p. 473, (1954b).

Taylor, G.I., "The Dispersion of Matter in Turbulent Flow Through a Pipe", Proceedings of the Royal Society (London), 223A, p. 446, (1954a).

Taylor, G.I., "Dispersion of Soluble Matter in Solvent Flowing Slowly Through a Tube", Proceedings of the Royal Society (London), 219A, p. 186, (1953).

Thilly, W. G., personal communication, (1987).

Thilly, W.G., M.I.T. Center For Environmental Health Sciences, 1986 Annual Report of Progress to N.I.E.H.S., (1986).

Tichacek, L.J., "Selectivity in Experimental Reactors", AIChE Journal, Vol. 9, No. 3, (1963).

Tompkins, E.E., and Long, R., "The Flux of Polycyclic Aromatic Hydrocarbons and of Insoluble Material in Premixed Acetylene-Oxygen Flames", Twelfth Symposium (International) on Combustion, p. 625, The Combustion Institute, Pittsburgh, PA (1969).

Toqan, M., Ph.D. Thesis, Massachusetts Institute of Technology, (1985).

Trost, B.M., Bright, G.M., Frihart, C., and Brittelli, D., Journal of the American Chemical Society, 93:3, pp. 4080-4086, February 10, (1971).

Tsang W., and Hampson, R.F., Journal of Physical Chemistry, Reference Data, 15, p. 3, (1986).

Tully, F.P., Ravishankara, A.R., Thompson, R.L., Nicovich, J.M., Shah, R,C., Kreutler, N.M., and Wine, P.H., Journal of Physical Chemistry, 85, p. 2262, (1981).

Vaughn, C.B., "Formation of Soot and Polycyclic Aromatic Hydrocarbons

in a Jet/Stirred Reactor", Ph.D. Thesis, Massachusetts Institute of Technology, (1985).

Vaughn, S.N., "A Single Pulse Shock Tube Study of the Chemical Mechanisms of Soot Formation From Benzene Pyrolysis", Ph.D. Thesis, Kansas State University, (1980).

Venkat, C., Brezinsky, K., and Glassman, I., Nineteenth Symposium (International) on Combustion, The Combustion Institute, (1982).

Warnatz, J., Combustion Science and Technology, 34, pp. 177-200, (1983).

Warnatz, J. in "Combustion Chemistry", W.C. Gardiner, Ed., Springer Verlag, New York, (1984).

Wenz, H.W., "Untersuchungen Zur Bildung Von Hohermoleckularen Kohlenwasserstoffen in Brennerstabilisierten Flammen Unterschiedlicher Brennstoffe und Gemischzusammensetzungen", Dissertation, Technischen Hochschule Darmstadt, (1983).

Westbrook, C.K. and Dryer, F.L., Progress in Energy Combustion, 10, pp. 1-57, (1984).

Westbrook, C.K., Combustion Science and Technology, 34, p. 201, (1983b).

Westbrook, C.K., Dryer, F.L., and Schug, K.P., Nineteenth Symposium (International) on Combustion, The Combustion Institute, (1983a).

Westmoreland, P.R., Dean, A.M., Howard, J.B., and Longwell, J.P., Journal of Physical Chemistry, pp. 1-23, (1988).

Westmoreland, P.R., "Advances in Soot Chemistry", sponsored by the Division of Fuel Chemistry, American Chemical Society, 194th National Meeting, New Orleans, LA, (1987).

Westmoreland, P.R., "Experimental And Theoretical Analysis of Oxidation and Growth Chemistry In a Fuel-Rich Acetylene Flame", Ph.D. thesis, Department of Chemical Engineering, Massachusetts Institute of Technology, Cambridge, MA, (1986c).

Westmoreland, P.R., Twenty-first Symposium (International) on Combustion, pp. 773-782, The Combustion Institute, (1986b).

Westmoreland, P.R., Dean, A.M., Howard, J.B., and Longwell, J.P., Journal of Physical Chemistry, pp. 1-24, (1986a).